

TECHNISCHE UNIVERSITÄT MÜNCHEN

WACKER Institut für Siliciumchemie

Professur für Siliciumchemie

**Novel Silyl Radicals and Disilenes: Reactivity Studies  
and Evaluation for Battery Application**

**Richard Holzner**

Vollständiger Abdruck der von der Fakultät für Chemie der Technischen Universität München zur Erlangung des akademischen Grades eines

**Doktors der Naturwissenschaften**

genehmigten Dissertation.

Vorsitzender: apl. Prof. Dr. Wolfgang Eisenreich  
Prüfer der Dissertation: 1. Prof. Dr. Shigeyoshi Inoue  
2. Prof. Dr. Dr. h.c. Bernhard Rieger

Die Dissertation wurde am 09.03.2020 bei der Technischen Universität München eingereicht und durch die Fakultät für Chemie am 13.04.2020 angenommen.

Diese Arbeit wurde in der Zeit von April 2016 bis Dezember 2019 im Rahmen der Professur für Siliciumchemie der Technischen Universität München unter Betreuung von Herrn Prof. Dr. Shigeyoshi Inoue durchgeführt.



## Acknowledgments

Mein herzlichster Dank gilt Herrn Prof. Dr. Shigeyoshi Inoue, für die Aufnahme an seinen Lehrstuhl und das Vertrauen, das er mir entgegengebracht hat, mein Promotionsthema mit vielen Freiheiten bearbeiten zu können. Er steckte mich mit seiner Begeisterung für Siliciumchemie an und brachte mein Forschungsprojekt stets mit produktiven Anregungen und Diskussionen voran.

Darüber hinaus bedanke ich mich beim gesamten AK Inoue und bei meinen Forschungspraktikanten für die gute Zusammenarbeit. Hier will ich besonders die restlichen zwei Drittel der „drei von der Tanke“ hervorheben: Meine besten Laborkollegen und guten Freunde Dominik Reiter und Philipp Frisch, mit denen es selbst während den anstrengendsten Zeiten immer etwas zu Lachen gab. Danke außerdem an Franziska Hanusch für ihr Organisationstalent, nicht nur während der spannenden Konferenzreise nach Asien.

Weiterhin möchte ich meinen ehemaligen Masterarbeitsbetreuern Herrn Prof. Dr. Dr. h.c. Bernhard Rieger und Herrn Dr. Carsten Troll vom Lehrstuhl für Makromolekulare Chemie danken. Sie haben unsere, anfangs noch im Aufbau befindliche, Gruppe stets großzügig unterstützt und uns an ihrer Ausrüstung und Geräten teilhaben lassen. Außerdem bedanke ich mich bei den Makro-Mitgliedern des Silicium-Instituts, besonders bei Dr. Daniel Wendel für die angenehme Arbeitsatmosphäre.

Diese Arbeit wurde in Kooperation mit der WACKER Chemie AG durchgeführt. Daher danke ich allen Partnern von der Industrieseite, besonders Herrn Dr. Richard Weidner, Herrn Dr. Thomas Renner, Frau Dr. Elke Fritz-Langhals, Herrn Dr. Jan Tillmann, sowie Herrn Dr. Niklas Wienkenhöver. Während der zahlreichen Treffen fand viel wissenschaftlicher Austausch statt, wobei oftmals neue Ideen entstanden.

Ein großes Dankeschön gebührt natürlich auch allen, die mich bei der Analytik unterstützt haben. Herr Dr. Alexander Pöthig, Herr Dr. Philipp Altmann und Philipp Frisch haben hervorragende Arbeit bei der Einkristall-Röntgendiffraktometrie gemacht und selbst die schlimmsten fehlgeordneten Kristalle nicht aufgegeben. Darüber hinaus danke ich Frau Dr. Oksana Storcheva (EPR Spektroskopie) und Ulrike Ammari (Elementaranalyse). Weiterhin bedanke ich mich bei Fabian Linsenmann für CV Messungen und den Grundkurs in Schwäbisch.

## Acknowledgments

---

Neben all meinen wissenschaftlichen Unterstützern will ich mich auch ganz besonders bei meinen Eltern Lia und Gerhard, sowie meiner ganzen Familie bedanken. Ihr habt mir durch eure großzügige Unterstützung und euren Rückhalt erst mein umfangreiches Studium ermöglicht.

Zu guter Letzt: Vielen Dank liebe Verena, dass du mich über meine gesamte Promotion begleitet hast. Zusammen haben wir währenddessen viele Höhen und Tiefen erlebt, aber du hast mich, wenn nötig, immer wieder aufgebaut. An dieser Stelle möchte ich dir nochmal sagen, wie wichtig mir deine Unterstützung während dieser ganzen Zeit war.

## List of Abbreviations

$\Delta E_{S,T}$	singlet-triplet energy gap	LiB	lithium ion battery
$\Theta$	<i>trans</i> -bent angle	LUMO	lowest unoccupied molecular orbital
$\tau$	twist angle	Mes	2,4,6-trimethylphenyl
CV	cyclic voltammetry	NHC	<i>N</i> -heterocyclic carbene
DCM	dichloromethane	NHI	<i>N</i> -heterocyclic imine
DFT	density functional theory	NHSi	<i>N</i> -heterocyclic silylene
Dipp	2,6-di <i>iso</i> -propylphenyl	NMR	nuclear magnetic resonance
DMAP	4- <i>N,N</i> -dimethylamino-pyridine	ORB	organic radical battery
DME	dimethoxyethane	ppm	parts per million
E	group 14 element	R	functional group
<i>e.g.</i>	latin: <i>exempli gratia</i> : "for example"	SC-XRD	single-crystal X-ray diffraction
EPR	electron paramagnetic resonance	SOMO	singly occupied molecular orbital
<i>et al.</i>	latin: <i>et alii</i> : "and others"	supersilyl	<sup>t</sup> Bu <sub>3</sub> Si
eV	electronvolt	Tbt	2,4,6-(CH(TMS) <sub>2</sub> ) <sub>3</sub> -C <sub>6</sub> H <sub>2</sub>
HBpin	pinacolborane	THF	tetrahydrofuran
HOMO	highest occupied molecular orbital	TMS	trimethylsilyl
hypersilyl	(TMS) <sub>3</sub> Si	Trityl	triphenylmethyl
<sup>i</sup> Pr <sub>2</sub> Me <sub>2</sub>	1,3-diisopropyl-4,5-dimethyl-imidazolin-2-ylidene	UV	ultra violet
IMe <sub>4</sub>	1,3,4,5-tetramethyl-imidazolin-2-ylidene	<i>vide infra</i>	latin: "see below"
<i>in situ</i>	latin: "on site"	<i>vide supra</i>	latin: "see above"
		VT	variable temperature
		X	Halogen atom or related substituent

## Abstract

Among the most important challenges for academia and industry of our time are the rising demand for electric energy storage and the improvement of catalytic processes with respect to sustainability. Therefore, this thesis aimed at the synthesis and electrochemical evaluation of low-coordinate silicon compounds, especially silyl radicals and disilenes in regard to application in organic radical batteries. Furthermore, the inherently high reactivity of these novel silicon compounds was utilized for the precise activation of industrially relevant small molecules, with respect to possible transition metal-free catalytic processes.

In an initial publication, the molecular structure of a silyl radical which has already been employed as anode material in batteries, was modified by introduction of a bulkier silyl group. The resulting silicon-centered radical is relatively air stable and promising for battery application because of its highly reversible redox behavior.

Furthermore, the synthesis of a tetra(silyl)disilene was reported. Interestingly, this disilene forms an equilibrium mixture with the isomeric silylene, thus being the first isolable free bis(silyl)silylene. Although it is not stable at room temperature and therefore not applicable in batteries, the mixture showed striking reactivity towards H<sub>2</sub> and ethylene. The silylene was investigated by isolation of base-stabilized (NHC and DMAP) derivatives, as well as by DFT calculations.

In a follow-up publication, the concept of stabilization of bis(silyl)silylenes by the weak Lewis base DMAP was further explored. Novel structures, which underwent unique thermally induced isomerization reaction were obtained. In addition, the ability of these silylene complexes to activate small molecules upon dissociation of the donor at elevated temperatures was demonstrated. Thus, these silylene-base adducts can be considered isolable synthetic equivalents of otherwise elusive bis(silyl)silylenes.

Another major part of this thesis was the investigation of iminodisilenes. In this regard, two novel disilenes were synthesized, which show much higher stability than the previously reported example. Due to a greatly facilitated purification process, a high isolable yield was achieved for one of these new iminodisilenes. The (*E/Z*)-isomerization of this compound was investigated thoroughly and interesting reactivities, such as formation of a cationic radical or activation of P<sub>4</sub> were observed.

The final manuscript focuses on the thermally induced, unprecedented and selective isomerization of this stable iminodisilene to an  $A_2Si=SiB_2$ -type disilene. With this unique disilene in hand, the reactivity towards carbon monoxide was explored. Resulting from an insertion of CO into the Si=Si double bond, a silene, containing a Si=C double bond was obtained.

## Kurzfassung

Zu den wichtigsten Herausforderungen für Wissenschaft und Industrie unserer Zeit gehören der steigende Bedarf an elektrischen Energiespeichern, sowie die Verbesserung katalytischer Prozesse im Hinblick auf ihre Nachhaltigkeit. Ziel dieser Arbeit war daher die Synthese und elektrochemische Bewertung von niedrigkoordinierten Siliciumverbindungen, insbesondere von Silylradikalen und Disilenen im Bezug auf ihre Anwendung in organischen Radikalbatterien. Darüber hinaus wurde die inhärent hohe Reaktivität dieser neuartigen Siliciumverbindungen zur präzisen Aktivierung von industriell relevanten kleinen Molekülen, im Hinblick auf mögliche übergangsmetallfreie katalytische Prozesse genutzt.

Zunächst wurde die molekulare Struktur eines Silyl-Radikals, das bereits als Anodenmaterial in Batterien eingesetzt wurde, durch Einführung einer größeren Silylgruppe modifiziert. Das resultierende Siliciumradikal ist relativ luftstabil und aufgrund seines hoch reversiblen Redoxverhaltens vielversprechend für mögliche Batterieanwendungen.

Darüberhinaus wurde ein Tetra(silyl)disilen synthetisiert, das mit dem isomeren Bis(silyl)silylen, dem ersten isolierbaren Vertreter dieser Klasse, ein Gleichgewichtsgemisch bildet. Obwohl es bei Raumtemperatur nicht stabil ist und somit nicht in Batterien eingesetzt werden kann, zeigte das Gemisch Additionsreaktionen mit  $H_2$  und Ethen. Das Silylen wurde durch Isolierung von basenstabilisierten (NHC und DMAP) Derivaten sowie durch DFT-Berechnungen untersucht.

In einer Folgeveröffentlichung wurde das Konzept der Stabilisierung von Bis(silyl)silylenen durch die schwache Lewis-Base DMAP weiter untersucht. Es wurden neuartige Strukturen erhalten, und ihre jeweils unterschiedlichen, thermisch induzierten Isomerisierungsreaktionen untersucht. Darüber hinaus wurde die Fähigkeit dieser Silylenkomplexe zur Aktivierung kleiner Moleküle nach der Dissoziation des Donors bei erhöhten Temperaturen nachgewiesen. Somit können diese Silylen-Basen Addukte als isolierbare synthetische Äquivalente von ansonsten instabilen Bis(silyl)silylenen betrachtet werden.

Ein weiterer wesentlicher Teil dieser Arbeit war die Untersuchung von Iminodisilenen. In diesem Zusammenhang wurden zwei neuartige Disilene

synthetisiert, die eine wesentlich höhere Stabilität als die bisher bekannte Verbindung zeigen. Durch einen stark vereinfachten Aufreinigungsprozess konnte für eines der neuen Iminodisilene eine hohe isolierbare Ausbeute erzielt werden. Die (*E/Z*)-Isomerisierung dieser Verbindung wurde eingehend untersucht und es konnten interessante Reaktivitäten, wie beispielsweise die Bildung eines kationischen Radikals, oder die Aktivierung von P<sub>4</sub> beobachtet werden.

Das abschließende Manuskript konzentriert sich auf die thermisch induzierte, bisher unbekannte und selektive Isomerisierung dieses stabilen Iminodisilens zu einem Disilen des A<sub>2</sub>Si=SiB<sub>2</sub>-Typs. Anhand dieses einzigartigen Disilens wurde die Reaktivität gegenüber Kohlenstoffmonoxid erforscht. Durch die Insertion von CO in die Si=Si-Doppelbindung wurde ein Silen mit einer Si=C Doppelbindung erhalten.

## Publication List

- R. Holzner, A. Kaushansky, B. Tumanskii, P. Frisch, F. Linsenmann, S. Inoue, *European Journal of Inorganic Chemistry* **2019**, 25, 2977-2981.  
Title: "Isolation of a Relatively Air-stable, Bulky Silyl-substituted, Neutral Silicon-centered Radical"  
DOI: [10.1002/ejic.201900522](https://doi.org/10.1002/ejic.201900522)
- D. Reiter,<sup>†</sup> R. Holzner,<sup>†</sup> A. Porzelt,<sup>†</sup> P. J. Altmann, P. Frisch, S. Inoue *Journal of the American Chemical Society* **2019**, 141, 13536-13546.  
Title: "Disilene-Silylene Interconversion: A Synthetically Accessible Acyclic Bis(silyl)silylene"  
DOI: [10.1021/jacs.9b05318](https://doi.org/10.1021/jacs.9b05318)
- R. Holzner,<sup>†</sup> D. Reiter,<sup>†</sup> P. Frisch, S. Inoue *RSC Advances* **2019**, 10, 3402-3406.  
Title: "DMAP-stabilized bis(silyl)silylenes as versatile synthons for organosilicon compounds"  
DOI: [10.1039/C9RA10628F](https://doi.org/10.1039/C9RA10628F)
- R. Holzner, P. Frisch, D. Wendel, S. Inoue  
Draft (Article)  
Title: "Iminodisilenes: Striking Reactivity in Small Molecule Activation"
- R. Holzner, P. Frisch, S. Inoue  
Draft (Communication)  
Title: "Formation of a Silene through CO Activation by a Polarized Iminodisilene"

<sup>†</sup> These authors contributed equally



Publications beyond the scope of this thesis:

- V. Nesterov, D. Reiter, P. Bag, P. Frisch, R. Holzner, A. Porzelt, S. Inoue, *Chemical Reviews* **2018**, 118, 9678-9842.  
Title: “NHCs in Main Group Chemistry”  
DOI: [10.1021/acs.chemrev.8b00079](https://doi.org/10.1021/acs.chemrev.8b00079)

## Poster List

- R. Holzner, S. Inoue,  
*The 7<sup>th</sup> Asian Silicon Symposium*, Singapur, July 28<sup>th</sup> – 31<sup>st</sup> **2019**,  
(<http://event.ntu.edu.sg/7ASC/Pages/default.aspx>)  
Title: “Reactivity of an Iminodisilene”
- R. Holzner, S. Inoue,  
*9<sup>th</sup> European Silicon Days*, Saarbrücken, September 09<sup>th</sup> – 12<sup>th</sup> **2018**,  
(<https://www.9esd.de/>)  
Title: “Iminodisilenes – Structures and Reactivities”

## Table of Contents

Acknowledgments.....	I
List of Abbreviations.....	III
Abstract.....	IV
Kurzfassung.....	VI
Publication List.....	VIII
Poster List.....	IX
1. Introduction.....	1
2. The Element Silicon.....	3
3. Low-coordinate Silicon Compounds.....	7
3.1 Silyl Radicals.....	7
3.2 Silylenes.....	11
3.3 Disilenes.....	21
4. Organic Radical Batteries.....	29
4.1 Lithium Ion Batteries and Related Technology.....	29
4.2 Silicon-based ORB.....	30
5. Transition Metal-free Catalysis.....	34
6. Scope of this Work.....	36
7. Isolation of a Relatively Air-Stable, Bulky Silyl-Substituted, Neutral Silicon-Centered Radical.....	39
8. Disilene–Silylene Interconversion: A Synthetically Accessible Acyclic Bis(silyl)silylene.....	45
9. DMAP-stabilized bis(silyl)silylenes as versatile synthons for organosilicon compounds.....	57
10. Iminodisilenes: Striking Reactivity in Small Molecule Activation.....	63
11. Formation of a Silene through CO Activation by a Polarized Iminodisilene.....	71
12. Summary and Outlook.....	76

## Table of Contents

---

12.1	Disilenes.....	76
12.2	Silyl radicals .....	79
12.3	Silylenes.....	82
12.4	Reactivities of Low-coordinate Silicon Compounds Towards Small Molecules.....	84
12.5	Outlook.....	86
<b>13.</b>	<b>Zusammenfassung und Ausblick.....</b>	<b>88</b>
13.1	Disilene .....	88
13.2	Silylradikale .....	91
13.3	Silylene.....	95
13.4	Reaktivität der niedervalenten Siliciumverbindungen gegenüber kleinen Molekülen .....	97
13.5	Ausblick.....	99
<b>14.</b>	<b>Bibliography.....</b>	<b>101</b>
<b>15.</b>	<b>Appendix .....</b>	<b>118</b>
15.1	Supporting Information Chapter 7 .....	118
15.2	Supporting Information Chapter 8 .....	131
15.3	Supporting Information Chapter 9 .....	223
15.4	Supporting Information Chapter 10 .....	249
15.5	Supporting Information Chapter 11 .....	291
15.6	Licenses for Copyrighted Content.....	311

## 1. Introduction

Dealing with limited resources, against the background of an ever-growing demand of energy and mobility is probably one of the biggest challenges, humanity has to face in the 21<sup>st</sup> century. Especially the finite supply of crude oil might become problematic.<sup>[1-2]</sup> This natural feedstock of hydrocarbons is the basic building block of modern economies. Chemical industry crucially requires crude oil as starting material for most commercially synthesized fine chemicals and plastics, as well as for the production of fuels for vehicles and homes. It is difficult to predict the point in time at which the natural oil resources will be exhausted, because new sources are discovered and the increasing price in combination with a more sophisticated oil production technology allows exploitation of non-conventional sources like oil sands. Nevertheless, this date will eventually come within the next decades. Furthermore, burning of fossil fuels through the resulting emission of CO<sub>2</sub> contributes to a man-made climate change.<sup>[3]</sup> It is widely recognized, that this global warming will bring up problems, even long before the last drop of crude oil is consumed.

Therefore, it is the task of science together with industry to tackle this challenge and provide solutions which allow preservation of our current life standard and further growth under sustainable conditions. Two key technologies in this regard are the storage of electric energy and catalysis. Transportation produces 23% of today's carbon dioxide emissions world-wide.<sup>[3]</sup> Hence, transition to electric mobility is required for a significant reduction of greenhouse gas emission. Moreover, in the course of transition from fossil fuels and nuclear energy to renewable sources, electric energy storage is imperative to compensate fluctuations from unsteady energy sources, such as wind- or solar-based power plants and guarantee a constant electrical energy supply. Although the current lithium ion battery technology has steadily been improved, it cannot meet the rising demand for energy storage alone. Since lithium is also a finite resource and its extraction process isn't particularly environmentally friendly,<sup>[4]</sup> it is important to utilize more abundant elements for this purpose. Silicon-based organic radical batteries might be a useful addition to the current electric energy storage technology in this respect and could even replace metal-containing batteries in some fields. Neutral silyl radicals have already been successfully applied as anode materials in metal-free organic radical batteries.<sup>[5]</sup> Further investigations, for example in regard to other low-coordinate silyl species might lead to more effective, sustainable batteries.

Therefore, the focus of this work is on the synthesis of novel low-coordinate silicon compounds, such as radicals or disilenes and their electrochemical evaluation.

Of course, not only storage, but also conservation of energy and in this regard, catalysis will become more important. Effective catalysts significantly reduce the activation barrier of chemical reactions and thus, the required energy. The multimillion-ton output of today's chemical industry would be absolutely inconceivable without catalysis. However, these processes are mainly relying on costly and sometimes toxic transition metals.<sup>[6]</sup> In general, replacement of these metals by highly abundant main group elements would mean a great step towards a "greener", more sustainable economy. A recent report demonstrated the catalytic activity of a cationic silicon compound in hydrosilylation of alkenes.<sup>[7]</sup> This silyliumylidene turned out to be as effective as the currently applied platinum-based catalysts and might therefore be soon implemented in the catalytic curing of polysiloxanes for the synthesis of silicone rubbers. Based on these promising results, the reactivity of the newly synthesized low-coordinate silicon compounds will be tested towards small molecules as the second main aim of this thesis. Selective activation of relatively inert small molecules, such as H<sub>2</sub> or CO is the key condition for a potential catalytic application of these species. The achieved results could probably pave the way for a further development of sustainable, non-toxic silicon compounds in catalysis.

## 2. The Element Silicon

Whereas carbon is the undisputable “carrier of life” among the elements, its direct heavier congener silicon has a totally different character. Nevertheless, the semiconductor silicon is an essential part of modern life, applied in computer chips or silicone polymers. Right behind oxygen with 45.5%, silicon is the second most abundant element in the lithosphere with a proportion of more than a quarter (27.2%) (Figure 1).<sup>[8]</sup> Akin to carbon, silicon in general adopts  $sp^3$  hybridization and forms bonds to four substituents, resulting in a tetrahedral coordination sphere. Silanes for example, show similar physical properties, such as melting and boiling points than their lighter analogues alkanes. In regard to their chemical reactivities however, they differ drastically. Silane ( $SiH_4$ ), disilane ( $Si_2H_6$ ) and chlorosilane ( $SiH_3Cl$ ) are highly pyrophoric and ignite immediately upon exposure to air. Methane and ethane on the other hand are relatively inert. Whereas dichloromethane is a common solvent, dichlorosilane hydrolyzes to a polymeric, potentially pyrophoric substance.<sup>[9]</sup> The reason for that is mainly the oxophilicity and the electropositive character of silicon, compared to carbon and hydrogen, which leads to an inversely polarized  $Si^{\delta+}-H^{\delta-}$  bond (Pauling electronegativity: Si = 1.9, C = 2.55, H = 2.2).

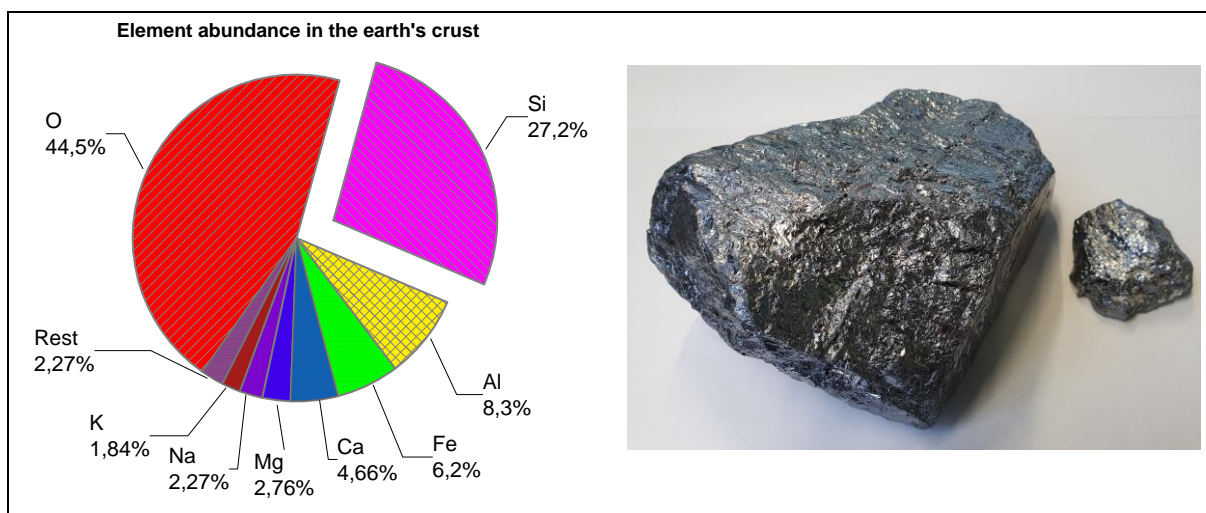


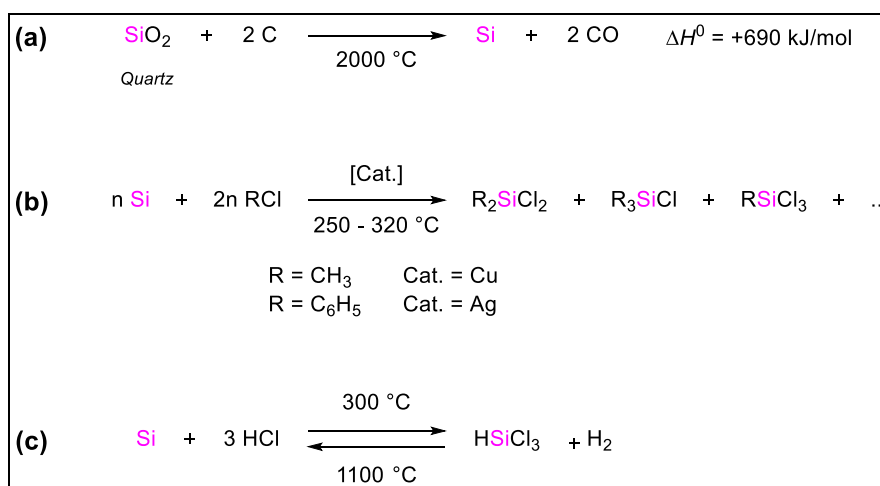
**Figure 1:** Left: abundance of the elements in the earth's crust; right: depiction of metallurgical grade silicon chunks.

Because of its high affinity towards oxygen, silicon never occurs in elemental form, but only oxidized as silicates with other elements or as  $SiO_2$  like in quartz, sea sand or pebble stone.<sup>[10]</sup> Even the name silicon derives from the Latin words *silex* or *silicis*, which translate to “flint” or “hard stone”. Despite its high abundance, the oxophilicity of silicon is the reason for its relatively late discovery compared to rarer elements.

Eventually in 1824, J. J. Berzelius obtained amorphous elemental silicon from the reduction of  $\text{SiF}_4$ .<sup>[10]</sup>

Although the output volume is declining since 2013, 6.7 million tons of silicon were produced in 2018.<sup>[11]</sup> On the industrial scale, silicon production is realized by the reduction of quartz with carbon in an electric arc furnace at 2000 °C (Scheme 1, (a)). This highly energy consuming process provides metallurgical grade silicon with a purity of 98.5–99.7 wt.%, which is already sufficient for steel production, as alloying component or deoxidizing agent.<sup>[10]</sup> Furthermore, it can be converted to organochlorosilanes in the so called “Müller-Rochow” process.<sup>[12]</sup> This transformation, also known as “direct synthesis” provides chloromethylsilanes and chlorophenylsilanes from reaction of elemental silicon with methylchloride or phenylchloride, respectively in presence of a catalyst (Cu or Ag) (Scheme 1, (b)). The ratio of the resulting crude chlorosilane mixture is strongly depending on the process control. Usually, the desired dimethyldichlorosilane is formed in 80% yield. After distillative separation, these chlorosilanes are mainly polymerized to polysiloxanes (silicones) or used as starting materials in synthetic organosilicon chemistry.

**Scheme 1:** (a) Synthesis of metallurgical grade silicon from reduction of quartz, (b) Direct synthesis of chlorosilanes, (c) *Siemens* process.



For the production of solar cells and semiconductors however, an even higher purity than metallurgical grade is required. Usually, this purification is industrially realized by the again highly energy consuming “*Siemens* process” (Scheme 1, (c)). In this process, crude silicon is reacted with hydrogen chloride to trichlorosilane, which is then purified in various distillation steps. Subsequently this trichlorosilane is reduced with hydrogen on the surface of heated (1100 °C) silicon rods, providing purities above 99.99%. In the so called “*Czochralski* process”, the highest silicon purity, which is required for the

production of semiconductors for microelectronic applications can be achieved. Here, a silicon seed crystal is dipped into a 1420 °C hot silicon melt and pulled upwards under simultaneous rotation. This results in a large, cylindrical silicon single crystal. Dopant impurities, e.g. boron, aluminum, phosphorus or arsenic can be added in this process to determine the electronic properties of the resulting semiconductor material. In the next production step, these monocrystalline silicon cylinders are cut into “wafers”, which in turn are further processed to computer chips.<sup>[10]</sup>

Besides in integrated circuits and solar cells, the element silicon finds numerous technical applications today, mostly in the oxidation state Si(IV). Amorphous SiO<sub>2</sub> powder is employed as thickener, pigment for coating, or reinforcing filler for polymers, especially rubbers, for example in tires. Furthermore, it is a key component in high performance concrete. Zeolites, which are based on aluminosilicates, find application in heterogeneous catalysis. In addition, silicon is the basis of glasses and high performance ceramics with excellent properties in regard to strength and hardness, even at high temperatures.<sup>[8]</sup>

Among the most important applications of silicon are polysiloxanes.<sup>[13]</sup> Historically, Kipping hydrolyzed silanes and obtained high-molecular linear and cyclic polymers, containing Si–O bonds. However, he mistook these sticky, colorless compounds as heavier analogues of ketones, which contain a Si=O double bond and therefore called them “silicoketones” or “silicones”. Thus, silicones is a misnomer for polysiloxanes, that persisted to this day, at least as a trivial name. Initially, polysiloxanes were considered useless. Kipping concluded his long-term work on this class of compounds that no applications are to be expected. Their immense potential was finally recognized in the 1940s, with the development of the *Müller-Rochow* process, which allowed facile access to organochlorosilanes, the monomers of polysiloxanes. Polysiloxanes display properties, which cannot be achieved with carbon-based polymers. The large Si–O–Si angle of 143° in the polysiloxane chain is much wider than the usual tetrahedral angle (~110°) and therefore allows inversion through the linear form and rotations with only a small energy barrier.<sup>[13]</sup> This characteristic feature accounts for the high dynamic flexibility and the low glass transition temperature of polysiloxanes. Due to the strong Si–O bond, these polymers show also high thermal stability and hence are applicable in a large temperature range. Among silicones, polydimethylsiloxane is the most commonly used representative. On an industrial scale, polydimethylsiloxanes are synthesized by hydrolysis of dichlorodimethylsilane. The resulting linear or cyclic



oligosiloxanes can be converted to high-molecular polysiloxanes by subsequent polycondensation or ring opening polymerization. Lower molecular polysiloxanes, so called silicone oils, find applications as defoaming agents or for lubrication purposes. Depending on the addition of other functional monomers, such as  $\text{MeSiCl}_3$  or  $\text{SiCl}_4$  during the production process, branched silicone resins, which are used as additives in coatings or as hydrophobic water repellants for concrete structures, can be obtained.<sup>[14]</sup> Another technically important application of polysiloxanes is the elastomeric form. For that purpose, monomers with polymerizable functional groups, which allow cross-linking are added. The elasticity of these silicone rubbers can be precisely tuned, through the monomer ratio.<sup>[13]</sup>

This brief overview on the achievable structures and the resulting applications of polysiloxanes demonstrates already the versatility and importance of these synthetic, silicon-based polymers. In summary, the element silicon became industrially relevant because of its natural abundance and its intriguing properties in the recent century and thus, we encounter it in many applications in our daily lives. However, silicon is mostly applied in elemental form  $\text{Si}(0)$  in semiconductors, or in the oxidation state  $\text{Si}(\text{IV})$ , in  $\text{SiO}_2$ , silanes and polysiloxanes. Nonetheless, silicon in different oxidation states and coordination modes (see the following chapters), which was unconceivable for a long time, might also become attractive for industrial processes in the future.

### 3. Low-coordinate Silicon Compounds

Akin to the lighter homologue carbon, most silicon compounds are present in a four-coordinate, tetrahedral state. Lower-coordinated silicon species are electronically extremely unfavored and therefore highly reactive.<sup>[15]</sup> Thus, they show strong tendencies to undergo oligomerization or disproportionation reactions to restore the preferred four-coordinate state. Examples of low-coordinate silicon compounds comprise silyliumylidene ions ( $\text{RSi}^+$ , one-coordinate), silylenes ( $\text{R}_2\text{Si}:$ , two-coordinate) and silyl radicals ( $\text{R}_3\text{Si}^\cdot$ ), silylium ions ( $\text{R}_3\text{Si}^+$ ) or disilenes ( $\text{R}_2\text{Si}=\text{SiR}_2$ , three-coordinate). Only tailor-made ligands which either provide kinetic stabilization by sterically shielding of the reactive center, stabilizing electronic effects from heteroatoms, or a combination of both allow for isolation of these elusive species. Utilization of these strategies has led to isolation of numerous low-coordinate silicon compounds in the recent decades. Within this chapter, the milestones and most outstanding discoveries in the field of silyl radicals will be presented. Furthermore, silylenes will be discussed briefly. Finally, disilenes, the formal dimers of silylenes will be shown, and their bonding nature and reactivity will be pointed out with selected examples.

#### 3.1 Silyl Radicals

The chemistry of carbon radicals ( $\text{R}_3\text{C}^\cdot$ ) has a long history and attracted much attention, both from academia and from industry. As early as 1900, Gomberg reported the persistent triphenylmethyl radical and demonstrated its radical character by the reaction with oxygen.<sup>[16-17]</sup> From this starting point on, a lot of persistent carbon radicals<sup>[17-19]</sup> and radical-based reactions were identified, for example biological processes of cell damage.<sup>[20]</sup> Furthermore, carbon radicals play an indispensable role in industrial processes (e.g. low-density polyethylene production) or organic transformations.<sup>[21-22]</sup>

In contrast to carbon radicals, the investigation of silyl radicals ( $\text{R}_3\text{Si}^\cdot$ ) is far less developed. Nevertheless, silyl radicals have also found application as active species in organic reactions, such as alkene hydrosilylation or halide abstraction.<sup>[23-25]</sup> In this cases, the silyl radicals were generated *in situ*. They are only short-lived intermediates and thus not isolable.

Akin to carbon radicals, silyl radicals bear three substituents and a singly occupied molecular orbital (SOMO).<sup>[24]</sup> A valuable tool for the characterization of these radicals is electron paramagnetic resonance (EPR) spectroscopy.<sup>[26]</sup> Besides the  $g$  value, which is slightly greater than 2 for silyl radicals, the hyperfine coupling constant (hfcc)  $a$  from coupling of the unpaired electron with the  $\alpha$ - $^{29}\text{Si}$  nucleus can be observed. The value of the hfcc provides information about the hybridization of the SOMO (whether it is rather an  $s$ - or  $\pi$ -type orbital) and thereby on the geometry around the radical center. This connection is depicted in Figure 2. A higher degree of pyramidalization around the radical center leads to a larger contribution of the  $3s$ -orbital to the SOMO and therefore an increasing value for  $a(\alpha\text{-}^{29}\text{Si})$ .<sup>[26]</sup>

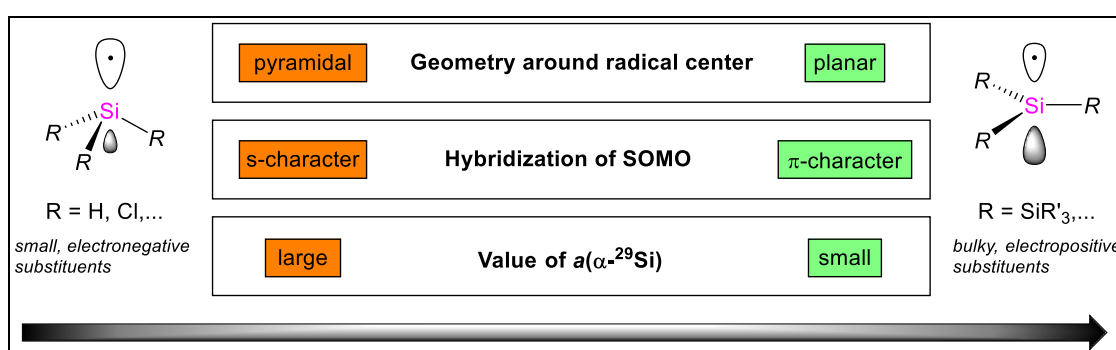


**Figure 2:** Connection between silyl radical geometry, hybridization of the SOMO and hyperfine coupling constant  $a$  with  $\alpha$ - $^{29}\text{Si}$  nucleus.

As early as 1966, parent group 14 radicals were investigated by means of matrix isolation. EPR studies of these transient species revealed, that the degree of pyramidalization is increasing, going down the group from the planar  $\text{H}_3\text{C}^\bullet$  to the pyramidal  $\text{H}_3\text{Sn}^\bullet$ .<sup>[27]</sup> Furthermore, it was shown that the degree of pyramidalization rises from  $\text{Me}_3\text{Si}$  to  $\text{Cl}_3\text{Si}$  by stepwise replacement of a methyl group by a chlorine atom. However, persistent silicon-centered radicals require bulkier substituents (kinetic stabilization) or delocalization of the spin density throughout the ligand system (thermodynamic stabilization). Therefore, they remained elusive.

The pioneering synthetic work in investigation of silyl radicals was done by Lappert *et al.* in the mid 1970s.<sup>[28-29]</sup> They irradiated a silane with UV light and obtained a silyl radical with a half-life of 10 minutes, which was characterized by EPR spectroscopy. Later, persistent polysilyl radicals were obtained from irradiation of polysilanes with UV light.<sup>[30-32]</sup> Further, even more stable tri(silyl)-substituted silicon-centered radicals were reported by the groups of Matsumoto and Kira.<sup>[33-35]</sup> In the EPR spectrum, these silyl substituted radicals generally display a large signal with additional satellite signals

deriving from coupling of the unpaired electron with  $\alpha$ - and  $\beta$ - $^{29}\text{Si}$  nuclei. Structural characterization however was yet to be achieved. This task was eventually accomplished by Sekiguchi and co-workers in 2001 with the isolation of a cyclotetrasilanyl radical **L1** (see Figure 3).<sup>[36]</sup>

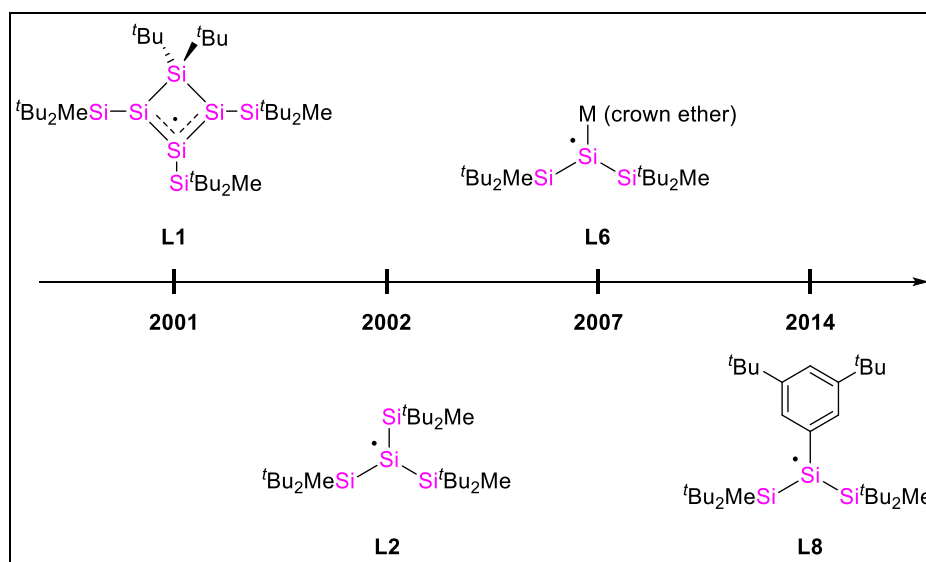


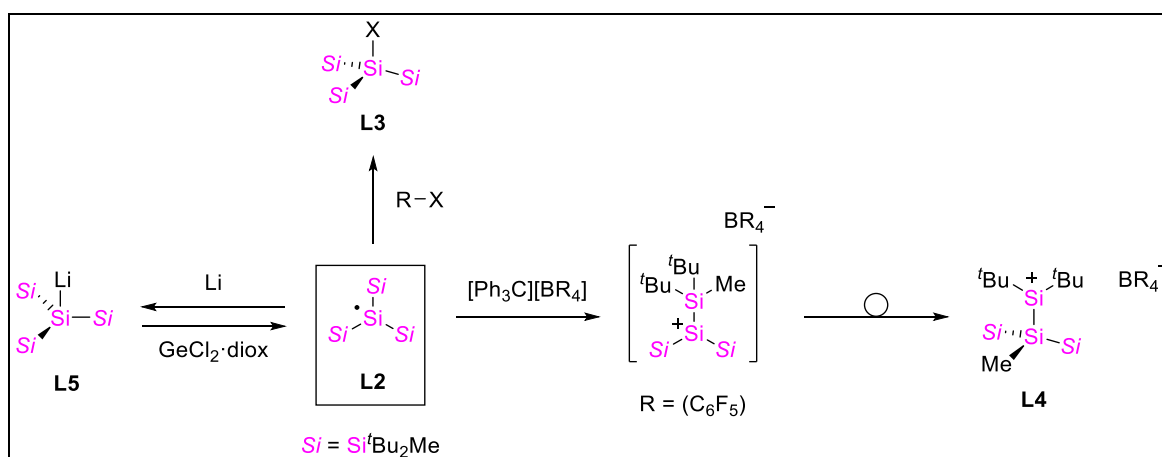
**Figure 3:** Milestones in silyl radical chemistry: structurally characterized examples by the group of Sekiguchi.

Compound **L1** was obtained from one-electron reduction of the corresponding silylium ion. The spin density is delocalized over three silicon centers, embedded in the four-membered, planar ring. This result is consistent with density functional theory (DFT) calculations on the substituent effects in silyl radicals. Electropositive substituents, such as silyl groups or alkali metals are stabilizing silyl radicals. Furthermore, bulky silyl groups have been predicted to lead to planar geometries, whereas electronegative substituents, which bear a lone pair of electrons, induce pyramidalization.<sup>[26,37]</sup>

The next milestone, only one year later was the report of the neutral silyl radical **L2**, which adopts a completely trigonal planar geometry.<sup>[38]</sup> This compound was generated by one-electron oxidation of the *in situ* formed silyl anion by the  $\text{GeCl}_2$ -dioxane complex. Apparently, the three  $t\text{Bu}_2\text{MeSi}$  groups are bulky enough to sterically protect the radical center from undergoing typical decomposition reactions, such as dimerization or hydrogen abstraction. In contrast to **L1**, radical **L2** is completely lacking stabilization by conjugation with  $\pi$ -bonds. The reactivity of compound **L2** was extensively studied and reaction patterns, characteristic for silyl radicals were identified (Scheme 2). With haloalkanes, radical **L2** readily undergoes halogen abstraction reactions, resulting in the corresponding chloro- and bromosilanes **L3**.<sup>[38]</sup> One-electron

oxidation of **L2** was also realized, by treatment with a trityl reagent.<sup>[39]</sup> The intermediary generated silylium ion however was only isolable as acetonitrile adduct. In dichloromethane, a non-coordinating solvent, a Wagner-Meerwein-type rearrangement took place, furnishing the isomeric silylium ion **L4**. The positive charge in this isomer is far better stabilized by silicon hyperconjugation ( $\beta$ -silicon effect).

**Scheme 2:** Reactivity of silyl radical **L2**.



Most interestingly, silyl radical **L2** was reduced with an excess of lithium dispersion to the corresponding silyl anion **L5** without greater change of the silyl structure.<sup>[40]</sup> In contrast to most four-coordinate alkali metal compounds of group 14 elements, which prefer a tetrahedral coordination sphere, all silicon atoms in compound **L5** are still in plane. This unusual structure was ascribed to the steric repulsion between the three <sup>t</sup>Bu<sub>2</sub>MeSi groups. By oxidation of **L5**, the radical starting material **L2** was regenerated, which already indicated the reversibility of the underlying redox process.<sup>[41]</sup> A similar reaction behavior was reported by Apeloig and co-workers for a tri(silyl)silyl radical, deriving from oxidation of a hydrosilane by an organic peroxide.<sup>[42]</sup> This reversible nature of the redox-couple (silyl radical  $\rightleftharpoons$  silyl anion) was later confirmed by cyclic voltammetric (CV) analysis for **L2** and eventually exploited for battery applications (see chapter 4.2).<sup>[5,43]</sup>

Examples of alkali metal-substituted silyl radicals were studied by EPR spectroscopy<sup>[44]</sup> and finally, compounds **L6** were structurally characterized.<sup>[45-46]</sup> Silyl radicals **L6** were obtained from reductive splitting of the tetra(silyl)disilene (<sup>t</sup>Bu<sub>2</sub>MeSi)<sub>2</sub>Si=Si(<sup>t</sup>Bu<sub>2</sub>Me)<sub>2</sub> (**L7**) by alkali metal naphthalenide in presence of the respective crown ether. In the case of lithium, there is no contact between the metal and the silicon center. This compound can be described as silylene radical anion. With sodium and potassium however, the structure is strongly depending on the amount of

crown ether and the solvent. In the solid state, with one equivalent of the respective crown ether, the Na- and K-containing compounds display planar alkali metal-substituted silyl radical structures. EPR spectroscopy revealed the nature of these radicals in solution: in toluene, coupling of the unpaired electron with the 3/2 spin nuclei (Na, K) was observable, clearly indicating contact ion pair character. In THF and 1,2-dimethoxyethane (DME) the radicals form solvent-separated ion pairs, hence no coupling with the alkali metals was observed.

Furthermore, aryl-substituted silyl radicals, such as the structurally characterized **L8** were obtained from reduction of the corresponding iodosilanes.<sup>[47]</sup> Notably, only iodosilanes could be selectively reduced to silyl radicals, whereas reduction of bromosilanes resulted in a 1:1 mixture of starting material and the corresponding silyl potassium species. This was attributed to the ability of the iodosilanes to convert the silyl anion to the radical *via* one-electron oxidation. With this versatile approach, Sekiguchi *et al.* were able to synthesize a variety of aryl-functionalized silicon-centered radicals, comprising even di- or tri-radical species.<sup>[48-49]</sup>

Besides these examples, there are also a number of NHC-,<sup>[50]</sup> amidinato-,<sup>[51]</sup> or cyclic alkyl amino carbene- (CAAC)-stabilized<sup>[21,52-54]</sup> silyl radicals. However, in the latter cases, the spin density is strongly delocalized over the carbon and nitrogen atoms of the ligand frameworks. Further isolated silyl radicals derive from oxidation or reduction of Si–Si multiple bonds. Reduction of a disilyne (Si≡Si triple bond) or of disilenes afforded anionic silyl radicals.<sup>[55-58]</sup> However, only one disilene radical cation was isolated so far (see chapter 3.3.4).<sup>[59]</sup> Although significant progress in the field of silyl radicals was achieved since the pioneering work of Lappert<sup>[28-29]</sup> and Sekiguchi,<sup>[36,38]</sup> structurally characterized silyl radicals with electronegative substituents have yet to be described.

## 3.2 Silylenes

Among the class of low-coordinate silicon compounds, silylenes ( $R_2Si:$ ) are probably the most intensively investigated species. Silylenes bear either two monodentate substituents or one bidentate, cyclic ligand and a lone pair of electrons. Their name derives from the lighter homologues carbenes. Carbenes are highly reactive electron sextet species and play an important role in organic transformations, such as the

*Simmons-Smith* cyclopropanation.<sup>[60]</sup> Furthermore, especially stable *N*-heterocyclic carbenes became indispensable as excellent  $\sigma$ -electron donating ligands<sup>[61]</sup> for transition metal<sup>[62-64]</sup> or main group element complexes.<sup>[65]</sup>

### 3.2.1 Electronic properties and concepts of silylene chemistry

Compared to carbenes, the electronic structure of silylenes in general differs significantly (Figure 4).<sup>[66]</sup> For two-coordinate carbon compounds like methylene ( $\text{H}_2\text{C}$ :) a triplet ground state is favored, hence the calculated corresponding singlet-triplet energy gap ( $\Delta E_{\text{S,T}} = -14.0 \text{ kcal/mol}$ ) is negative. This means that  $\text{H}_2\text{C}$ : displays biradical character with two electrons with parallel spin in two  $\text{sp}^2$ -type orbitals.

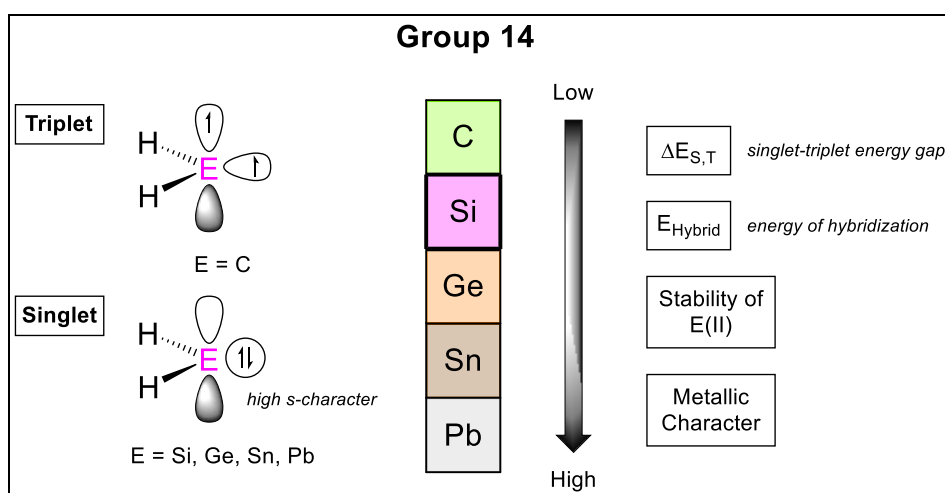


**Figure 4:** Frontier orbitals in tetrylenes and general trends of electronic properties of group 14 elements.

In sharp contrast, the value of the singlet-triplet splitting energy for  $\text{H}_2\text{Si}$ : ( $\Delta E_{\text{S,T}}$ ) is 16.7 kcal/mol and even further increasing, going down group 14 to 34.8 kcal/mol for  $\text{H}_2\text{Pb}$ :. These calculations demonstrate that heavier tetrylenes clearly prefer the singlet ground state configuration with the electron lone pair located in a low-lying orbital with high s-character and an energetically higher, vacant p-orbital.

A similar trend is true for the energy of hybridization and the relative stability of the oxidation state  $\text{E(II)}$ : s/p hybridization becomes more difficult for heavier group 14 elements. The reason for this is the increasing energetic separation between the s- and p-orbitals with increasing nuclear charge, which results in the relativistic “inert s-pair effect”. This means, only the p electrons take part in chemical bonding.<sup>[66-68]</sup>

Although the singlet electronic ground state is preferred for silylenes, theoretical calculations predict that a triplet silylene should also be accessible.<sup>[69-76]</sup> Apparently,

the angle  $\alpha$  between the substituents (R–Si–R) has a crucial influence on the hybridization of the silicon center (Figure 5, adapted from Gaspar *et al.*).<sup>[76]</sup> Small angles lead to singlet ground state multiplicities, whereas widening of  $\alpha$  increases the p-character of the  $\sigma$ -orbital. This lowers the  $\sigma \rightarrow p$  promotion energy, thus eventually producing a triplet ground state.<sup>[76]</sup> The angle from which on the triplet ground state is energetically favored is called “crossover angle” and was first calculated by Gordon in 1985 to be  $129^\circ$  for  $\text{H}_2\text{Si}$ :.<sup>[75]</sup> However, deviating values, depending on the methods of theory were reported. The crossover angle in turn, is strongly depending on the electronegativity of the substituents. Gaspar, who investigated triplet state silylenes intensively, calculated the crossover angle of  $\text{Me}_2\text{Si}$ : with  $140^\circ$  to be much larger than for  $\text{H}_2\text{Si}$ : and attributed the striking difference on the differing electronegativity of carbon, compared to hydrogen.

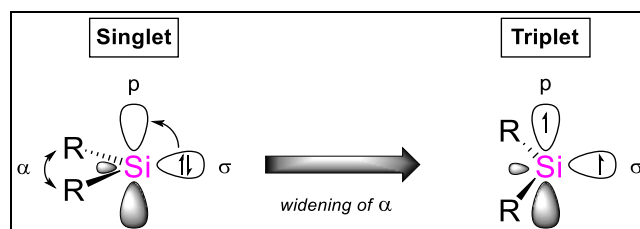


**Figure 5:** Effect of bond angle  $\alpha$  on electronic ground state of silylenes.

More electronegative substituents increase the crossover angle. With silyl substituents on the other hand, the crossover angle decreases even further to  $120^\circ$ .<sup>[71]</sup> Therefore, bulky, electropositive silyl groups were identified to be the most promising ligands for the generation of triplet ground state silylenes. However, to date, no stable, two-coordinate bis(silyl)silylene could be isolated. All synthetic attempts failed because of the extreme reactivity of the created species and resulted either in C–H bond activation of the ligand framework<sup>[77]</sup> or in silyl group migration.<sup>[78-80]</sup> Remarkably, Sekiguchi and co-workers were able to generate triplet silylenes bearing two extremely sterically demanding supersilyl groups ( $^t\text{Bu}_3\text{Si}$ ) or one supersilyl group and one alkali metal substituent, by irradiation of a corresponding silirene with UV light.<sup>[77,81]</sup> Although they were able to prove the paramagnetic nature of these species by EPR spectroscopy *in situ* below 15 K, the silylenes immediately decomposed upon warming up. Therefore, the quest for stable bis(silyl)silylenes, which might even display triplet character is still ongoing.

Stabilization of two-coordinate silylenes is a challenging task that requires precise design of the substituents. Because of their electron lone pair and their vacant p-orbital,



singlet ground state silylenes are ambiphilic, which means they can react as Lewis acids and bases. Whereas the electron lone pair is considered rather inert, due to its high s-character,<sup>[66]</sup> the extreme electrophilicity of silylenes, resulting from the empty p-orbital however makes them vulnerable against nucleophiles. Therefore, one of two basic concepts of stabilization or a combination of both has to be applied in order to produce stable silylenes (Figure 6, adapted from Tokitoh *et al.*).<sup>[66]</sup> Electronegative,  $\sigma$ -accepting substituents, that further possess lone pairs of electrons, such as oxygen, nitrogen, sulfur or phosphorus are ideal candidates for thermodynamic stabilization of silylenes. On the one hand, their inductive effect increases the s-character of the HOMO, thus promoting the singlet ground state and leading to a higher singlet-triplet energy gap ( $\Delta E_{S,T}$ ). On the other hand, these substituents can act as  $\pi$ -electron donors (mesomeric effect) to the vacant p-orbital (LUMO) and thereby reduce the extensive electrophilicity. The second basic concept for the generation of stable silylenes is the kinetic stabilization by sterically encumbered ligands. Like an umbrella, these bulky substituents protect the reactive, low-coordinate silicon center from nucleophilic attacks and prevent dimerization or oligomerization by steric repulsion. Since this concept works for the stabilization of all kinds of reactive species, a plethora of these bulky substituents with fine-tunable steric demand and various electronic properties has been developed. Prominent examples comprise alkyl based (trityl), aryl based (terphenyl, Dipp,...) and silyl based (supersilyl, hypersilyl, <sup>t</sup>Bu<sub>2</sub>MeSi,...) ligands.

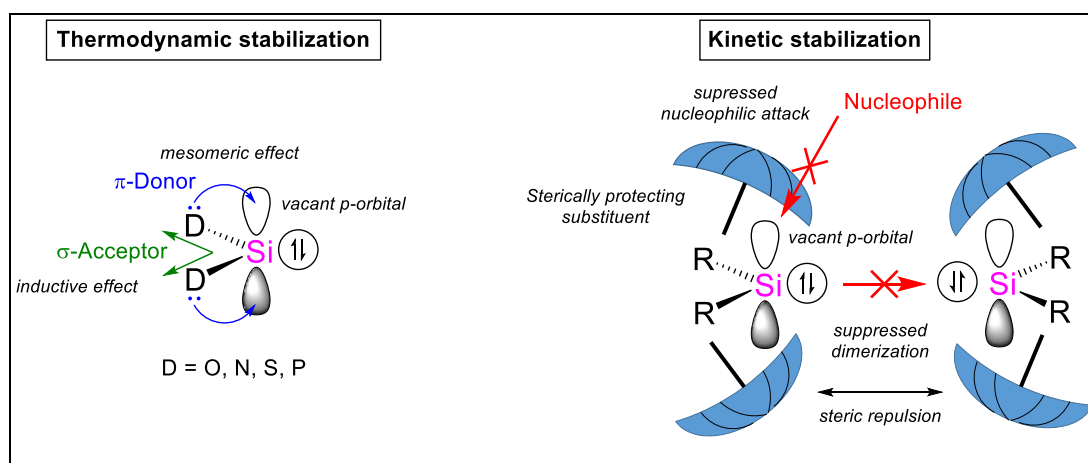


**Figure 6:** Thermodynamic and kinetic stabilization of silylenes.

A new, promising class of stabilizing substituents are the imidazolin-2-iminato ligands or *N*-heterocyclic imines (NHIs).<sup>[82-83]</sup> As reflected in the resonance structures, NHIs are excellent  $\pi$ -electron donors because of the electron lone pair at the exocyclic

nitrogen atom, which can readily be shared with the central atom (Figure 7). The resulting positive charge is further delocalized throughout the imidazoline scaffold.

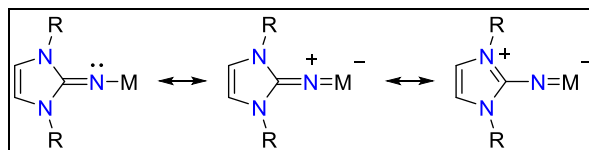


**Figure 7:** Selected resonance structures of an NHI-metal complex.

Consequently, the contribution of the allenic resonance structures results in a shortening of the N–M bond and a widening of the C–N–M angle. NHIs are conveniently accessible from the *Staudinger*-type reaction of the respective NHC with trimethylsilyl azide.<sup>[83]</sup> Therefore, the wide variety of NHC structures can be transferred to NHIs, allowing a precisely tuned steric demand of the wingtips R. NHI-TMS can either be introduced to a main group center *via* TMS halide elimination, or it can be hydrolyzed in methanol to the corresponding N–H species. The free imine in turn can be deprotonated to a highly nucleophilic imidinato compound (NHI–Li). In general, these flexible methods of introduction, in combination with its strong  $\pi$ -donor ability, easy accessibility and the opportunity for adjusting of the steric bulk make NHIs valuable and versatile ligands, which have found considerable applications in modern main group chemistry.<sup>[82]</sup>

Besides of  $\pi$ -donors and bulky ligands, the stabilization of silylene moieties by electron donation of an additional Lewis base (*e.g.* amine,<sup>[84]</sup> NHC,<sup>[65]</sup> isonitrile)<sup>[85]</sup> to the vacant p-orbital is a viable approach for isolation of otherwise elusive species. This Lewis base coordination can either be intramolecular, or an external donor can be applied. Depending on the structure of the donor, additional steric protection for the silylene center is provided as well. Thus, this versatile concept of stabilization has become widely used throughout modern main group chemistry. However, the resulting stable silylenes are three-coordinate and their reactivity is oftentimes significantly hampered.

In summary, the ambiphilic, highly reactive silylene center (Si:) needs appropriate stabilization by the adjacent substituents to prevent oligomerization and decomposition reactions. Here, two basic concepts come into play. Thermodynamic stabilization can be provided by ligands, which possess electron lone pairs and thus lower the electrophilicity by effective  $\pi$ -electron-donation to the vacant  $p_z$ -orbital. Bulky ligands

on the other hand, sterically shield the reactive center and prevent nucleophilic attacks and oligomerization reactions (kinetic stabilization).

### 3.2.2 Landmarks in silylene chemistry

Historically, silylenes were considered intensely reactive intermediates, which cannot be stable at room temperature. Initial studies were performed by Skell and Goldstein in 1964, generating dimethylsilylene by reduction of the corresponding dichlorosilane with sodium/potassium vapor at almost 300 °C.<sup>[86]</sup> Although of course, no stable silylene was obtained, typical silylene reactions, such as insertion into Si–H bonds<sup>[86]</sup> or silacyclopropane (silirane) formation<sup>[87]</sup> were identified. In the early 1980s, matrix isolation techniques in argon or hydrocarbons were utilized to investigate elusive silylene species, for example the parent silylene H<sub>2</sub>Si,<sup>[88]</sup> spectroscopically. Yet, the synthetic breakthrough of an isolable silylene had not been achieved.

In 1986, Jutzi *et al.* synthesized decamethylsilicocene (**L9**), the first mononuclear Si(II) compound.<sup>[89]</sup> This compound and further selected milestones of isolated silylenes are depicted in Figure 8 and briefly discussed within this chapter. Although, **L9** is unprecedented (first silicon  $\pi$ -complex), it does not meet the definition of a silylene because the silicon center is hyper-coordinate ( $\eta^{10}$ ).<sup>[90]</sup> Four years later, the group of Karsch described a  $\sigma$ -bonded, four-coordinate silylene species, which is thermodynamically stabilized by intramolecular electron donation from P atoms of the substituents.<sup>[91]</sup> The first “true” silylene, which meets the criteria of a two-coordinate Si center was reported by Denk and co-workers in 1994. In this compound **L10** the low-coordinate silylene center is stabilized by the adjacent,  $\pi$ -donating nitrogen atoms which are embedded in a cyclic framework. The resonance for the two-coordinate silyl center was observed at 78.3 ppm in the <sup>29</sup>Si NMR spectrum.<sup>[92]</sup> Compound **L10** is the first representative of the class of *N*-heterocyclic silylenes (NHSis), which to this day has been subject of extensive studies.<sup>[61,93]</sup> In 1997, Tokitoh and Okazaki were the first to employ Lewis bases (isonitriles) to stabilize the otherwise transient silylene fragment of **L11**.<sup>[85]</sup> Although **L11** is not a true silylene, due to the three-coordinate Si center, it can be considered an important progress in this field of research. The approach of isolating elusive silylene species as Lewis acid base adducts found widespread application and was for example later used to stabilize a bis(silyl)silylene (<sup>t</sup>Bu<sub>3</sub>Si)<sub>2</sub>Si.<sup>[50]</sup> The next landmark in silylene chemistry was the report of the dicarbon-substituted

example **L12** by the group of Kira.<sup>[94]</sup> Again, the low-coordinate silicon center is part of a five-membered ring and sterically protected by TMS groups adjacent to the  $\alpha$ -carbon atoms. Based on this compound, a plethora of characteristic silylene reactivity was discovered and interesting novel compounds,<sup>[95]</sup> for example a silanone ( $R_2Si=O$ , a heavier ketone analogue) were synthesized.<sup>[96]</sup>

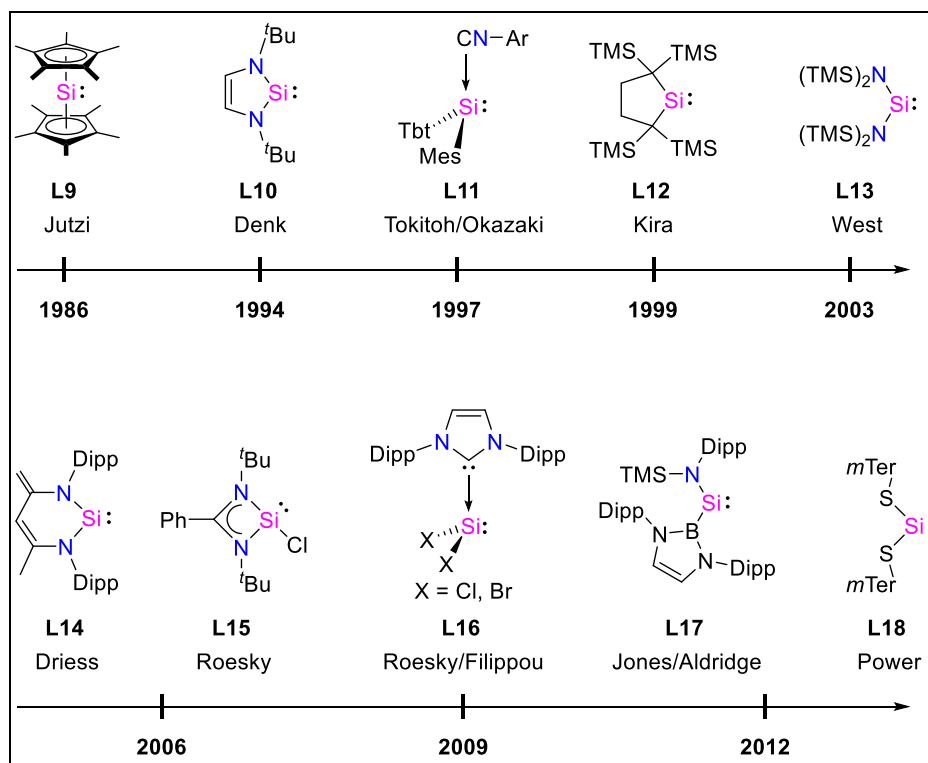


**Figure 8:** Selected milestones in silylene chemistry.

The first acyclic silylene **L13** was described by West.<sup>[97]</sup> As in the NHSis, the N-substituents serve the purpose of stabilizing the silylene center by  $\pi$ -electron donation. In contrast to the cyclic NHSi **L10**, the  $^{29}\text{Si}$  NMR signal of **L13** is strongly downfield-shifted to 223.9 ppm. Eventually however, this compound decomposes at temperatures above  $-20\text{ }^\circ\text{C}$ . Driess and colleagues extended the well-established class of NHSis by the cyclic, six-membered silylene **L14**.<sup>[98]</sup> The bidentate  $\beta$ -ketiminato ligand of **L14** was also employed for the isolation of a number of other low-coordinate main group compounds.<sup>[99]</sup> In the same year, a three-coordinate chloro silylene **L15** with an amidinato ligand was reported.<sup>[84]</sup> This first halosilylene complex is an ideal precursor for novel silylene structures, because it allows facile conversion to functionalized silylenes *via* salt metathesis reactions.<sup>[99-102]</sup> The same is true for the next innovative silylene milestones **L16**. With the help of a bulky NHC, Roesky was able to isolate a monomeric  $\text{SiCl}_2$  unit.<sup>[103]</sup> These molecules were previously only observed in the gas phase and polymerize immediately to perchlorinated polysilane

(SiCl<sub>2</sub>)<sub>n</sub>. Interestingly, the synthesis of the chloro silylene was achieved by treating HSiCl<sub>3</sub> with two equivalents of NHC by reductive dehydrochlorination. This result nicely pointed out the suitability of carbenes for HCl elimination. Essentially at the same time, the analogue bromo silylene<sup>[104]</sup> and later the iodo derivative<sup>[105]</sup> were reported by Filippou and co-workers. Bishalosilylenes have since been employed as valuable building blocks for interesting low-coordinate silicon species.<sup>[106]</sup> 2012 finally became the year of stable, two-coordinate, acyclic silylenes. Independently and simultaneously, Power's group, as well as Jones, Aldridge and co-workers reported the synthesis of the silylenes **L17**<sup>[107]</sup> and **L18**.<sup>[108]</sup> Silylene **L17** was obtained from reduction of the corresponding dibromosilane and shows a <sup>29</sup>Si NMR signal at 285.5 ppm, whereas the silicon center of **L18** resonates strongly downfield-shifted at 439.7 ppm. Strikingly, compound **L17** also displays a significantly wider R–Si–R angle than **L18** and thus a smaller HOMO-LUMO energy gap. Acyclic silylenes like **L17** which combine small HOMO-LUMO gaps with structural flexibility, are able to mimic transition metal reactivity to some extent and are therefore considered promising candidates in regard of bond activation and main group catalysis.<sup>[109-110]</sup> These long sought after compounds promoted a deeper understanding of the nature of silylenes and opened up a completely new field of low-coordinate silicon chemistry. Of course, there are numerous other interesting silylenes aside from the presented examples, including bis-silylene structures, which contain two silylene centers per molecule, either interconnected, or separated by a spacer.<sup>[111]</sup> To date, thorough investigation of silylenes over the last decades has provided a good understanding of this class of low-coordinate silicon compounds in general. However, some puzzle parts are still missing, especially in respect to triplet ground state bis(silyl)silylenes and their particular reactivities.

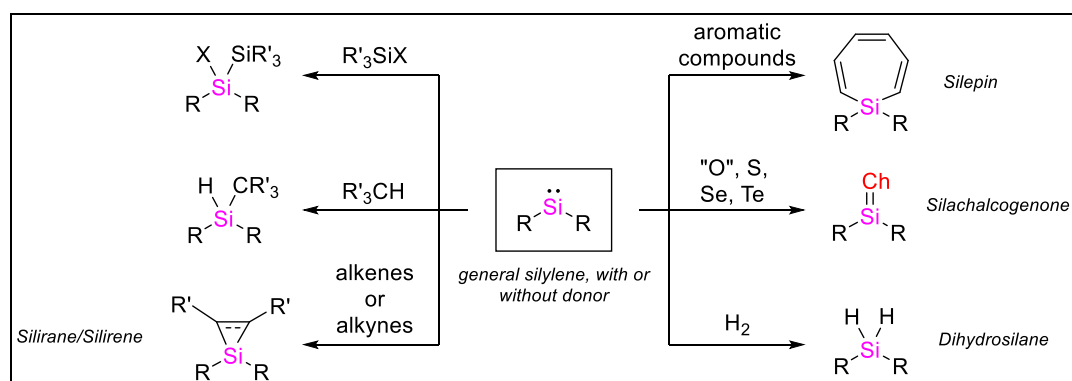
#### 3.2.3 Reactivity of silylenes

Owing to their electron deficient state of only six valence electrons, silylenes in general show intense reactivity. Their vacant p-orbital makes them strong electrophiles and their electron lone pair allows application in coordination chemistry, for example with transition metals.<sup>[37]</sup> In this chapter, selected, characteristic silylene reactivities, especially in regard to small molecule activation are shown and discussed briefly.

Silylenes tend to insert readily into Si–X bonds of halosilanes. This was demonstrated by the group of Kira with their cyclic dialkylsilylene **L12** (Scheme 3).<sup>[66]</sup>

Generally speaking, bond insertion is a commonly observed reaction pattern of silylenes.<sup>[37,61,93,95,112]</sup> Examples comprise alkyl-halogen bonds,  $\text{NH}_3$ , B–H and B–B bonds,<sup>[113-114]</sup> as well as O–H bonds of alcohols. Therefore, the latter have frequently been used to trap transient silylene species, furnishing the corresponding alkoxy-silanes  $\text{R}_2\text{Si}(\text{OR}')\text{H}$ .

**Scheme 3:** Selected examples of silylene reactivities.



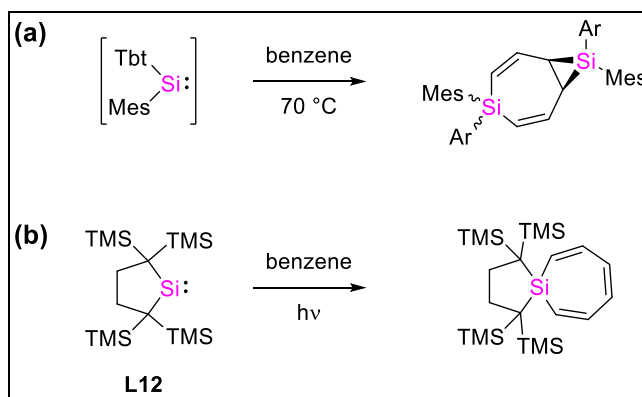
Furthermore, intramolecular bond activation of ligand framework is oftentimes the reason for silylene decomposition. The elusive bis(supersilyl)silylene ( ${}^t\text{Bu}_3\text{Si}$ ) $_2\text{Si}$ : for example inserts into a C–H bond of a  ${}^t\text{Bu}$  group to the isomeric disiletane.<sup>[77]</sup>

Another classical silylene reactivity, that was already observed by Skell and Goldstein in 1964 is [1+2] cycloaddition with unsaturated compounds.<sup>[87]</sup> In fact, silylenes readily undergo silirane or silacyclopropene (silirene) formation upon treatment with alkenes or alkynes, respectively. Siliranes in turn are useful synthons in organosilicon chemistry.<sup>[115]</sup>

Interestingly, silylenes are also able to insert into aromatic compounds, generating silaheptatrienes (silepins) by dearomative ring expansion.<sup>[116]</sup> Tokitoh and Okazaki observed activation of benzene in this fashion by the *in situ* generated bis(aryl)silylene, which was later stabilized as base adduct **L11**.<sup>[117-118]</sup> Apparently, the resulting silepin is so reactive in a subsequent [1+2] cycloaddition with another silylene molecule, that it could not be isolated, even with a great excess of benzene (Scheme 4 (a)).<sup>[117]</sup> In contrast to this thermally induced silepin formation, activation of silylene **L12** into a singlet excited state by irradiation in presence of benzene resulted in the selective insertion into an aromatic C–C bond (Scheme 4 (b)).<sup>[119-120]</sup> Kira *et al.* observed this photochemically induced reaction also for 1,4-functionalized benzene derivatives, such as xylene, difluorobenzene or dimethoxybenzene.<sup>[119]</sup> Not only benzene derivatives

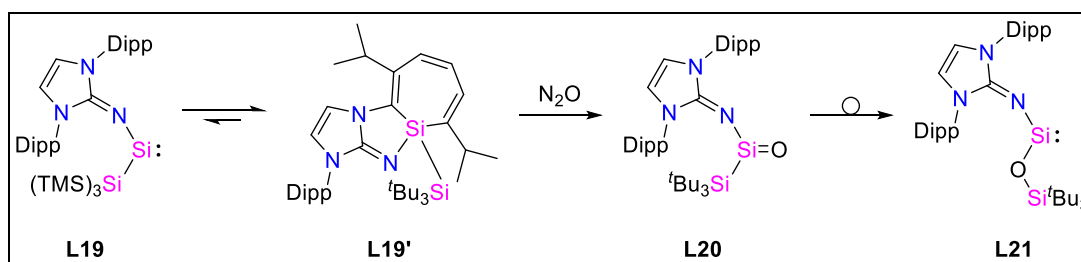
were activated in this fashion, but also heterocyclic aromatic compounds, such as pyridine<sup>[121]</sup> or pyrazine.<sup>[116]</sup>

**Scheme 4:** Thermally (a) and photochemically (b) induced silepin formation by silylenes.



Recently, our group presented an acyclic silylene **L19**, which reversibly undergoes isomerization *via* silepin formation **L19'** (Scheme 5).<sup>[122]</sup> Therefore, to a certain extent, silepins, as well as siliranes can be considered as stable synthetic equivalents for free silylenes.

**Scheme 5:** Oxidation of a silylene/silepin equilibrium to a silanone and subsequent rearrangement.



Oxidation reactions of silylenes with chalcogens have been intensively studied in recent years. Kira's cyclic silylene **L12** selectively reacts with sulfur, selenium and tellurium to the stable corresponding silachalcogenones.<sup>[95]</sup> However, the synthesis of silanones, the formal monomers of silicones, which were a long term dream of silicon chemistry pioneer Frederic S. Kipping, turned out to be far more challenging. Because of the high difference in electronegativity, the Si=O double bond is extremely polarized and silanones therefore have a high propensity towards polymerization reactions. Nevertheless, several examples have been reported. The group of Driess oxidized a donor-stabilized (NHC or DMAP) derivative of their NHSi **L14** with the oxygen transfer reagent  $\text{N}_2\text{O}$  to the respective silanone species. The remarkably stable, three-coordinate silanone **L20** was obtained by our group by oxidation of silepin **L19'**,

underlining the partial silylene character of this compound.<sup>[123]</sup> Eventually, silanone **L20** undergoes rearrangement to the isomeric, acyclic, oxygen-substituted silylene **L21**.

One of the most remarkable silylene reactivities is the single-site activation of the apolar, enthalpically strong dihydrogen molecule. This was achieved by the acyclic silylene **L17**.<sup>[108]</sup> The acyclic bis(arythio)silylene **L18** with the larger HOMO-LUMO gap in contrast showed no reactivity towards H<sub>2</sub>.<sup>[124]</sup> Nonetheless, to date, two further examples of H<sub>2</sub> addition to silylenes have been reported, including the silylene silepin equilibrium mixture **L19/L19'**.<sup>[122,125]</sup> Donor-stabilized silylenes however, haven't yet achieved this challenge.

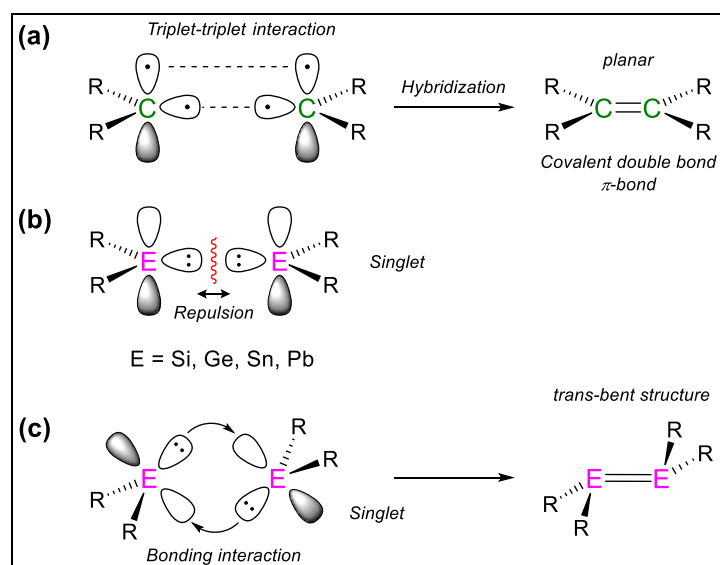
### 3.3 Disilenes

Disilenes are the heavier analogues of alkenes. Until the pioneering work of West and co-workers in 1981, they remained elusive species. To date, a plethora of disilenes with various combinations of substituents and a resulting multitude of reactivities has been reported.<sup>[126-135]</sup> Within this chapter, the milestones in this field of research and the key features of disilenes will be pointed out briefly.

#### 3.3.1 Bonding situation in disilenes

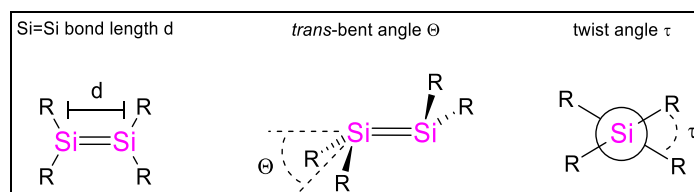
Unsaturated carbon compounds are ubiquitous in organic and biochemistry. Whether in hormones, fatty acids or monomers for commodity plastics, especially the alkene moiety can be found in every part of life. The reason behind the planar structure of the C=C double bond is the triplet multiplicity of the formal monomeric carbene fragments. They readily undergo sp<sup>2</sup> hybridization, forming π-bonding interactions (Figure 9, (a), adapted from Weidenbruch).<sup>[128,136]</sup> As pointed out, heavier tetrylenes prefer the singlet ground state instead (*vide supra*). Here, the repulsive interactions between inner-shell electrons (Pauli repulsion) and the decreasing overlap of p-orbitals play a role. Together with the repulsion between the electron lone pairs, these effects prevent π-bond formation as in alkenes (Figure 9, (b)). Based on these principles, the so-called "double bond rule" was widely accepted, stating that elements with a principal quantum number greater than 2 cannot form π-bonds, either with themselves or other elements.<sup>[137-138]</sup> Thus, the chemical community was flabbergasted as in the early 1980s, this common hypothesis was finally disproven by the isolation of the first disilene **L22** by the group of West<sup>[139]</sup> and the first silene (Si=C) by Brook and co-workers.<sup>[140]</sup>





**Figure 9:** (a) Bonding model in alkenes; (b) Repulsion between singlet tetrylenes; (c) CGMT bonding model for heavier group 14 elements.

Accordingly, a model which explains the bonding situation in these unprecedented compounds was developed by Carter, Goddard, Malrieu and Trinquier (CGMT) (Figure 9, (c)).<sup>[141-143]</sup> In order to avoid repulsion between the electron lone pairs, the singlet tetrylene fragments have to rotate in relation to each other, forming bonding interactions between the doubly-occupied s-type orbitals and the vacant p-orbitals. This results in *trans*-bending between the  $\text{SiR}_2$  planes and the  $\text{Si}=\text{Si}$  axis, reflected by the *trans*-bent angle  $\Theta$ . The extent of the donor-acceptor interaction and thereby the angle  $\Theta$  are strongly depending on the singlet-triplet gap of the involved tetrylenes fragments: a small  $\Delta E_{s,\tau}$  induces planar dimetallenes.<sup>[127,134]</sup> The influence of the ligands on the structure and thus the singlet-triplet energy gap of silylenes has already been discussed (see chapter 3.2.1). Accordingly, the choice of substituents is crucial for the degree of *trans*-bending in the corresponding disilenes.

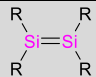
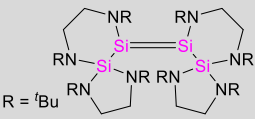


**Figure 10:** Key structural features of disilenes.

Besides *trans*-bending, twisting between the two  $\text{SiR}_2$  planes, described by the twist angle  $\tau$  is another characteristic structural feature of disilenes (Figure 10). A large twist angle correlates with a smaller  $\pi-\pi^*$  energy separation because of the unfavored orbital overlap. Hence, the HOMO-LUMO gap becomes narrower upon twisting,

resulting in a red-shifted absorption signal for the longest wavelength in the UV-vis spectrum of the disilene.<sup>[144]</sup> In the case of carbon, there is only little variation between C=C double bond lengths, even in sterically crowded alkenes. For silicon, the values of Si=Si distances  $d$  vary more and the shortening from Si=Si double bonds compared to Si–Si single bonds is less pronounced.<sup>[128]</sup> The effects of the adjacent substituents on the geometrical features of disilenes are briefly illustrated by the examples in Table 1. Tetra(aryl)disilene **L22** features a short Si=Si bond length and moderate degrees of *trans*-bending and twisting.<sup>[145-146]</sup> Introduction of bulky, electropositive silyl substituents (**L23**<sup>[147]</sup> and **L7**)<sup>[57]</sup> results in (almost) planar disilene structures. Interestingly, the bulky <sup>t</sup>Bu<sub>2</sub>MeSi groups in **L7** induce a large twist angle. In sharp contrast, an increasing number of electronegative,  $\pi$ -donating substituents (such as nitrogen) promotes *trans*-bending. Since there are no structurally characterized disilenes bearing four nitrogen ligands, Kira, Müller and Apeloig calculated the structure of (<sup>i</sup>PrN)<sub>2</sub>Si=Si(N<sup>i</sup>Pr<sub>2</sub>) (**L24**).<sup>[148]</sup> The authors concluded that disilene **L24** should adopt an extreme *trans*-bent angle of 42.6° and furthermore a highly twisted geometry. Compound **L25**, one of few isolated *N*-substituted disilenes also displays a large *trans*-bent angle, thus confirming this effect.<sup>[149]</sup>

**Table 1:** Structural features of selected disilenes (\*values calculated).

R =					
	Mes	<sup>i</sup> Pr <sub>3</sub> Si	<sup>t</sup> Bu <sub>2</sub> MeSi	<sup>i</sup> Pr <sub>2</sub> N	
#	<b>L22</b> <sup>[146]</sup>	<b>L23</b> <sup>[147]</sup>	<b>L7</b> <sup>[57]</sup>	<b>L24</b> <sup>[148]</sup>	<b>L25</b> <sup>[149]</sup>
$d$ [Å]	2.143	2.251(1)	2.2598(18)	2.472*	2.2890(14)
Avg. $\Theta$ [°]	13	10.2	5.9	42.6*	33.1
$\tau$ [°]	3	0	54.5	55.5*	25.1

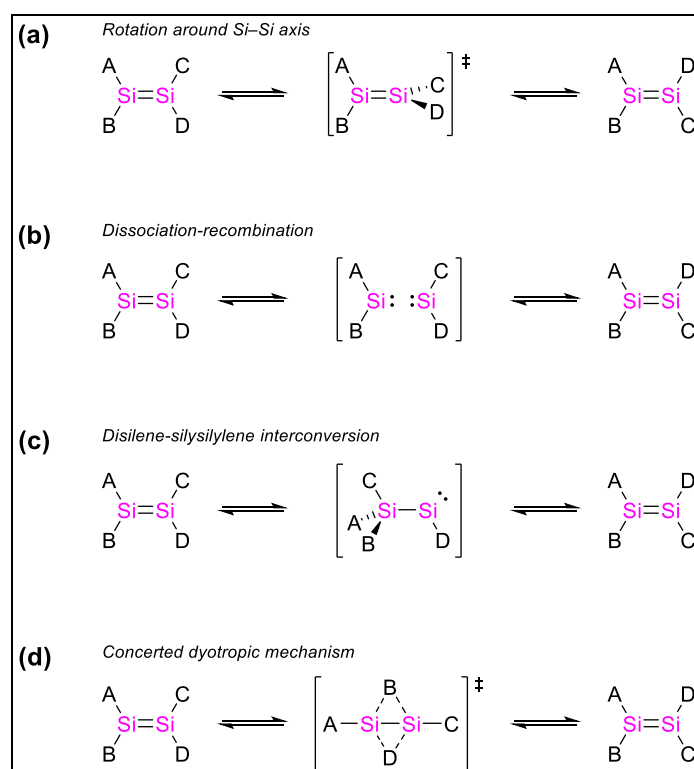
These studies impressively demonstrated the structural variability of disilenes and the possibilities to influence their structural parameters und thereby the chemical behavior by introduction of specifically designed substituents.

### 3.3.2 Isomerization reactions of disilenes

Whereas thermal (*E/Z*)-isomerization of alkenes takes place *via* rotation around the C=C bond, there are four mechanisms that should be taken into consideration for this kind of isomerization reaction in disilenes (Scheme 6, adapted from Kira).<sup>[131]</sup> Comparable to alkene (*E/Z*)-isomerization, there is the possibility of rotation around

the Si=Si axis (a). Examples of disilenes which undergo isomerization in this fashion are Mes(<sup>t</sup>Bu)Si=Si(<sup>t</sup>Bu)Mes and the tetra(aryl)disilene Mes(Dipp)Si=Si(Dipp)Mes from the group of West.<sup>[126]</sup> Tetra(silyl)disilene **L7** was investigated by Sekiguchi and Apeloig in this regard.<sup>[150]</sup> EPR studies and theoretical calculations showed that rotation of the substituents of the already highly twisted disilene around the Si=Si bond at elevated temperatures, results in a triplet state diradical. Isomerization by thermally induced dissociation of a tetra(aryl)disilene **L26** into the respective silylene fragments (b) has also been reported.<sup>[118]</sup> Okazaki *et al.* were even able to trap the resulting silylene with various reagents, including benzene, *via* silepin formation. Furthermore, the first silylene Lewis base adduct **L11** was obtained from this reaction (*vide supra*).

**Scheme 6:** Possible mechanism for (*E/Z*)-isomerization in disilenes.



In contrast to the first two pathways, mechanisms (c) and (d) not only provide access to the (*E/Z*)-isomerization product, but also allow  $A_2Si=SiB_2 \leftrightarrow ABSi=SiAB$  transformation. Upon 1,2-migration of a substituent, a disilene can isomerize to the corresponding silylsilylene. From this state, the reaction to the starting material or rotation around the Si-Si single bond and subsequent substituent shift under formation of the (*E/Z*)-isomerization product can take place. However, also ligand scrambling to an isomeric disilene is possible. Kira and co-workers made no final conclusion, on whether the formal dyotropic isomerization of their tetra(silyl)disilene occurred *via* this

type of rearrangement reaction.<sup>[151]</sup> Very recently however, this mechanism was proposed for the (*E/Z*)-isomerization of a silene.<sup>[152]</sup>

Finally, there is a concerted dyotropic rearrangement.<sup>[153]</sup> This mechanism *via* a 1,3-disilabicylcobutane-like transition state was proposed by West and colleagues for the isomerization of tetra(aryl)disilenes.<sup>[154-155]</sup>

### 3.3.3 Historic milestones in disilene chemistry

Without a doubt, the isolation of the first compound, containing a Si=Si double bond was a striking landmark in modern silicon chemistry. This pioneering work was accomplished by West, Fink and Michl. In 1981, they reported the synthesis of Mes<sub>2</sub>Si=SiMes<sub>2</sub> (**L22**) and thereby finally disproved the long existing “double bond rule” (Figure 11). Irradiation of the silane Mes<sub>2</sub>Si(TMS)<sub>2</sub> with UV light resulted in the intermediary formation of the silylene Mes<sub>2</sub>Si:, that ultimately undergoes dimerization, furnishing **L22**. Its discovery opened up an entirely new, flourishing field of silicon chemistry. The most prominent, structurally characterized disilene examples are shown and briefly discussed below.

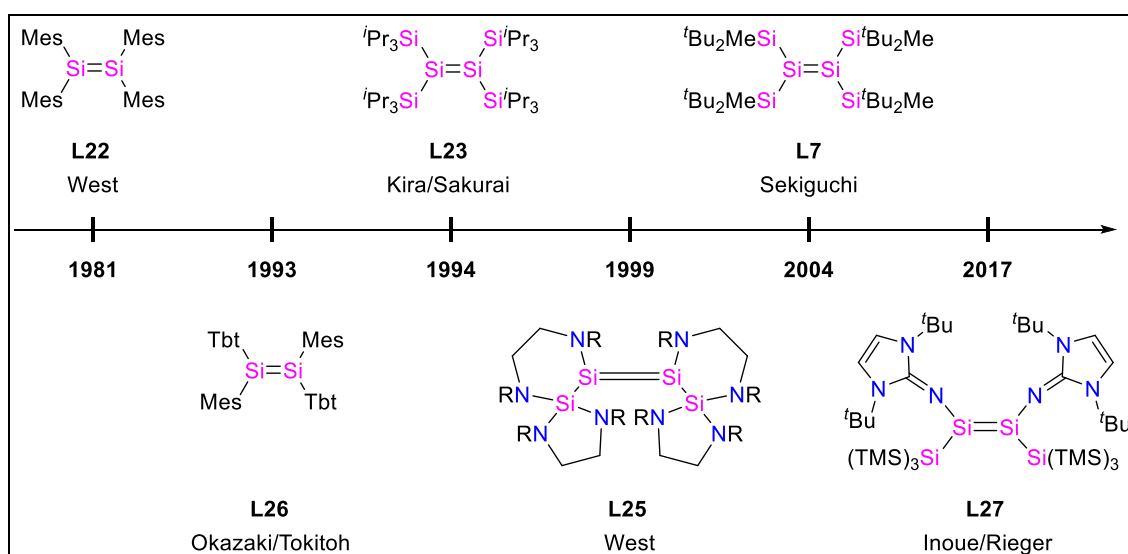


**Figure 11:** Selected examples of disilenes.

West *et al.* continued their studies on disilenes and synthesized derivatives with alkyl and amine substituents.<sup>[156-157]</sup> Disilene **L26** can thermally be cleaved into the corresponding silylene units and thus undergo (*E/Z*)-isomerization. Furthermore, this dissociation at elevated temperatures allowed exploration of bis(aryl)silylene chemistry. Only one year later, the first representative of the class of tetra(silyl)disilenes **L23** was structurally characterized.<sup>[147]</sup> Due to the sterically

demanding, electropositive silyl groups, these compounds generally display a relatively planar geometry, compared to tetra(aryl)disilenes. In 1999, the first completely characterized *N*-substituted disilene was reported.<sup>[149]</sup> Compound **L25** resulted from tetramerization of an NHSi and exhibits a large *trans*-bent angle of 33.1°, due to the  $\pi$ -donating effect of the ligands. Another tetra(silyl)disilene **L7** was presented in 2004.<sup>[57]</sup> This remarkable example from the group of Sekiguchi is relatively air stable because of the kinetic stabilization by the bulky silyl groups. Furthermore, it enabled the exploration of the redox chemistry of disilenes (*vide infra*). On a final note, our group recently reported the disilene **L27** bearing sterically protecting hypersilyl groups and strongly  $\pi$ -donating *N*-heterocyclic imines.<sup>[158]</sup> This was the first multiply bonded silicon compound, able to activate dihydrogen, even at ambient temperature.

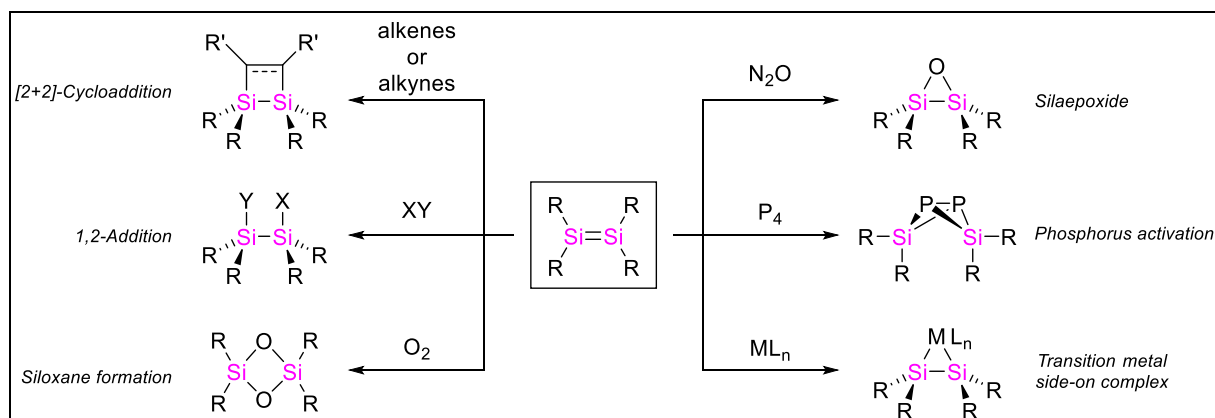
To date, numerous more of these heavier alkene congeners have been isolated. Among them are cyclic disilenes<sup>[159-161]</sup> and disilenes with conjugated<sup>[162-163]</sup> or cumulated Si=Si double bonds.<sup>[164]</sup> Furthermore, there is a halogen-substituted example, which was later converted to a disilyne, a compound containing a Si $\equiv$ Si triple bond.<sup>[165]</sup> These disilynes in turn, readily undergo 1,2-addition reactions, furnishing again disilenes.<sup>[165-167]</sup> Metal-substituted disilenes<sup>[163,168]</sup> allow facile functionalization with electrophiles *via* salt metathesis. Scheschkewitz and co-workers successfully employed their Li-substituted disilene (disilenide) as precursor for a heavier benzene derivative.<sup>[169]</sup>

#### 3.3.4 Reactivity of disilenes

With their unprecedented tetra(aryl)disilenes in hand, West and co-workers proceeded to thoroughly investigate their reactivities. The most characteristic examples are depicted in Scheme 7. Expectably, the double bond character of disilenes enables facile [2+2] cycloaddition reactions with alkenes and alkynes. However, not only unsaturated hydrocarbons, but also other multiply bonded compounds (*e.g.* C=N, C=O, N=O) generally react in the same fashion with disilenes, furnishing four-membered heterocycles, which are otherwise difficult to synthesize.<sup>[126]</sup> Not only [2+2], but also [3+2] cycloadditions with azides and [4+2] cycloadditions with conjugated dienes were observed. Disilenes are prone to react with halogens and polarized hydrogen containing compounds, such as alcohols, hydrogen halides or hydrosilanes to the respective 1,2-addition products. The corresponding dihydrosilane of disilenes can be obtained from the reduction with lithium aluminum hydride or tin hydride.<sup>[126]</sup> To date,

the only disilene to activate elemental H<sub>2</sub> in a 1,2-addition reaction is the NHI-substituted compound **L27**.<sup>[158]</sup> Theoretical calculations revealed a concerted *anti*-addition pathway for this reaction.

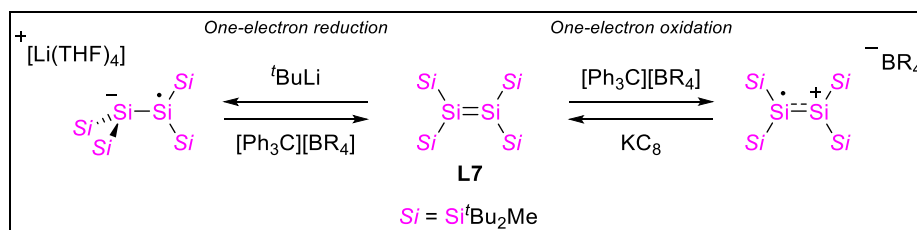
**Scheme 7:** Selected examples of disilene reactivities.



With oxygen, disilenes initially undergo a [2+2] cycloaddition to a 1,2-dioxo-3,4-disilacyclobutane intermediate, which rearranges to the isomeric cyclic disiloxane. Oxidation by N<sub>2</sub>O, which is a milder oxygen transfer reagent instead furnishes a silaepoxide. Similar [2+1] cycloaddition products were obtained from the oxidation of disilenes with elemental sulfur, selenium and tellurium.

Rather unexpected reactions were observed by West *et al.* from treatment of disilenes with white phosphorous. Selective formation of a butterfly-shaped structure of the two former low-coordinate silicon atoms, bridged by two phosphorous atoms took place upon cleavage of the Si=Si double bond.<sup>[170-171]</sup> Furthermore, disilenes were applied as ligands for transition metal complexes, for example with platinum, iron, or hafnium.<sup>[126,172-174]</sup>

Most interestingly however, especially in regard to potential battery applications is of course the reversible redox behavior of the tetra(silyl)disilene **L7**, which was impressively demonstrated by the group of Sekiguchi (Scheme 8).<sup>[57,59]</sup> One-electron reduction of the disilene by <sup>t</sup>BuLi afforded the corresponding radical anion, which can be reoxidized to the starting material. On the other hand, also the cationic radical was accessible by one-electron oxidation with a trityl reagent. Remarkably, the anionic and cationic radical were both structurally characterized, providing deeper insight into the bonding situation of disilenes. Notably, with 88°, the anionic radical is even stronger twisted than disilene **L7**. So far, only one additional example of a disilene radical anion has been reported.<sup>[58]</sup>

**Scheme 8:** Reversible reduction and oxidation of tetra(silyl)disilene **L7**.

In summary, disilenes have shown an immense structural diversity. Due to their reactive Si=Si double bond moiety, they provide great synthetic potential as building blocks in organosilicon chemistry. Additionally, the reversible redox nature of tetra(silyl)disilenes might even be exploited for the purpose of electric energy storage.

## 4. Organic Radical Batteries

Electrochemical energy storage is of utmost importance in the information era. Batteries with high energy density and long lifetimes are inevitable for portable devices, such as cellular phones and laptop computers.<sup>[175-179]</sup> An additional demand for batteries is further arising from the emphasis on electromobility in the face of finite fossil fuels and climate change.<sup>[3]</sup> Furthermore, energy storage will become an increasing issue with respect to the transition of current electricity generation to renewable sources, in order to grant a continuous power supply.

### 4.1 Lithium Ion Batteries and Related Technology

Currently, industry is mainly relying on the lithium ion battery (LiB). The origins of this technology are dating back to the 1970s and 80s and the pioneers in this field of energy storage were honored by the 2019 Nobel Prize for chemistry, which underlines the fundamental importance of lithium ion batteries. Since they were made commercially available in 1991 by the *Sony Corporation*, these batteries have found application in almost every aspect of daily life and their performance has continuously been improved.<sup>[179]</sup> In general, lithium ion batteries consist of two half cells, as depicted in Figure 12.<sup>[177]</sup> Usually, transition metal oxides, which can intercalate lithium ions without significant structural modifications (e.g.  $\text{LiCoO}_2$ ,  $\text{LiNi}_{0.8}\text{Co}_{0.15}\text{O}_2$ ,  $\alpha\text{-NaFeO}_2$ ) are employed as cathode materials.<sup>[179]</sup>

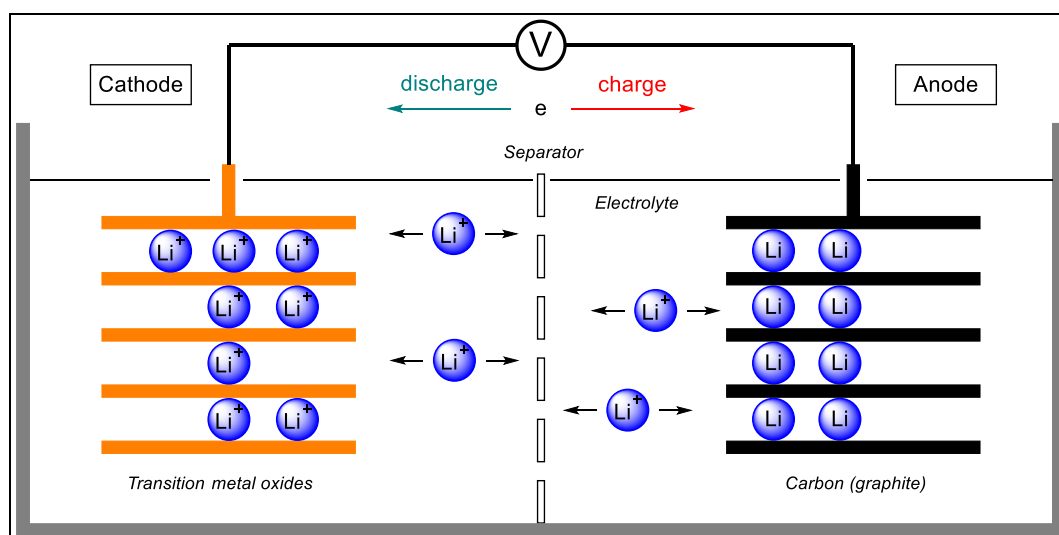


**Figure 12:** Principle of a lithium ion battery.

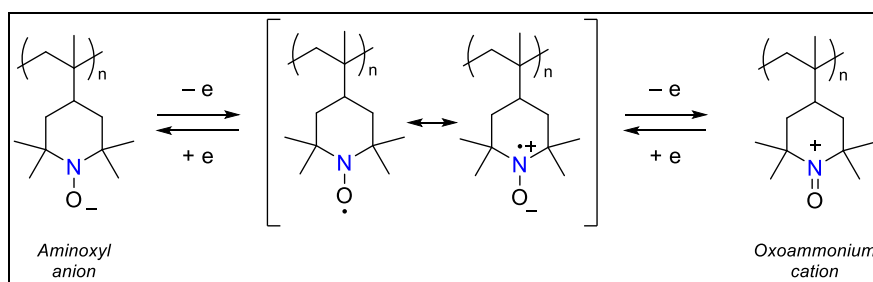
During the charging process, lithium ions diffuse through the porous separator and are forced to intercalate between the graphite layers of the anode. Organic solvents, such



as ethylene carbonate, diethyl carbonate or DME are used as electrolytes. The battery's energy density and capacity are mainly limited by the cathode.<sup>[180]</sup>

Furthermore, there have been toxicity and safety issues with the lithium transition metal oxide cathodes. Hence, the organic radical battery (ORB) was developed. This relatively new energy storage technology mostly relies on a conventional lithium/graphite anode and a cathode, which consists of stable organic radicals. Oftentimes nitroxyl radicals, such as 2,2,6,6-tetramethylpiperidine-1-oxyl (TEMPO) are applied (Scheme 9). They are adjacent to a polymer backbone to avoid dissolving in the electrolyte.<sup>[180-181]</sup> The nitroxide radical offers two redox couples. One is based on the reversible oxidation of the resonance-stabilized radical to the stable oxoammonium cation.

**Scheme 9:** Nitroxide polymers as cathode material in the battery process.



This process can be utilized in cathodes of ORBs. The second process is the one-electron reduction of the radical to the aminoxyl anion. However, this reaction is rarely applied because of its lower reversibility.<sup>[182]</sup> Although, these batteries are transition metal-free and might provide higher energy densities, they still require lithium, which is also a finite resource. Furthermore, elemental lithium in the anode in combination with highly flammable organic solvents poses a serious safety threat in case of a breach of the battery cell. So far however, reports on fully organic-based batteries are scarce. The group of Nishide developed a battery, which is completely based on bipolar redox-active radical polymers.<sup>[183]</sup>

## 4.2 Silicon-based ORB

An even more visionary approach was presented from a cooperation of the group of Sekiguchi together with the *R&D Labs. of Toyota* in 2014.<sup>[5]</sup> For the first time, heavier group 14 radicals ( $(\text{tBu}_2\text{MeSi})_3\text{E}^\bullet$ , E = Si, Ge, Sn) were utilized for the purpose of energy storage in a totally alkali- and transition metal-free battery cell with rapid charge/discharge properties. These radicals were previously electrochemically

investigated by cyclic voltammetry and showed highly reversible redox processes.<sup>[184]</sup> Furthermore, the reversible redox nature has already been demonstrated chemically for silyl radical **L2**. Among these tetryl radicals, the silyl derivative **L2** was concluded to be the most suitable, because it provides the largest capacity and the highest reaction rate. The general setup of this battery type is depicted in Figure 13.<sup>[5]</sup>

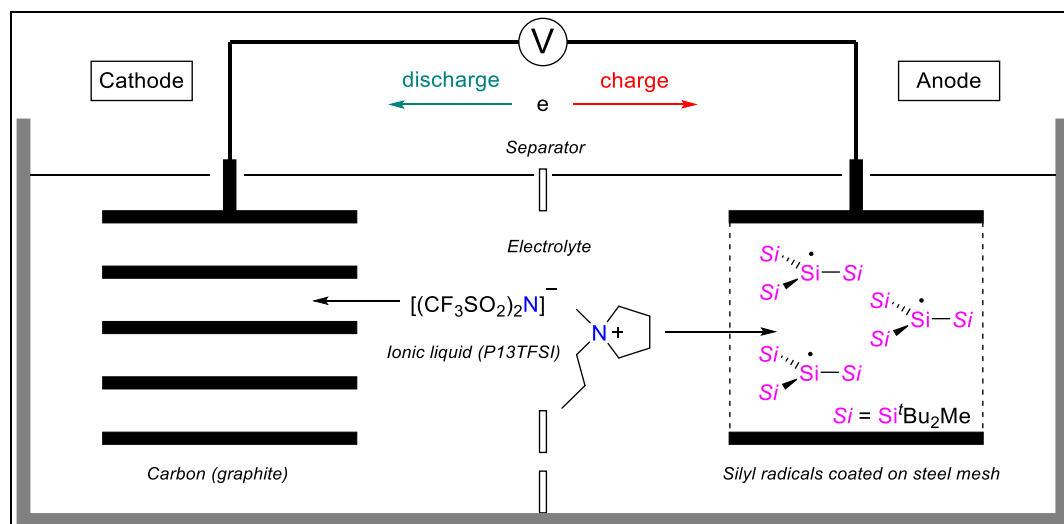
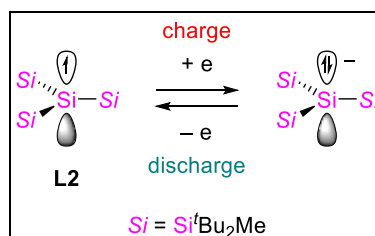


**Figure 13:** Schematic representation of a silicon radical battery cell.

The anode in this case consists of tri(silyl)-substituted silyl radical **L2**, coated on a stainless steel mesh. Graphite was also coated on steel and employed as cathode. Both half cells are separated by a porous polyethylene membrane and the ionic liquid P13TFSI serves as electrolyte. During the charge process, the silyl radicals are reduced to the corresponding anionic species (Scheme 10). Cations from the ionic liquid diffuse into the silyl scaffold for charge balance. At the same time, TFSI anions are intercalated into the graphite of the cathode. Upon discharge, the reversed processes take place.

**Scheme 10:** Anode process in silyl radical batteries.



Sekiguchi *et al.* achieved already remarkable cyclic stability with their experimental cells. After 100 charge/discharge cycles at an operating temperature of 28 °C, the battery still possessed 98% of the original capacity. Later, the carbon cathode was

replaced by hyper-valent sulfur and selenium radicals.<sup>[43]</sup> Deriving from the operating principle of the battery cells the requirements for the anode materials were defined:

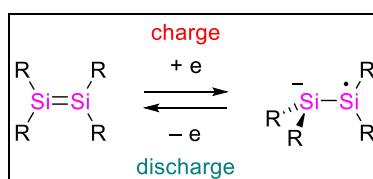
- Highly reversible redox behavior for long lifetimes and cyclic stability
- Suitable reduction potential (determining the resulting battery charge)
- Electrode material must be absolutely insoluble in the electrolyte to provide cyclic stability
- Sufficient space between the charge centers (radical centers) to allow rapid counter ion diffusion into the crystal lattice
- Structural change upon reduction/oxidation must be minimal to avoid cracking of the anode
- Convenient accessibility, high purity
- Stability, even at elevated temperatures
- Preferably tolerance against various solvents and air to facilitate cell construction process

Compared to lithium ion batteries, this silyl radical battery can operate at much higher charge/discharge rates, because the silyl radical exhibits a larger diffusion constant, than cathode active materials commonly used in LiBs.<sup>[5]</sup> Therefore, silyl radical batteries might be suitable for electric vehicles or power-grid applications. This advantage however, comes with the downside of lower energy density. Due to the sterically demanding substituents, which are necessary to stabilize the radical, silyl radical-based anodes provide fewer charges per volume than graphite/Li anodes, which can basically reach one charge per phenyl ring ( $\text{LiC}_6$ ).<sup>[176]</sup>

Nevertheless, the development of the silyl radical battery can be considered as progress towards safe and sustainable energy storage. The great advantage of this battery type is their completely metal free operation and they also provide the intriguing opportunity to employ silicon for the purpose of electric energy storage. Of course, the question arises: How can these energy storage devices be improved, regarding capacity and performance? Probably, a silyl radical with bulkier substituents could minimize structural change upon reduction even further and thus increase cyclic stability. This might also affect the distance between the radical centers and thus have an effect on charge/discharge rates. The battery voltage and therefore the energy density could be improved by anode materials with lower reduction potentials. This might be achieved by functionalization of the silyl radicals, or by utilization of a different

redox active material. In this context, disilenes could be promising candidates. At the example of tetra(silyl)disilene **L7**, it was already demonstrated, that these heavier alkenes can offer reversible redox couples. The reduction to the corresponding anionic radical could be employed for electric energy storage (Scheme 11). But also novel, heteroatom-substituted disilenes might be promising in regard to reversible redox chemistry, which has not been explored so far. Their potential for battery applications can be determined by electrochemical investigation, such as cyclic voltammetry.

**Scheme 11:** Possible redox process of disilenes in batteries.



Eventually however, the structural behavior of the coated anode material upon repeated reduction and oxidation processes has to be tested in experimental battery cells.

## 5. Transition Metal-free Catalysis

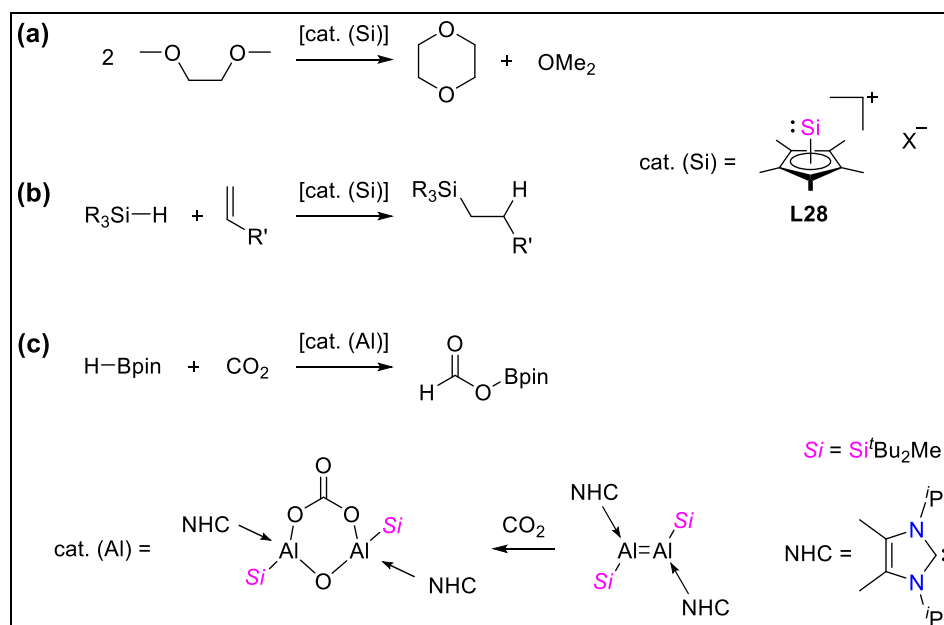
There is no doubt that the concept of catalysis is fundamental for modern chemistry, whether in laboratory scale, or for multi-million ton scale industrial processes.<sup>[6]</sup> As early as in the beginning of the 19<sup>th</sup> century, J. J. Berzelius, who also achieved the first isolation of elemental silicon (*vide supra*), coined the term “catalysis” to describe the acceleration of chemical reactions by substances which remain unchanged during these transformations. Today, it is estimated that more than 80% of all commercially produced chemicals require at least one catalytic step during their synthesis process.<sup>[185-186]</sup> The fundamental importance of catalysis is further reflected by a number of Nobel Prizes in this field of research, starting with Ostwald in 1909. Furthermore, Nobel Prizes were also awarded for the discovery of the *Haber-Bosch* process, the catalytic synthesis of ammonia from the elements and for the *Ziegler-Natta* catalysis for olefin polymerization. The vast majority of catalysts applied in industrial processes are heterogeneous. Nevertheless, also homogeneous catalysts are utilized. A prominent example in this regard is the Pt(0)-based Karstedt’s catalyst, which highly effectively catalyzes hydrosilylation reactions and is therefore applied for the cross-linking of polysiloxanes.<sup>[187]</sup> This is not optimal, because the expensive catalyst remains in the polymer and cannot be recovered.

Most of the industrial relevant catalytic transformation rely on transition metals as active species. Due to their electronic structure with partially occupied valence d-orbitals which are close in energy, these elements readily interact with small molecules, such as CO, ethylene or H<sub>2</sub>. Furthermore, transition metals can adopt multiple oxidation states and therefore are ideal to undergo oxidative addition and subsequent reductive elimination of these substrates in a catalytic cycle.<sup>[188]</sup> On the downside however, these metals are often toxic or rare and thus expensive. This becomes especially problematic in cases where the catalyst cannot be recovered, as in the Pt-based curing of polysiloxanes. Hence, the question arises, whether highly abundant, main group elements can mimic transition metal behavior and therefore be applied as catalysts.<sup>[110,188]</sup> Silicon-based catalysis is considered particularly attractive, because silicon and its derivatives are generally non-toxic and available in almost infinite quantities.

In this chapter, selected examples of main group element catalysis are briefly presented. With regard to silicon, the list of catalytic applications is rather short so far.

Silylium ions ( $R_3Si^+$ ) have been employed in Lewis acid catalysis or for the purpose of C–F bond activation.<sup>[189]</sup> Notably, the pentamethylcyclopentadienyl silyliumylidene ion **L28** from Jutzi and co-workers showed some intriguing catalytic activity (Scheme 12 (a) and (b)). The precise transformation of ethyleneglycol ethers, such as DME to 1,4-dioxane was observed in the presence of silyliumylidene **L28**.<sup>[190]</sup> A probably more industrially relevant catalytic application of this compound, the hydrosilylation of alkenes was reported recently. This catalytic reaction is key for the curing of polysiloxanes in the process of silicone rubber production. Remarkably, the catalytic activity of **L28** is even comparable with the currently applied Pt-based catalysts and thus might offer a sustainable alternative to transition metal-catalysis in this field.

**Scheme 12:** Examples of main group element catalysis: (a) Degradation of DME; (b) Hydrosilylation; (c) Hydroboration.



Right behind silicon, aluminum is the third most abundant element in the earth's crust and therefore also an attractive candidate to be integrated into catalytic processes. Very recently, the catalytic hydroboration of  $\text{CO}_2$  by a silyl-substituted aluminum compound was presented (Scheme 12 (c)).<sup>[191]</sup> The catalytically active species in this case is a six-membered heterocycle of two aluminum centers, bridged by a carbonate group and an oxygen atom, which is generated from the reaction of the  $\text{Al}=\text{Al}$  double bonded precursor with  $\text{CO}_2$ . Similar heterocyclic rings were obtained from exposure of iminodisilene **L27** to carbon dioxide. Thus, disilenes might not only be considered for battery applications, but also as possible molecular catalysts.

## 6. Scope of this Work

As pointed out in the introduction, it is of significant importance to find sustainable electric energy storage systems in the course of the transition from fossil fuels to renewable energy sources. With the application of a neutral silyl radical in organic radical batteries, an intriguing way of employing the abundantly available element silicon in this process was presented. However, several further obstacles such as low energy density and difficult preparation processes have to be overcome for this technology to find widespread application. The challenges can be tackled both on the molecular level, as well as on the level of cell construction. Within this thesis, only the molecular design of possible anode materials will be addressed. In order to be suitable for battery application, silyl radicals have to meet several criteria:

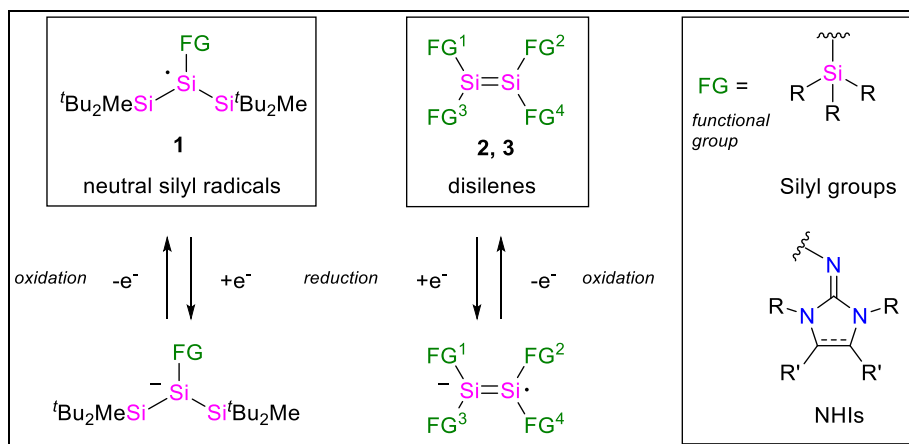
- Easy accessibility
- Stability in solution (probably tolerance against air/moisture to some extent)
- Ability to undergo reversible reduction/oxidation processes
- Low reduction potential
- Minimal steric change during redox processes
- Enough distance between the radical centers in the solid state to allow for fast counter-ion diffusion during the battery process

Prior to this work, only few structurally characterized, neutral silicon-centered radicals have been reported.<sup>[36,38,47-49]</sup> Therefore, one focus of this thesis lays on the synthesis of novel silyl radicals **1** (Scheme 13), which meet the above mentioned criteria. These radicals are supposed to be kinetically stabilized by bulky silyl groups, or even bear other functional groups, such as NHIs. Electrochemical investigations (cyclic voltammetry) should give information about, whether these compounds can be employed in organic radical batteries. Not only silyl radicals, but also a disilene (**L7**) has been reported to reversibly undergo a reduction reaction.<sup>[57,59]</sup> Thus, another goal of this work is to determine if disilenes can also be considered suitable candidates for anode materials. Therefore, literature reported as well as novel disilenes **2** and **3** (Scheme 13) should be synthesized and evaluated electrochemically.

To obtain neutral silicon centered radicals, the approach of Sekiguchi and co-workers for **L2** (Approach 1, Scheme 14) should be reproduced and eventually modified with the goal of increasing the yield and the steric protection of the resulting

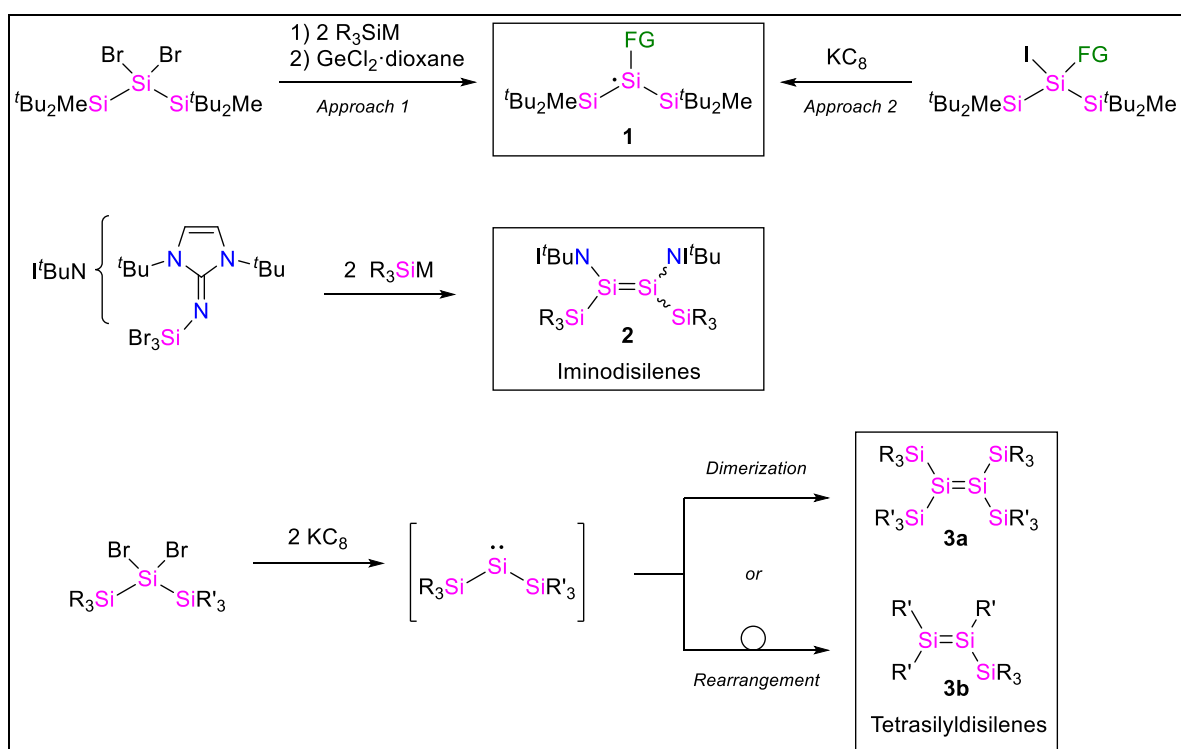
radicals. Approach 2 however, could directly afford functionalized radicals from the corresponding iodosilanes.

**Scheme 13:** Synthetically targeted neutral silyl radicals **1** and disilenes **2** and **3** for reversible redox processes.



In addition, the synthesis of various disilenes is planned. On the one hand, the novel class of iminodisilenes **2** should be complemented by new structures, following our established synthetic route *via* treating the tribromoiminosilane with two equivalents of a bulky silanide.<sup>[158]</sup> The focus will be put on the isolation of a more stable disilene, that allows for exploration of new reactivities, especially in regard to redox behavior.

**Scheme 14:** Planned synthetic approaches for neutral silyl radicals **1**, iminodisilenes **2** and tetrasilyldisilenes **3**.





On the other hand, tetra(silyl)disilenes **3** are synthetic targets of this thesis. Reduction of bis(silyl)-substituted dibromosilanes might lead to the intermediary formation of a bis(silyl)silylene. Depending on the steric demand of the silyl groups and their propensity towards silyl migration, this silylene could undergo dimerization - as in the case of  $(t\text{Bu}_2\text{MeSi})_2\text{Si}=\text{Si}(\text{Si}^t\text{Bu}_2\text{Me})_2$  (**L7**)<sup>[57]</sup> - or a rearrangement to the isomeric disilene might take place.<sup>[79-80]</sup>

Besides investigation of their suitability for battery application, the inherent reactivity of these newly developed, low-coordinate silicon species is also of great interest. Thus, the second main focus of this thesis is on detailed studies in respect to small molecule activation. Classical examples are, of course, industrially relevant molecules such as dihydrogen, ethylene,  $\text{O}_2$ , phosphorus, carbon dioxide and carbon monoxide. Silyl radicals are prone to abstract halogens and will be investigated in this regard. Especially the chemistry of iminodisilenes which display a unique electronic structure, resulting from the strongly  $\pi$ -donating NHI substituents and the silyl groups as  $\sigma$ -donors, might provide interesting addition products (for plausible structures see Figure 14).

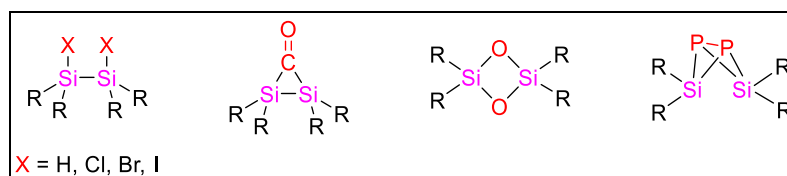


**Figure 14:** Expected products from small molecule activation by disilenes.

With dihydrogen or halogens, disilenes might undergo 1,2-additions. The chemistry of disilenes towards  $\text{CO}$  is relatively underdeveloped, however formation of bis(sila)ketones is conceivable. From oxidation with oxygen transfer reagents or phosphorus, bridged structures, similar to previous reports might be obtained. However, entirely different reaction modes are possible, since iminodisilenes can also react as formal monomeric silylene units.

In summary, novel silyl radicals and disilenes should be synthesized, with the aim to improve organic radical battery technology. Furthermore, their behavior in oxidative addition reactions will be investigated. This might hopefully lead to new structures or even pave the way for possible, future, main-group element-based catalytic cycles.

## 7. Isolation of a Relatively Air-Stable, Bulky Silyl-Substituted, Neutral Silicon-Centered Radical

**Title:** Isolation of a Relatively Air-Stable, Bulky Silyl-Substituted, Neutral Silicon-Centered Radical

**Status:** Article, published online June 5<sup>th</sup>, 2019

**Journal:** *European Journal of Inorganic Chemistry*, **2019**, 2977-2981.

**Publisher:** WILEY-VCH Verlag GmbH & Co. KGaA, Weinheim

**DOI:** [10.1002/ejic.201900522](https://doi.org/10.1002/ejic.201900522)

**Authors:** Richard Holzner, Alexander Kaushansky, Boris Tumanskii, Philipp Frisch, Fabian Linsenmann, Shigeyoshi Inoue<sup>a</sup>

*Reprinted with permission. © 2019 Wiley-VCH Verlag GmbH & Co. KGaA.*

**Content:** In regard to electrochemical energy storage systems, organic radical batteries containing silicon-based anodes can be considered a metal-free and thus sustainable option. However, a big drawback is their low energy density and the sensitivity of the silyl radical that complicates the manufacturing process. Addressing these problems, this contribution aims at providing a more stable silicon-centered radical, suitable for battery application.

Indeed, pursuing a modified, literature-reported approach, resulted in the isolation of a novel, neutral silyl radical bearing an extremely sterically demanding supersilyl group (<sup>t</sup>Bu<sub>3</sub>Si). This unprecedented kinetic stabilization gives the silyl radical a remarkable stability: in the solid state, it shows no signs of decomposition, even after being exposed to air for 16 hours. Furthermore, SC-XRD analysis revealed a slightly shorter distance between the radical centers than in the silyl radical that was applied in the reported battery. The redox potential was determined to be similar to the reported silyl radical and the redox process turned out to be highly reversible.

In summary, the initially reported and battery applied silyl radical structure was enhanced in regard to stability towards air and moisture, which might facilitate the cell construction process. Furthermore, the shorter radical center distance promises higher energy density and the improved synthetic approach lowers the required expense and thus paves the way for an advanced, silicon-based organic radical battery.

---

<sup>a</sup>R. Holzner planned and executed all experiments regarding synthetic methods A and B for the title compound, its reactivity and wrote the manuscript. A. Kaushanski and B. Tumanskii contributed synthetic method C and the EPR simulation. P. Frisch conducted the SC-XRD analysis and processed the respective data. F. Linsenmann performed the CV measurements. All work was done under the supervision of S. Inoue.

## Silyl Radicals | Very Important Paper |

## VIP Isolation of a Relatively Air-Stable, Bulky Silyl-Substituted, Neutral Silicon-Centered Radical

Richard Holzner,<sup>[a]</sup> Alexander Kaushansky,<sup>[b]</sup> Boris Tumanskii,<sup>[b]</sup> Philipp Frisch,<sup>[a]</sup> Fabian Linsenmann,<sup>[c]</sup> and Shigeyoshi Inoue<sup>\*[a]</sup>

**Abstract:** The bulky supersilyl-substituted (<sup>t</sup>Bu<sub>3</sub>Si) silicon-centered radical **1** was synthesized and fully characterized by single-crystal X-ray crystallography, cyclic voltammetry (CV), and EPR spectroscopy. With its extremely sterically encumbered radical center, **1** is stable in the solid state in air for 16 hours without showing signs of decomposition. Thus **1** is the most robust

trisilyl-substituted silyl radical to date and a promising candidate for application as electrode material in organic radical batteries. Furthermore, it was found to be a strong dehalogenation reagent and therefore might find application in organic syntheses.

## Introduction

For a long time, silyl radicals have been employed as active species in various organic transformations, such as alkene hydrosilylation or halide abstraction reactions.<sup>[1]</sup> However, these radicals are short lived intermediates and can only be generated in situ and observed by EPR spectroscopy. In the 1970s, Lappert and co-workers prepared an alkyl-substituted, silicon centered radical by the irradiation of a silane with UV light.<sup>[2]</sup> This species showed a half-life time of 10 minutes and was characterized by EPR measurements. Nonetheless, several examples of persistent<sup>[3]</sup> and even isolable silicon centered radicals have been reported.<sup>[4]</sup> Sekiguchi and co-workers were able to isolate and structurally characterize the first isolable silyl radical **I** (Figure 1).<sup>[5]</sup> In this cyclotetrasilanyl radical, the spin density is spread over three silicon centers. Shortly after their pioneering work in this field, the neutral, three-coordinate silyl radical **II** without any  $\pi$  conjugation was also presented (Figure 1).<sup>[6]</sup> This molecule bears three bulky trialkylsilyl groups (<sup>t</sup>Bu<sub>2</sub>MeSi), which shield the reactive radical center and prevent decomposition reactions, such as dimerization or hydrogen abstraction, though it is air-sensitive. Trialkylsilyl groups have already been proven to be ideal substituents for highly reactive main group compounds. Because of the alkyl groups at the silicon atom, that do not tend to migrate, are relatively inert and allow fine tuning

of the steric demand, as well as the  $\sigma$ -electron-donating effect of the silicon, these groups are suitable for stabilization of elusive species.<sup>[7]</sup> Recent examples of these reactive compounds stabilized by trialkylsilyl substituent from our group comprise hydrosilylenes,<sup>[8]</sup> silylene-transition metal complexes<sup>[9]</sup> and silanones.<sup>[10]</sup> For the synthesis of **II**, (<sup>t</sup>Bu<sub>2</sub>MeSi)<sub>2</sub>SiBr<sub>2</sub> is treated with two equivalents of <sup>t</sup>Bu<sub>2</sub>MeSiNa and the in situ generated silanide is subsequently oxidized with GeCl<sub>4</sub>-dioxane. Later, the yield was improved via an alternate synthetic approach by Apeloig and co-workers.<sup>[11]</sup> Furthermore, one silyl substituent can be replaced by various aryl groups (compounds **III**).<sup>[12]</sup>

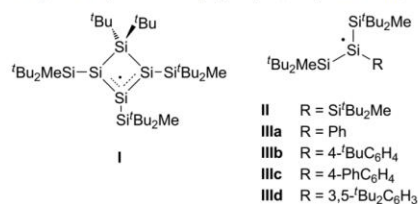


Figure 1. Selected examples of isolated silyl radicals.

Besides the shown examples, there are various other stable silyl radicals, including cyclic alkyl amino carbene- (CAAC),<sup>[13]</sup> N-heterocyclic carbene- (NHC)<sup>[14]</sup> and amidinato-stabilized,<sup>[15]</sup> as well as alkali metal-substituted<sup>[16]</sup> compounds. However, in the cases of the CAAC- and amidinato-stabilized radicals, the spin density not only resides at the silicon center, but is also delocalized over the neighboring C- and N-atoms, respectively.<sup>[13,15]</sup> Furthermore, structures with two or three radical centers, linked by aryl groups<sup>[17]</sup> and silyl radicals deriving from oxidation or reduction of Si-Si multiple bonds have been reported.<sup>[18]</sup> Most interestingly, Sekiguchi and co-workers demonstrated the application of silyl radical **II** in organic radical batteries.<sup>[19]</sup> They constructed an experimental, lithium-free cell with **II** as redox active anode material, which can be considered an

[a] Department of Chemistry, WACKER-Institute of Silicon Chemistry and Catalysis Research Center, Technische Universität München, Lichtenbergstraße 4, 85748 Garching bei München, Germany  
E-mail: s.inoue@tum.de  
<https://www.si.ch.tum.de>

[b] Shulich Faculty of Chemistry, Technion-Israel Institute of Technology, Haifa 32000, Israel

[c] Chair of Technical Electrochemistry, Department of Chemistry, Technische Universität München, Lichtenbergstrasse 4, 85748 Garching, Germany

Supporting information and ORCID(s) from the author(s) for this article are available on the WWW under <https://doi.org/10.1002/ejic.201900522>.

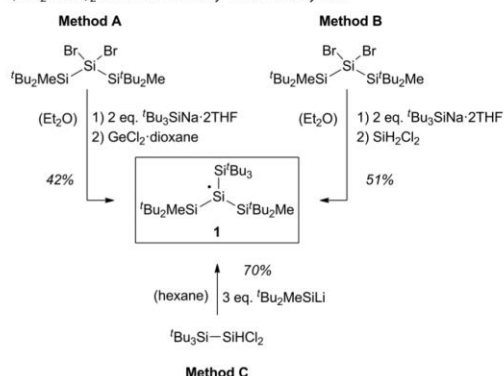


## 7. Isolation of a Relatively Air-Stable, Bulky Silyl-Substituted, Neutral Silicon-Centered Radical

important milestone in the development of main group element-based electric energy storage systems. Although this battery already showed remarkable cyclic stability, there is still room for improvement. An important feature of the silyl radical to be used as battery material is of course the stability. This can be achieved by kinetic stabilization of the reactive center by three bulky silyl substituents. Another crucial requirement is the distance between the radical centers in the solid state. During the charging process, the radical is reduced to the corresponding silyl anion. Cations from the electrolyte intercalate into the silyl framework for the charge balance. Therefore, it is important for high charge- and discharge rates to have enough space within the silicon scaffold, to enable a fast diffusion process.

### Results and Discussion

Motivated by these reports, we set out to synthesize a more stable silyl radical, that lends itself very well for battery applications and we succeeded in isolating compound **1** bearing a bulky supersilyl (<sup>t</sup>Bu<sub>3</sub>Si) group (Scheme 1). This was achieved by three different approaches (Scheme 1, A, B and C). In method A, similar to Sekiguchi's synthetic route,<sup>[6]</sup> the extremely sterically demanding supersilyl group is introduced by reacting the corresponding dibromosilane (<sup>t</sup>Bu<sub>2</sub>MeSi)<sub>2</sub>SiBr<sub>2</sub> with supersilylsodium (<sup>t</sup>Bu<sub>3</sub>SiNa·2THF). The resulting green suspension of in situ formed silanide was poured on GeCl<sub>2</sub>-dioxane complex to undergo a one-electron oxidation reaction, leading to the formation of **1**. In method B, dichlorosilane, instead of germanium dichloride, is employed to oxidize the intermediary formed silanide. This avoids the formation of a Ge-containing by-product, thus facilitating the crystallization and improving the yield to 51%. Method C is based on the improved approach.<sup>[11]</sup> Treatment of (<sup>t</sup>Bu<sub>3</sub>Si)SiHCl<sub>2</sub> with 3 equivalents of silanide (<sup>t</sup>Bu<sub>2</sub>MeSiLi) furnishes silyl radical **1** in 70% yield, a much higher yield, than provided by methods A and B. The use of the nonpolar solvent hexane in method C is crucial for this reaction. Even trace amounts of THF lead to the formation of (<sup>t</sup>Bu<sub>3</sub>Si)-(<sup>t</sup>Bu<sub>2</sub>MeSi)<sub>2</sub>SiLi and thereby lower the yield.



Scheme 1. Synthesis of silicon-centered radical **1** by method A, B, and C.

Compound **1** was obtained as yellow crystals and characterized by X-ray diffraction analysis and EPR spectroscopy.

Single crystal X-ray diffraction (SC-XRD) analysis of radical **1** revealed a planar silicon center (sum of the bond angles  $\Sigma\theta = 359.7^\circ$ ) (Figure 2). As in compound **II**, this structural motif is a result of the steric repulsion of the bulky substituents, which does not allow a pyramidal geometry that is typical for trisilyl-substituted silyl radicals.<sup>[20]</sup>

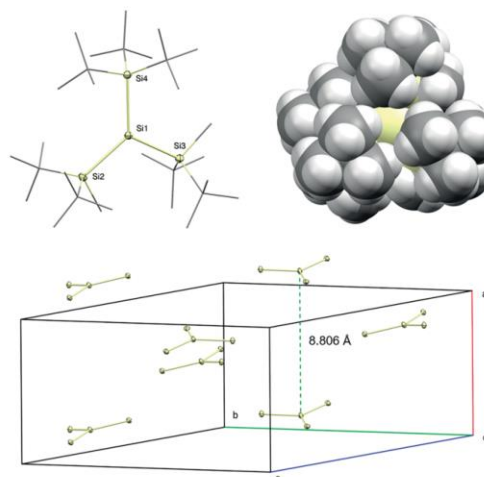


Figure 2. Solid state structure of **1** with thermal ellipsoids drawn at the 50% probability level. Hydrogen atoms are omitted for clarity and <sup>t</sup>Bu- and Me-groups are simplified as wire frame (top left). Space-filling model of **1** (top right, yellow: silicon, grey: carbon, white: hydrogen). Crystal packing diagram of **1** (bottom, carbon and hydrogen atoms are omitted for clarity). Selected bond lengths [Å] and angles [°]: Si1–Si2 2.4533(6), Si1–Si3 2.4480(5), Si1–Si4 2.4834(6), Si4–Si1–Si3 118.61(2), Si4–Si1–Si2 128.95(2), Si2–Si1–Si3 112.16(2).

Furthermore, the high steric demand of the supersilyl group is reflected by the longer distance of the Si1–Si4 bond (2.4834(6) Å) compared to the Si–Si bond lengths of the other two silyl substituents (2.4533(6) Å and 2.4480(5) Å, respectively), as well as by the narrowing of the Si2–Si1–Si3 angle (112.2°). The space-filling model of **1** shows the strong shielding of the radical center by its silyl substituents. With 8.806 Å, the distance between the radical centers in the crystal lattice is minimally shorter than in compound **I** (9.08 Å). This space is sufficient for counterion diffusion at high rates and promising slightly higher energy densities in the battery cell.

In the EPR spectrum of **1**, a strong signal with a *g* value of 2.00541 is observable (Figure 3). This *g* value compares very well to that of Sekiguchi's radical **II** (2.0056)<sup>[6]</sup> and is within the typical range for silicon-centered radicals bearing three silyl substituents.<sup>[3,5,6,21]</sup> Furthermore, satellite signals from the coupling of the unpaired electron with the central  $\alpha$ -<sup>29</sup>Si nucleus (hyperfine coupling constant *hfcc a* = 6.047 mT), as well as with the three  $\beta$ -<sup>29</sup>Si nuclei (*a* = 0.80 mT) are visible. Apparently, the silicon nuclei of the <sup>t</sup>Bu<sub>3</sub>Si-group and the <sup>t</sup>Bu<sub>2</sub>MeSi-groups are equivalent in the EPR spectrum since no further splitting pattern can be observed. This observation is backed up by a simulation, fitting the experimental data, using the *Easyspin* toolbox for *Matlab* (Figure 3).<sup>[22]</sup>

## 7. Isolation of a Relatively Air-Stable, Bulky Silyl-Substituted, Neutral Silicon-Centered Radical

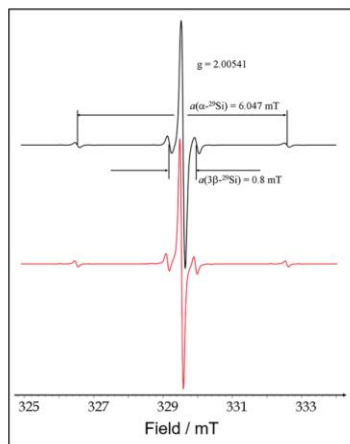


Figure 3. X-band EPR spectrum of silyl radical **1** recorded at room temperature in *n*-hexane; (black) experimental, (red) simulation.

Remarkably, silyl radical **1** shows high stability against air and moisture: even after exposing the crystals to air for 16 hours, no sign of decomposition was observed. Within 4 days, the crystal surface turned colorless, however, the characteristic EPR signal of **1** was still detected. In solution, the degradation process proceeds much faster. EPR experiments with an uncapped tube showed decreasing of the initial signal intensity to 16% after 5 hours (Figure 4). The structures of the decomposition products were not clarified.

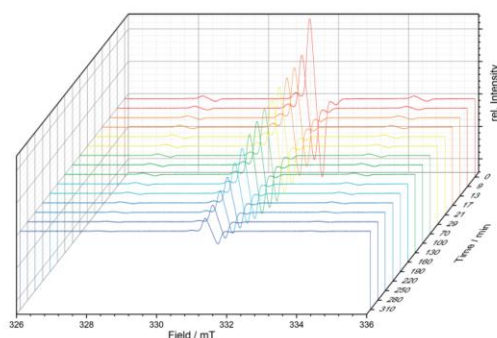


Figure 4. Kinetic studies on the degradation of silyl radical **1** in solution upon exposure to air. EPR spectra were recorded with a starting concentration of  $4 \times 10^{-3}$  M of **1** in *n*-hexane in an uncapped EPR tube at room temperature.

In regard to a battery application as anode material, the redox behavior of **1** is of particular interest. Although a chemical reduction was not achieved, the electrochemical reduction is possible. In the CV chart, a highly reversible reduction wave with reduction and oxidation peaks at 1.40 V vs. Li/Li<sup>+</sup> and 1.50 V vs. Li/Li<sup>+</sup>, respectively can be observed (Figure 5). This

reduction of **1** occurs at a slightly lower potential than of silyl radical **II**, that was measured under the same conditions for comparison (see Figure S5). Furthermore, we scanned to higher potentials (Figure S6). An irreversible oxidation can be observed at 3.5 V vs. Li/Li<sup>+</sup>, suggesting the formation of a cationic species.

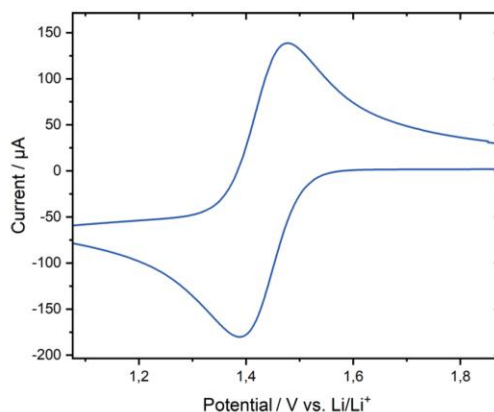
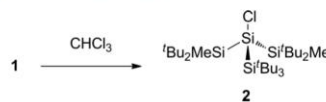


Figure 5. Cyclic voltammogram of **1** measured in a three-electrode setup using a lithium metal reference electrode at scan rate of 100 mV/s (0.1 M (*n*Bu<sub>4</sub>N)TFSI in THF at room temperature).

To gain further insight into the propensity of **1** towards hydrogen abstraction reactions, it was treated with an excess amount of chloroform (Scheme 2). The conversion proceeded in a selective fashion at room temperature within 2 minutes and provided the corresponding chlorosilane **2** in almost quantitative yield. This high reaction rate is attributed to the concentration of chlorine donating-molecules and presumably the radical nature of the reaction mechanism.



Scheme 2. Halogenation of radical **1** to chlorosilane **2**.

### Conclusion

From three different synthetic procedures, we obtained silyl radical **1** which bears two <sup>t</sup>Bu<sub>2</sub>MeSi-groups and one even more sterically demanding supersilyl group. Because of this increased kinetic stabilization, compound **1** in the crystalline state does not decompose even being exposed to air for 16 hours and is probably the most stable silicon-centered radical to date. This feature makes it an ideal candidate for application as anode material in organic radical batteries, as it facilitates the cell construction process and most likely enhances the life time. Additional CV analysis showed the high reversibility of the reduction process of **1**, thus underlining the suitability for battery purposes. Furthermore, we demonstrated the dehalogenation by compound **1**, which reacts readily to yield the corresponding



## 7. Isolation of a Relatively Air-Stable, Bulky Silyl-Substituted, Neutral Silicon-Centered Radical



chlorinated derivative **2**. Investigations of **1** with regard to further reactivity and application in lithium-free batteries are currently on-going in our research group.

### Conflict of Interest

The authors declare no conflict of interest.

## Experimental Section

### General Methods and Instrumentation

All reactions and manipulations were carried out under an atmosphere of argon (4.6 (≥ 99.996 %) by using standard Schlenk and glovebox techniques. The glassware used was heat dried under high vacuum prior to use. All solvents were refluxed over sodium/benzophenone, freshly distilled under argon and deoxygenated prior to use. Deuterated benzene (C<sub>6</sub>D<sub>6</sub>) was obtained from *Sigma-Aldrich*, dried over Na/K alloy, flask-to-flask condensed, deoxygenated by three freeze-pump-thaw cycles and stored over 4 Å molecular sieves. All NMR samples were prepared under argon in *J. Young* PTFE valve NMR tubes. The NMR spectra were recorded on a *Bruker* DRX400 (<sup>1</sup>H: 400.13 MHz, <sup>13</sup>C: 100.62 MHz, <sup>29</sup>Si: 79.49 MHz), or AV500C (<sup>1</sup>H: 500.36 MHz, <sup>13</sup>C: 125.83 MHz, <sup>29</sup>Si: 99.41 MHz) spectrometer at ambient temperature (300 K). The <sup>1</sup>H, <sup>13</sup>C{<sup>1</sup>H} and <sup>29</sup>Si{<sup>1</sup>H} NMR spectroscopic chemical shifts δ are reported in ppm relative to tetramethylsilane. <sup>1</sup>H and <sup>13</sup>C{<sup>1</sup>H} NMR spectra are calibrated against the residual proton and natural abundance carbon resonances of the respective deuterated solvent as internal standard: C<sub>6</sub>D<sub>6</sub>; δ(<sup>1</sup>H) = 7.16 ppm and δ(<sup>13</sup>C) = 128.1 ppm.<sup>[23]</sup> The following abbreviation is used to describe signal multiplicities: s = singlet.

EPR spectra were recorded on a *Bruker* EMX-10/12 X-band (spectrometer frequency: 9.3 GHz) digital EPR spectrometer. The spectra were recorded with a microwave power of 1.0 mW, 100 kHz magnetic field modulation of 0.5 G amplitude. Digital field resolution was 2048 points per spectrum. Spectra processing and simulation were performed with the *Bruker* WIN-EPR and *SimFonia* Software and *Easyspin* toolbox for *Matlab*.

Melting points (m.p.) were determined in sealed glass capillaries under inert gas by a *Büchi* M-565 melting point apparatus. Unless otherwise stated, all commercially available chemicals were purchased from *abc* or *Sigma-Aldrich* and used without further purification. The compounds (<sup>t</sup>Bu<sub>2</sub>MeSi)<sub>2</sub>SiBr<sub>2</sub>,<sup>[6]</sup> <sup>t</sup>Bu<sub>2</sub>MeSiLi,<sup>[24]</sup> (<sup>t</sup>Bu<sub>3</sub>Si)SiCl<sub>2</sub>H,<sup>[25]</sup> (<sup>t</sup>Bu<sub>2</sub>MeSi)<sub>3</sub>Si,<sup>[6]</sup> and <sup>t</sup>Bu<sub>3</sub>SiNa·2THF<sup>[7]</sup> were prepared according to literature procedures.

**Silyl radical 1 Method A:** Diethyl ether (4 mL) was added to (<sup>t</sup>Bu<sub>2</sub>MeSi)<sub>2</sub>SiBr<sub>2</sub> (350 mg, 696 μmol, 1.0 eq.) and supersilylsodium (638 mg, 1.74 mmol, 2.5 eq.) at room temperature, resulting in a dark green suspension. After stirring for 2.5 h, this mixture was poured on GeCl<sub>2</sub>-dioxane complex (161 mg, 696 μmol, 1.0 eq.) and stirred for 3 h. All volatiles were removed under reduced pressure and silyl radical **1** was obtained by recrystallization from *n*-hexane (161 mg, 297 μmol, 42% yield). Single crystals suitable for XRD were obtained from a cooled (−34 °C) solution of **1** in *n*-hexane. EPR (*n*-hexane, 286 K) *g* = 2.00541, *a*(<sup>29</sup>Si<sub>1</sub>) = 6.047 mT, *a*(<sup>29</sup>Si<sub>β</sub>) = 0.80 mT; m.p. 149 °C. Anal. Calcd. [%] for Si<sub>4</sub>C<sub>27</sub>H<sub>63</sub>: C, 66.45; H, 12.83. Found [%]: C, 66.00; H 12.94.

**Method B:** Diethyl ether (3 mL) was added to (<sup>t</sup>Bu<sub>2</sub>MeSi)<sub>2</sub>SiBr<sub>2</sub> (200 mg, 398 μmol, 1.0 eq.) and supersilylsodium (365 mg, 995 μmol, 2.5 eq.) at room temperature, resulting in a dark green suspension. After stirring for 2.5 h, a solution of dichlorosilane in toluene (37.4 %wt., 144 mg, 398 μmol, 1.0 eq.) was added. The color

changed to blue due to a minor formation of the disilene (<sup>t</sup>Bu<sub>2</sub>MeSi)<sub>2</sub>Si=Si(<sup>t</sup>Bu<sub>2</sub>MeSi)<sub>2</sub>. After stirring for 2 h at room temperature, all volatiles were removed in vacuo and silyl radical **1** was obtained by recrystallization from *n*-hexane (110 mg, 203 μmol, 51% yield).

**Method C:** A solution of <sup>t</sup>Bu<sub>2</sub>MeSiLi (492 mg, 3.00 mmol, 3.00 eq.) in hexane (3 mL) was added to a frozen (−196 °C) solution of (<sup>t</sup>Bu<sub>3</sub>Si)SiCl<sub>2</sub>H (299 mg, 1.00 mmol, 1.00 eq.) in hexane (5 mL). The frozen mixture was warmed up to room temperature under rapid stirring for 1 hour. After filtration and evaporation of all volatile compounds under reduced pressure, silyl radical **1** was obtained by recrystallization from *n*-hexane at 0 °C (380 mg, 700 μmol, 70% yield).

**Chlorosilane 2:** A solution of compound **1** (10.0 mg, 18.4 μmol, 1.0 eq.) in benzene (0.5 mL) was treated with CDCl<sub>3</sub> (10.4 μL, 130 μmol, 7 eq.). Immediate decolorization occurred and chlorosilane **2** was obtained after evaporation of solvent in vacuo as colorless solid (10 mg, 94% yield).

<sup>1</sup>H NMR (500 MHz, C<sub>6</sub>D<sub>6</sub>, 300 K): δ = 1.14 (s, 36H, (<sup>t</sup>Bu<sub>2</sub>MeSi)), 1.10 (s, 27H, (<sup>t</sup>Bu<sub>3</sub>Si)), 0.20 (s, 6H, (<sup>t</sup>Bu<sub>2</sub>MeSi)). <sup>13</sup>C{<sup>1</sup>H} NMR (126 MHz, C<sub>6</sub>D<sub>6</sub>, 300 K): δ = 29.9 ((Me<sub>3</sub>C)<sub>3</sub>Si), 29.8 ((Me<sub>3</sub>C)<sub>2</sub>MeSi), 24.4 ((Me<sub>3</sub>C)<sub>2</sub>Si), 22.5 ((Me<sub>3</sub>C)<sub>2</sub>MeSi), −6.3 ((Me<sub>3</sub>C)<sub>2</sub>MeSi). <sup>29</sup>Si{<sup>1</sup>H} NMR (99 MHz, C<sub>6</sub>D<sub>6</sub>, 300 K): 38.9, 33.5, 6.3.

### X-ray Crystallography

The X-ray intensity data of **1** was collected on an X-ray single crystal diffractometer equipped with a CMOS detector (*Bruker* Photon-100), a rotating anode (*Bruker* TXS) with MoK<sub>α</sub> radiation (λ = 0.71073 Å) and a Helios mirror optic by using the APEX III software package.<sup>[26]</sup> The measurements were performed on single crystals coated with the perfluorinated ether Fomblin® Y. The crystal was fixed on the top of a micro sampler, transferred to the diffractometer and frozen under a stream of cold nitrogen. A matrix scan was used to determine the initial lattice parameters. Reflections were merged and corrected for Lorentz and polarization effects, scan speed, and background using SAINT.<sup>[27]</sup> Absorption corrections, including odd and even ordered spherical harmonics were performed using SADABS.<sup>[27]</sup> Space group assignments were based upon systematic absences, E statistics, and successful refinement of the structures. Structures were solved by direct methods with the aid of successive difference Fourier maps, and were refined against all data using the APEX III software in conjunction with SHELXL-2014<sup>[28]</sup> and SHELXL.<sup>[29]</sup> All H atoms were placed in calculated positions and refined using a riding model, with methylene and aromatic C–H distances of 0.99 and 0.95 Å, respectively, and U<sub>iso</sub>(H) = 1.2·U<sub>eq</sub>(C). Full-matrix least-squares refinements were carried out by minimizing Δw(F<sub>o</sub><sup>2</sup>−F<sub>c</sub><sup>2</sup>)<sup>[27]</sup> with SHELXL-97 weighting scheme.<sup>[30]</sup> Neutral atom scattering factors for all atoms and anomalous dispersion corrections for the non-hydrogen atoms were taken from International Tables for Crystallography.<sup>[31]</sup> The images of the crystal structures were generated by Mercury.<sup>[32]</sup>

CCDC 1899751 (for **1**) contains the supplementary crystallographic data for this paper. These data can be obtained free of charge from The Cambridge Crystallographic Data Centre.

### Acknowledgments

We thank WACKER Chemie AG and the European Research Council (SILION 637394) for continued financial support. We are also thankful to Dr. Oksana Storcheva for conducting the EPR measurements.

## 7. Isolation of a Relatively Air-Stable, Bulky Silyl-Substituted, Neutral Silicon-Centered Radical



**Keywords:** Silicon · Radicals · Steric hindrance · Materials science · Dehalogenation

- [1] a) C. Chatgillaloglu, C. H. Schiesser in *The Chemistry of Organic Silicon Compounds*, Vol. 3 (Eds.: Z. Rappoport, Y. Apeloig), **2001**; b) C. Chatgillaloglu, *Acc. Chem. Res.* **1992**, *25*, 188–194.
- [2] a) J. D. Cotton, C. S. Cundy, D. H. Harris, A. Hudson, M. F. Lappert, P. W. Lednor, *J. Chem. Soc., Chem. Commun.* **1974**, 651–652; b) A. Hudson, M. F. Lappert, P. W. Lednor, *J. Chem. Soc., Dalton Trans.* **1976**, 2369–2375.
- [3] a) S. Kyushin, H. Sakurai, T. Betsuyaku, H. Matsumoto, *Organometallics* **1997**, *16*, 5386–5388; b) M. Kira, T. Obata, I. Kon, H. Hashimoto, M. Ichinohe, H. Sakurai, S. Kyushin, H. Matsumoto, *Chem. Lett.* **1998**, *27*, 1097–1098.
- [4] V. Y. Lee, A. Sekiguchi, *Eur. J. Inorg. Chem.* **2005**, *2005*, 1209–1222.
- [5] A. Sekiguchi, T. Matsuno, M. Ichinohe, *J. Am. Chem. Soc.* **2001**, *123*, 12436–12437.
- [6] A. Sekiguchi, T. Fukawa, M. Nakamoto, V. Y. Lee, M. Ichinohe, *J. Am. Chem. Soc.* **2002**, *124*, 9865–9869.
- [7] N. Wiberg, K. Amelunxen, H. W. Lerner, H. Schuster, H. Nöth, I. Krossing, M. Schmidt-Amelunxen, T. Seifert, *J. Organomet. Chem.* **1997**, *542*, 1–18.
- [8] S. Inoue, C. Eisenhut, *J. Am. Chem. Soc.* **2013**, *135*, 18315–18318.
- [9] C. Eisenhut, T. Szilvási, G. Dübek, N. C. Breit, S. Inoue, *Inorg. Chem.* **2017**, *56*, 10061–10069.
- [10] D. Wendel, D. Reiter, A. Porzelt, P. J. Altmann, S. Inoue, B. Rieger, *J. Am. Chem. Soc.* **2017**, *139*, 17193–17198.
- [11] G. Molev, B. Tumanskii, D. Sheberla, M. Botoshansky, D. Bravo-Zhivotovskii, Y. Apeloig, *J. Am. Chem. Soc.* **2009**, *131*, 11698–11700.
- [12] K. Taira, M. Ichinohe, A. Sekiguchi, *Chem. Eur. J.* **2014**, *20*, 9342–9348.
- [13] a) K. C. Mondal, H. W. Roesky, A. C. Stückli, F. Ehret, W. Kaim, B. Ditttrich, B. Maity, D. Koley, *Angew. Chem. Int. Ed.* **2013**, *52*, 11804–11807; *Angew. Chem.* **2013**, *125*, 12020–12023; b) Y. Li, Y.-C. Chan, B.-X. Leong, Y. Li, E. Richards, I. Purushothaman, S. De, P. Parameswaran, C.-W. So, *Angew. Chem. Int. Ed.* **2017**, *56*, 7573–7578; *Angew. Chem.* **2017**, *129*, 7681–7686; c) B. Tumanskii, M. Karni, Y. Apeloig, in *Encyclopedia of Radicals in Chemistry, Biology and Materials* (Eds.: C. Chatgillaloglu, A. Studer), **2012**.
- [14] a) H. Tanaka, M. Ichinohe, A. Sekiguchi, *J. Am. Chem. Soc.* **2012**, *134*, 5540–5543; b) V. Nesterov, D. Reiter, P. Bag, P. Frisch, R. Holzner, A. Porzelt, S. Inoue, *Chem. Rev.* **2018**, *118*, 9678–9842.
- [15] S.-H. Zhang, E. Carter, H.-W. Xi, Y. Li, K. H. Lim, C.-W. So, *Inorg. Chem.* **2017**, *56*, 701–704.
- [16] a) S. Inoue, M. Ichinohe, A. Sekiguchi, *Organometallics* **2008**, *27*, 1358–1360; b) G. Molev, D. Bravo-Zhivotovskii, M. Karni, B. Tumanskii, M. Botoshansky, Y. Apeloig, *J. Am. Chem. Soc.* **2006**, *128*, 2784–2785; c) S. Ishida, T. Iwamoto, M. Kira, *J. Am. Chem. Soc.* **2003**, *125*, 3212–3213; d) S. Inoue, M. Ichinohe, A. Sekiguchi, *J. Am. Chem. Soc.* **2007**, *129*, 6096–6097; e) D. Bravo-Zhivotovskii, I. Ruderfer, S. Melamed, M. Botoshansky, B. Tumanskii, Y. Apeloig, *Angew. Chem. Int. Ed.* **2005**, *44*, 739–743; *Angew. Chem.* **2005**, *117*, 749–753.
- [17] a) T. Nozawa, M. Nagata, M. Ichinohe, A. Sekiguchi, *J. Am. Chem. Soc.* **2011**, *133*, 5773–5775; b) T. Nozawa, M. Ichinohe, A. Sekiguchi, *Chem. Lett.* **2015**, *44*, 56–57.
- [18] a) A. Sekiguchi, S. Inoue, M. Ichinohe, Y. Arai, *J. Am. Chem. Soc.* **2004**, *126*, 9626–9629; b) S. Inoue, M. Ichinohe, A. Sekiguchi, *J. Am. Chem. Soc.* **2008**, *130*, 6078–6079; c) A. Sekiguchi, R. Kinjo, M. Ichinohe, *Synth. Met.* **2009**, *159*, 773–775; d) R. Kinjo, M. Ichinohe, A. Sekiguchi, *J. Am. Chem. Soc.* **2007**, *129*, 26–27; e) A. Tsurusaki, S. Kyushin, *Chem. Eur. J.* **2016**, *22*, 134–137.
- [19] H. Maruyama, H. Nakano, M. Nakamoto, A. Sekiguchi, *Angew. Chem. Int. Ed.* **2014**, *53*, 1324–1328; *Angew. Chem.* **2014**, *126*, 1348–1352.
- [20] V. Y. Lee, *Organosilicon Compounds*, Vol. 1, Academic Press, **2017**.
- [21] a) S. W. Bennett, C. Eaborn, A. Hudson, R. A. Jackson, K. D. J. Root, *J. Chem. Soc. A* **1970**, 348–351; b) Y. Apeloig, D. Bravo-Zhivotovskii, M. Yuzefovich, M. Bendikov, A. I. Shames, *Appl. Magn. Reson.* **2000**, *18*, 425–434; c) S. Kyushin, H. Sakurai, H. Matsumoto, *Chem. Lett.* **1998**, *27*, 107–108.
- [22] S. Stoll, A. Schweiger, *J. Magn. Reson.* **2006**, *178*, 42–55.
- [23] H. E. Gottlieb, V. Kotlyar, A. Nudelman, *J. Org. Chem.* **1997**, *62*, 7512–7515.
- [24] D. Pinchuk, J. Mathew, A. Kaushansky, D. Bravo-Zhivotovskii, Y. Apeloig, *Angew. Chem. Int. Ed.* **2016**, *55*, 10258–10262; *Angew. Chem.* **2016**, *128*, 10414–10418.
- [25] N. Wiberg, W. Niedermayer, H. Nöth, J. Knizek, W. Ponikwar, K. Polborn, *Z. Naturforsch. B* **2000**, *55*, 389–405.
- [26] APEX suite of crystallographic software, APEX 3 version 2015.5-2; Bruker AXS Inc.: Madison, Wisconsin, USA, **2015**.
- [27] SAINT, Version 7.56a and SADABS Version 2008/1; Bruker AXS Inc.: Madison, Wisconsin, USA, **2008**.
- [28] G. M. Sheldrick, SHELXL-2014, University of Göttingen, Göttingen, Germany, **2014**.
- [29] C. B. Hübschle, G. M. Sheldrick, B. Ditttrich, *J. Appl. Crystallogr.* **2011**, *44*, 1281–1284.
- [30] G. M. Sheldrick, SHELXL-97, University of Göttingen, Göttingen, Germany, **1998**.
- [31] A. J. C. Wilson, in *International Tables for Crystallography*, Volume C, Tables 6.1.1.4 (pp. 500–502), 4.2.6.8 (pp. 219–222), and 4.2.4.2 (pp. 193–199), Kluwer Academic Publishers: Dordrecht, The Netherlands, **1992**.
- [32] C. F. Macrae, I. J. Bruno, J. A. Chisholm, P. R. Edgington, P. McCabe, E. Pidcock, L. Rodriguez-Monge, R. Taylor, J. van de Streek, P. A. Wood, *J. Appl. Crystallogr.* **2008**, *41*, 466–470.

Received: May 10, 2019

## 8. Disilene–Silylene Interconversion: A Synthetically Accessible Acyclic Bis(silyl)silylene

**Title:** Disilene–Silylene Interconversion: A Synthetically Accessible Acyclic Bis(silyl)silylene

**Status:** Article, published online July 28<sup>th</sup>, 2019

**Journal:** *Journal of the American Chemical Society*, **2019**, *141*, 13536-13546.

**Publisher:** American Chemical Society

**DOI:** [10.1021/jacs.9b05318](https://doi.org/10.1021/jacs.9b05318)

**Authors:** Dominik Reiter, Richard Holzner, Amelie Porzelt, Philipp J. Altmann, Philipp Frisch, Shigeyoshi Inoue<sup>a</sup>

*Reprinted with permission. © 2019 American Chemical Society*

**Content:** The well-known propensity of the hypersilyl group ((TMS)<sub>3</sub>Si) towards silyl migration reactions is exploited in this publication to synthesize a tetra(silyl)disilene. Unfortunately, this disilene is not stable in solution at ambient temperature and therefore not suitable for battery applications.

Interestingly however, the disilene displays an equilibrium with the isomeric silylene form, the first isolable bis(silyl)silylene so far. The extreme reactivity of this compound was investigated in detailed reactivity studies towards industrial relevant small molecules, such as dihydrogen, ammonia and ethylene. In fact, oxidative addition of H<sub>2</sub> was observed, even at –40 °C. Theoretical calculations predicted the silylene to be in a triplet ground state. To determine the inherent ground state multiplicity, cycloaddition experiments with olefins regarding the Skell rule were performed. However, no conclusive results were obtained from this study. Additionally, intermediary formed silylenes were isolated as Lewis base adducts with NHCs and DMAP respectively. On a final note, an NHC-stabilized silylene was oxidized with N<sub>2</sub>O to an NHC-coordinated silaester complex.

In summary, the first acyclic bis(silyl)silylene was isolated and thoroughly investigated. Thereby, this contribution provides both theoretical and experimental insights into disilene-silylene rearrangement reactions. Furthermore, the suitability of this extremely reactive species for the facile activation of small molecules was demonstrated.

---

<sup>a</sup>D. Reiter and R. Holzner planned and executed all experiments and co-wrote the manuscript. A. Porzelt performed the DFT calculations. P. J. Altmann and P. Frisch conducted all SC-XRD measurements and processed the resulting data. All work was performed under the supervision of S. Inoue.



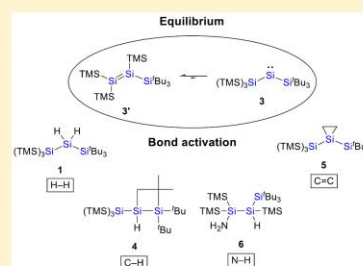
## Disilene–Silylene Interconversion: A Synthetically Accessible Acyclic Bis(silyl)silylene

Dominik Reiter,<sup>†</sup> Richard Holzner,<sup>†</sup> Amelie Porzelt,<sup>†</sup> Philipp J. Altmann, Philipp Frisch, and Shigeyoshi Inoue\*<sup>✉</sup>

Department of Chemistry, WACKER-Institute of Silicon Chemistry and Catalysis Research Center, Technische Universität München, Lichtenbergstraße 4, 85748 Garching bei München, Germany

Supporting Information

**ABSTRACT:** Silylenes have recently shown fascinating reactivity patterns, which are normally observed almost exclusively for transition-metal complexes. In particular, very reactive representatives are considered to be promising candidates, which may become powerful and economical alternatives for catalytic applications in the future. Here, we present the isolation of an equilibrium mixture consisting of a tetrasilyldisilene and its isomeric bis(silyl)silylene, the first isolable silylene of this type. Preliminary investigations demonstrate the extreme inherent reactivity via facile small-molecule activation even under very mild conditions. Thus, the oxidative addition of challenging targets such as H<sub>2</sub> and NH<sub>3</sub> was achieved. In addition, by synthesizing donor-stabilized bis(silyl)silylenes we gained further insights into the disilene–silylene rearrangement by 1,2-silyl migrations. Thorough theoretical calculations support the observed experimental results.



### INTRODUCTION

Low-valent silicon compounds have attracted considerable attention and nowadays make an important contribution to modern main group chemistry.<sup>1</sup> In particular, two-coordinate silylenes (RR'Si:), the silicon analogues of carbenes (RR'C:), play an important role because of their ambiphilic nature, which is reflected in a wide variety of reactivity patterns. Silylenes have a free 3p<sub>z</sub> orbital and a lone pair of electrons and, in contrast to carbenes, are almost exclusively in the singlet ground state.<sup>2</sup> To ensure the isolation of silylenes, sufficient kinetic and/or thermodynamic stabilization by adjacent, tailor-made substituents is essential. Therefore, a vast majority of stable silylenes are embedded in cyclic frameworks, including the well-established group of *N*-heterocyclic silylenes (NHSis), the silicon version of *N*-heterocyclic carbenes (NHCs).<sup>3</sup>

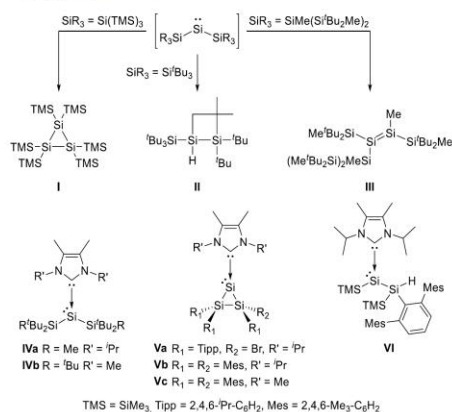
In contrast to their diverse counterparts, there are only scarce examples of stable acyclic silylenes reported.<sup>4</sup> Their true potential is revealed by silylenes bearing nucleophilic boryl and/or electropositive silyl substituents, leading to wide RSiR' angles and small HOMO–LUMO gaps. Thus, these highly reactive compounds are to a certain extent capable of mimicking transition-metal complexes in the activation of small molecules. Remarkably, acyclic silylenes can even undergo the oxidative addition of enthalpically strong molecules such as H<sub>2</sub>.<sup>4a,d,g</sup> Very recently, the reductive coupling of CO by an isolable aminoborylsilylene was also reported.<sup>5</sup> Bis(silyl)silylenes with sterically demanding substituents are considered to be even more reactive species

because of their wider RSiR' angles, smaller HOMO–LUMO gaps, and potential triplet ground state.<sup>2a–d,6</sup> Lately, the intrinsic nature of triplet ground state silylenes was experimentally proven by in situ generated silylenes analyzed by low-temperature glass matrix EPR studies;<sup>7</sup> however, typical triplet silylene reactivity is still unexplored.<sup>2f</sup> Nevertheless, no isolable two-coordinate acyclic bis(silyl)silylene has been reported so far. In situ generated, extremely reactive (R<sub>3</sub>Si)<sub>2</sub>Si: species are verifiable only as stable tetravalent silicon compounds, formed as products of subsequent intra- and intermolecular reactions. The general decomposition pathways include dimerization to disilenes (heavier alkene congeners), 1,2-silyl migration, and/or intramolecular C–H/Si–Si bond activation affording disilenes or cyclic silanes (Scheme 1).

Klinkhammer, for example, observed the formation of hexakis(trimethylsilyl)cyclotrisilane **I** as the formal decomposition product of bis(hypersilyl)silylene ((TMS)<sub>3</sub>Si)<sub>2</sub>Si: by treating HSiCl<sub>3</sub> with alkali metal hypersilanides (silyl anions).<sup>8</sup> The experimentally evidenced triplet ground state bis(supersilyl)silylene ((<sup>t</sup>Bu<sub>3</sub>Si)<sub>2</sub>Si:) undergoes an intramolecular C–H activation reaction (occurring from the singlet state<sup>2f</sup>) even at very low temperatures, providing disiletane **II**.<sup>7a</sup> Sekiguchi et al. pursued the isolation of the sterically crowded bis(silyl)silylene ((<sup>t</sup>Bu<sub>2</sub>MeSi)<sub>2</sub>MeSi)<sub>2</sub>Si:, but irreversible formation of disilene **III** occurred via a 1,2-silyl migration.<sup>9</sup> To

Received: May 17, 2019

Published: July 28, 2019

**Scheme 1. Isomerization Reactions of Transient Bis(silyl)silylenes I–III and Reported Examples of Bis(silyl)silylene NHC Adducts IV–VI**

date, isolable bis(silyl)silylenes are accessible only with the aid of additional  $\sigma$ -donor molecules such as NHCs.<sup>10</sup> The first examples of acyclic bis(silyl)silylene NHC adducts **IV** were obtained by reductive debromination of the corresponding dibromosilanes with  $\text{KC}_8$  in the presence of NHCs.<sup>11</sup> Scheschkewitz et al. and the Lips group reported cyclic derivatives **V** with a  $\text{Si}_3$  scaffold via the reaction of NHC:SiBr<sub>4</sub> with a disilylithium reagent and the coreduction of NHC:SiCl<sub>4</sub> and  $\text{Mes}_2\text{SiCl}_2$  ( $\text{Mes} = 2,4,6\text{-Me}_3\text{-C}_6\text{H}_2$ ), respectively.<sup>12</sup> Very recently, Cowley and colleagues experimentally demonstrated the disilene–silylsilylene equilibrium<sup>13</sup> for the first time by synthesizing and isolating NHC-stabilized bis(silyl)silylene **VI** from the corresponding donor-supported disilene.<sup>14</sup> Thus, the quest for isolable, acyclic two-coordinate bis(silyl)silylenes is ongoing.

Sterically demanding silyl groups are ideal candidates for the stabilization of otherwise elusive species because they are strong  $\sigma$ -donors and provide kinetic stabilization; however, they sometimes tend to migrate.<sup>1</sup> On the basis of the previous

results achieved with the hypersilyl- and supersilyl groups, we envisioned a combination of both substituents as a promising approach to gaining access to unprecedented low-coordinate silicon compounds through controlled 1,2-silyl shifts. Herein, we present the isolation of a novel tetrasilyldisilene displaying bis(silyl)silylene reactivity.

## RESULTS AND DISCUSSION

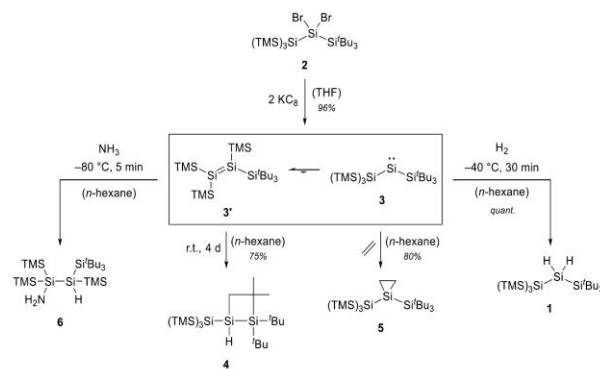
### Bis(silyl)silylene–Tetrasilyldisilene Interconversion.

The entry into this chemistry provided the isolation of the silane  $((\text{TMS})_3\text{Si})(\text{Bu}_3\text{Si})\text{SiH}_2$  (**1**).<sup>15</sup> Bromination of **1** in *n*-pentane furnished the corresponding dibromosilane **2**, which was isolated as colorless crystals in high yield and fully characterized (Scheme 2).

Subsequent reductive debromination of **2** with 2 equiv of  $\text{KC}_8$  at low temperatures resulted in a color change from colorless to blood red with the concomitant formation of black graphite. Multinuclear and 2D NMR analyses of the isolated product suggested the formation of tetrasilyldisilene **3'**, the isomer of (hypersilyl)(supersilyl)silylene **3**. The three-coordinate silicon nuclei of **3'** resonate at  $\delta = 161.9$  ppm ( $\text{SiTMS}_2$ ) and  $\delta = 132.4$  ppm ( $\text{Si}(\text{TMS})\text{Si}^\text{tipp}$ ) in the <sup>29</sup>Si NMR spectrum, which is in line with the signals for disilene **III** ( $\delta = 158.9$  and  $103.8$  ppm).<sup>9</sup> However, all attempts to crystallize the reaction product have been unsuccessful so far. Calculations performed at the M06-2X/6-31+g(d,p) level of density functional theory revealed a bent and twisted structure for tetrasilyldisilene **3'** (Figure 2)<sup>16</sup> comparable to that for disilene **III**.<sup>9</sup> The calculated <sup>29</sup>Si NMR resonances at  $\delta = 162.5$  and  $140.5$  ppm (gauge-independent atomic orbital (GIAO)/M06-L/6-311++(2d,2p); solvent model based on density (SMD); benzene) are in good agreement with the experimental values. (For details see the Supporting Information<sup>16</sup>).

Variable-temperature (VT) UV–vis spectroscopy revealed only two characteristic absorption bands at  $\lambda_{\text{max}} = 352$  and  $469$  nm. The calculated transitions, by means of time-dependent density functional theory (TD-DFT), at  $335$  and  $467$  nm are assigned to the HOMO–1  $\rightarrow$  LUMO and HOMO  $\rightarrow$  LUMO transitions of disilene **3'**, respectively.

Keeping a product solution at room temperature results in a rather slow decomposition and the selective formation of disilene **4**. Nevertheless, full conversion was not observed

**Scheme 2. Synthesis and Reactivity of Bis(silyl)silylene **3** and Its More Stable Isomer Tetrasilyldisilene **3'****

13537

DOI: 10.1021/jacs.9b05318  
J. Am. Chem. Soc. 2019, 141, 13536–13546



until after 4 days. Monitoring the decomposition reaction by NMR spectroscopy revealed no signals other than those assigned to **3'** and **4**. In addition, no signs of decomposition were observed when a product solution was stored at  $-35\text{ }^{\circ}\text{C}$  in a glovebox for at least 1 year. Disiletane **4** was fully characterized, and its molecular structure was unambiguously confirmed by single-crystal X-ray diffraction (SC-XRD) (Figure 1). As already shown in the case of **II**,<sup>7a</sup> the formation

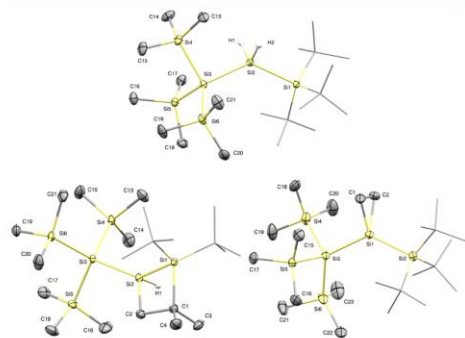


**Figure 1.** Molecular structures of **1** (top), **4** (bottom left), and **5** (bottom right). Ellipsoids are set at 50% probability. Hydrogen atoms are omitted for clarity, except for the respective Si–H nuclei of silane **1** and disiletane **4**. Selected bond lengths (Å) and angles ( $^{\circ}$ ): **1**: Si1–Si2 2.369(1), Si2–Si3 2.350(1); Si1–Si2–Si3 132.1(1). **4**: Si1–Si2 2.345(1), Si1–C1 1.957(2), C1–C2 1.572(2), Si2–C2 1.916(2), Si2–Si3 2.346(1); C1–Si1–Si2 76.3(1), Si1–Si2–C2 76.6(1), Si1–C1–C2 97.3(1), C1–C2–Si2 99.7(1). **5**: Si1–C1 1.885(2), Si1–C2 1.890(2), C1–C2 1.542(3), Si1–Si2 2.372(1), Si1–Si3 2.371(1); Si1–C1–C2 66.1(1), C1–C2–Si1 65.7(1), C2–Si1–C1 48.2(1), Si2–Si1–Si3 131.7(1).

of **4** quite likely originates from C–H bond activation of a *tert*-butyl group of bis(silyl)silylene **3**. Thus, the slow conversion of **3'** to **4** already indicates the existence of an equilibrium between bis(silyl)silylene **3** and disilene **3'** in solution. DFT calculations concerning **3** revealed the silylene located 5.7 kcal/mol in energy above its disilene isomer **3'** as well as its triplet state 2.5 kcal/mol lower in energy (Si–Si–Si bond angles:  $140.7^{\circ}$  (triplet) and  $116.2^{\circ}$  (singlet)) (Figure 2).<sup>16</sup> Several theoretical studies concerning possible triplet ground

state silylenes have been published in the last few decades. For different bis(silyl)silylenes, however, deviating values for the respective singlet–triplet energy gaps were found, depending on the methods and basis sets used.<sup>2b,f,6a</sup> Clearly, the singlet–triplet gap of **3** with a value of 2.5 kcal/mol is not high enough to readily take it for granted and judge the ground state multiplicity of **3** at the moment.

Therefore, we intended to experimentally elucidate the ground state multiplicity of bis(silyl)silylene isomer **3**. Because NMR spectroscopy provided no further insights (possible resonances for the singlet silylene of **3** were not observed), we used EPR spectroscopy (X-band: 9.267 GHz), the method of choice for potential triplet ground state detection. However, all EPR spectra obtained from a solution containing the equilibrium mixture of **3/3'**, measured in the temperature range of 133–286 K, exhibited only a strong EPR signal at around 331 mT ( $g = 2.0067$ ), corresponding to a typical silyl radical of still unknown structure. Sekiguchi et al. observed similar species (at around 340 mT,  $g = 2.0055$ ) when measuring the in situ generated triplet silylenes.<sup>7</sup> Nonetheless, under our measurement conditions, no analogous weak, broad signal at around 800 mT, assignable to the triplet silylene of **3**, was observed. Thus, the combined results suggest the position of the equilibrium being either almost entirely shifted to disilene **3'** or the decomposition to disiletane **4** being too rapid and beyond the detection limit for both the singlet and triplet ground state bis(silyl)silylene **3**.

As further evidence for the equilibrium, we intended  $[2 + 1]$  or  $[2 + 2]$  cycloaddition reactions with unsaturated organic substrates under the formation of defined trapping products. Whereas the reaction of **3/3'** with phenylacetylene, diphenylacetylene, and anthracene led to complicated mixtures of products, exposure to ethylene resulted in the clean formation of silirane **5** as the sole product, clearly indicating silylene reactivity (Scheme 2). Interestingly, no  $[2 + 2]$  cycloaddition reaction of tetrasilyl-disilene **3'** with ethylene was observed. Silirane **5** was fully characterized, including its solid-state structure (Figure 1). The ring silicon nucleus resonates at  $\delta = -164.3$  ppm in the  $^{29}\text{Si}$  NMR spectrum and exhibits a large Si–Si–Si bond angle of  $131.7(1)^{\circ}$  due to the sterically congested electropositive silyl groups.

According to the ethylene addition selectivity, we pursued  $[2 + 1]$  cycloaddition reactions of (*E*)/(*Z*) alkenes with respect to the Skell rule to further investigate the ground state multiplicity of bis(silyl)silylene **3**.<sup>17</sup> The Skell rule originates

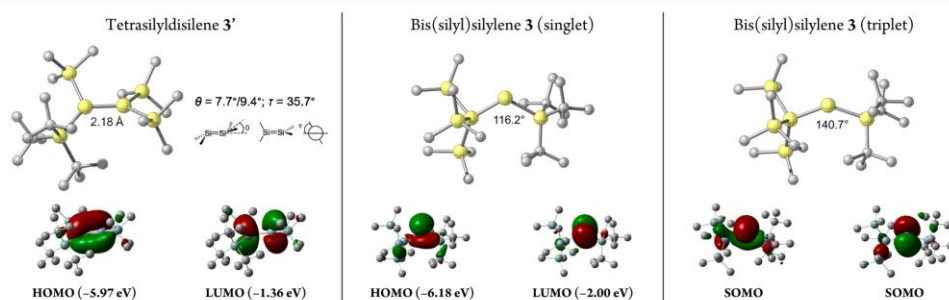
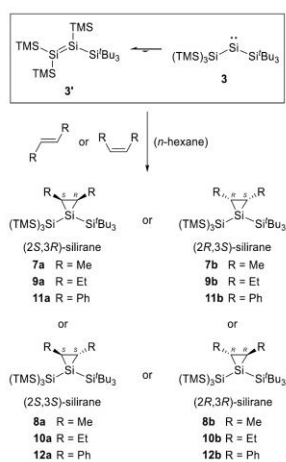


**Figure 2.** Calculated structures of tetrasilyl-disilene **3'** and bis(silyl)silylene **3** (singlet/triplet state) with their corresponding frontier orbitals.

from carbene chemistry and predicts the stereospecific olefin addition of singlet carbenes. Triplet carbenes undergo a nonstereospecific cycloaddition via a diradical intermediate, allowing for facile rotation and a loss of initial stereochemistry. In the case of silylenes, however, the situation might be more complicated, and a failure of the Skell rule cannot be ruled out.<sup>2c,f,6a</sup> Nonetheless, investigated singlet silylenes react according to the rule, and intended cycloaddition reactions of the transient triplet silylene (<sup>3</sup>Bu<sub>3</sub>Si)<sub>2</sub>Si: did not furnish any corresponding silirane.<sup>6a,7a,18</sup> This prompted us to investigate the stereochemistry of olefin cycloaddition with the equilibrium mixture of 3/3'. Because of the different silyl groups, not only two silirane isomers (*cis* and *trans*) but four different stereoisomers can be formed (Scheme 3). Therefore, we

**Scheme 3. Plausible Silirane Stereoisomers Formed Upon [2 + 1] Cycloaddition Reaction of (Hypersilyl)(supersilyl)silylene 3 with (E)- and (Z)-Alkenes**



initially used the simplest isomers, (*E*)- and (*Z*)-2-butenes. The exposure of 3/3' to (*Z*)-2-butene selectively afforded *cis*-silirane 7. Compound 7 was sufficiently characterized by multinuclear and 2D NMR spectroscopy, albeit not being able to resolve its stereochemistry ((2*S*,3*R*)-silirane 7a or (2*R*,3*S*)-silirane 7b). The observed <sup>29</sup>Si NMR resonance at  $\delta = -131.7$  ppm for the silirane silicon nucleus is shifted to slightly lower field compared to those observed for reported *cis*-bis-(trialkylsilyl)siliranes ( $\delta = -154.5$  to  $-159.1$  ppm) and silirane 5.<sup>6a,18c</sup> On the other hand, the reaction of 3/3' with (*E*)-2-butene furnished approximately a 50:50 mixture of *cis*-silirane 7 and *trans*-silirane 8. Again, the absolute configuration of 8 remains unclear, but the silirane silicon atom exhibits a similar downfield shift in the <sup>29</sup>Si NMR spectrum ( $\delta = -123.3$  ppm) in comparison to reported bis-(trialkylsilyl)siliranes ( $\delta = -144.1$  to  $-149.6$  ppm) and 5.<sup>6a,18c</sup> The observed nonstereospecificity most likely originates from (*Z*)-2-butene contamination (~1.3%) because the purity of the utilized alkenes is crucial to the silirane product ratio. This was already recognized in the initially observed nonstereospecific cycloadditions of 2-butenes to dimethylsilylene, in which gas contamination of the respective other isomer led to misinter-

pretations.<sup>18b,19</sup> Accordingly, the reaction of 3/3' with an approximately 50:50 mixture of both stereogenic alkenes provided *cis*-silirane 7 as the sole product because of the higher reactivity of the (*Z*)-isomer.

To gain deeper insight, we turned to sterically more demanding alkenes with higher isomeric purity. However, the utilization of 3-hexenes and stilbenes (1,2-diphenylethylenes) led to significantly slower or even no (stilbene) cycloaddition reactions with the concomitant formation of disilene 4, especially with the respective (*E*)-isomer. The most satisfying result was obtained with (*Z*)-3-hexene, with <sup>29</sup>Si NMR analysis ( $\delta = -133.2$  ppm) indicating the selective formation of *cis*-silirane 9. The reaction of 3/3' with (*E*)-3-hexene, on the contrary, led to the formation of a mixture of products. However, *trans*-silirane 10 was identified by <sup>1</sup>H and <sup>29</sup>Si NMR ( $\delta = -127.1$  ppm; typical downfield shift compared to the *cis*-isomer) spectroscopy. Interestingly, no resonances for *cis*-silirane 9 were observed. Therefore, we conclude that [2 + 1] cycloaddition reactions of bis(silyl)silylene 3 with stereogenic alkenes are most likely stereospecific.

Overall, the outcome of the cycloaddition reactions with stereogenic alkenes cannot yet reveal with certainty the ground state multiplicity of bis(silyl)silylene 3 because even triplet ground state silylenes could react via their singlet state.<sup>2c,f,6a</sup> Therefore, further examinations are essential and both a reliable method for determining the ground state multiplicity (besides EPR spectroscopy) and typical triplet silylene reactivity have yet to be found.

Surprisingly, the disilene/silylene equilibrium mixture is also capable of activating dihydrogen via oxidative addition. So far, only a few examples of low-coordinate silicon compounds are known to react similarly. This series consists of three acyclic silylenes and one disilene with small HOMO–LUMO gaps (2.0–3.0 eV), which undergo fast reactions under relatively mild conditions (from 2 h at 0 °C to up to 2 days at 50 °C).<sup>4a,4b,20</sup> Recently, Iwamoto et al. reported hydrogen splitting reactions by boryldisilenes.<sup>21</sup> Although no observable sign of reaction was detectable at  $-80$  °C (3 h), treating an *n*-hexane solution of 3/3' at  $-40$  °C with H<sub>2</sub> (1 bar) resulted in a color change from blood red to pale yellow within 30 min. The quantitative formation of silane 1 was detected by NMR spectroscopy (Scheme 2). Again, no formation of the respective disilene addition product was detected. The molecular structure of 1 revealed a large Si–Si–Si bond angle of 132.1(1)° comparable to that of silirane 5, indicating a large Si–Si–Si bond angle for bis(silyl)silylene 3 (Figure 1). Contrary to reported acyclic silylenes, which are able to activate H<sub>2</sub>, singlet bis(silyl)silylene 3 exhibits a large HOMO–LUMO gap of 4.18 eV (Figure 2). Because acyclic silylenes with a comparable large HOMO–LUMO gap have shown no reaction toward H<sub>2</sub>,<sup>4b</sup> the extreme reactivity of bis(silyl)silylene 3 is rather astonishing. Thus, we performed additional calculations concerning the bimolecular reaction of H<sub>2</sub> and singlet 3 and determined a very low effective barrier of 4.2 kcal/mol. The calculated barrier is significantly lower than that reported for Aldridge's acyclic aminoborylsilylene (23.2 kcal/mol),<sup>4a</sup> which therefore rationalizes the observed fast reaction of bis(silyl)silylene 3. These results contrast with the generally assumed connectivity of a low HOMO–LUMO gap and the activation of dihydrogen for acyclic silylenes. Thus, this correlation presumably does not account for acyclic bis(silyl)silylenes. Additionally, this observation represents the first example of dihydrogen activation by a bis(silyl)silylene



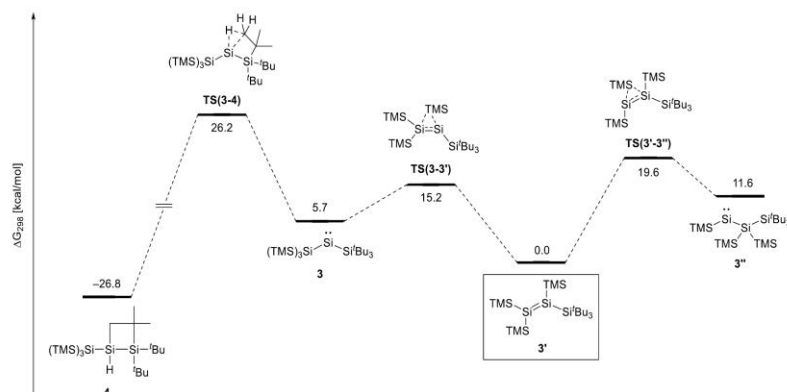


**Figure 3.** DFT-derived energy profile for the silylene–disilene–silylene equilibrium at the M06-2X/6-311+G(d,p)(SMD = benzene)//M06-2X/6-31+G(d,p) level of theory.

and the fastest reaction of a low-coordinate silicon compound toward  $H_2$  to date.

DLPNO-CCSD(T)/cc-pVQZ single-point calculations based on the PBEh-3c optimized structures of **3** revealed the singlet state of **3** located 4.6 kcal/mol lower in energy than the triplet, thus supporting the assumed reactivity toward  $H_2$ .<sup>22</sup>

Besides dihydrogen, the activation of ammonia via oxidative addition is still a challenging target even for transition-metal complexes.<sup>23</sup> However, the rapid growth of main group chemistry in recent decades has revealed various reactive compounds capable of activating ammonia under mild conditions.<sup>24</sup> Among them are only a few silicon compounds, all of which bear low-coordinate centers, represented by their most prominent examples, silylenes<sup>24,25</sup> and disilenes.<sup>26</sup> On the basis of the results so far, we envisaged the reaction of **3/3'** with ammonia as a promising target. Indeed, a facile reaction was observed even at  $-80^\circ C$  by treating an *n*-hexane solution of **3/3'** with an equimolar amount of  $NH_3$  (0.4 M solution in 1,4-dioxane). The successful hydroamination reaction was clearly evident by the immediate color change from blood red to pale yellow. Multinuclear and 2D NMR spectroscopy identified the major product formed as aminosilane **6**, the addition product derived from tetrasilyl-disilene **3'**. The reaction is completely regioselective, with the preferred regioisomer bearing the amino group attached to the silicon nucleus with the two TMS groups, presumably for steric reasons. A similar observation was reported by Scheschkewitz and colleagues.<sup>26b</sup> The Si– $NH_2$  atom resonates at  $\delta = -35.7$  ppm in the  $^{29}Si$  NMR spectrum, which agrees well with those observed for similar compounds ( $\delta = -14.7$  to  $-48.6$  ppm)<sup>26</sup> and the theoretically calculated value ( $\delta = -36.8$  ppm). The Si–H nucleus exhibits a high-field shift in the  $^{29}Si$  NMR spectrum at  $\delta = -119.9$  ppm compared to the reported ones ( $\delta = -57.1$  to  $-72.4$  ppm) but is in good accordance with the calculated shift ( $\delta = -116.6$  ppm). Performing the reaction at elevated temperatures leads to less-selective product formation, presumably also affording the respective regioisomer and the adduct of bis(silyl)silylene **3**. Besides proving the existence of tetrasilyl-disilene **3'**, these results further strengthen the assumption of an equilibrium between silylene **3** and disilene **3'**. Further calculations to obtain a conclusive mechanistic

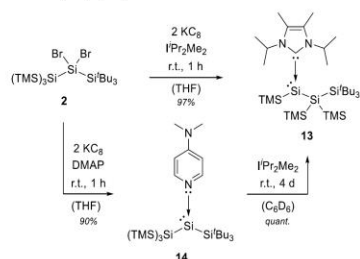
picture concerning ammonia activation are under current investigation.

In addition, very fast reactions of **3/3'** with small molecules  $O_2$ ,  $CO_2$ , and  $P_4$  were observed, but in all cases, nonselective reactions occurred, leading to product mixtures. However, these observations underline the high reactivity of the equilibrium mixture containing bis(silyl)silylene **3** and tetrasilyl-disilene **3'**.

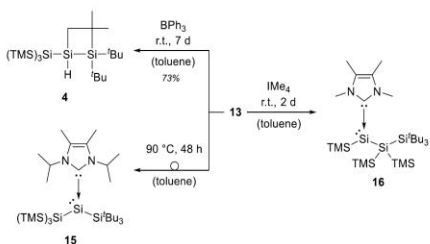
As previously investigated theoretically for  $((H_3Si)H_2Si)-(H)Si$ : and  $(H_3Si)HSi=SiH_2$ ,<sup>13b</sup> further verification of the experimentally observed equilibrium was provided by DFT calculations (Figure 3). Accordingly, disilene **3'** represents the most stable isomer, with an effective barrier of 15.2 kcal/mol for the TMS group migration affording bis(silyl)silylene **3**. Interestingly, another regioisomeric bis(silyl)silylene  $(TMS)_2((Bu_3Si)Si)Si$ : **3''** is accessible via a second 1,2-silyl shift with its formation connected to an effective barrier of 19.6 kcal/mol. Thus, the isomerization reactions between bis(silyl)silylenes **3/3''** and disilene **3'** via TMS group migrations represent an equilibrium, with disilene **3'** as the kinetic product. The decomposition of disilene **3'**/silylene **3** proceeds via C–H activation, connected to a substantially higher barrier of 26.2 kcal/mol, affording thermodynamic product **4** in an irreversible reaction.

**Lewis Base-Stabilized Bis(silyl)silylenes.** To gain deeper insight into the disilene–silylene interconversion, we attempted to trap **3** and/or **3'** with additional Lewis bases such as phosphines and NHCs. However, treating the equilibrium mixture of **3/3'** with  $PMe_3$  and NHCs with varying steric demand did not furnish a clean donor–acceptor product. The resulting mixtures contained several donor-stabilized species, presumably including both bis(silyl)silylene and disilene adducts. Instead, the reductive debromination of **2** with  $KC_8$  in the presence of 1,3-diisopropyl-4,5-dimethylimidazolin-2-ylidene ( $iPr_2Me_2$ ) selectively furnished NHC-stabilized bis(silyl)silylene **13** in excellent yield (Scheme 4). Interestingly, the formation of initially targeted bis(silyl)silylene NHC adduct **15** (Scheme 5) was not observed, but two consecutive 1,2-silyl migrations from silylene **3** through disilene **3'** to silylene **3''** occurred and finally NHC-stabilized regioisomeric silylene **13** was obtained. Presumably, **13** is

Scheme 4. Synthesis and Interconversion of Novel Donor-Stabilized Bis(silyl)silylenes



Scheme 5. Reactivity of NHC-Stabilized Bis(silyl)silylene 13



formed as the preferred product as a result of less steric congestion between  $\text{IPr}_2\text{Me}_2$  and silylene  $3''$  compared to silylene 3. The divalent silicon nucleus of **13** exhibits a downfield-shifted resonance in the  $^{29}\text{Si}$  NMR spectrum ( $\delta = -104.7$  ppm) relative to those observed for reported bis(silyl)silylenes **IV–VI** ( $\delta = -110.5$  to  $-136.6$  ppm). The molecular structure of **13** was unambiguously confirmed by SC-XRD analysis (Figure 4). The  $\text{IPr}_2\text{Me}_2$ -stabilized divalent silicon center adopts a trigonal pyramidal geometry with the sum of bond angles amounting to  $340.9^\circ$  (**IVb**,  $344.3^\circ$ ; **Va**,  $302.7^\circ$ ; **Vb**,  $293.4^\circ$ ; **Vc**,  $255.5^\circ$ ; and **VI**,  $317.3^\circ$ ). The low degree of pyramidalization indicates less-pronounced s character of the lone pair of electrons at the three-coordinate

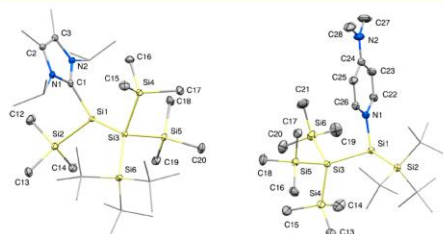


Figure 4. Molecular structures of **13** (left) and **14** (right). Ellipsoids are set at 50% probability. Hydrogen atoms and solvent molecules are omitted for clarity. Selected bond lengths (Å) and angles ( $^\circ$ ): **13**: Si1–Si2 2.360(1), Si1–Si3 2.437(1), Si1–C1 1.961(2); C1–Si1–Si2 99.3(1), C1–Si1–Si3 115.6(1), Si2–Si1–Si3 126.0(1). **14**: Si1–Si2 2.433(1), Si1–Si3 2.420(1), Si1–N1 1.942(2); N1–Si1–Si2 104.5(1), N1–Si1–Si3 98.1(1), Si2–Si1–Si3 116.1(1).

silylenes. The  $\text{C}_{\text{NHC}}\text{–Si}$  bond length is 1.961(2) Å, which is in the typical range for  $\text{C}_{\text{NHC}}\text{–Si}$  bonds<sup>10b</sup> but elongated in comparison to **IV–VI** (1.933–1.960 Å) and thus displaying a weaker interaction between the NHC  $\text{IPr}_2\text{Me}_2$  and the silylene moiety in complex **13**.

In contrast, the utilization of weaker Lewis base 4-*N,N*-dimethylaminopyridine (DMAP) afforded DMAP-coordinated silylene **14** in 90% yield. In this case, regioisomeric (hypersilyl)(supersilyl)silylene **3** was trapped as donor–acceptor complex **14**. The less-shielded three-coordinate silicon atom shows a significant downfield shift in the  $^{29}\text{Si}$  NMR spectrum at  $\delta = 68.8$  ppm. A similar trend was observed for donor-stabilized  $\beta$ -diketiminato silylenes ( $\delta = -12.0$  to 37.4 ppm)<sup>27</sup> reported by Driess et al. However, that case is far less pronounced because the respective donor-free silylene resonates only at  $\delta = 88.4$  ppm.<sup>28</sup> The solid-state structure (Figure 4) revealed a higher degree of pyramidalization around the divalent silicon nucleus (sum of bond angles:  $318.7^\circ$ ) and therefore illustrates the increased s character of base-stabilized silylene **14**. The  $\text{N}_{\text{DMAP}}\text{–Si}$  bond length of 1.942(2) Å agrees well with those observed for previously reported DMAP-stabilized low-valent silicon complexes ( $d_{\text{N–Si}} = 1.85\text{–}2.01$  Å).<sup>27b,29</sup> Surprisingly, the treatment of silylene **14** with an equimolar amount of  $\text{IPr}_2\text{Me}_2$  does not afford corresponding NHC-stabilized silylene **15** but, selectively again, provides rearranged silylene NHC adduct **13**. This observation for the Lewis base exchange further indicates the presence of the silylene–disilene–silylene equilibrium discussed above. In addition, our results are an extension of the recent findings regarding the disilene–silylene rearrangement, reported by Cowley, Holthausen, and colleagues.<sup>14</sup>

To gain more profound knowledge concerning the accessibility of all isomers in equilibrium, we investigated the reactivity of silylene **13** with respect to Lewis base abstraction and exchange. The reaction of **13** with 1 equiv of Lewis acid  $\text{BPh}_3$  provided disilene **4** through NHC abstraction and the concomitant formation of the NHC–borane adduct  $\text{IPr}_2\text{Me}_2\cdot\text{BPh}_3$  (Scheme 5). Full conversion, however, was observed only after a reaction time of 1 week at ambient temperature. Monitoring the reaction with  $^1\text{H}$  and  $^{29}\text{Si}$  NMR spectroscopy revealed the intermediary formation of tetrasilyl-disilene  $3'$ . Therefore, NHC abstraction initially affords respective donor-free silylene  $3''$  being in equilibrium with disilene  $3'$  and silylene 3. As already mentioned, the irreversible decomposition of the equilibrium mixture is kinetically limited but thermodynamically preferred, thus accounting for the long reaction times.

Silylene **13** is completely stable as a solid and in solution at room temperature. However, heating a solution of **13** to  $90^\circ\text{C}$  results again in a double TMS migration and the formation of initially targeted NHC-supported silylene **15** (Scheme 5) in 58% yield (NMR). Additional DFT calculations revealed that **15** is slightly more stable than **13** with an effective activation barrier of 30.0 kcal/mol for the interconversion, thus being in line with the required elevated temperature and prolonged reaction time for the isomerization. Nevertheless, silylene **15** could not be isolated in its pure form because of incomplete conversion and concomitant decomposition via the formation of disilene **4** and free  $\text{IPr}_2\text{Me}_2$ . Neither prolonged heating (at different temperatures) nor solvent change to benzene, *n*-hexane, or THF affected the outcome of the reaction in favor of silylene **15**, thus further confirming the existence of the equilibrium. Nonetheless, **15** was unambiguously characterized



by a combination of multinuclear and 2D NMR studies, supported by the results obtained from DFT calculations. The  $^{29}\text{Si}$  resonance of the three-coordinate Si nucleus is shifted to higher field ( $\delta = -120.6$  ppm) compared to that for donor-stabilized silylenes **13** and **14** and agrees well with its GIAO-predicted chemical shift ( $\delta = -127.2$  ppm). In particular, the huge difference from that observed for analogous DMAP-stabilized silylene **14** emphasizes the stronger interaction between bis(silyl)silylene **3** and the better  $\sigma$ -donor molecule.

Furthermore, an even stronger donor–acceptor interaction was shown by the successful exchange of  $\text{I}^+\text{Pr}_2\text{Me}_2$  with the stronger  $\sigma$ -donating NHC, 1,3,4,5-tetramethylimidazolin-2-ylidene ( $\text{IME}_4$ ).  $\text{IME}_4$ -stabilized bis(silyl)silylene **16** was sufficiently characterized by multinuclear NMR spectroscopy (Scheme 5). The low-valent silicon nucleus exhibits a signal observed at  $\delta = -117.1$  ppm in the  $^{29}\text{Si}$  NMR spectrum. The high-field-shifted resonance compared to that observed for **13** indicates a stronger interaction between NHC and bis(silyl)silylene **3**. The theoretically determined resonance at  $\delta = -115.2$  ppm supports the formation of NHC adduct **16**. However, it was neither possible to remove free  $\text{I}^+\text{Pr}_2\text{Me}_2$ , nor to observe a rearrangement to the corresponding  $\text{IME}_4$ -stabilized bis(silyl)silylene adduct of **3** because of an even more facile decomposition reaction.

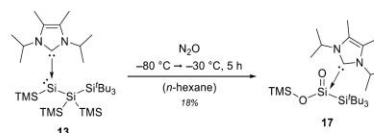
Additional DFT calculations also reflect the trend observed for the  $\sigma$ -donor–silylene interactions by  $^{29}\text{Si}$  NMR spectroscopy (details in Tables S9 and S11 in the Supporting Information), and thus the gas-phase Gibbs free bond-dissociation energy increases from 15.3 kcal/mol (**14**) to 16.3 kcal/mol (**15**) to 22.0 kcal/mol (**13**) and finally to 27.6 kcal/mol (**16**). These observations correlate well with the increasing donor strength of the Lewis base used and also confirm the inability to access  $((\text{TMS})_2\text{Si})(^t\text{Bu}_3\text{Si})\text{Si}:(\text{IME}_4)$ , the regioisomeric product of **16**. In addition to the higher gas-phase Gibbs free bond-dissociation energy, the reduced steric demand of  $\text{IME}_4$  makes **16** more susceptible for subsequent reactions. This is evidenced by the slow decomposition of **16** in solution. In the case of NHC-stabilized silylene **13**, rearrangement to **15** is still the preferred pathway, although decomposition and disiletane **4** formation occur during heating. For DMAP-stabilized silylene **14**, the isomerization equilibrium finally providing **13** appears to be the only accessible pathway subsequent to Lewis base dissociation.

**NHC-Stabilized Silanoic Ester.** Even though the oxygenation of **3/3'** led only to complicated mixtures with no isolable products, we investigated the reaction of **13** toward various oxidizing agents because the last decades have witnessed significant attention in the synthesis of heavier analogues of carbonyl compounds. However, in particular, the isolation of organosilicon compounds bearing a  $\text{Si}=\text{O}$  moiety is a rather demanding task because of their extreme reactivity. The origin of this reactivity lies in the kinetic and thermodynamic instability of the weak  $\text{Si}=\text{O}$   $\pi$ -bond attributed to the unfavorable  $p_\pi$ -orbital overlap of silicon and oxygen.<sup>30</sup> In addition, the Pauling electronegativity difference between silicon and oxygen ( $\Delta\chi_{(\text{Si}-\text{O})} = 1.54$ ) is much larger than that between carbon and oxygen ( $\Delta\chi_{(\text{C}-\text{O})} = 0.89$ ).<sup>31</sup> Thus, the zwitterionic, ylide-like  $\text{Si}^{\delta+}=\text{O}^{\delta-}$  resonance form makes a large contribution to the nature of the strongly polarized  $\text{Si}=\text{O}$  double bond.<sup>32</sup> As a consequence, the  $\text{Si}=\text{O}$  double bond is prone to barrierless, rapid head-to-tail oligomerization affording oligosiloxanes via  $\text{Si}-\text{O}$   $\sigma$ -bond formation.<sup>33</sup> Despite this challenge, the  $\text{Si}=\text{O}$  moiety could be tamed<sup>10b,34</sup> and a

series of donor-<sup>27a,c,35</sup> and donor–acceptor-stabilized<sup>27b,36</sup> heavier carbonyl compounds have been reported. Even a few examples of donor-free, three-coordinate silanones (silicon analogues of ketones) have been isolated.<sup>4b,37</sup> Nevertheless, silanoic esters, the heavier congeners of carboxylate esters, remain rather elusive compounds with scarcely any reported example species.<sup>38</sup>

Because we recently reported the isolation of a stable silyl-substituted silanone,<sup>4b</sup> we assumed that **13**, with two silyl groups, was a promising precursor for gaining access to silanone derivatives. However, the reaction of NHC-stabilized silylene **13** toward  $\text{Me}_3\text{NO}$ ,  $\text{CO}_2$ , and  $\text{O}_2$  resulted in either no reaction or the formation of a complicated mixture of products. Interestingly, the exposure of an *n*-hexane solution of **13** to  $\text{N}_2\text{O}$  results in a color change from purple-red to pale red with the concomitant formation of a white precipitate. After workup, unique NHC-supported silanoic ester **17** was isolated in 18% yield (Scheme 6). The exact mechanism of the

**Scheme 6.** Oxygenation of Silylene **13** Furnishing NHC-Stabilized Silanoic Ester **17**



formation of **17** is unclear but presumably includes the initial generation of a silanone. Subsequent silyl migration, further oxidation, and rearrangement might eventually lead to **17**. In  $^{29}\text{Si}$  NMR, the  $\text{Si}=\text{O}$  silicon nucleus exhibits a resonance at  $\delta = -50.8$  ppm, which exactly matches the GIAO-DFT value and agrees with those reported for related species ( $\delta = -49.1$  to  $-91.5$  ppm).<sup>38</sup> The  $^1\text{H}$  NMR spectrum provided the most intriguing spectroscopic feature of **17**, an unusual broad splitting of the NHC wingtip methine protons ( $\Delta\delta = 2.68$  ppm). The reason for this observation is presumably hydrogen bonding of one isopropyl C–H proton to the oxygen atom of the  $\text{Si}=\text{O}$  bond. The solid-state structure of **17** (Figure 5) revealed a close  $\text{O}\cdots\text{H}$  distance of 2.143 Å, being much shorter than the sum of the van der Waals radii of hydrogen and oxygen (2.72 Å) and thus supporting this assumption.<sup>39</sup> The

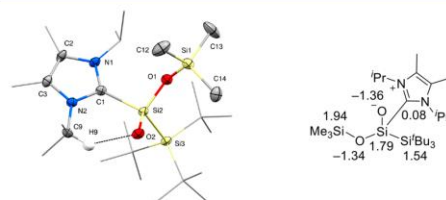


**Figure 5.** Molecular structure of **17** with ellipsoids set at 50% probability (left) and the results of NBO analysis of **17** (right). Hydrogen atoms, except for H9 involved in hydrogen bonding (visualized by the dashed line), are omitted for clarity. Selected bond lengths (Å) and angles ( $^\circ$ ): Si1–O1 1.641(2), Si2–O2 1.556(2), Si2–O1 1.655(3), Si2–Si3 2.415(1), Si2–C1 1.984(3), O2–Si2–O1 115.5(1), O2–Si2–C1 106.9(1), O1–Si2–C1 101.2(1), O2–Si2–Si3 111.7(1), O1–Si2–Si3 107.0(1), C1–Si2–Si3 114.3(1).

experimentally determined Si=O bond length of 1.556(2) Å is in the range observed for similar compounds ( $d_{\text{Si=O}} = 1.52\text{--}1.59$  Å) and much shorter than the measured Si–O single bonds ( $d_{\text{Si–O}} = 1.641(2)$  and  $1.655(3)$  Å).<sup>38</sup> Interestingly, the TMS–O  $\sigma$ -bond is shorter than the Si2–O1 bond and the C<sub>NHC</sub>–Si bond is elongated compared to that observed for the precursor, silylene NHC adduct **13** ( $d_{\text{C–Si}} = 1.961(2)$  Å).

Characteristic Si=O and Si–O–Si stretching vibrations at  $\tilde{\nu} = 1069$  and  $971\text{ cm}^{-1}$ , respectively, were found in the IR spectrum of **17**. NHC-stabilized silanoic ester **17** is not a particularly stable compound because decomposition to an unidentified mixture of products was observed in solution at temperatures higher than  $-30\text{ }^{\circ}\text{C}$ . Possible multiple bonding in four-coordinate silanoic esters and related thioesters has already been investigated in detail by Driess, Apeloig, and co-workers.<sup>35a</sup> Nevertheless, our entirely silyl-substituted silanoic ester is the first example of its kind. Natural bond orbital (NBO) analysis revealed strong polarization for both central silicon oxygen bonds (details in the Supporting Information). The Wiberg bond indices (WBIs) of the Si2–O1 (0.47) and Si2–O2 (0.91) bonds are relatively low, contradictory to the short Si2–O2 bond observed in the solid state. Natural resonance theory (NRT) revealed the zwitterionic formulation as the major resonance structure (Table S15). However, NBO analysis further features negative hyperconjugation of the lone pairs of O2 into the  $\sigma^*$  orbitals of Si2–C1 and Si2–O1, thus rationalizing the observed short Si2–O2 bond as well as the elongated O1–Si2 and Si2–C1 bonds (Figure S81). Moreover, both highly polarized Si–O bonds and the reduced C<sub>NHC</sub>–Si interaction account for the limited thermal stability of **17**.

## CONCLUSIONS

We used the novel dibromosilane ((TMS)<sub>3</sub>Si)(<sup>t</sup>Bu<sub>3</sub>Si)SiBr<sub>2</sub> (**2**) to gain access to the equilibrium mixture of tetrasilyldisilene **3'** and the first example of an isolable bis(silyl)silylene **3**. The highly reactive nature of **3/3'** was demonstrated by the facile activation of small molecules under very mild conditions. In particular, the fastest reactions discovered for a low-valent silicon compound toward dihydrogen and ammonia via oxidative addition were observed. These results further demonstrate the potential of main group compounds as transition-metal mimics and possible catalysts for the future. In the course of our study, we further isolated unprecedented donor-stabilized bis(silyl)silylenes **13** and **14** and revealed deeper insights into the disilene–silylene rearrangement. In addition, the first acyclic NHC-stabilized silanoic ester, **17**, was isolated. Currently, the synthesis of bis(silyl)silylene transition-metal complexes to examine the inherent  $\sigma$ -donor strength and further studies regarding the ground state multiplicity of **3** are under active investigation in our laboratories.

## ASSOCIATED CONTENT

### Supporting Information

The Supporting Information is available free of charge on the ACS Publications website at DOI: 10.1021/jacs.9b05318.

Experimental details, including synthesis, spectroscopic, crystallographic, and computational data (PDF)

Crystallographic data (CCDC 1915625–1915631) (CIF)

## AUTHOR INFORMATION

### Corresponding Author

\*s.inoue@tum.de

### ORCID

Shigeyoshi Inoue: 0000-0001-6685-6352

### Author Contributions

<sup>†</sup>D.R., R.H., and A.P. contributed equally to this work.

### Notes

The authors declare no competing financial interest.

## ACKNOWLEDGMENTS

We are exceptionally grateful to the WACKER Chemie AG and the European Research Council (SILION 637394) for continued financial support. We thank Dr. Daniel Wendel for revising the manuscript, Maria Matthews for the low-temperature NMR studies, and Dr. Oksana Storcheva for the EPR measurements. We also thank Prof. Dr. M. C. Holthausen (Goethe-Universität Frankfurt am Main) and J. I. Schweizer for fruitful discussions, computational resources, and advice. Quantum chemical calculations were performed in parts at the Leibniz Supercomputing Center of the Bavarian Academy of Science and Humanities.

## REFERENCES

- Lee, V. Y. *Organosilicon Compounds: Theory and Experiment (Synthesis)*; Academic Press: New York, 2017.
- (a) Grev, R. S.; Schaefer, H. F., III; Gaspar, P. P. In search of triplet silylenes. *J. Am. Chem. Soc.* **1991**, *113*, 5638–5643. (b) Holthausen, M. C.; Koch, W.; Apeloig, Y. Theory Predicts Triplet Ground-State Organic Silylenes. *J. Am. Chem. Soc.* **1999**, *121*, 2623–2624. (c) Gaspar, P. P.; Xiao, M.; Pae, D. H.; Berger, D. J.; Haile, T.; Chen, T.; Lei, D.; Winchester, W. R.; Jiang, P. The quest for triplet ground state silylenes. *J. Organomet. Chem.* **2002**, *646*, 68–79. (d) Yoshida, M.; Tamaoki, N. DFT Study on Triplet Ground State Silylenes Revisited: The Quest for the Triplet Silylene Must Go On. *Organometallics* **2002**, *21*, 2587–2589. (e) Apeloig, Y.; Pauncz, R.; Karni, M.; West, R.; Steiner, W.; Chapman, D. Why Is Methylene a Ground State Triplet while Silylene Is a Ground State Singlet? *Organometallics* **2003**, *22*, 3250–3256. (f) Kosa, M.; Karni, M.; Apeloig, Y. Were Reactions of Triplet Silylenes Observed? *J. Am. Chem. Soc.* **2013**, *135*, 9032–9040.
- (3) For recent reviews on silylenes, see (a) Haaf, M.; Schmedake, T. A.; West, R. Stable Silylenes. *Acc. Chem. Res.* **2000**, *33*, 704–714. (b) Gehrhus, B.; Lappert, M. F. Chemistry of thermally stable bis(amino)silylenes. *J. Organomet. Chem.* **2001**, *617–618*, 209–223. (c) Nagendran, S.; Roesky, H. W. The Chemistry of Aluminum(I), Silicon(II), and Germanium(II). *Organometallics* **2008**, *27*, 457–492. (d) Mizuhata, Y.; Sasamori, T.; Tokitoh, N. Stable Heavier Carbene Analogues. *Chem. Rev.* **2009**, *109*, 3479–3511. (e) Kira, M. An isolable dialkylsilylene and its derivatives. A step toward comprehension of heavy unsaturated bonds. *Chem. Commun.* **2010**, *46*, 2893–2903. (f) Asay, M.; Jones, C.; Driess, M. N-Heterocyclic Carbene Analogues with Low-Valent Group 13 and Group 14 Elements: Syntheses, Structures, and Reactivities of a New Generation of Multitalented Ligands. *Chem. Rev.* **2011**, *111*, 354–396. (g) Yao, S.; Xiong, Y.; Driess, M. Zwitterionic and Donor-Stabilized N-Heterocyclic Silylenes (NHSis) for Metal-Free Activation of Small Molecules. *Organometallics* **2011**, *30*, 1748–1767. (h) Sen, S. S.; Khan, S.; Samuel, P. P.; Roesky, H. W. Chemistry of functionalized silylenes. *Chem. Sci.* **2012**, *3*, 659–682. (i) Sen, S. S.; Khan, S.; Nagendran, S.; Roesky, H. W. Interconnected Bis-Silylenes: A New Dimension in Organosilicon Chemistry. *Acc. Chem. Res.* **2012**, *45*, 578–587.
- (4) (a) Protchenko, A. V.; Birjumar, K. H.; Dange, D.; Schwarz, A. D.; Vidovic, D.; Jones, C.; Kaltsoyannis, N.; Mountford, P.; Aldridge,



- S. A Stable Two-Coordinate Acyclic Silylene. *J. Am. Chem. Soc.* **2012**, *134*, 6500–6503. (b) Rekken, B. D.; Brown, T. M.; Fetting, J. C.; Tuononen, H. M.; Power, P. P. Isolation of a Stable, Acyclic, Two-Coordinate Silylene. *J. Am. Chem. Soc.* **2012**, *134*, 6504–6507. (c) Inoue, S.; Leszczynska, K. An Acyclic Imino-Substituted Silylene: Synthesis, Isolation, and its Facile Conversion into a Zwitterionic Silimine. *Angew. Chem., Int. Ed.* **2012**, *51*, 8589–8593. (d) Protchenko, A. V.; Schwarz, A. D.; Blake, M. P.; Jones, C.; Kaltsayannis, N.; Mountford, P.; Aldridge, S. A Generic One-Pot Route to Acyclic Two-Coordinate Silylenes from Silicon(IV) Precursors: Synthesis and Structural Characterization of a Silylsilylene. *Angew. Chem., Int. Ed.* **2013**, *52*, 568–571. (e) Rekken, B. D.; Brown, T. M.; Fetting, J. C.; Lips, F.; Tuononen, H. M.; Herber, R. H.; Power, P. P. Dispersion Forces and Counterintuitive Steric Effects in Main Group Molecules: Heavier Group 14 (Si–Pb) Dichalcogenolate Carbene Analogues with Sub-90° Interligand Bond Angles. *J. Am. Chem. Soc.* **2013**, *135*, 10134–10148. (f) Hadlington, T. J.; Abdalla, J. A. B.; Tirfoin, R.; Aldridge, S.; Jones, C. Stabilization of a two-coordinate, acyclic diaminosilylene (ADASI): completion of the series of isolable diaminoalkylsilylenes, E(NR<sub>2</sub>)<sub>2</sub> (E = group 14 element). *Chem. Commun.* **2016**, *52*, 1717–1720. (g) Wendel, D.; Porzelt, A.; Herz, F. A. D.; Sarkar, D.; Jandl, C.; Inoue, S.; Rieger, B. From Si(II) to Si(IV) and Back: Reversible Intramolecular Carbon–Carbon Bond Activation by an Acyclic Iminosilylene. *J. Am. Chem. Soc.* **2017**, *139*, 8134–8137. (h) Wendel, D.; Reiter, D.; Porzelt, A.; Altmann, P. J.; Inoue, S.; Rieger, B. Silicon and Oxygen's Bond of Affection: An Acyclic Three-Coordinate Silanone and Its Transformation to an Iminosiloxysilylene. *J. Am. Chem. Soc.* **2017**, *139*, 17193–17198. (i) Loh, Y. K.; Ying, L.; Angeles Fuentes, M.; Do, D. C. H.; Aldridge, S. An N-Heterocyclic Boryloxy Ligand Isoelectronic with N-Heterocyclic Imines: Access to an Acyclic Dioxysilylene and its Heavier Congeners. *Angew. Chem., Int. Ed.* **2019**, *58*, 4847–4851.
- (5) Protchenko, A. V.; Vasko, P.; Do, D. C. H.; Hicks, J.; Angeles Fuentes, M.; Jones, C.; Aldridge, S. Reduction of carbon oxides by an acyclic silylene: reductive coupling of CO. *Angew. Chem., Int. Ed.* **2019**, *58*, 1808–1812.
- (6) (a) Gaspar, P. P.; Beatty, A. M.; Chen, T.; Haile, T.; Lei, D.; Winchester, W. R.; Braddock-Wilking, J.; Rath, N. P.; Klooster, W. T.; Koetzle, T. F.; Mason, S. A.; Albinati, A. Tris(triisopropylsilyl)silane and the Generation of Bis(triisopropylsilyl)silylene. *Organometallics* **1999**, *18*, 3921–3932. (b) Jiang, P.; Gaspar, P. P. Tri-tert-butylsilyl(triisopropylsilyl)silylene (tBu)<sub>3</sub>Si–Si–Si(iPr)<sub>3</sub> and Chemical Evidence for Its Reactions from a Triplet Electronic State. *J. Am. Chem. Soc.* **2001**, *123*, 8622–8623.
- (7) (a) Sekiguchi, A.; Tanaka, T.; Ichinohe, M.; Akiyama, K.; Tero-Kubota, S. Bis(tri-tert-butylsilyl)silylene: Triplet Ground State Silylene. *J. Am. Chem. Soc.* **2003**, *125*, 4962–4963. (b) Sekiguchi, A.; Tanaka, T.; Ichinohe, M.; Akiyama, K.; Gaspar, P. P. Tri-tert-butylsilylsilylenes with Alkali Metal Substituents (tBu<sub>3</sub>Si)SiM (M = Li, K): Electronically and Sterically Accessible Triplet Ground States. *J. Am. Chem. Soc.* **2008**, *130*, 426–427.
- (8) (a) Klinkhammer, K. W. Tris(trimethylsilyl)silanides of the Heavier Alkali Metals—A Structural Study. *Chem. - Eur. J.* **1997**, *3*, 1418–1431. (b) Klinkhammer, K. W. In *Organosilicon Chemistry III: From Molecules to Materials*; Auner, N., Weis, J., Eds.; Wiley-VCH: Weinheim, 1998.
- (9) Ichinohe, M.; Kinjo, R.; Sekiguchi, A. The First Stable Methyl-Substituted Disilene: Synthesis, Crystal Structure, and Regiospecific MeLi Addition. *Organometallics* **2003**, *22*, 4621–4623.
- (10) (a) Marschner, C. Silylated Group 14 Ylenes: An Emerging Class of Reactive Compounds. *Eur. J. Inorg. Chem.* **2015**, *2015*, 3805–3820. (b) Nesterov, V.; Reiter, D.; Bag, P.; Frisch, P.; Holzner, R.; Porzelt, A.; Inoue, S. NHCs in Main Group Chemistry. *Chem. Rev.* **2018**, *118*, 9678–9842.
- (11) Tanaka, H.; Ichinohe, M.; Sekiguchi, A. An Isolable NHC-Stabilized Silylene Radical Cation: Synthesis and Structural Characterization. *J. Am. Chem. Soc.* **2012**, *134*, 5540–5543.
- (12) (a) Jana, A.; Omlor, I.; Huch, V.; Rzepa, H. S.; Scheschkewitz, D. N-Heterocyclic Carbene Coordinated Neutral and Cationic Heavier Cyclopropylidenes. *Angew. Chem., Int. Ed.* **2014**, *53*, 9953–9956. (b) Guddorf, B. J.; Hepp, A.; Lips, F. Efficient Synthesis of a NHC-Coordinated Trisilacyclopropylidene and Its Coordination Behavior. *Chem. - Eur. J.* **2018**, *24*, 10334–10338.
- (13) (a) Sakurai, H.; Nakadaira, Y.; Sakaba, H. Chemistry of organosilicon compounds. 181. Silylene-to-disilene and disilene-to-silylene rearrangements. *Organometallics* **1983**, *2*, 1484–1486. (b) Nagase, S.; Kudo, T. Silylene-disilene isomerizations. A theoretical study. *Organometallics* **1984**, *3*, 1320–1322.
- (14) Stanford, M. W.; Schweizer, J. L.; Menche, M.; Nichol, G. S.; Holthausen, M. C.; Cowley, M. J. Intercepting the Disilene-Silylsilylene Equilibrium. *Angew. Chem., Int. Ed.* **2019**, *58*, 1329–1333.
- (15) Detailed experimental and analytical data for the preparation of **1** and its precursors can be found in the Supporting Information.
- (16) Geometry optimizations and harmonic frequency calculations were performed at the M06-2X/6-31+G(d,p) level of density functional theory. NMR chemical shift values were calculated using the gauge-independent atomic orbital (GIAO) method implemented in *Gaussian 09* and the M06-L functional along with the 6-311G(2,p) basis set and the SMD solvent model for the structures obtained at the M06-2X/6-31+G(d,p) level of theory. For detailed information, see the Supporting Information.
- (17) Skell, P. S.; Woodworth, R. C. Structure of Carbene, CH<sub>2</sub>. *J. Am. Chem. Soc.* **1956**, *78*, 4496–4497.
- (18) (a) Pae, D. H.; Xiao, M.; Chiang, M. Y.; Gaspar, P. P. Diadamantylsilylene and its stereochemistry of addition. *J. Am. Chem. Soc.* **1991**, *113*, 1281–1288. (b) Zhang, S.; Wagenseller, P. E.; Conlin, R. T. Addition of dimethylsilylene to olefins. A reinvestigation. *J. Am. Chem. Soc.* **1991**, *113*, 4278–4281. (c) Kira, M.; Iwamoto, T.; Maruyama, T.; Kuzuguchi, T.; Yin, D.; Kabuto, C.; Sakurai, H. Hexakis(trialkylsilyl)cyclotrisilanes and photochemical generation of bis(trialkylsilyl)silylenes. *J. Chem. Soc., Dalton Trans.* **2002**, 1539–1544.
- (19) Ando, W.; Fujita, M.; Yoshida, H.; Sekiguchi, A. Stereochemistry of the addition of diarylsilylenes to *cis*- and *trans*-2-butenes. *J. Am. Chem. Soc.* **1988**, *110*, 3310–3311.
- (20) Wendel, D.; Szilvási, T.; Jandl, C.; Inoue, S.; Rieger, B. Twist of a Silicon–Silicon Double Bond: Selective Anti-Addition of Hydrogen to an Iminodisilene. *J. Am. Chem. Soc.* **2017**, *139*, 9156–9159.
- (21) (a) Kosai, T.; Iwamoto, T. Stable Push–Pull Disilene: Substantial Donor–Acceptor Interactions through the Si = Si Double Bond. *J. Am. Chem. Soc.* **2017**, *139*, 18146–18149. (b) Kosai, T.; Iwamoto, T. Cleavage of Two Hydrogen Molecules by Boryldisilenes. *Chem. - Eur. J.* **2018**, *24*, 7774–7780.
- (22) Personal communication: Prof. M. C. Holthausen (Goethe-Universität Frankfurt am Main); References for the additional calculations: (a) Riplinger, C.; Neese, F. An efficient and near linear scaling pair natural orbital based local coupled cluster method. *J. Chem. Phys.* **2013**, *138*, 034106. (b) Riplinger, C.; Sandhoefer, B.; Hansen, A.; Neese, F. Natural triple excitations in local coupled cluster calculations with pair natural orbitals. *J. Chem. Phys.* **2013**, *139*, 134101. (c) Kendall, R. A.; Dunning, T. H., Jr. Electron affinities of the first-row atoms revisited. Systematic basis sets and wave functions. *J. Chem. Phys.* **1992**, *96*, 6796–6806. (d) Woon, D. E.; Dunning, T. H., Jr. Gaussian basis sets for use in correlated molecular calculations. III. The atoms aluminum through argon. *J. Chem. Phys.* **1993**, *98*, 1358–1371. (e) Grimme, S.; Brandenburg, J. G.; Bannwarth, C.; Hansen, A. Consistent structures and interactions by density functional theory with small atomic orbital basis sets. *J. Chem. Phys.* **2015**, *143*, 054107.
- (23) Hoover, J. Ammonia activation at a metal. *Science* **2016**, *354*, 707–708.
- (24) (a) Power, P. P. Interaction of Multiple Bonded and Unsaturated Heavier Main Group Compounds with Hydrogen, Ammonia, Olefins, and Related Molecules. *Acc. Chem. Res.* **2011**, *44*, 627–637. (b) Yadav, S.; Saha, S.; Sen, S. S. Compounds with Low-Valent p-Block Elements for Small Molecule Activation and Catalysis. *ChemCatChem* **2016**, *8*, 486–501.



- (25) (a) Jana, A.; Schulzke, C.; Roesky, H. W. Oxidative Addition of Ammonia at a Silicon(II) Center and an Unprecedented Hydrogenation Reaction of Compounds with Low-Valent Group 14 Elements Using Ammonia Borane. *J. Am. Chem. Soc.* **2009**, *131*, 4600–4601. (b) Protchenko, A. V.; Bates, J. L.; Saleh, L. M. A.; Blake, M. P.; Schwarz, A. D.; Kolychev, E. L.; Thompson, A. L.; Jones, C.; Mountford, P.; Aldridge, S. Enabling and Probing Oxidative Addition and Reductive Elimination at a Group 14 Metal Center: Cleavage and Functionalization of E–H Bonds by a Bis(boryl)stannylenes. *J. Am. Chem. Soc.* **2016**, *138*, 4555–4564.
- (26) (a) Boomgaarden, S.; Saak, W.; Weidenbruch, M.; Marsmann, H. Ammonia and Chlorine Additions to a Tetrasilabuta-1,3-diene: Conglomerate versus Racemate Crystallization. *Z. Anorg. Allg. Chem.* **2001**, *627*, 349–352. (b) Meltzer, A.; Majumdar, M.; White, A. J. P.; Huch, V.; Scheschkevit, D. Potential Protecting Group Strategy for Disila Analogues of Vinylolithiums: Synthesis and Reactivity of a 2,4,6-Trimethoxyphenyl-Substituted Disilene. *Organometallics* **2013**, *32*, 6844–6850. (c) Wendel, D.; Szilvási, T.; Henschel, D.; Altmann, P. J.; Jandl, C.; Inoue, S.; Rieger, B. Precise Activation of Ammonia and Carbon Dioxide by an Iminodisilene. *Angew. Chem., Int. Ed.* **2018**, *57*, 14575–14579.
- (27) (a) Xiong, Y.; Yao, S.; Driess, M. An Isolable NHC-Supported Silanone. *J. Am. Chem. Soc.* **2009**, *131*, 7562–7563. (b) Xiong, Y.; Yao, S.; Müller, R.; Kaupp, M.; Driess, M. Activation of Ammonia by a Si = O Double Bond and Formation of a Unique Pair of Sila-Hemiaminal and Silanoic Amide Tautomers. *J. Am. Chem. Soc.* **2010**, *132*, 6912–6913. (c) Yao, S.; Xiong, Y.; Driess, M. N-Heterocyclic Carbene (NHC)-Stabilized Silanochalcogenones: NHC-Si(R)<sub>2</sub>=E (E = O, S, Se, Te). *Chem. - Eur. J.* **2010**, *16*, 1281–1288.
- (28) Driess, M.; Yao, S.; Brym, M.; Van Wüllen, C.; Lentz, D. A New Type of N-Heterocyclic Silylene with Ambivalent Reactivity. *J. Am. Chem. Soc.* **2006**, *128*, 9628–9629.
- (29) Yeong, H.-X.; Xi, H.-W.; Li, Y.; Lim, K. H.; So, C.-W. A Silyliumylidene Cation Stabilized by an Amidinate Ligand and 4-Dimethylaminopyridine. *Chem. - Eur. J.* **2013**, *19*, 11786–11790.
- (30) Avakyan, V. G.; Sidorkin, V. F.; Belogolova, E. F.; Gusevnikov, S. L.; Gusevnikov, L. E. AIM and ELF Electronic Structure/G2 and G3  $\pi$ -Bond Energy Relationship for Doubly Bonded Silicon Species, H<sub>2</sub>Si = X (X = E<sup>14</sup>H<sub>2</sub>, E<sup>15</sup>H, E<sup>16</sup>). *Organometallics* **2006**, *25*, 6007–6013.
- (31) Allred, A. L. Electronegativity values from thermochemical data. *J. Inorg. Nucl. Chem.* **1961**, *17*, 215–221.
- (32) Kapp, J.; Remko, M.; Schleyer, P. v. R. H<sub>2</sub>XO and (CH<sub>3</sub>)<sub>2</sub>XO Compounds (X = C, Si, Ge, Sn, Pb): Double Bonds vs Carbene-Like Structures—Can the Metal Compounds Exist at All? *J. Am. Chem. Soc.* **1996**, *118*, 5745–5751.
- (33) (a) Kudo, T.; Nagase, S. Theoretical study on the dimerization of silanone and the properties of the polymeric products (H<sub>2</sub>SiO)<sub>n</sub> (n = 2, 3, and 4). Comparison with dimers (H<sub>2</sub>SiS)<sub>2</sub> and (H<sub>2</sub>CO)<sub>2</sub>. *J. Am. Chem. Soc.* **1985**, *107*, 2589–2595. (b) Kimura, M.; Nagase, S. The Quest of Stable Silanones: Substituent Effects. *Chem. Lett.* **2001**, *30*, 1098–1099.
- (34) Xiong, Y.; Yao, S.; Driess, M. Chemical Tricks To Stabilize Silanones and Their Heavier Homologues with E = O Bonds (E = Si–Pb): From Elusive Species to Isolable Building Blocks. *Angew. Chem., Int. Ed.* **2013**, *52*, 4302–4311.
- (35) (a) Epping, J. D.; Yao, S.; Karni, M.; Apeloig, Y.; Driess, M. Si = X Multiple Bonding with Four-Coordinate Silicon? Insights into the Nature of the Si = O and Si = S Double Bonds in Stable Silanoic Esters and Related Thioesters: A Combined NMR Spectroscopic and Computational Study. *J. Am. Chem. Soc.* **2010**, *132*, 5443–5455. (b) Xiong, Y.; Yao, S.; Müller, R.; Kaupp, M.; Driess, M. From silicon(II)-based dioxigen activation to adducts of elusive dioxasiliranes and sila-ureas stable at room temperature. *Nat. Chem.* **2010**, *2*, 577–580. (c) Ahmad, S. U.; Szilvási, T.; Irran, E.; Inoue, S. An NHC-Stabilized Silicon Analogue of Acylium Ion: Synthesis, Structure, Reactivity, and Theoretical Studies. *J. Am. Chem. Soc.* **2015**, *137*, 5828–5836. (d) Hansen, K.; Szilvási, T.; Blom, B.; Irran, E.; Driess, M. From an Isolable Acyclic Phosphinosilylene Adduct to Donor-Stabilized Si = E Compounds (E = O, S, Se). *Chem. - Eur. J.* **2015**, *21*, 18930–18933. (e) Troadec, T.; Lopez Reyes, M.; Rodriguez, R.; Baceiredo, A.; Saffon-Merceron, N.; Kato, T. Donor-Stabilized Silacyclobutanone: A Precursor of 1-Silaketene via Retro-[2 + 2]-Cycloaddition Reaction at Room Temperature. *J. Am. Chem. Soc.* **2016**, *138*, 2965–2968.
- (36) (a) Yao, S.; Brym, M.; van Wüllen, C.; Driess, M. From a Stable Silylene to a Mixed-Valent Disiloxane and an Isolable Silaformamide–Borane Complex with Considerable Silicon–Oxygen Double-Bond Character. *Angew. Chem., Int. Ed.* **2007**, *46*, 4159–4162. (b) Xiong, Y.; Yao, S.; Driess, M. Silicon Analogues of Carboxylic Acids: Synthesis of Isolable Silanoic Acids by Donor–Acceptor Stabilization. *Angew. Chem., Int. Ed.* **2010**, *49*, 6642–6645. (c) Xiong, Y.; Yao, S.; Driess, M. Coordination of a Si = O subunit to metals: complexes of donor-stabilized silanone featuring a terminal Si = O→M coordination (M = Zn, Al). *Dalton Trans* **2010**, *39*, 9282–9287. (d) Gao, Y.; Hu, H.; Cui, C. The Reactivity of a Silacyclopentadienylidene towards Aldehydes: Silole Ring Expansion and the Formation of Base-Stabilized Silacyclohexadienones. *Chem. - Eur. J.* **2011**, *17*, 8803–8806. (e) Muraoka, T.; Abe, K.; Haga, Y.; Nakamura, T.; Ueno, K. Synthesis of a Base-Stabilized Silanone-Coordinated Complex by Oxygenation of a (Silyl)silylenetungsten Complex. *J. Am. Chem. Soc.* **2011**, *133*, 15365–15367. (f) Ghadwal, R. S.; Azhakar, R.; Roesky, H. W.; Pröpper, K.; Ditttrich, B.; Goedecke, C.; Frenking, G. Donor–acceptor stabilized silaformyl chloride. *Chem. Commun.* **2012**, *48*, 8186–8188. (g) Muraoka, T.; Abe, K.; Kimura, H.; Haga, Y.; Ueno, K.; Sunada, Y. Synthesis, structures, and reactivity of the base-stabilized silanone molybdenum complexes. *Dalton Trans* **2014**, *43*, 16610–16613. (h) Fukuda, T.; Hashimoto, H.; Sakaki, S.; Tobita, H. Stabilization of a Sila-aldehyde by its  $\eta_2$  Coordination to Tungsten. *Angew. Chem., Int. Ed.* **2016**, *55*, 188–192. (i) Lopez Reyes, M.; Troadec, T.; Rodriguez, R.; Baceiredo, A.; Saffon-Merceron, N.; Branchadell, V.; Kato, T. Donor/Acceptor-Stabilized 1-Silaketene: Reversible [2 + 2] Cycloaddition with Pyridine and Evolution by an Olefin Metathesis Reaction. *Chem. - Eur. J.* **2016**, *22*, 10247–10253. (j) Muraoka, T.; Kimura, H.; Trigagema, G.; Nakagaki, M.; Sakaki, S.; Ueno, K. Reactions of Silanone(silyl)tungsten and -molybdenum Complexes with MesCNO, (Me<sub>2</sub>SiO)<sub>3</sub>, MeOH, and H<sub>2</sub>O: Experimental and Theoretical Studies. *Organometallics* **2017**, *36*, 1009–1018.
- (37) (a) Filippou, A. C.; Baars, B.; Chernov, O.; Lebedev, Y. N.; Schnakenburg, G. Silicon–Oxygen Double Bonds: A Stable Silanone with a Trigonal-Planar Coordinated Silicon Center. *Angew. Chem., Int. Ed.* **2014**, *53*, 565–570. (b) Ishida, S.; Abe, T.; Hirakawa, F.; Kosai, T.; Sato, K.; Kira, M.; Iwamoto, T. Persistent Dialkylsilanone Generated by Dehydrobromination of Dialkylbromosilanol. *Chem. - Eur. J.* **2015**, *21*, 15100–15103. (c) Alvarado-Beltran, I.; Rosas-Sánchez, A.; Baceiredo, A.; Saffon-Merceron, N.; Branchadell, V.; Kato, T. A Fairly Stable Crystalline Silanone. *Angew. Chem., Int. Ed.* **2017**, *56*, 10481–10485. (d) Rosas-Sánchez, A.; Alvarado-Beltran, I.; Baceiredo, A.; Saffon-Merceron, N.; Massou, S.; Hashizume, D.; Branchadell, V.; Kato, T. Cyclic (Amino)(Phosphonium-Bora-Ylide)-Silanone: A Remarkably Room Temperature Persistent Silanone. *Angew. Chem., Int. Ed.* **2017**, *56*, 15916–15920.
- (38) (a) Yao, S.; Xiong, Y.; Brym, M.; Driess, M. An Isolable Silanoic Ester by Oxygenation of a Stable Silylene. *J. Am. Chem. Soc.* **2007**, *129*, 7268–7269. (b) Ghadwal, R. S.; Azhakar, R.; Roesky, H. W.; Pröpper, K.; Ditttrich, B.; Klein, S.; Frenking, G. Donor–Acceptor-Stabilized Silicon Analogue of an Acid Anhydride. *J. Am. Chem. Soc.* **2011**, *133*, 17552–17555. (c) Rodriguez, R.; Gau, D.; Troadec, T.; Saffon-Merceron, N.; Branchadell, V.; Baceiredo, A.; Kato, T. A Base-Stabilized Sila- $\beta$ -Lactone and a Donor/Acceptor-Stabilized Silanoic Acid. *Angew. Chem., Int. Ed.* **2013**, *52*, 8980–8983. (d) Rodriguez, R.; Troadec, T.; Gau, D.; Saffon-Merceron, N.; Hashizume, D.; Miquieu, K.; Sotiropoulos, J.-M.; Baceiredo, A.; Kato, T. Synthesis of a Donor-Stabilized Silacyclopropan-1-one. *Angew. Chem., Int. Ed.* **2013**, *52*, 4426–4430. (e) Wang, Y.; Chen, M.; Xie, Y.; Wei, P.; Schaefer, H. F., III; Robinson, G. H. Stabilization of Silicon–Carbon Mixed Oxides. *J. Am. Chem. Soc.* **2015**, *137*, 8396–8399. (f) Wang, Y.; Chen, M.; Xie,

Y.; Wei, P.; Schaefer, H. F., III; Schleyer, P. v. R.; Robinson, G. H. Stabilization of elusive silicon oxides. *Nat. Chem.* **2015**, *7*, 509–513. (g) Rodriguez, R.; Gau, D.; Saouli, J.; Baceiredo, A.; Saffon-Merceron, N.; Branchadell, V.; Kato, T. A Stable Monomeric SiO<sub>2</sub> Complex with Donor–Acceptor Ligands. *Angew. Chem., Int. Ed.* **2017**, *56*, 3935–3939. (h) Do, D. C. H.; Protchenko, A. V.; Angeles Fuentes, M.; Hicks, J.; Kolychev, E. L.; Vasko, P.; Aldridge, S. A  $\beta$ -diketiminato stabilized sila-acyl chloride: systematic access to base-stabilised silicon analogues of classical carbonyl compounds. *Angew. Chem., Int. Ed.* **2018**, *57*, 13907–13911. (i) Rodriguez, R.; Alvarado-Beltran, I.; Saouli, J.; Saffon-Merceron, N.; Baceiredo, A.; Branchadell, V.; Kato, T. Reversible CO<sub>2</sub> Addition to a Si = O Bond and Synthesis of a Persistent SiO<sub>2</sub>–CO<sub>2</sub> Cycloadduct Stabilized by a Lewis Donor–Acceptor Ligand. *Angew. Chem., Int. Ed.* **2018**, *57*, 2635–2638. (39) Bondi, A. van der Waals Volumes and Radii. *J. Phys. Chem.* **1964**, *68*, 441–451.

## 9. DMAP-stabilized bis(silyl)silylenes as versatile synthons for organosilicon compounds

**Title:** DMAP-stabilized bis(silyl)silylenes as versatile synthons for organosilicon compounds

**Status:** Article, published online January 21<sup>st</sup>, 2020

**Journal:** *RSC Advances*, **2020**, *10*, 3402-3406.

**Publisher:** Royal Society of Chemistry

**DOI:** [10.1039/C9RA10628F](https://doi.org/10.1039/C9RA10628F)

**Authors:** Richard Holzner, Dominik Reiter, Philipp Frisch, Shigeyoshi Inoue<sup>a</sup>

*Reprinted with permission. © 2020 The Royal Society of Chemistry*

**Content:** Electron donation of Lewis bases, such as NHCs to the vacant p-orbital of silylenes is oftentimes the only possibility to control their electrophilicity and to isolate these transient species. However, the reactivity of the resulting donor-acceptor adducts is significantly reduced.

DMAP, a weaker Lewis base, compared to NHCs was utilized in this publication to stabilize different bis(silyl)silylenes. Among these complexes was the first isolated bis(hypersilyl)silylene derivative. The weaker donor-acceptor interaction allowed for facile dissociation of DMAP at elevated temperatures, providing the extremely reactive free silylenes. Interestingly, all three silylene complexes showed distinctly different, thermally induced decomposition reactions: C–H bond activation, dearomative ring expansion of DMAP by the silylene fragment to an azasilepin and rearrangement in combination with TMS migrations were observed. Furthermore, the silylene complexes underwent H<sub>2</sub> and ethylene addition upon elevated temperatures, furnishing the corresponding dihydrosilanes and siliranes. DMAP-coordinated silaimines were obtained from the reactions with trimethylsilyl azide. Remarkably, over-reduction of (<sup>t</sup>Bu<sub>3</sub>Si)<sub>2</sub>SiBr<sub>2</sub> provided the corresponding K-substituted silyl radical.

In summary, novel, stable DMAP-bis(silyl)silylene complexes were synthesized and their thermal isomerization behavior was investigated. The weakly-coordinating DMAP allowed dissociation upon heating. Therefore, these complexes can be considered convenient synthetic equivalents for elusive bis(silyl)silylene species. In fact, the first single-site dihydrogen activation by donor-stabilized silylenes was achieved. The K-substituted silyl radical might allow access to functionalized silyl radicals *via* salt metathesis.

---

<sup>a</sup>R. Holzner and D. Reiter planned and executed all experiments and co-wrote the manuscript. P. Frisch conducted all SC-XRD measurements and processed the resulting data. All work was performed under the supervision of S. Inoue.



Cite this: *RSC Adv.*, 2020, 10, 3402Received 17th December 2019  
Accepted 6th January 2020

DOI: 10.1039/c9ra10628f

rsc.li/rsc-advances

## DMAP-stabilized bis(silyl)silylenes as versatile synthons for organosilicon compounds†

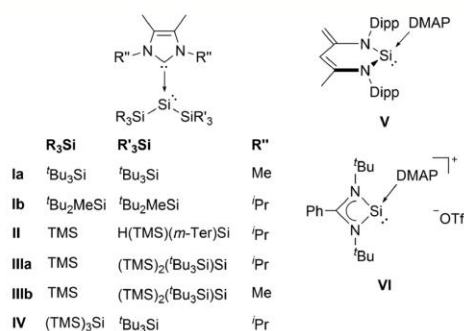
Richard Holzner,<sup>‡</sup> Dominik Reiter,<sup>‡</sup> Philipp Frisch and Shigeyoshi Inoue<sup>\*,†</sup>

DMAP-stabilized silylenes **1a–c** are obtained from the reductive debromination of the corresponding dibromosilanes in the presence of DMAP. Their distinctly different thermal isomerization reactions via C–H bond activation, dearomative ring expansion and silyl migration are discussed. Furthermore, complexes **1** dissociate at elevated temperatures, providing the corresponding free silylenes *in situ*, which are even capable of single-site activation of H<sub>2</sub>. Additionally, a potassium-substituted silicon-centered radical **2** is isolated from overreduction of (tBu<sub>3</sub>Si)<sub>2</sub>SiBr<sub>2</sub>.

### Introduction

Silylenes (R<sub>2</sub>Si), the heavier congeners of carbenes (R<sub>2</sub>C:) have attracted much attention in modern main group chemistry in recent years.<sup>1</sup> The substituents R can either be monodentate, or cyclic, bidentate ligands, as in the case of the extensively studied class of *N*-heterocyclic silylenes (NHSis). In general, silylenes possess a lone pair of electrons and an empty 3p<sub>z</sub> orbital and can therefore display amphiphilic reaction behaviour both as Lewis bases and Lewis acids. This particular reactivity profile even enables the facile activation of small molecules.<sup>2</sup> Thus, silylenes are considered to be promising candidates for metal-free catalysis.<sup>2</sup> In contrast to carbenes, however, the singlet ground state is energetically favoured for almost all reported silylenes. The two sole exceptions are transient silylenes bearing two bulky and strongly electropositive supersilyl (tBu<sub>3</sub>Si) substituents, or both supersilyl groups and alkali metal substituents. However, these species were only generated and analyzed *in situ* at temperatures below 15 K.<sup>3</sup> These reports already underline the peculiarity of bis(silyl)silylenes. In fact, no room temperature stable, two-coordinate derivative has been isolated to date. In all synthetic attempts the extremely reactive bis(silyl)silylene was not stable and either silyl migration<sup>4</sup> or C–H bond activation occurred, even at low temperatures.<sup>3a</sup> Very recently, we presented a bis(silyl)silylene that undergoes reversible isomerization to the corresponding tetra(silyl)disilene.<sup>5</sup> Although this compound is relatively stable, it eventually decomposes *via* insertion of the silylene moiety into a C–H bond of a substituent. A convenient method to stabilize silylenes is to

control their excessive electrophilicity by coordination of a Lewis base, as already recognized by Tokitoh and co-workers in 1997.<sup>6</sup> In fact, electron donation from *N*-heterocyclic carbenes (NHCs) was the only way so far to isolate bis(silyl)silylenes.<sup>7</sup> Sekiguchi *et al.* successfully employed this approach and obtained the NHC-stabilized silylenes **I** (Fig. 1).<sup>8</sup> Lately, several additional examples of acyclic bis(silyl)silylene NHC complexes were reported by Cowley (**II**)<sup>9</sup> and by our group (**III** and **IV**).<sup>5</sup> Besides those acyclic representatives, the groups of Scheschkewitz<sup>10</sup> and Lips<sup>11</sup> synthesized NHC-stabilized silylenes with the low-coordinate silicon center being embedded in a three-membered silicon cycle. Although electron-donation of NHCs to the vacant p-orbital of silylenes is an effective method to allow isolation of these compounds, it brings the downside of a significantly reduced reactivity. Accordingly, none of the



TMS = Me<sub>3</sub>Si; DMAP = 4-*N,N*-dimethylaminopyridine,  
*m*-Ter = 2,6-(2,4,6-Me<sub>3</sub>-C<sub>6</sub>H<sub>2</sub>)<sub>2</sub>-C<sub>6</sub>H<sub>3</sub>; Dipp = 2,6-Pr<sub>2</sub>-C<sub>6</sub>H<sub>3</sub>

Fig. 1 Acyclic NHC-stabilized bis(silyl)silylenes **I–IV** and low-coordinate silicon DMAP complexes **V** and **VI**.

Department of Chemistry, WACKER-Institute of Silicon Chemistry and Catalysis Research Center, Lichtenbergstraße 4, 85748 Garching bei München, Germany. E-mail: s.inoue@tum.de

† Electronic supplementary information (ESI) available: Experimental details and crystallographic data. CCDC 1967942–1967945. For ESI and crystallographic data in CIF or other electronic format see DOI: 10.1039/c9ra10628f

‡ R. H. and D. R. contributed equally to this work.



examples listed is capable of activating small molecules such as dihydrogen. Therefore, a weaker donor–acceptor interaction is necessary to achieve a balance between reactivity and stability of the respective bis(silyl)silylene compounds. 4-*N,N*-Dimethylaminopyridine (DMAP) is a much weaker Lewis base, compared to NHCs and was already applied by the groups of Driess<sup>12</sup> and So<sup>13</sup> to isolate the low-coordinate silicon donor–acceptor complexes **V** and **VI**. Thus, we envisioned DMAP to be a suitable Lewis base, strong enough to stabilize elusive bis(silyl)silylenes, yet weak enough to partially maintain their reactivity. Very recently, we reported the first acyclic bis(silyl)silylene–DMAP adduct **1a** (cf. Scheme 1).<sup>5</sup>

Herein, we extend this class of donor-stabilized, highly reactive bis(silyl)silylenes. Decomposition pathways and reactivity of these novel silylenes are presented and discussed in detail. Additionally, we report the synthesis and characterization of the potassium-substituted silyl radical **2**.

## Results and discussion

### Synthesis of novel DMAP–silylene complexes **1** and radical **2**

In an approach analogue to the synthesis of **1a**, we obtained the donor-stabilized bis(silyl)silylene **1b** from the reductive debromination of the corresponding dibromosilane with  $\text{KC}_8$  in presence of DMAP (Scheme 1). Silylene **1b** was obtained as red-brown crystals in excellent yield (92%) and fully characterized. Neither the formation of any decomposition products, nor of the disilene  $(^t\text{Bu}_2\text{MeSi})_2\text{Si}=\text{Si}(^t\text{Bu}_2\text{Me})_2$ <sup>14</sup> was observed during the synthesis. Compared to compound **1a**, the <sup>29</sup>Si NMR signal of the silylene Si atom in **1b** is slightly upfield-shifted to 61.5 ppm (68.8 ppm in **1a**). Single crystal X-ray diffraction (SC-XRD) analysis revealed a Si–N<sup>DMAP</sup> bond length in compound **1b** of 1.937(5) Å (Fig. 2). This value is essentially identical to that in **1a** (1.942(2) Å)<sup>5</sup> and clearly within the range of previously reported low-coordinate silicon–DMAP donor–acceptor complexes (1.84–2.01 Å).<sup>9,12,13,15</sup> The high degree of pyramidalization around the silylene center in **1b** (sum of bond angles  $\Sigma\theta = 318.1^\circ$ ) results from the stereo-chemically active electron lone pair and also compares very well to **1a** ( $\Sigma\theta = 318.7^\circ$ ).<sup>5</sup>

Additionally, the steric hindrance of the silylene center was increased by introducing bulky hypersilyl groups ( $(\text{TMS})_3\text{Si}$ ), resulting in complex **1c**. Compound **1c**, which is the first stable bis(hypersilyl)silylene species, was identified by the characteristic <sup>29</sup>Si NMR signal of the low-coordinate silicon nucleus (72.5 ppm), similar to the resonances of **1a** and **1b**.<sup>5</sup> Remarkably, in

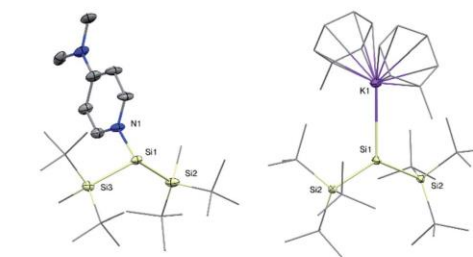
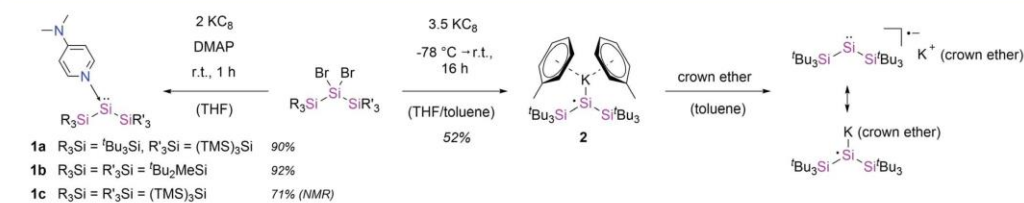


Fig. 2 Molecular structures of silylene **1b** (left) and silyl radical **2** (right) with thermal ellipsoids drawn at the 30% probability level. Hydrogen atoms are omitted for clarity. Selected bond lengths [Å] and angles [°]: **1b**: Si1–N1 1.937(5), Si1–Si2 2.390(3), Si1–Si3 2.378(3), Si2–Si1–Si3 123.1(1), Si2–Si1–N1 96.2(2), Si3–Si1–N1 98.8(2); **2**: Si1–Si2 2.3936(14), Si1–K1 3.315(2), K1–Si1–Si2 114.91(2), Si2–Si1–Si2\* 130.19(3).

this case, the facile TMS-migrations were prevented by the coordination of DMAP and the silylene could be stabilized successfully. In sharp contrast, we were not able to isolate the bis(hypersilyl)silylene moiety with NHCs. This result underlines the difference in reactivity between NHCs and the weaker Lewis base DMAP. Unfortunately, the reaction was accompanied by the by-product formation of hexakis(trimethylsilyl)trisilirane (**4**) and  $\text{Si}(\text{TMS})_4$ , reflecting the high propensity of hypersilyl groups towards TMS-group migrations.

Despite several attempts, we were not able to isolate the DMAP-stabilized bis(supersilyl) silylene  $(^t\text{Bu}_3\text{Si})_2\text{Si} \leftarrow \text{DMAP}$  with the same approach used for the syntheses of **1**. Even at low temperatures, the reduction of the corresponding dibromosilane only afforded the decomposition product of the free silylene (disilene from C–H bond activation).<sup>3a</sup> With an excess of 3.5 equivalents of  $\text{KC}_8$ , however the potassium-substituted silyl radical **2** was generated, even in the presence of DMAP. The solid state structure of **2** was unambiguously determined by SC-XRD analysis (Fig. 2). Silyl radical **2** exhibits a completely planar geometry (sum of bond angles  $\Sigma\theta = 360.0^\circ$ ) which is typical for alkali metal-substituted silyl radicals.<sup>16</sup> The Si–K bond distance (3.315(2) Å) is in the same range as observed in four-coordinate potassium silanides, such as hypersilyl potassium (3.352(4) Å).<sup>16</sup> Thus compound **2** is clearly a contact ion pair in the solid state. Unfortunately, **2** is extremely sensitive and decomposes in toluene solution. Therefore, no satisfactory spectroscopic data was obtained. After synthesis in absence of DMAP and



Scheme 1 Synthesis of DMAP-stabilized silylenes **1a–c** and silyl radical **2**.



stabilization by crown ether (18-C-6) however, we were able to obtain an EPR spectrum which contains a signal with a  $g$  value of 2.0056 and a hyperfine coupling  $a(\alpha\text{-}^{29}\text{Si}) = 2.92$  mT (see ESI, Fig. S7†). Coupling with the  $\beta\text{-}^{29}\text{Si}$  nuclei was not observable. This  $g$  value is in the same range, as it was reported for other alkali metal-substituted silyl radicals.<sup>16,17</sup> Furthermore, no signal splitting from coupling of the unpaired electron with the K nucleus was observed. Presumably, in solution, compound 2 in presence of crown ether exists as solvent-separated ion pair. This observation is consistent with reports of a potassium substituted silyl radical.<sup>16</sup>

### Thermally induced isomerization of 1

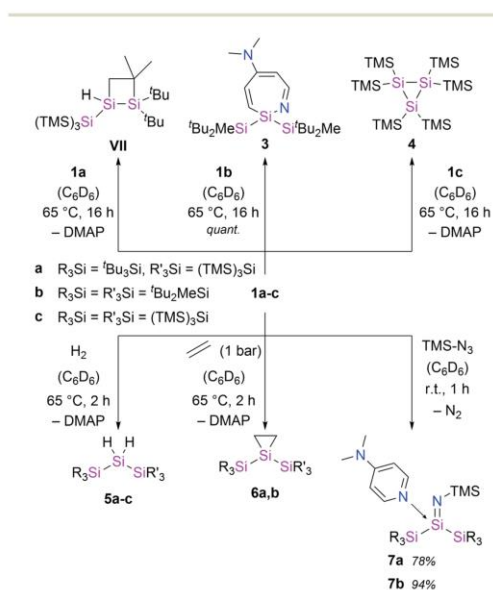
With the novel silylene complexes 1 in hand, we initially tested their thermal stability. Silylene 1a isomerizes to the respective disilene VII via DMAP dissociation and subsequent C–H bond activation at elevated temperatures (Scheme 2). The same product, that was observed for the decomposition of the donor-free disilene/silylene equilibrium mixture.<sup>5</sup> Surprisingly, upon heating compound 1b to 65 °C, the silylene fragment inserts into the pyridine ring of DMAP, generating azasilepin 3 by dearomatic ring expansion in quantitative yield. Silepin formation via insertion of a silylene into an aromatic ring system has previously been reported,<sup>18</sup> oftentimes either thermally<sup>19</sup> or photochemically<sup>20</sup> induced. After transformation from 1b to 3 and thus increase of the coordination number, the <sup>29</sup>Si NMR signal of the central silicon atom is strongly upfield-shifted to –28.1 ppm. This value is comparable to that of a similar compound, reported by Tokitoh *et al.* from the

reaction of a transient, *in situ* generated bis(aryl)silylene with DMAP (–20.8 ppm).<sup>21</sup> In comparison to 1b, the Si–N bond distance in 3 is shortened by 10% to 1.750(1) Å, indicating a covalent bonding-type instead of the dative interaction in 1b. This bond length is identical to that in Tokitoh's azasilepin.<sup>21</sup> Furthermore, the Si center adopts a tetrahedral coordination sphere within the boat-shaped, seven-membered heterocyclic ring (*cf.* Fig. 3). In sharp contrast to the related compounds 1a and 1b however, the thermal decomposition of silylene 1c does not proceed via C–H, or C–N bond activation, but in fact by silyl migration. At 65 °C, 1c isomerizes under liberation of DMAP to the cyclic silane 4, which was already observed from rearrangement of ((TMS)<sub>3</sub>Si)<sub>2</sub>Si: in the attempted synthesis of the free silylene.<sup>14,d</sup>

### Small molecule activation by silylenes 1

Single-site activation of the enthalpically strong, apolar dihydrogen molecule remains a challenging task for low-coordinate silicon compounds. So far, this was only achieved by few acyclic, donor-free silylenes and a masked iminosilyl silylene.<sup>5,18a,22</sup> In fact, to date, there are no reports of H<sub>2</sub> activation by a silylene base complex.

Although, the thermal decomposition reactions of 1a–c strongly depend on the silyl substituents and proceed via three different mechanisms, they are all based on the extreme reactivity of the respective free silylene. Furthermore, the calculated Gibbs free bond-dissociation energy of 1a (15.3 kcal mol<sup>–1</sup>),<sup>5</sup> which is lower than for the analogous, NHC-coordinated (hypersilyl)(supersilyl)silylene IV<sup>5</sup> (16.3 kcal mol<sup>–1</sup>)<sup>5</sup> also suggests a higher reactivity of the DMAP–silylene complexes, compared to the NHC-stabilized bis(silyl)silylenes. Therefore, we conceived compounds 1a–c to be easily accessible synthetic equivalents for these unstable, elusive, donor-free bis(silyl)silylenes and conducted a reactivity study towards activation of small molecules. Indeed, all three DMAP–silylenes underwent dihydrogen addition reactions upon heating to 65 °C, furnishing the reported corresponding dihydrosilanes 5a–c in



Scheme 2 Thermally-induced decomposition of silylenes 1 and synthesis of hydrosilanes 5, siliranes 6 and silaimines 7.

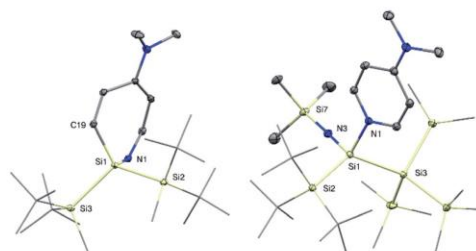


Fig. 3 Molecular structures of azasilepin 3 (left) and silaimine 7a (right) with thermal ellipsoids drawn at the 30% probability level. Hydrogen atoms are omitted for clarity. Selected bond lengths [Å] and angles [°]: 3: Si1–N1 1.750(1), Si1–C19 1.878(1), Si1–Si2 2.4144(6), Si2–Si1–Si3 113.74(2), Si2–Si1–N1 109.08(4), N1–Si1–C19 104.71(5); 7a: Si1–Si2 2.453(1), Si1–N1 1.928(2), Si1–N3 1.616(2), N3–Si7 1.660(2), Si2–Si1–Si3 125.08(3), N1–Si1–N3 106.08(8), Si1–N3–Si7 177.1(1).



quantitative yields. (Scheme 2).<sup>5,23</sup> Remarkably, the oxidative addition of dihydrogen to the DMAP-silylene complexes proceeds in a selective fashion, without the formation of the respective decomposition products. Free DMAP was simply removed from the product by precipitation with one equivalent of SiBr<sub>4</sub> and subsequent filtration. Notably, no reaction was observed upon exposure of NHC-stabilized bis(silyl)silylenes **1a** and **11a** to H<sub>2</sub>, even at elevated temperatures. This result underlines the inherently high reactivity of bis(silyl)silylene–DMAP complexes upon thermal dissociation of the stabilizing donor. Presumably, the H<sub>2</sub> addition to the silylene fragments of **1** proceeds *via* a bimolecular reaction similar to that proposed for the free silylene (tBu<sub>3</sub>Si)((TMS)<sub>3</sub>Si)Si.<sup>5</sup>

Additional reactivity investigations were carried out with **1a** and **1b** due to their easier accessibility. Silirane formation – was observed after treatment of **1a** and **1b** with ethylene, yielding compounds **6**. The <sup>29</sup>Si NMR shift of the central Si-atom in **6b** (–174.5 ppm) is similar to that of the earlier reported **6a** (–164.3 ppm).<sup>5</sup>

Since the isolation of the first silimine by Wiberg *et al.* in 1985,<sup>24</sup> a number of these heavier imine analogues have been published. Besides donor free examples,<sup>25</sup> many silimines need additional stabilization by a coordinating Lewis base, such as NHCs.<sup>7</sup> Interestingly, reaction of **1a** and **1b** with trimethylsilyl azide furnishes the DMAP-coordinated silimines **7** under liberation of gaseous N<sub>2</sub>. The <sup>29</sup>Si NMR signals of the central Si atoms in **7a** and **7b** were observed at –25.9 ppm and –25.5 ppm, respectively. Compared to a silimine–pyridine adduct (<sup>29</sup>Si = –12.6 ppm),<sup>25b</sup> these resonances are slightly upfield-shifted, presumably due to the electropositive silyl groups. In the solid state, compound **7a** displays a tetrahedral coordination sphere around the silicon center. Silimine **7a** contains three unique Si–N bonds, distinguishable by their characteristic lengths: a short Si=N bond (1.616(2) Å), a significantly longer Si7–N3 single bond to the TMS group (1.660(2) Å) and an even further elongated, dative Si–N<sup>DMAP</sup> bond (1.928(2) Å). The central Si=N distance is slightly longer, than in the donor-free silimines, from the groups of Wiberg and Kira (1.57–1.59 Å)<sup>25a,25c</sup> and essentially identical to Klingebiel's silimine–pyridine adduct (1.611(2) Å).<sup>25b</sup> Interestingly, the geometry of the imino group is almost linear ( $\theta = 177.1(1)^\circ$ ). A similar observation was reported by Kira *et al.* and attributed to the electronic properties of the TMS group.<sup>25c</sup> Notably, compound **7a** slowly decomposes in solution under liberation of DMAP and probably formation of the donor-free silimine, which decomposes further to a mixture of unidentified species. Complex **7b** instead is stable in solution.

## Conclusions

In summary, we utilized our recently published method to synthesize two novel DMAP-stabilized silylenes **1b** and **1c**. Compound **1c** is the first stable bis(hypersilyl)silylene complex, which could be synthesized so far. Surprisingly, silyl radical **2** was obtained in a related fashion from the over-reduction of the corresponding dibromosilane. The silylene complexes **1a–c** turned out to undergo facile oxidative addition with dihydrogen

and ethylene at relatively mild conditions. This remarkable reactivity originates from the respective free silylenes, which are generated *in situ* from dissociation of complexes **1**. Stabilization of transient bis(silyl)silylenes with DMAP is the only method so far to isolate these species and reactivate their extreme reactivity upon dissociation. Therefore, complexes **1** can be considered easily accessible, stable synthetic equivalents of otherwise elusive bis(silyl)silylenes. Additionally, the unprecedented, DMAP-coordinated silimines **7** were isolated from the reactions of the silylene complexes with trimethylsilyl azide.

## Conflicts of interest

The authors declare no conflict of interest.

## Acknowledgements

We are exceptionally grateful to the WACKER Chemie AG and the European Research Council (SILION 637394) for continued financial support. We thank Dr Oksana Storcheva for the EPR measurements.

## Notes and references

- For selected reviews on silylenes see: (a) M. Haaf, T. A. Schmedake and R. West, *Acc. Chem. Res.*, 2000, **33**, 704–714; (b) B. Gehrhus and M. F. Lappert, *J. Organomet. Chem.*, 2001, **617–618**, 209–223; (c) S. Nagendran and H. W. Roesky, *Organometallics*, 2008, **27**, 457–492; (d) Y. Mizuhata, T. Sasamori and N. Tokitoh, *Chem. Rev.*, 2009, **109**, 3479–3511; (e) M. Kira, *Chem. Commun.*, 2010, **46**, 2893–2903; (f) M. Asay, C. Jones and M. Driess, *Chem. Rev.*, 2011, **111**, 354–396; (g) S. Yao, Y. Xiong and M. Driess, *Organometallics*, 2011, **30**, 1748–1767; (h) S. S. Sen, S. Khan, S. Nagendran and H. W. Roesky, *Acc. Chem. Res.*, 2012, **45**, 578–587; (i) S. S. Sen, S. Khan, P. P. Samuel and H. W. Roesky, *Chem. Sci.*, 2012, **3**, 659–682; (j) B. Blom and M. Driess, in *Functional Molecular Silicon Compounds II*, ed. D. Scheschkewitz, Springer, Cham, 2013, vol. 156, pp. 85–123.
- (a) P. P. Power, *Nature*, 2010, **463**, 171–177; (b) C. Weetman and S. Inoue, *ChemCatChem*, 2018, **10**, 4213–4228.
- (a) A. Sekiguchi, T. Tanaka, M. Ichinohe, K. Akiyama and S. Tero-Kubota, *J. Am. Chem. Soc.*, 2003, **125**, 4962–4963; (b) A. Sekiguchi, T. Tanaka, M. Ichinohe, K. Akiyama and P. P. Gaspar, *J. Am. Chem. Soc.*, 2008, **130**, 426–427.
- (a) K. W. Klinkhammer, *Chem.–Eur. J.*, 1997, **3**, 1418–1431; (b) M. Ichinohe, R. Kinjo and A. Sekiguchi, *Organometallics*, 2003, **22**, 4621–4623; (c) K. Hassler, A. Dzambaski and J. Baumgartner, *Silicon Chem.*, 2008, **3**, 271–288; (d) C. Marschner, *Eur. J. Inorg. Chem.*, 2015, **2015**, 3805–3820; (e) S. K. Mueller, A. Dzambaski, N. Altenhuber, A. Torvisco, K. Hassler and M. Flock, *J. Mol. Struct.*, 2015, **1099**, 197–203; (f) M. Haas, A. Knoechl, T. Wiesner, A. Torvisco, R. Fischer and C. Jones, *Organometallics*, 2019, **38**, 4158–4170.





- 5 D. Reiter, R. Holzner, A. Porzelt, P. J. Altmann, P. Frisch and S. Inoue, *J. Am. Chem. Soc.*, 2019, **141**, 13536–13546.
- 6 N. Takeda, H. Suzuki, N. Tokitoh, R. Okazaki and S. Nagase, *J. Am. Chem. Soc.*, 1997, **119**, 1456–1457.
- 7 V. Nesterov, D. Reiter, P. Bag, P. Frisch, R. Holzner, A. Porzelt and S. Inoue, *Chem. Rev.*, 2018, **118**, 9678–9842.
- 8 H. Tanaka, M. Ichinohe and A. Sekiguchi, *J. Am. Chem. Soc.*, 2012, **134**, 5540–5543.
- 9 M. W. Stanford, J. I. Schweizer, M. Menche, G. S. Nichol, M. C. Holthausen and M. J. Cowley, *Angew. Chem., Int. Ed.*, 2019, **58**, 1329–1333.
- 10 A. Jana, I. Omlor, V. Huch, H. S. Rzepa and D. Scheschkewitz, *Angew. Chem., Int. Ed.*, 2014, **53**, 9953–9956.
- 11 B. J. Guddorf, A. Hepp and F. Lips, *Chem.–Eur. J.*, 2018, **24**, 10334–10338.
- 12 Y. Xiong, S. Yao, R. Müller, M. Kaupp and M. Driess, *J. Am. Chem. Soc.*, 2010, **132**, 6912–6913.
- 13 H.-X. Yeong, H.-W. Xi, Y. Li, K. H. Lim and C.-W. So, *Chem.–Eur. J.*, 2013, **19**, 11786–11790.
- 14 A. Sekiguchi, S. Inoue, M. Ichinohe and Y. Arai, *J. Am. Chem. Soc.*, 2004, **126**, 9626–9629.
- 15 T. Yamaguchi and A. Sekiguchi, *J. Am. Chem. Soc.*, 2011, **133**, 7352–7354.
- 16 S. Inoue, M. Ichinohe and A. Sekiguchi, *Organometallics*, 2008, **27**, 1358–1360.
- 17 (a) D. Bravo-Zhivotovskii, I. Ruderfer, S. Melamed, M. Botoshansky, B. Tumanskii and Y. Apeloig, *Angew. Chem., Int. Ed.*, 2005, **44**, 739–743; (b) S. Ishida, T. Iwamoto and M. Kira, *J. Am. Chem. Soc.*, 2003, **125**, 3212–3213; (c) G. Molev, D. Bravo-Zhivotovskii, M. Karni, B. Tumanskii, M. Botoshansky and Y. Apeloig, *J. Am. Chem. Soc.*, 2006, **128**, 2784–2785; (d) S. Inoue, M. Ichinohe and A. Sekiguchi, *J. Am. Chem. Soc.*, 2007, **129**, 6096–6097.
- 18 (a) D. Wendel, A. Porzelt, F. A. D. Herz, D. Sarkar, C. Jandl, S. Inoue and B. Rieger, *J. Am. Chem. Soc.*, 2017, **139**, 8134–8137; (b) S. Ishida, T. Tamura and T. Iwamoto, *Dalton Trans.*, 2018, **47**, 11317–11321.
- 19 (a) H. Suzuki, N. Tokitoh and R. Okazaki, *J. Am. Chem. Soc.*, 1994, **116**, 11572–11573; (b) H. Suzuki, N. Tokitoh and R. Okazaki, *Bull. Chem. Soc. Jpn.*, 1995, **68**, 2471–2481.
- 20 (a) M. Kira, S. Ishida, T. Iwamoto and C. Kabuto, *J. Am. Chem. Soc.*, 2002, **124**, 3830–3831; (b) M. Kira, S. Ishida, T. Iwamoto, A. de Meijere, M. Fujitsuka and O. Ito, *Angew. Chem., Int. Ed.*, 2004, **43**, 4510–4512; (c) T. Kosai, S. Ishida and T. Iwamoto, *Chem. Commun.*, 2015, **51**, 10707–10709.
- 21 Y. Mizuhata, T. Sato and N. Tokitoh, *Heterocycles*, 2012, **84**, 413–418.
- 22 (a) A. V. Protchenko, K. H. Birjkumar, D. Dange, A. D. Schwarz, D. Vidovic, C. Jones, N. Kaltsoyannis, P. Mountford and S. Aldridge, *J. Am. Chem. Soc.*, 2012, **134**, 6500–6503; (b) A. V. Protchenko, A. D. Schwarz, M. P. Blake, C. Jones, N. Kaltsoyannis, P. Mountford and S. Aldridge, *Angew. Chem., Int. Ed.*, 2013, **52**, 568–571.
- 23 (a) T. Gross, H. Reinke and H. Oehme, *Can. J. Chem.*, 2000, **78**, 1399–1404; (b) A. Sekiguchi, T. Fukawa, M. Nakamoto, V. Y. Lee and M. Ichinohe, *J. Am. Chem. Soc.*, 2002, **124**, 9865–9869.
- 24 N. Wiberg, K. Schurz and G. Fischer, *Angew. Chem., Int. Ed. Engl.*, 1985, **24**, 1053–1054.
- 25 (a) N. Wiberg, K. Schurz, G. Reber and G. Müller, *J. Chem. Soc., Chem. Commun.*, 1986, 591–592; (b) J. Niesmann, U. Klingebiel, M. Schäfer and R. Boese, *Organometallics*, 1998, **17**, 947–953; (c) T. Iwamoto, N. Ohnishi, Z. Gui, S. Ishida, H. Isobe, S. Maeda, K. Ohno and M. Kira, *New J. Chem.*, 2010, **34**, 1637–1645; (d) S. Inoue and K. Leszczyńska, *Angew. Chem., Int. Ed.*, 2012, **51**, 8589–8593; (e) J. Keuter, A. Hepp, C. Mück-Lichtenfeld and F. Lips, *Angew. Chem., Int. Ed.*, 2019, **58**, 4395–4399; (f) A. V. Protchenko, P. Vasko, D. C. H. Do, J. Hicks, M. Ángeles Fuentes, C. Jones and S. Aldridge, *Angew. Chem., Int. Ed.*, 2019, **58**, 1808–1812.



## 10. Iminodisilenes: Striking Reactivity in Small Molecule Activation

**Title:** Iminodisilenes: Striking Reactivity in Small Molecule Activation

**Status:** Draft (Article)

**Authors:** Richard Holzner, Philipp Frisch, Daniel Wendel, Shigeyoshi Inoue<sup>a</sup>

**Content:** Hypersilyl-substituted iminosilyldisilene **L27** has already shown interesting reactivity towards small molecules, such as dihydrogen, CO<sub>2</sub>, NH<sub>3</sub> and N<sub>2</sub>O. However, further investigation of this novel class of disilenes is difficult due to the instability of **L27** in solution at room temperature and the moderate achievable yield.

Hence, the disilene structure was modified by introducing different silyl groups. The extremely bulky supersilyl group forced the resulting iminodisilene **2a** to adopt (*E*)-configuration, in contrast to **L27**. Introduction of <sup>t</sup>Bu<sub>2</sub>MeSi groups on the other hand, provided the completely stable **2b**, which can be isolated in high yields, because of the simplified removal of the byproduct *via* sublimation. Interestingly, **2b** shows (*E/Z*)-isomerization to a temperature-dependent equilibrium mixture which was monitored by VT NMR spectroscopy. Initial reactivity studies towards H<sub>2</sub> and oxygen transfer reagents confirmed the similarity to **L27**. Furthermore, the corresponding cationic radical of **2b** was obtained by one-electron oxidation. EPR spectroscopy revealed coupling of the unpaired electron with the <sup>14</sup>N nuclei of the NHI ligand. On a final note, this manuscript outlines the unique activation of white phosphorus by iminodisilene **2b**. In the resulting unprecedented product, the base of the P<sub>4</sub> tetrahedron is substituted by the former low-coordinate silicon centers.

In total, this contribution provides two novel iminodisilenes **2**, of which **2b** is easily accessible and highly stable, even at elevated temperatures. Based on this compound, the second example of a disilene radical cation and the activation of P<sub>4</sub> were achieved. The disilenes and their addition products were thoroughly characterized. Furthermore, the stable nature of **2b** will allow further reactivity investigations of iminodisilenes, possibly even in regard to transition metal-free catalysis.

Notably, this is not the final version of the draft. In order to shed light on the isomerization mechanism and to gain further insight into the electronic structure and the observed reactivity of iminodisilene **2b**, DFT calculations are currently ongoing. These additional results will be incorporated and discussed in the final manuscript.

---

<sup>a</sup>R. Holzner planned and executed all experiments and wrote the manuscript. P. Frisch conducted all SC-XRD measurements and processed the resulting data. D. Wendel obtained single crystals from compound **2a**. All work was performed under the supervision of S. Inoue.

### Iminosilyldisilenes: Striking Reactivity in Small Molecule Activation

Richard Holzner, Philipp Frisch, Daniel Wendel, and Shigeyoshi Inoue\*

Department of Chemistry, WACKER-Institute of Silicon Chemistry and Catalysis Research Center, Lichtenbergstraße 4, 85748 Garching bei München, Germany

Supporting Information Placeholder

**ABSTRACT:** Iminodisilenes have shown intriguing reactivity, especially in the activation of small molecules such as H<sub>2</sub>. Herein we greatly enhanced their versatility by variation of the kinetically stabilizing silyl groups and thereby creating highly stable compounds **1** and **2** with indefinite lifetimes in solution. Disilene **2**, which shows temperature-dependent (*E/Z*)-isomerization was thoroughly investigated experimentally. The reaction products with H<sub>2</sub>, oxygenation- and bromination reagents were isolated and analyzed. Additionally, **2** was converted to the corresponding radical cation **8**. Furthermore, a novel silaphosphide structure **9**, based on the tetrahedral P<sub>4</sub> cage was synthesized and conclusions on iminodisilene reactivity, compared to tetraaryl and tetrasilyl disilenes, are drawn.

#### INTRODUCTION

Without a doubt, the isolation of Mes<sub>2</sub>Si=SiMes<sub>2</sub> (**1**), the first disilene by West et al. in 1981 was one of the biggest milestones in modern main group chemistry (Chart 1).<sup>1</sup> With that, the long existing so called "double bond rule"<sup>2</sup> was finally disproven and a large field of research in low-valent silicon chemistry was opened up. To date, a plethora of these heavier alkene analogues have been reported.<sup>3-9</sup> In strong contrast to alkenes, disilenes can adopt *trans*-bent geometries due to their electronic structures. Since the silylene fragments are in a singlet ground state, they have to rotate in relation to each other, in order to form bonding interactions between the doubly-occupied *s*-type orbitals and the vacant *p*-orbitals. This results in a *trans*-bent angle  $\theta$  between the SiR<sub>2</sub> planes and the Si=Si axis. Furthermore, a twist of the two SiR<sub>2</sub> planes can occur, described by the twist angle  $\tau$ , thereby allowing a large range of possible disilene structures (for definition of  $\theta$  and  $\tau$ , see Chart 1).<sup>5</sup> This structural flexibility is an intriguing feature of disilenes and allows for design of their geometry.

In the majority of reported disilenes, the highly reactive Si=Si double bond is kinetically stabilized by sterically demanding substituents, such as aryl or silyl groups. The choice of these substituents has a profound impact on the structural configuration (cf. Chart 1). Bulky silyl groups, for example lead to the planar disilenes **II**<sup>10</sup> and **III**<sup>11</sup>. With increased steric demand of the silyl group, however, the twisted character becomes more pronounced, thus minimizing the steric repulsion between the substituents. On the other hand, an increasing number of  $\pi$ -do-

nating substituents like nitrogen induces stronger *trans*-bending in disilenes. Since no example with four *N*-substituents is known, Kira, Müller and Apeloig demonstrated this effect by calculating the structure of (Pr<sub>2</sub>N)<sub>2</sub>Si=Si(NPr<sub>2</sub>)<sub>2</sub> (**IV**), which features a large *trans*-bent angle of 42.6°. <sup>12</sup> Nevertheless, a number of *N*-substituted disilenes are structurally characterized. Compound **V**, which is in equilibrium with its monomeric *N*-heterocyclic silylene (NHSi), also displays a strongly twisted and *trans*-bent geometry around the Si=Si double bond.<sup>13</sup> Further examples comprise N(TMS)<sub>2</sub> containing structures,<sup>14-15</sup> like the one deriving from Jutzi's silyliumylidene ion.<sup>16</sup> Besides that, Sekiguchi and co-workers presented diaza-disilabenzene derivatives, generated from the reaction of their famous disilyne with silanitriles, bearing an iminodisilene moiety.<sup>17-18</sup> Recently, our group employed the convenient approach from Rivard et al. of introducing *N*-heterocyclic imines (NHIs) to silicon centers,<sup>19</sup> and prepared the first acyclic iminodisilene **VI**.<sup>20</sup> This compound has already shown interesting reactivity, however, its potential is strictly limited by its thermal instability, as well as the low isolable yield, resulting from the difficult removal of the byproduct (TMS)<sub>3</sub>SiBr.<sup>20-21</sup> Therefore, we aimed at synthesizing iminodisilenes with increased stability, combining bulky silyl groups and strong  $\pi$ -donating NHI ligands.

Herein, we extend this class of disilenes by two novel compounds **1** and **2**. Their surprisingly different structures are investigated and discussed in detail. Furthermore, an in-depth reactivity study of the highly stable and easily accessible **2** is presented. The focus lies not only on understanding of the

Chart 1. Selected Examples of Disilenes I-VI with Key Structural Features

	R = Mes	<sup>t</sup> Pr <sub>3</sub> Si	<sup>t</sup> Bu <sub>2</sub> MeSi	<sup>t</sup> Pr <sub>2</sub> N	R = <sup>t</sup> Bu	
#	<b>I</b> <sup>22</sup>	<b>II</b> <sup>10</sup>	<b>III</b> <sup>11</sup>	<b>IV</b> <sup>12</sup>	<b>V</b> <sup>13</sup>	<b>VI</b> <sup>20</sup>
d(Si=Si) [Å]	2.1602	2.251(1)	2.2598(18)	2.472	2.2890(14)	2.3124(7)
avg. θ [°]	18.4	10.2	5.9	42.6	33.1	38.5
τ [°]	11.8	0	54.5	55.5	25.1	23.1

\*structure calculated

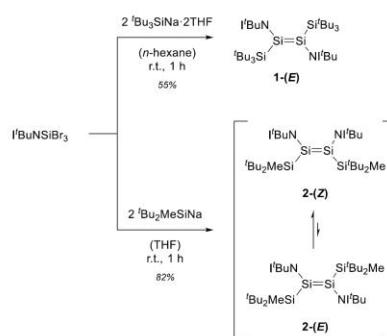
difference in reactivity between iminodisilenes and other compounds containing Si=Si double bonds, but also on the conversion to elusive compounds. In this regard, we took advantage of the strong  $\pi$ -donating ability of the NHI ligand to stabilize the cationic radical **8**. Moreover, we present the activation of white phosphorus by iminodisilene **2**.

## RESULTS AND DISCUSSION

Synthesis and properties of novel Iminodisilenes. Recently, our group presented the NHI-substituted disilene **VI** and thereby introduced a new class of disilenes.<sup>20</sup> Iminodisilene **VI** undergoes facile activation reactions with hydrogen and ammonia. In the latter case, a 1,2-addition of NH<sub>3</sub> to the Si=Si double bond can be observed, or **VI** can react as the formal monomeric silylene resulting in the formation of (TMS<sub>3</sub>Si)(<sup>t</sup>BuN)SiH(NH<sub>2</sub>).<sup>21</sup> The outcome of this reaction strongly depends on the warm up rate of the reaction mixture. Furthermore, the oxidation reactions with CO<sub>2</sub>, N<sub>2</sub>O and O<sub>2</sub> have been reported. However, further investigations of iminodisilene **VI** are limited, because it decomposes at room temperature, especially in solution. Another drawback of **VI** is the relatively low isolable yield resulting from the difficult separation process of the byproduct (TMS)<sub>3</sub>SiBr, that is generated during the synthesis and hampers the crystallization of **VI**.<sup>20</sup>

Inspired by these promising initial results, we focused on improving the disilene stability. Although the decomposition pathway is unclear, it is conceivable that the hypersilyl group ((TMS)<sub>3</sub>Si) with its well-known tendency toward rearrangement reactions is the reason for the low stability of **VI**.<sup>23-24</sup> We intended to replace the hypersilyl group by a supersilyl group (<sup>t</sup>Bu<sub>3</sub>Si), comparable in regard to the steric demand and  $\sigma$ -donating ability, with the additional benefit of being significantly more inert because of the alkyl groups. The synthesis was conducted in the same fashion as for **VI**, with supersilyl sodium (<sup>t</sup>Bu<sub>3</sub>SiNa·2THF) instead of (TMS)<sub>3</sub>SiK (Scheme 1). Immediately upon addition of the silanide solution, the reaction mixture turned dark green. Iminodisilene **1** was separated from the byproducts NaBr and <sup>t</sup>Bu<sub>3</sub>SiBr by filtration and subsequent crystallization and was obtained as green crystals in a moderate yield of 55%. Interestingly, treatment of <sup>t</sup>BuNSiBr<sub>3</sub> with supersilyl sodium in THF results in the formation of a dark purple compound instead of **1**. Unfortunately, this species is not stable above -40 °C and various trapping attempts were unsuccessful. Apparently, the choice of the solvent seems to be crucial for the synthesis of **1** and *n*-hexane turned out to work well. Indeed, compound **1** is stable in the solid state and in benzene solution

at ambient temperatures. However, it decomposes at elevated temperatures (50 °C). Hence, with the aim to obtain an even more stable iminodisilene, <sup>t</sup>BuNSiBr<sub>3</sub> was treated with <sup>t</sup>Bu<sub>2</sub>MeSiNa to generate compound **2**. This disilene turned out to be completely stable in the solid state and dissolved in various solvents, even at temperatures up to 90 °C. Because of this remarkable thermal stability, the bromosilane byproduct <sup>t</sup>Bu<sub>2</sub>MeSiBr can easily be removed via sublimation, thus increasing the isolable yield of **2** to 82% of a dark red solid. Notably, for the synthesis of **2**, the best results were achieved in THF. The configuration of **1** and **2** in the solid state was determined by single crystal X-ray diffraction (SC-XRD) analysis to be **1-(E)** and **2-(Z)** (Figure 1).

Scheme 1. Synthesis of Iminodisilenes **1** and **2**

In the <sup>29</sup>Si NMR spectra, the central silicon atoms of **1** and **2-(Z)** resonate at 72.5 ppm and 67.4 ppm, respectively. These low-field shifts are typical for disilenes (50 ppm – 157 ppm)<sup>5,8</sup> and the values compare well to that of iminodisilene **VI** (72.0 ppm)<sup>20</sup> and tetraaryl disilene **1** (63.6 ppm).<sup>1</sup> Neither for disilene **1**, nor for **2**, any signals of the monomeric silylene unit were observed. Interestingly, the multinuclear NMR spectra of compound **2** contain a second set of signals (<sup>29</sup>Si NMR  $\delta$  = 71.4 ppm, for the low-coordinate Si center, Figure S8) which clearly indicates the presence of the isomeric disilene **2-(E)**. Variable temperature NMR studies of **2** revealed a temperature-dependent equilibrium between the (*E/Z*)-isomers in



## 10. Iminodisilenes: Striking Reactivity in Small Molecule Activation

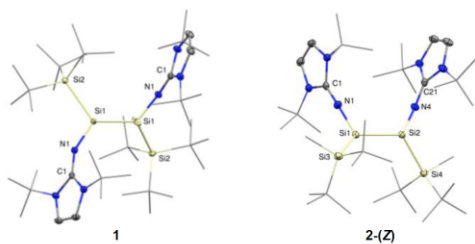


**Figure 1.** Molecular structures of iminodisilenes **1** (left) and **2-(Z)** (right) with thermal ellipsoids drawn at the 50% probability level. Hydrogen atoms are omitted for clarity. <sup>t</sup>Bu- and Me-groups are simplified as wireframes. Selected bond lengths [Å] and angles [°]: **1** Si1–Si1 2.2534(7), Si1–Si2 2.4142(6), Si1–N1 1.682(1), N1–C1 1.285(2), N1–Si1–Si1 122.97(5), Si2–Si1–Si1 124.52(3), Si2–Si1–N1 110.56(4) **2-(Z)** Si1–Si2 2.2844(7), Si1–Si3 2.3922(7), Si2–Si4 2.4001(7), Si1–N1 1.683(1), Si2–N4 1.680(1), N1–C1 1.283(2), N4–C21 1.278(2), Si3–Si1–N1 104.35(5), Si4–Si2–N4 103.84(5), Si2–Si1–Si3 121.28(2), Si2–Si1–N1 119.25(5).

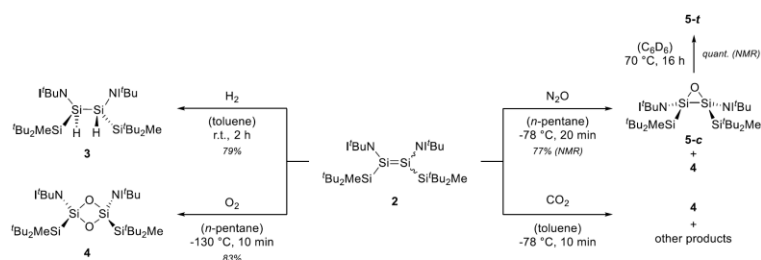
solution, ranging from 18% of **2-(E)** at 25 °C to 24% of **2-(E)** at 80 °C (Figure S12). Whereas the steric repulsion between the extremely bulky supersilyl groups in **1** forces the molecule to solely adopt (*E*)-configuration, the smaller <sup>t</sup>Bu<sub>2</sub>MeSi groups in **2** allow for (*E/Z*)-isomerization. Besides the conformation, crystal structure analysis shows further geometric differences between compounds **1** and **2-(Z)** (Figure 1). Despite several attempts, no crystal structure of sufficient quality was obtained for **2-(E)**. Nonetheless, the measured structure (Figure S13) clearly proves the existence of the (*E*) isomer of **2**. Key structural features of iminodisilenes **1** and **2** are presented in Table 1. Disilene **2-(Z)** displays a highly *trans*-bent ( $\theta_1 = 36.3^\circ$ ,  $\theta_2 = 34.7^\circ$ ) and slightly twisted structure ( $\tau = 25.5^\circ$ ), very similar to that of **VI** ( $\theta_1 = 37.9^\circ$ ,  $\theta_2 = 39.0^\circ$ ,  $\tau = 23.1^\circ$ ) (see Chart 1 for definition of *trans*-bent and twist angle). Because of the lower steric demand of the <sup>t</sup>Bu<sub>2</sub>MeSi group, compared to the hypersilyl group ((TMS)<sub>3</sub>Si), the Si=Si bond length of **2-(Z)** (2.284 Å) is shorter than in **VI** (2.312 Å), indicating a stronger double bond. In sharp contrast to **2-(Z)** and **VI**, compound **1** features a completely different geometry. It is strongly twisted ( $\tau = 40.2^\circ$ ) and shows smaller *trans*-bent angles ( $\theta_1 = 12.8^\circ$ ,  $\theta_2 = 12.8^\circ$ ) with the substituents arranged in (*E*)-configuration. This conformation minimizes the steric repulsion of the substituents and thus leads to a shortened Si=Si distance (2.253 Å), compared to **2-(Z)**.

**Table 1.** Selected Structural Features and <sup>29</sup>Si NMR Shifts of Iminodisilenes **1**, **2** and **VI**<sup>20</sup>

#	d(Si=Si) [Å]	twist angle $\tau$ [°]	<i>trans</i> -bent angles $\theta$ [°]	$\delta(^{29}\text{Si}_{\text{Si}=\text{Si}})$ [ppm]
<b>1</b>	2.2534(7)	40.2	12.8, 12.8	72.5
<b>2-(Z)</b>	2.2844(7)	25.5	36.3, 34.7	67.4
<b>VI</b>	2.3124(7)	23.1	37.9, 39.0	72.0

**Oxidation Reactions.** Activation of dihydrogen remains a challenging task for low-valent silicon compounds. Thus, only few examples of oxidative H<sub>2</sub> addition are reported to date.<sup>20,25–29</sup> Iminodisilene **VI** is among these highly reactive species. Therefore, we conceived, compounds **1** and **2** might also undergo hydrogenation reactions. As expected, the deep-red color of an *n*-hexane solution of **2** vanished upon exposure to dihydrogen (1 bar) within 2 hours and the *anti*-addition product **3** was formed in high yield (Scheme 2). SC-XRD analysis of hydrosilane **3** unambiguously proves the *anti*-conformation of H1 and H2 (Figure 2). Furthermore, the Si–Si bond is elongated to 2.4102(7) Å, which is within the range of Si–Si single bonds.<sup>30</sup> Both, the Si–Si bond length in **3**, as well as the <sup>29</sup>Si NMR shifts of the central Si atoms (–69.1 ppm) are in good agreement with the values observed for the hydrogenation product of **VI** (2.4142(7) Å, –62.4 ppm).<sup>20</sup> Presumably, this reaction proceeds via the same concerted addition mechanism, that was calculated for the H<sub>2</sub> activation by compound **VI**.<sup>20</sup> Disilene **1** on the other hand turned out not to react with dihydrogen. In order to get a better understanding for the correlation of structural features and the ability to activate dihydrogen, we attempted a similar reaction with highly twisted tetrasilyl-disilene **III**,<sup>11</sup> which however, showed no reaction with H<sub>2</sub> either. Concluding from these observations, a twisted disilene structure by itself is not enough to activate hydrogen. A *trans*-bent geometry of some extent seems also to be necessary. Therefore, and because of the lower stability and accessibility of **1**, compared to **2**, further investigations were based on the latter. In order to gain further insight into the chemical behavior of **2**, we reacted it with O<sub>2</sub>, N<sub>2</sub>O, as well as CO<sub>2</sub> and compared the outcome to the already reported reactivities of disilene **VI**.<sup>21</sup> With molecular oxygen, disilene **2** reacts immediately, even at –130 °C, furnishing exclusively dioxadisilene **4**. The <sup>29</sup>Si NMR signal of the central Si atoms, that are now bridged by two oxygen atoms, is strongly upfield shifted to –47.3 ppm.

**Scheme 2.** Reaction of Iminodisilene **2** with H<sub>2</sub>, O<sub>2</sub>, N<sub>2</sub>O and CO<sub>2</sub> to the Oxidation Products **3**, **4** and **5**



## 10. Iminodisilenes: Striking Reactivity in Small Molecule Activation

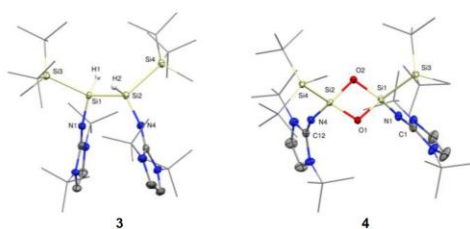
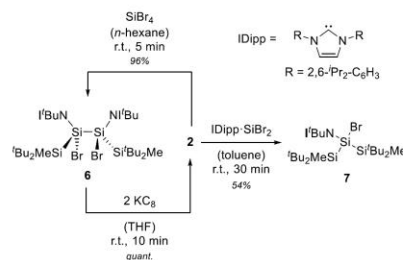


**Figure 2.** Molecular structures of hydrosilane **3** (left) and silanone dimer **4** (right). Thermal ellipsoids are drawn at the 50% probability level and hydrogen atoms omitted for clarity (except H1 and H2 in **3**). <sup>t</sup>Bu- and Me-groups are simplified as wireframes. Selected bond lengths [Å] and angles [°]: **3** Si1–Si2 2.4184(6), Si1–H1 1.43(1), Si1–Si3 2.4085(6), Si1–N1 1.682(1), Si2–H2 1.42(2), H1–Si1–Si3 101.1(6), N1–Si1–H1 113.9(6), N1–Si1–Si2 111.91(4), Si2–Si1–Si3 120.40(2) **4** Si1–O1 1.686(1), Si1–O2 1.695(1), Si1–Si3 2.3897(6), Si1–N1 1.641(1), N1–C1 1.274(2), Si2–O1 1.698(1), Si2–O2 1.691(1), Si3–Si1–O1 119.63(4), Si3–Si1–O2 114.96(4), Si3–Si1–N1 106.06(5), Si1–O1–Si2 91.77(5).

In the solid state, compound **4** displays *cis*-conformation of the substituents which are arranged perpendicular to the central Si<sub>2</sub>O<sub>2</sub>-plane (Figure 2). Again, this result is perfectly in line with the reaction of **VI** and other disilenes with O<sub>2</sub>.<sup>7,21,31</sup> For the reactions with N<sub>2</sub>O and CO<sub>2</sub>, disilene **2** shows a different reactivity, compared to **VI**. Treatment of iminodisilene **2** with one atmosphere of N<sub>2</sub>O at room temperature leads to decomposition to unidentified products. The same reaction conducted at –80 °C, however, furnishes an initial mixture of the two products **4** (25%) and **5-c** (75%), which were identified by comparison of multinuclear and 2D NMR spectroscopic data with the oxidation products of **VI**.<sup>21</sup> In contrast to **VI**, the corresponding disiloxirane **5-c** does not isomerize at room temperature. Nonetheless, it can be selectively transformed into the *trans*-isomer **5-t**, by heating to 70 °C overnight. At ambient temperatures, **2** decomposes upon exposure to CO<sub>2</sub>. Even at low temperatures (–80 °C), **2** shows no selective reactivity toward CO<sub>2</sub>. Dioxadisiletane **4** was observed to be the main product, but at least two additional species occurred. Despite all efforts (variation of solvents and temperatures), these compounds could not be isolated, or identified. Presumably, these are cycloaddition products of CO<sub>2</sub> with the Si=Si double bond akin to that, observed from the reaction of **VI** with carbon dioxide.<sup>21</sup>

**Bromination Reactions.** Because of its high stability, disilene **2** is suitable for further exploration of iminodisilene reactivities that were not possible with compound **VI**. In contrast to the halogenation of alkenes, there are only few examples for their heavier congeners. Wiberg and co-workers treated (<sup>t</sup>Bu<sub>3</sub>Si)PhSi=SiPh(<sup>t</sup>Bu<sub>3</sub>Si) with elemental chlorine and bromine and obtained exclusively the corresponding *syn*-addition product,<sup>32</sup> which is preferred according to calculations of Kira et al.<sup>33</sup> Nevertheless, the group of Sekiguchi demonstrated selective *anti*-halogenation of cyclic disilenes by CCl<sub>4</sub>, PbCl<sub>2</sub> and 1,2-dibromoethane.<sup>34–35</sup> We now report the 1,2-bromination of iminodisilene **2** by tetrabromosilane (Scheme 3). Obviously, iminodisilenes **1** and **2** do not react with bulkier bromosilanes like <sup>t</sup>Bu<sub>2</sub>MeSiBr or <sup>t</sup>Bu<sub>3</sub>SiBr, since these are byproducts of the respective syntheses. Nonetheless, addition of SiBr<sub>4</sub> to an *n*-hexane solution of disilene **2** leads to rapid decolorization and concomitant precipitation of compound **6** in excellent yield (96%).

**Scheme 3.** Synthesis of 1,2-Dibromosilane **6** and Bromosilane **7**



Multinuclear NMR spectroscopy revealed the exclusive formation of only one of two conceivable diastereomers, resulting either from *syn*- or *anti*-addition to the Si=Si double bond. The splitting of the <sup>1</sup>H and <sup>13</sup>C NMR signals for the Si=Si double bond of **6** suggests an asymmetric product. In the <sup>29</sup>Si NMR spectrum, the central Si atoms are strongly upfield-shifted from 64.4 ppm to –51.9 ppm, which compares very well to the shifts observed by Sekiguchi et al. after bromination of a cyclic disilene (δ = –53.2 ppm).<sup>34</sup> It is important to note, that dibromosilane **6** can quantitatively be reconverted to iminodisilene **2** by reductive dehalogenation with 2 equivalents of potassium graphite in THF. The solid state structure of **6** was determined by SC-XRD analysis (Figure 3). Surprisingly, the central Si–Si bond is even further elongated, compared to the hydrogenation product **3**, to 2.479(2) Å, but still within the range of Si–Si single bonds.<sup>36</sup>

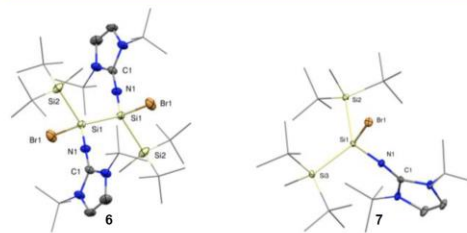


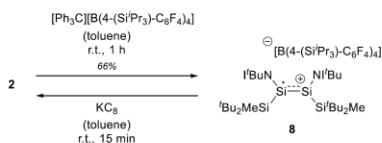
**Figure 3.** Molecular structures of dibromosilane **6** (left) and bromosilane **7** (right). Thermal ellipsoids are drawn at the 50% probability level and hydrogen atoms omitted for clarity. <sup>t</sup>Bu- and Me-groups are simplified as wireframes. Selected bond lengths [Å] and angles [°]: **6** Si1–Si1 2.479(2), Si1–N1 1.658(3), Si1–Br1 2.340(2), Si1–Si2 2.427(3), Br1–Si1–Si2 99.32(8), Br1–Si1–N1 111.1(2), Br1–Si1–Si1 100.14(8) **7** Si1–Br1 2.3555(5), Si1–Si2 2.4663(5), Si1–Si3 2.4637(6), Si1–N1 1.651(1), Br1–Si1–Si2 98.30(2), Br1–Si1–Si3 98.33(2), Br1–Si1–N1 106.53(5), Si2–Si1–Si3 123.75(2).

Presumably for the reason of minimized steric repulsion, the bulky NHI and silyl substituents are arranged in *trans*-position. Assuming, that only the main isomer **2-(Z)** has reacted with SiBr<sub>4</sub>, selective *syn*-addition occurred. However, the exact reaction mechanism was not clarified. Recently, Filippou and co-workers obtained the first NHC-stabilized bromo(silyl)silylene from reaction of a disilene with an NHC-dibromosilylene adduct.<sup>37</sup> Inspired by these results, we performed an analogue reaction, treating iminodisilene **2** with an equimolar amount of IDipp-SiBr<sub>2</sub> (Scheme 3). The reaction proceeded within 30 min

at ambient temperature, accompanied by decolorization and formation of colorless precipitate. Instead of an NHC-coordinated species, however,  $^1\text{H}$  NMR spectroscopy indicated free IDipp and the selective formation of a compound with an NHI to  $^t\text{Bu}_2\text{MeSi}$  substituents ratio of 1:2. After precipitation of the NHC, by exposure of the mixture to  $\text{CO}_2$ , as IDipp- $\text{CO}_2$  adduct, the soluble compound **7** was separated via filtration and isolated in moderate yield (54%). In fact, crystal structure analysis of **7** revealed a tetrahedral coordination sphere around the  $\text{Si}^{\text{IV}}$  center, bearing two silyl groups, one NHI substituent and one bromine atom (Figure 3). Compared to the other bromination product **6**, the  $^{29}\text{Si}$  NMR signal of the silicon center in **7** is about 20 ppm down-field shifted to  $-35.6$  ppm. Apparently, a 1,2-silyl migration of one  $^t\text{Bu}_2\text{MeSi}$  group and a dissociation of the Si=Si bond took place. Because of the insolubility of the concomitantly formed precipitate, we were not able to conclude the fate of the missing  $\text{SiN}^i\text{Bu}$  fragment. Therefore, the formation mechanism of **7** could not be further elucidated.

**Conversion to Radical Species.** Although a plethora of disilenes, both cyclic and acyclic, with various substituents is known,<sup>7-9</sup> only one example of a stable cationic radical deriving from one-electron oxidation of disilene **II** has been reported to date.<sup>38</sup> Since our group has already shown, the potential of the strongly  $\pi$ -donating NHI substituent for stabilization of elusive, cationic silicon species,<sup>39</sup> we conceived the bis-NHI substituted disilene **2** to be the perfect precursor for such a radical cation. The initially recorded cyclic voltammogram of **2** showed an oxidation wave, which occurred at lower potentials than required for the oxidation of **II**, indicating the accessibility of a cationic compound (Figure S15). Indeed, treatment of **2** with a trityl reagent resulted in the formation of the green, ionic species **8** in 66% yield (Scheme 4).

#### Scheme 4. One-Electron Oxidation of **2** to Radical Cation **8**



Compound **8**, which is highly soluble in difluorobenzene and slightly in toluene was identified by EPR spectroscopy and elemental analysis. The large EPR signal clearly confirms the paramagnetic nature of **8** (Figure 4). Signal splitting from coupling of the unpaired electron with different  $^{14}\text{N}$  nuclei indicates a distribution of spin density over the imino ligands, comparable to So's observation from an amidinato-stabilized silyl radical.<sup>40</sup> Upon treatment of radical **8** with  $\text{KC}_8$ , fast color change to deep red occurred, originating from the formation of iminodisilene **2**. This reversibility is in line with the reduction results of Sekiguchi's tetrasilyl disilene radical cation.<sup>38</sup> In order to enhance crystallization of **8**, the trityl reagent with a TIPS- ( $^t\text{Pr}_3\text{Si}$ ) functionalized borate  $\text{BAR}_4^-$  anion was synthesized<sup>41</sup> and used instead of the commercially available  $\text{B}(\text{C}_6\text{F}_5)_4^-$ . Unfortunately, despite these efforts, we were not able to obtain a crystal structure of sufficient quality to discuss all structural features of **8** because of twinning and disorder. Nonetheless, the measured crystal (Figure S34) reveals the (*E*)-configuration of the substituents and

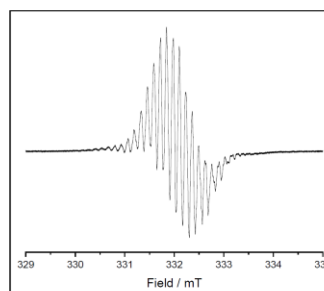
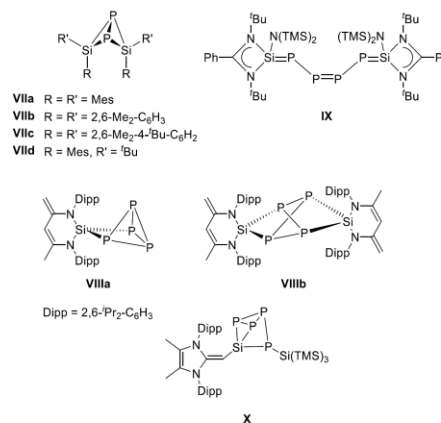


Figure 4. X-band EPR spectrum of cation **8** in toluene ( $2 \times 10^{-3}$  M) at 286 K.

three-coordinate silicon centers without interaction with solvent molecules or anions. In contrast to **II**<sup>+</sup>, twisting of the central Si-Si bond is less pronounced.<sup>38</sup>

**Activation of  $\text{P}_4$**  Since silaphosphines and silaphosphides are essential starting materials for the synthesis of nanomaterials,<sup>42-43</sup> as well as for organophosphines,<sup>44</sup> it is of great interest for silicon chemists, to provide access to these molecules. West's early disilenes turned out to react with white phosphorus, furnishing compounds **VII**, in which the silicon centers are bridged by two P atoms (Chart 2).<sup>45-46</sup> To date, these are the only examples of  $\text{P}_4$  activation by disilenes.<sup>47</sup> Besides that, three further  $\text{P}_4$  functionalizations by  $\text{Si}(\text{II})$  species are reported, all based on silylenes. Driess et al. successively treated  $\text{P}_4$  with one and two equivalents of an *N*-heterocyclic silylene to obtain the mono- and disubstituted  $\text{P}_4$  moieties **VIIIa** and **VIIIb**, respectively.<sup>48</sup> Further examples comprise  $\text{P}_4$  activation products like the  $\text{P}_4$  chain-containing **IX**, based on amidinato silylenes from the group of Roesky<sup>49-50</sup> and compound **X** from Rivard<sup>51</sup> and co-workers. Encouraged by the intriguing reactivity of iminodisilene **2**, especially toward the non-polar dihydrogen molecule, we treated **2** with 1 equivalent of  $\text{P}_4$  (Scheme 5). This reaction proceeded cleanly and straightforward at room temperature, furnishing exclusively compound **9**.

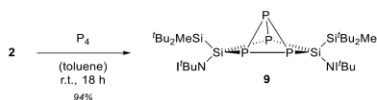
#### Chart 2. Activation Products of $\text{P}_4$ by Low-coordinate Si Compounds





The  $^{31}\text{P}$  NMR spectrum, containing three sets of signals, however, ruled out the possibility of a structure bridged by two P atoms, as in West's **VII**. The unique functionalized  $\text{P}_4$  structure of **9** was unambiguously determined by SC-XRD analysis (Figure 5). Compound **9** displays two silyl centers, bridged by the three P atoms of the  $\text{P}_4$  tetrahedron base. In the  $^{31}\text{P}$  NMR spectrum, the top P atom of the tetrahedron (P2) resonates at  $-217.6$  ppm and shows coupling with two chemically inequivalent Si functionalized P atoms ( $^1J_{\text{P-P}} = 157.9$  Hz,  $^1J_{\text{P-Si}} = 129.0$  Hz). This signal is strongly downfield-shifted compared to the  $\text{PP}_3$  atoms in Driess' **VIIIa** ( $-342.4$  ppm,  $-348.0$  ppm)<sup>48</sup> and Rivard's **X** ( $-316.2$  ppm).<sup>51</sup> The  $^{29}\text{Si}$  NMR signals of the P-substituted silicon centers in **9** can be observed at  $-52.2$  ppm as multiplet due to coupling with the 4 P atoms.

#### Scheme 5. Activation of $\text{P}_4$ by Iminodisilene **2**



This shift compares best to  $\text{P}_4$  activation product by tetraaryl disilene **VIIc** ( $-49.8$  ppm).<sup>46</sup> In order to elucidate whether **2** reacts as disilene, or as silylene, the reaction was repeated with differing amounts of white phosphorus. Addition of either excess (4 eq.) or 0.5 eq. still resulted in the selective formation of **9**. In the latter case, the reaction stopped at 50% conversion. Upon heating the sample mixtures to  $70$  °C, full decomposition occurred. Since no possible silylene reaction products, such as **VIII** – **X** were generated, we assume that the reaction proceeds via insertion of the  $\text{P}_4$  cage into the Si=Si double bond of **2**.

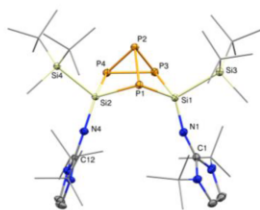


**Figure 5.** Molecular structure of compound **9** with thermal ellipsoids drawn at the 50% probability level. Hydrogen atoms are omitted for clarity,  $t\text{Bu}$ - and  $\text{Me}$ -groups are simplified as wireframes. Selected bond lengths [Å] and angles [°]: Si1–P1 2.2785(8), Si1–P3 2.2723(7), P1–P2 2.2937(7), P3–P2 2.2301(8), N1–Si1–Si3 109.32(4), P1–Si1–P3 94.22(2), P1–P2–P3 94.95(2), Si1–P1–Si2 106.69(2).

#### CONCLUSIONS

In summary, we synthesized two new iminodisilenes **1** and **2**, of which especially **2** is easily accessible in good yield and shows high thermal stability. The structural differences between **1** and **2** in the solid state as well as the (*E/Z*)-isomerization of **2** in solution were investigated using VT-NMR and SC-XRD analysis. With highly stable, but nonetheless reactive **2** in hand, we were able to activate dihydrogen at ambient temperature and investigate oxidation reactions with  $\text{O}_2$ ,  $\text{N}_2\text{O}$  and  $\text{CO}_2$ . Additionally, bromination products **6** and **7** were synthesized from reactions of **2** with  $\text{SiBr}_4$  and  $\text{IDipp-SiBr}_2$  and fully characterized. Furthermore, radical cation **8**, which shows reversible

redox behavior, was obtained. It is the second example of a disilene radical cation and underlines again the suitability of the NHI substituent for stabilizing cationic silicon species. Furthermore, we isolated the unprecedented bisilyl-functionalized  $\text{P}_4$  cage **9** from the unique reaction of the Si=Si double bond of **2** with white phosphorus.

#### ASSOCIATED CONTENT

Supporting Information

#### AUTHOR INFORMATION

Corresponding Author

\*s.inoue@tum.de

ORCID

Shigeyoshi Inoue: 0000-0001-6685-6352

Notes

The authors declare no conflict of interest.

#### ACKNOWLEDGMENT

We thank WACKER Chemie AG and the European Research Council (SILION 637394) for continued financial support. We are also thankful to Dr. Oksana Storcheva for conducting the EPR measurements and to Fabian Linsenmann for the CV analysis.

#### REFERENCES

- West, R.; Fink, M. J.; Michl, J., Tetramesityldisilene, a Stable Compound Containing a Silicon-Silicon Double Bond. *Science* **1981**, *214*, 1343.
- Jutz, P., New Element-Carbon (p-p) $\pi$  Bonds. *Angew. Chem. Int. Ed. Engl.* **1975**, *14*, 232-245.
- Okazaki, R.; West, R., Chemistry of Stable Disilenes. In *Advances in Organometallic Chemistry*, Gordon, F.; Stone, A.; West, R., Eds. Academic Press, **1996**.
- Power, P. P.,  $\pi$ -Bonding and the Lone Pair Effect in Multiple Bonds between Heavier Main Group Elements. *Chem. Rev.* **1999**, *99*, 3463-3504.
- Weidenbruch, M., Recent Advances in the Chemistry of Silicon-Silicon Multiple Bonds. In *The Chemistry of Organic Silicon Compounds*, Rappoport, Z.; Apeloig, Y., Eds. John Wiley & Sons, Ltd., **2001**.
- Weidenbruch, M., Some recent advances in the chemistry of silicon and its homologues in low coordination states. *J. Organomet. Chem.* **2002**, *646*, 39-52.
- Kira, M.; Iwamoto, T., Progress in the Chemistry of Stable Disilenes. In *Advances in Organometallic Chemistry*, West, R.; Hill, A. F., Eds. Academic Press, **2006**.
- Kira, M., Bonding and structure of disilenes and related unsaturated group-14 element compounds. *Proc. Jpn. Acad., Ser. B, Phys. Biol. Sci.* **2012**, *88*, 167-191.
- Präsang, C.; Scheschke, D., Reactivity in the periphery of functionalised multiple bonds of heavier group 14 elements. *Chem. Soc. Rev.* **2016**, *45*, 900-921.
- Kira, M.; Maruyama, T.; Kabuto, C.; Ebata, K.; Sakurai, H., Stable Tetrakis(trialkylsilyl)disilenes; Synthesis, X-Ray Structures, and UV/VIS Spectra. *Angew. Chem. Int. Ed. Engl.* **1994**, *33*, 1489-1491.
- Sekiguchi, A.; Inoue, S.; Ichinohe, M.; Arai, Y., Isolable Anion Radical of Blue Disilene  $(t\text{Bu}_2\text{MeSi})_2\text{Si}=\text{Si}(\text{SiMe}_2\text{Bu}_2)_2$  Formed upon One-Electron Reduction: Synthesis and Characterization. *J. Am. Chem. Soc.* **2004**, *126*, 9626-9629.



## 10. Iminodisilenes: Striking Reactivity in Small Molecule Activation

- (12) Takahashi, M.; Tsutsui, S.; Sakamoto, K.; Kira, M.; Müller, T.; Apeloig, Y., Dimers of Diaminosilylenes: Doubly Bonded or Bridged? The Dimers of (*i*-Pr<sub>2</sub>N)<sub>2</sub>Si. *J. Am. Chem. Soc.* **2001**, *123*, 347-348.
- (13) Schmedake, T. A.; Haaf, M.; Apeloig, Y.; Müller, T.; Bukalov, S.; West, R., Reversible Transformation between a Diaminosilylene and a Novel Disilene. *J. Am. Chem. Soc.* **1999**, *121*, 9479-9480.
- (14) Michalczyk, M. J.; West, R.; Michl, J., Kinetics of Thermal Cis-Trans Isomerizations in Disilenes. *Organometallics* **1985**, *4*, 826-829.
- (15) Khan, S.; Sen, S. S.; Roesky, H. W.; Kratzert, D.; Michel, R.; Stalke, D., One Pot Synthesis of Disilatricycloheptene Analogue and Jutzl's Disilene. *Inorg. Chem.* **2010**, *49*, 9689-9693.
- (16) Jutzl, P.; Mix, A.; Rummel, B.; Schoeller, W. W.; Neumann, B.; Stammer, H.-G., The (Me<sub>3</sub>C)<sub>3</sub>Si<sup>+</sup> Cation: A Stable Derivative of HSi<sup>+</sup>. *Science* **2004**, *305*, 849-851.
- (17) Takeuchi, K.; Ichinohe, M.; Sekiguchi, A., Reactivity of the Disilyne RSi≡SiR (R = Si<sup>i</sup>Pr[CH(SiMe<sub>3</sub>)<sub>2</sub>]<sub>2</sub>) toward Silylcyanide: Two Pathways To Form the Bis-Adduct [RSiSiR(CNSiMe<sub>3</sub>)<sub>2</sub>] with Some Silaketiminic Character and a 1,4-Diaza-2,3-disilabenzene Analogue. *J. Am. Chem. Soc.* **2008**, *130*, 16848-16849.
- (18) Takeuchi, K.; Ichinohe, M.; Sekiguchi, A.; Guo, J.-D.; Nagase, S., Reactivity of the disilyne RSi≡SiR (R = Si<sup>i</sup>Pr[CH(SiMe<sub>3</sub>)<sub>2</sub>]<sub>2</sub>) toward bis(silylcyanide) forming a 1,4-diaza-2,3-disilabenzene analog. *J. Phys. Org. Chem.* **2010**, *23*, 390-394.
- (19) Lui, M. W.; Merten, C.; Ferguson, M. J.; McDonald, R.; Xu, Y.; Rivard, E., Contrasting Reactivities of Silicon and Germanium Complexes Supported by an N-Heterocyclic Guanidine Ligand. *Inorg. Chem.* **2015**, *54*, 2040-2049.
- (20) Wendel, D.; Szilvási, T.; Jandl, C.; Inoue, S.; Rieger, B., Twist of a Silicon-Silicon Double Bond: Selective *Anti*-Addition of Hydrogen to an Iminodisilene. *J. Am. Chem. Soc.* **2017**, *139*, 9156-9159.
- (21) Wendel, D.; Szilvási, T.; Henschel, D.; Altmann, P. J.; Jandl, C.; Inoue, S.; Rieger, B., Precise Activation of Ammonia and Carbon Dioxide by an Iminodisilene. *Angew. Chem. Int. Ed.* **2018**, *57*, 14575-14579.
- (22) Fink, M. J.; Michalczyk, M. J.; Haller, K. J.; West, R.; Michl, J., The X-Ray Crystal Structure of Tetramesityldisilene. *J. Chem. Soc., Chem. Commun.* **1983**, 1010-1011.
- (23) Marschner, C., Silylated Group 14 Ylenes: An Emerging Class of Reactive Compounds. *Eur. J. Inorg. Chem.* **2015**, *2015*, 3805-3820.
- (24) Stanford, M. W.; Schweizer, J. I.; Menche, M.; Nichol, G. S.; Holthausen, M. C.; Cowley, M. J., Intercepting the Disilene-Silylsilylene Equilibrium. *Angew. Chem. Int. Ed.* **2019**, *58*, 1329-1333.
- (25) Protchenko, A. V.; Schwarz, A. D.; Blake, M. P.; Jones, C.; Kaltsoyannis, N.; Mountford, P.; Aldridge, S., A Generic One-Pot Route to Acyclic Two-Coordinate Silylenes from Silicon(IV) Precursors: Synthesis and Structural Characterization of a Silylsilylene. *Angew. Chem. Int. Ed.* **2013**, *52*, 568-571.
- (26) Kosai, T.; Iwamoto, T., Cleavage of Two Hydrogen Molecules by Boryldisilenes. *Chem. Eur. J.* **2018**, *24*, 7774-7780.
- (27) Kosai, T.; Iwamoto, T., Stable Push-Pull Disilene: Substantial Donor-Acceptor Interactions through the Si=Si Double Bond. *J. Am. Chem. Soc.* **2017**, *139*, 18146-18149.
- (28) Protchenko, A. V.; Birjkumar, K. H.; Dange, D.; Schwarz, A. D.; Vidovic, D.; Jones, C.; Kaltsoyannis, N.; Mountford, P.; Aldridge, S., A Stable Two-Coordinate Acyclic Silylene. *J. Am. Chem. Soc.* **2012**, *134*, 6500-6503.
- (29) Wendel, D.; Porzelt, A.; Herz, F. A. D.; Sarkar, D.; Jandl, C.; Inoue, S.; Rieger, B., From Si(II) to Si(IV) and Back: Reversible Intramolecular Carbon-Carbon Bond Activation by an Acyclic Iminodisilylene. *J. Am. Chem. Soc.* **2017**, *139*, 8134-8137.
- (30) Krempner, C.; Chtchian, S.; Reinke, H., First synthesis of a dihydrido functionalized double-cored oligosilane dendrimer. *Inorg. Chim. Acta* **2004**, *357*, 3733-3738.
- (31) Khan, S.; Michel, R.; Koley, D.; Roesky, H. W.; Stalke, D., Reactivity Studies of a Disilene with N<sub>2</sub>O and Elemental Sulfur. *Inorg. Chem.* **2011**, *50*, 10878-10883.
- (32) Wiberg, N.; Niedermayer, W.; Polborn, K.; Mayer, P., Reactivity of the Isolable Disilene R<sup>+</sup>PhSi=SiPhR<sup>+</sup> (R<sup>+</sup>=Si<sup>i</sup>Bu<sub>3</sub>). *Chem. Eur. J.* **2002**, *8*, 2730-2739.
- (33) Takahashi, M.; Veszprémi, T.; Hajgató, B.; Kira, M., Theoretical Study on Stereochemical Diversity in the Addition of Water to Disilene. *Organometallics* **2000**, *19*, 4660-4662.
- (34) Lee, V. Y.; Matsuno, T.; Ichinohe, M.; Sekiguchi, A., Interconversion of Cyclotrimetallanes and Dihalocyclotrimetallanes Consisting of Group 14 Elements. *Heteroat. Chem.* **2001**, *12*, 223-226.
- (35) Lee, V. Y.; Ito, Y.; Sekiguchi, A., 1,2-Dibromo-<sup>3</sup>Δ-1,2,3,4-disiladigermetene. *Phosphorus Sulfur Silicon Relat. Elem.* **2011**, *186*, 1351-1355.
- (36) Wiberg, N.; Schuster, H.; Simon, A.; Peters, K., Hexa-*tert*-butyldisilane—the Molecule with the Longest Si-Si Bond. *Angew. Chem. Int. Ed. Engl.* **1986**, *25*, 79-80.
- (37) Ghana, P.; Arz, M. I.; Das, U.; Schnakenburg, G.; Filippou, A. C., Si=Si Double Bonds: Synthesis of an NHC-Stabilized Disilavinylidene. *Angew. Chem. Int. Ed.* **2015**, *54*, 9980-9985.
- (38) Inoue, S.; Ichinohe, M.; Sekiguchi, A., The Isolable Cation Radical of Disilene: Synthesis, Characterization, and a Reversible One-Electron Redox System. *J. Am. Chem. Soc.* **2008**, *130*, 6078-6079.
- (39) Ochiai, T.; Szilvási, T.; Inoue, S., Facile Access to Stable Silylium Ions Stabilized by *N*-Heterocyclic Imines. *Molecules* **2016**, *21*, 1155.
- (40) Zhang, S.-H.; Carter, E.; Xi, H.-W.; Li, Y.; Lim, K. H.; So, C.-W., Delocalized Hypervalent Silyl Radical Supported by Amidinate and Imino Substituents. *Inorg. Chem.* **2017**, *56*, 701-704.
- (41) Jia, L.; Yang, X.; Ishihara, A.; Marks, T. J., Protected (Fluoroaryl)borates as Effective Counteranions for Cationic Metallocene Polymerization Catalysts. *Organometallics* **1995**, *14*, 3135-3137.
- (42) Gary, D. C.; Cossairt, B. M., Role of Acid in Precursor Conversion During InP Quantum Dot Synthesis. *Chem. Mater.* **2013**, *25*, 2463-2469.
- (43) Gary, D. C.; Glassy, B. A.; Cossairt, B. M., Investigation of Indium Phosphide Quantum Dot Nucleation and Growth Utilizing Triarylsilylphosphine Precursors. *Chem. Mater.* **2014**, *26*, 1734-1744.
- (44) Geeson, M. B.; Cummins, C. C., Phosphoric acid as a precursor to chemicals traditionally synthesized from white phosphorus. *Science* **2018**, *359*, 1383-1385.
- (45) Driess, M.; Fanta, A. D.; Powell, D. R.; West, R., Synthesis, Characterization, and Complexation of an Unusual P<sub>2</sub>Si<sub>2</sub>: Bicyclobutane with Butterfly-Structure: 2,2,4,4-Tetramesityl-1,3-diphospha-2,4-disilabicyclo[1.1.0]butane. *Angew. Chem. Int. Ed. Engl.* **1989**, *28*, 1038-1040.
- (46) Fanta, A. D.; Tan, R. P.; Comerlato, N. M.; Driess, M.; Powell, D. R.; West, R., The reaction of disilenes with P<sub>4</sub> and As<sub>4</sub>. *Inorg. Chim. Acta* **1992**, *198-200*, 733-739.
- (47) Scheer, M.; Balázs, G.; Seitz, A., P<sub>4</sub> Activation by Main Group Elements and Compounds. *Chem. Rev.* **2010**, *110*, 4236-4256.
- (48) Xiong, Y.; Yao, S.; Brym, M.; Driess, M., Consecutive Insertion of a Silylene into the P<sub>4</sub> Tetrahedron: Facile Access to Strained SiP<sub>4</sub> and Si<sub>2</sub>P<sub>4</sub> Cage Compounds. *Angew. Chem. Int. Ed.* **2007**, *46*, 4511-4513.
- (49) Khan, S.; Michel, R.; Sen, S. S.; Roesky, H. W.; Stalke, D., A P<sub>4</sub> Chain and Cage from Silylene-Activated White Phosphorus. *Angew. Chem. Int. Ed.* **2011**, *50*, 11786-11789.
- (50) Sen, S. S.; Khan, S.; Roesky, H. W.; Kratzert, D.; Meindl, K.; Henn, J.; Stalke, D.; Demers, J.-P.; Lange, A., Zwitterionic Si-C-Si-P and Si-P-Si-P Four-Membered Rings with Two-Coordinate Phosphorus Atoms. *Angew. Chem. Int. Ed.* **2011**, *50*, 2322-2325.
- (51) Roy, M. M. D.; Ferguson, M. J.; McDonald, R.; Zhou, Y.; Rivard, E., A vinyl silylsilylene and its activation of strong homo- and heteroatomic bonds. *Chem. Sci.* **2019**, *10*, 6476-6481.

## 11. Formation of a Silene through CO Activation by a Polarized Iminodisilene

**Title:** Formation of a Silene through CO Activation by a Polarized Iminodisilene

**Status:** Draft (Communication)

**Authors:** Richard Holzner, Philipp Frisch, Shigeyoshi Inoue<sup>a</sup>

**Content:** Despite numerous examples of disilenes with various substituents, reports on reactivities towards carbon monoxide are scarce. Therefore, investigations in this regard were conducted with the previously presented stable iminodisilene **2b**.

Although **2b** immediately reacts with CO, the reaction does not proceed in a selective fashion. Nevertheless, the neutral, NHI-substituted silyl radical **1b** was obtained from these reactions and fully characterized. The formation of **1b** proves, that these heteroatom-substituted silyl radicals can be stable and isolated, yet the reproducibility of this reaction is limited and the provided yield is poor. Most interestingly, iminodisilene **2b** selectively and irreversibly undergoes isomerization to the corresponding  $A_2Si=SiB_2$  type disilene **2c** upon heating to 115 °C for a prolonged time. Both, <sup>29</sup>Si NMR spectroscopy and SC-XRD analysis demonstrated the highly zwitterionic nature of **2c** with the positive charge stabilized by the two adjacent NHI ligands and the negatively polarized =SiSi<sub>2</sub> center. This unprecedented disilene **2c** in turn shows facile activation of carbon monoxide at ambient temperature, resulting in the formation of silene **15a** *via* insertion of CO into the Si=Si double bond. A similar product was obtained from the reaction of the tetra(silyl)disilene **L7** with CO, however this activation requires elevated temperatures, presumably because of the non-polar nature of the disilene.

In summary, the thermally induced isomerization of iminodisilene **2b** was investigated and the resulting polarized disilene **2c** was characterized thoroughly. Furthermore, this manuscript outlined the synthetic approach to silenes through the activation of CO by disilenes.

By now, this draft is still in preparation. The so far unique isomerization of **2b** to disilene **2c** is currently under investigation by DFT calculations to clarify the underlying mechanism. Furthermore, crystal structure analysis is ongoing. Additional results will be included in the final version of the manuscript.

---

<sup>a</sup>R. Holzner planned and executed all experiments and wrote the manuscript. P. Frisch conducted all SC-XRD measurements and processed the resulting data. All work was performed under the supervision of S. Inoue.

## Formation of a Silene through CO Activation by a Polarized Iminodisilene

Richard Holzner, Philipp Frisch and Shigeyoshi Inoue\*

Department of Chemistry, WACKER-Institute of Silicon Chemistry and Catalysis Research Center, Technische Universität München, Lichtenbergstraße 4, 85748 Garching bei München (Germany)

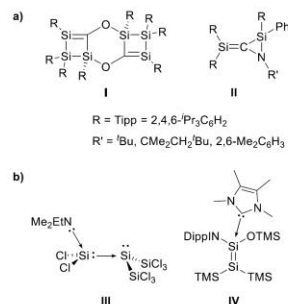
Supporting Information Placeholder

**ABSTRACT:** The thermally induced rearrangement of iminodisilene ( $(t\text{-BuN})(t\text{-Bu}_2\text{MeSi})\text{Si}=\text{Si}(\text{Si}^i\text{Bu}_2\text{Me})(\text{N}^i\text{Bu})$ ) produced the highly polarized disilene **1** of the  $\text{A}_2\text{Si}=\text{SiB}_2$  type. Compound **1** was fully characterized and displays one positively charged planar and one negatively charged pyramidal Si-center with a twist angle of  $46.9^\circ$ . Interestingly, formation of **1** proceeds in an irreversible fashion. In addition, a facile insertion of CO into the Si=Si double bond of **1** was observed, furnishing silene **2**.

Carbon monoxide is a common C1 building block in organic transformations, for example in the Pauson-Khand reaction.<sup>1-3</sup> Furthermore, CO is employed as carbon feedstock in the industrial Fischer-Tropsch process together with dihydrogen to produce liquid hydrocarbons.<sup>4-5</sup> Because the C=O triple bond in carbon monoxide is one of the strongest bonds in chemistry<sup>6</sup> (dissociation energy CO: 256.1 kcal/mol),<sup>7</sup> these reactions typically require transition-metal catalysis. Nevertheless, a number of CO activations by main group element compounds have been reported to date. The reaction of CO with diboron hydride<sup>8</sup> has been known for a long time and various other boron compounds have been found to activate carbon monoxide as well.<sup>9-17</sup> Other main group examples of CO activations comprise magnesium,<sup>18</sup> carbenes,<sup>19-21</sup> frustrated Lewis pairs (FLP)<sup>22-24</sup> and phosphinidenes.<sup>25-26</sup> Very recently, the groups of Aldridge<sup>27</sup> and Driess<sup>28-29</sup> observed reactions of their silylenes towards CO and also Sekiguchi<sup>30</sup> and Scheschkewitz<sup>31-32</sup> investigated silicon compounds in this regard. Since the synthesis and characterization of the first disilene by West et al. in 1981,<sup>33</sup> a plethora of these heavier alkene congeners has been reported to date and their reactivity was studied extensively.<sup>34-40</sup> Considering these efforts, the activation of carbon monoxide by disilenes has received only little attention so far. The only disilene-CO addition product is the insoluble compound **I** (Chart 1), obtained by Sekiguchi, Scheschkewitz and co-workers from a cyclic disilene.<sup>41</sup> Additionally, insertion reactions of isocyanides which are isoelectronic with CO into a Si=Si double bond of a disilene were observed (compounds **II**).<sup>42</sup> Besides "classical" disilenes, kinetically stabilized by bulky aryl or silyl substituents, there are also zwitterionic compounds with a rather dative-type bonding interaction between the low-coordinate silicon centers. Usually, these highly polarized molecules need electron donation from coordinated Lewis bases to stabilize the positively charged fragment like in the disilene base adduct **III** from Holthausen et al. Further examples were isolated from

the reaction of a disilyne with 4-dimethylamino pyridine (DMAP)<sup>43</sup> and from rearrangement of a silanone (**IV**).<sup>44</sup> Very recently, compounds with interactions between the central Si atoms similar to those in **III**, however, stabilized by *N*-heterocyclic carbenes (NHCs) or a DMAP derivative instead of an amine were published. Herein, we report the thermally induced, irreversible isomerization of an ABSi=SiAB-type iminodisilene **V** to a zwitterionic, donor-free  $\text{A}_2\text{Si}=\text{SiB}_2$ -type disilene **1**. Additionally, the fascinating nature of **1** is underlined by the activation of CO at ambient temperature, affording silene **2a**.

**Chart 1. a) Reaction Products of Disilenes with CO (I) and Isonitriles (II). b) Selected Examples of Polarized Disilene Base Adducts (III, IV)**

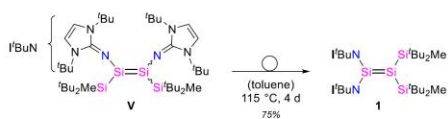


In our recent work, we presented iminodisilene **V** (Scheme 1), which shows remarkable thermal stability. Within a temperature range up to 90 °C, reversible (*E/Z*)-isomerization but no decomposition was observed. Heating of a toluene solution of **V** over 100 °C, however, lead to an irreversible rearrangement of the substituents, furnishing disilene **1** in good yield (75%) after crystallization. Compound **1** was obtained as purple crystals which are indefinitely stable in various solvents under inert atmosphere. Compared to the starting material **V**, the <sup>29</sup>Si NMR shifts of the central Si atoms in **1** are significantly upfield shifted from 67.4 ppm (**V-Z**) to 30.4 ppm (=Si N<sub>2</sub>) and -176.1 ppm (=Si Si<sub>2</sub>). These surprising shifts, which are not in the typical range for disilenes (about 50 ppm – 157 ppm),<sup>34,36</sup> indicate a highly polarized bonding situation for the central Si-Si bond in compound **1**, reflected in the zwitterionic Lewis structure **1'** (cf. Chart 2).



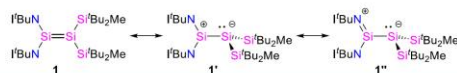
# 11. Formation of a Silene through CO Activation by a Polarized Iminodisilene

**Scheme 1. Thermally Induced Isomerization of Disilene V to Compound 1**



The positively polarized Si center is stabilized by the two adjacent,  $\pi$ -donating imino substituents (**1'**), whereas the negatively charged Si center bears two bulky trialkylsilyl substituents. In the  $^{29}\text{Si}$  NMR spectrum, the signal for this negatively polarized Si atom can be observed at  $-176.1$  ppm, which is in the region of resonances of trisilyl-substituted silicon anions, such as hypersilane ( $(\text{TMS})_3\text{SiK}$ ).<sup>45</sup> In fact, the  $^{29}\text{Si}$  NMR shifts of **1** are comparable to the polar disilene base adduct **III** ( $\delta = 43.7$  ppm ( $\text{Si}^{\delta+}$ ),  $-155.6$  ppm ( $\text{Si}^{\delta-}$ )<sup>46</sup> and to the NHC-stabilized, zwitterionic disilene **IV**, reported by our group ( $\delta = -35.2$  ppm ( $\text{Si}^{\delta+}$ ),  $-174.6$  ppm ( $\text{Si}^{\delta-}$ )).<sup>44</sup> In sharp contrast to these examples, however, disilene **1** is stable without an additional external donor.

**Chart 2. Plausible Lewis Structure Representations of 1.**



Although the molecular connectivity of **1** was unambiguously determined by single crystal X-ray diffraction (SC-XRD) analysis, specific bonding parameters are difficult to discuss because of twinning and disorder in the crystal (Figure 1). Upon isomerization, the Si=Si bond length seems to be shortened from 2.2844(7) Å (**V-Z**) to 2.219(4) Å in **1**. This value is significantly smaller than in disilene base adducts **III** (2.324(2) Å) and **IV** (2.3297(7) Å) and clearly suggests double bond character between the central Si atoms. Disilene **1** is highly twisted (46.9°) and displays different geometries at the two Si centers, resulting from the asymmetric substitution pattern (for definition of twist- and *trans*-bent angle see Table 1). The bisimino substituted Si1 is almost planar (sum of bond angles  $\Sigma\theta = 359.2^\circ$ ), whereas the Si2 center adopts a more pyramidal coordination sphere. This pyramidalization at Si2, reflected also by the *trans*-bent angle ( $\theta = 40.3^\circ$ ), indicates the presence

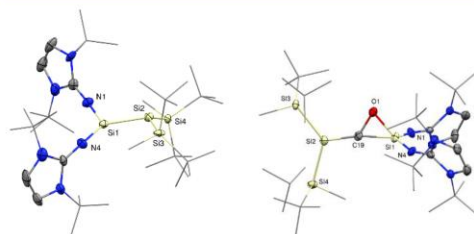


**Figure 1.** Molecular structures of disilene **1** (left) and silene **2a** (right) with thermal ellipsoids drawn at the 30% probability level. Hydrogen atoms are omitted for clarity, <sup>t</sup>Bu- and Me-groups are simplified as wireframes. Selected bond lengths [Å] and angles [°]: **1** Si1–Si2 2.219(4), Si1–N1 1.659(4), Si1–N4 1.604(4), Si2–Si3 2.360(6), Si2–Si4 2.343(5), N1–Si1–N4 113.1(2), Si3–Si2–Si4 138.2(2), Si1–Si2–Si3 106.3(2), Si2–Si1–N1 115.4(2), **2a**

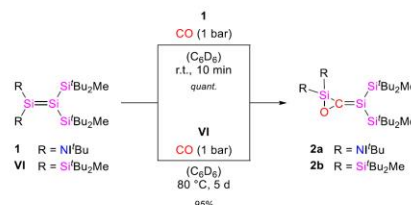
**Table 1. Selected Structural Features and  $^{29}\text{Si}$  NMR Shifts of Iminodisilenes I and 1**

#	d(Si=Si) [Å]	$\tau^a$ [°]	$\theta^b$ [°]	$\delta^{29}\text{Si}$ [ppm]
<b>V-Z</b>	2.2844(7)	25.5	36.3, 34.7	67.4 (Si=Si)
<b>1</b>	2.219(4)	46.9	8.1 (=Si <sup>+</sup> N <sub>2</sub> ) 40.3 (=Si <sup>-</sup> Si <sub>2</sub> )	30.4 (=Si <sup>+</sup> N <sub>2</sub> ) -176.1 (=Si <sup>-</sup> Si <sub>2</sub> )



of a stereochemically active lone pair (cf. structures **1'** and **1''** in Chart 2), comparable to compound **III**. Rearrangement of substituents in disilenes has already been observed for tetraaryl-<sup>47</sup> and tetrasilyl-substituted<sup>48</sup> examples. In contrast to our results however, in these cases, only equilibria between the  $\text{ABSi}=\text{SiAB}$  and  $\text{A}_2\text{Si}=\text{SiB}_2$  forms were observed and dyotropic isomerization mechanisms were concluded.<sup>47-48</sup> With the unique compound **1** in hand, we set out to explore the reactivity toward carbon monoxide, since this is a rather undeveloped field of disilene chemistry. Indeed, **1** readily reacts with CO, under mild conditions, selectively furnishing the Brook-type<sup>49</sup> silene **2a** in quantitative yield (Scheme 2).

**Scheme 2. Reaction of Disilenes 1 and VI to Silenes 2**



In the  $^1\text{H}$  NMR spectrum of **2a**, splitting of the <sup>t</sup>Bu- and Me-signals of the silyl groups is observable, because of the reduced symmetry compared to compound **1**. The Si<sub>2</sub>Si atom in **2a** resonates at 10.1 ppm in the  $^{29}\text{Si}$  NMR spectrum. Since previously reported silenes cover a wide range of  $^{29}\text{Si}$  NMR shifts ( $-78.7$  ppm to 144.2 ppm),<sup>50</sup> this value is not very characteristic. For comparison, Scheschkewitz et al. presented a cyclic silene **VII**, which also has an oxygen substituent adjacent to the  $\text{C}^{\text{sp}2}$  center and displays a comparable  $^{29}\text{Si}$  NMR shift of 17.5 ppm.<sup>51</sup> In the  $^{13}\text{C}$  NMR spectrum of **2a**, the  $\text{C}^{\text{sp}2}$  signal can be observed at 231.1 ppm, which is within the typical range for silenes<sup>50</sup> and also compares well to **VII** (213.4 ppm).<sup>51</sup> Notably, both <sup>t</sup>Bu<sub>2</sub>MeSi groups and the three-membered silaoxirane ring are in-plane with the central Si=C atoms. The NHi substituents are arranged perpendicular to this plane, thus minimizing steric repulsion between the <sup>t</sup>Bu-wingtips and the bulky silyl groups. Presumably, the formation of **2a** proceeds via coordination of carbon monoxide to the positively polarized Si atom in disilene **1** (see Scheme S1). This kind of donor-acceptor transition state was also assumed for the formation of **II**,<sup>42</sup> as well as for the addition of isocyanides to Brook's silene.<sup>52-53</sup> Subsequently, a three-membered transition state (bis(sila)ketone) is formed, that rearranges to silene **2a**. In order to examine whether a strongly polarized disilene structure like in **1** is necessary to activate carbon monoxide in this fashion, we utilized the previously reported and structurally related (via the Si=Si(<sup>t</sup>Bu<sub>2</sub>Me)<sub>2</sub> moiety) tetrasilyldisilene

(<sup>t</sup>Bu<sub>2</sub>MeSi)<sub>2</sub>Si=Si(Si<sup>t</sup>Bu<sub>2</sub>Me)<sub>2</sub> (**VI**)<sup>54</sup> (Scheme 2) in the same conversion. In fact, **VI** turned out to react with carbon monoxide, however, at a much lower rate than **1**. Heating of the reaction mixture to 80 °C for 5 days is required to achieve full conversion to silene **2b**. The slow formation of compound **2b** which also displays a cyclic silene structure, similar to **2a**, also indicates the presumed mechanism. Since the polarization in **1** greatly facilitates coordination of the Lewis-basic carbon monoxide, formation of the initial donor-acceptor transition state should take place significantly easier than with the non-polar disilene **VI**.

In summary, we isolated and fully characterized an A<sub>2</sub>Si=SiB<sub>2</sub>-type imino-silyl disilene **1** from the thermally induced rearrangement reaction of ABSi=SiAB-type disilene **V**. Interestingly, compound **1** features a strongly polarized Si=Si double bond. Nonetheless, it is stable without coordination of a Lewis-base donor, because of the π-donating effects of the NHI substituents. In addition, we presented the facile activation of carbon monoxide by disilene **1**, resulting in the formation of the stable silene **2a**.

## ASSOCIATED CONTENT

Supporting Information

## AUTHOR INFORMATION

Corresponding Author

\*s.inoue@tum.de

ORCID

Shigeyoshi Inoue: 0000-0001-6685-6352

Notes

The authors declare no conflict of interest.

## ACKNOWLEDGMENT

We thank WACKER Chemie AG and the European Research Council (SILION 637394) for continued financial support. We are also thankful to Dr. Oksana Storcheva for conducting the EPR measurements

## REFERENCES

- (1) Peng, J.-B.; Geng, H.-Q.; Wu, X.-F., The Chemistry of CO: Carbonylation. *Chem* **2019**, *5*, 526-552.
- (2) Gibson, S. E.; Stevenazzi, A., The Pauson-Khand Reaction: the Catalytic Age Is Here! *Angew. Chem. Int. Ed.* **2003**, *42*, 1800-1810.
- (3) Khand, I. U.; Knox, G. R.; Pauson, P. L.; Watts, W. E.; Foreman, M. L., Organocobalt Complexes. Part II. Reaction of Acetylenehexacarbonyldicobalt Complexes, (R<sup>1</sup>C<sub>2</sub>R<sup>2</sup>)Co<sub>2</sub>(CO)<sub>6</sub>, with Norbornene and its Derivatives. *J. Chem. Soc., Perkin Trans. 1* **1973**, 977-981.
- (4) Fischer, F.; Trotsch, H., Über die direkte Synthese von Erdöl-Kohlenwasserstoffen bei gewöhnlichem Druck. (Erste Mitteilung). *Ber. Dtsch. Chem. Ges. (A and B Series)* **1926**, *59*, 830-831.
- (5) Khodakov, A. Y.; Chu, W.; Fongarland, P., Advances in the Development of Novel Cobalt Fischer-Tropsch Catalysts for Synthesis of Long-Chain Hydrocarbons and Clean Fuels. *Chem. Rev.* **2007**, *107*, 1692-1744.
- (6) Kalescky, R.; Kraka, E.; Cremer, D., Identification of the Strongest Bonds in Chemistry. *J. Phys. Chem. A* **2013**, *117*, 8981-8995.
- (7) Gaydon, A. G.; Penney, W. G., The Dissociation Energies of CO, N<sub>2</sub>, NO and CN. *Proc. R. Soc. A* **1945**, *183*, 374-388.
- (8) Burg, A. B.; Schlesinger, H. I., Hydrides of Boron. VII. Evidence of the Transitory Existence of Borine (BH<sub>3</sub>): Borine Carbonyl and Borine Trimethylamine. *J. Am. Chem. Soc.* **1937**, *59*, 780-787.
- (9) Dahcheh, F.; Martin, D.; Stephan, D. W.; Bertrand, G., Synthesis and Reactivity of a CAAC-Aminoborylene Adduct: A Hetero-Allene or an Organoboron Isoelectronic with Singlet Carbenes. *Angew. Chem. Int. Ed.* **2014**, *53*, 13159-13163.
- (10) Braunschweig, H.; Dewhurst, R. D.; Hupp, F.; Nutz, M.; Radacki, K.; Tate, C. W.; Vargas, A.; Ye, Q., Multiple complexation of CO and related ligands to a main-group element. *Nature* **2015**, *522*, 327-330.
- (11) Braunschweig, H.; Krummenacher, I.; Légaré, M.-A.; Matler, A.; Radacki, K.; Ye, Q., Main-Group Metallomimetics: Transition Metal-like Photolytic CO Substitution at Boron. *J. Am. Chem. Soc.* **2017**, *139*, 1802-1805.
- (12) Wang, H.; Wu, L.; Lin, Z.; Xie, Z., Transition-Metal-Like Behavior of Monovalent Boron Compounds: Reduction, Migration, and Complete Cleavage of CO at a Boron Center. *Angew. Chem. Int. Ed.* **2018**, *57*, 8708-8713.
- (13) Légaré, M.-A.; Pranckevicius, C.; Braunschweig, H., Metallomimetic Chemistry of Boron. *Chem. Rev.* **2019**, *119*, 8231-8261.
- (14) Braunschweig, H.; Dellermann, T.; Dewhurst, R. D.; Ewing, W. C.; Hammond, K.; Jimenez-Halla, J. O. C.; Kramer, T.; Krummenacher, I.; Mies, J.; Phukan, A. K.; Vargas, A., Metal-free binding and coupling of carbon monoxide at a boron-boron triple bond. *Nat. Chem.* **2013**, *5*, 1025-1028.
- (15) Böhnke, J.; Braunschweig, H.; Dellermann, T.; Ewing, W. C.; Hammond, K.; Jimenez-Halla, J. O. C.; Kramer, T.; Mies, J., The Synthesis of B<sub>2</sub>(SIDip)<sub>2</sub> and its Reactivity Between the Diboracumulenic and Diborynic Extremes. *Angew. Chem. Int. Ed.* **2015**, *54*, 13801-13805.
- (16) Arrowsmith, M.; Böhnke, J.; Braunschweig, H.; Celik, M. A., Reactivity of a Dihydrodiborene with CO: Coordination, Insertion, Cleavage, and Spontaneous Formation of a Cyclic Alkyne. *Angew. Chem. Int. Ed.* **2017**, *56*, 14287-14292.
- (17) Zhang, H.; Cao, Z.; Wu, W.; Mo, Y., The Transition-Metal-Like Behavior of B<sub>2</sub>(NHC)<sub>2</sub> in the Activation of CO: HOMO-LUMO Swap Without Photoinduction. *Angew. Chem. Int. Ed.* **2018**, *57*, 13076-13081.
- (18) Yuvaraj, K.; Douair, I.; Paparo, A.; Maron, L.; Jones, C., Reductive Trimerization of CO to the Deltate Dianion Using Activated Magnesium(I) Compounds. *J. Am. Chem. Soc.* **2019**, *141*, 8764-8768.
- (19) Lavallo, V.; Canac, Y.; Donnadiu, B.; Schoeller, W. W.; Bertrand, G., CO Fixation to Stable Acyclic and Cyclic Alkyl Amino Carbenes: Stable Amino Ketenes with a Small HOMO-LUMO Gap. *Angew. Chem. Int. Ed.* **2006**, *45*, 3488-3491.
- (20) Hudnall, T. W.; Bielawski, C. W., An *N,N'*-Diamidocarbene: Studies in C-H Insertion, Reversible Carbonylation, and Transition-Metal Coordination Chemistry. *J. Am. Chem. Soc.* **2009**, *131*, 16039-16041.
- (21) Siemeling, U.; Färber, C.; Bruhn, C.; Leibold, M.; Selent, D.; Baumann, W.; von Hopffgarten, M.; Goedecke, C.; Frenking, G., *N*-heterocyclic carbenes which readily add ammonia, carbon monoxide and other small molecules. *Chem. Sci.* **2010**, *1*, 697-704.
- (22) Dobrovetsky, R.; Stephan, D. W., Stoichiometric Metal-Free Reduction of CO in Syn-Gas. *J. Am. Chem. Soc.* **2013**, *135*, 4974-4977.
- (23) Stephan, D. W., The broadening reach of frustrated Lewis pair chemistry. *Science* **2016**, *354*, aaf7229.
- (24) Devillard, M.; de Bruin, B.; Siegler, M. A.; van der Lugt, J. I., Transition-Metal-Free Cleavage of CO. *Chem. Eur. J.* **2017**, *23*, 13628-13632.
- (25) Hansmann, M. M.; Bertrand, G., Transition-Metal-like Behavior of Main Group Elements: Ligand Exchange at a Phosphinidene. *J. Am. Chem. Soc.* **2016**, *138*, 15885-15888.
- (26) Hansmann, M. M.; Jazzar, R.; Bertrand, G., Singlet (Phosphino)phosphinidenes are Electrophilic. *J. Am. Chem. Soc.* **2016**, *138*, 8356-8359.
- (27) Protchenko, A. V.; Vasko, P.; Do, D. C. H.; Hicks, J.; Fuentes, M. Á.; Jones, C.; Aldridge, S., Reduction of Carbon Oxides by an Acyclic Silylene: Reductive Coupling of CO. *Angew. Chem. Int. Ed.* **2019**, *58*, 1808-1812.
- (28) Luecke, M.-P.; Kostenko, A.; Wang, Y.; Yao, S.; Driess, M., Silicon-Mediated Coupling of Carbon Monoxide, Ammonia, and

## 11. Formation of a Silene through CO Activation by a Polarized Iminodisilene

- Primary Amines to Form Acetamides. *Angew. Chem. Int. Ed.* **2019**, *58*, 12940-12944.
- (29) Wang, Y.; Kostenko, A.; Hadlington, T. J.; Luecke, M.-P.; Yao, S.; Driess, M., Silicon-Mediated Selective Homo- and Heterocoupling of Carbon Monoxide. *J. Am. Chem. Soc.* **2019**, *141*, 626-634.
- (30) Nakata, N.; Oikawa, T.; Matsumoto, T.; Kabe, Y.; Sekiguchi, A., Silyl-Substituted 1,4-Disila(Dewar benzene): New Synthesis and Unexpected Insertion of CO into the Si-Si Bond To Form a Disilyl Ketone. *Organometallics* **2005**, *24*, 3368-3370.
- (31) Cowley, M. J.; Huch, V.; Scheschkewitz, D., Donor-Acceptor Adducts of a 1,3-Disila-2-oxallyl Zwitterion. *Chem. Eur. J.* **2014**, *20*, 9221-9224.
- (32) Majumdar, M.; Omlor, I.; Yildiz, C. B.; Azizoglu, A.; Huch, V.; Scheschkewitz, D., Reductive Cleavage of Carbon Monoxide by a Disilene. *Angew. Chem. Int. Ed.* **2015**, *54*, 8746-8750.
- (33) West, R.; Fink, M. J.; Michl, J., Tetramethylidisilene, a Stable Compound Containing a Silicon-Silicon Double Bond. *Science* **1981**, *214*, 1343.
- (34) Kira, M., Bonding and structure of disilenes and related unsaturated group-14 element compounds. *Proc. Jpn. Acad., Ser. B, Phys. Biol. Sci.* **2012**, *88*, 167-191.
- (35) Iwamoto, T.; Ishida, S., Multiple Bonds with Silicon: Recent Advances in Synthesis, Structure, and Functions of Stable Disilenes. In *Functional Molecular Silicon Compounds II: Low Oxidation States*, Scheschkewitz, D., Ed. Springer International Publishing Switzerland, **2014**.
- (36) Weidenbruch, M., Recent Advances in the Chemistry of Silicon-Silicon Multiple Bonds. In *The Chemistry of Organic Silicon Compounds*, Rappoport, Z.; Apeloig, Y., Eds. John Wiley & Sons, Ltd., **2001**.
- (37) Präsang, C.; Scheschkewitz, D., Reactivity in the periphery of functionalised multiple bonds of heavier group 14 elements. *Chem. Soc. Rev.* **2016**, *45*, 900-921.
- (38) Okazaki, R.; West, R., Chemistry of Stable Disilenes. In *Advances in Organometallic Chemistry*, Gordon, F.; Stone, A.; West, R., Eds. Academic Press, **1996**.
- (39) Kira, M.; Iwamoto, T., Progress in the Chemistry of Stable Disilenes. In *Advances in Organometallic Chemistry*, West, R.; Hill, A. F., Eds. Academic Press, **2006**.
- (40) Rammo, A.; Scheschkewitz, D., Functional Disilenes in Synthesis. *Chem. Eur. J.* **2018**, *24*, 6866-6885.
- (41) Cowley, M. J.; Ohmori, Y.; Huch, V.; Ichinohe, M.; Sekiguchi, A.; Scheschkewitz, D., Carbonylation of Cyclotrisilenes. *Angew. Chem. Int. Ed.* **2013**, *52*, 13247-13250.
- (42) Majumdar, M.; Huch, V.; Bejan, I.; Meltzer, A.; Scheschkewitz, D., Reversible, Complete Cleavage of Si=Si Double Bonds by Isocyanide Insertion. *Angew. Chem. Int. Ed.* **2013**, *52*, 3516-3520.
- (43) Yamaguchi, T.; Sekiguchi, A., Unusual Reactivity of a Disilyne with 4-Dimethylaminopyridine: Formation of an Intramolecularly N-Coordinated Silylene and Its Isomerization to a Zwitterionic Silyl Anion. *J. Am. Chem. Soc.* **2011**, *133*, 7352-7354.
- (44) Wendel, D.; Reiter, D.; Porzelt, A.; Altmann, P. J.; Inoue, S.; Rieger, B., Silicon and Oxygen's Bond of Affection: An Acyclic Three-Coordinate Silanone and Its Transformation to an Iminosiloxysilylene. *J. Am. Chem. Soc.* **2017**, *139*, 17193-17198.
- (45) Marschner, C., A New and Easy Route to Polysilylanylpotassium Compounds. *Eur. J. Inorg. Chem.* **1998**, *1998*, 221-226.
- (46) Schweizer, J. I.; Scheibel, M. G.; Diefenbach, M.; Neumeyer, F.; Würtele, C.; Kulminkaya, N.; Linsler, R.; Auner, N.; Schneider, S.; Holthausen, M. C., A Disilene Base Adduct with a Dative Si-Si Single Bond. *Angew. Chem. Int. Ed.* **2016**, *55*, 1782-1786.
- (47) Yokelson, H. B.; Siegel, D. A.; Millevoite, A. J.; Maxka, J.; West, R., 1,2-Diaryl Rearrangement in Tetraaryldisilenes. *Organometallics* **1990**, *9*, 1005-1010.
- (48) Iwamoto, T.; Okita, J.; Kabuto, C.; Kira, M., Synthesis, structure and isomerization of A<sub>2</sub>Si=SiB<sub>2</sub>-type tetrakis(trialkylsilyl)disilenes. *J. Organomet. Chem.* **2003**, *686*, 105-111.
- (49) Brook, A. G.; Nyburg, S. C.; Abdesaken, F.; Gutekunst, B.; Gutekunst, G.; Krishna, R.; Kallury, M. R.; Poon, Y. C.; Chang, Y. M.; Winnie, W. N., Stable Solid Silaethylenes. *J. Am. Chem. Soc.* **1982**, *104*, 5667-5672.
- (50) Ottosson, H.; Eklöf, A. M., Silenes: Connectors between classical alkenes and nonclassical heavy alkenes. *Coord. Chem. Rev.* **2008**, *252*, 1287-1314.
- (51) Bejan, I.; Güclü, D.; Inoue, S.; Ichinohe, M.; Sekiguchi, A.; Scheschkewitz, D., Stable Cyclic Silenes from Reaction of Disilenes with Carboxylic Acid Chlorides. *Angew. Chem. Int. Ed.* **2007**, *46*, 3349-3352.
- (52) Brook, A. G.; Saxena, A. K.; Sawyer, J. F., 1-Sila-3-azacyclobutanes: the Insertion of Isocyanides into Silaaziridines. *Organometallics* **1989**, *8*, 850-852.
- (53) Brook, A. G.; Kong, Y. K.; Saxena, A. K.; Sawyer, J. F., Silaaziridines from the Reaction of Isonitriles with Stable Silenes. *Organometallics* **1988**, *7*, 2245-2247.
- (54) Sekiguchi, A.; Inoue, S.; Ichinohe, M.; Arai, Y., Soluble Anion Radical of Blue Disilene (t-Bu<sub>2</sub>MeSi)<sub>2</sub>Si=Si(SiMe<sub>2</sub>t-Bu)<sub>2</sub> Formed upon One-Electron Reduction: Synthesis and Characterization. *J. Am. Chem. Soc.* **2004**, *126*, 9626-9629.



## 12. Summary and Outlook

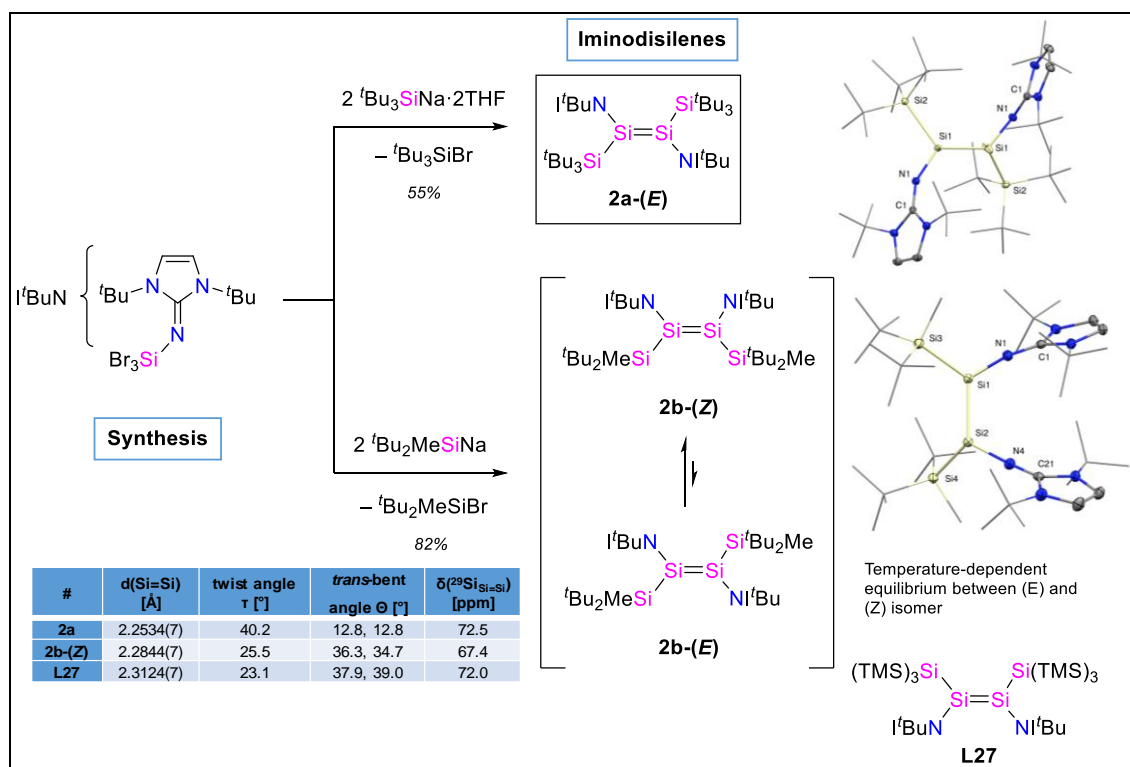
The isolation and structural characterization of the first disilene **L22** by West *et al.* in 1985<sup>[139,145]</sup> and of the first silyl radical **L1** by Sekiguchi in 2001<sup>[36]</sup> can be considered to be among the most important milestones in modern main group chemistry. Ever since, these low-coordinate silicon species have been thoroughly investigated and reactivities and applications have been identified. Disilenes have demonstrated interesting reactivity patterns towards small molecules<sup>[133]</sup> and silyl radicals have already been successfully applied in organic radical batteries.<sup>[5]</sup>

The goal of this thesis was to extend these highly reactive classes of low-coordinate silicon species, to enhance their stability and to further explore their reactivities and electrochemical properties.

### 12.1 Disilenes

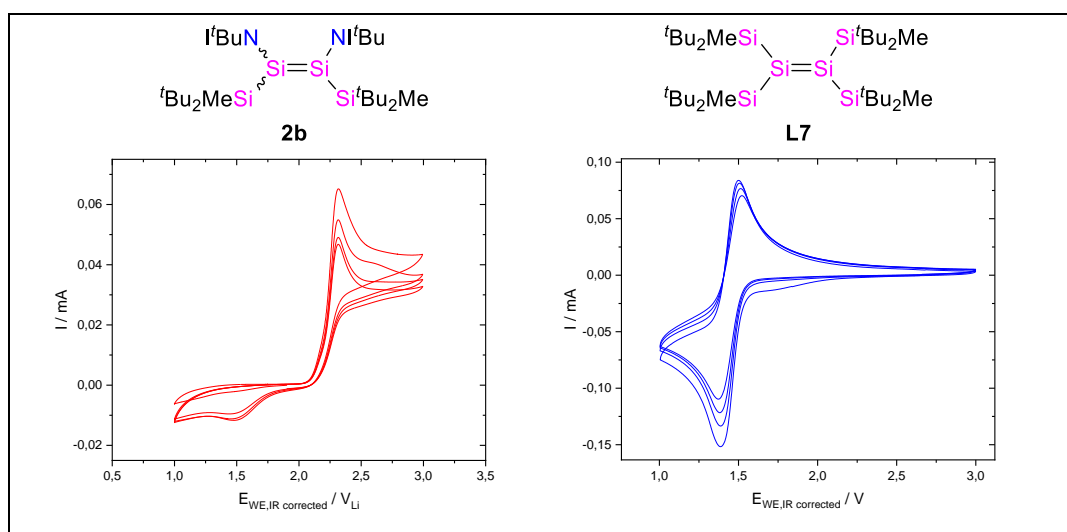
Besides neutral silicon-centered radicals, disilenes might also be suitable anode materials for organic radical batteries because of their reversible redox behavior which has been demonstrated for tetra(silyl)disilene **L7**.<sup>[57,59]</sup>

**Scheme 15:** Synthesis and structures of iminodisilenes **2a** and **2b**.



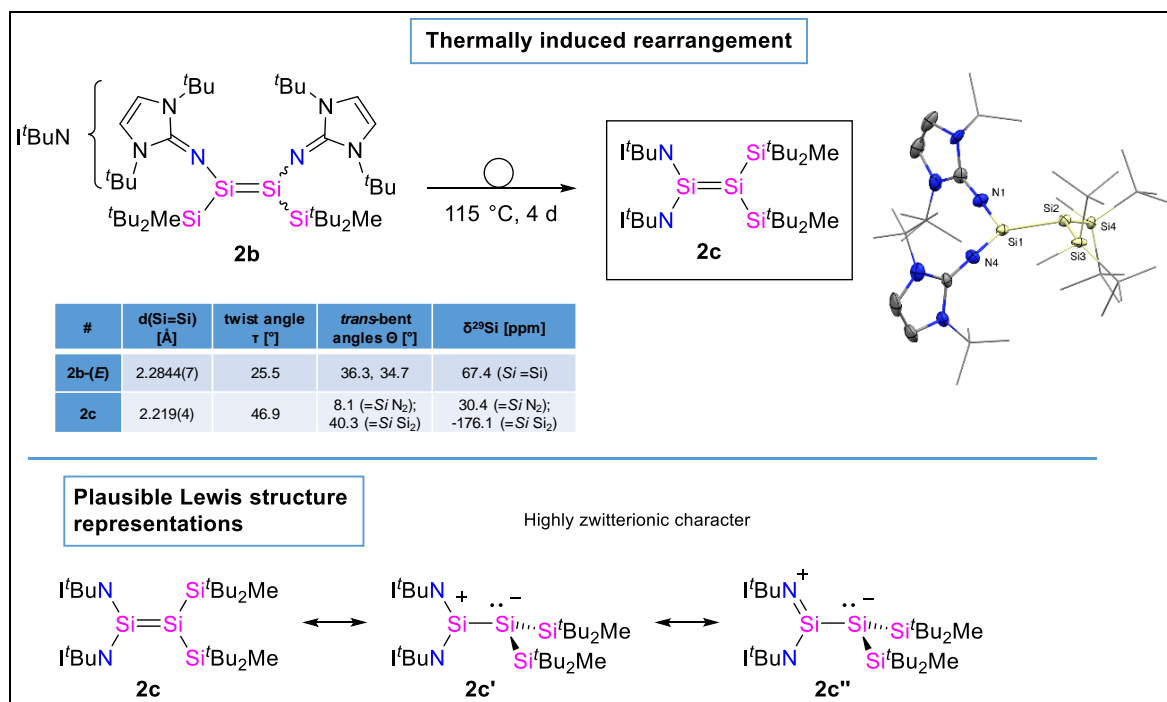
Of special interest was of course also the class of *N*-heterocyclic imino-substituted disilenes, since the first representative **L27** already showed interesting reactivity in the

activation of small molecules, such as H<sub>2</sub>, N<sub>2</sub>O, CO<sub>2</sub> and NH<sub>3</sub>.<sup>[158,192]</sup> However, **L27** is not stable at room temperature and its redox chemistry remained unexplored. Driven by these promising results, a novel iminodisilene **2a** was synthesized by the established approach of treating I<sup>t</sup>BuN–SiBr<sub>3</sub> with two equivalents of supersilanide (Scheme 15). In contrast to **L27**, **2a** adopts (*E*)-configuration in the solid state, because of the steric repulsion of the extremely bulky supersilyl groups. Although **2a** is completely stable at ambient temperature, its yield is limited by the difficult separation process from the concomitantly generated byproduct <sup>t</sup>Bu<sub>3</sub>SiBr. Thus, the disilene structure was further varied by introducing <sup>t</sup>Bu<sub>2</sub>MeSi groups, resulting in the formation of **2b**. Compound **2b** is stable, even at elevated temperatures up to 90 °C. Therefore, the byproduct can easily be removed by sublimation, increasing the isolable yield of **2b** to 82%. In the solid state, **2b**, exhibits (*Z*)-configuration whereas in solution, a temperature-dependent equilibrium between (*E*)- and (*Z*)-isomers was observed. The kinetic of this isomerization was monitored by VT NMR spectroscopy. With the initial motive of battery application in mind, CV investigations were conducted (Figure 15).



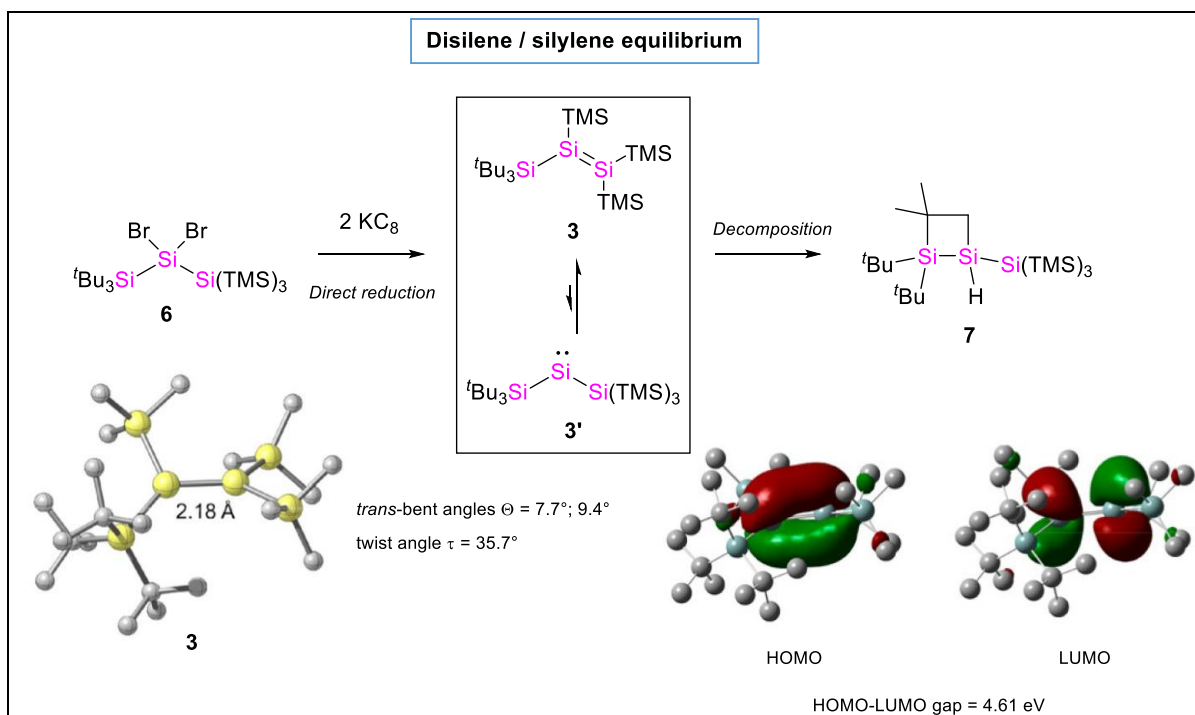
**Figure 15:** CV analysis of disilenes **2b** and **L7**.

Unfortunately, these studies showed that only a cationic species is accessible and that reversible reduction might not work. In fact, no experimental reduction of **2b** was achieved either, thus excluding the possibility of battery application of these ABSi=SiAB-type iminodisilenes. Nonetheless, compound **2b** showed interesting reactivity towards small molecules and also a cationic radical **4** was isolable (*vide infra*). Most interestingly however, compound **2b** isomerizes to the A<sub>2</sub>Si=SiB<sub>2</sub> type iminodisilene (I<sup>t</sup>BuN)<sub>2</sub>Si=Si(Si<sup>t</sup>Bu<sub>2</sub>Me)<sub>2</sub> (**2c**) upon heating to 115 °C for four days.

Scheme 16: Synthesis and structure of iminodisilene **2c**.

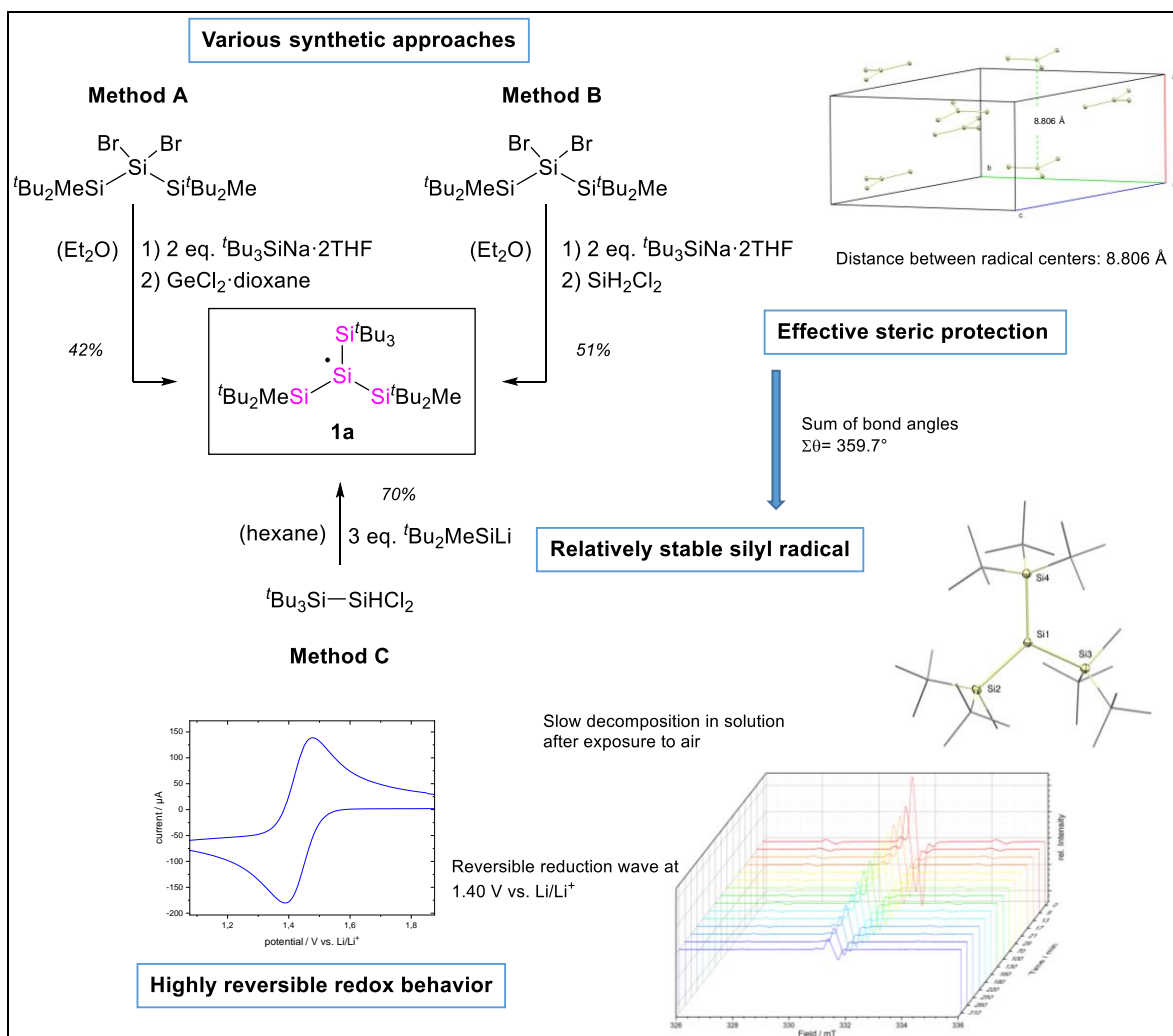
$^{29}\text{Si}$  NMR spectroscopy and single crystal XRD analysis revealed the strong zwitterionic character of **2c** with a positively polarized  $\text{N}_2\text{Si}$ -center and a negative  $\text{Si}_2\text{Si}$ -moiety (Scheme 16). Although a facile activation of CO by compound **2c** to silene **5a** was demonstrated (see chapter 12.4.1), the electrochemistry of **2c** has yet to be investigated.

Based on the CV results with **2b**, tetra(silyl)disilenes seemed to be more suitable for battery applications (Figure 15). Compound **L7** was synthesized by reductive debromination of the corresponding dibromosilane and dimerization of the intermediary formed silylene. Accordingly, a novel dibromosilane **6**, bearing both, a supersilyl and a hypersilyl group was synthesized. Reduction of this dibromosilane however, did not afford the dimerization product, but instead tetra(silyl)disilene **3** after TMS migration (Scheme 17). Unfortunately, **3** decomposes at room temperature, thus disqualifying this compound as anode material. Nevertheless, the decomposition product disiletane **7** (formed *via* C–H bond activation of a  $^t\text{Bu}$ -group), as well DFT calculations and further reactivity studies (*vide infra*) revealed an equilibrium between tetra(silyl)disilene **3** and the isomeric bis(silyl)silylene **3'** which was successfully stabilized as Lewis base adduct (see chapter 12.3).

**Scheme 17:** Synthesis and decomposition of disilene / silylene equilibrium mixture **3/3'**.

## 12.2 Silyl radicals

In 2014, the group of Sekiguchi together with the *Toyota R&D Labs.* constructed alkali- and transition metal-free organic radical battery cells, based on their neutral, heavier group 14 radicals ( $t\text{Bu}_2\text{MeSi}$ ) $_3\text{E}^\bullet$  [E = Si, Ge, Sn]. These compounds seemed to be promising candidates as anode materials because of the low reduction potentials and their highly reversible redox behavior. Indeed, the experimental cells showed remarkable cyclic stability (98% capacity after 100 cycles) with high charge and discharge rates. Among the applied group 14 radicals, the silyl compound **L2** was considered to be the most suitable because it provided the highest capacity and the fastest reaction rate.<sup>[5]</sup> Based on these promising results, this thesis aimed at improving this novel energy storage technology on the molecular level. In fact, silyl radical **1a**, which is even more kinetically stabilized than **L2**, was obtained from three different approaches in a good yield of 70% (Scheme 18). In the solid state, compound **1a** adopts a completely planar geometry, typical for silyl radical with bulky, electropositive substituents such as silyl groups. Furthermore, the distance of over 8.8 Å between the radical centers promises high diffusion rates in battery processes. In combination with the complete reversibility of the redox reaction, radical **1a** might find application as anode material in long living organic radical batteries and allow for fast charge / discharge rates.

**Scheme 18:** Synthesis and properties of silicon-centered radical **1a**.

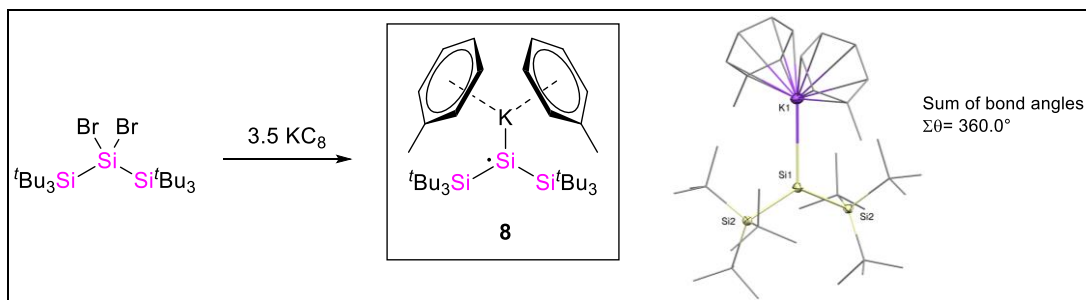
Most interestingly however, the effective steric shielding of the radical center by the extremely bulky supersilyl group makes compound **1a** relatively inert towards air and moisture. This feature might facilitate battery cell construction and thus lead to a wider spread of this sustainable technology.

An alternative synthetic approach for functionalized silicon-centered radicals could be the reaction of an alkali metal-substituted silyl radical with an electrophile *via* salt metathesis. From over-reduction of  $(\text{tBu}_3\text{Si})_2\text{SiBr}_2$  with 3.5 equivalents  $\text{KC}_8$ , the potassium-substituted radical **8** was obtained (Scheme 19). Despite the extreme sensitivity of **8** towards air and moisture and the fact that it decomposes in toluene solution, a crystal structure was obtained. Compound **8** displays a completely planar geometry (sum of bond angles  $\Sigma\theta = 360.0^\circ$ ), typical for alkali metal-substituted silyl radicals. Furthermore, the Si–K distance, which is comparable to hypersilyl potassium, demonstrates the contact ion pair character of compound **8** in the solid state.



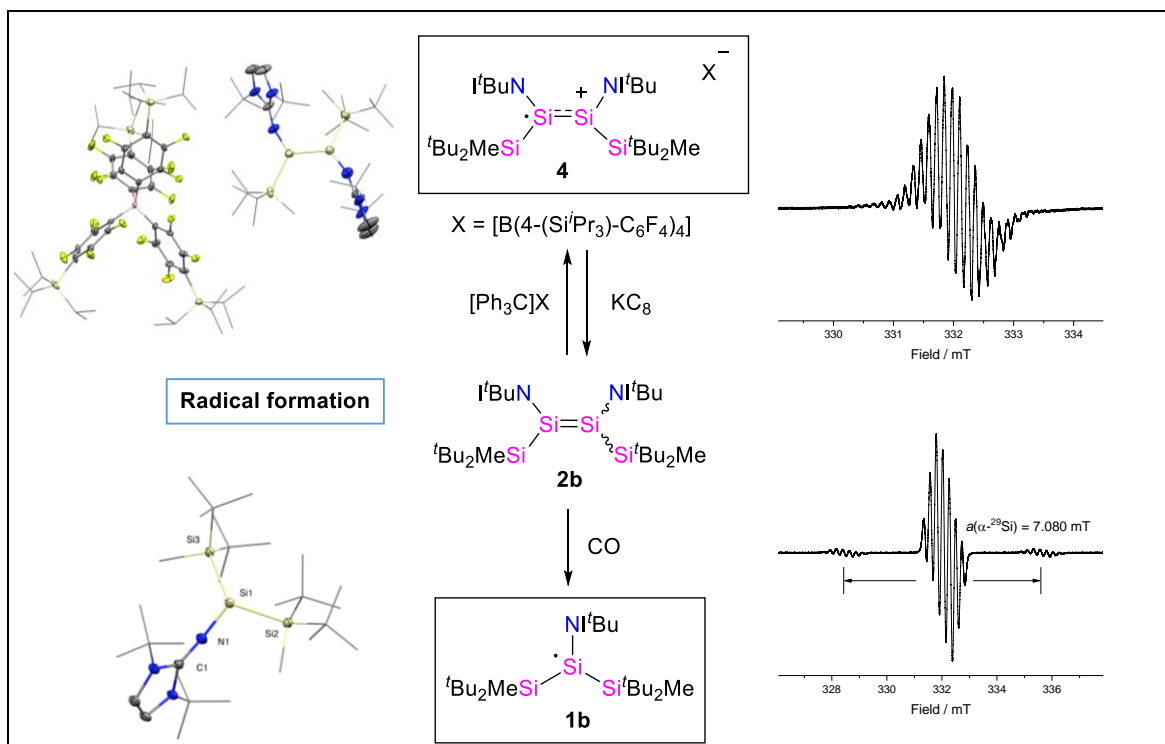
Unfortunately, attempts to introduce the silyl radical moiety of **8** to electrophiles, in order to produce functionalized silicon radicals, remained unsuccessful so far.

**Scheme 19:** Synthesis and structure of potassium-substituted silyl radical **8**.



Prior to this thesis, no silyl radical with electronegative substituents, as for example nitrogen, has been structurally characterized. By one-electron oxidation of iminodisilene **2b** the cationic radical **4** was obtained (Scheme 20). It is the second reported example of a disilene radical cation (after **L7<sup>•+</sup>**), the first with heteroatom substituents. Remarkably, reduction of **4** with  $\text{KC}_8$  furnished the starting material **2b**. CV analysis showed, that the oxidation of the iminodisilene **2b** takes place at lower potentials (about 1 V), than required for tetra(silyl)disilene **L7**. Splitting of the EPR signal of **4** indicated coupling of the unpaired electron with the  $^{14}\text{N}$  nuclei of the imino group. This result underlined the suitability of the NHI substituent to effectively stabilize cationic silyl centers.

Neutral silicon radicals with imino and silyl substituents might be of great significance for battery applications. Targeted synthesis *via* one-electron reduction of the corresponding halosilane did not afford the desired radical. Serendipitously however, decomposition of disilene **2b** in presence of CO afforded the NHI-substituted silyl radical **1b**. The synthesis of **1b** was not perfectly reproducible, provided only poor yield and the mechanism for the formation remains unclear. Nevertheless, it is an unambiguous evidence, that these kinds of heteroatom-substituted silyl radicals are stable and isolable. In fact, **1b** was even structurally characterized by SC-XRD analysis. Compound **1b** adopts a slightly pyramidalized geometry ( $\Sigma\theta = 353.5^\circ$ ), in contrast to the tri(silyl)silyl radicals **L2** and **1a**. This can be attributed to effect of the electronegative NHI substituent.<sup>[26]</sup> However, the electrochemical properties of imino-substituted silyl radicals have yet to be determined.

Scheme 20: Formation and properties of silyl radicals **4** and **1b**.

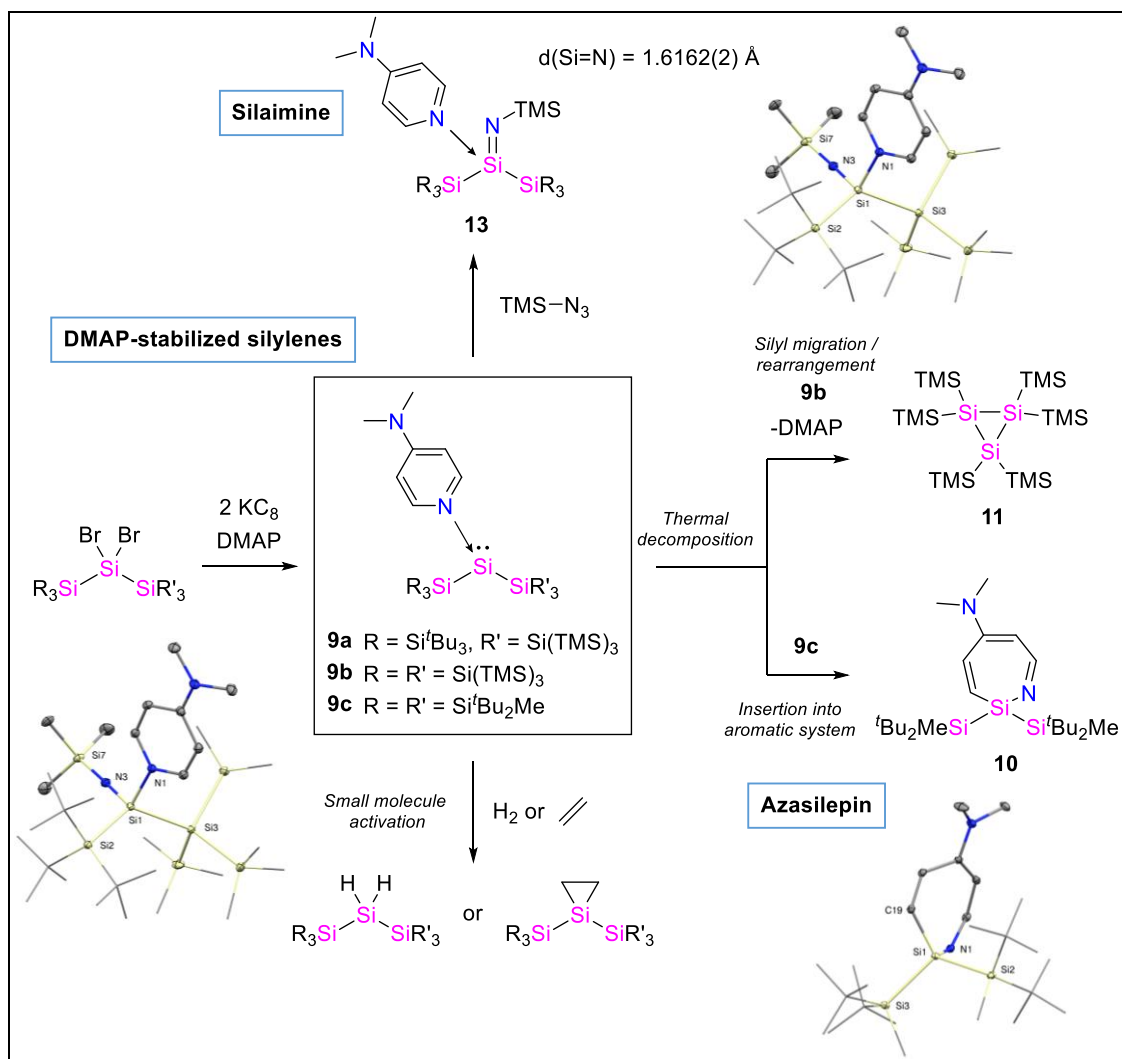
### 12.3 Silylenes

During the studies of silyl radicals and disilenes, also a number of silylenes were obtained in the course of this work. Although, these low-coordinate silicon species are not particularly promising in regard to organic radical batteries, they are considered to be potential candidates for transition metal-free catalysis, because their ambiphilic character enables facile small molecule activation. For the most part, electron donation to the empty 3p<sub>z</sub>-orbital of silylenes is necessary to control their excessive electrophilicity and allow isolation as Lewis base adducts. Therefore, reports on donor-free silylenes are scarce. Prior to this thesis, no isolable, room temperature-stable bis(silyl)silylenes were known. All synthetic attempts resulted in decomposition reactions, either *via* C–H bond activation or silyl migration.<sup>[77-80]</sup>

By reduction of dibromosilane **6** however, an equilibrium mixture consisting of tetra(silyl)disilene **3** (*vide supra*) and the isomeric bis(silyl)silylene **3'** was obtained (Scheme 17). This unique behavior results from the tailor-made combination of supersilyl and hypersilyl substituents. On the one hand, they provide kinetic stabilization (supersilyl group) but on the other hand also allow for facile TMS group migration (hypersilyl group). Because of this tautomerism, silylene **3'** is indefinitely stable at –35 °C and thus the only isolable bis(silyl)silylene derivative to date. However,

the silylene moiety of **3'** eventually inserts into a C–H bond of a <sup>t</sup>Bu-group at room temperature, generating disiletane **7**.

**Scheme 21:** Synthesis and reactivity of DMAP silylene complexes **9**.



To gain further insight into the TMS group shifts, the reduction of **6** was conducted in the presence of Lewis bases. Interestingly, with the NHC  $i\text{Pr}_2\text{Me}_2$ , a TMS-substituted silylene, isomeric to **3'** was obtained. With the weaker Lewis base DMAP instead, the silylene fragment **3'** was stabilized as donor-acceptor complex **9a** (Scheme 21). Compound **9a** is stable in solution up to  $60 \text{ }^\circ\text{C}$ . Above this temperature it decomposes to disiletane **7** under liberation of DMAP. This observation already indicated the suitability of DMAP-stabilization for the isolation of otherwise elusive bis(silyl)silylenes under conservation of their unique reactivity. Driven by these initial results, two additional DMAP-bis(silyl)silylene complexes **9b** and **9c** were synthesized analogously. In contrast to **9a**, **9b** and **9c** undergo completely different thermally induced isomerization reactions. At  $65 \text{ }^\circ\text{C}$  the silylene moiety of **9b** inserts into the

C–N bond of DMAP under dearomative ring expansion, generating azasilepin **10**. Upon heating to 65 °C, compound **9c**, the first stable bis(hypersilyl)silylene derivative, rearranges to the cyclic silane **11** under liberation of DMAP. The attempted synthesis of DMAP-stabilized bis(supersilyl)silylene was unsuccessful and afforded only the C–H bond activation product, that was observed from decomposition of the free silylene. Over-reduction of the corresponding dibromosilane however, furnished the bis(supersilyl)-substituted silicon radical **8** (*vide supra*).

## 12.4 Reactivities of Low-coordinate Silicon Compounds Towards Small Molecules

Conversion of small molecules such as H<sub>2</sub>, CO, CO<sub>2</sub> and P<sub>4</sub> to value added products is a task that is realized on industrial scale by transition metal catalysis. A promising way to substitute precious, expensive or toxic transition metals in these processes might be to mimic their behavior with main group element compounds. In order to achieve this ambitious goal, highly reactive main group species, which selectively undergo oxidative addition with these small molecules are required. Disilenes and silylenes are among those promising considered compounds.

### 12.4.1 Activation by disilenes

In general, disilenes display intense colors because of their inherently small HOMO-LUMO gaps (Figure 16). Iminodisilenes **2** are no exception to this trend and thus promising with respect to small molecule activation.

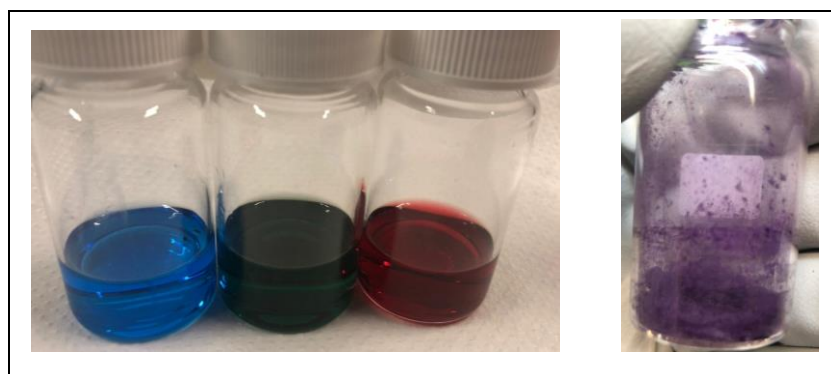
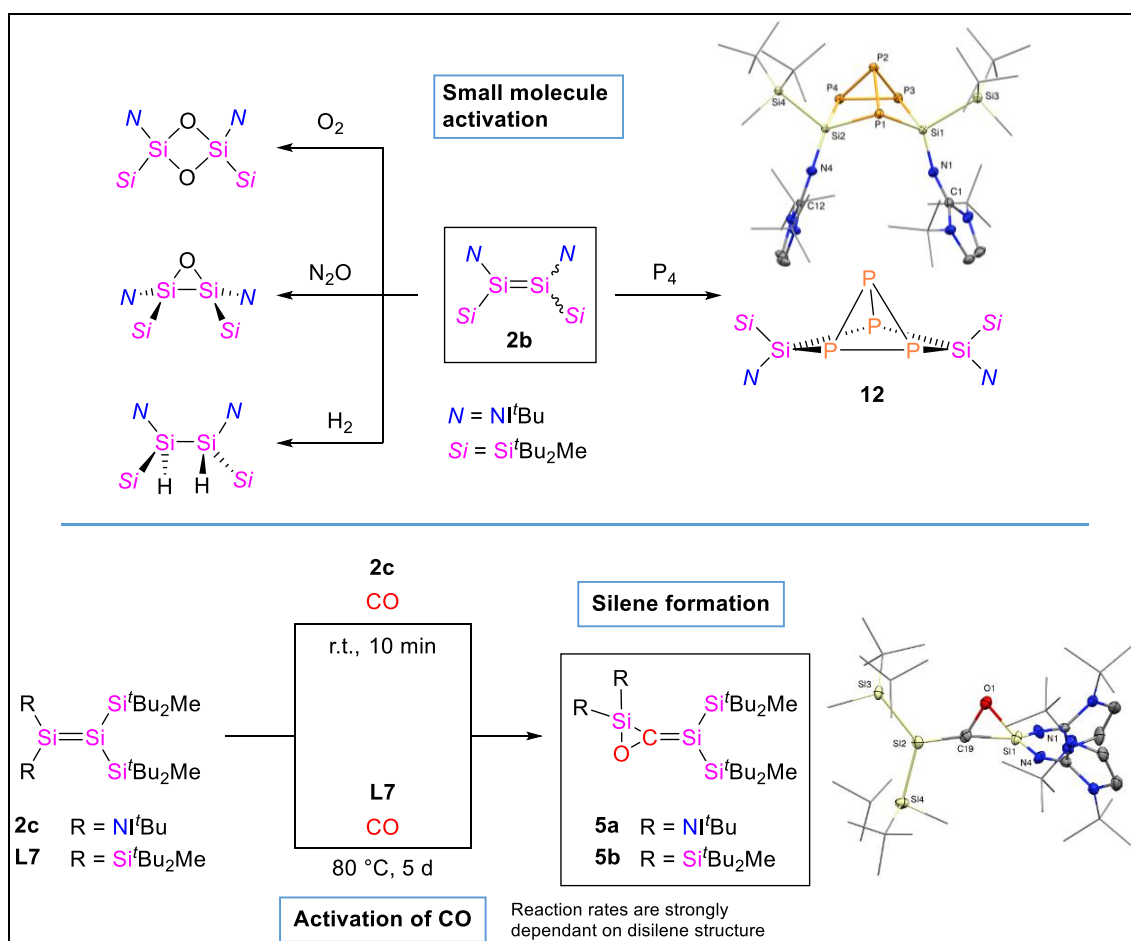


**Figure 16:** Depiction of disilenes in solution, or in solid state. From left: **L7**, **2a**, **2b** and **2c**.

Previous to this work, iminodisilene **L27** has already demonstrated remarkable reactivity towards H<sub>2</sub>, N<sub>2</sub>O, O<sub>2</sub>, CO<sub>2</sub> and NH<sub>3</sub>. Disilene **2b** showed comparable reaction behavior. Facile activation of dihydrogen to the 1,2-addition product was observed even at ambient temperature (Scheme 22). Besides that, a silaepoxide and a four-

membered cyclic siloxane were obtained from oxidation of **2b** with  $\text{N}_2\text{O}$  and  $\text{O}_2$ , respectively. Most interestingly however, white phosphorus was activated in a unique fashion, furnishing compound **12**. In **12**, the two former low-coordinate silicon centers are bridged by three P atoms of the  $\text{P}_4$  tetrahedron. Additionally, silenes **5** were synthesized by exposing the  $\text{A}_2\text{Si}=\text{SiB}_2$  type disilene **2c** and the literature-reported, symmetric disilene  $(^t\text{Bu}_2\text{MeSi})_2\text{Si}=\text{Si}(^t\text{Bu}_2\text{Me})_2$  (**L7**) to carbon monoxide. Notably, iminodisilene **2c** reacts within minutes at room temperature, whereas **L7** requires heating to  $80\text{ }^\circ\text{C}$  for 4 days. Presumably, the highly polarized character of **2c** is the reason for this significant difference in reaction rates.

**Scheme 22:** Small molecule activation by disilenes.



The equilibrium mixture of tetra(silyl)disilene **3** and the isomeric bis(silyl)silylene **3'** was also investigated in regard of small molecule activation. However, only with ammonia, the disilene 1,2-addition product was obtained. In the cases of  $\text{H}_2$  and ethylene, exclusively reaction of the silylene **3'** was observed.



### 12.4.2 Activation by silylenes

Silylene **3'** which is in equilibrium with disilene **3** is the first isolable example of a bis(silyl)silylene and showed according reactivity. It inserts into the H–H bond in dihydrogen, even at  $-40\text{ }^{\circ}\text{C}$ , thus representing the fastest  $\text{H}_2$  activation by silicon compounds to date. It was further shown, that upon exposure of **3/3'** to ethylene selective silirane formation takes place.

In sharp contrast to donor-free examples, the reactivity of NHC-stabilized silylenes is strictly limited. Hence, no  $\text{H}_2$  activation by an NHC-silylene complex has been reported. Due to the lower Lewis basicity of DMAP, compared to NHCs, the respective complexes are far more reactive. In fact, it was demonstrated that DMAP silylene complexes **9** show bis(silyl)silylene reactivity upon dissociation of the donor at elevated temperatures (Scheme 21). Also, silirane formation was observed and DMAP-stabilized silaimines **13** were obtained from the reaction of **9a** and **9b** with trimethylsilyl azide. Therefore, these novel donor-stabilized silylenes can be considered easily accessible synthetic equivalents for otherwise elusive bis(silyl)silylenes.

## 12.5 Outlook

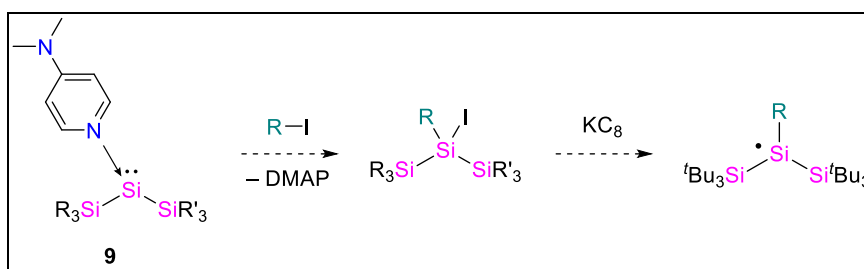
Disilene **2b** is completely stable in solution, even at elevated temperatures and thus easier to handle than **L27**. Nevertheless, it shows comparably strong reactivity, which in combination with the high isolable yield make it the perfect test compound for further reactivity exploration of the class of iminodisilenes. Because of its ability to activate small molecules, compound **2b** might even be applicable as catalyst for example for hydroboration or transfer hydrogenation of suitable substrates. The isomeric, zwitterionic disilene **2c** is absolutely unprecedented and its reactivity except towards carbon monoxide remains unexplored. With the polarized Si=Si double bond, this compound might be ideal for facile small molecule activation, probably even in a catalytic context. The CV analysis of the literature-reported tetra(silyl)disilene ( $^t\text{Bu}_2\text{MeSi}$ )<sub>2</sub>Si=Si(Si $^t\text{Bu}_2\text{Me}$ )<sub>2</sub> (**L7**) confirmed the reversible reduction to the anionic species. Therefore, an experimental battery cell, containing **L7** as anode material should be constructed to verify the suitability of disilenes for organic radical batteries.

Intended for battery applications, a relatively air-stable, tri(silyl)-substituted silicon-centered radical **1a** was obtained. This modification of the current state-of-the-art might facilitate organic radical battery cell construction and contribute to the further

development of this technology. The isolation and characterization of the NHI-substituted silyl radical **1b** is an unambiguous evidence for the accessibility of silicon radical species bearing electronegative ligands. A straight-forward synthetic approach should be looked for, in order to further investigate the properties of this class of compounds, especially in regard to electrochemistry.

It was demonstrated, that silylene stabilization by the Lewis base DMAP is a suitable way to isolate otherwise elusive bis(silyl)silylene structures under retention of their unique reactivity. Thus, these DMAP-silylene complexes can probably find application in chemical syntheses, as synthons for novel organosilicon compounds, for example functionalized silyl radicals (Scheme 23). Probably, these compounds could contain multiple radical centers in one molecule, thus increasing the energy density of a radical battery.

**Scheme 23:** Possible utilization of DMAP-silylenes **9** as precursors for silyl radicals.



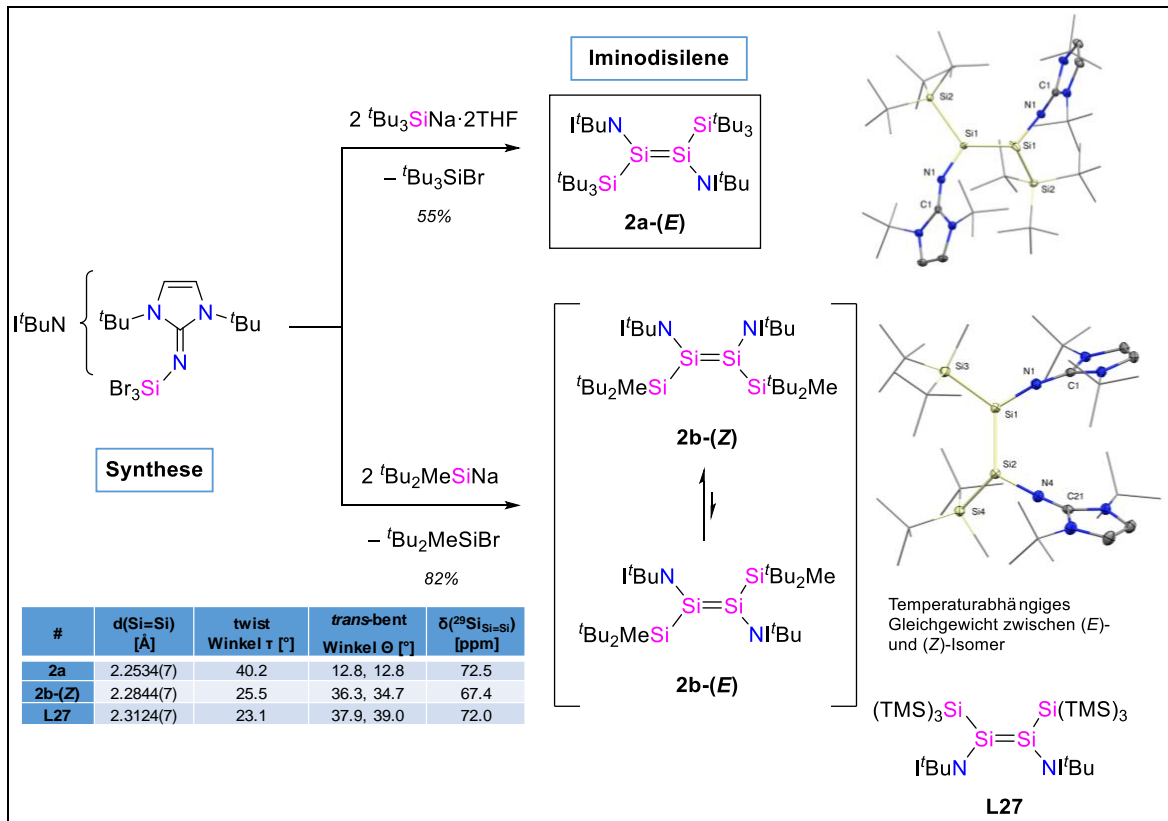
## 13. Zusammenfassung und Ausblick

Zweifellos können die Isolierung und strukturelle Charakterisierung des ersten Disilens **L22** durch West *et al.* in 1985,<sup>[139,145]</sup> sowie des ersten Silylradikals **L2** durch Sekiguchi in 2001<sup>[36]</sup> als Meilensteine der modernen Organosiliciumchemie angesehen werden. Disilene haben interessante Reaktivitätsmuster gegenüber kleinen Molekülen gezeigt<sup>[133]</sup> und Silylradikale wurden bereits erfolgreich in organischen Radikalbatterien eingesetzt.<sup>[5]</sup> Das Ziel dieser Arbeit war es, diese hochreaktiven Klassen von niedrigkoordinierten Silicium-Spezies zu erweitern, um ihre Stabilität zu verbessern und ihre Reaktivitäten und elektrochemischen Eigenschaften weiter zu untersuchen.

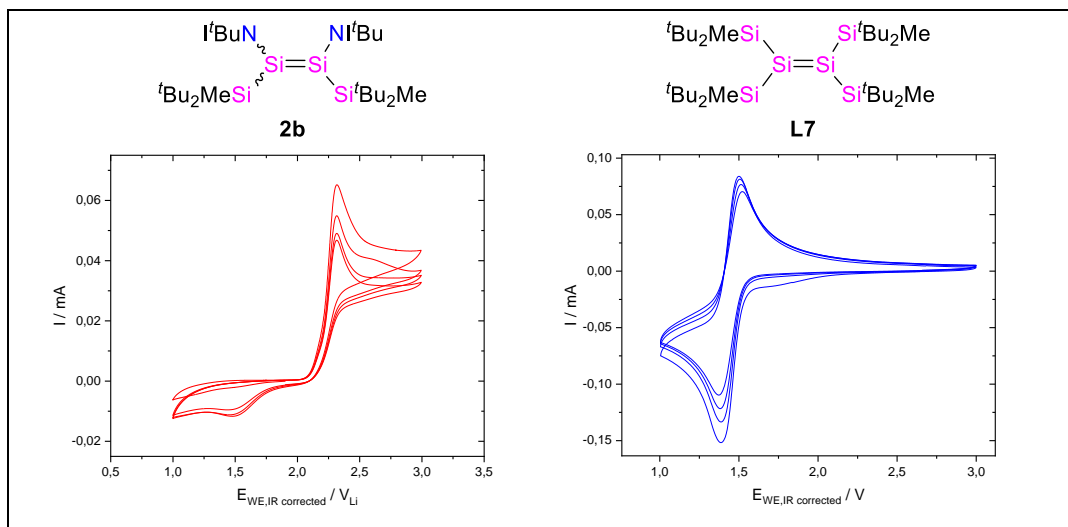
### 13.1 Disilene

Neben neutralen Siliciumradikalen könnten Disilene auch aufgrund ihres reversiblen Redoxverhaltens für organische Radikalbatterien geeignet sein. Eine entsprechende Reaktivität wurde bereits für das Tetra(silyl)disilene **L7** nachgewiesen.<sup>[57,59]</sup> Von besonderem Interesse war natürlich auch die Klasse der *N*-heterocyclischen Imino-substituierten Disilene, da der erste Vertreter **L27** bereits interessante Reaktivität bei der Aktivierung kleiner Moleküle wie H<sub>2</sub>, O<sub>2</sub>, CO<sub>2</sub> und Ammoniak zeigte.<sup>[158,192]</sup> Verbindung **L27** ist jedoch bei Raumtemperatur nicht stabil und seine Redoxchemie wurde bisher nicht erforscht.

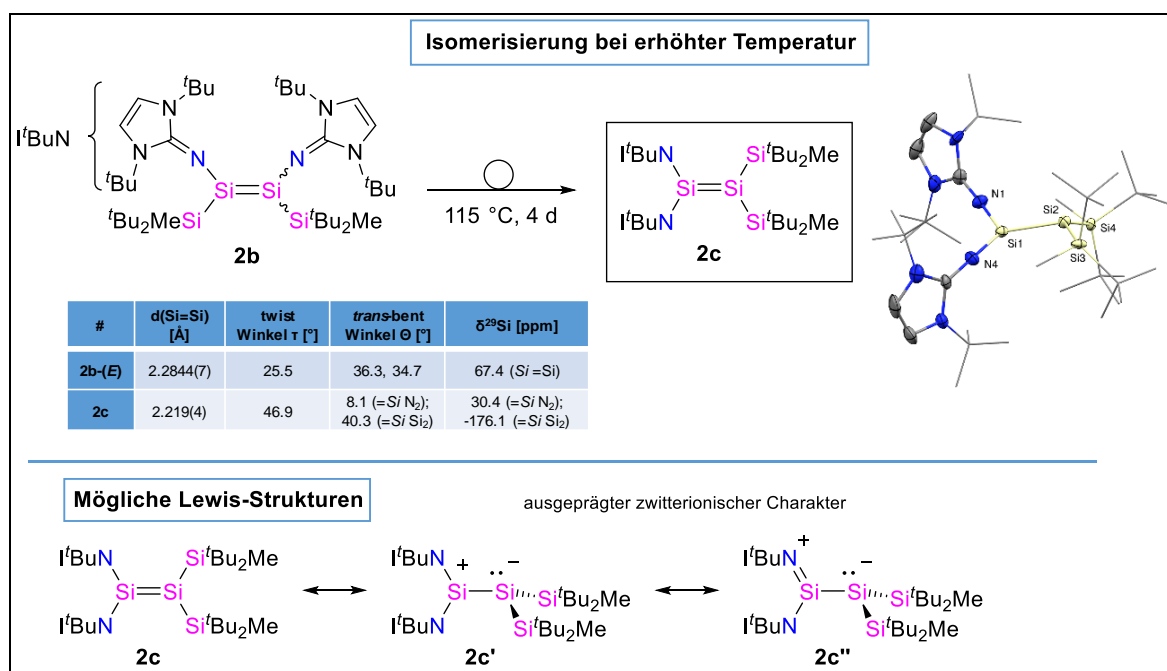
Aufgrund dieser vielversprechenden Ergebnisse wurde ein neuartiges Iminodisilen **2a** durch den etablierten Ansatz (Reaktion von <sup>t</sup>BuN–SiBr<sub>3</sub> mit zwei Äquivalenten Supersilanid) synthetisiert (Abbildung 17). Im Gegensatz zu **L27** weist **2a** aufgrund der sterischen Abstoßung zwischen den Supersilylgruppen im Kristall (*E*)-Konfiguration auf. Obwohl **2a** bei Raumtemperatur absolut stabil ist, ist seine Verwendung durch den schwierigen Abtrennprozess von dem gleichzeitig entstehenden Nebenprodukt <sup>t</sup>Bu<sub>3</sub>SiBr eingeschränkt. Daher wurde die Disilenstruktur durch die Einführung von <sup>t</sup>Bu<sub>2</sub>MeSi-Gruppen weiter variiert, was zur Isolierung von **2b** führte. Verbindung **2b** ist auch bei erhöhten Temperaturen bis 90 °C stabil. Deshalb kann das Nebenprodukt leicht durch Sublimation entfernt werden, was die isolierbaren Ausbeute von **2b** auf 82% erhöht. Verbindung **2b** zeigt in der Kristallstruktur (*Z*)-Konfiguration, wohingegen in Lösung ein temperaturabhängiges Gleichgewicht zwischen (*E*)- und (*Z*)-Isomeren beobachtet wurde.


 Abbildung 17: Synthese und Strukturen der Iminodisilene **2a** und **2b**.

Die Kinetik dieser Isomerisierung wurde mit Hilfe von VT NMR Spektroskopie verfolgt. Im Hinblick auf mögliche Batterieanwendungen wurden CV Untersuchungen durchgeführt (Abbildung 18). Leider haben diese Studien gezeigt, dass nur eine kationische Spezies zugänglich ist und dass eine reversible Reduktion möglicherweise nicht funktioniert.


 Abbildung 18: CV Analyse der Disilene **2b** und **L7**.

Tatsächlich wurde auch keine experimentelle Reduktion von **2b** erreicht, was die Möglichkeit der Batterieanwendung dieser Iminodisilene vom ABSi=SiAB-Typ ausschließt. Dennoch zeigte die Verbindung **2b** interessante Reaktivität gegenüber kleinen Molekülen und auch ein kationisches Radikal **4** war isolierbar (siehe unten). Interessanterweise isomerisiert Verbindung **2b** zu dem A<sub>2</sub>Si=SiB<sub>2</sub>-Typ Iminodisilen ((<sup>t</sup>BuN)<sub>2</sub>Si=Si(Si<sup>t</sup>Bu<sub>2</sub>Me)<sub>2</sub> (**2c**) durch Erhitzen auf 115 °C über vier Tage.



**Abbildung 19:** Synthese und Struktur von Iminodisilen **2c**.

Sowohl <sup>29</sup>Si-NMR Spektroskopie als auch Einkristall Röntgenstrukturanalyse belegten den zwitterionischen Charakter von **2c**, der sich in einem positiv polarisierten N<sub>2</sub>Si-Zentrum und einem negativen Si<sub>2</sub>Si-Teil widerspiegelt (Abbildung 19). Außerdem konnte eine Aktivierung von CO durch Verbindung **2c** zum Silen **5a** nachgewiesen werden (siehe unten). Das elektrochemische Verhalten von **2c** wurde jedoch noch nicht untersucht.

Basierend auf den CV-Ergebnissen mit **2b** schienen Tetra(silyl)disilene besser für Batterieanwendungen geeignet zu sein (Abbildung 18). Verbindung **L7** wurde durch reduktive Debromierung des entsprechenden Dibromosilans und Dimerisierung des intermediär erzeugten Silylens erhalten. Daher wurde ein neuartiges Dibromosilan **6** synthetisiert, das sowohl eine Supersilyl- als auch eine Hypersilylgruppe trägt. Die Reduktion dieses Dibromosilans führte jedoch nicht zum Dimerisierungsprodukt, sondern stattdessen wurde Tetra(silyl)disilene **3** durch TMS-Migration gebildet (Abbildung 20). Leider zersetzt sich Verbindung **3** bei Raumtemperatur, wodurch sie



als Anodenmaterial ausscheidet. Dennoch zeigten das Zersetzungsprodukt Disiletan **7** (gebildet durch C–H-Bindungsaktivierung einer <sup>t</sup>Bu-Gruppe), DFT-Berechnungen und weitere Reaktivitätsstudien (siehe unten) ein Gleichgewicht zwischen Tetra(silyl)disilene **3** und dem isomeren Bis(silyl)silylen **3'**, das als Lewis-Basenaddukt erfolgreich stabilisiert wurde (siehe Kapitel 13.3).

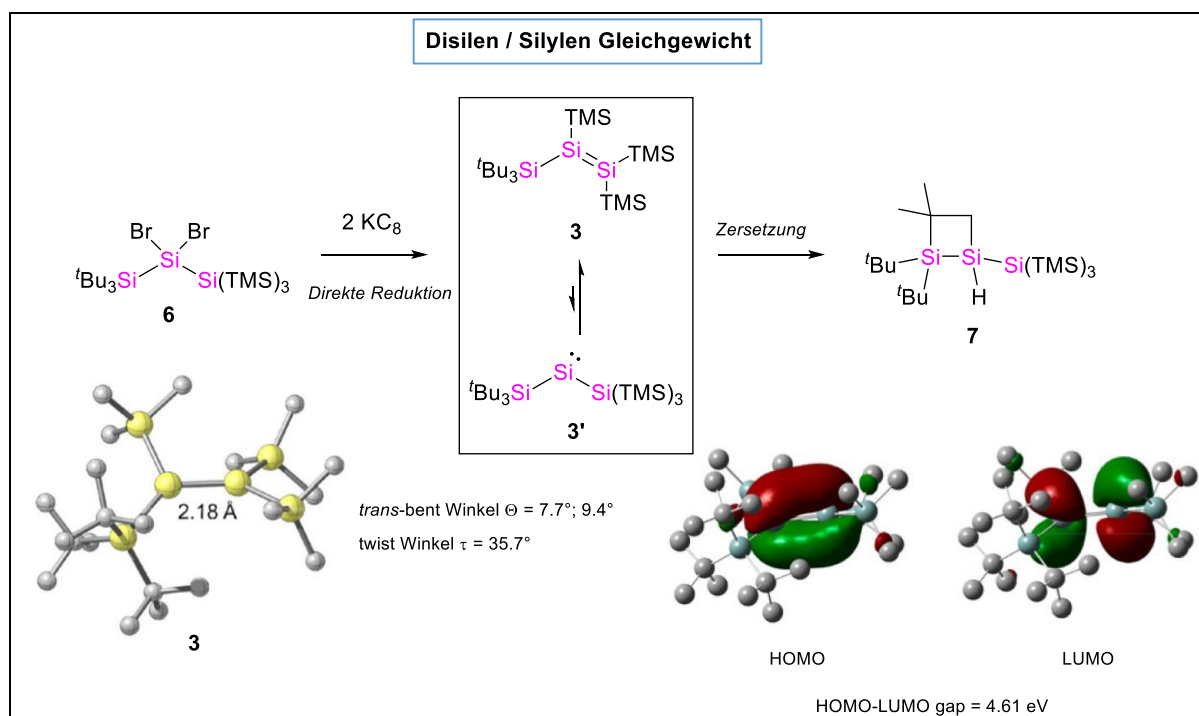


**Abbildung 20:** Synthese und Zersetzung der Disilen / Silylen Gleichgewichtsmischung **3/3'**.

## 13.2 Silylradikale

Im Jahr 2014 konstruierte die Gruppe von Sekiguchi zusammen mit den Forschungs- und Entwicklungslabors von *Toyota* Alkali- und Übergangsmetallfreie organische Radikalbatteriezellen, basierend auf ihren neutralen, schwereren Gruppe 14 Radikalen (<sup>t</sup>Bu<sub>2</sub>MeSi)<sub>3</sub>E<sup>•</sup> [E = Si, Ge, Sn]. Diese Verbindungen schienen aufgrund der geringen Reduktionspotenziale und ihres hochreversiblen Redoxverhaltens vielversprechende Kandidaten für Anodenmaterialien zu sein. Tatsächlich zeigten die experimentellen Zellen eine bemerkenswerte zyklische Stabilität (98% Kapazität nach 100 Zyklen) bei hohen Lade- und Entladeraten. Unter den getesteten Radikalen der Gruppe 14 erwies sich die Silylverbindung **L2** als die am besten geeignete, da sie die höchste Kapazität und die schnellste Reaktionsgeschwindigkeit ermöglicht.<sup>[5]</sup> Basierend auf diesen vielversprechenden Ergebnissen zielte diese Arbeit darauf ab, die neuartige Energiespeichertechnologie auf molekularer Ebene zu verbessern. Tatsächlich wurde

das Siliciumradikal **1a**, das noch besser kinetisch stabilisiert ist als **L2**, über drei verschiedenen Routen mit einer guten Ausbeute von 70% gewonnen (Abbildung 21).

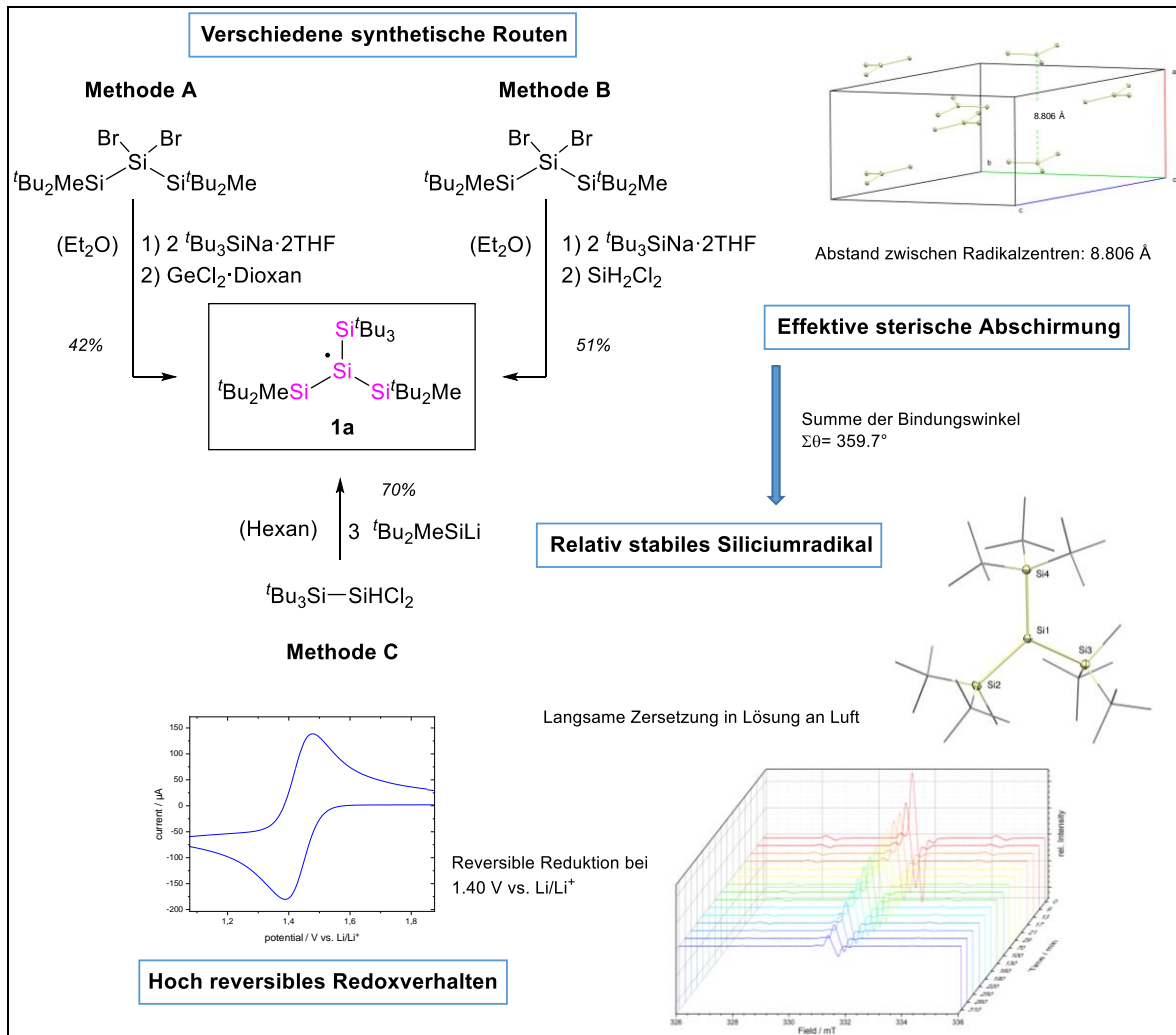


**Abbildung 21:** Synthese und Eigenschaften von Siliciumradikal **1a**.

Im Kristall zeigt die Verbindung **1a** eine vollständig planare Geometrie, die typisch für Silylradikale mit sterisch anspruchsvollen, elektropositiven Substituenten wie Silylgruppen ist. Darüber hinaus verspricht der Abstand von über 8,8 Å zwischen den Radikalzentren hohe Diffusionsraten bei Batterieprozessen. In Kombination mit der vollständigen Reversibilität der Redoxreaktion könnte das Radikal **1a** daher als Anodenmaterial in langlebigen organischen Radikalbatterien Anwendung finden und schnelle Lade-/Entladeraten ermöglichen. Vor allem aber macht die effektive sterische Abschirmung des Radikalzentrums durch die extrem große Supersilylgruppe die Verbindung **1a** relativ inert gegenüber Luft und Feuchtigkeit. Diese Eigenschaft könnte den Bau von Batteriezellen erleichtern und somit zu einer weiteren Verbreitung dieser nachhaltigen Technologie führen.

Ein alternativer synthetischer Ansatz für funktionalisierte Siliciumradikale könnte die Reaktion eines Alkalimetall-substituierten Silylradikals mit einem Elektrophil sein. Aus der Überreduktion von  $(t\text{Bu}_3\text{Si})_2\text{SiBr}_2$  mit 3,5 Äquivalenten  $\text{KC}_8$  wurde das Kalium-substituierte Radikal **8** erhalten (Abbildung 22). Trotz der extremen Empfindlichkeit von **8** gegenüber Luft und Feuchtigkeit, sowie der Tatsache, dass es sich in Toluollösung zersetzt, konnte eine Kristallstruktur erhalten werden. Verbindung **8** weist eine vollständig planare Geometrie auf (Summe der Bindungswinkel  $\Sigma\theta = 360.0^\circ$ ), typisch für Alkalimetall-substituierte Silylradikale. Darüber hinaus zeigt der Si–K-Abstand, der mit Hypersilylkalium vergleichbar ist, den “contact-ion-pair” Charakter von Verbindung **8** im festen Zustand. Leider blieben die bisherigen Versuche, das Silylradikalfragment von **8** mit Elektrophilen zu koppeln, um funktionalisierte Siliciumradikale zu erhalten, erfolglos.

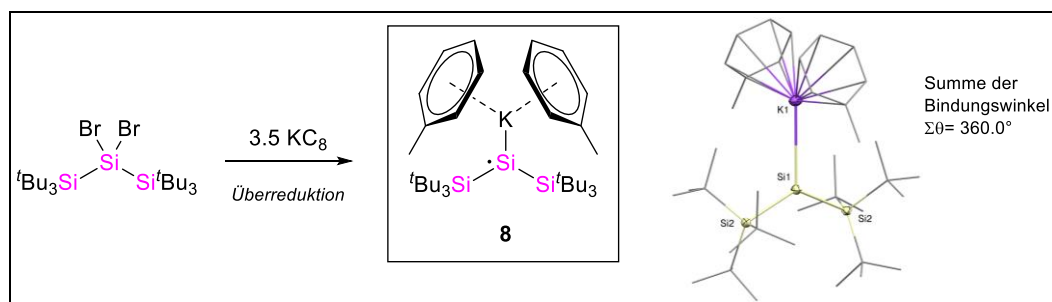


**Abbildung 22:** Synthese und Struktur von Siliciumradikal **8**.

Im Vorfeld dieser Arbeit wurde noch kein Silylradikal mit elektronegativen Substituenten, wie beispielsweise Stickstoff, strukturell charakterisiert. Durch Ein-Elektronen-Oxidation von Iminodisilen **2b** wurde das kationische Radikal **4** erhalten (Abbildung 23). Es ist das zweite bekannte Beispiel für ein Disilenradikal-Kation (nach **L7<sup>•+</sup>**) und das erste mit Heteroatomsubstituenten. Bemerkenswert ist, dass die Reduktion von **4** durch  $\text{KC}_8$  wieder die Ausgangsverbindung **2b** ergab. Die CV Analyse zeigte, dass die Oxidation des Iminodisilens **2b** bereits bei niedrigeren Potentialen (etwa 1 V) stattfindet, als für die Oxidation von Tetra(silyl)disilen **L7** erforderlich ist. Die Aufspaltung des EPR Signals von Verbindung **4** weist auf eine Kopplung des ungepaarten Elektrons mit den  $^{14}\text{N}$  Kernen der Iminogruppe hin. Dieses Ergebnis stellt die Eignung des NHI-Substituenten zur effektiven Stabilisierung kationischer Silylzentren heraus.

Neutrale Siliciumradikale mit Imino- und Silylsubstituenten könnten für Batterieanwendungen von größerer Bedeutung sein. Die gezielte Synthese durch Ein-

Elektronen-Reduktion des entsprechenden Halogensilans lieferte jedoch nicht das gewünschte Radikal. Zufälligerweise führte die Zersetzung von Disilen **2b** in Gegenwart von CO jedoch zum NHI-substituierten Silylradikal **1b** (Abbildung 23). Die Synthese von **1b** war nicht perfekt reproduzierbar, lieferte nur geringe Ausbeute und der Mechanismus für die Bildung blieb ungeklärt. Dennoch ist es ein eindeutiger Beweis dafür, dass diese Art von heteroatom-substituierten Silylradikalen stabil und isolierbar sind. Es war sogar möglich, **1b** strukturell durch Einkristall-Röntgenstrukturanalyse zu charakterisieren. Die Verbindung **1b** zeigt eine leicht pyramidalisierte Geometrie ( $\Sigma\theta = 353.5^\circ$ ), im Gegensatz zu den Tri(silyl)silylradikalen **L2** und **1a**. Dies ist auf den elektronegativen NHI-Substituenten zurückzuführen.<sup>[26]</sup> Die elektrochemischen Eigenschaften von iminosubstituierten Silylradikalen wurden jedoch noch nicht erforscht.

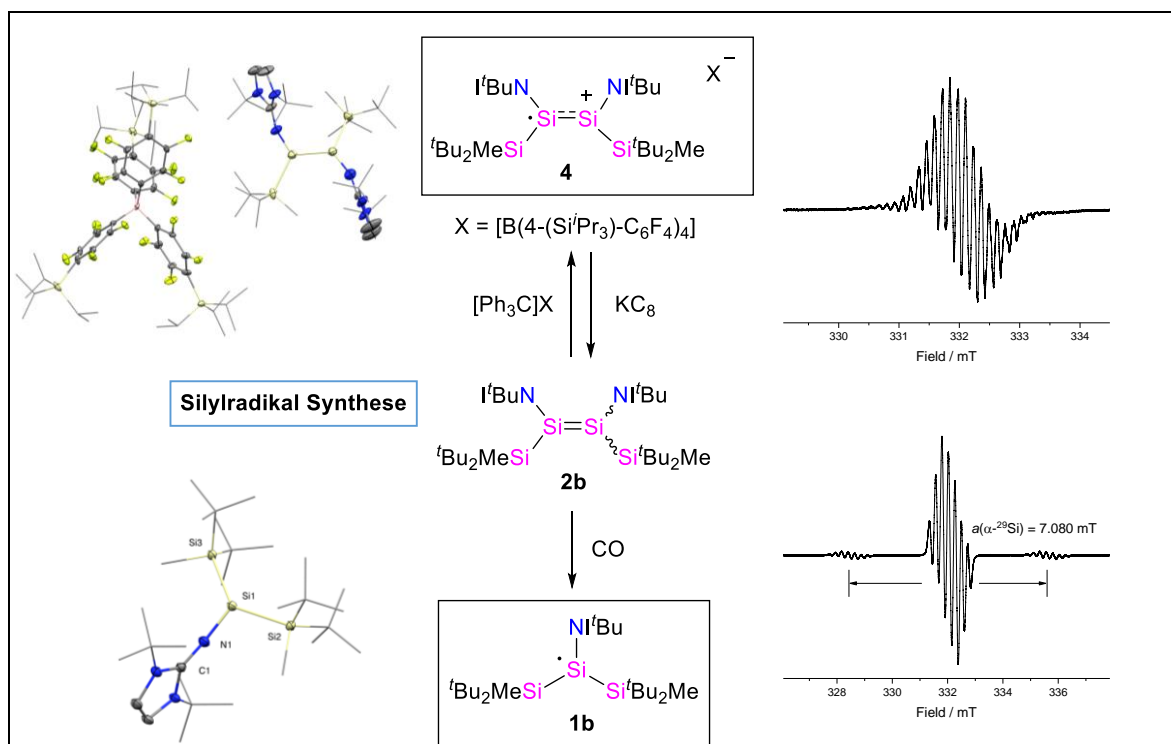


**Abbildung 23:** Herstellung und Charakterisierung der Siliciumradikale **1b** und **4**.

### 13.3 Silylene

Während der Untersuchung von Silylradikalen und Disilenen konnten im Rahmen dieser Arbeit auch eine Reihe von Silylenen synthetisiert werden. Obwohl diese niedervalenten Siliciumverbindungen in Bezug auf organische Radikalbatterien noch nie eingesetzt wurden, gelten sie als vielversprechende Kandidaten für die Übergangsmetallfreie Katalyse, da ihr ambiphiler Charakter eine einfache Aktivierung kleiner Moleküle ermöglicht. In den meisten Fällen ist die Koordination eines Elektronendonors an das leere  $3p_z$ -Orbital von Silylenen notwendig, um ihre übermäßige Elektrophilie zu kontrollieren und eine Isolierung als Lewis-Baseaddukte zu ermöglichen. Daher gibt es bis jetzt nur wenige Beispiele von donorfreen Silylenen. Vor dieser Arbeit waren keine isolierbaren, raumtemperaturstabilen Bis(silyl)silylene bekannt. Alle synthetischen Versuche führten zu Zersetzungsreaktionen, entweder durch Aktivierung der C–H-Bindung von Substituenten, oder durch Silylmigration.<sup>[77-80]</sup>

Durch Reduktion von Dibromsilan **6** konnte ein Gleichgewichtsgemisch aus Tetra(silyl)disilen **3** und dem isomeren Bis(silyl)silylen **3'** erhalten werden (Abbildung 20). Dieses einzigartige Isomerisierungsverhalten resultiert aus der maßgeschneiderten Kombination von Supersilyl- und Hypersilylsubstituenten. Sie bieten einerseits eine kinetische Stabilisierung (Supersilylgruppe), ermöglichen aber andererseits auch eine einfache Migration von TMS-Gruppen (Hypersilylgruppe). Aufgrund dieser Tautomerie ist Silylen **3'** bei  $-35\text{ °C}$  unbegrenzt stabil und damit das bisher einzige isolierbare Bis(silyl)silylenderivat. Das Silylenzentrum von **3'** insertiert jedoch bei Raumtemperatur in die C–H-Bindung einer <sup>t</sup>Bu-Gruppe und bildet dadurch Disiletan **7**.

Zum besseren Verständnis der TMS-Gruppenwanderung wurde die Reduktion von Dibromsilan **6** in Anwesenheit von Lewis-Basen durchgeführt. Interessanterweise wurde mit  $i\text{Pr}_2\text{Me}_2$ , ein TMS-substituiertes Silylen, isomer zu **3'** erhalten. Mit der schwächeren Lewis-Base DMAP hingegen konnte das Silylenfragment **3'** als Donor-Akzeptor-Komplex **9a** stabilisiert werden (Abbildung 24). Verbindung **9a** ist in Lösung bis zu  $60\text{ °C}$  stabil. Oberhalb dieser Temperatur zerfällt es zu Disiletan **7** unter Freisetzung von DMAP. Diese Beobachtung zeigte bereits die Eignung von DMAP für die Isolierung von sonst instabilen Bis(silyl)silylenen unter Erhalt ihrer einzigartigen Reaktivität. Aufgrund dieser ersten Ergebnisse wurden zwei weitere DMAP-Bis(silyl)silylen-Komplexe **9b** und **9c** auf analoge Weise synthetisiert. Im Gegensatz



zu **9a**, verlaufen die thermisch induzierten Isomerisierungsreaktionen von **9b** und **9c** völlig unterschiedlich ab: Bei 65 °C insertiert der Silylenteil von **9b** in die aromatische C–N-Bindung von DMAP und erzeugt Azasilepin **10**. Beim Erwärmen von Verbindung **9c** auf 65 °C lagert dieses erste stabile Bis(hypersilyl)silylenderivat, unter Freisetzung von DMAP zum cyclische Silan **11** um. Die versuchte Synthese des DMAP-stabilisierten Bis(supersilyl)silylens war hingegen erfolglos und lieferte nur das C–H-Bindungsaktivierungsprodukt, das auch beim Zerfall des freien Silylens beobachtet wurde. Eine Überreduktion des entsprechenden Dibromsilans führte jedoch zum Bis(supersilyl)-substituierten Siliciumradikal **8** (siehe oben).

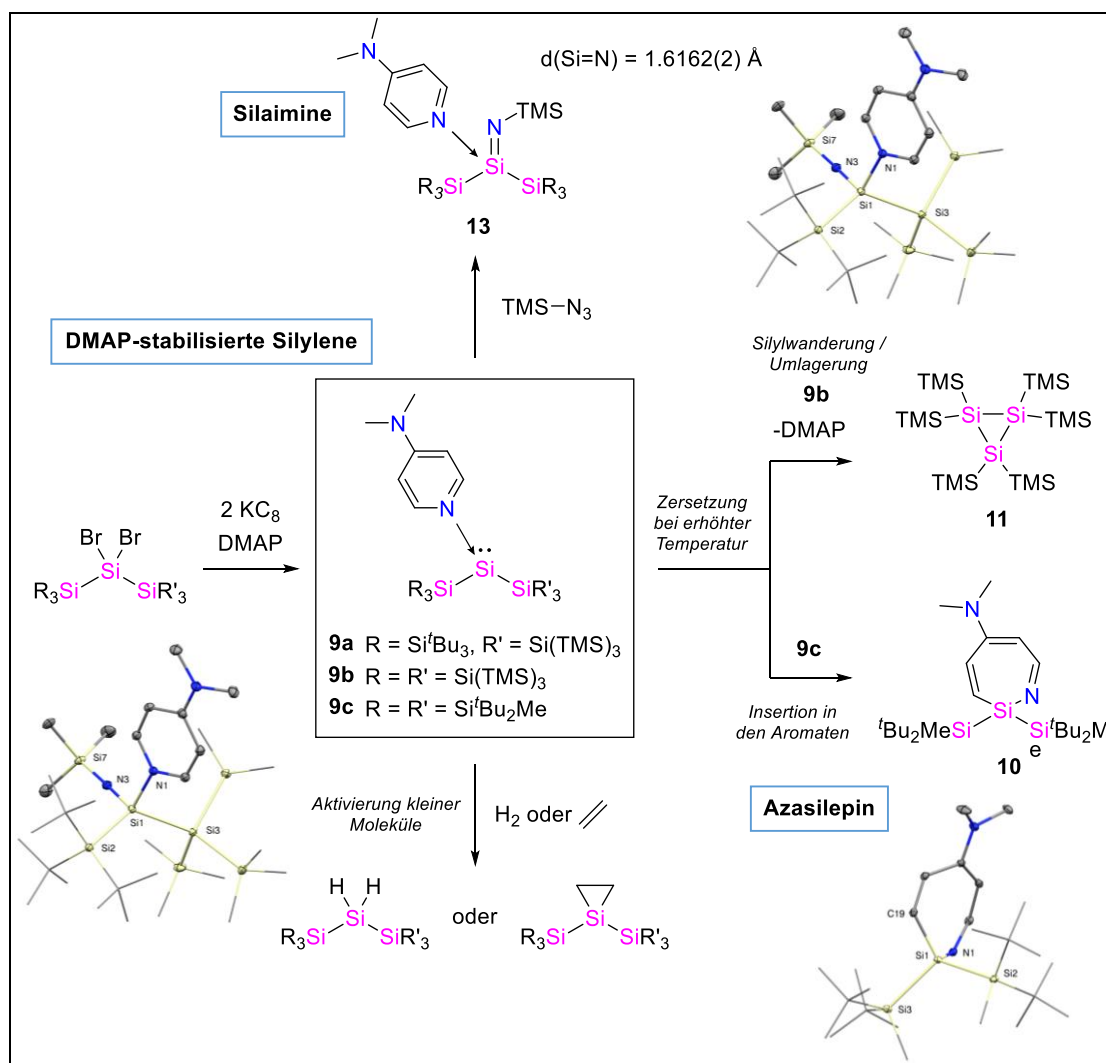


Abbildung 24: Synthese und Reaktivität der DMAP-Silylen Komplexe **9**.

## 13.4 Reaktivität der niedervalenten Siliciumverbindungen gegenüber kleinen Molekülen

Die Umwandlung von kleinen Molekülen wie  $H_2$ ,  $CO$ ,  $CO_2$  und  $P_4$  zu höherwertigen Chemikalien wird im industriellen Maßstab meist durch Übergangsmetallkatalyse realisiert. Ein vielversprechender Weg, seltene, teure oder toxische Übergangsmetalle in diesen Prozessen zu ersetzen, könnte darin bestehen, ihr Verhalten mit Hauptgruppenelementverbindungen nachzuahmen. Um dieses ehrgeizige Ziel zu erreichen, sind hochreaktive Hauptgruppenverbindungen erforderlich, die selektiv diese kleinen Moleküle durch oxidative Addition aktivieren. Disilene und Silylene gehören dabei zu den vielversprechendsten Verbindungen.

### 13.4.1 Aktivierung durch Disilene

Im Allgemeinen sind Disilene aufgrund ihres geringen energetischen Unterschieds zwischen HOMO und LUMO intensiv gefärbt (Abbildung 25). Die Iminodisilene **2** zeigen ebenfalls intensive Farben und sind daher im Hinblick auf die Aktivierung kleiner Moleküle vielversprechend.

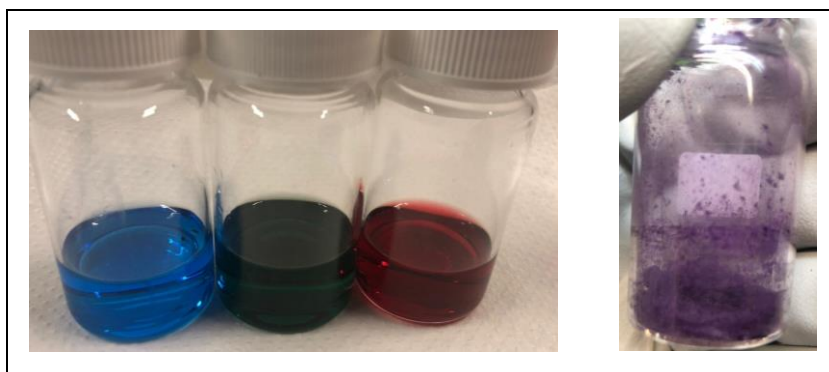


**Abbildung 25:** Disilene in Lösung oder als Feststoff. Von links: **L7**, **2a**, **2b** und **2c**.

Iminodisilen **L27** zeigte bereits vor dieser Arbeit eine bemerkenswerte Reaktivität gegenüber  $H_2$ ,  $N_2O$ ,  $CO_2$  und  $NH_3$ . Für Disilen **2b** wurde ein vergleichbares Reaktionsverhalten beobachtet. Die Aktivierung von Wasserstoff zum 1,2-Additionsprodukt wurde selbst bei Raumtemperatur beobachtet (Abbildung 26). Außerdem wurden ein Silaepoxid und ein viergliedriges cyclisches Siloxan durch Oxidation von **2b** mit  $N_2O$  bzw.  $O_2$  erhalten. Interessanterweise führte eine Aktivierung von weißem Phosphor zum Additionsprodukt **12**. In **12** werden die beiden ehemaligen niedrigkoordinierten Siliciumzentren durch drei P-Atome der Grundfläche des  $P_4$ -Tetraeders verbrückt. Zusätzlich wurden die Silene **5** synthetisiert, indem das Disilen

**2c** und das bereits literaturbekannte, symmetrische Disilen ( ${}^t\text{Bu}_2\text{MeSi}$ )<sub>2</sub>Si=Si(Si<sup>t</sup>Bu<sub>2</sub>Me)<sub>2</sub> (**L7**) mit Kohlenstoffmonoxid umgesetzt wurden. Iminodisilen **2c** reagiert innerhalb von Minuten bei Raumtemperatur, wohingegen **L7** vier Tage lang auf 80 °C erhitzt werden muss. Anscheinend ist der stark polarisierte Charakter von **2c** der Grund für diesen signifikanten Unterschied in der Reaktionsgeschwindigkeit.

Das Gleichgewichtsgemisch von Tetra(silyl)disilen **3** und dem isomeren Bis(silyl)silylen **3'** wurde ebenfalls im Hinblick auf die Aktivierung kleiner Moleküle untersucht. Allerdings wurde lediglich mit Ammoniak das Disilen-1,2-Additionsprodukt erhalten. Mit H<sub>2</sub> und Ethylen wurde jeweils nur die Reaktion des Silylens **3'** beobachtet.

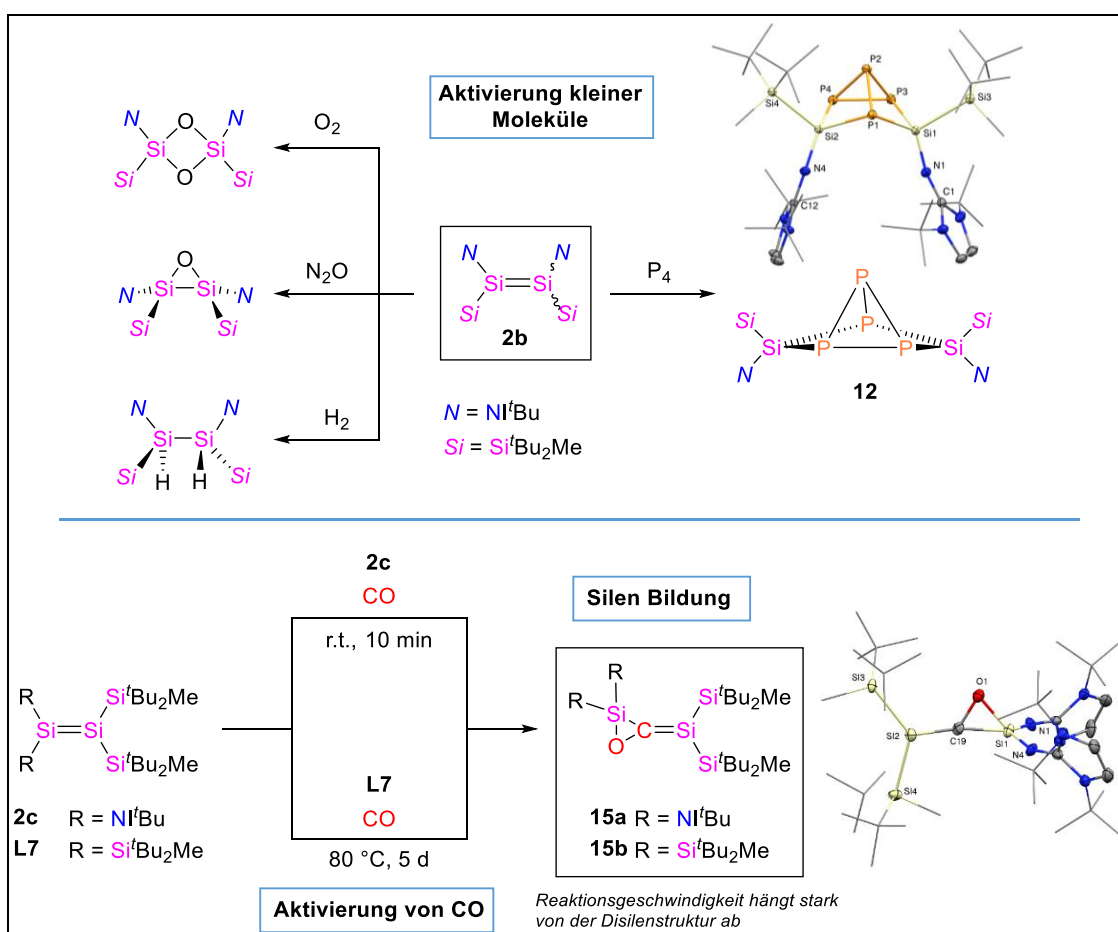


**Abbildung 26:** Aktivierung kleiner Moleküle durch Disilene.

### 13.4.2 Aktivierung durch Silylene

Silylen **3'**, das sich im Gleichgewicht mit Disilene **3** befindet, ist das erste isolierbare Beispiel für ein Bis(silyl)silylen und zeigte eine entsprechende Reaktivität. Es insertiert bereits bei –40 °C in die H–H-Bindung von Wasserstoff, was die bislang schnellste H<sub>2</sub>-

Aktivierung durch Siliciumverbindungen darstellt. Weiterhin wurde gezeigt, dass bei der Reaktion von **3/3'** mit Ethylen selektiv die Bildung von Silirane stattfindet.

Im Gegensatz zu donorfreen Silylenen ist die Reaktivität von NHC-stabilisierten Silylenen stark eingeschränkt. Daher wurde bislang keine H<sub>2</sub>-Aktivierung durch einen NHC-Silylenkomplex beobachtet. Aufgrund der im Vergleich zu NHCs geringeren Lewis-Basizität von DMAP sind die entsprechenden DMAP-Komplexe wesentlich reaktiver. Tatsächlich konnte nachgewiesen werden, dass die DMAP-Silylenkomplexe **9** nach der Dissoziation des Donors bei erhöhten Temperaturen Bis(silyl)silylenreaktivität zeigen (Abbildung 24). Darüberhinaus wurde Siliranbildung beobachtet und die DMAP-stabilisierten Silaimine **13** wurden aus der Reaktion von **9a** und **9b** mit Trimethylsilylazid gewonnen. Von daher können diese neuartigen donorstabilisierten Silylene als leicht zugängliche synthetische Äquivalente für ansonsten nicht isolierbare Bis(silyl)silylene angesehen werden.

#### 13.5 Ausblick

Iminodisilen **2b** ist stabil in Lösung bei Raumtemperatur und daher viel einfacher zu Handhaben als **L27**. Trotzdem zeigt es vergleichbar ausgeprägte Reaktivität. In Kombination mit der hohen isolierbaren Ausbeute ist es daher die perfekte Testverbindung für weitere Reaktivitätserforschung der Klasse der Iminodisilene. Aufgrund ihrer Fähigkeit, kleine Moleküle zu aktivieren, könnte Verbindung **2b** sogar möglicherweise als Katalysator eingesetzt werden, z.B. zur Hydroborierung oder Transferhydrierung geeigneter Substrate. Die Reaktivität des isomeren, zwitterionischen Disilens **2c** blieb unerforscht, mit Ausnahme der beobachteten CO Addition. Die polarisierte Si=Si-Doppelbindung könnte ideal für die einfache Aktivierung kleiner Moleküle sein, möglicherweise sogar in einem katalytischen Kontext. CV Analyse des literaturbekannten Tetra(silyl)disilens (<sup>t</sup>Bu<sub>2</sub>MeSi)<sub>2</sub>Si=Si(Si<sup>t</sup>Bu<sub>2</sub>Me)<sub>2</sub> (**L7**) bestätigte die reversible Reduktion zur entsprechenden anionischen Spezies. Daher sollte eine experimentelle Batteriezelle mit **L7** als Anodenmaterial konstruiert werden, um die Eignung von Disilenen für organische Radikalbatterien zu überprüfen.

Im Hinblick auf Batterieanwendungen wurde ein relativ luftstabiles, tri(silyl)-substituiertes Siliciumradikal **1a** erhalten. Diese Verbesserung des bisher eingesetzten Silylradikals **L2** könnte die Konstruktion von organischen Radikalbatteriezellen erleichtern und zur weiteren Verbreitung dieser Technologie beitragen. Die Isolierung

und Charakterisierung des NHI-substituierten Silylradikals **1b** ist ein eindeutiger Beweis dafür, dass Siliciumradikale mit elektronegativen Liganden stabil und isolierbar sein können. Es sollte nach einem passenden synthetischen Ansatz für diese Radikale gesucht werden, um die Eigenschaften dieser Verbindungsklasse, insbesondere im Bezug auf die Elektrochemie, weiter zu untersuchen.

Es konnte weiterhin gezeigt werden, dass die Stabilisierung von Silylenen durch die Lewis-Base-DMAP eine geeignete Methode ist, um ansonsten unzugängliche Bis(silyl)silylenstrukturen unter Beibehaltung ihrer einzigartigen Reaktivität zu isolieren. So könnten diese DMAP-Silylenkomplexe möglicherweise Anwendung in chemischen Synthesen, als Synthone für neuartige Organosiliciumverbindungen, wie beispielsweise funktionalisierten Silylradikalen finden (Abbildung 27). Es wäre denkbar, dass diese Verbindungen mehrere Radikalzentren pro Molekül enthalten und dadurch die Energiedichte einer organischen Radikalbatterie gesteigert werden kann.

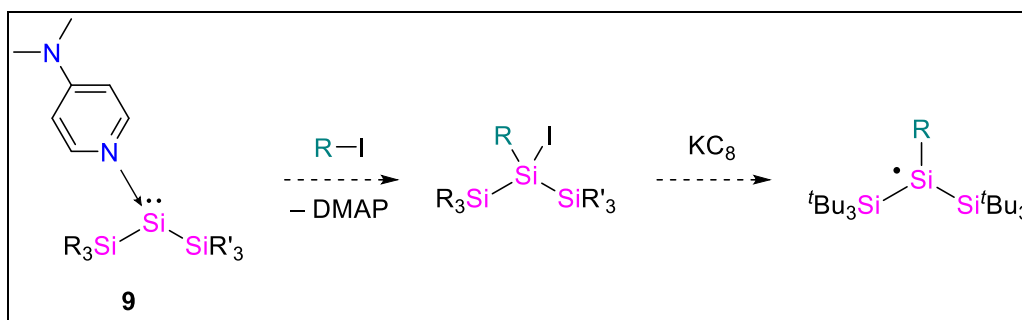


**Abbildung 27:** Mögliche Anwendung von DMAP-Silylenen **9** als Edukte für Siliciumradikale.



## 14. Bibliography

- [1] R. A. Kerr, Bumpy Road Ahead for World's Oil. *Science*, 2005, 310, 1106-1108.
- [2] R. G. Miller, S. R. Sorrell, The future of oil supply. *Phil. Trans. R. Soc. A*, **2014**, 372, 1-27.
- [3] O. Gröger, H. A. Gasteiger, J.-P. Suchsland, Review—Electromobility: Batteries or Fuel Cells? *J. Electrochem. Soc.*, **2015**, 162, A2605-A2622.
- [4] H. Ambrose, A. Kendall, Understanding the future of lithium: Part 2, temporally and spatially resolved life-cycle assessment modeling. *J. Ind. Ecol.*, **2020**, 24, 90-100.
- [5] H. Maruyama, H. Nakano, M. Nakamoto, A. Sekiguchi, High-Power Electrochemical Energy Storage System Employing Stable Radical Pseudocapacitors. *Angew. Chem. Int. Ed.*, **2014**, 53, 1324-1328.
- [6] R. A. van Santen, *Modern Heterogeneous Catalysis*. Wiley-VCH, Weinheim, **2017**.
- [7] E. Fritz-Langhals, Silicon(II) Cation  $Cp^*Si^+ X^-$ : A New Class of Efficient Catalysts in Organosilicon Chemistry. *Org. Process. Res. Dev.*, **2019**, 23, 2369-2377.
- [8] E. Riedel, C. Janiak, *Anorganische Chemie*. Walter de Gruyter, Berlin, **2007**.
- [9] B. Arkles, Silicon Compounds, Silanes. in *Kirk-Othmer Encyclopedia of Chemical Technology*. John Wiley & Sons, Inc., **2000**.
- [10] A. F. Holleman, E. Wiberg, N. Wiberg, *Lehrbuch der Anorganischen Chemie*. Walter de Gruyter & Co., Berlin, **2007**.
- [11] Silicon production worldwide from 2010 to 2018. <https://www.statista.com/statistics/573585/global-silicon-production/> (accessed 2019-12-23).
- [12] L. Rösch, P. John, R. Reitmeier, Silicon Compounds, Organic. in *Ullmann's Encyclopedia of Industrial Chemistry*. Wiley-VCH Verlag GmbH & Co. KGaA, Weinheim, **2012**.
- [13] J. E. Mark, D. W. Schaefer, G. Lin, *The Polysiloxanes*. Oxford University Press, New York, **2015**.

- [14] H.-G. Elias, *Makromoleküle*. Wiley-VCH Verlag GmbH, Weinheim, **2001**.
- [15] V. Y. Lee, A. Sekiguchi, *Organometallic Compounds of Low-Coordinate Si, Ge, Sn and Pb: From Phantom Species to Stable Compounds*. John Wiley & Sons, Ltd., Chichester, **2010**.
- [16] M. Gomberg, Triphenylmethyl, ein Fall von dreierwertigem Kohlenstoff. *Ber. Dtsch. Chem. Ges.*, **1900**, 33, 3150-3163.
- [17] R. G. Hicks, *Stable radicals : fundamentals and applied aspects of odd-electron compounds*. John Wiley & Sons, Ltd., Chichester, **2010**.
- [18] D. Griller, K. U. Ingold, Persistent carbon-centered radicals. *Acc. Chem. Res.*, **1976**, 9, 13-19.
- [19] R. G. Hicks, What's new in stable radical chemistry? *Organic & Biomolecular Chemistry*, **2007**, 5, 1321-1338.
- [20] *Encyclopedia of Radicals in Chemistry, Biology and Materials* C. Chatgililoglu; A. Studer, Eds. John Wiley & Sons, Ltd., Chichester, **2012**.
- [21] S. Kundu, S. Sinhababu, V. Chandrasekhar, H. W. Roesky, Stable cyclic (alkyl)(amino)carbene (cAAC) radicals with main group substituents. *Chem. Sci.*, **2019**, 10, 4727-4741.
- [22] K. Chandra Mondal, S. Roy, H. W. Roesky, Silicon based radicals, radical ions, diradicals and diradicaloids. *Chem. Soc. Rev.*, **2016**, 45, 1080-1111.
- [23] C. Chatgililoglu, Organosilanes as radical-based reducing agents in synthesis. *Acc. Chem. Res.*, **1992**, 25, 188-194.
- [24] C. Chatgililoglu, Structural and Chemical Properties of Silyl Radicals. *Chem. Rev.*, **1995**, 95, 1229-1251.
- [25] C. Chatgililoglu, C. H. Schiesser, Silyl Radicals. in *The Chemistry of Organic Silicon Compounds*. Z. Rappoport; Y. Apeloig, Eds. **2001**.
- [26] B. Tumanskii, M. Karni, Y. Apeloig, Persistent and Stable Silyl Radicals. in *Encyclopedia of Radicals in Chemistry, Biology and Materials*. C. Chatgililoglu; A. Studer, Eds. **2012**.
- [27] R. L. Morehouse, J. J. Christiansen, W. Gordy, ESR of Free Radicals Trapped in Inert Matrices at Low Temperature: CH<sub>3</sub>, SiH<sub>3</sub>, GeH<sub>3</sub>, and SnH<sub>3</sub>. *J. Chem. Phys.*, **1966**, 45, 1751-1758.

- [28] J. D. Cotton, C. S. Cundy, D. H. Harris, A. Hudson, M. F. Lappert, P. W. Lednor, Photochemical synthesis and electron spin resonance characterisation of stable trivalent metal alkyls (Si, Ge, Sn) and amides (Ge and Sn) of Group IV elements. *J. Chem. Soc., Chem. Commun.*, **1974**, 651-652.
- [29] A. Hudson, M. F. Lappert, P. W. Lednor, Subvalent Group 4B Metal Alkyls and Amides. Part 4. An Electron Spin Resonance Study of Some Long-lived Photochemically Synthesised Trisubstituted Silyl, Germyl, and Stannyl Radicals. *J. Chem. Soc., Dalton Trans.*, **1976**, 2369-2375.
- [30] A. J. McKinley, T. Karatsu, G. M. Wallraff, R. D. Miller, R. Sooriyakumaran, J. Michl, Photodegradation of poly(dialkylsilane)s in solution: the persistent radicals have an unexpected structure. *Organometallics*, **1988**, 7, 2567-2569.
- [31] A. J. McKinley, T. Karatsu, G. M. Wallraff, D. P. Thompson, R. D. Miller, J. Michl, Solution photochemistry of poly(di-n-alkylsilanes). An EPR-ENDOR study of the structure of the persistent radicals. *J. Am. Chem. Soc.*, **1991**, 113, 2003-2010.
- [32] Y. Apeloig, D. Bravo-Zhivotovskii, M. Yuzefovich, M. Bendikov, A. I. Shames, Polysilyl radicals: EPR study of the formation and decomposition of star polysilanes. *Appl. Magn. Reson.*, **2000**, 18, 425-434.
- [33] S. Kyushin, H. Sakurai, T. Betsuyaku, H. Matsumoto, Highly Stable Silyl Radicals  $(Et_nMe_{3-n}Si)_3Si\cdot$  ( $n = 1-3$ ). *Organometallics*, **1997**, 16, 5386-5388.
- [34] M. Kira, T. Obata, I. Kon, H. Hashimoto, M. Ichinohe, H. Sakurai, S. Kyushin, H. Matsumoto, Persistent Tris(*t*-butyldimethylsilyl)silyl Radical and Its New Generation Methods. *Chem. Lett.*, **1998**, 27, 1097-1098.
- [35] S. Kyushin, H. Sakurai, H. Matsumoto, Highly Planar Silane  $[(i\text{-Pr})_3Si]_3SiH$  and Silyl Radical  $[(i\text{-Pr})_3Si]_3Si\cdot$ . *Chem. Lett.*, **1998**, 27, 107-108.
- [36] A. Sekiguchi, T. Matsuno, M. Ichinohe, Cyclotetrasilenylyl: The First Isolable Silyl Radical. *J. Am. Chem. Soc.*, **2001**, 123, 12436-12437.
- [37] V. Y. Lee, *Organosilicon Compounds*. Academic Press, London, **2017**.
- [38] A. Sekiguchi, T. Fukawa, M. Nakamoto, V. Y. Lee, M. Ichinohe, Isolable Silyl and Germyl Radicals Lacking Conjugation with  $\pi$ -Bonds: Synthesis, Characterization, and Reactivity. *J. Am. Chem. Soc.*, **2002**, 124, 9865-9869.

- [39] N. Masaaki, F. Tomohide, S. Akira, Silylium Ion to Silylium Ion Rearrangement Caused by 1,3-Methyl Migration. *Chem. Lett.*, **2004**, 33, 38-39.
- [40] M. Nakamoto, T. Fukawa, V. Y. Lee, A. Sekiguchi, Nearly Planar Nonsolvated Monomeric Silyl- and Germyllithiums as a Result of an Intramolecular CH-Li Agostic Interaction. *J. Am. Chem. Soc.*, **2002**, 124, 15160-15161.
- [41] V. Y. Lee, A. Sekiguchi, Si-, Ge-, and Sn-Centered Free Radicals: From Phantom Species to Grams-Order-Scale Materials. *Eur. J. Inorg. Chem.*, **2005**, 1209-1222.
- [42] G. Molev, B. Tumanskii, D. Sheberla, M. Botoshansky, D. Bravo-Zhivotovskii, Y. Apeloig, Isolable Photoreactive Polysilyl Radicals. *J. Am. Chem. Soc.*, **2009**, 131, 11698-11700.
- [43] Y. Imada, H. Nakano, K. Furukawa, R. Kishi, M. Nakano, H. Maruyama, M. Nakamoto, A. Sekiguchi, M. Ogawa, T. Ohta, Y. Yamamoto, Isolation of Hypervalent Group-16 Radicals and Their Application in Organic-Radical Batteries. *J. Am. Chem. Soc.*, **2016**, 138, 479-482.
- [44] G. Molev, D. Bravo-Zhivotovskii, M. Karni, B. Tumanskii, M. Botoshansky, Y. Apeloig, Synthesis, Molecular Structure, and Reactivity of the Isolable Silylenoid with a Tricoordinate Silicon. *J. Am. Chem. Soc.*, **2006**, 128, 2784-2785.
- [45] S. Inoue, M. Ichinohe, A. Sekiguchi, Isolable Silylene Anion Radical: Structural Characteristics in the Solid State and in Solution. *J. Am. Chem. Soc.*, **2007**, 129, 6096-6097.
- [46] S. Inoue, M. Ichinohe, A. Sekiguchi, Isolable Alkali-Metal-Substituted Silyl Radicals ( $(t\text{Bu}_2\text{MeSi})_2\text{SiM}$  (M = Li, Na, K): Electronically and Sterically Accessible Planar Silyl Radicals. *Organometallics*, **2008**, 27, 1358-1360.
- [47] K. Taira, M. Ichinohe, A. Sekiguchi, Isolable Aryl-Substituted Silyl Radicals: Synthesis, Characterization, and Reactivity. *Chem. Eur. J.*, **2014**, 20, 9342-9348.
- [48] T. Nozawa, M. Nagata, M. Ichinohe, A. Sekiguchi, Isolable *p*- and *m*- $[(t\text{Bu}_2\text{MeSi})_2\text{Si}]_2\text{C}_6\text{H}_4$ : Disilaquinodimethane vs Triplet Bis(silyl radical). *J. Am. Chem. Soc.*, **2011**, 133, 5773-5775.

- [49] T. Nozawa, M. Ichinohe, A. Sekiguchi, 1,3,5-[(<sup>t</sup>Bu<sub>2</sub>MeSi)<sub>2</sub>Si]<sub>3</sub>C<sub>6</sub>H<sub>3</sub>: Isolable Si-centered Triradical with a High-spin Quartet Ground State. *Chem. Lett.*, **2015**, *44*, 56-57.
- [50] H. Tanaka, M. Ichinohe, A. Sekiguchi, An Isolable NHC-Stabilized Silylene Radical Cation: Synthesis and Structural Characterization. *J. Am. Chem. Soc.*, **2012**, *134*, 5540-5543.
- [51] S.-H. Zhang, E. Carter, H.-W. Xi, Y. Li, K. H. Lim, C.-W. So, Delocalized Hypervalent Silyl Radical Supported by Amidinate and Imino Substituents. *Inorg. Chem.*, **2017**, *56*, 701-704.
- [52] Y. Li, Y.-C. Chan, B.-X. Leong, Y. Li, E. Richards, I. Purushothaman, S. De, P. Parameswaran, C.-W. So, Trapping a Silicon(I) Radical with Carbenes: A Cationic cAAC–Silicon(I) Radical and an NHC–Parent-Silyliumylidene Cation. *Angew. Chem. Int. Ed.*, **2017**, *56*, 7573-7578.
- [53] K. C. Mondal, H. W. Roesky, A. C. Stückl, F. Ehret, W. Kaim, B. Dittrich, B. Maity, D. Koley, Formation of Trichlorosilyl-Substituted Carbon-Centered Stable Radicals through the Use of π-Accepting Carbenes. *Angew. Chem. Int. Ed.*, **2013**, *52*, 11804-11807.
- [54] W. Li, S. Kundu, C. Köhler, J. Li, S. Dutta, Z. Yang, D. Stalke, R. Herbst-Irmer, A. C. Stückl, B. Schwederski, D. Koley, W. Kaim, H. W. Roesky, Cyclic Alkyl(amino) Carbene-Stabilized Monoradicals of Organosilicon(IV) Compounds with Small Substituents. *Organometallics*, **2019**, *38*, 1939-1945.
- [55] R. Kinjo, M. Ichinohe, A. Sekiguchi, An Isolable Disilyne Anion Radical and a New Route to the Disilenide Ion upon Reduction of a Disilyne. *J. Am. Chem. Soc.*, **2007**, *129*, 26-27.
- [56] A. Sekiguchi, R. Kinjo, M. Ichinohe, Interaction of π-bonds of the silicon–silicon triple bond with alkali metals: An isolable anion radical upon reduction of a disilyne. *Synth. Met.*, **2009**, *159*, 773-775.
- [57] A. Sekiguchi, S. Inoue, M. Ichinohe, Y. Arai, Isolable Anion Radical of Blue Disilene (<sup>t</sup>Bu<sub>2</sub>MeSi)<sub>2</sub>Si=Si(SiMe<sup>t</sup>Bu<sub>2</sub>)<sub>2</sub> Formed upon One-Electron Reduction: Synthesis and Characterization. *J. Am. Chem. Soc.*, **2004**, *126*, 9626-9629.
- [58] A. Tsurusaki, S. Kyushin, The Radical Anion of Cyclopentasilane-Fused Hexasilabenzvalene. *Chem. Eur. J.*, **2016**, *22*, 134-137.



- [59] S. Inoue, M. Ichinohe, A. Sekiguchi, The Isolable Cation Radical of Disilene: Synthesis, Characterization, and a Reversible One-Electron Redox System. *J. Am. Chem. Soc.*, **2008**, *130*, 6078-6079.
- [60] H. E. Simmons, R. D. Smith, A NEW SYNTHESIS OF CYCLOPROPANES FROM OLEFINS. *J. Am. Chem. Soc.*, **1958**, *80*, 5323-5324.
- [61] B. Gehrhus, M. F. Lappert, Chemistry of thermally stable bis(amino)silylenes. *J. Organomet. Chem.*, **2001**, *617-618*, 209-223.
- [62] S. Díez-González, N. Marion, S. P. Nolan, N-Heterocyclic Carbenes in Late Transition Metal Catalysis. *Chem. Rev.*, **2009**, *109*, 3612-3676.
- [63] M. G. Gardiner, C. C. Ho, Recent advances in bidentate bis(*N*-heterocyclic carbene) transition metal complexes and their applications in metal-mediated reactions. *Coord. Chem. Rev.*, **2018**, *375*, 373-388.
- [64] E. Peris, Smart N-Heterocyclic Carbene Ligands in Catalysis. *Chem. Rev.*, **2018**, *118*, 9988-10031.
- [65] V. Nesterov, D. Reiter, P. Bag, P. Frisch, R. Holzner, A. Porzelt, S. Inoue, NHCs in Main Group Chemistry. *Chem. Rev.*, **2018**, *118*, 9678-9842.
- [66] Y. Mizuhata, T. Sasamori, N. Tokitoh, Stable Heavier Carbene Analogues. *Chem. Rev.*, **2009**, *109*, 3479-3511.
- [67] V. S. V. S. N. Swamy, S. Pal, S. Khan, S. S. Sen, Cations and dications of heavier group 14 elements in low oxidation states. *Dalton Trans.*, **2015**, *44*, 12903-12923.
- [68] P. Pyykkö, Relativistic effects in structural chemistry. *Chem. Rev.*, **1988**, *88*, 563-594.
- [69] R. S. Grev, H. F. Schaefer, P. P. Gaspar, In Search of Triplet Silylenes. *J. Am. Chem. Soc.*, **1991**, *113*, 5638-5643.
- [70] M. C. Holthausen, W. Koch, Y. Apeloig, Theory Predicts Triplet Ground-State Organic Silylenes. *J. Am. Chem. Soc.*, **1999**, *121*, 2623-2624.
- [71] P. P. Gaspar, M. Xiao, D. H. Pae, D. J. Berger, T. Haile, T. Chen, D. Lei, W. R. Winchester, P. Jiang, The quest for triplet ground state silylenes. *J. Organomet. Chem.*, **2002**, *646*, 68-79.

- [72] M. Yoshida, N. Tamaoki, DFT Study on Triplet Ground State Silylenes Revisited: The Quest for the Triplet Silylene Must Go On. *Organometallics*, **2002**, *21*, 2587-2589.
- [73] Y. Apeloig, R. Pauncz, M. Karni, R. West, W. Steiner, D. Chapman, Why Is Methylene a Ground State Triplet while Silylene Is a Ground State Singlet? *Organometallics*, **2003**, *22*, 3250-3256.
- [74] M. Kosa, M. Karni, Y. Apeloig, Were Reactions of Triplet Silylenes Observed? *J. Am. Chem. Soc.*, **2013**, *135*, 9032-9040.
- [75] M. S. Gordon, POTENTIAL-ENERGY SURFACES IN SINGLET AND TRIPLET SILYLENE. *Chem. Phys. Lett.*, **1985**, *114*, 348-352.
- [76] P. P. Gaspar, A. M. Beatty, T. Chen, T. Haile, D. Lei, W. R. Winchester, J. Braddock-Wilking, N. P. Rath, W. T. Klooster, T. F. Koetzle, S. A. Mason, A. Albinati, Tris(triisopropylsilyl)silane and the Generation of Bis(triisopropylsilyl)silylene. *Organometallics*, **1999**, *18*, 3921-3932.
- [77] A. Sekiguchi, T. Tanaka, M. Ichinohe, K. Akiyama, S. Tero-Kubota, Bis(tri-*tert*-butylsilyl)silylene: Triplet Ground State Silylene. *J. Am. Chem. Soc.*, **2003**, *125*, 4962-4963.
- [78] K. Hassler, A. Dzambaski, J. Baumgartner, Dihalohexasilanes  $X_2Si[SiMe(SiMe_3)_2]_2$  as potential precursors for silylenes, disilenes and cyclotrisilanes. *Silicon Chem.*, **2008**, *3*, 271-288.
- [79] M. Haas, A. Knoechl, T. Wiesner, A. Torvisco, R. Fischer, C. Jones, Attempted Synthesis of a Homocyclic Bis(silyl)silylene Leads to the Formation of a Tricyclo[3,1,1,12,4]octasilane. *Organometallics*, **2019**, *38*, 4158-4170.
- [80] M. Ichinohe, R. Kinjo, A. Sekiguchi, The First Stable Methyl-Substituted Disilene: Synthesis, Crystal Structure, and Regiospecific MeLi Addition. *Organometallics*, **2003**, *22*, 4621-4623.
- [81] A. Sekiguchi, T. Tanaka, M. Ichinohe, K. Akiyama, P. P. Gaspar, Tri-*tert*-butylsilylsilylenes with Alkali Metal Substituents ( $tBu_3Si$ )SiM (M = Li, K): Electronically and Sterically Accessible Triplet Ground States. *J. Am. Chem. Soc.*, **2008**, *130*, 426-427.

- [82] T. Ochiai, D. Franz, S. Inoue, Applications of N-heterocyclic imines in main group chemistry. *Chem. Soc. Rev.*, **2016**, *45*, 6327-6344.
- [83] X. Wu, M. Tamm, Transition metal complexes supported by highly basic imidazolin-2-iminato and imidazolin-2-imine N-donor ligands. *Coord. Chem. Rev.*, **2014**, *260*, 116-138.
- [84] C.-W. So, H. W. Roesky, J. Magull, R. B. Oswald, Synthesis and Characterization of  $[\text{PhC}(\text{N}t\text{Bu})_2]\text{SiCl}$ : A Stable Monomeric Chlorosilylene. *Angew. Chem. Int. Ed.*, **2006**, *45*, 3948-3950.
- [85] N. Takeda, H. Suzuki, N. Tokitoh, R. Okazaki, S. Nagase, Reaction of a Sterically Hindered Silylene with Isocyanides: The First Stable Silylene–Lewis Base Complexes. *J. Am. Chem. Soc.*, **1997**, *119*, 1456-1457.
- [86] P. S. Skell, E. J. Goldstein, Dimethylsilene:  $\text{CH}_3\text{SiCH}_3$ . *J. Am. Chem. Soc.*, **1964**, *86*, 1442-1443.
- [87] P. S. Skell, E. J. Goldstein, Silacyclopropanes. *J. Am. Chem. Soc.*, **1964**, *86*, 1442-1442.
- [88] L. Fredin, R. H. Hauge, Z. H. Kafafi, J. L. Margrave, Matrix isolation studies of the reactions of silicon atoms with molecular hydrogen. The infrared spectrum of silylene. *J. Chem. Phys.*, **1985**, *82*, 3542-3545.
- [89] P. Jutzi, D. Kanne, C. Krüger, Decamethylsilicocene—Synthesis and Structure. *Angew. Chem. Int. Ed. Engl.*, **1986**, *25*, 164-164.
- [90] T. Kühler, P. Jutzi, Decamethylsilicocene: Synthesis, Structure, Bonding and Chemistry. in *Advances in Organometallic Chemistry*. Academic Press, **2003**.
- [91] H. H. Karsch, U. Keller, S. Gamper, G. Müller,  $\text{Si}[(\text{Me}_2\text{P})_2\text{C}(\text{SiMe}_3)]_2$ , a Stable  $\sigma$ -Bonded Compound Containing Divalent Silicon. *Angew. Chem. Int. Ed. Engl.*, **1990**, *29*, 295-296.
- [92] M. Denk, R. Lennon, R. Hayashi, R. West, A. V. Belyakov, H. P. Verne, A. Haaland, M. Wagner, N. Metzler, Synthesis and Structure of a Stable Silylene. *J. Am. Chem. Soc.*, **1994**, *116*, 2691-2692.
- [93] M. Haaf, T. A. Schmedake, R. West, Stable Silylenes. *Acc. Chem. Res.*, **2000**, *33*, 704-714.

- [94] M. Kira, S. Ishida, T. Iwamoto, C. Kabuto, The First Isolable Dialkylsilylene. *J. Am. Chem. Soc.*, **1999**, *121*, 9722-9723.
- [95] M. Kira, An isolable dialkylsilylene and its derivatives. A step toward comprehension of heavy unsaturated bonds. *Chem. Commun.*, **2010**, *46*, 2893-2903.
- [96] S. Ishida, T. Abe, F. Hirakawa, T. Kosai, K. Sato, M. Kira, T. Iwamoto, Persistent Dialkylsilanone Generated by Dehydrobromination of Dialkylbromosilanol. *Chem. Eur. J.*, **2015**, *21*, 15100-15103.
- [97] G.-H. Lee, R. West, T. Müller, Bis[bis(trimethylsilyl)amino]silylene, an Unstable Divalent Silicon Compound. *J. Am. Chem. Soc.*, **2003**, *125*, 8114-8115.
- [98] M. Driess, S. Yao, M. Brym, C. van Wüllen, D. Lentz, A New Type of N-Heterocyclic Silylene with Ambivalent Reactivity. *J. Am. Chem. Soc.*, **2006**, *128*, 9628-9629.
- [99] S. Nagendran, H. W. Roesky, The Chemistry of Aluminum(I), Silicon(II), and Germanium(II). *Organometallics*, **2008**, *27*, 457-492.
- [100] M. Asay, C. Jones, M. Driess, N-Heterocyclic Carbene Analogues with Low-Valent Group 13 and Group 14 Elements: Syntheses, Structures, and Reactivities of a New Generation of Multitalented Ligands. *Chem. Rev.*, **2011**, *111*, 354-396.
- [101] S. Yao, Y. Xiong, M. Driess, Zwitterionic and Donor-Stabilized N-Heterocyclic Silylenes (NHSis) for Metal-Free Activation of Small Molecules. *Organometallics*, **2011**, *30*, 1748-1767.
- [102] S. S. Sen, S. Khan, P. P. Samuel, H. W. Roesky, Chemistry of functionalized silylenes. *Chem. Sci.*, **2012**, *3*, 659-682.
- [103] R. S. Ghadwal, H. W. Roesky, S. Merkel, J. Henn, D. Stalke, Lewis Base Stabilized Dichlorosilylene. *Angew. Chem. Int. Ed.*, **2009**, *48*, 5683-5686.
- [104] A. C. Filippou, O. Chernov, G. Schnakenburg, SiBr<sub>2</sub>(Idipp): A Stable N-Heterocyclic Carbene Adduct of Dibromosilylene. *Angew. Chem. Int. Ed.*, **2009**, *48*, 5687-5690.

- [105] A. C. Filippou, Y. N. Lebedev, O. Chernov, M. Straßmann, G. Schnakenburg, Silicon(II) Coordination Chemistry: N-Heterocyclic Carbene Complexes of Si<sup>2+</sup> and Si<sup>1+</sup>. *Angew. Chem. Int. Ed.*, **2013**, *52*, 6974-6978.
- [106] R. S. Ghadwal, R. Azhakar, H. W. Roesky, Dichlorosilylene: A High Temperature Transient Species to an Indispensable Building Block. *Acc. Chem. Res.*, **2013**, *46*, 444-456.
- [107] B. D. Rekken, T. M. Brown, J. C. Fettinger, H. M. Tuononen, P. P. Power, Isolation of a Stable, Acyclic, Two-Coordinate Silylene. *J. Am. Chem. Soc.*, **2012**, *134*, 6504-6507.
- [108] A. V. Protchenko, K. H. Birjkumar, D. Dange, A. D. Schwarz, D. Vidovic, C. Jones, N. Kaltsoyannis, P. Mountford, S. Aldridge, A Stable Two-Coordinate Acyclic Silylene. *J. Am. Chem. Soc.*, **2012**, *134*, 6500-6503.
- [109] S. Yadav, S. Saha, S. S. Sen, Compounds with Low-Valent p-Block Elements for Small Molecule Activation and Catalysis. *ChemCatChem*, **2016**, *8*, 486-501.
- [110] C. Weetman, S. Inoue, The Road Travelled: After Main-Group Elements as Transition Metals. *ChemCatChem*, **2018**, *10*, 4213-4228.
- [111] S. S. Sen, S. Khan, S. Nagendran, H. W. Roesky, Interconnected Bis-Silylenes: A New Dimension in Organosilicon Chemistry. *Acc. Chem. Res.*, **2012**, *45*, 578-587.
- [112] T. Chu, G. I. Nikonov, Oxidative Addition and Reductive Elimination at Main-Group Element Centers. *Chem. Rev.*, **2018**, *118*, 3608-3680.
- [113] T. Kajiwara, N. Takeda, T. Sasamori, N. Tokitoh, Insertion of an Overcrowded Silylene into Hydro- and Haloboranes: A Novel Synthesis of Silylborane Derivatives and Their Properties. *Organometallics*, **2004**, *23*, 4723-4734.
- [114] T. Kajiwara, N. Takeda, T. Sasamori, N. Tokitoh, Synthesis of Alkali Metal Salts of Borylsilyl Anions Utilizing Highly Crowded Silylboranes and Their Properties. *Organometallics*, **2008**, *27*, 880-893.
- [115] C. C. Ventocilla, K. A. Woerpel, Synthesis of Silyloxy Dienes by Silylene Transfer to Divinyl Ketones: Application to the Asymmetric Synthesis of Substituted Cyclohexanes. *J. Org. Chem.*, **2012**, *77*, 3277-3283.

- [116] S. Ishida, T. Tamura, T. Iwamoto, Dearomative cycloadditions of a silylene with pyrazine and quinoxaline. *Dalton Trans.*, **2018**, 47, 11317-11321.
- [117] H. Suzuki, N. Tokitoh, R. Okazaki, A Novel Reactivity of a Silylene: The First Examples of [1 + 2] Cycloaddition with Aromatic Compounds. *J. Am. Chem. Soc.*, **1994**, 116, 11572-11573.
- [118] H. Suzuki, N. Tokitoh, R. Okazaki, Thermal Dissociation of Disilenes into Silylenes. *Bull. Chem. Soc. Jpn.*, **1995**, 68, 2471-2481.
- [119] M. Kira, S. Ishida, T. Iwamoto, C. Kabuto, Excited-State Reactions of an Isolable Silylene with Aromatic Compounds. *J. Am. Chem. Soc.*, **2002**, 124, 3830-3831.
- [120] M. Kira, S. Ishida, T. Iwamoto, A. de Meijere, M. Fujitsuka, O. Ito, The Singlet Excited State of a Stable Dialkylsilylene Is Responsible for Its Photoreactions. *Angew. Chem. Int. Ed.*, **2004**, 43, 4510-4512.
- [121] Y. Mizuhata, T. Sato, N. Tokitoh, Reactions of an Overcrowded Silylene with Pyridines: Formation of a Novel 2H-1,2-Azasilole and its Further Cycloaddition. *Heterocycles*, **2012**, 84, 413-418.
- [122] D. Wendel, A. Porzelt, F. A. D. Herz, D. Sarkar, C. Jandl, S. Inoue, B. Rieger, From Si(II) to Si(IV) and Back: Reversible Intramolecular Carbon–Carbon Bond Activation by an Acyclic Iminosilylene. *J. Am. Chem. Soc.*, **2017**, 139, 8134-8137.
- [123] D. Wendel, D. Reiter, A. Porzelt, P. J. Altmann, S. Inoue, B. Rieger, Silicon and Oxygen's Bond of Affection: An Acyclic Three-Coordinate Silanone and Its Transformation to an Iminosiloxysilylene. *J. Am. Chem. Soc.*, **2017**, 139, 17193-17198.
- [124] M. Driess, Breaking the limits with silylenes. *Nature Chemistry*, **2012**, 4, 525.
- [125] A. V. Protchenko, A. D. Schwarz, M. P. Blake, C. Jones, N. Kaltsoyannis, P. Mountford, S. Aldridge, A Generic One-Pot Route to Acyclic Two-Coordinate Silylenes from Silicon(IV) Precursors: Synthesis and Structural Characterization of a Silylsilylene. *Angew. Chem. Int. Ed.*, **2013**, 52, 568-571.
- [126] R. Okazaki, R. West, Chemistry of Stable Disilenes. in *Advances in Organometallic Chemistry*. F. Gordon; A. Stone; R. West, Eds. Academic Press, **1996**.



- [127] P. P. Power,  $\pi$ -Bonding and the Lone Pair Effect in Multiple Bonds between Heavier Main Group Elements. *Chem. Rev.*, **1999**, *99*, 3463-3504.
- [128] M. Weidenbruch, Recent Advances in the Chemistry of Silicon–Silicon Multiple Bonds. in *The Chemistry of Organic Silicon Compounds*. Z. Rappoport; Y. Apeloig, Eds. **2001**.
- [129] M. Weidenbruch, Some recent advances in the chemistry of silicon and its homologues in low coordination states. *J. Organomet. Chem.*, **2002**, *646*, 39-52.
- [130] M. Kira, T. Iwamoto, Progress in the Chemistry of Stable Disilenes. in *Advances in Organometallic Chemistry*. R. West; A. F. Hill, Eds. Academic Press, **2006**.
- [131] M. Kira, Bonding and structure of disilenes and related unsaturated group-14 element compounds. *Proc. Jpn. Acad., Ser. B, Phys. Biol. Sci.*, **2012**, *88*, 167-191.
- [132] T. Iwamoto, S. Ishida, Multiple Bonds with Silicon: Recent Advances in Synthesis, Structure, and Functions of Stable Disilenes. in *Functional Molecular Silicon Compounds II: Low Oxidation States*. D. Scheschkewitz, Ed. Springer International Publishing Switzerland, **2014**.
- [133] C. Präsang, D. Scheschkewitz, Reactivity in the periphery of functionalised multiple bonds of heavier group 14 elements. *Chem. Soc. Rev.*, **2016**, *45*, 900-921.
- [134] R. C. Fischer, P. P. Power,  $\pi$ -Bonding and the Lone Pair Effect in Multiple Bonds Involving Heavier Main Group Elements: Developments in the New Millennium. *Chem. Rev.*, **2010**, *110*, 3877-3923.
- [135] K. K. Milnes, L. C. Pavelka, K. M. Baines, Cycloaddition of carbonyl compounds and alkynes to (di)silenes and (di)germenes: reactivity and mechanism. *Chem. Soc. Rev.*, **2016**, *45*, 1019-1035.
- [136] G. Trinquier, Double bonds and bridged structures in the heavier analogs of ethylene. *J. Am. Chem. Soc.*, **1990**, *112*, 2130-2137.
- [137] P. Jutzi, New Element-Carbon (p-p) $\pi$  Bonds. *Angew. Chem. Int. Ed. Engl.*, **1975**, *14*, 232-245.

- [138] L. E. Gusel'nikov, N. S. Nametkin, Formation and Properties of Unstable Intermediates Containing Multiple  $p_{\pi}-p_{\pi}$  Bonded Group 4B Metals. *Chem. Rev.*, **1979**, *79*, 529-577.
- [139] R. West, M. J. Fink, J. Michl, Tetramesityldisilene, a Stable Compound Containing a Silicon-Silicon Double Bond. *Science*, **1981**, *214*, 1343.
- [140] A. G. Brook, S. C. Nyburg, F. Abdesaken, B. Gutekunst, G. Gutekunst, R. Krishna, M. R. Kallury, Y. C. Poon, Y. M. Chang, W. N. Winnie, Stable Solid Silaethylenes. *J. Am. Chem. Soc.*, **1982**, *104*, 5667-5672.
- [141] E. A. Carter, W. A. Goddard, Relation between Singlet-Triplet Gaps and Bond Energies. *J. Phys. Chem.*, **1986**, *90*, 998-1001.
- [142] G. Trinquier, J. P. Malrieu, Nonclassical Distortions at Multiple Bonds. *J. Am. Chem. Soc.*, **1987**, *109*, 5303-5315.
- [143] M. Driess, H. Grützmacher, Main Group Element Analogues of Carbenes, Olefins, and Small Rings. *Angew. Chem. Int. Ed. Engl.*, **1996**, *35*, 828-856.
- [144] S. David, The Versatile Chemistry of Disilenides: Disila Analogues of Vinyl Anions as Synthons in Low-valent Silicon Chemistry. *Chem. Lett.*, **2011**, *40*, 2-11.
- [145] M. J. Fink, M. J. Michalczyk, K. J. Haller, R. West, J. Michl, The X-Ray Crystal Structure of Tetramesityldisilene. *J. Chem. Soc., Chem. Commun.*, **1983**, 1010-1011.
- [146] B. D. Shepherd, C. F. Campana, R. West, Crystallographic Analysis of Thermochromic, Unsolvated Tetramesityldisilene at 173 K and 295 K. *Heteroat. Chem.*, **1990**, *1*, 1-7.
- [147] M. Kira, T. Maruyama, C. Kabuto, K. Ebata, H. Sakurai, Stable Tetrakis(trialkylsilyl)disilenes; Synthesis, X-Ray Structures, and UV/VIS Spectra. *Angew. Chem. Int. Ed. Engl.*, **1994**, *33*, 1489-1491.
- [148] M. Takahashi, S. Tsutsui, K. Sakamoto, M. Kira, T. Müller, Y. Apeloig, Dimers of Diaminosilylenes: Doubly Bonded or Bridged? The Dimers of  $(i\text{-Pr}_2\text{N})_2\text{Si}$ . *J. Am. Chem. Soc.*, **2001**, *123*, 347-348.

- [149] T. A. Schmedake, M. Haaf, Y. Apeloig, T. Müller, S. Bukalov, R. West, Reversible Transformation between a Diaminosilylene and a Novel Disilene. *J. Am. Chem. Soc.*, **1999**, *121*, 9479-9480.
- [150] A. Kostenko, B. Tumanskii, M. Karni, S. Inoue, M. Ichinohe, A. Sekiguchi, Y. Apeloig, Observation of a Thermally Accessible Triplet State Resulting from Rotation around a Main-Group  $\pi$  Bond. *Angew. Chem. Int. Ed.*, **2015**, *54*, 12144-12148.
- [151] T. Iwamoto, J. Okita, C. Kabuto, M. Kira, Synthesis, structure and isomerization of  $A_2Si=SiB_2$ -type tetrakis(trialkylsilyl)disilenes. *J. Organomet. Chem.*, **2003**, *686*, 105-111.
- [152] L. Zborovsky, A. Kostenko, D. Bravo-Zhivotovskii, Y. Apeloig, Mechanism of the Thermal  $Z \rightleftharpoons E$  Isomerization of a Stable Silene. Experiment and Theory. *Angew. Chem. Int. Ed.*, **2019**, *58*, 14524-14528.
- [153] M. T. Reetz, Dyotropic Rearrangements and Related  $\sigma$ - $\sigma$  Exchange Processes. in *Advances in Organometallic Chemistry*. F. G. A. Stone; R. West, Eds. Academic Press, **1977**.
- [154] H. B. Yokelson, J. Maxka, D. A. Siegel, R. West,  $^{29}Si$  NMR Observation of an Unprecedented Rearrangement in Tetraaryldisilenes. *J. Am. Chem. Soc.*, **1986**, *108*, 4239-4241.
- [155] H. B. Yokelson, D. A. Siegel, A. J. Millevolte, J. Maxka, R. West, 1,2-Diaryl Rearrangement in Tetraaryldisilenes. *Organometallics*, **1990**, *9*, 1005-1010.
- [156] M. J. Michalczyk, R. West, J. Michl, Kinetics of Thermal Cis-Trans Isomerizations in Disilenes. *Organometallics*, **1985**, *4*, 826-829.
- [157] R. West, Chemistry of the Silicon-Silicon Double Bond. *Angew. Chem. Int. Ed. Engl.*, **1987**, *26*, 1201-1211.
- [158] D. Wendel, T. Szilvási, C. Jandl, S. Inoue, B. Rieger, Twist of a Silicon-Silicon Double Bond: Selective *Anti*-Addition of Hydrogen to an Iminodisilene. *J. Am. Chem. Soc.*, **2017**, *139*, 9156-9159.
- [159] M. Kira, T. Iwamoto, C. Kabuto, The First Stable Cyclic Disilene: Hexakis(trialkylsilyl)tetrasilacyclobutene. *J. Am. Chem. Soc.*, **1996**, *118*, 10303-10304.

- [160] H. Kobayashi, T. Iwamoto, M. Kira, A Stable Fused Bicyclic Disilene as a Model for Silicon Surface. *J. Am. Chem. Soc.*, **2005**, *127*, 15376-15377.
- [161] A. Tsurusaki, C. Iizuka, K. Otsuka, S. Kyushin, Cyclopentasilane-Fused Hexasilabenzvalene. *J. Am. Chem. Soc.*, **2013**, *135*, 16340-16343.
- [162] M. Weidenbruch, S. Willms, W. Saak, G. Henkel, Hexaaryltetrasilabuta-1,3-diene: A Molecule with Conjugated Si–Si Double Bonds. *Angew. Chem. Int. Ed. Engl.*, **1997**, *36*, 2503-2504.
- [163] D. Scheschkewitz, A Silicon Analogue of Vinylolithium: Structural Characterization of a Disilenide. *Angew. Chem. Int. Ed.*, **2004**, *43*, 2965-2967.
- [164] S. Ishida, T. Iwamoto, C. Kabuto, M. Kira, A stable silicon-based allene analogue with a formally sp-hybridized silicon atom. *Nature*, **2003**, *421*, 725-727.
- [165] N. Wiberg, S. K. Vasisht, G. Fischer, P. Mayer, Disilynes. III [1] A Relatively Stable Disilyne  $\text{RSi}\equiv\text{SiR}$  ( $\text{R} = \text{SiMe}(\text{Si}^t\text{Bu}_3)_2$ ). *Z. Anorg. Allg. Chem.*, **2004**, *630*, 1823-1828.
- [166] K. Takeuchi, M. Ichinohe, A. Sekiguchi, Reactivity of the Disilyne  $\text{RSi}\equiv\text{SiR}$  ( $\text{R} = \text{Si}^i\text{Pr}[\text{CH}(\text{SiMe}_3)_2]_2$ ) toward Silylcyanide: Two Pathways To Form the Bis-Adduct  $[\text{RSiSiR}(\text{CNSiMe}_3)_2]$  with Some Silaketenimine Character and a 1,4-Diaza-2,3-disilabenzene Analogue. *J. Am. Chem. Soc.*, **2008**, *130*, 16848-16849.
- [167] A. Sekiguchi, R. Kinjo, M. Ichinohe, A Stable Compound Containing a Silicon-Silicon Triple Bond. *Science*, **2004**, *305*, 1755-1757.
- [168] M. Ichinohe, K. Sanuki, S. Inoue, A. Sekiguchi, Disilynyllithium from Tetrasilabuta-1,3-butadiene: A Silicon Analogue of a Vinylolithium. *Organometallics*, **2004**, *23*, 3088-3090.
- [169] K. Abersfelder, A. J. P. White, H. S. Rzepa, D. Scheschkewitz, A Tricyclic Aromatic Isomer of Hexasilabenzene. *Science*, **2010**, *327*, 564-566.
- [170] M. Driess, A. D. Fanta, D. R. Powell, R. West, Synthesis, Characterization, and Complexation of an Unusual  $\text{P}_2\text{Si}_2$  Bicyclobutane with Butterfly-Structure: 2,2,4,4-Tetramesityl-1,3-diphospha-2,4-disilabicyclo[1.1.0]butane. *Angew. Chem. Int. Ed. Engl.*, **1989**, *28*, 1038-1040.

- [171] A. D. Fanta, R. P. Tan, N. M. Comerlato, M. Driess, D. R. Powell, R. West, The reaction of disilenes with P<sub>4</sub> and As<sub>4</sub>. *Inorganica Chimica Acta*, **1992**, 198-200, 733-739.
- [172] R. Fischer, M. Zirngast, M. Flock, J. Baumgartner, C. Marschner, Synthesis of a Hafnocene Disilene Complex. *J. Am. Chem. Soc.*, **2005**, 127, 70-71.
- [173] H. Hashimoto, K. Suzuki, W. Setaka, C. Kabuto, M. Kira, Iron Complexes of (*E*- and (*Z*)-1,2-Dichlorodisilenes. *J. Am. Chem. Soc.*, **2004**, 126, 13628-13629.
- [174] H. Hashimoto, Y. Sekiguchi, Y. Sekiguchi, T. Iwamoto, C. Kabuto, M. Kira, Comparison of structures between platinum and palladium complexes of a tetrasilyldisilene. *Can. J. Chem.*, **2003**, 81, 1241-1245.
- [175] B. Scrosati, J. Garche, Lithium batteries: Status, prospects and future. *J. Power Sources*, **2010**, 195, 2419-2430.
- [176] J. M. Tarascon, M. Armand, Issues and challenges facing rechargeable lithium batteries. *Nature*, **2001**, 414, 359-367.
- [177] M. Wakihara, Recent developments in lithium ion batteries. *Mater. Sci. Eng. R Rep.*, **2001**, 33, 109-134.
- [178] P. G. Bruce, B. Scrosati, J.-M. Tarascon, Nanomaterials for Rechargeable Lithium Batteries. *Angew. Chem. Int. Ed.*, **2008**, 47, 2930-2946.
- [179] G. E. Blomgren, The Development and Future of Lithium Ion Batteries. *J. Electrochem. Soc.*, **2017**, 164, A5019-A5025.
- [180] N. Kentaro, O. Kenichi, N. Hiroyuki, Organic Radical Battery Approaching Practical Use. *Chem. Lett.*, **2011**, 40, 222-227.
- [181] H. Nishide, S. Iwasa, Y.-J. Pu, T. Suga, K. Nakahara, M. Satoh, Organic radical battery: nitroxide polymers as a cathode-active material. *Electrochim. Acta*, **2004**, 50, 827-831.
- [182] C. Friebe, U. S. Schubert, High-Power-Density Organic Radical Batteries. *Top. Curr. Chem.*, **2017**, 375, 19.
- [183] S. Takeo, S. Shuhei, O. Hiroki, O. Kenichi, N. Hiroyuki, p- and n-Type Bipolar Redox-Active Radical Polymer: Toward Totally Organic Polymer-Based Rechargeable Devices with Variable Configuration. *Advanced Materials*, **2011**, 23, 751-754.

- [184] J. Y. Becker, V. Y. Lee, M. Nakamoto, A. Sekiguchi, A. Chrostowska, A. Dargelos, Electrochemical Properties and Computations of Stable Radicals of the Heavy Group 14 Elements (Si, Ge, and Sn). *Chem. Eur. J.*, **2009**, *15*, 8480-8484.
- [185] J. Hagen, Economic Importance of Catalysts. in *Industrial Catalysis*. Wiley-VCH Verlag GmbH & Co. KGaA, Weinheim, **2015**.
- [186] C. R. Catlow, M. Davidson, C. Hardacre, G. J. Hutchings, Catalysis making the world a better place. *Phil. Trans. R. Soc. A*, **2016**, *374*, 20150089.
- [187] L. N. Lewis, J. Stein, Y. Gao, R. E. Colborn, G. Hutchings, Platinum Catalysts Used in the Silicones Industry. *Platinum Metals Rev.*, **1997**, *41*, 66-75.
- [188] P. P. Power, Main-group elements as transition metals. *Nature*, **2010**, *463*, 171-177.
- [189] H. F. T. Klare, M. Oestreich, Silylium ions in catalysis. *Dalton Trans.*, **2010**, *39*, 9176-9184.
- [190] K. Leszczyńska, A. Mix, R. J. F. Berger, B. Rummel, B. Neumann, H.-G. Stammler, P. Jutzi, The Pentamethylcyclopentadienylsilicon(II) Cation as a Catalyst for the Specific Degradation of Oligo(ethyleneglycol) Diethers. *Angew. Chem. Int. Ed.*, **2011**, *50*, 6843-6846.
- [191] S. Inoue, C. Weetman, P. Bag, T. Szilvási, C. Jandl, CO<sub>2</sub> Fixation and Catalytic Reduction by a Neutral Aluminium Double bond. *Angew. Chem. Int. Ed.*, **2019**, *58*, 10961-10965.
- [192] D. Wendel, T. Szilvási, D. Henschel, P. J. Altmann, C. Jandl, S. Inoue, B. Rieger, Precise Activation of Ammonia and Carbon Dioxide by an Iminodisilene. *Angew. Chem. Int. Ed.*, **2018**, *57*, 14575-14579.



## 15. Appendix

### 15.1 Supporting Information Chapter 7



#### Supporting Information

#### **Isolation of a Relatively Air-Stable, Bulky Silyl-Substituted, Neutral Silicon-Centered Radical**

Richard Holzner, Alexander Kaushansky, Boris Tumanskii, Philipp Frisch, Fabian Linsenmann, and Shigeyoshi Inoue\*

[ejic201900522-sup-0001-SupMat.pdf](#)

## Supporting Information

### Table of Contents

1. Experimental Section	S2
1.1. General Methods and Instrumentation.....	S2
1.2. Silyl radical <b>1</b> .....	S3
1.4. ( <sup>t</sup> Bu <sub>2</sub> MeSi) <sub>2</sub> ( <sup>t</sup> Bu <sub>3</sub> Si)SiCl ( <b>2</b> ).....	S4
2. Cyclic Voltammetry (CV)	S6
2.1 General Information.....	S6
2.2 CV Diagrams.....	S7
3. X-ray Crystallographic Data	S9
3.1. General Information.....	S9
3.2 Crystal Structure of <b>1</b> .....	S10
4. References	S12

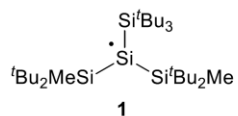
## 1. Experimental Section

### 1.1. General Methods and Instrumentation

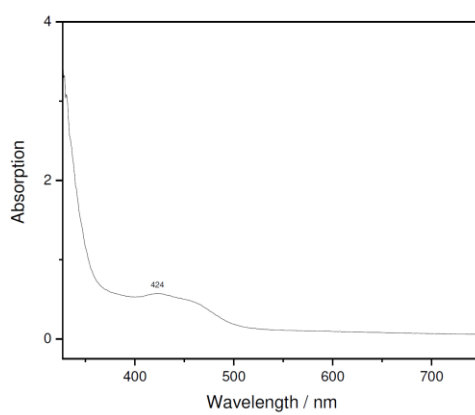
All reactions and manipulations were carried out under an atmosphere of argon 4.6 ( $\geq 99.996\%$ ) by using standard Schlenk and glovebox techniques. The glassware used was heat dried under high vacuum prior to use. All solvents were refluxed over sodium/benzophenone, freshly distilled under argon and deoxygenated prior to use. Deuterated benzene ( $C_6D_6$ ) was obtained from *Sigma-Aldrich*, dried over Na/K alloy, flask-to-flask condensed, deoxygenated by three freeze-pump-thaw cycles and stored over 4 Å molecular sieves. All NMR samples were prepared under argon in *J. Young* PTFE valve NMR tubes. The NMR spectra were recorded on a *Bruker* DRX400 ( $^1H$ : 400.13 MHz,  $^{13}C$ : 100.62 MHz,  $^{29}Si$ : 79.49 MHz), or AV500C ( $^1H$ : 500.36 MHz,  $^{13}C$ : 125.83 MHz,  $^{29}Si$ : 99.41 MHz) spectrometer at ambient temperature (300 K). The  $^1H$ ,  $^{13}C\{^1H\}$  and  $^{29}Si\{^1H\}$  NMR spectroscopic chemical shifts  $\delta$  are reported in ppm relative to tetramethylsilane.  $^1H$  and  $^{13}C\{^1H\}$  NMR spectra are calibrated against the residual proton and natural abundance carbon resonances of the respective deuterated solvent as internal standard:  $C_6D_6$ :  $\delta$  ( $^1H$ ) = 7.16 ppm and  $\delta$  ( $^{13}C$ ) = 128.1 ppm.<sup>[S1]</sup> The following abbreviation is used to describe signal multiplicities: s = singlet.

EPR spectra were recorded on a *Bruker* EMX-10/12 X-band (spectrometer frequency: 9.3 GHz) digital EPR spectrometer. The spectra were recorded with a microwave power of 1.0 mW, 100 kHz magnetic field modulation of 0.5 G amplitude. Digital field resolution was 2048 points per spectrum. Spectra processing and simulation were performed with the *Bruker* WIN-EPR and *SimFonia* Software and *Easyspin* toolbox for *Matlab*.

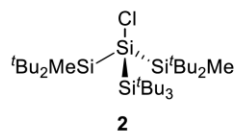
Melting points (m.p.) were determined in sealed glass capillaries under inert gas by a *Büchi* M-565 melting point apparatus. Unless otherwise stated, all commercially available chemicals were purchased from *abc* or *Sigma-Aldrich* and used without further purification. The compounds  $(^tBu_2MeSi)_2SiBr_2$ ,<sup>[S2]</sup>  $^tBu_2MeSiLi$ ,<sup>[S3]</sup>  $(^tBu_3Si)SiCl_2H$ ,<sup>[S4]</sup>  $(^tBu_2MeSi)_3Si$ <sup>[S2]</sup> and  $^tBu_3SiNa \cdot 2THF$ <sup>[S5]</sup> were prepared according to literature procedures.

1.2. Silyl radical **1** $\text{Si}_4\text{C}_{27}\text{H}_{63}$ 

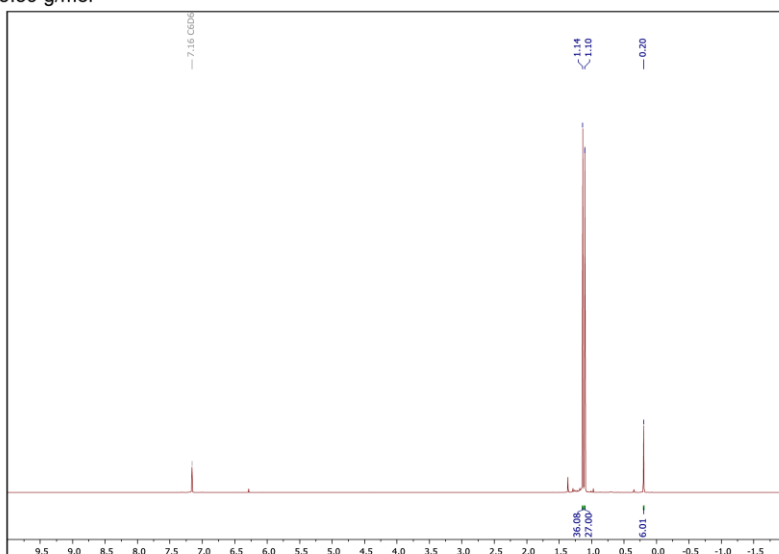
500.14 g/mol



**Figure S1:** UV-Vis spectrum of compound **1** ( $3 \times 10^{-3}$  M in *n*-hexane) at room temperature.

1.4. (<sup>t</sup>Bu<sub>2</sub>MeSi)<sub>2</sub>(<sup>t</sup>Bu<sub>3</sub>Si)SiCl (**2**) $\text{Si}_4\text{C}_{27}\text{H}_{63}\text{Cl}$ 

535.59 g/mol

**Figure S2:** <sup>1</sup>H NMR spectrum of (<sup>t</sup>Bu<sub>2</sub>MeSi)<sub>2</sub>(<sup>t</sup>Bu<sub>3</sub>Si)SiCl (**2**) in C<sub>6</sub>D<sub>6</sub> at 300 K.

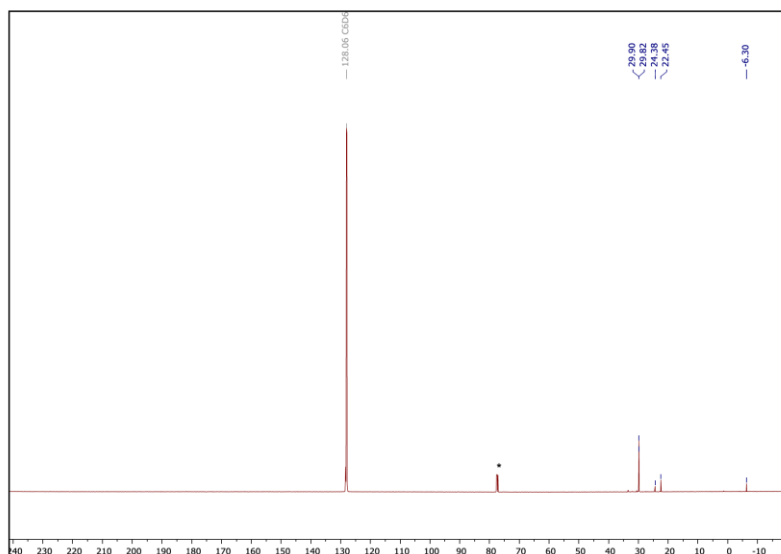


**Figure S3:**  $^{13}\text{C}\{^1\text{H}\}$  NMR spectrum of  $(^t\text{Bu}_2\text{MeSi})_2(^t\text{Bu}_3\text{Si})\text{SiCl}$  (**2**) in  $\text{C}_6\text{D}_6$  at 300 K ( $^*\text{CDCl}_3$ ).

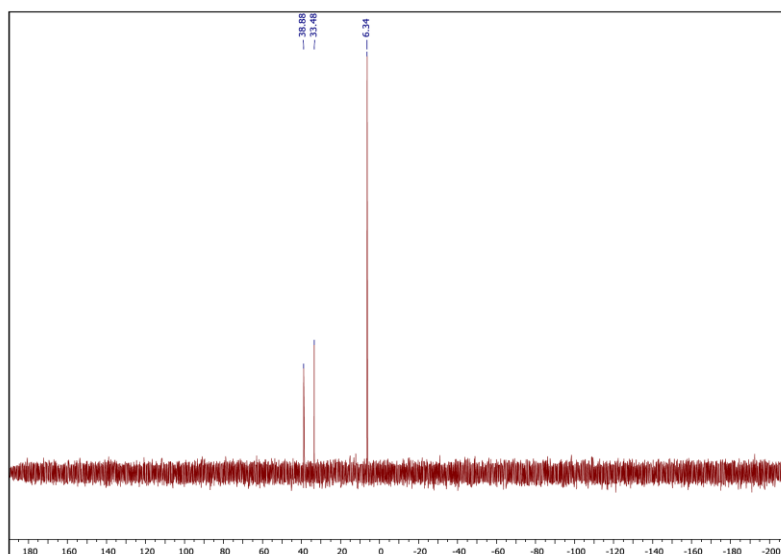


**Figure S4:**  $^{29}\text{Si}\{^1\text{H}\}$  NMR spectrum of  $(^t\text{Bu}_2\text{MeSi})_2(^t\text{Bu}_3\text{Si})\text{SiCl}$  (**2**) in  $\text{C}_6\text{D}_6$  at 300 K.

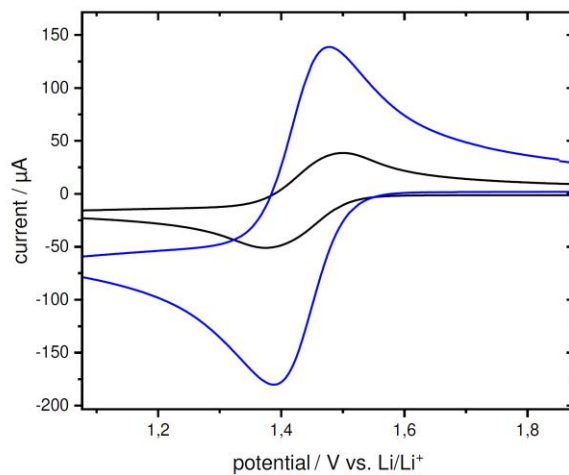


## 2. Cyclic Voltammetry (CV)

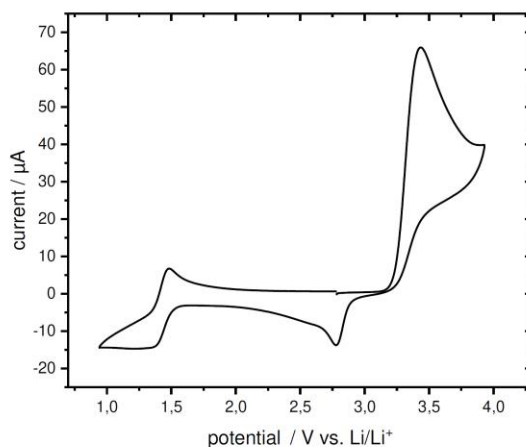
### 2.1 General Information

The CV measurements were performed in an Ar-filled glovebox (*MBraun*, oxygen and water content < 0.1 ppm). The electrochemical three-electrode glass cell was custom made with a gold (*Alfa Aesar*, 99.999% purity) working electrode (WE), a platinum (*Advent*, 99.99+% purity) counter electrode (CE), and a lithium (99.9%, foil, *Rockwood Lithium*, 0.45 mm thickness) reference electrode (RE). The electrolyte in the main and the CE compartment consisted of THF (*Sigma-Aldrich*) and 0.1 M tetrabutylammonium bis(trifluoromethane)sulfonimide (TBATFSI). For the RE compartment a solution of 0.1 M LiTFSI in THF was used. The cell compartments were separated by porous glass frits. For the separation of the RE compartment a *Vycor 7930* frit (*Advanced Glass & Ceramics, Holden, MA*) was used in order to diminish the diffusion between the Li-ion containing RE electrolyte and the electrolyte in the main compartment. The electrodes of the cell compartments were connected *via* fused-in tungsten wires. Before the first CV was recorded, the high frequency resistance (HFR) of the glass cell setup was measured *via* Electrochemical Impedance Spectroscopy (EIS) and used for ohmic drop correction of the measured WE potential. At the end of the CVs, about 10 mg of ferrocenium hexafluorophosphate ( $\text{FcPF}_6$ , *Sigma-Aldrich*) were added to the electrolyte in the main compartment in order to calibrate the potential of the Li RE versus the  $\text{Fc}/\text{Fc}^+$  couple. The CVs were recorded using a *Biologic VMP3* potentiostat/galvanostat.

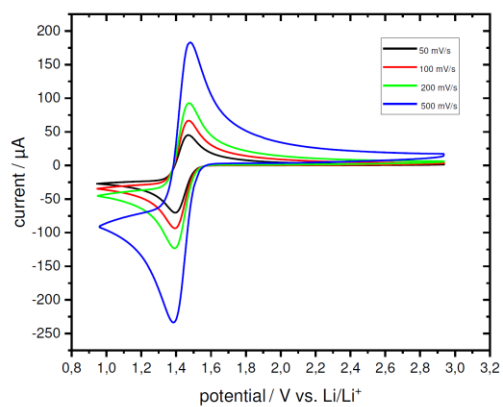
## 2.2 CV Diagrams



**Figure S5:** Cyclic voltammogram of **1** (blue, measured at a scan rate of 100 mV/s) and **2** (black, measured at a scan rate of 500 mV/s) measured in a three-electrode setup using a lithium metal reference electrode (0.1 M (*n*-Bu<sub>4</sub>N)TFSI in THF at room temperature).



**Figure S6:** Cyclic voltammogram of **1** measured in a three-electrode setup using a lithium metal reference electrode at scan rate of 100 mV/s (0.1 M (*n*-Bu<sub>4</sub>N)TFSI in THF at room temperature).

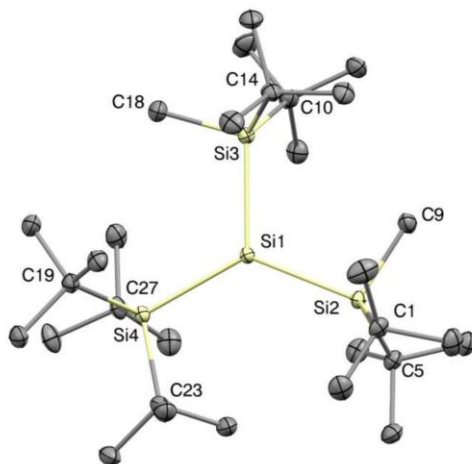


**Figure S7:** Cyclic voltammogram of **1** measured in a three-electrode setup using a lithium metal reference electrode at various scan rates (0.1 M (*n*-Bu<sub>4</sub>N)TFSI in THF at room temperature).

### 3. X-ray Crystallographic Data

#### 3.1. General Information

The X-ray intensity data of **1** was collected on an X-ray single crystal diffractometer equipped with a CMOS detector (*Bruker* Photon-100), a rotating anode (*Bruker* TXS) with MoK $\alpha$  radiation ( $\lambda = 0.71073 \text{ \AA}$ ) and a Helios mirror optic by using the APEX III software package.<sup>[S6]</sup> The measurements were performed on single crystals coated with the perfluorinated ether Fomblin<sup>®</sup> Y. The crystal was fixed on the top of a micro sampler, transferred to the diffractometer and frozen under a stream of cold nitrogen. A matrix scan was used to determine the initial lattice parameters. Reflections were merged and corrected for Lorentz and polarization effects, scan speed, and background using SAINT.<sup>[S7]</sup> Absorption corrections, including odd and even ordered spherical harmonics were performed using SADABS.<sup>[S7]</sup> Space group assignments were based upon systematic absences, E statistics, and successful refinement of the structures. Structures were solved by direct methods with the aid of successive difference Fourier maps, and were refined against all data using the APEX III software in conjunction with SHELXL-2014<sup>[S8]</sup> and SHELXL.<sup>[S9]</sup> All H atoms were placed in calculated positions and refined using a riding model, with methylene and aromatic C–H distances of 0.99 and 0.95 Å, respectively, and  $U_{\text{iso}}(\text{H}) = 1.2 \cdot U_{\text{eq}}(\text{C})$ . Full-matrix least-squares refinements were carried out by minimizing  $\Delta w(F_o^2 - F_c^2)$ <sup>[S7]</sup> with SHELXL-97 weighting scheme.<sup>[S10]</sup> Neutral atom scattering factors for all atoms and anomalous dispersion corrections for the non-hydrogen atoms were taken from International Tables for Crystallography.<sup>[S11]</sup> The images of the crystal structures were generated by Mercury.<sup>[S12]</sup> The CCDC number CCDC-1899751 (**1**) contains the supplementary crystallographic data for the structure. These data can be obtained free of charge from the Cambridge Crystallographic Data Centre via <https://www.ccdc.cam.ac.uk/structures/>.

3.2 Crystal Structure of **1**

**Figure S8:** Molecular structure of **1** with ellipsoids set at 50% probability. Hydrogen atoms are omitted for clarity. Selected bond lengths [Å] and angles [°]: Si1–Si2 2.4533(6), Si1–Si3 2.4480(5), Si1–Si4 2.4834(6), Si4–Si1–Si3 118.61(2), Si4–Si1–Si2 128.95(2), Si2–Si1–Si3 112.16(2).

## 15. Appendix

Table S1. Crystal data and structure refinement for compound 1.

Compound #	1
Chemical formula	C <sub>30</sub> H <sub>69</sub> Si <sub>4</sub>
Formula weight	524.21 g/mol
Temperature	115(2) K
Wavelength	0.71073 Å
Crystal size	0.143 × 0.152 × 0.531 mm
Crystal habit	clear yellow fragment
Crystal system	monoclinic
Space group	P 1 21/n 1
Unit cell dimensions	a = 8.8055(4) Å, α = 90° b = 18.8124(9) Å, β = 93.457(2)° c = 20.7199(10) Å, γ = 90°
Volume	3426(1) Å <sup>3</sup>
Z	4
Density (calculated)	1.051 g/cm <sup>3</sup>
Absorption coefficient	0.190 mm <sup>-1</sup>
F(000)	1220
Diffractometer	Bruker D8 Venture
Radiation source	TXS rotating anode (Mo)
Theta range for data collection	2.25 to 25.68°
Index ranges	-10 ≤ h ≤ 10, -22 ≤ k ≤ 22, -25 ≤ l ≤ 25
Reflections collected	79214
Independent reflections	6508 [R(int) = 0.0276]
Coverage of independent reflections	100.0%
Absorption correction	Multi-Scan
Max. and min. transmission	0.7028 and 0.7465
Refinement method	Full-matrix least-squares on F <sup>2</sup>
Refinement program	SHELXL-2014/7 (Sheldrick, 2014)
Function minimized	Σ w(F <sub>o</sub> <sup>2</sup> - F <sub>c</sub> <sup>2</sup> ) <sup>2</sup>
Data / restraints / parameters	6508 / 0 / 330
Goodness-of-fit on F <sup>2</sup>	1.092
Δ/σ <sub>max</sub>	0.002
Final R indices	5898 data; I > 2σ(I): R1 = 0.0279, wR2 = 0.0695 all data: R1 = 0.0321, wR2 = 0.0722
Weighting scheme	w = 1/[σ <sup>2</sup> (F <sub>o</sub> <sup>2</sup> ) + (0.0287P) <sup>2</sup> + 1.8551P] where P = (F <sub>o</sub> <sup>2</sup> + 2F <sub>c</sub> <sup>2</sup> )/3
Largest diff. peak and hole	0.242 and -0.265 eÅ <sup>-3</sup>
R.M.S. deviation from mean	0.049 eÅ <sup>-3</sup>



#### 4. References

- [S1] H. E. Gottlieb, V. Kotlyar, A. Nudelman, *J. Org. Chem.* **1997**, *62*, 7512-7515.
- [S2] A. Sekiguchi, T. Fukawa, M. Nakamoto, V. Y. Lee, M. Ichinohe, *J. Am. Chem. Soc.* **2002**, *124*, 9865-9869.
- [S3] D. Pinchuk, J. Mathew, A. Kaushansky, D. Bravo-Zhivotovskii, Y. Apeloig, *Angew. Chem. Int. Ed.* **2016**, *55*, 10258-10262; *Angew. Chem.* **2016**, *128*, 10414-10418.
- [S4] N. Wiberg, W. Niedermayer, H. Nöth, J. Knizek, W. Ponikwar, K. Polborn, *Z. Naturforsch.* **2000**, *55 b*, 389 - 405.
- [S5] N. Wiberg, K. Amelunxen, H. W. Lerner, H. Schuster, H. Nöth, I. Krossing, M. Schmidt-Amelunxen, T. Seifert, *J. Organomet. Chem.* **1997**, *542*, 1-18.
- [S6] *APEX suite of crystallographic software*, APEX 3 version 2015.5-2; Bruker AXS Inc.: Madison, Wisconsin, USA, 2015.
- [S7] *SAINT*, Version 7.56a and *SADABS* Version 2008/1; Bruker AXS Inc.: Madison, Wisconsin, USA, 2008.
- [S8] G. M. Sheldrick, *SHELXL-2014*, University of Göttingen, Göttingen, Germany, 2014.
- [S9] C. B. Hübschle, G. M. Sheldrick, B. Dittrich, *J. Appl. Cryst.* **2011**, *44*, 1281-1284.
- [S10] G. M. Sheldrick, *SHELXL-97*, University of Göttingen, Göttingen, Germany, 1998.
- [S11] A. J. C. Wilson, *International Tables for Crystallography*, Volume C, Tables 6.1.1.4 (pp. 500-502), 4.2.6.8 (pp. 219-222), and 4.2.4.2 (pp. 193-199), Kluwer Academic Publishers: Dordrecht, The Netherlands, **1992**.
- [S12] C. F. Macrae, I. J. Bruno, J. A. Chisholm, P. R. Edgington, P. McCabe, E. Pidcock, L. Rodriguez-Monge, R. Taylor, J. van de Streek, P. A. Wood, *J. Appl. Cryst.* **2008**, *41*, 466-470.

## 15.2 Supporting Information Chapter 8

## Supporting Information

**Disilene-Silylene Interconversion: A Synthetically Accessible Acyclic Bis(silyl)silylene**

*Dominik Reiter,<sup>†</sup> Richard Holzner,<sup>†</sup> Amelie Porzelt,<sup>†</sup> Philipp J. Altmann, Philipp Frisch, and Shigeyoshi Inoue\**

## Table of Contents

1. Experimental Section.....	S2
1.1 General Methods and Instrumentation.....	S2
1.2 Synthesis of ((TMS) <sub>3</sub> Si)SiH <sub>2</sub> Cl ( <b>18</b> ).....	S3
1.3 Synthesis of ((TMS) <sub>3</sub> Si)( <sup>t</sup> Bu <sub>3</sub> Si)SiH <sub>2</sub> ( <b>1</b> ).....	S5
1.4 Synthesis of ((TMS) <sub>3</sub> Si)( <sup>t</sup> Bu <sub>3</sub> Si)SiBr <sub>2</sub> ( <b>2</b> ).....	S7
1.5 Synthesis and reactivity of bis(silyl)silylene <b>3</b> /tetrasilyldisilene <b>3'</b> .....	S9
1.6 Synthesis of disiletane <b>4</b> .....	S13
1.7 Synthesis of ((TMS) <sub>3</sub> Si)( <sup>t</sup> Bu <sub>3</sub> Si)Si(CH <sub>2</sub> CH <sub>2</sub> ) ( <b>5</b> ).....	S18
1.8 [2+1] cycloaddition reactions of <b>3/3'</b> with ( <i>E</i> )-/( <i>Z</i> )-alkenes.....	S20
1.9 Synthesis of aminosilane <b>6</b> .....	S35
1.10 Synthesis of (TMS)((TMS) <sub>2</sub> ( <sup>t</sup> Bu <sub>3</sub> Si)Si)Si( <sup>i</sup> Pr <sub>2</sub> Me <sub>2</sub> ) ( <b>13</b> ).....	S37
1.11 Synthesis and reactivity of ((TMS) <sub>3</sub> Si)( <sup>t</sup> Bu <sub>3</sub> Si)Si(DMAP) ( <b>14</b> ).....	S41
1.12 Synthesis of ((TMS) <sub>3</sub> Si)( <sup>t</sup> Bu <sub>3</sub> Si)Si( <sup>i</sup> Pr <sub>2</sub> Me <sub>2</sub> ) ( <b>15</b> ).....	S44
1.13 Synthesis of (TMS)((TMS) <sub>2</sub> ( <sup>t</sup> Bu <sub>3</sub> Si)Si)Si(IME <sub>4</sub> ) ( <b>16</b> ).....	S47
1.14 Synthesis of (TMSO)( <sup>t</sup> Bu <sub>3</sub> Si)Si=O( <sup>i</sup> Pr <sub>2</sub> Me <sub>2</sub> ) ( <b>17</b> ).....	S49
2. X-ray Crystallographic Data.....	S52
3. DFT Calculations.....	S67
4. References.....	S91

## 1. Experimental Section

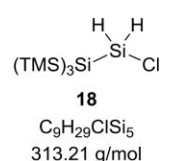
### 1.1 General Methods and Instrumentation

All manipulations were carried out under exclusion of H<sub>2</sub>O and O<sub>2</sub> under an atmosphere of argon 4.6 (≥99.996%; *Westfalen AG*) using standard *Schlenk* techniques or in a *LABstar* glovebox from *MBraun Inertgas-Systeme GmbH* with H<sub>2</sub>O and O<sub>2</sub> levels below 0.5 ppm. The glassware used was heat dried under fine vacuum prior to use with *Triboflon III* grease (mixture of polytetrafluoroethylene (PTFE) and perfluoropolyether (PFPE)) from *Freudenberg & Co. KG* as sealant. All solvents were refluxed over sodium/benzophenone, freshly distilled under argon and deoxygenated before use. The deuterated solvents benzene (C<sub>6</sub>D<sub>6</sub>), THF (THF-*d*<sub>8</sub>) and toluene (toluene-*d*<sub>8</sub>) were obtained from *Sigma-Aldrich Chemie GmbH*, dried over Na/K alloy, flask-to-flask condensed, deoxygenated by three freeze-pump-thaw cycles and stored over 3 Å molecular sieves in the glovebox. All NMR samples were prepared under argon in *J. Young* PTFE valve NMR tubes. The NMR spectra were recorded on *Bruker AV400US* (<sup>1</sup>H: 400.13 MHz) *AV500* (<sup>1</sup>H: 500.13 MHz) or *AV500C* (<sup>1</sup>H: 500.36 MHz, <sup>13</sup>C: 125.83 MHz, <sup>29</sup>Si: 99.41 MHz) spectrometers at ambient temperature (300 K). Low temperature NMR spectra were recorded on a *Bruker DRX400* (<sup>1</sup>H: 400.13 MHz, <sup>13</sup>C: 100.62 MHz, <sup>29</sup>Si: 79.49 MHz) spectrometer. The <sup>1</sup>H, <sup>13</sup>C{<sup>1</sup>H} and <sup>29</sup>Si{<sup>1</sup>H} NMR spectroscopic chemical shifts  $\delta$  are reported in ppm relative to tetramethylsilane. <sup>1</sup>H and <sup>13</sup>C{<sup>1</sup>H} NMR spectra are calibrated against the residual proton and natural abundance carbon resonances of the respective deuterated solvent as internal standard (C<sub>6</sub>D<sub>6</sub>:  $\delta(^1\text{H}) = 7.16$  ppm and  $\delta(^{13}\text{C}) = 128.1$  ppm, THF-*d*<sub>8</sub>:  $\delta(^1\text{H}) = 1.73$  ppm and  $\delta(^{13}\text{C}) = 25.4$  ppm, toluene-*d*<sub>8</sub>:  $\delta(^1\text{H}) = 2.09$  ppm and  $\delta(^{13}\text{C}) = 20.4$  ppm).<sup>[S1]</sup> The following abbreviations are used to describe signal multiplicities: s = singlet, d = doublet, dd = doublet of doublets, dq = doublet of quartets, t = triplet, sept = septet, m = multiplet, br = broad. Some NMR spectra include resonances for silicone grease (C<sub>6</sub>D<sub>6</sub>:  $\delta(^1\text{H}) = 0.29$  ppm,  $\delta(^{13}\text{C}) = 1.4$  ppm and  $\delta(^{29}\text{Si}) = -21.8$  ppm) derived from *B. Braun Melsungen AG Sterican®* cannulas. EPR spectra were recorded on a *Jeol jes-Fa200 esr* spectrometer with a spectrometer frequency of 9.267 GHz (X-band). Quantitative elemental analyses (EA) were carried out using a *EURO EA (HEKAtech)* instrument equipped with a CHNS combustion analyzer at the *Laboratory for Microanalysis* at the *TUM Catalysis Research Center*. IR spectra were recorded on a *Perkin Elmer FT-IR* spectrometer (diamond ATR, Spectrum Two) in a range of 400–4000 cm<sup>-1</sup> at room temperature inside an argon-filled glovebox. The intensities of the IR bands are abbreviated as following: s = strong, m = medium, w = weak. The UV-Vis spectrum was taken on a *Varian, Inc. Cary 50* spectrophotometer with a *Schlenk* quartz cuvette.

S2

Melting Points (m.p.) were determined in sealed glass capillaries under inert gas by a *Büchi M-565* melting point apparatus. Unless otherwise stated, all commercially available chemicals were purchased from *aber GmbH*, *Sigma-Aldrich Chemie GmbH* or *Tokyo Chemical Industry Co., Ltd.* and used without further purification. Dinitrogen monoxide (N<sub>2</sub>O) 5.0 (≥99.999%), ethylene 3.5 (≥99.95%) and hydrogen 5.0 (≥99.999%) were purchased from *Westfalen AG* and used as received. (*E*)-2-butene and (*Z*)-2-butene (technical grade, estimated purity between 2.0 (≥99%) and 3.5 (≥99.5%) with lower isomeric purity) were obtained from *GHC Gerling, Holz & Co. Handels GmbH* and degassed by three freeze-pump-thaw cycles to remove ethylene contamination. The compounds tris(trimethylsilyl)silyl potassium (KSi(TMS)<sub>3</sub>)<sup>[S2]</sup>, tri(*tert*-butyl)silyl sodium (NaSi<sup>*t*</sup>Bu<sub>3</sub>(THF)<sub>2</sub>)<sup>[S3]</sup>, 1,3,4,5-tetramethylimidazol-2-ylidene (IMe<sub>4</sub>) and 1,3-diisopropyl-4,5-dimethylimidazol-2-ylidene (IPr<sub>2</sub>Me<sub>2</sub>)<sup>[S4]</sup> were prepared as described in the corresponding references. Potassium graphite (KC<sub>8</sub>) was synthesized following a literature reported procedure upon heating a 1:8 mixture of potassium and graphite in a thick-walled, PTFE-capped pressurizeable Schlenk flask to 500 °C until a homogenous bronze powder was obtained.<sup>[S5]</sup>

### 1.2 Synthesis of ((TMS)<sub>3</sub>Si)SiH<sub>2</sub>Cl (**18**)



**18**  
C<sub>9</sub>H<sub>29</sub>ClSi<sub>5</sub>  
313.21 g/mol

A solution of dichlorosilane in toluene (38.9 wt%, 7.63 g, 75.5 mmol, 2.5 eq.) was diluted with toluene (200 mL) and cooled to -78 °C. Solvent-free KSi(TMS)<sub>3</sub> (8.66 g, 30.2 mmol, 1.0 eq.) in toluene (400 mL) was slowly added over a period of 7 hours. Subsequently, the reaction mixture was stirred for 16 hours and thereby gradually warmed to room temperature. KCl was separated from the mixture by filtration and the solvent removed *in vacuo*. The crude product, containing ~3% of the di-substituted compound bis[tris(trimethylsilyl)silyl]silane (((TMS)<sub>3</sub>Si)<sub>2</sub>SiH<sub>2</sub>)<sup>[S6]</sup>, was purified by sublimation (90 °C / 5.0 × 10<sup>-3</sup> mbar) providing **18** as a colorless, waxy solid (8.51 g, 27.2 mmol, 90%).

**m.p.:** 207-208 °C.

**<sup>1</sup>H NMR (500 MHz, C<sub>6</sub>D<sub>6</sub>, 300 K):** δ [ppm] = 5.21 (s, 2H, SiH), 0.24 (s, 27H, TMS).

**<sup>13</sup>C{<sup>1</sup>H} NMR (126 MHz, C<sub>6</sub>D<sub>6</sub>, 300 K):** δ [ppm] = 2.1 (TMS).

**<sup>29</sup>Si{<sup>1</sup>H} NMR (99 MHz, C<sub>6</sub>D<sub>6</sub>, 300 K):** δ [ppm] = -9.1 (TMS), -17.0 (SiH<sub>2</sub>Cl), -133.2 (Si(TMS)<sub>3</sub>).

**Anal. Calcd. [%] for C<sub>9</sub>H<sub>29</sub>ClSi<sub>5</sub>:** C, 34.51; H, 9.33. Found [%]: C, 33.95; H, 9.34.

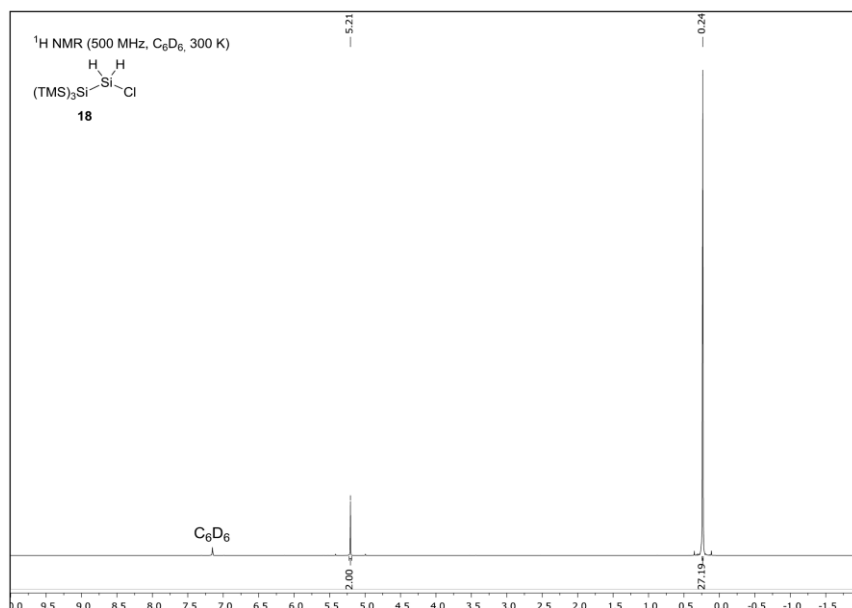


Figure S1. <sup>1</sup>H NMR spectrum of ((TMS)<sub>3</sub>Si)SiH<sub>2</sub>Cl (**18**) in C<sub>6</sub>D<sub>6</sub> at 300 K.

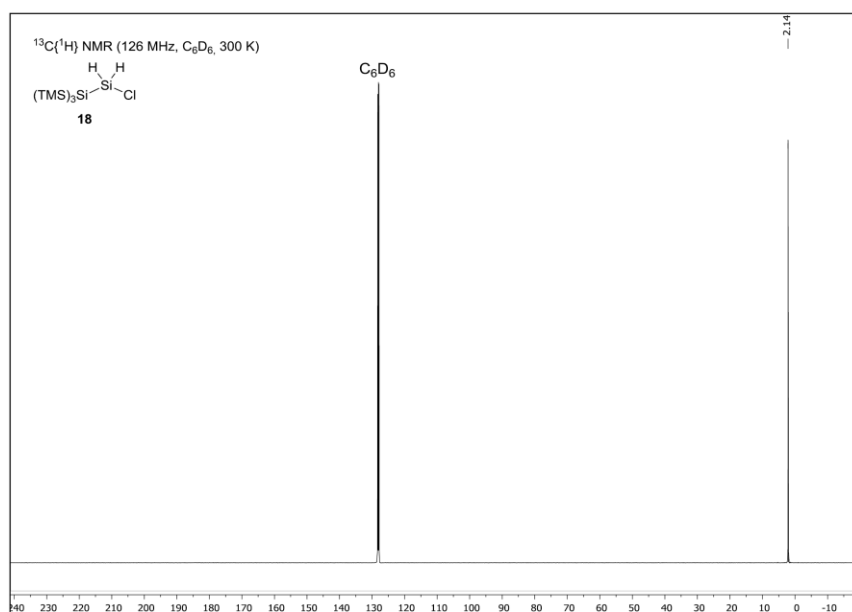
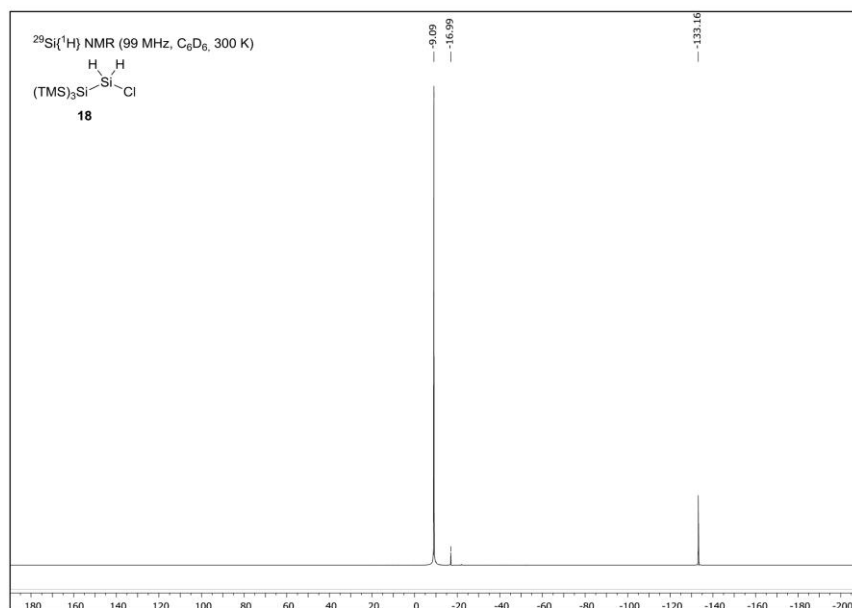


Figure S2. <sup>13</sup>C{<sup>1</sup>H} NMR spectrum of ((TMS)<sub>3</sub>Si)SiH<sub>2</sub>Cl (**18**) in C<sub>6</sub>D<sub>6</sub> at 300 K.



**Figure S3.** <sup>29</sup>Si{<sup>1</sup>H} NMR spectrum of ((TMS)<sub>3</sub>Si)SiH<sub>2</sub>Cl (**18**) in C<sub>6</sub>D<sub>6</sub> at 300 K.

### 1.3 Synthesis of ((TMS)<sub>3</sub>Si)(<sup>i</sup>Bu<sub>3</sub>Si)SiH<sub>2</sub> (**1**)

$$\begin{array}{c} \text{H} \quad \text{H} \\ \diagdown \quad \diagup \\ \text{Si} \\ \diagup \quad \diagdown \\ (\text{TMS})_3\text{Si} \quad \text{Si}^i\text{Bu}_3 \\ \mathbf{1} \\ \text{C}_{21}\text{H}_{56}\text{Si}_6 \\ 477.19 \text{ g/mol} \end{array}$$

A solution of NaSi<sup>i</sup>Bu<sub>3</sub>(THF)<sub>2</sub> (7.98 g, 21.8 mmol, 1.0 eq.) in THF (45 mL) was slowly added to a solution of **18** (6.82 g, 21.8 mmol, 1.0 eq.) in THF (60 mL) at -78 °C. The reaction mixture was warmed to room temperature and subsequently stirred for one hour. The solvent was removed *in vacuo* and the residue extracted with *n*-pentane (60 mL). NaCl was separated from the mixture by filtration and the solvent removed under high vacuum, yielding **1** as a colorless solid (10.2 g, 21.3 mmol, 98%). The product was of sufficient purity and used in following reactions without further purification. Block-shaped crystals, suitable for single-crystal X-ray diffraction (SC-XRD) analysis, were obtained by storing a saturated *n*-hexane solution of **1** at -35 °C overnight.

**m.p.:** 163-164 °C.

**<sup>1</sup>H NMR (500 MHz, C<sub>6</sub>D<sub>6</sub>, 300 K):** δ [ppm] = 3.39 (s, 2H, SiH<sub>2</sub>), 1.23 (s, 27H, C(CH<sub>3</sub>)<sub>3</sub>), 0.36 (s, 27H, TMS).

**<sup>13</sup>C{<sup>1</sup>H} NMR (126 MHz, C<sub>6</sub>D<sub>6</sub>, 300 K):** δ [ppm] = 31.8 (C(CH<sub>3</sub>)<sub>3</sub>), 23.8 (C(CH<sub>3</sub>)<sub>3</sub>), 2.9 (TMS).

**<sup>29</sup>Si{<sup>1</sup>H} NMR (99 MHz, C<sub>6</sub>D<sub>6</sub>, 300 K):** δ [ppm] = 21.2 (Si<sup>i</sup>Bu<sub>3</sub>), -8.6 (TMS), -114.1 (SiH<sub>2</sub>), -132.9 (Si(TMS)<sub>3</sub>).



Anal. Calcd. [%] for  $C_{21}H_{56}Si_6$ : C, 52.86; H, 11.83. Found [%]: C, 52.73; H, 11.89.

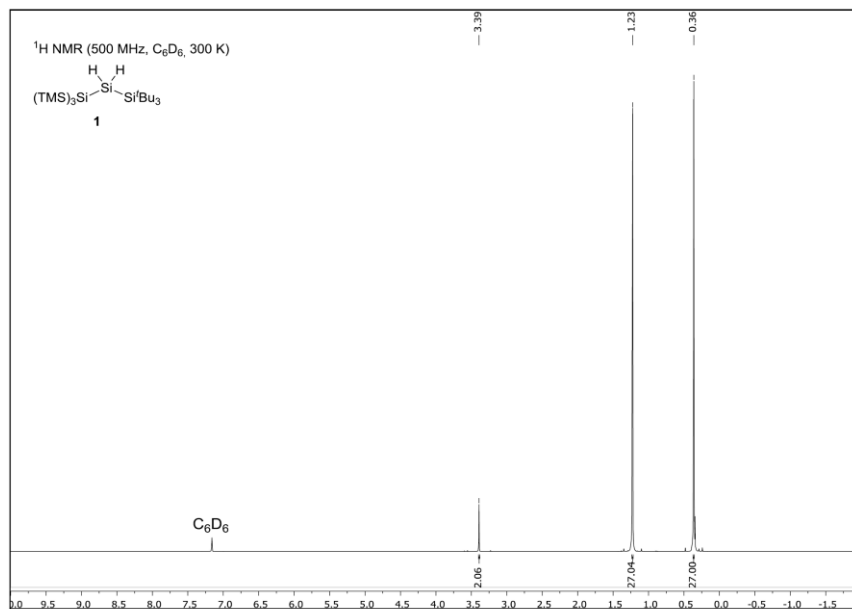


Figure S4.  $^1H$  NMR spectrum of  $((TMS)_3Si)(tBu_3Si)SiH_2$  (**1**) in  $C_6D_6$  at 300 K.

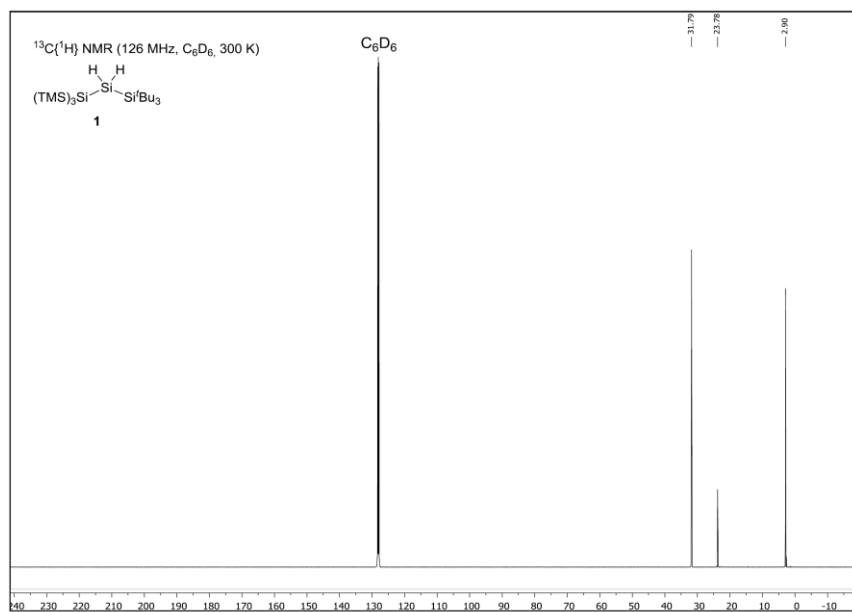
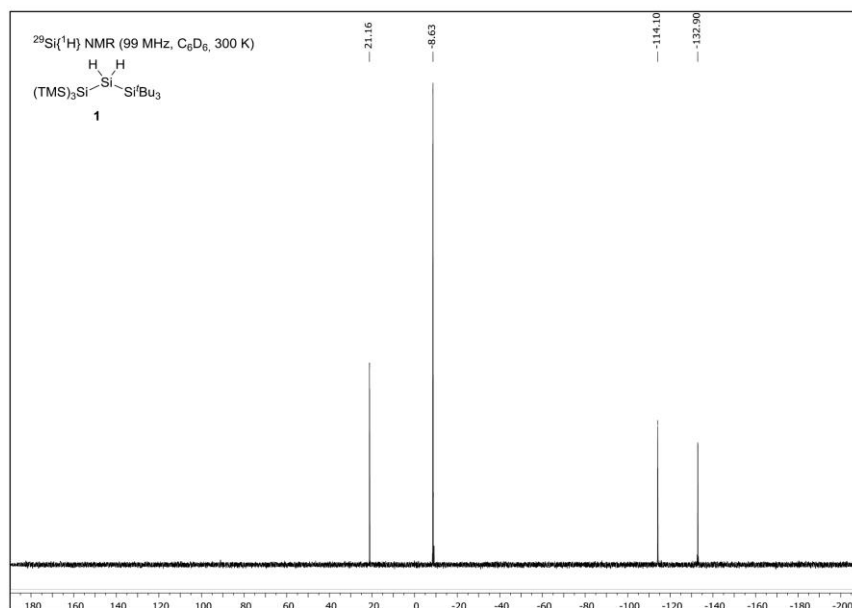


Figure S5.  $^{13}C\{^1H\}$  NMR spectrum of  $((TMS)_3Si)(tBu_3Si)SiH_2$  (**1**) in  $C_6D_6$  at 300 K.



**Figure S6.** <sup>29</sup>Si{<sup>1</sup>H} NMR spectrum of ((TMS)<sub>3</sub>Si)(Bu<sub>3</sub>Si)SiH<sub>2</sub> (**1**) in C<sub>6</sub>D<sub>6</sub> at 300 K.

#### 1.4 Synthesis of ((TMS)<sub>3</sub>Si)(Bu<sub>3</sub>Si)SiBr<sub>2</sub> (**2**)

$$\begin{array}{c} \text{Br} \quad \text{Br} \\ \diagdown \quad / \\ \text{Si} \\ / \quad \backslash \\ (\text{TMS})_3\text{Si} \quad \text{Si}^t\text{Bu}_3 \end{array}$$
**2**  
 C<sub>21</sub>H<sub>54</sub>Br<sub>2</sub>Si<sub>6</sub>  
 634.98 g/mol

To a cooled (0 °C) solution of **1** (9.86 g, 20.7 mmol, 1.0 eq.) in *n*-pentane (100 mL) was added bromine (2.12 mL, 6.61 g, 41.3 mmol, 2.0 eq.) dropwise *via* a syringe. Subsequently, the reaction mixture was warmed to room temperature and stirred for 15 minutes. All volatiles were removed *in vacuo*. Recrystallization of the residue from *n*-hexane afforded colorless crystals of **2** (11.2 g, 17.7 mmol, 86%). The molecular structure of **2** could not be obtained *via* X-ray crystallography, since all suitable crystals revealed highly disordered structures or crystal twinning.

**m.p.:** 186-187 °C.

**<sup>1</sup>H NMR (500 MHz, C<sub>6</sub>D<sub>6</sub>, 300 K):** δ [ppm] = 1.35 (s, 27H, C(CH<sub>3</sub>)<sub>3</sub>), 0.45 (s, 27H, TMS).

**<sup>13</sup>C{<sup>1</sup>H} NMR (126 MHz, C<sub>6</sub>D<sub>6</sub>, 300 K):** δ [ppm] = 32.3 (C(CH<sub>3</sub>)<sub>3</sub>), 26.1 (C(CH<sub>3</sub>)<sub>3</sub>), 4.4 (TMS).

**<sup>29</sup>Si{<sup>1</sup>H} NMR (99 MHz, C<sub>6</sub>D<sub>6</sub>, 300 K):** δ [ppm] = 27.9 (Si<sup>t</sup>Bu<sub>3</sub>), 16.3 (SiBr<sub>2</sub>), -7.2 (TMS), -88.5 (Si(TMS)<sub>3</sub>).

**Anal. Calcd. [%] for C<sub>21</sub>H<sub>54</sub>Br<sub>2</sub>Si<sub>6</sub>:** C, 39.72; H, 8.57; Br, 25.17. Found [%]: C, 39.55; H, 8.67; Br, 25.40.

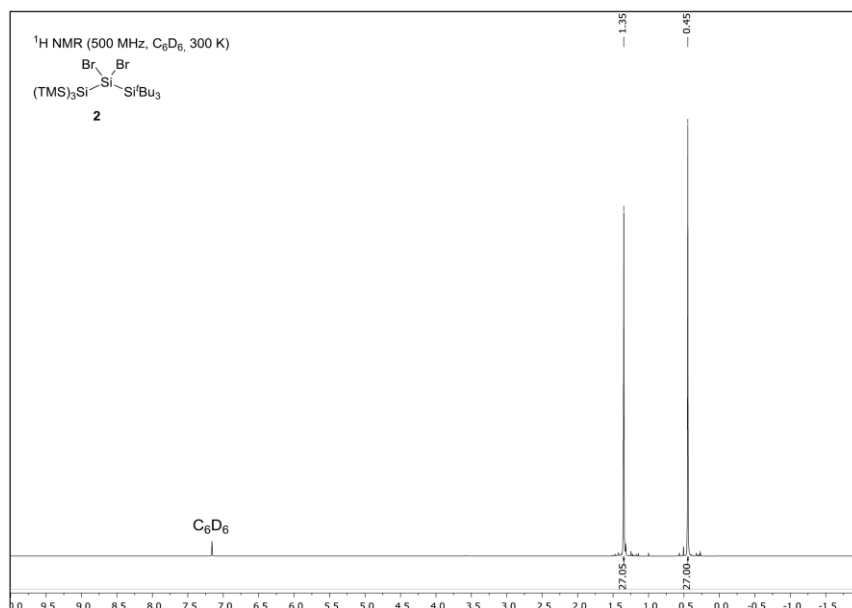


Figure S7. <sup>1</sup>H NMR spectrum of ((TMS)<sub>3</sub>Si)(<sup>t</sup>Bu<sub>3</sub>Si)SiBr<sub>2</sub> (**2**) in C<sub>6</sub>D<sub>6</sub> at 300 K.

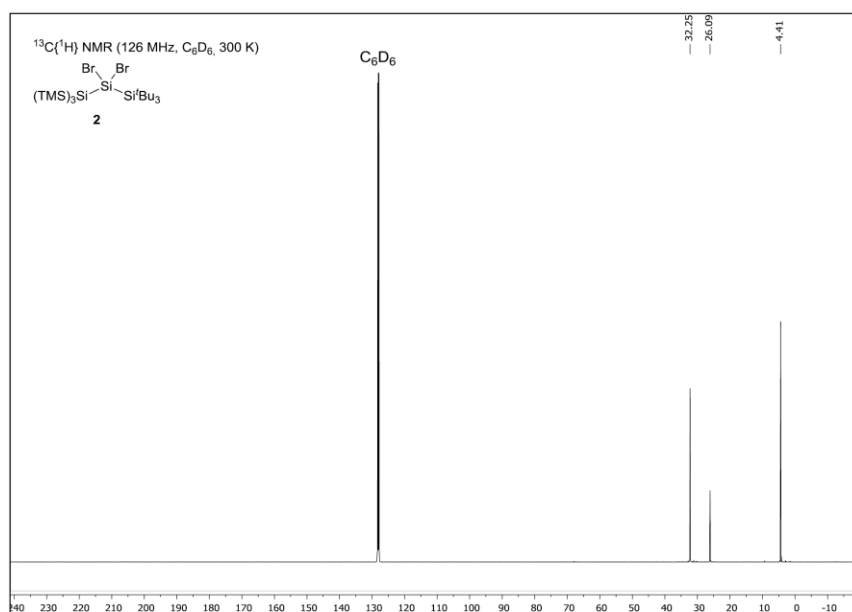
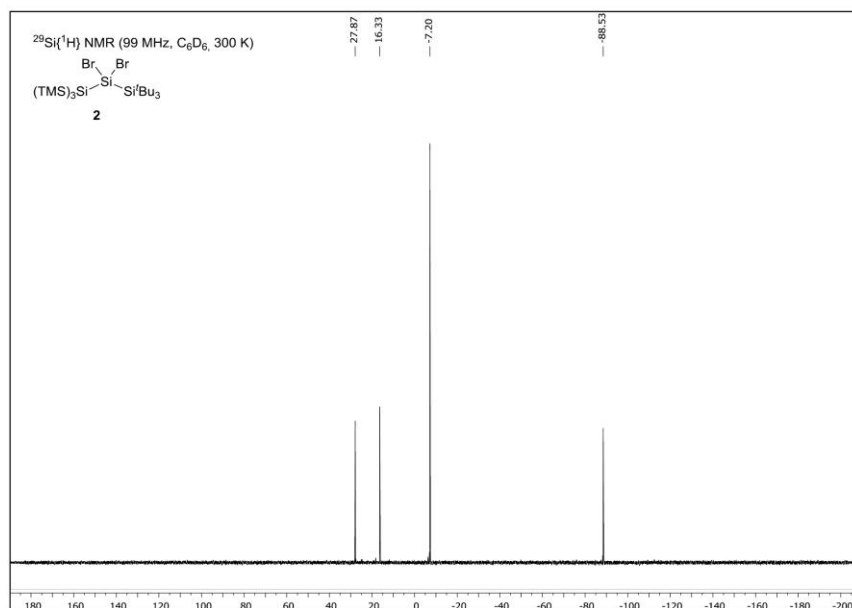
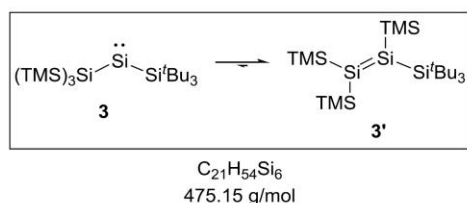


Figure S8. <sup>13</sup>C{<sup>1</sup>H} NMR spectrum of ((TMS)<sub>3</sub>Si)(<sup>t</sup>Bu<sub>3</sub>Si)SiBr<sub>2</sub> (**2**) in C<sub>6</sub>D<sub>6</sub> at 300 K.



**Figure S9.** <sup>29</sup>Si{<sup>1</sup>H} NMR spectrum of ((TMS)<sub>3</sub>Si)(*t*Bu<sub>3</sub>Si)SiBr<sub>2</sub> (**2**) in C<sub>6</sub>D<sub>6</sub> at 300 K.

### 1.5 Synthesis and reactivity of bis(silyl)silylene **3**/tetrasilyldisilene **3'**



Precooled THF (35 mL, -78 °C) was added to a mixture of **2** (3.00 g, 4.72 mmol, 1.0 eq.) and K<sub>2</sub>C<sub>8</sub> (1.28 g, 9.45 mmol, 2.0 eq.) at -78 °C. The reaction mixture was stirred for 16 hours and thereby gradually warmed to -15 °C using a cryostat. Subsequently, the solvent was removed *in vacuo* and the residue extracted with precooled *n*-pentane (3 × 15 mL, -78 °C) at -78 °C. Graphite and KBr were separated from the mixture by filtration. Removal of the solvent *in vacuo* at -15 °C furnished the equilibrium mixture of bis(silyl)silylene **3** and tetrasilyldisilene **3'** as a blood red waxy solid (2.15 g, 4.52 mmol, 96%). **3/3'** is stable as a solid and in solution at -35 °C for at least 1 year, however slowly decomposes in solution at room temperature to disiletane **4** (*vide infra*). By using variable temperature (VT) NMR and UV-Vis spectroscopic studies, only tetrasilyldisilene **3'** and disiletane **4** were detected. Performed EPR spectroscopy, to possibly observe the triplet ground state of bis(silyl)silylene **3**, revealed solely a strong signal around 331 mT (*g* = 2.0067), corresponding to a typical silyl radical

of unknown structure. Sekiguchi *et al.* observed comparable EPR signals in the measurement of *in situ* generated triplet silylenes.<sup>[S7]</sup>

**<sup>1</sup>H NMR (400 MHz, toluene-*d*<sub>8</sub>, 258 K):** δ [ppm] = 1.31 (s, 27H, C(CH<sub>3</sub>)<sub>3</sub>), 0.59 (s, 9H, TMS), 0.51 (s, 9H, TMS), 0.46 (s, 9H, TMS).

**<sup>13</sup>C{<sup>1</sup>H} NMR (101 MHz, toluene-*d*<sub>8</sub>, 258 K):** δ [ppm] = 32.4 (C(CH<sub>3</sub>)<sub>3</sub>), 24.3 (C(CH<sub>3</sub>)<sub>3</sub>), 5.8 (TMS), 4.1 (TMS), 3.5 (TMS).

**<sup>29</sup>Si{<sup>1</sup>H} NMR (79 MHz, toluene-*d*<sub>8</sub>, 258 K):** δ [ppm] = 161.3 (SiTMS<sub>2</sub>), 131.3 (Si(TMS)Si'Bu<sub>3</sub>), 31.1 (Si'Bu<sub>3</sub>), -6.3 (TMS), -6.7 (TMS), -7.0 (TMS).

**<sup>29</sup>Si{<sup>1</sup>H} NMR (99 MHz, C<sub>6</sub>D<sub>6</sub>, 300 K):** δ [ppm] = 161.9 (SiTMS<sub>2</sub>), 132.4 (Si(TMS)Si'Bu<sub>3</sub>), 31.7 (Si'Bu<sub>3</sub>), -6.8 (TMS), -7.7 (TMS).

**Anal. Calcd. [%] for C<sub>21</sub>H<sub>54</sub>Si<sub>6</sub>:** C, 53.08; H, 11.46. Found [%]: C, 52.25; H, 11.54.

**UV-Vis (*n*-hexane, 273 K):** λ<sub>max</sub> [nm] = 352 (theo.: 335; HOMO-1→LUMO), 469 (theo.: 467; HOMO→LUMO).

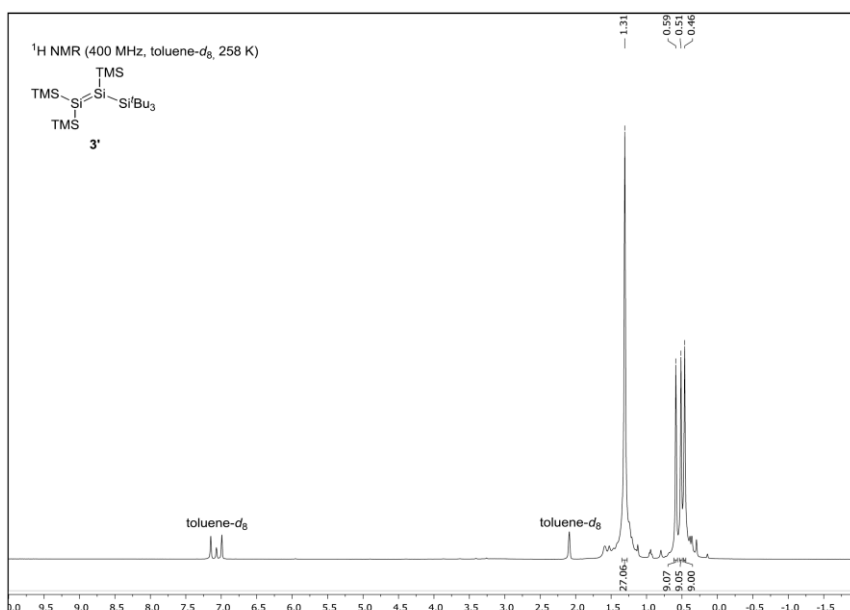


**Figure S10.** <sup>1</sup>H NMR spectrum of bis(silyl)silylene **3**/tetrasilyldisilene **3\*** in toluene-*d*<sub>8</sub> at 258 K.

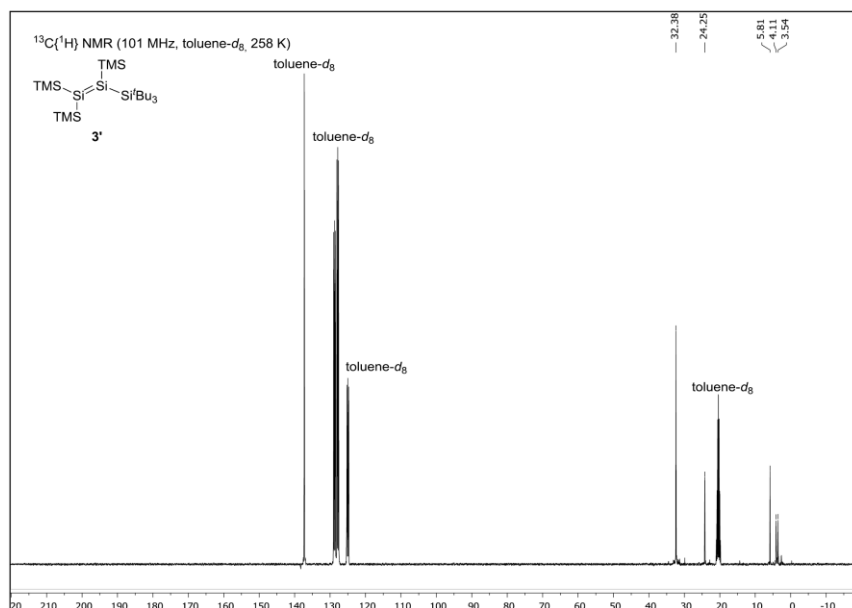


Figure S11.  $^{13}\text{C}\{^1\text{H}\}$  NMR spectrum of bis(silyl)silylene **3**/tetrasilyldisilene **3\*** in toluene- $d_8$  at 258 K.

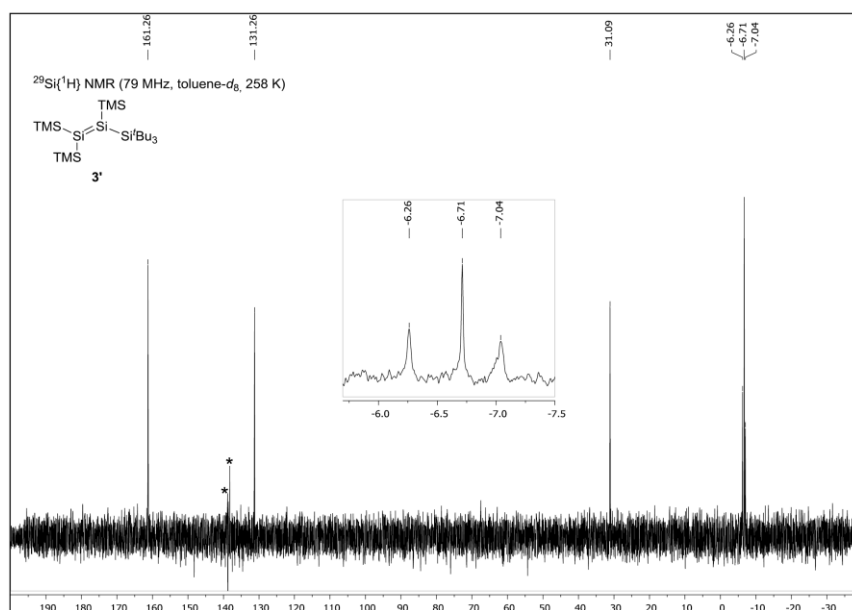
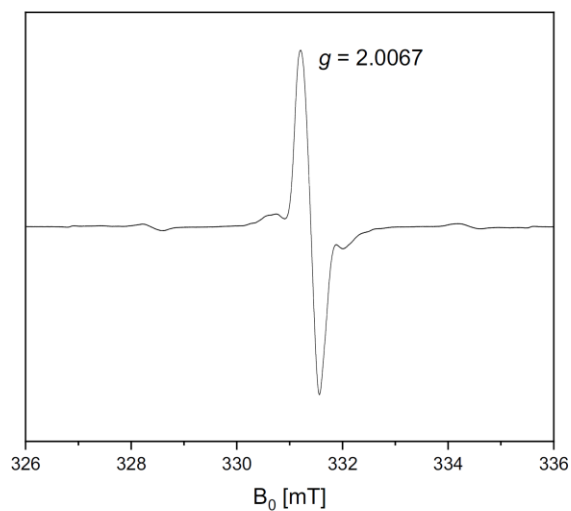
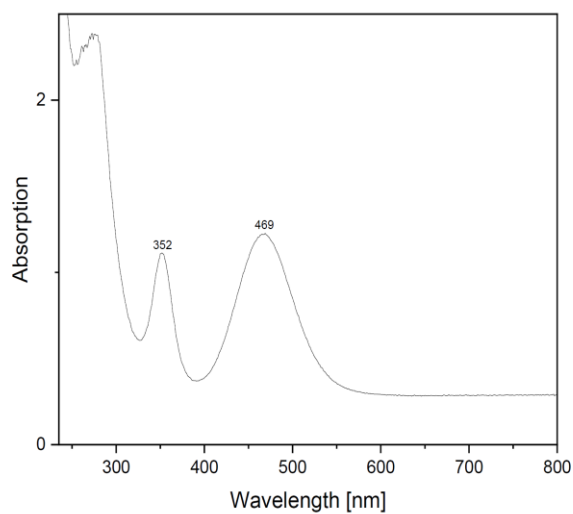


Figure S12.  $^{29}\text{Si}\{^1\text{H}\}$  NMR spectrum of bis(silyl)silylene **3**/tetrasilyldisilene **3\*** in toluene- $d_8$  at 258 K. Spectrometer related artefacts are marked with asterisks \*.

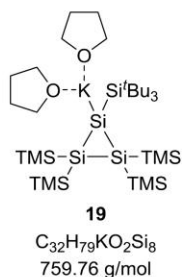




**Figure S13.** EPR spectrum of bis(silyl)silylene **3**/tetrasilyldisilene **3'** in *n*-pentane at 258 K measured with a spectrometer frequency of 9.267 GHz (X-band). The detected signal originates from a silyl radical with unknown structure.



**Figure S14.** UV-Vis spectrum of bis(silyl)silylene **3**/tetrasilyldisilene **3'** in *n*-hexane ( $c = 3.0 \times 10^{-4}$  M). The two characteristic disilene absorption bands at  $\lambda_{\text{max}} = 352$  and 469 nm are presumably based on the HOMO-1  $\rightarrow$  LUMO (theo.: 335 nm) and HOMO  $\rightarrow$  LUMO (theo.: 467 nm) transitions.

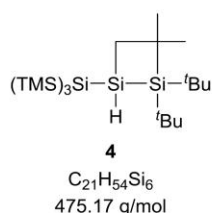
**Reduction of bis(silyl)silylene 3/tetrasilyldisilene 3'**

Utilization of excessive amounts of KC<sub>8</sub> for the reductive debromination of ((TMS)<sub>3</sub>Si)(t-Bu<sub>3</sub>Si)SiBr<sub>2</sub> (**2**) led to formation of a mixture of products, presumably also including radical species. Comparable results were obtained by reduction of bis(silyl)silylene **3**/tetrasilyldisilene **3'** with different equivalents of KC<sub>8</sub>. The only product identified so far was the novel cyclic potassium silanide **19** by SC-XRD analysis (*vide infra*). However, selective formation and further characterization was not possible.

**Oxidative addition of H<sub>2</sub> to bis(silyl)silylene 3/tetrasilyldisilene 3' providing 1**

A solution of **3/3'** (50 mg, 105 μmol) in *n*-hexane (5 mL) was frozen in liquid nitrogen, degassed and warmed to -40 °C. Subsequently, the solution was exposed to H<sub>2</sub> (1 bar) under vigorous stirring. The observed color change from blood red to colorless within 30 min indicated successful dihydrogen activation. All volatiles were removed *in vacuo* and <sup>1</sup>H NMR spectroscopy revealed quantitative conversion of **3/3'** to ((TMS)<sub>3</sub>Si)(t-Bu<sub>3</sub>Si)SiH<sub>2</sub> (**1**).

Note: At least within 3 hours, no sign of reaction was observed at -80 °C, however, dihydrogen activation could still work at temperatures below -40 °C.

**1.6 Synthesis of disiletane 4**

The 1,3-disilacyclobutane **4** was obtained by two different methods, either by slow decomposition of bis(silyl)silylene **3**/tetrasilyldisilene **3'** in solution (Method A) or by NHC abstraction from the NHC-stabilized bis(silyl)silylene **13** (*vide infra*) (Method B). The long reaction time for the formation of **4** originates from the thermal stability of the equilibrium mixture of **3/3'**, which isomerizes to bis(silyl)silylene **3** and subsequently undergoes a C-H activation finally affording disiletane **4**. The even longer reaction time observed for Method B results from the NHC abstraction and the additional isomerization step from the corresponding donor-free silylene **3''** of **13** to **3/3'**.

**Method A:**

A solution of **3/3'** (150 mg, 316 μmol) in *n*-hexane (5 mL) was stirred for 4 days at room temperature. The observed color change from blood red to colorless indicated complete conversion.

Subsequently, the solution was concentrated and stored at  $-35\text{ }^{\circ}\text{C}$  furnishing **4** as colorless crystals (112 mg, 236  $\mu\text{mol}$ , 75%), which were suitable for SC-XRD analysis. A comparable long reaction time was observed in benzene, THF or toluene.

**Method B:**

To a mixture of **13** (100 mg, 153  $\mu\text{mol}$ , 1.0 eq.) and  $\text{BPh}_3$  (36.9 mg, 153  $\mu\text{mol}$ , 1.0 eq.) was added toluene (3 mL). The reaction mixture was stirred for 7 days, whereby the color of the solution changed from purple-red to colorless. The solvent was removed *in vacuo*. Treatment of the residue with *n*-hexane resulted in the formation of a colorless precipitate (byproduct carbene-borane adduct  $\text{I}^{\text{Pr}}\text{Pr}_2\text{Me}_2\cdot\text{BPh}_3^{[\text{S}8]}$ ) which was removed by filtration. Cooling the concentrated filtrate to  $-35\text{ }^{\circ}\text{C}$  for several days afforded colorless crystals of **4** (53.1 mg, 112  $\mu\text{mol}$ , 73%).

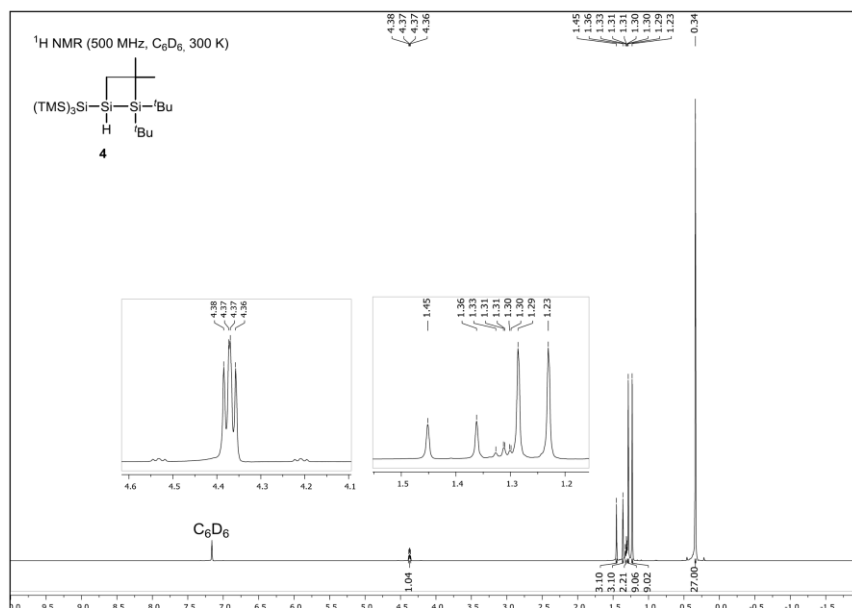
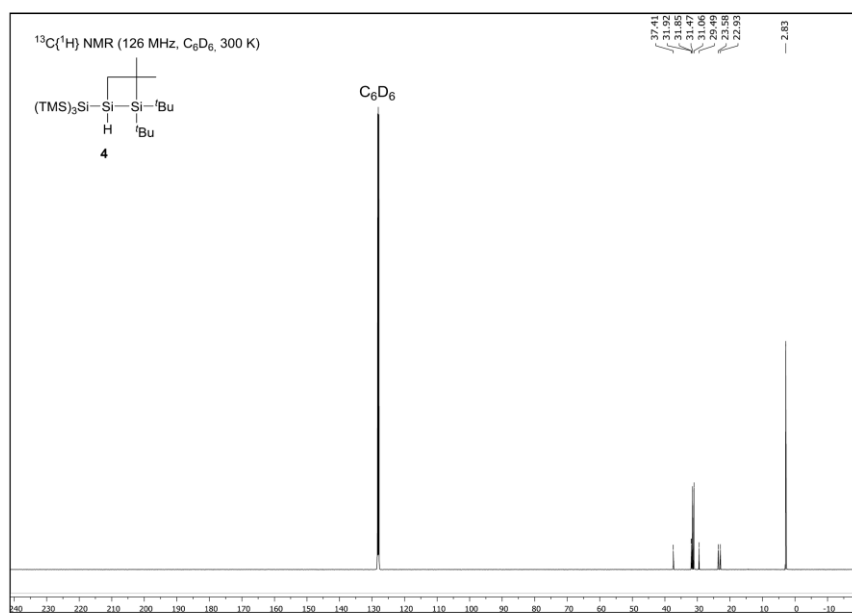
**m.p.:** 141-142  $^{\circ}\text{C}$ .

**$^1\text{H}$  NMR (500 MHz,  $\text{C}_6\text{D}_6$ , 300 K):**  $\delta$  [ppm] = 4.37 (dd,  $^3J = 7.8\text{ Hz}$ ,  $^3J = 5.9\text{ Hz}$ , 1H,  $\text{SiH}$ ), 1.45 (s, 3H,  $\text{C}(\text{CH}_3)_2$ ), 1.36 (s, 3H,  $\text{C}(\text{CH}_3)_2$ ), 1.33–1.30 (m, 2H,  $\text{CH}_2$ ), 1.29 (s, 9H,  $\text{C}(\text{CH}_3)_3$ ), 1.23 (s, 9H,  $\text{C}(\text{CH}_3)_3$ ), 0.34 (s, 27H,  $\text{TMS}$ ).

**$^{13}\text{C}\{^1\text{H}\}$  NMR (126 MHz,  $\text{C}_6\text{D}_6$ , 300 K):**  $\delta$  [ppm] = 37.4 ( $\underline{\text{C}}(\text{CH}_3)_2$ ), 31.9 ( $\text{C}(\underline{\text{C}}\text{H}_3)_2$ ), 31.9 ( $\text{C}(\underline{\text{C}}\text{H}_3)_2$ ), 31.5 ( $\text{C}(\underline{\text{C}}\text{H}_3)_3$ ), 31.0 ( $\text{C}(\underline{\text{C}}\text{H}_3)_3$ ), 29.5 ( $\underline{\text{C}}\text{H}_2$ ), 23.6 ( $\underline{\text{C}}(\text{CH}_3)_3$ ), 22.9 ( $\underline{\text{C}}(\text{CH}_3)_3$ ), 2.8 ( $\text{TMS}$ ).

**$^{29}\text{Si}\{^1\text{H}\}$  NMR (99 MHz,  $\text{C}_6\text{D}_6$ , 300 K):**  $\delta$  [ppm] = 35.6 ( $\underline{\text{Si}}^{\text{t}}\text{Bu}_2$ ),  $-9.2$  ( $\text{TMS}$ ),  $-60.4$  ( $\underline{\text{Si}}\text{H}$ ),  $-133.8$  ( $\underline{\text{Si}}(\text{TMS})_3$ ).

**Anal. Calcd. [%] for  $\text{C}_{21}\text{H}_{54}\text{Si}_6$ :** C, 53.08; H, 11.46. Found [%]: C, 53.11; H, 11.55.

Figure S15. <sup>1</sup>H NMR spectrum of disiletane **4** in C<sub>6</sub>D<sub>6</sub> at 300 K.Figure S16. <sup>13</sup>C{<sup>1</sup>H} NMR spectrum of disiletane **4** in C<sub>6</sub>D<sub>6</sub> at 300 K.

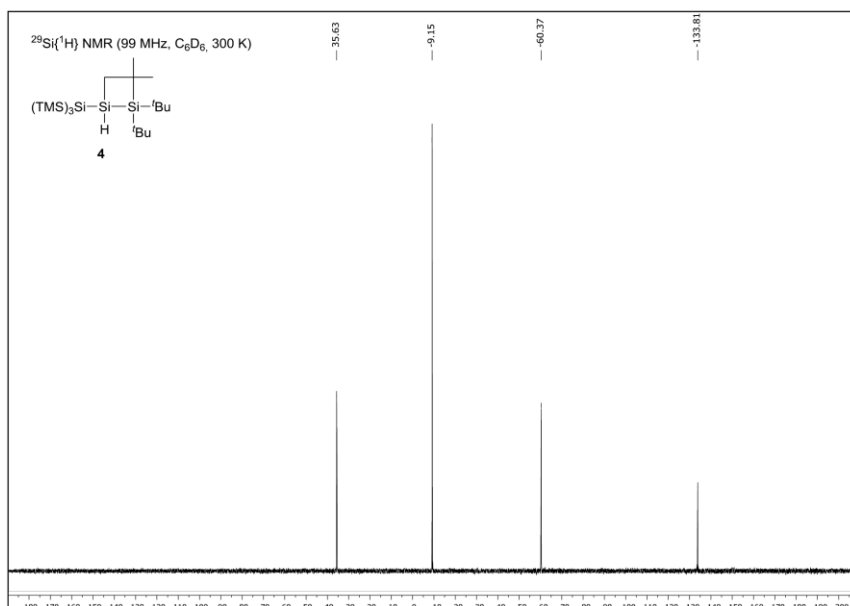


Figure S17.  $^{29}\text{Si}\{^1\text{H}\}$  NMR spectrum of disiletane **4** in  $\text{C}_6\text{D}_6$  at 300 K.

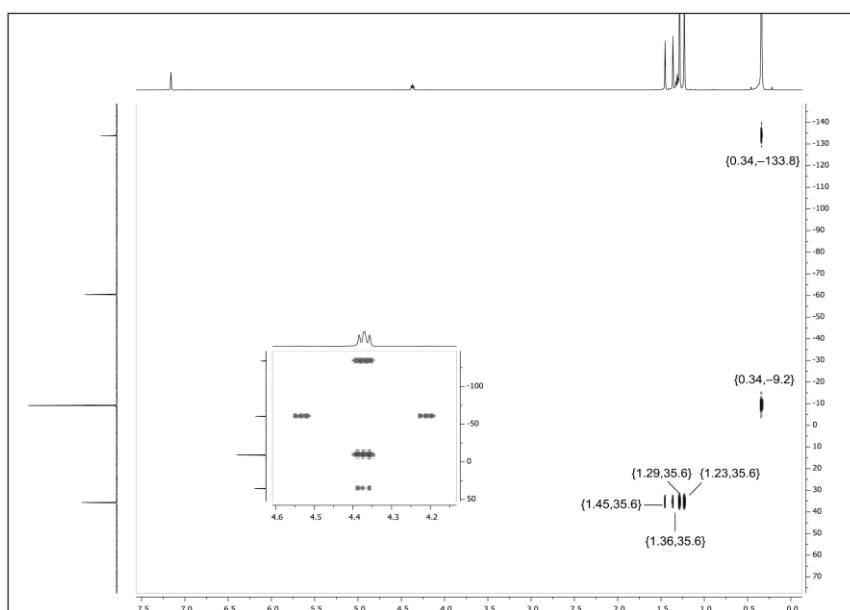
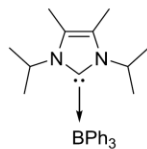


Figure S18.  $^1\text{H}/^{29}\text{Si}$  HMBC NMR spectrum of disiletane **4** in  $\text{C}_6\text{D}_6$  at 300 K.

Byproduct NHC-borane adduct  $\text{I}^i\text{Pr}_2\text{Me}_2\cdot\text{BPh}_3$  (Method B):

$\text{I}^i\text{Pr}_2\text{Me}_2\cdot\text{BPh}_3$   
 $\text{C}_{29}\text{H}_{35}\text{BN}_2$   
 422.42 g/mol

$^1\text{H}$  NMR (400 MHz,  $\text{C}_6\text{D}_6$ , 300 K):  $\delta$  [ppm] = 7.68 (d,  $^3J = 7.0$  Hz, 6H,  $\text{C}_{\text{ar}}\text{H}$ ), 7.32 (t,  $^3J = 7.5$  Hz, 6H,  $\text{C}_{\text{ar}}\text{H}$ ), 7.19 (d,  $^3J = 7.3$  Hz, 3H,  $\text{C}_{\text{ar}}\text{H}$ ), 5.04 (sept,  $^3J = 7.1$  Hz, 2H,  $\text{NCH}(\text{CH}_3)_2$ ), 1.52 (s, 6H,  $\text{CCH}_3$ ), 0.70 (d,  $^3J = 7.0$  Hz, 12H,  $\text{NCH}(\text{CH}_3)_2$ ).

The spectroscopic data match those previously reported.<sup>[S8]</sup>

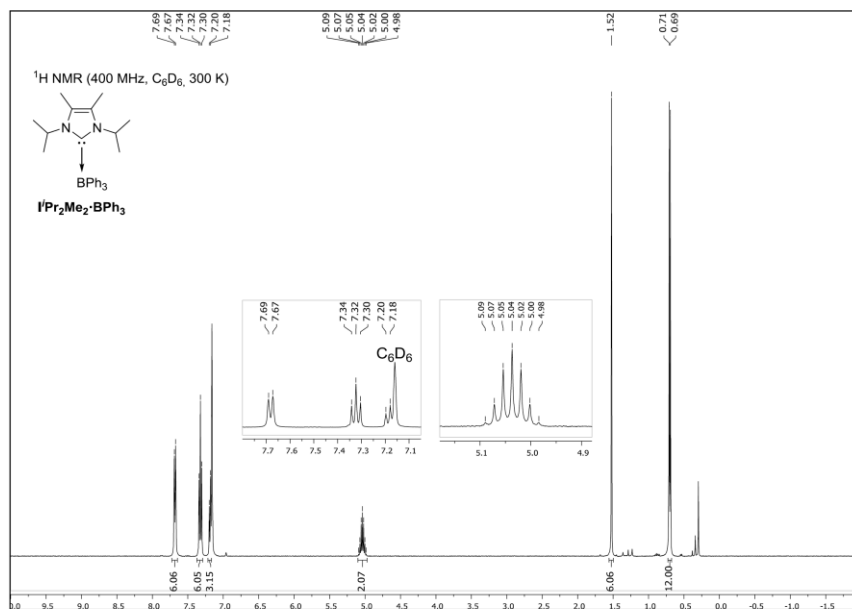


Figure S19.  $^1\text{H}$  NMR spectrum of the byproduct NHC-borane adduct  $\text{I}^i\text{Pr}_2\text{Me}_2\cdot\text{BPh}_3$  in  $\text{C}_6\text{D}_6$  at 300 K.



1.7 Synthesis of ((TMS)<sub>3</sub>Si)(<sup>*i*</sup>Bu<sub>3</sub>Si)Si(CH<sub>2</sub>CH<sub>2</sub>) (**5**)

A solution of **3/3'** (150 mg, 316 μmol) in *n*-hexane (5 mL) was frozen in liquid nitrogen, degassed and warmed to −80 °C. Subsequently, the solution was exposed to ethylene (1 bar) under vigorous stirring. The reaction mixture was warmed to ambient temperature, whereby the color changed from blood red to pale yellow. The solvent was removed *in vacuo* and the residue recrystallized from a saturated Et<sub>2</sub>O solution at −35 °C. Silirane **5** was obtained as colorless crystals (127 mg, 252 μmol, 80%), which were suitable for single-crystal X-ray diffraction analysis.

**m.p.:** 142–143 °C (gas formation, sticky colorless oil).

<sup>1</sup>H NMR (500 MHz, C<sub>6</sub>D<sub>6</sub>, 300 K): δ [ppm] = 1.21 (s, 27H, C(CH<sub>3</sub>)<sub>3</sub>), 0.96–0.93 (m, 2H, CH<sub>2</sub>CH<sub>2</sub>), 0.78–0.75 (m, 2H, CH<sub>2</sub>CH<sub>2</sub>), 0.37 (s, 27H, TMS).

<sup>13</sup>C{<sup>1</sup>H} NMR (126 MHz, C<sub>6</sub>D<sub>6</sub>, 300 K): δ [ppm] = 32.4 (C(CH<sub>3</sub>)<sub>3</sub>), 24.9 (C(CH<sub>3</sub>)<sub>3</sub>), 4.1 (TMS), 1.2 (CH<sub>2</sub>CH<sub>2</sub>).

<sup>29</sup>Si{<sup>1</sup>H} NMR (99 MHz, C<sub>6</sub>D<sub>6</sub>, 300 K): δ [ppm] = 20.2 (<sup>*i*</sup>SiBu<sub>3</sub>), −8.3 (TMS), −113.7 (<sup>*i*</sup>Si(TMS)<sub>3</sub>), −164.3 (<sup>*i*</sup>SiCH<sub>2</sub>CH<sub>2</sub>).

**Anal. Calcd. [%] for C<sub>23</sub>H<sub>58</sub>Si<sub>6</sub>:** C, 54.90; H, 11.62. Found [%]: C, 54.73; H, 11.39.

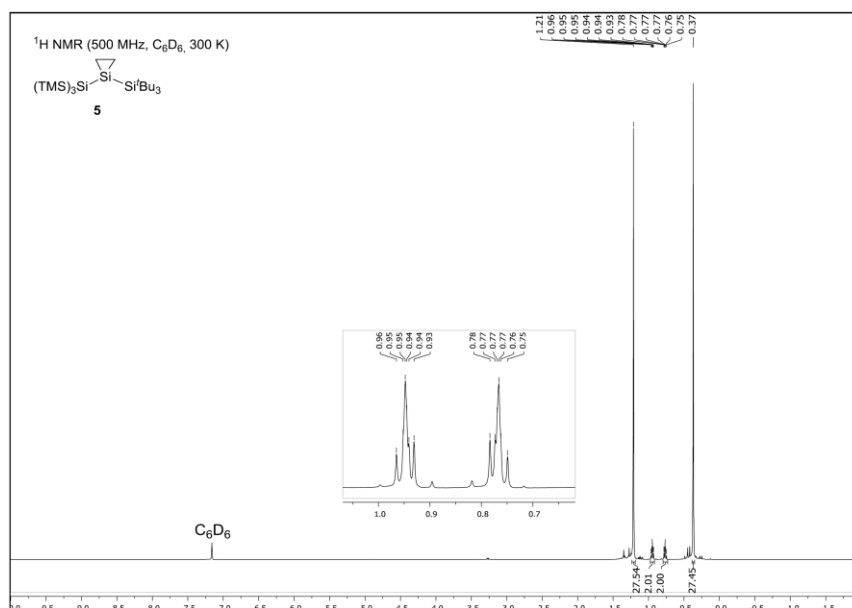


**Figure S20.** <sup>1</sup>H NMR spectrum of ((TMS)<sub>3</sub>Si)(<sup>*i*</sup>Bu<sub>3</sub>Si)Si(CH<sub>2</sub>CH<sub>2</sub>) (**5**) in C<sub>6</sub>D<sub>6</sub> at 300 K.

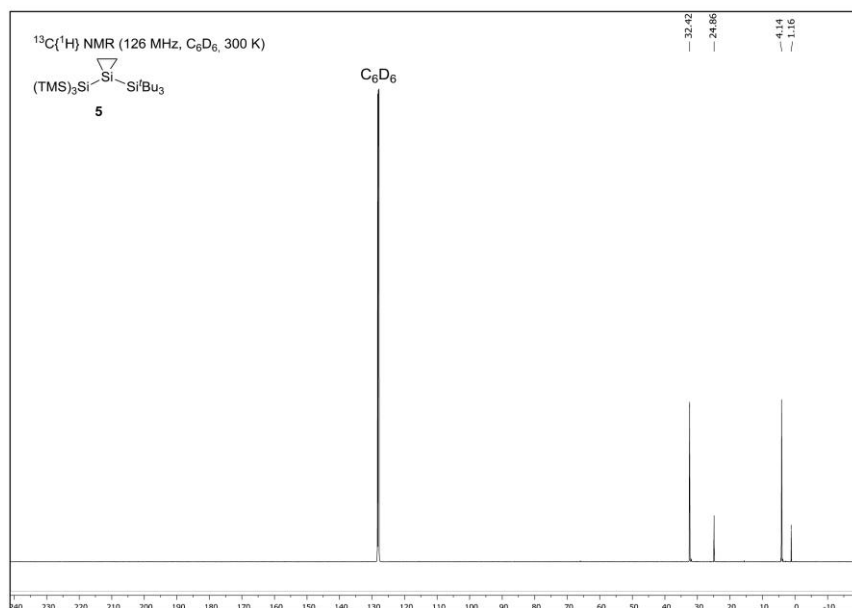


Figure S21.  $^{13}\text{C}\{^1\text{H}\}$  NMR spectrum of  $((\text{TMS})_3\text{Si})(\text{Bu}_3\text{Si})\text{Si}(\text{CH}_2\text{CH}_2)$  (**5**) in  $\text{C}_6\text{D}_6$  at 300 K.

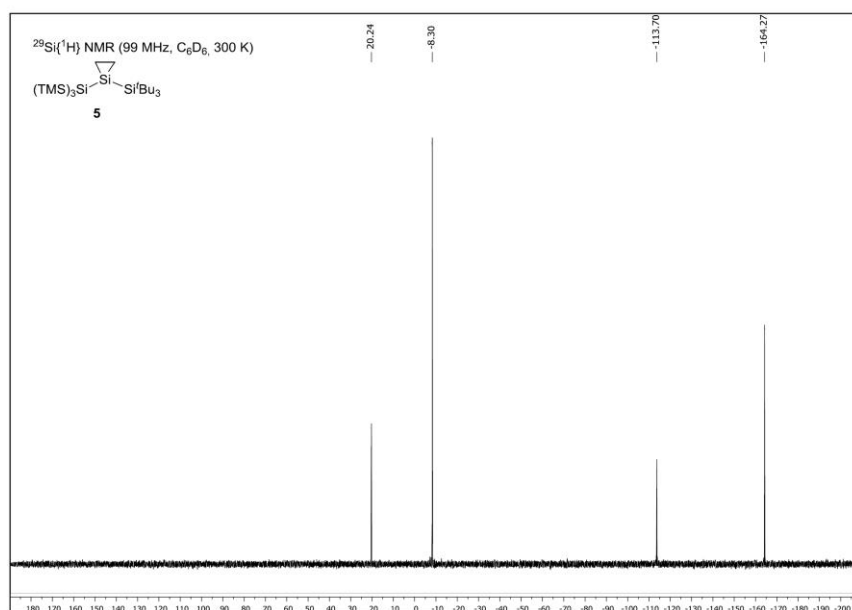
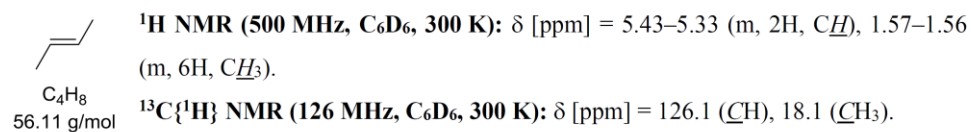
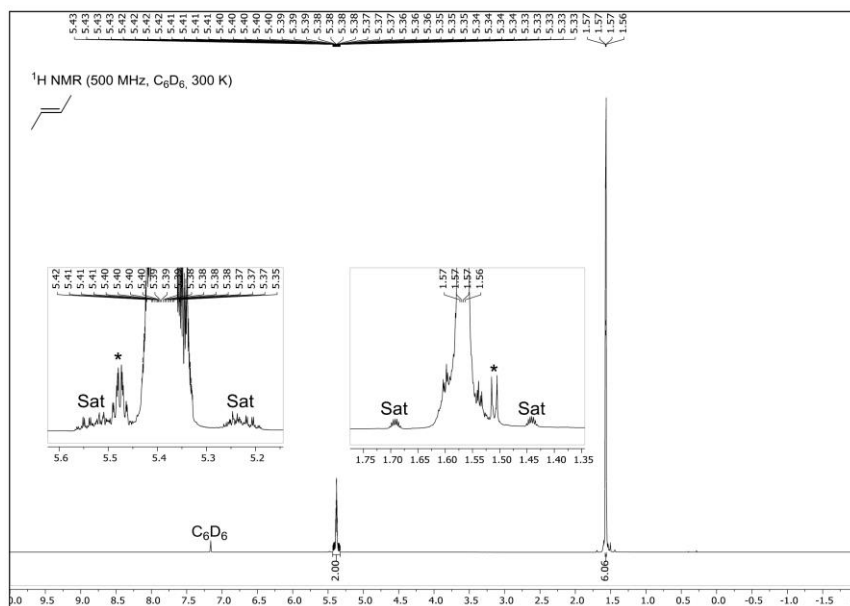


Figure S22.  $^{29}\text{Si}\{^1\text{H}\}$  NMR spectrum of  $((\text{TMS})_3\text{Si})(\text{Bu}_3\text{Si})\text{Si}(\text{CH}_2\text{CH}_2)$  (**5**) in  $\text{C}_6\text{D}_6$  at 300 K.

1.8 [2+1] cycloaddition reactions of 3/3' with (*E*)-/(*Z*)-alkenes**General information:**

As observed previously, the purity of stereogenic alkenes investigated for [2+1] cycloaddition reactions with silylenes is decisive for the resulting silirane product ratio.<sup>[S9]</sup> However, high purity alkenes, especially with respect to contamination with other stereoisomers, are often difficult to obtain due to their similar physical data and thus associated separation issues. For our studies we purchased (*E*)-2-butene and (*Z*)-2-butene (technical grade, estimated purity between 2.0 (≥99%) and 3.5 (≥99.5%) with lower isomeric purity) from *GHC Gerling, Holz & Co. Handels GmbH*. The corresponding approximate amounts of contamination with the other stereoisomers were determined via <sup>1</sup>H and <sup>13</sup>C NMR (1 bar in 0.5 mL C<sub>6</sub>D<sub>6</sub>; *vide infra*): (*E*)-2-butene (~1.3% (*Z*)-2-butene) and (*Z*)-2-butene (~0.7% (*E*)-2-butene). Utilized (*E*)-3-hexene (>99.0%) and (*Z*)-3-hexene (>97.0%) were obtained from *Tokyo Chemical Industry Co., Ltd.* and dried over 4 Å molecular sieves.

**Spectroscopic data for (*E*)-2-butene:**



**Figure S23.** <sup>1</sup>H NMR spectrum of (*E*)-2-butene in C<sub>6</sub>D<sub>6</sub> at 300 K. The respective resonances of the (*Z*)-2-butene contamination are marked with asterisks \* and <sup>13</sup>C satellites with Sat.

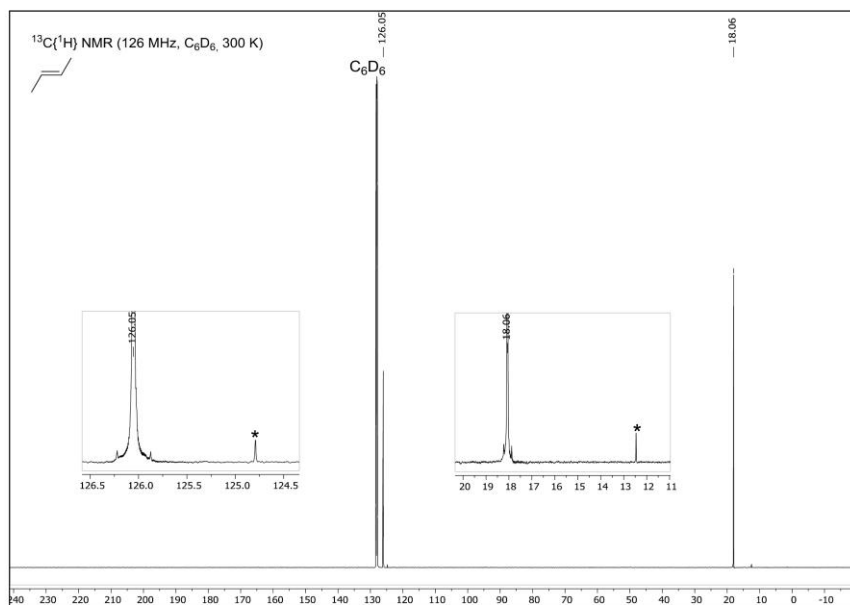


**Figure S24.** <sup>13</sup>C{<sup>1</sup>H} NMR spectrum of (*E*)-2-butene in C<sub>6</sub>D<sub>6</sub> at 300 K. The respective resonances of the (*Z*)-2-butene contamination are marked with asterisks \*.

Spectroscopic data for (*Z*)-2-butene:

C/C=C/C  $^1\text{H}$  NMR (500 MHz,  $\text{C}_6\text{D}_6$ , 300 K):  $\delta$  [ppm] = 5.52–5.44 (m, 2H,  $\underline{\text{C}}\underline{\text{H}}$ ), 1.52–1.50 (m, 6H,  $\underline{\text{C}}\underline{\text{H}}_3$ ).  
 $\text{C}_4\text{H}_8$   
 56.11 g/mol  $^{13}\text{C}\{^1\text{H}\}$  NMR (126 MHz,  $\text{C}_6\text{D}_6$ , 300 K):  $\delta$  [ppm] = 124.8 ( $\underline{\text{C}}\underline{\text{H}}$ ), 12.5 ( $\underline{\text{C}}\underline{\text{H}}_3$ ).

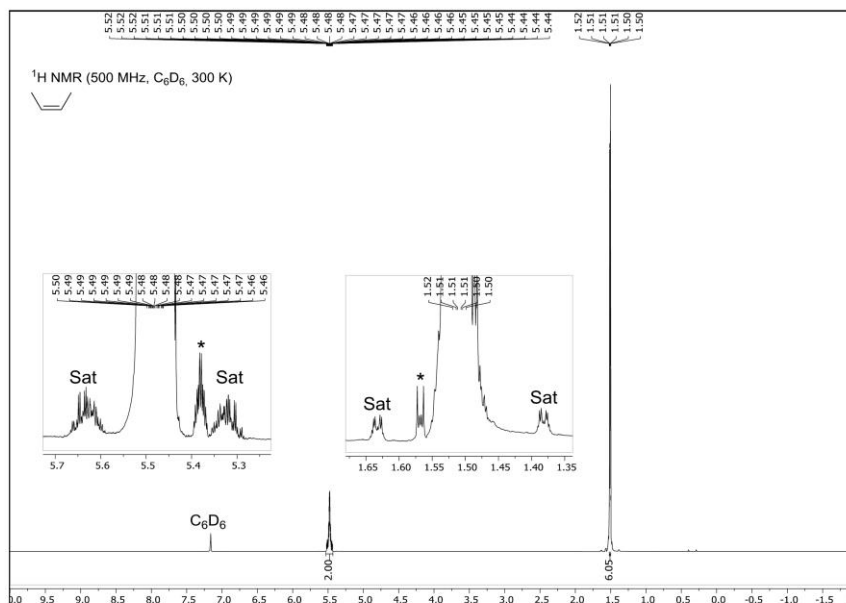


**Figure S25.**  $^1\text{H}$  NMR spectrum of (*Z*)-2-butene in  $\text{C}_6\text{D}_6$  at 300 K. The respective resonances of the (*E*)-2-butene contamination are marked with asterisks \* and  $^{13}\text{C}$  satellites with Sat.

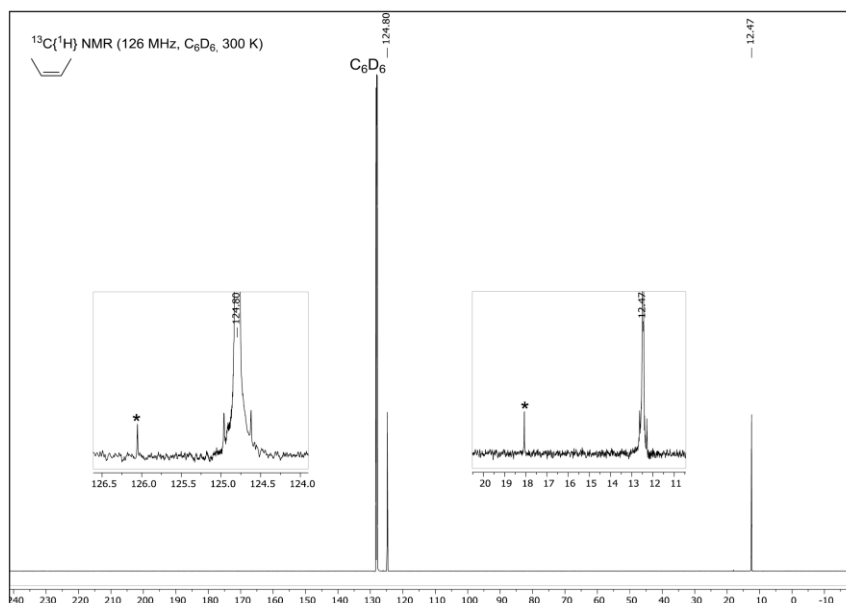
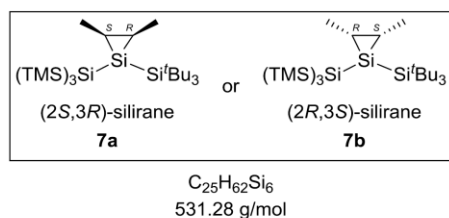


**Figure S26.**  $^{13}\text{C}\{^1\text{H}\}$  NMR spectrum of (*Z*)-2-butene in  $\text{C}_6\text{D}_6$  at 300 K. The respective resonances of the (*E*)-2-butene contamination are marked with asterisks \*.

#### Reaction with (*Z*)-2-butene: synthesis of *cis*-silirane **7**



A solution of **3/3'** (150 mg, 316  $\mu\text{mol}$ ) in *n*-hexane (5 mL) was frozen in liquid nitrogen, degassed and warmed to  $-30\text{ }^\circ\text{C}$ . Subsequently, the solution was exposed to (*Z*)-2-butene (1 bar) under vigorous stirring. The reaction mixture was warmed to ambient temperature, whereby the color changed from blood red to pale yellow. Removal of all volatiles *in vacuo* furnished *cis*-silirane **7** as an off-white solid (168 mg, 316  $\mu\text{mol}$ , quantitative yield).

$^1\text{H}$  NMR (500 MHz,  $\text{C}_6\text{D}_6$ , 300 K):  $\delta$  [ppm] = 1.57 (d,  $^3J = 2.3$  Hz, 3H,  $\text{CHCH}_3$ ), 1.56 (d,  $^3J = 2.3$  Hz, 3H,  $\text{CHCH}_3$ ), 1.34–1.31 (m, 2H,  $\text{CHCH}_3$ ), 1.26 (s, 27H,  $\text{C}(\text{CH}_3)_3$ ), 0.39 (s, 27H, *TMS*).  
 $^{13}\text{C}\{^1\text{H}\}$  NMR (101 MHz,  $\text{C}_6\text{D}_6$ , 300 K):  $\delta$  [ppm] = 32.9 ( $\text{C}(\text{CH}_3)_3$ ), 24.3 ( $\text{C}(\text{CH}_3)_3$ ), 17.7 ( $\text{CHCH}_3$ ), 13.7 ( $\text{CHCH}_3$ ), 4.5 (*TMS*).

$^{29}\text{Si}\{^1\text{H}\}$  NMR (79 MHz,  $\text{C}_6\text{D}_6$ , 300 K):  $\delta$  [ppm] = 27.3 ( $\text{Si}'\text{Bu}_3$ ),  $-8.4$  (*TMS*),  $-100.5$  ( $\text{Si}(\text{TMS})_3$ ),  $-131.7$  (*central Si*).



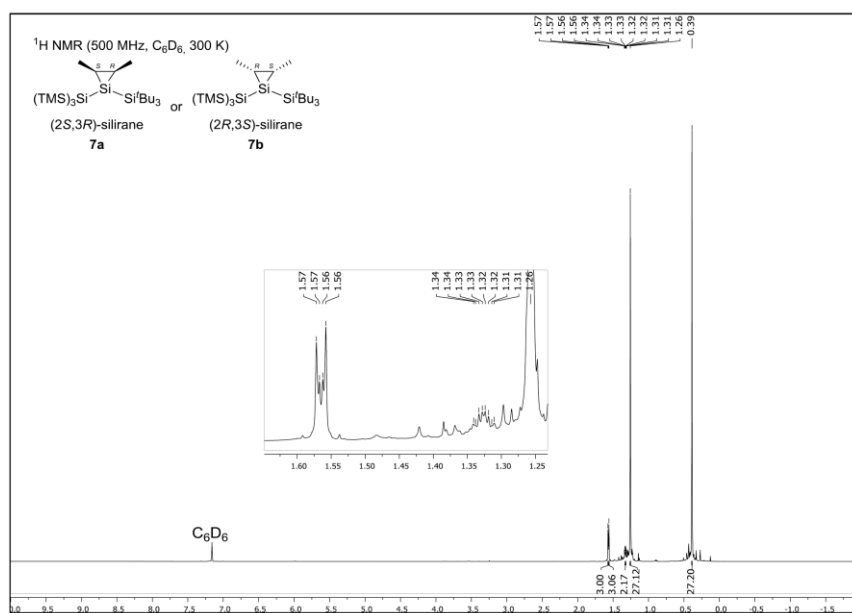


Figure S27. <sup>1</sup>H NMR spectrum of *cis*-silirane **7** in C<sub>6</sub>D<sub>6</sub> at 300 K.

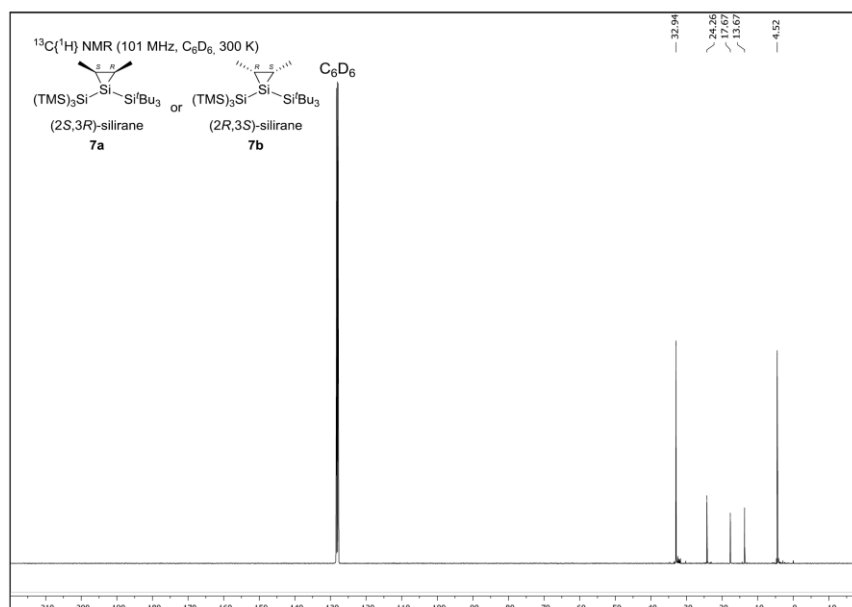


Figure S28. <sup>13</sup>C{<sup>1</sup>H} NMR spectrum of *cis*-silirane **7** in C<sub>6</sub>D<sub>6</sub> at 300 K.

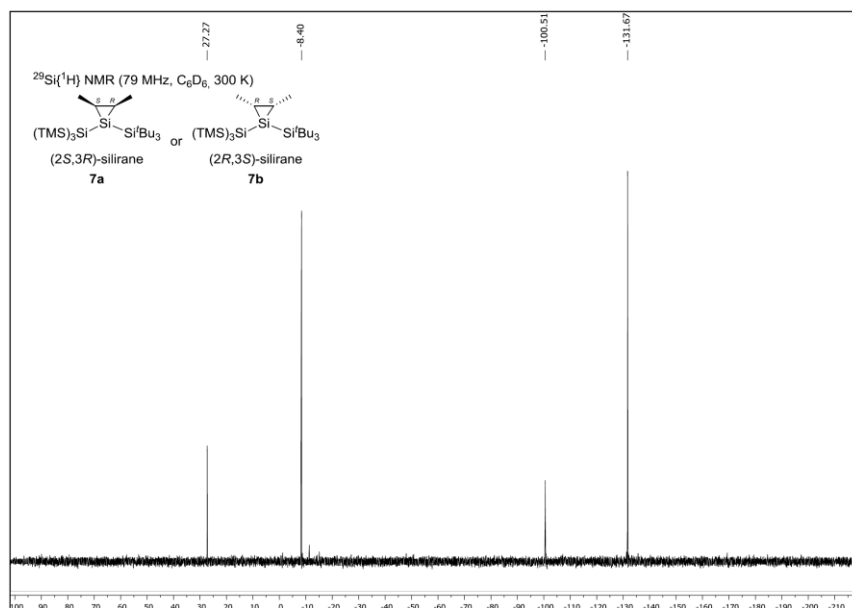


Figure S29.  $^{29}\text{Si}\{^1\text{H}\}$  NMR spectrum of *cis*-silirane **7** in  $\text{C}_6\text{D}_6$  at 300 K.

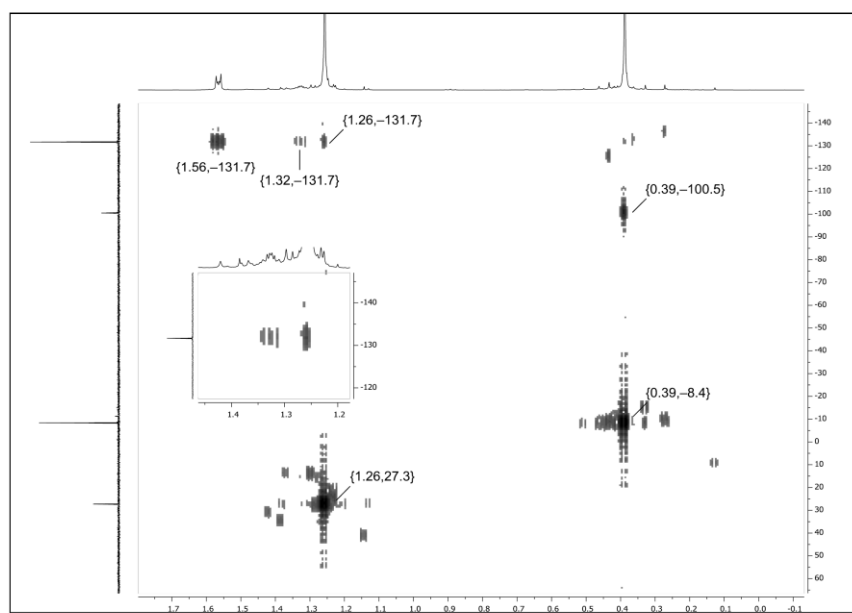
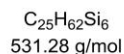
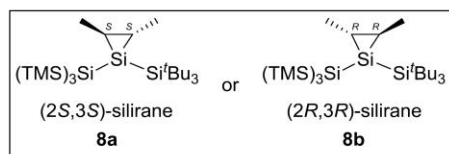


Figure S30.  $^1\text{H}/^{29}\text{Si}$  HMBC NMR spectrum of *cis*-silirane **7** in  $\text{C}_6\text{D}_6$  at 300 K.

Reaction with (*E*)-2-butene: synthesis of *trans*-silirane **8** (& *cis*-silirane **7**)

A solution of **3/3'** (150 mg, 316  $\mu\text{mol}$ ) in *n*-hexane (5 mL) was frozen in liquid nitrogen, degassed and warmed to  $-30\text{ }^\circ\text{C}$ . Subsequently, the solution was exposed to (*E*)-2-butene (1 bar) under vigorous stirring. The reaction mixture was warmed to ambient temperature, whereby the color changed

from blood red to pale yellow. Removal of all volatiles *in vacuo* provided a ~50:50 mixture of *trans*-silirane **8** and *cis*-silirane **7** as an off-white oil (168 mg, 316  $\mu\text{mol}$ , quantitative yield).

NMR characterization of *trans*-silirane **8**:

$^1\text{H}$  NMR (500 MHz,  $\text{C}_6\text{D}_6$ , 300 K):  $\delta$  [ppm] = 1.68 (d,  $^3J = 6.9$  Hz, 3H,  $\text{CHCH}_3$ ), 1.60 (d,  $^3J = 6.9$  Hz, 3H,  $\text{CHCH}_3$ ), 1.24 (s, 27H,  $\text{C}(\text{CH}_3)_3$ ), 1.05 (dq,  $^3J = 12.1$  Hz,  $^3J = 6.9$  Hz, 1H,  $\text{CHCH}_3$ ), 0.79 (dq,  $^3J = 12.1$  Hz,  $^3J = 6.9$  Hz, 1H,  $\text{CHCH}_3$ ), 0.40 (s, 27H, *TMS*).

$^{13}\text{C}\{^1\text{H}\}$  NMR (101 MHz,  $\text{C}_6\text{D}_6$ , 300 K):  $\delta$  [ppm] = 33.0 ( $\text{C}(\text{CH}_3)_3$ ), 24.5 ( $\text{C}(\text{CH}_3)_3$ ), 23.8 ( $\text{CHCH}_3$ ), 20.5 ( $\text{CHCH}_3$ ), 19.7 ( $\text{CHCH}_3$ ), 18.3 ( $\text{CHCH}_3$ ), 5.0 (*TMS*).

$^{29}\text{Si}\{^1\text{H}\}$  NMR (79 MHz,  $\text{C}_6\text{D}_6$ , 300 K):  $\delta$  [ppm] = 25.2 ( $\text{Si}^i\text{Bu}_3$ ),  $-8.5$  (*TMS*),  $-109.2$  ( $\text{Si}(\text{TMS})_3$ ),  $-123.3$  (*central Si*).

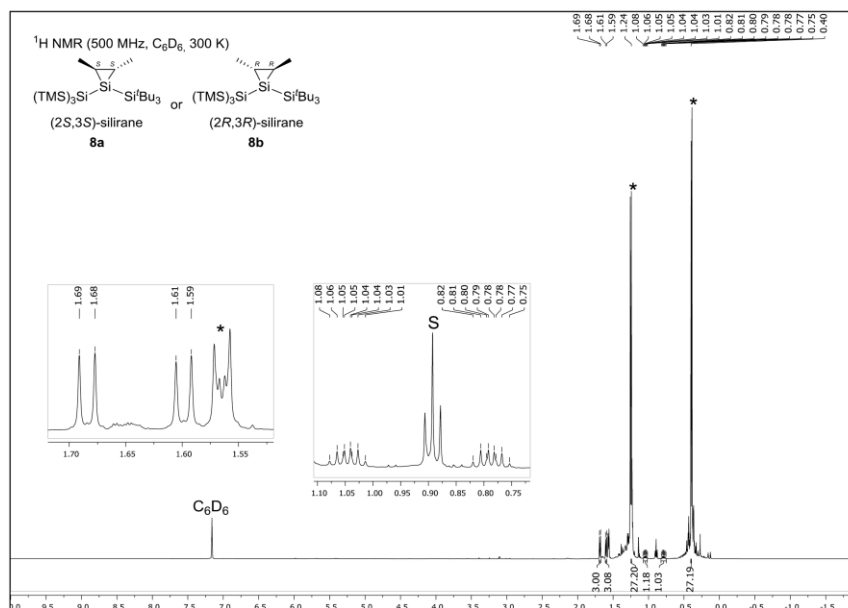


**Figure S31.**  $^1\text{H}$  NMR spectrum of *trans*-silirane **8** and **7** in  $\text{C}_6\text{D}_6$  at 300 K. The respective resonances of *cis*-silirane **7** are marked with asterisks \* and residual *n*-hexane with an S.

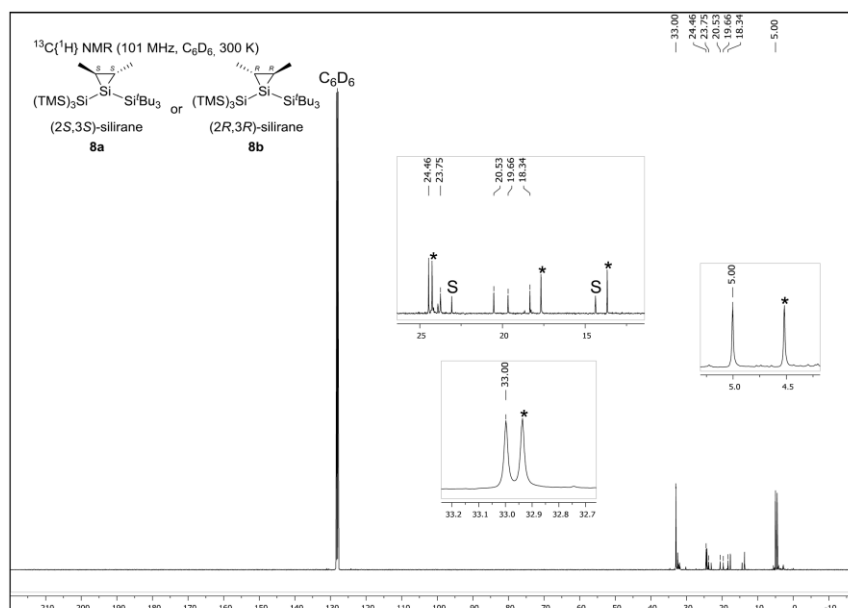


**Figure S32.**  $^{13}\text{C}\{^1\text{H}\}$  NMR spectrum of *trans*-silirane **8** and **7** in  $\text{C}_6\text{D}_6$  at 300 K. The respective resonances of *cis*-silirane **7** are marked with asterisks \* and residual *n*-hexane with an S.

S27

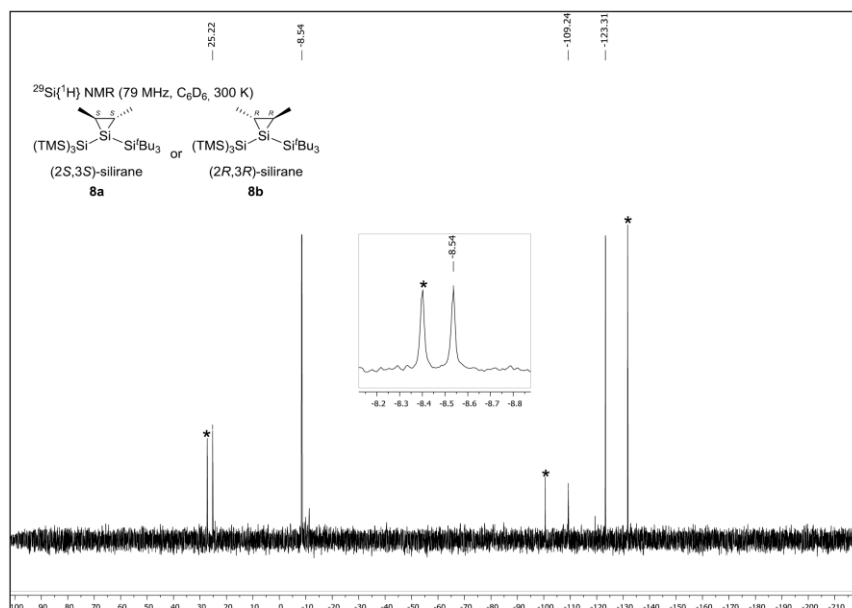


**Figure S33.**  $^{29}\text{Si}\{^1\text{H}\}$  NMR spectrum of *trans*-silirane **8** and **7** in  $\text{C}_6\text{D}_6$  at 300 K. The respective resonances of *cis*-silirane **7** are marked with asterisks \*.

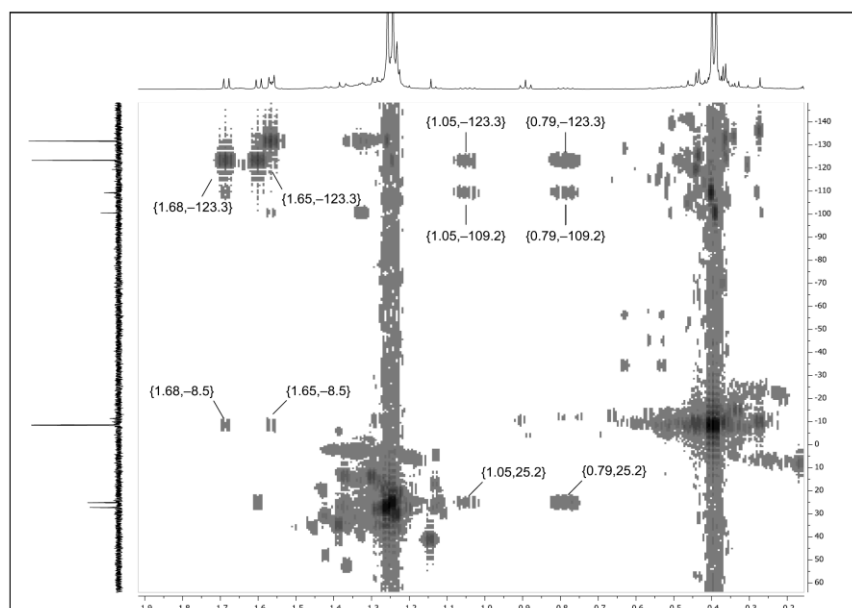


**Figure S34.**  $^1\text{H}/^{29}\text{Si}$  HMBC NMR spectrum of *trans*-silirane **8** and **7** in  $\text{C}_6\text{D}_6$  at 300 K.

**Reaction with an approx. 50/50 mixture of (*E*)-2-butene and (*Z*)-2-butene:**

Two thick-walled, PTFE-capped pressurizeable Schlenk flasks were evacuated and subsequently filled with (*E*)-2-butene and (*Z*)-2-butene, respectively (1 bar each). Both gases were transferred *via* vacuum to another thick-walled, PTFE-capped pressurizeable, cooled (−30 °C) *Schlenk* flask. The liquefied gases were vigorously stirred and vacuum transferred to a cooled (−30 °C) *J. Young* PTFE valve NMR tube containing frozen C<sub>6</sub>D<sub>6</sub> (0.5 mL). The thus prepared gas mixture was analyzed by <sup>1</sup>H and <sup>13</sup>C NMR spectroscopy (*vide infra*).

In a second experiment, the prepared gas mixture was vacuum transferred to a cooled (−30 °C) *J. Young* PTFE valve NMR tube containing a solution of **3/3'** (10.0 mg, 21.0 μmol) in *n*-hexane (0.5 mL). Subsequently, the reaction mixture was warmed to ambient temperature under shaking, whereby the color changed from blood red to pale yellow. All volatiles were removed *in vacuo* and the resulting off-white solid dissolved in C<sub>6</sub>D<sub>6</sub>. NMR spectroscopy revealed quantitative formation of *cis*-silirane **7**.

According to this result, the non-stereospecific addition of **3/3'** to (*E*)-2-butene (formation of both *trans*-silirane **8** and *cis*-silirane **7**) presumably stems from the (*Z*)-2-butene contamination, since the reactivity of the (*Z*)-isomer is expected to be significantly higher. Similar conclusions were already drawn during the reinvestigation of [2+1] cycloaddition reactions of dimesitylsilylene to stereogenic alkenes.<sup>[S9b]</sup> In addition, it was assumed that smaller alkene substituents lead to a higher preference of the respective (*Z*)-isomer by sterically demanding silylenes. Therefore, further experiments with (*E*)/(*Z*)-3-hexene and (*E*)/(*Z*)-stilbene (1,2-diphenylethylene) were performed to prove the contamination assumption as a potential source for the loss of stereochemistry (*vide infra*).



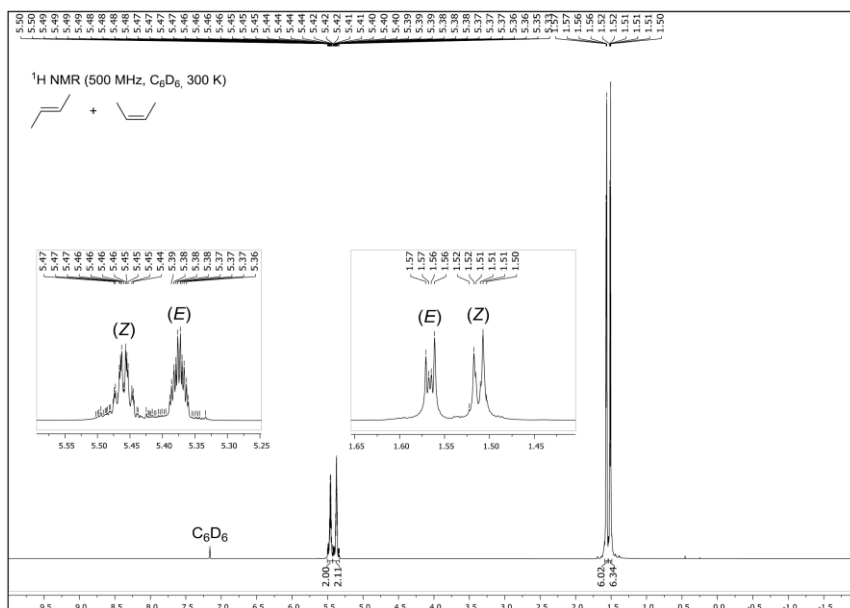


Figure S35. <sup>1</sup>H NMR spectrum of an approx. 50/50 mixture of (*E*)-2-butene and (*Z*)-2-butene in C<sub>6</sub>D<sub>6</sub> at 300 K.

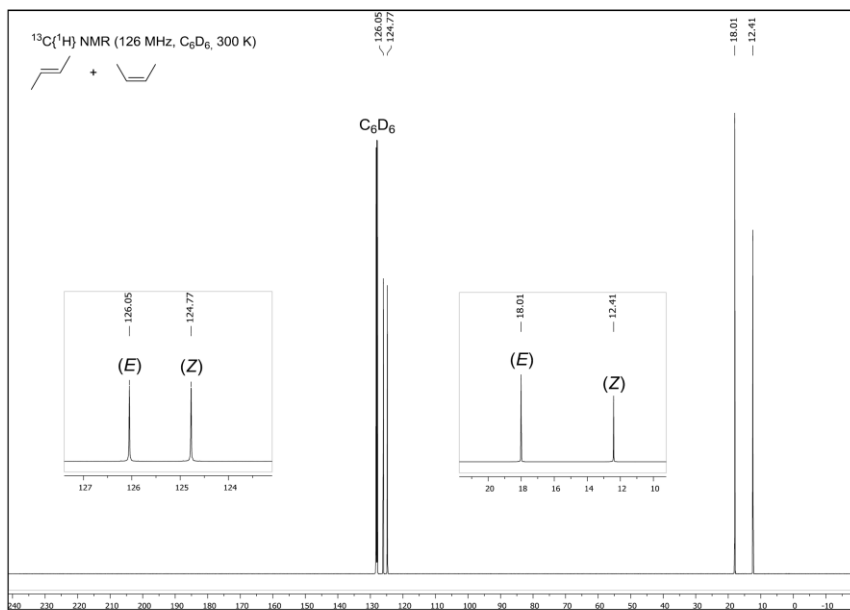
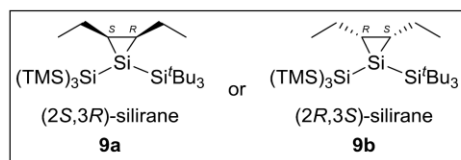


Figure S36. <sup>13</sup>C{<sup>1</sup>H} NMR spectrum of an approx. 50/50 mixture of (*E*)-2-butene and (*Z*)-2-butene in C<sub>6</sub>D<sub>6</sub> at 300 K.

Reaction with (*Z*)-3-hexene: synthesis of *cis*-silirane **9**

$C_{27}H_{66}Si_6$   
559.34 g/mol

To a cooled ( $-30\text{ }^{\circ}\text{C}$ ) solution of **3/3'** (30.0 mg,  $63.1\text{ }\mu\text{mol}$ , 1.0 eq.) in *n*-hexane (1 mL) was added (*Z*)-3-hexene (5.31 mg,  $63.1\text{ }\mu\text{mol}$ , 1.0 eq.) under vigorous stirring. Subsequently, the reaction mixture was warmed to ambient temperature, whereby the color changed from

blood red to pale yellow. Removal of all volatiles *in vacuo* furnished *cis*-silirane **9** as an off-white solid (35.1 mg,  $63.1\text{ }\mu\text{mol}$ , quantitative yield).

$^1\text{H NMR}$  (500 MHz,  $C_6D_6$ , 300 K):  $\delta$  [ppm] = 1.92–1.86 (m, 4H,  $CH_2CH_3$ ), 1.26 (s, 27H,  $C(CH_3)_3$ ), 0.40 (s, 27H, *TMS*). The resonances for the  $CHCH_2$  and  $CH_2CH_3$  protons could not be clearly assigned due to overlapping signals.

$^{29}\text{Si}\{^1\text{H}\}$  NMR (99 MHz,  $C_6D_6$ , 300 K):  $\delta$  [ppm] = 27.3 ( $Si^iBu_3$ ),  $-8.6$  (*TMS*),  $-100.3$  ( $Si^i(TMS)_3$ ),  $-133.2$  (*central Si*).

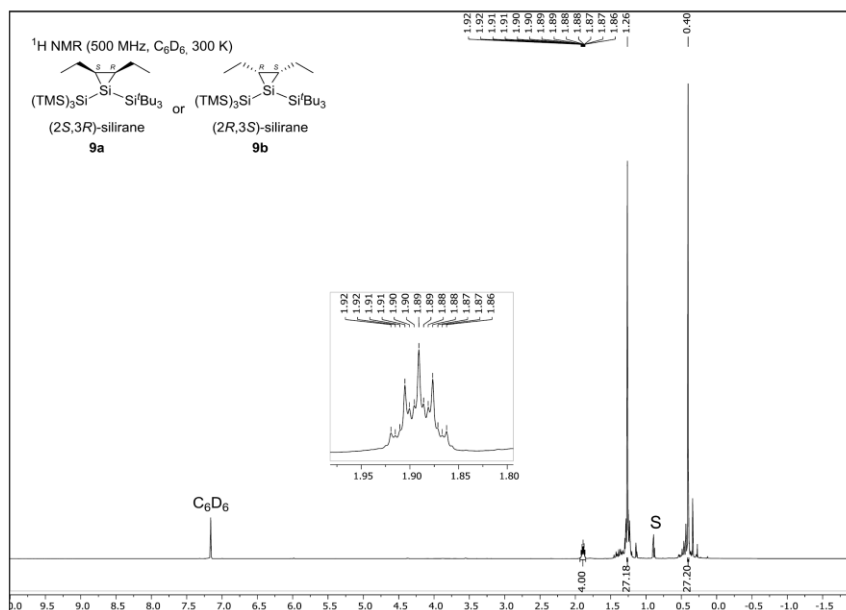


**Figure S37.**  $^1\text{H NMR}$  spectrum of *cis*-silirane **9** in  $C_6D_6$  at 300 K. Residual *n*-hexane is marked with an S.

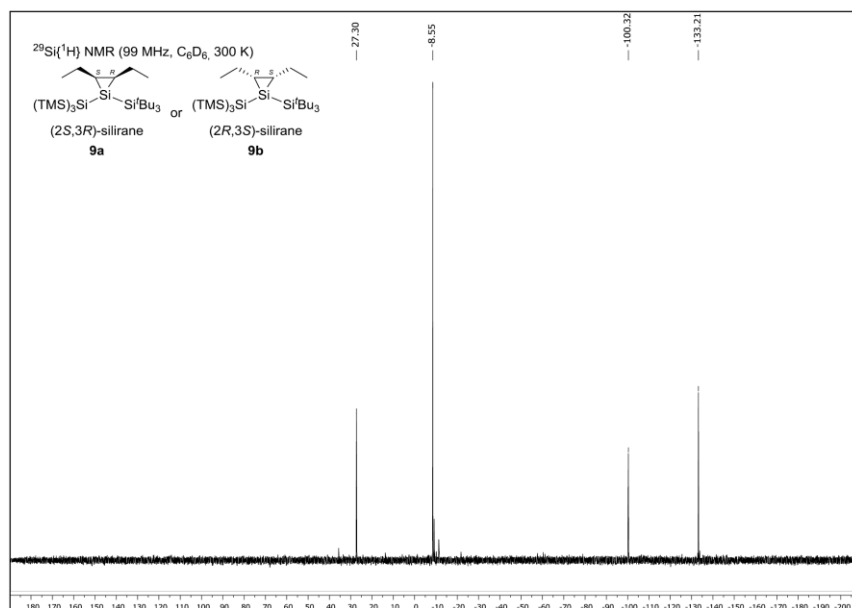


Figure S38.  $^{29}\text{Si}\{^1\text{H}\}$  NMR spectrum of *cis*-silirane **9** in  $\text{C}_6\text{D}_6$  at 300 K.

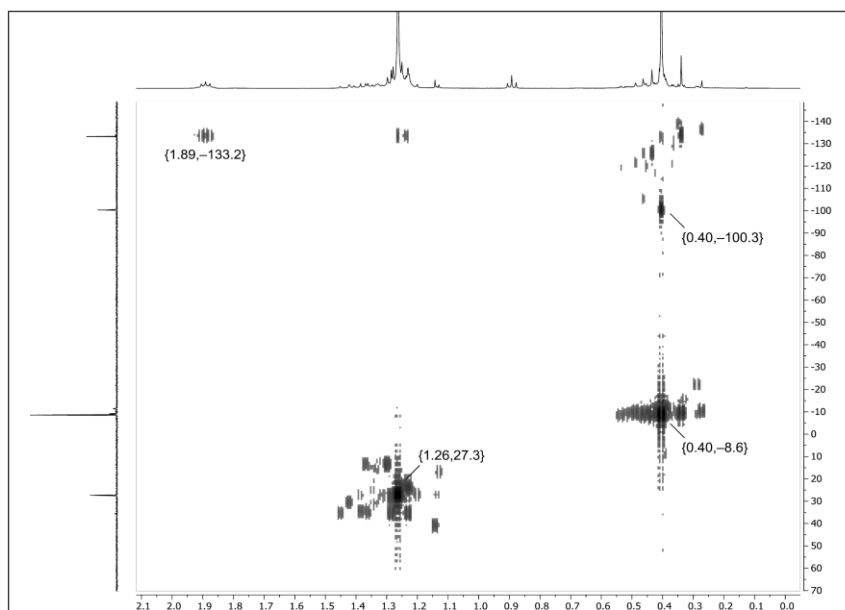
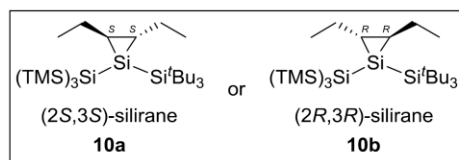


Figure S39.  $^1\text{H}/^{29}\text{Si}$  HMBC NMR spectrum of *cis*-silirane **9** in  $\text{C}_6\text{D}_6$  at 300 K.

Reaction with (*E*)-3-hexene: synthesis of *trans*-silirane **10**

$\text{C}_{27}\text{H}_{66}\text{Si}_6$   
 559.34 g/mol

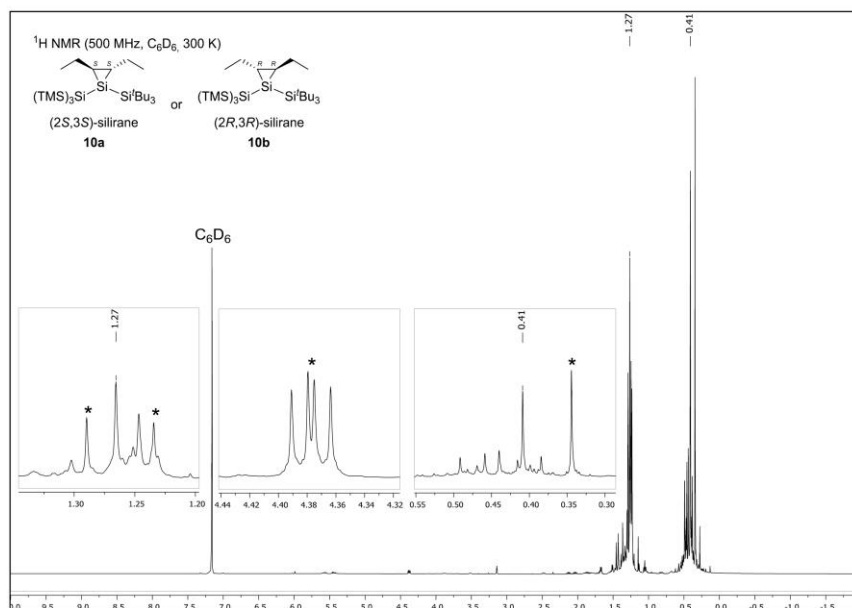
To a cooled ( $-30\text{ }^\circ\text{C}$ ) solution of **3/3'** (30.0 mg, 63.1  $\mu\text{mol}$ , 1.0 eq.) in *n*-hexane (1 mL) was added (*E*)-3-hexene (5.31 mg, 63.1  $\mu\text{mol}$ , 1.0 eq.) under vigorous stirring. Subsequently, the reaction mixture was warmed to ambient temperature, whereby the color changed from

blood red to pale yellow. Removal of all volatiles *in vacuo* provided a mixture of *trans*-silirane **10**, disiletane **4** and other impurities as an off-white oil.

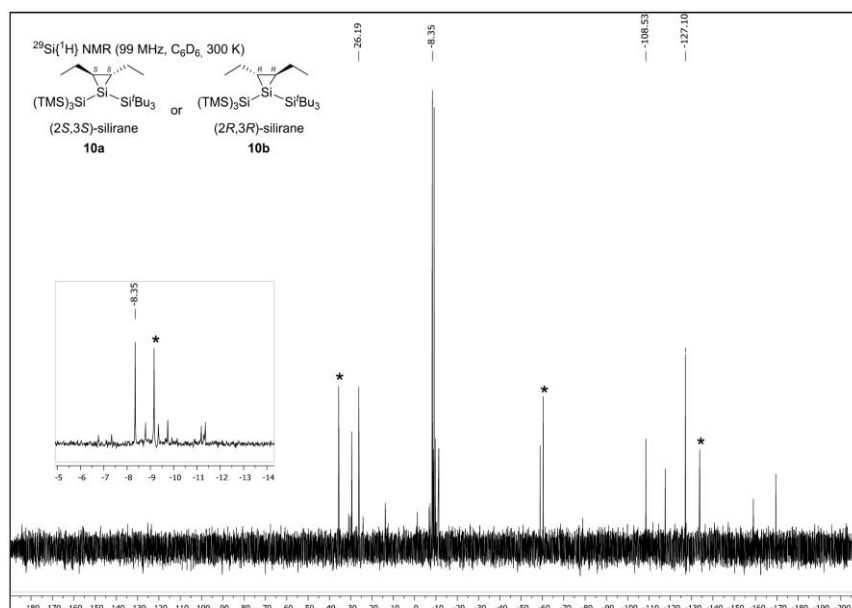
NMR characterization of *trans*-silirane **10**:

$^1\text{H}$  NMR (500 MHz,  $\text{C}_6\text{D}_6$ , 300 K):  $\delta$  [ppm] = 1.27 (s, 27H, C( $\underline{\text{H}}_3$ )<sub>3</sub>), 0.41 (s, 27H,  $\underline{\text{TMS}}$ ). The resonances for the  $\underline{\text{C}}\underline{\text{H}}\underline{\text{C}}\underline{\text{H}}_2$ ,  $\underline{\text{C}}\underline{\text{H}}_2\underline{\text{C}}\underline{\text{H}}_3$  and  $\text{C}\underline{\text{H}}_2\underline{\text{C}}\underline{\text{H}}_3$  protons could not be clearly assigned due to overlapping signals.

$^{29}\text{Si}\{^1\text{H}\}$  NMR (99 MHz,  $\text{C}_6\text{D}_6$ , 300 K):  $\delta$  [ppm] = 26.2 ( $\underline{\text{S}}\underline{\text{i}}^t\text{Bu}_3$ ),  $-8.4$  ( $\underline{\text{TMS}}$ ),  $-108.5$  ( $\underline{\text{S}}\underline{\text{i}}(\text{TMS})_3$ ),  $-127.1$  (*central Si*).



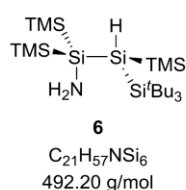
**Figure S40.** <sup>1</sup>H NMR spectrum of *trans*-silirane **10** and **4** in C<sub>6</sub>D<sub>6</sub> at 300 K. The respective resonances of disiletane **4** are marked with asterisks \*.



**Figure S41.** <sup>29</sup>Si{<sup>1</sup>H} NMR spectrum of *trans*-silirane **10** and **4** in C<sub>6</sub>D<sub>6</sub> at 300 K. The respective resonances of disiletane **4** are marked with asterisks \*.

**Reaction with (*E*)-stilbene and (*Z*)-stilbene:**

Exposure of **3/3'** to (*E*)-stilbene and (*Z*)-stilbene resulted in no reaction but disiletane **4** formation, presumably due to steric reasons.

**1.9 Synthesis of aminosilane **6****

To a cooled (−80 °C) solution of **3/3'** (375 mg, 789 μmol, 1.0 eq.) in *n*-hexane (60 mL) was added a 0.4 M NH<sub>3</sub> solution in 1,4-dioxane (1.97 mL, 13.4 mg, 789 μmol, 1.0 eq.) under vigorous stirring. An immediate color change from blood red to pale yellow with concomitant precipitation (1,4-dioxane) was observed. Stirring was continued at −80 °C for one hour and subsequently the solution was warmed to ambient temperature. All volatiles were removed *in vacuo*, providing crude aminosilane **6** as an orange oil. Multinuclear and 2D NMR analysis clearly revealed **6** as the major product. However, all further purification attempts *via* crystallization, distillation or washing were unsuccessful so far.

<sup>1</sup>H NMR (500 MHz, C<sub>6</sub>D<sub>6</sub>, 300 K): δ [ppm] = 3.08 (s, 1H, SiH), 1.24 (s, 27H, C(CH<sub>3</sub>)<sub>3</sub>), 0.37 (s, 9H, TMS), 0.32 (s, 18H, TMS), −0.17 (br s, 2H, SiNH<sub>2</sub>).

<sup>13</sup>C{<sup>1</sup>H} NMR (126 MHz, C<sub>6</sub>D<sub>6</sub>, 300 K): δ [ppm] = 32.1 (C(CH<sub>3</sub>)<sub>3</sub>), 23.6 (C(CH<sub>3</sub>)<sub>3</sub>), 4.6 (TMS), 1.2 (TMS), 0.5 (TMS).

<sup>29</sup>Si{<sup>1</sup>H} NMR (99 MHz, C<sub>6</sub>D<sub>6</sub>, 300 K): δ [ppm] = 29.6 (Si'Bu<sub>3</sub>), −11.5 (TMS), −12.2 (TMS), −12.9 (TMS), −35.7 (SiNH<sub>2</sub>), −119.9 (SiH).

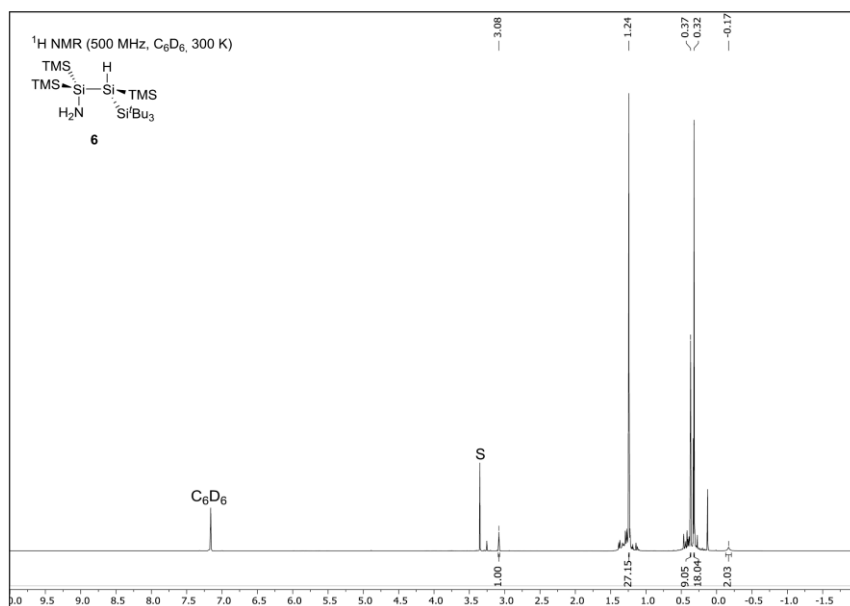


Figure S42. <sup>1</sup>H NMR spectrum of aminosilane **6** in C<sub>6</sub>D<sub>6</sub> at 300 K. Residual 1,4-dioxane is marked with an S.

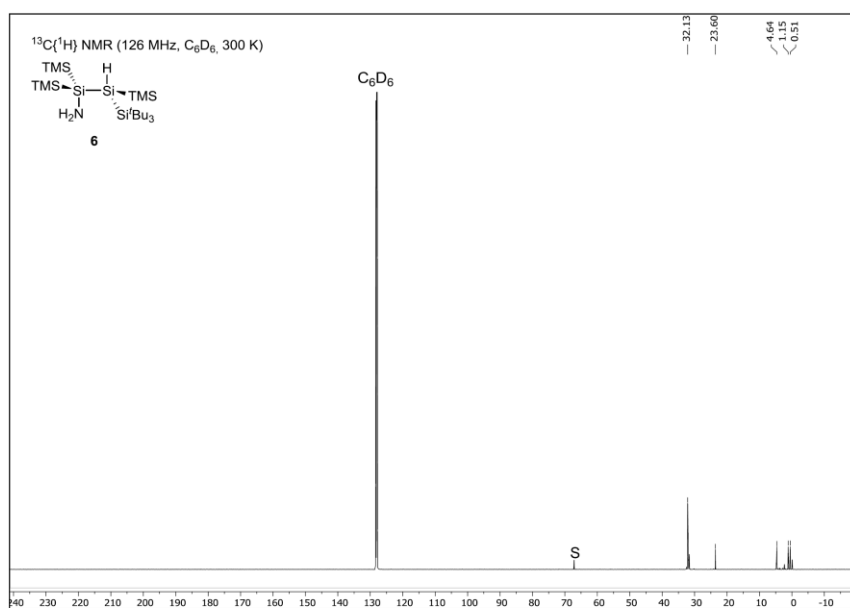


Figure S43. <sup>13</sup>C{<sup>1</sup>H} NMR spectrum of aminosilane **6** in C<sub>6</sub>D<sub>6</sub> at 300 K. Residual 1,4-dioxane is marked with an S.



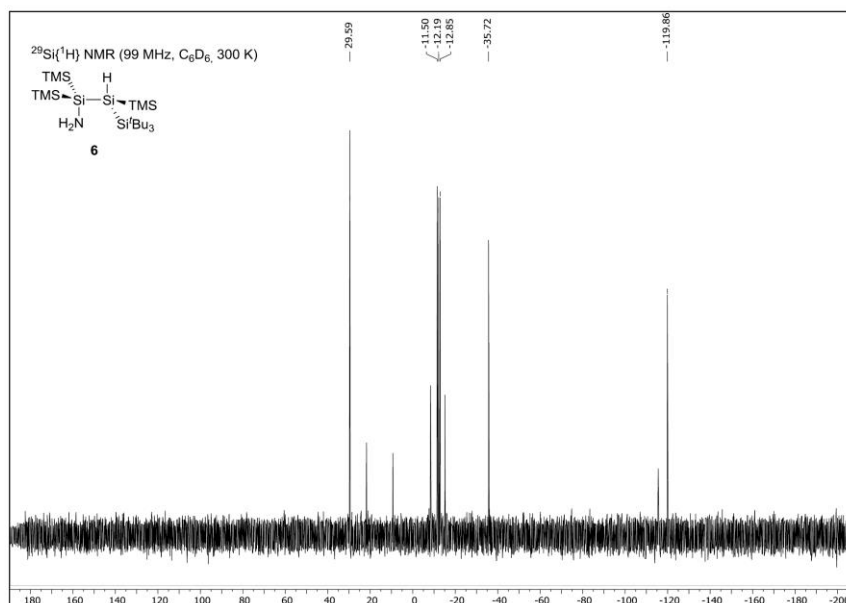
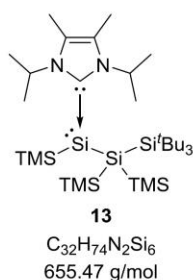


Figure S44.  $^{29}\text{Si}\{^1\text{H}\}$  NMR spectrum of aminosilane **6** in  $\text{C}_6\text{D}_6$  at 300 K.

### 1.10 Synthesis of $(\text{TMS})((\text{TMS})_2(\text{Bu}_3\text{Si})\text{Si})\text{Si}(\text{I}^t\text{Pr}_2\text{Me}_2)$ (**13**)



THF (60 mL) was added to a mixture of **2** (3.00 g, 4.72 mmol, 1.0 eq.),  $\text{I}^t\text{Pr}_2\text{Me}_2$  (852 mg, 4.72 mmol, 1.0 eq.) and  $\text{KC}_8$  (1.28 g, 9.45 mmol, 2.0 eq.) at ambient temperature. After stirring the reaction mixture for 1 h, the solvent was removed *in vacuo* and the residue was extracted with toluene ( $3 \times 20$  mL). Graphite and KBr were separated from the mixture by filtration and the solvent was removed under high vacuum to furnish **13** as a purple-red solid (3.01 g, 4.59 mmol, 97%). Crystals suitable for SC-XRD analysis were obtained by cooling a concentrated THF solution of **13** to  $-35$  °C for several days. The NHC-stabilized bis(silyl)silylene **13** is completely stable as a solid and in solution at room temperature, but partially isomerizes to  $((\text{TMS})_3\text{Si})(\text{Bu}_3\text{Si})\text{Si}(\text{I}^t\text{Pr}_2\text{Me}_2)$  (**15**) (*vide infra*) at elevated temperatures.

**m.p.:** 160-161 °C (decomposition; color change from purple-red to orange).

$^1\text{H}$  NMR (500 MHz,  $\text{C}_6\text{D}_6$ , 300 K):  $\delta$  [ppm] = 6.58 (sept,  $^3J = 7.1$  Hz, 2H,  $\text{NCH}(\text{CH}_3)_2$ ), 1.57 (s, 6H,  $\text{CCH}_3$ ), 1.42 (s, 27H,  $\text{C}(\text{CH}_3)_3$ ), 1.28 (d,  $^3J = 7.1$  Hz, 6H,  $\text{NCH}(\text{CH}_3)_2$ ), 1.24 (d,  $^3J = 7.1$  Hz, 6H,  $\text{NCH}(\text{CH}_3)_2$ ), 0.63 (s, 18H,  $\text{TMS}$ ), 0.37 (s, 9H,  $\text{TMS}$ ).

$^{13}\text{C}\{^1\text{H}\}$  NMR (126 MHz,  $\text{C}_6\text{D}_6$ , 300 K):  $\delta$  [ppm] = 171.9 (*carbene C*), 126.5 ( $\text{CCH}_3$ ), 53.3 ( $\text{NCH}(\text{CH}_3)_2$ ), 33.7 ( $\text{C}(\text{CH}_3)_3$ ), 25.0 ( $\text{C}(\text{CH}_3)_3$ ), 22.5 ( $\text{NCH}(\text{CH}_3)_2$ ), 22.2 ( $\text{NCH}(\text{CH}_3)_2$ ), 10.5 ( $\text{CCH}_3$ ), 7.2 (*TMS*), 6.3 (*TMS*).

$^{29}\text{Si}\{^1\text{H}\}$  NMR (99 MHz,  $\text{C}_6\text{D}_6$ , 300 K):  $\delta$  [ppm] = 29.4 (*Si*<sup>t</sup>Bu<sub>3</sub>), -9.1 (*TMS*), -11.9 (*TMS*), -104.7 (*silylene Si*), -117.4 (*Si*(TMS)<sub>2</sub>).

**IR (solid):**  $\tilde{\nu}$  [ $\text{cm}^{-1}$ ] = 2949 (m), 2884 (m), 2851 (m), 1632 (w), 1477 (w), 1352 (m), 1238 (m), 1103 (w), 1014 (w), 828 (s), 749 (m), 673 (m), 618 (m), 492 (m).

**Anal. Calcd. [%] for  $\text{C}_{32}\text{H}_{74}\text{N}_2\text{Si}_6$ :** C, 58.64; H, 11.38; N, 4.27. Found [%]: C, 58.41; H, 11.49; N, 4.36.

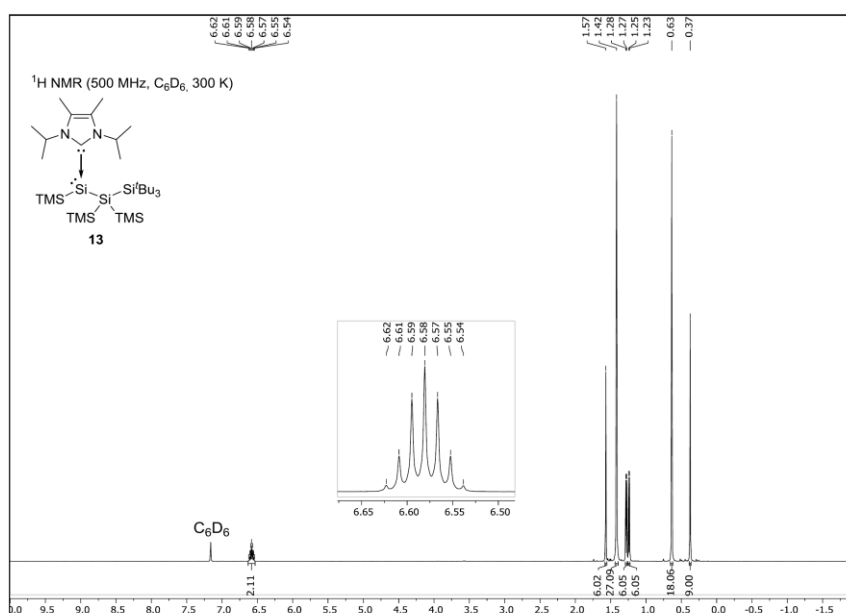


**Figure S45.**  $^1\text{H}$  NMR spectrum of  $(\text{TMS})(\text{TMS})_2(\text{Bu}_3\text{Si})\text{Si}(\text{I}^t\text{Pr}_2\text{Me}_2)$  (**13**) in  $\text{C}_6\text{D}_6$  at 300 K.

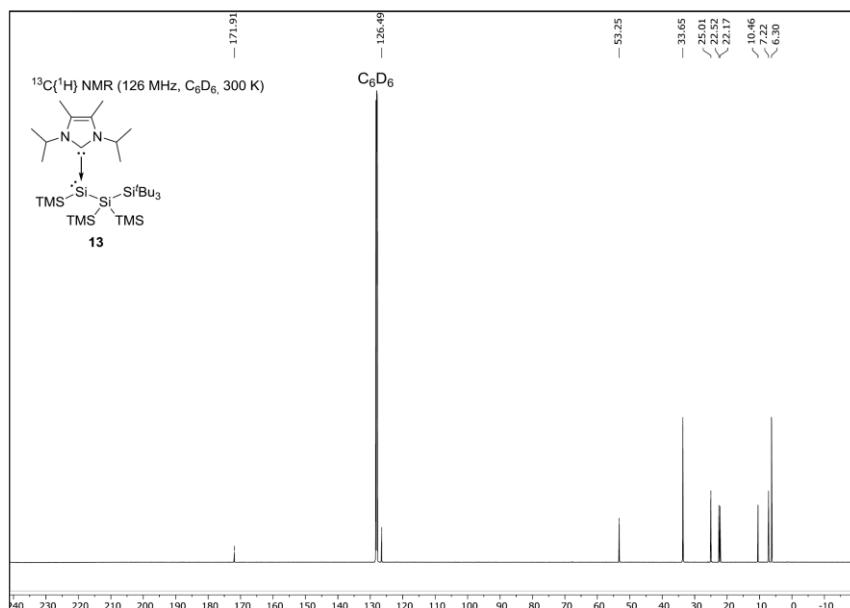


Figure S46.  $^{13}\text{C}\{^1\text{H}\}$  NMR spectrum of  $(\text{TMS})(\text{TMS})_2(\text{Bu}_3\text{Si})\text{Si}(\text{IPr}_2\text{Me}_2)$  (**13**) in  $\text{C}_6\text{D}_6$  at 300 K.

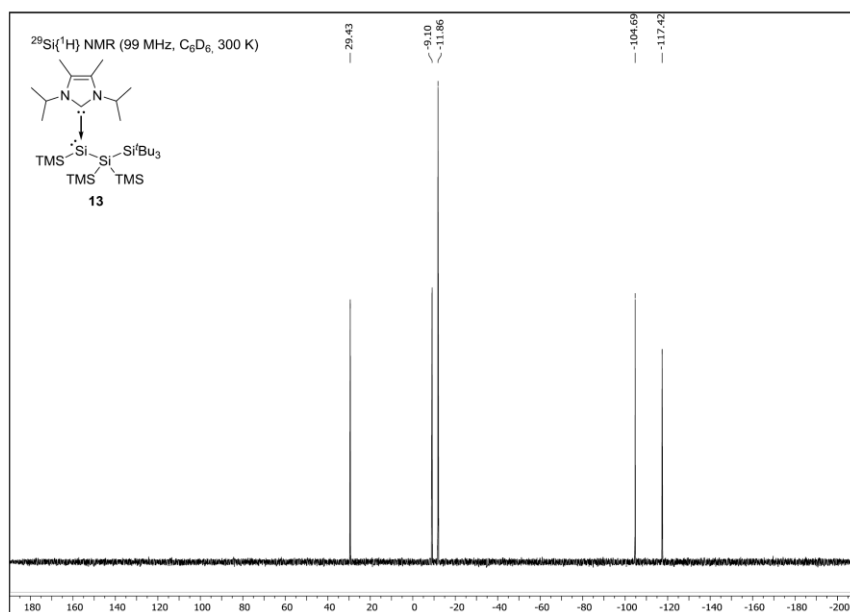
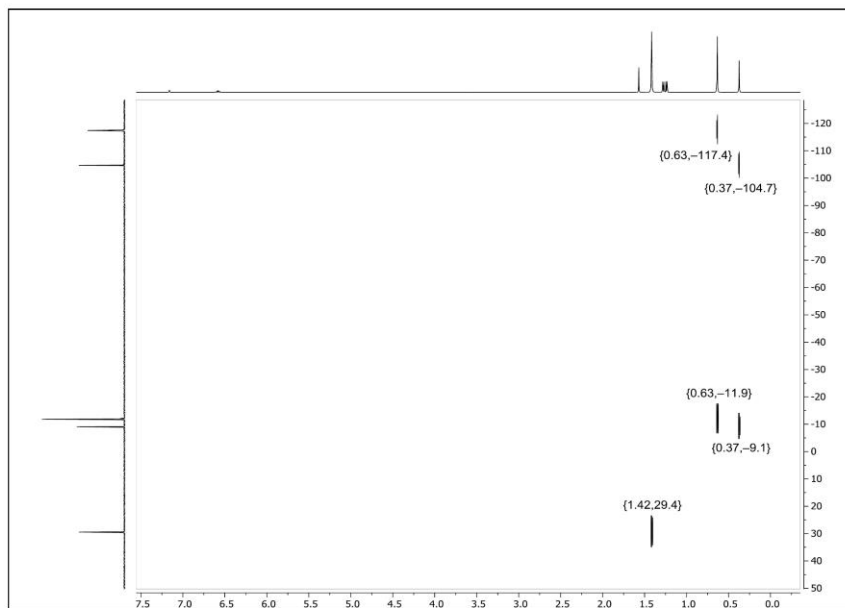
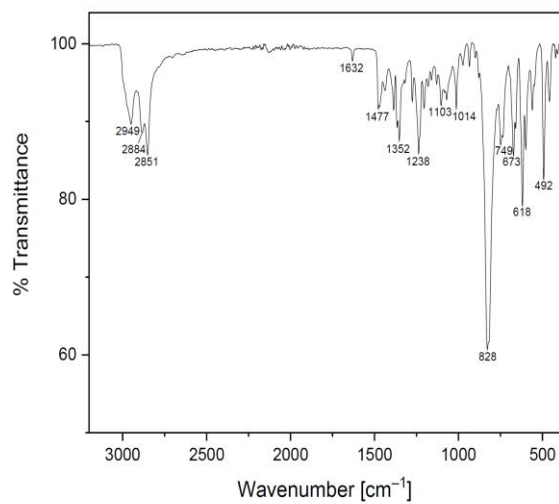


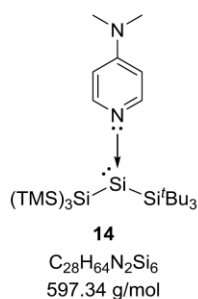
Figure S47.  $^{29}\text{Si}\{^1\text{H}\}$  NMR spectrum of  $(\text{TMS})(\text{TMS})_2(\text{Bu}_3\text{Si})\text{Si}(\text{IPr}_2\text{Me}_2)$  (**13**) in  $\text{C}_6\text{D}_6$  at 300 K.



**Figure S48.**  $^1\text{H}/^{29}\text{Si}$  HMBC NMR spectrum of  $(\text{TMS})((\text{TMS})_2(\text{Bu}_3\text{Si})\text{Si})\text{Si}(\text{iPr}_2\text{Me}_2)$  (**13**) in  $\text{C}_6\text{D}_6$  at 300 K.



**Figure S49.** Solid-state FT-IR spectrum of  $(\text{TMS})((\text{TMS})_2(\text{Bu}_3\text{Si})\text{Si})\text{Si}(\text{iPr}_2\text{Me}_2)$  (**13**).

1.11 Synthesis and reactivity of ((TMS)<sub>3</sub>Si)(<sup>i</sup>Bu<sub>3</sub>Si)Si(DMAP) (**14**)

THF (10 mL) was added to a mixture of **2** (200 mg, 315  $\mu$ mol, 1.0 eq.), DMAP (38.5 mg, 315  $\mu$ mol) and K<sub>2</sub>C<sub>8</sub> (85.2 mg, 630  $\mu$ mol, 1.0 eq.) at ambient temperature. After stirring the reaction mixture for 1 h, the solvent was removed *in vacuo* and the residue extracted with toluene (3  $\times$  3 mL). Graphite and KBr were separated from the mixture by filtration and the solvent was removed under high vacuum to furnish **14** as a red-brown solid (170 mg, 285  $\mu$ mol, 90%). Crystals suitable for SC-XRD analysis were obtained by cooling a concentrated THF solution to  $-35$   $^{\circ}$ C for several days.

**m.p.:** 59-60  $^{\circ}$ C (decomposition; color change from red-brown to black)

**<sup>1</sup>H NMR (500 MHz, C<sub>6</sub>D<sub>6</sub>, 300 K):**  $\delta$  [ppm] = 8.79 (d, <sup>3</sup>J = 7.1 Hz, 2H, *o*-C<sub>DMAP</sub>H), 5.62 (br s, 2H, *m*-C<sub>DMAP</sub>H), 1.72 (s, 6H, N(CH<sub>3</sub>)<sub>2</sub>), 1.47 (s, 27H, C(CH<sub>3</sub>)<sub>3</sub>), 0.51 (s, 27H, TMS).

**<sup>13</sup>C{<sup>1</sup>H} NMR (126 MHz, C<sub>6</sub>D<sub>6</sub>, 300 K):**  $\delta$  [ppm] = 154.7 (*p*-C<sub>DMAP</sub>), 105.3 (*m*-C<sub>DMAP</sub>), 38.1 (N(CH<sub>3</sub>)<sub>2</sub>), 33.2 (C(CH<sub>3</sub>)<sub>3</sub>), 25.5 (C(CH<sub>3</sub>)<sub>3</sub>), 4.9 (TMS). Due to a presumable overlap with the solvent signal, the resonance for the *o*-C<sub>DMAP</sub> nuclei was not directly observed.

**<sup>29</sup>Si{<sup>1</sup>H} NMR (99 MHz, C<sub>6</sub>D<sub>6</sub>, 300 K):**  $\delta$  [ppm] = 68.8 (*silylene Si*), 20.4 (*Si*<sup>i</sup>Bu<sub>3</sub>),  $-9.3$  (TMS),  $-121.6$  (*Si*(TMS)<sub>3</sub>).

**Anal. Calcd. [%] for C<sub>28</sub>H<sub>64</sub>N<sub>2</sub>Si<sub>6</sub>:** C, 56.30; H, 10.80; N, 4.69. Found [%]: C, 55.98; H, 10.77; N, 4.40.

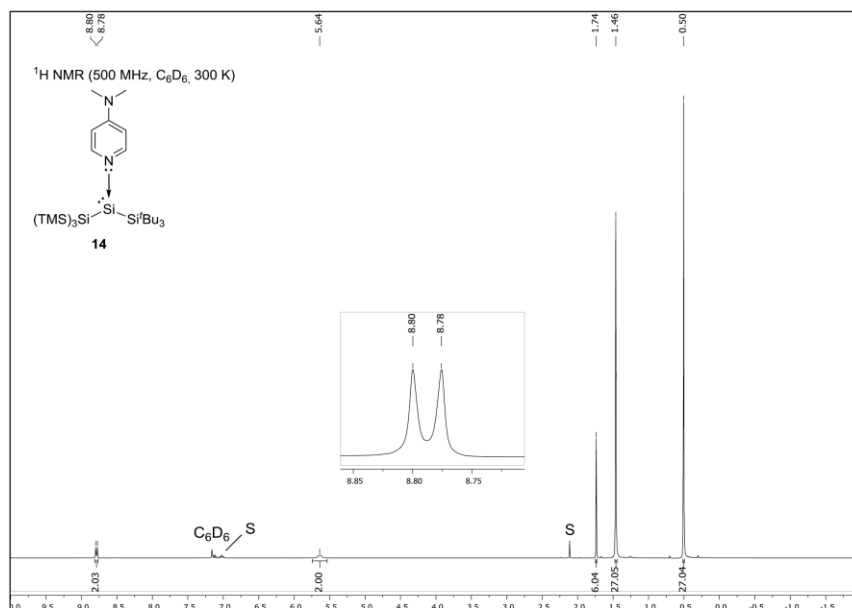


**Figure S50.** <sup>1</sup>H NMR spectrum of ((TMS)<sub>3</sub>Si)(<sup>t</sup>Bu<sub>3</sub>Si)Si(DMAP) (**14**) in C<sub>6</sub>D<sub>6</sub> at 300 K. Residual toluene is labeled with an S.

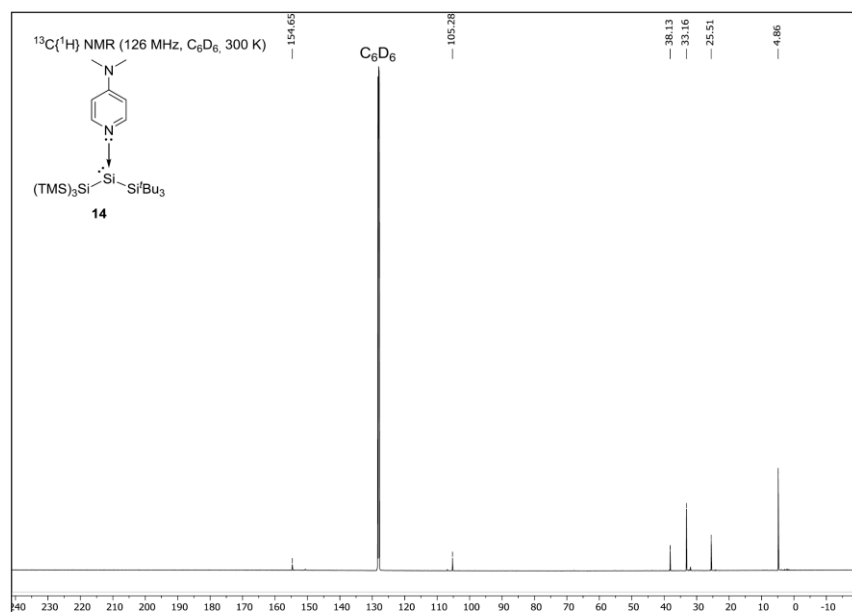


**Figure S51.** <sup>13</sup>C{<sup>1</sup>H} NMR spectrum of ((TMS)<sub>3</sub>Si)(<sup>t</sup>Bu<sub>3</sub>Si)Si(DMAP) (**14**) in C<sub>6</sub>D<sub>6</sub> at 300 K.

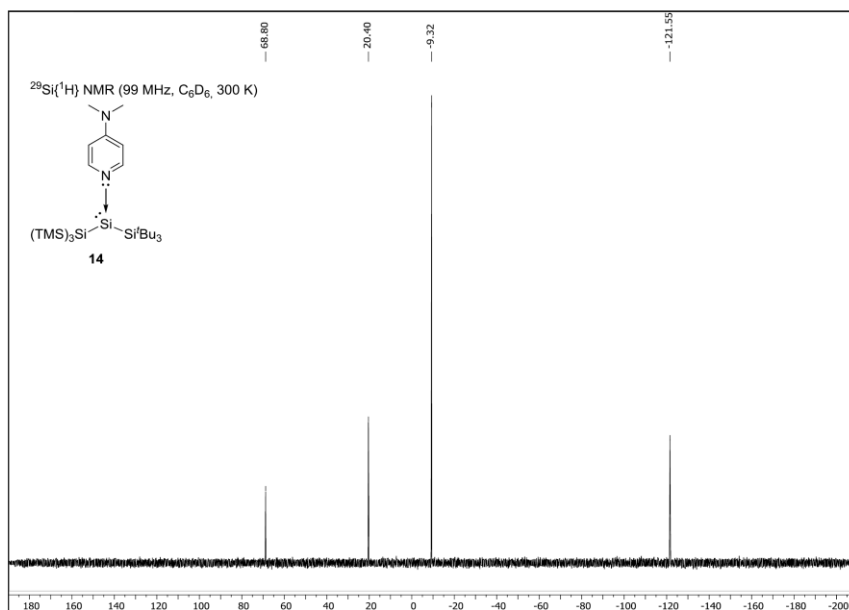


Figure S52.  $^{29}\text{Si}\{^1\text{H}\}$  NMR spectrum of  $((\text{TMS})_3\text{Si})(\text{Bu}_3\text{Si})\text{Si}(\text{DMAP})$  (**14**) in  $\text{C}_6\text{D}_6$  at 300 K.

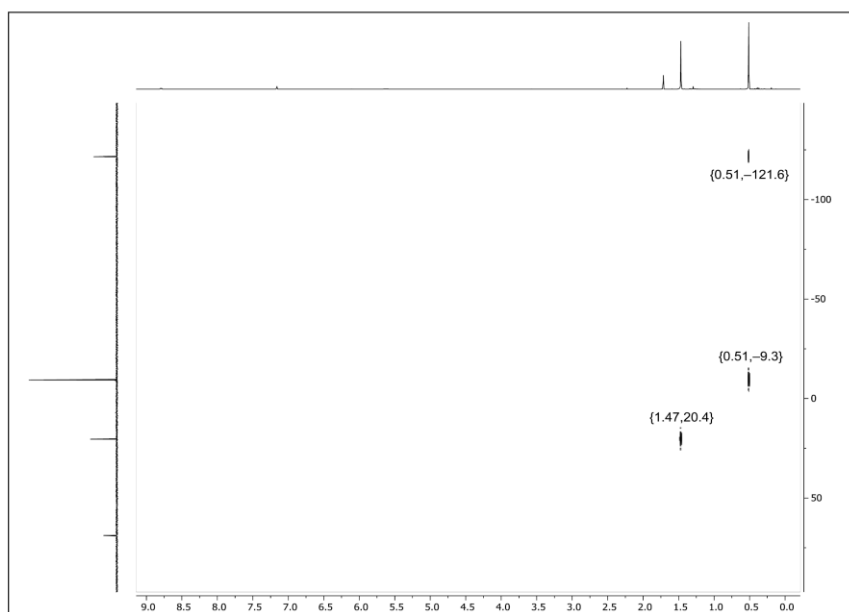
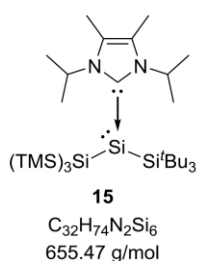


Figure S53.  $^1\text{H}/^{29}\text{Si}$  HMBC NMR spectrum of  $((\text{TMS})_3\text{Si})(\text{Bu}_3\text{Si})\text{Si}(\text{DMAP})$  (**14**) in  $\text{C}_6\text{D}_6$  at 300 K.



**Lewis base exchange reaction: synthesis of (TMS)((TMS)<sub>2</sub>(<sup>t</sup>Bu<sub>3</sub>Si)Si)Si(<sup>i</sup>Pr<sub>2</sub>Me<sub>2</sub>) (13)**

A *J. Young* PTFE valve NMR tube was filled with a solution of **14** (20.0 mg, 33.5 μmol, 1.0 eq.) and <sup>i</sup>Pr<sub>2</sub>Me<sub>2</sub> (6.04 mg, 33.5 μmol, 1.0 eq.) in C<sub>6</sub>D<sub>6</sub> (0.5 mL). Monitoring of the reaction mixture by <sup>1</sup>H NMR spectroscopy revealed quantitative conversion of **14** to the NHC-stabilized bis(silyl)silylene **13** with concomitant release of DMAP after 4 days.

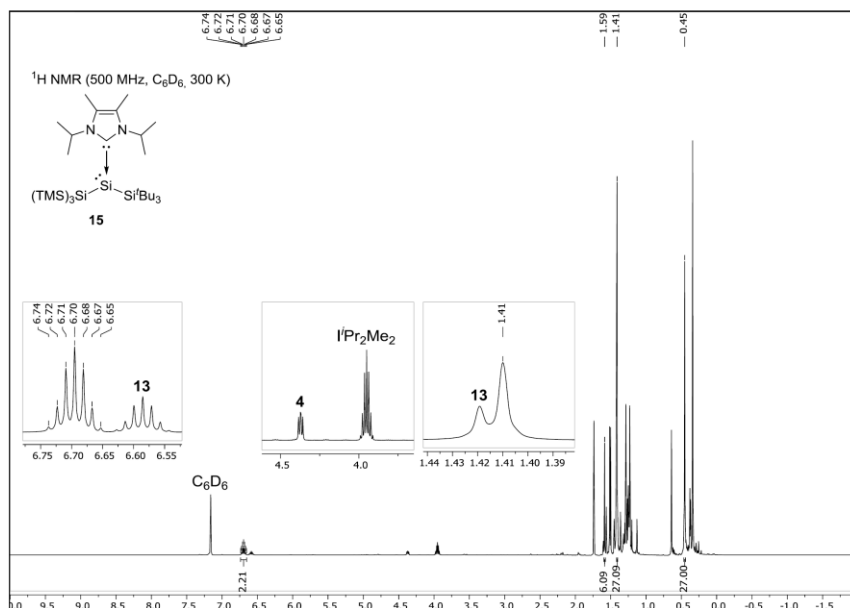
**1.12 Synthesis of ((TMS)<sub>3</sub>Si)(<sup>t</sup>Bu<sub>3</sub>Si)Si(<sup>i</sup>Pr<sub>2</sub>Me<sub>2</sub>) (15)**

A solution of **13** (500 mg, 763 μmol) in toluene (10 mL) was heated to 90 °C for 48 h. Subsequently, the solvent was removed *in vacuo*. Multinuclear and 2D NMR spectroscopic analysis of the residue revealed the NHC-stabilized bis(silyl)silylene **15** as the major product (58%). In addition to remaining starting material **13** (16%), the simultaneous formation of disiletane **4** (13%) and free <sup>i</sup>Pr<sub>2</sub>Me<sub>2</sub> (13%) was detected. Neither prolonged heating (at different temperatures), nor solvent change to THF, benzene or *n*-hexane affected the outcome of the reaction in favour of **15**. Therefore, the isomerization is presumably an equilibrium reaction, with initial NHC dissociation ultimately competing with re-coordination providing **15** or NHC release and disiletane **4** formation. DFT calculations support this assumption (*vide infra*). Nevertheless, all attempts to purify the residue and isolate **15** *via* crystallization, washing, or sublimation were unsuccessful so far.

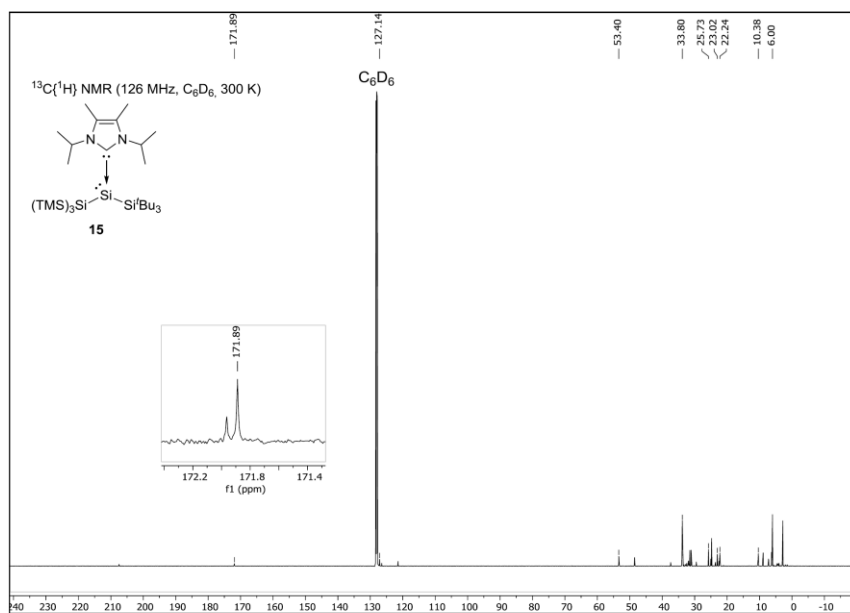
<sup>1</sup>H NMR (500 MHz, C<sub>6</sub>D<sub>6</sub>, 300 K): δ [ppm] = 6.70 (sept, <sup>3</sup>J = 7.0 Hz, 2H, NCH(CH<sub>3</sub>)<sub>2</sub>), 1.59 (s, 6H, CCH<sub>3</sub>), 1.41 (s, 27H, C(CH<sub>3</sub>)<sub>3</sub>), 0.45 (s, 27H, TMS). The resonances for the NCH(CH<sub>3</sub>)<sub>2</sub> protons could not be clearly assigned due to overlapping signals.

<sup>13</sup>C{<sup>1</sup>H} NMR (126 MHz, C<sub>6</sub>D<sub>6</sub>, 300 K): δ [ppm] = 171.9 (*carbene C*), 127.1 (CCH<sub>3</sub>), 53.4 (NCH(CH<sub>3</sub>)<sub>2</sub>), 33.8 (C(CH<sub>3</sub>)<sub>3</sub>), 25.7 (C(CH<sub>3</sub>)<sub>3</sub>), 23.0 (NCH(CH<sub>3</sub>)<sub>2</sub>), 22.2 (NCH(CH<sub>3</sub>)<sub>2</sub>), 10.4 (CCH<sub>3</sub>), 6.0 (TMS).

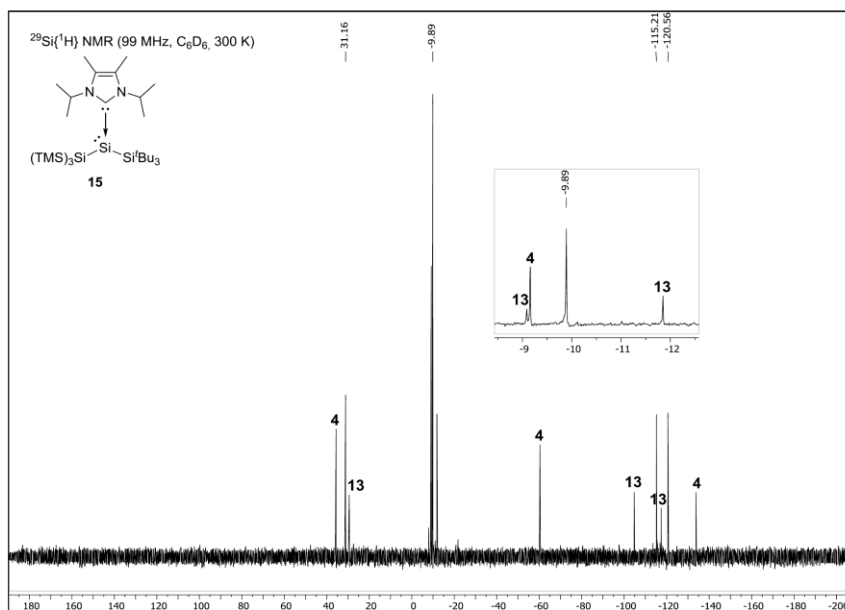
<sup>29</sup>Si{<sup>1</sup>H} NMR (99 MHz, C<sub>6</sub>D<sub>6</sub>, 300 K): δ [ppm] = 31.2 (*Si<sup>t</sup>Bu<sub>3</sub>*), -9.9 (TMS), -115.2 (*Si(TMS)<sub>3</sub>*), -120.6 (*silylene Si*).



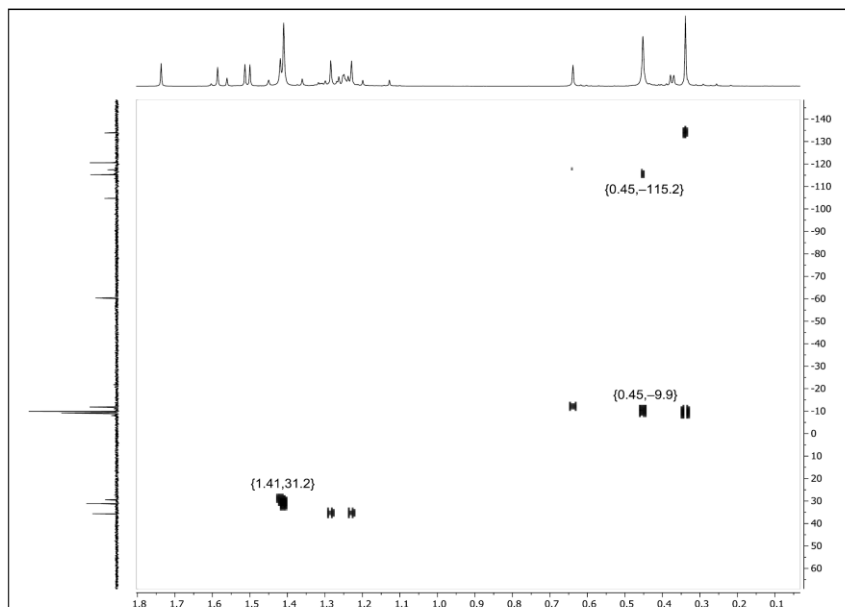
**Figure S54.** <sup>1</sup>H NMR spectrum of ((TMS)<sub>3</sub>Si)(Bu<sub>3</sub>Si)Si(IPr<sub>2</sub>Me<sub>2</sub>) (**15**) in C<sub>6</sub>D<sub>6</sub> at 300 K. Significant resonances for the side products (TMS)((TMS)<sub>2</sub>(Bu<sub>3</sub>Si)Si)Si(IPr<sub>2</sub>Me<sub>2</sub>) (**13**), disilene **4** and IPr<sub>2</sub>Me<sub>2</sub> are labeled accordingly.



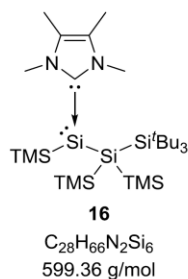
**Figure S55.** <sup>13</sup>C{<sup>1</sup>H} NMR spectrum of ((TMS)<sub>3</sub>Si)(Bu<sub>3</sub>Si)Si(IPr<sub>2</sub>Me<sub>2</sub>) (**15**) in C<sub>6</sub>D<sub>6</sub> at 300 K. Here, only the resonances for **15** are assigned.



**Figure S56.**  $^{29}\text{Si}\{^1\text{H}\}$  spectrum of  $(\text{TMS})_3\text{Si}(\text{Bu}_3\text{Si})\text{Si}(\text{I}^*\text{Pr}_2\text{Me}_2)$  (**15**) in  $\text{C}_6\text{D}_6$  at 300 K. The resonances for the side products  $(\text{TMS})(\text{TMS})_2(\text{Bu}_3\text{Si})\text{Si}(\text{I}^*\text{Pr}_2\text{Me}_2)$  (**13**) and disilene **4** are labeled accordingly.



**Figure S57.**  $^1\text{H}/^{29}\text{Si}$  HMBC NMR spectrum of  $(\text{TMS})_3\text{Si}(\text{Bu}_3\text{Si})\text{Si}(\text{I}^*\text{Pr}_2\text{Me}_2)$  (**15**) in  $\text{C}_6\text{D}_6$  at 300 K. Here, only the correlations for **15** are assigned.

1.13 Synthesis of (TMS)((TMS)<sub>2</sub>(<sup>t</sup>Bu<sub>3</sub>Si)Si)Si(IME<sub>4</sub>) (**16**)

Toluene (10 mL) was added to a mixture of **13** (300 mg, 458  $\mu$ mol, 1.0 eq.) and IMe<sub>4</sub> (56.8 g, 458  $\mu$ mol, 1.0 eq.) at ambient temperature. After stirring the reaction mixture for 2 days, the solvent was removed *in vacuo*. Multinuclear and 2D NMR spectroscopic analysis of the residue revealed formation of the NHC-stabilized bis(silyl)silylene **16** and I'Pr<sub>2</sub>Me<sub>2</sub>. Nevertheless, all attempts to purify the residue and isolate **16** *via* crystallization, washing, or sublimation were unsuccessful so far. NHC adduct **16** even slowly decomposes in solution to an unidentified product mixture.

<sup>1</sup>H NMR (500 MHz, C<sub>6</sub>D<sub>6</sub>, 300 K):  $\delta$  [ppm] = 3.68 (s, 6H, NCH<sub>3</sub>), 1.43 (s, 27H, C(CH<sub>3</sub>)<sub>3</sub>), 1.31 (s, 6H, CCH<sub>3</sub>), 0.53 (s, 18H, TMS), 0.39 (s, 9H, TMS).

<sup>13</sup>C{<sup>1</sup>H} NMR (126 MHz, C<sub>6</sub>D<sub>6</sub>, 300 K):  $\delta$  [ppm] = 172.1 (*carbene* C), 125.4 (C(CH<sub>3</sub>)<sub>3</sub>), 36.8 (NCH<sub>3</sub>), 33.3 (C(CH<sub>3</sub>)<sub>3</sub>), 25.1 (C(CH<sub>3</sub>)<sub>3</sub>), 8.6 (CCH<sub>3</sub>), 6.3 (TMS), 5.9 (TMS).

<sup>29</sup>Si{<sup>1</sup>H} NMR (99 MHz, C<sub>6</sub>D<sub>6</sub>, 300 K):  $\delta$  [ppm] = 30.6 (*Si*<sup>t</sup>Bu<sub>3</sub>), -9.2 (TMS), -11.4 (TMS), -117.1 (*silylene* Si), -118.9 (*Si*(TMS)<sub>2</sub>).

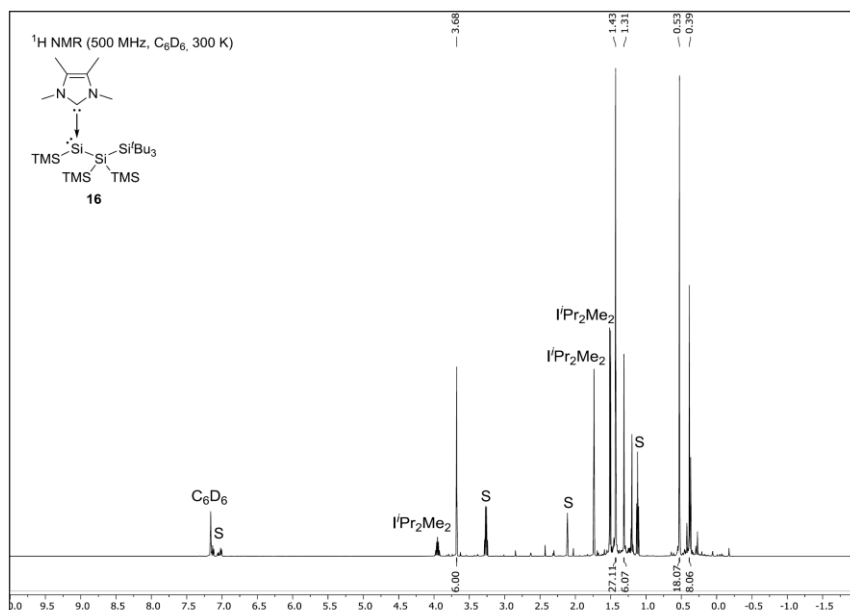


**Figure S58.** <sup>1</sup>H NMR spectrum of (TMS)((TMS)<sub>2</sub>(<sup>t</sup>Bu<sub>3</sub>Si)Si)Si(IME<sub>4</sub>) (**16**) in C<sub>6</sub>D<sub>6</sub> at 300 K. Residual solvents (S; toluene and Et<sub>2</sub>O from a crystallization attempt) and I'Pr<sub>2</sub>Me<sub>2</sub> are labeled accordingly.

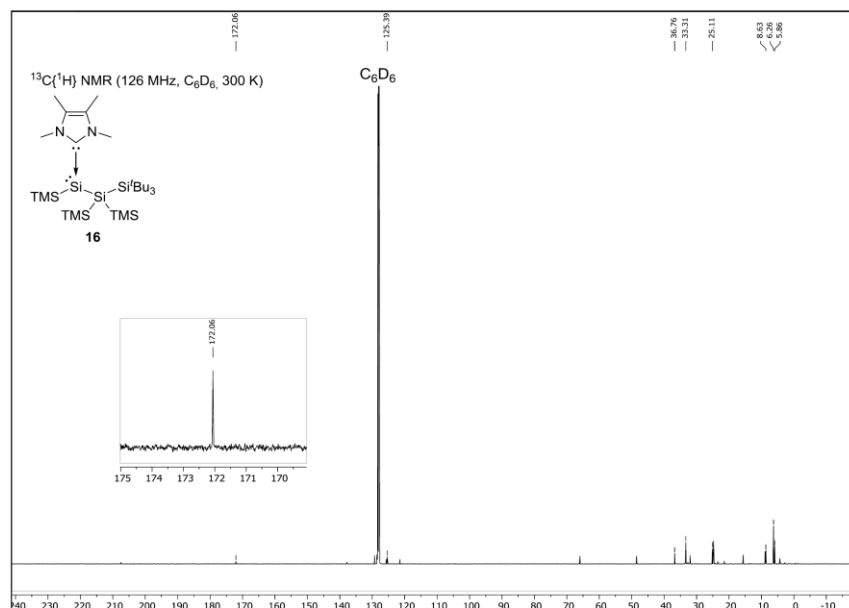


**Figure S59.**  $^{13}\text{C}\{^1\text{H}\}$  NMR spectrum of  $(\text{TMS})(\text{TMS})_2(\text{Bu}_3\text{Si})\text{Si}(\text{IME}_4)$  (**16**) in  $\text{C}_6\text{D}_6$  at 300 K. Here, only the resonances for **16** are assigned.

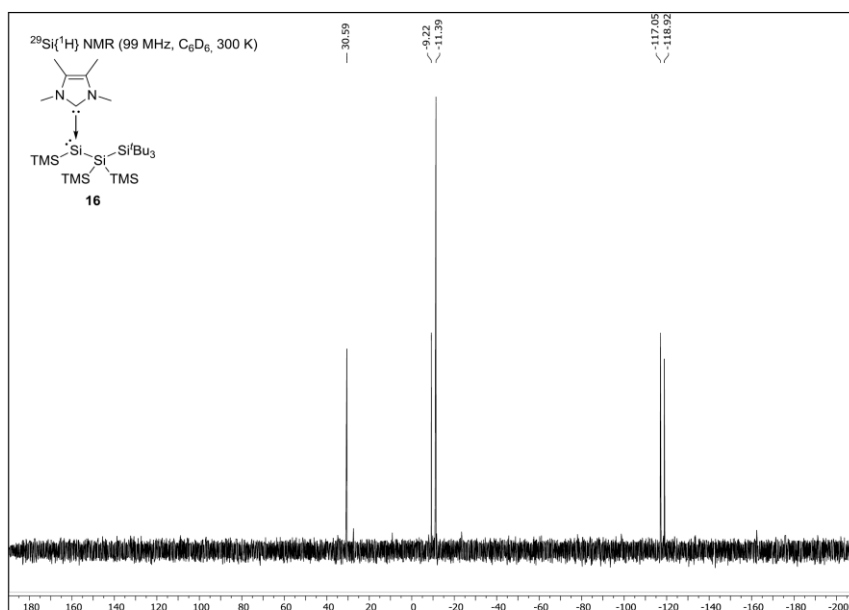


**Figure S60.**  $^{29}\text{Si}\{^1\text{H}\}$  NMR spectrum of  $(\text{TMS})(\text{TMS})_2(\text{Bu}_3\text{Si})\text{Si}(\text{IME}_4)$  (**16**) in  $\text{C}_6\text{D}_6$  at 300 K.

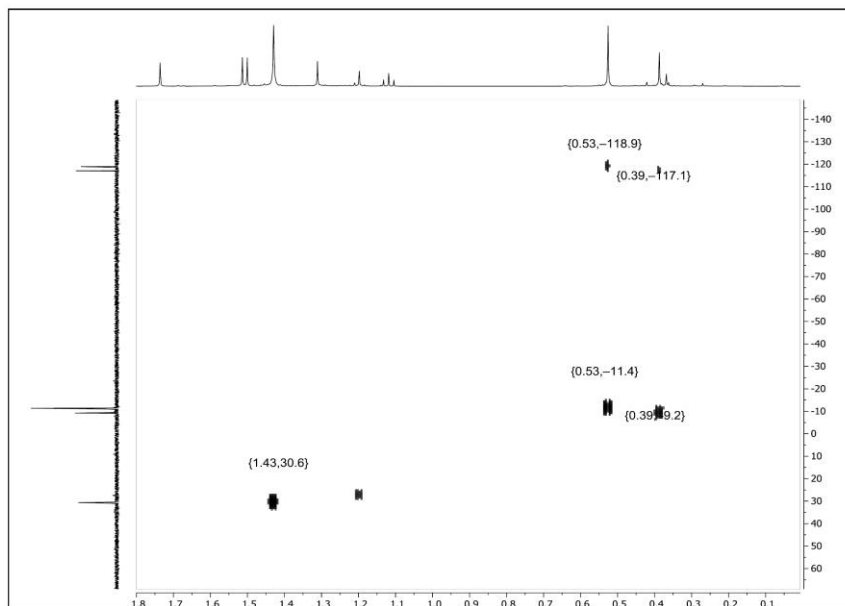
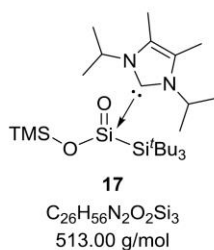


**Figure S61.**  $^1\text{H}/^{29}\text{Si}$  HMBC NMR spectrum of  $(\text{TMS})((\text{TMS})_2(\text{Bu}_3\text{Si})\text{Si})\text{Si}(\text{Ime}_4)$  (**16**) in  $\text{C}_6\text{D}_6$  at 300 K.

#### 1.14 Synthesis of $(\text{TMSO})(\text{Bu}_3\text{Si})\text{Si}=\text{O}(\text{I}^i\text{Pr}_2\text{Me}_2)$ (**17**)



A solution of **13** (300 mg, 458  $\mu\text{mol}$ ) in *n*-hexane (15 mL) was frozen in liquid nitrogen and degassed. The solution was warmed to  $-80\text{ }^\circ\text{C}$  and exposed to  $\text{N}_2\text{O}$  (1 bar) under vigorous stirring. Subsequently, the reaction mixture was allowed to warm to  $-30\text{ }^\circ\text{C}$  over a period of 5 h, whereby the color changed from purple-red to pale red and a fine white precipitate formed. The solid was immediately separated *via* filtration, washed with cold *n*-hexane and dried *in vacuo* to provide the NHC-stabilized silanoic silylester **17** as a colorless powder (41.5 mg, 80.9  $\mu\text{mol}$ , 18%). Suitable crystals for SC-XRD analysis were obtained by slow diffusion of *n*-hexane into a saturated THF solution at  $-35\text{ }^\circ\text{C}$  for several days. The NHC-stabilized silanoic silylester **17** decomposes in solution at temperatures higher than  $-30\text{ }^\circ\text{C}$  to an unidentified mixture of products. Thus, NMR characterization was performed at  $-30\text{ }^\circ\text{C}$ . The observed unusual broad splitting of the NHC wingtip methine protons ( $\Delta\delta = 2.68\text{ ppm}$ ) in the  $^1\text{H}$  NMR spectrum might originate from hydrogen bonding of one isopropyl C–H proton to the oxygen atom of the Si=O bond. This assumption is supported by the solid-state

analysis were obtained by slow diffusion of *n*-hexane into a saturated THF solution at  $-35\text{ }^\circ\text{C}$  for several days. The NHC-stabilized silanoic silylester **17** decomposes in solution at temperatures higher than  $-30\text{ }^\circ\text{C}$  to an unidentified mixture of products. Thus, NMR characterization was performed at  $-30\text{ }^\circ\text{C}$ . The observed unusual broad splitting of the NHC wingtip methine protons ( $\Delta\delta = 2.68\text{ ppm}$ ) in the  $^1\text{H}$  NMR spectrum might originate from hydrogen bonding of one isopropyl C–H proton to the oxygen atom of the Si=O bond. This assumption is supported by the solid-state

structure of **17** (*vide infra*), which revealed a close O $\cdots$ H distance of 2.143 Å, being much shorter than the sum of the van der Waals radii of hydrogen and oxygen (2.72 Å).

**m.p.:** 97 °C (decomposition, color change from colorless to red).

**<sup>1</sup>H NMR (400 MHz, THF-*d*<sub>8</sub>, 243 K):** δ [ppm] = 8.23 (sept, <sup>3</sup>J = 7.0 Hz, 1H, NCH(CH<sub>3</sub>)<sub>2</sub>), 5.55 (sept, <sup>3</sup>J = 6.9 Hz, 1H, NCH(CH<sub>3</sub>)<sub>2</sub>), 2.35 (s, 3H, CCH<sub>3</sub>), 2.33 (s, 3H, CCH<sub>3</sub>), 1.55 (d, <sup>3</sup>J = 6.9 Hz, 3H, NCH(CH<sub>3</sub>)<sub>2</sub>), 1.51 (d, <sup>3</sup>J = 6.5 Hz, 3H, NCH(CH<sub>3</sub>)<sub>2</sub>), 1.43 (d, <sup>3</sup>J = 6.4 Hz, 3H, NCH(CH<sub>3</sub>)<sub>2</sub>), 1.39 (d, <sup>3</sup>J = 7.2 Hz, 3H, NCH(CH<sub>3</sub>)<sub>2</sub>), 1.22 (s, 27H, C(CH<sub>3</sub>)<sub>3</sub>), 0.12 (s, 9H, OTMS).

**<sup>13</sup>C{<sup>1</sup>H} NMR (101 MHz, THF-*d*<sub>8</sub>, 243 K):** δ [ppm] = 156.8 (*carbene C*), 129.1 (CCH<sub>3</sub>), 127.0 (CCH<sub>3</sub>), 51.6 (NCH(CH<sub>3</sub>)<sub>2</sub>), 50.2 (NCH(CH<sub>3</sub>)<sub>2</sub>), 32.5 (C(CH<sub>3</sub>)<sub>3</sub>), 24.6 (C(CH<sub>3</sub>)<sub>3</sub>), 23.4 (NCH(CH<sub>3</sub>)<sub>2</sub>), 23.2 (NCH(CH<sub>3</sub>)<sub>2</sub>), 21.8 (NCH(CH<sub>3</sub>)<sub>2</sub>), 20.6 (NCH(CH<sub>3</sub>)<sub>2</sub>), 11.0 (CCH<sub>3</sub>), 10.7 (CCH<sub>3</sub>), 3.3 (TMS).

**<sup>29</sup>Si{<sup>1</sup>H} NMR (79 MHz, THF-*d*<sub>8</sub>, 243 K):** δ [ppm] = 6.6 (Si<sup>i</sup>Bu<sub>3</sub>), -3.4 (TMS), -50.8 (Si=O).

**IR (solid):**  $\tilde{\nu}$  [cm<sup>-1</sup>] = 2957 (w), 2847 (m), 1626 (w), 1469 (w), 1371 (m), 1244 (m), 1069 (m) ( $\tilde{\nu}_{\text{Si=O}}$ ), 971 (s) ( $\tilde{\nu}_{\text{Si-O}}$ ), 840 (s), 755 (m), 598 (w), 453 (m), 428 (m).

**Anal. Calcd. [%] for C<sub>26</sub>H<sub>56</sub>N<sub>2</sub>O<sub>2</sub>Si<sub>3</sub>:** C, 60.87; H, 11.00; N, 5.46. Found [%]: C, 60.04; H, 10.92; N, 5.36.

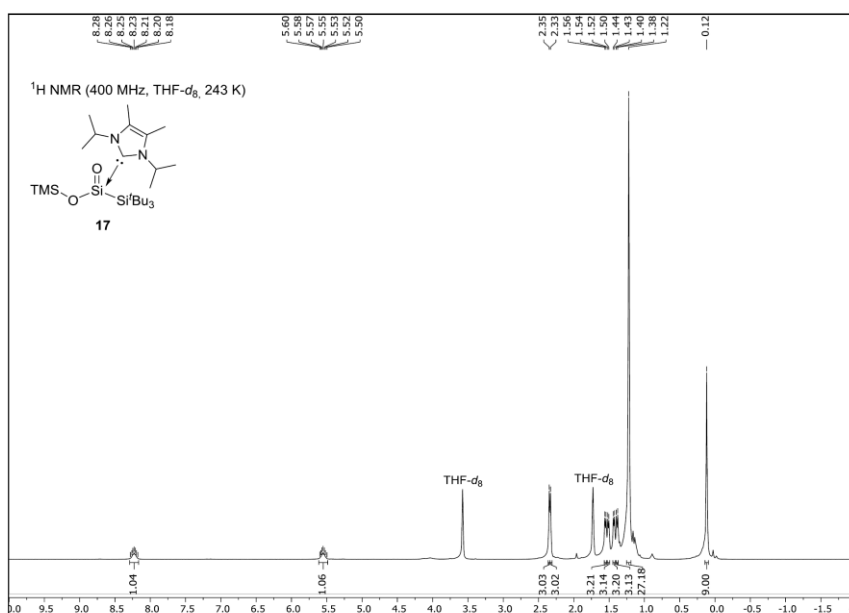


**Figure S62.** <sup>1</sup>H NMR spectrum of (TMSO)(Bu<sub>3</sub>Si)Si=O(I'Pr<sub>2</sub>Me<sub>2</sub>) (**17**) in THF-*d*<sub>8</sub> at 243 K.



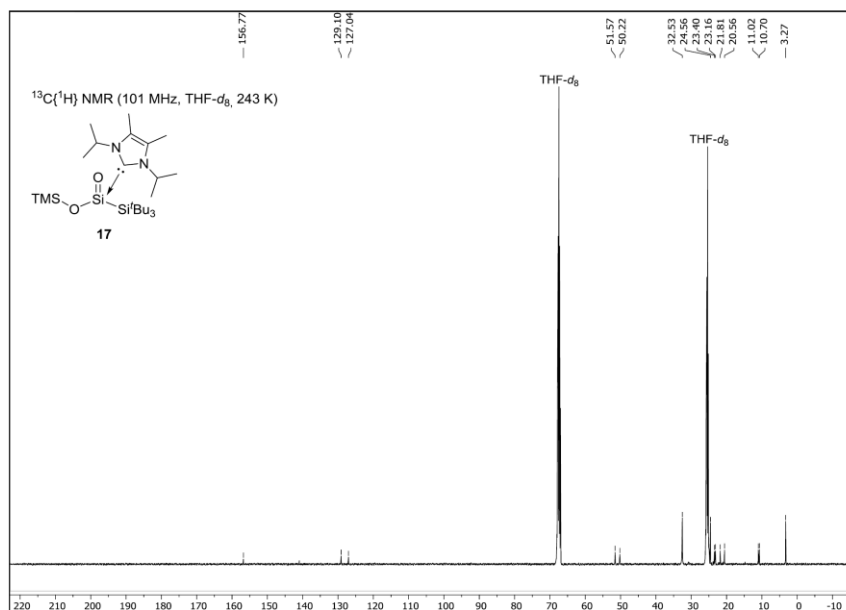


Figure S63. <sup>13</sup>C{<sup>1</sup>H} NMR spectrum of (TMSO)(*Bu*<sub>3</sub>Si)Si=O(*i*Pr<sub>2</sub>Me<sub>2</sub>) (17) in THF-*d*<sub>8</sub> at 243 K.

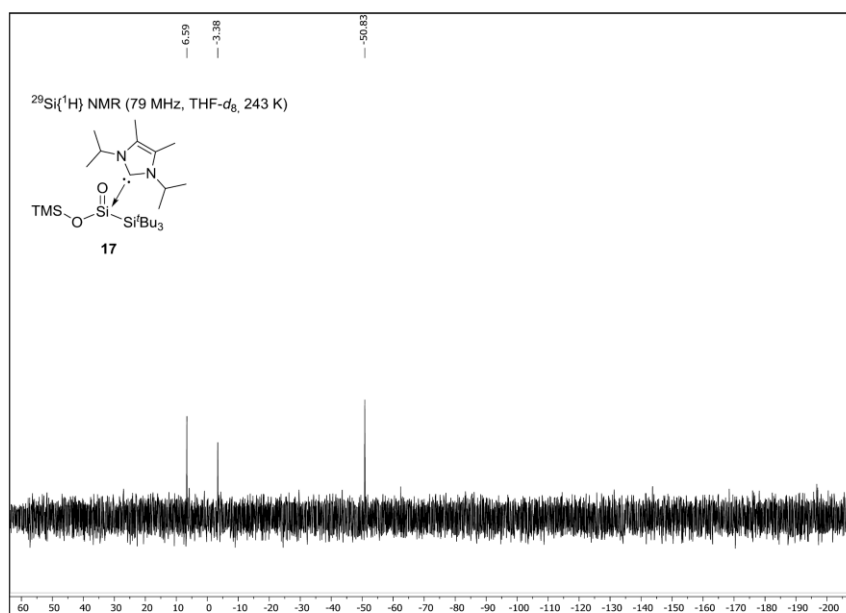
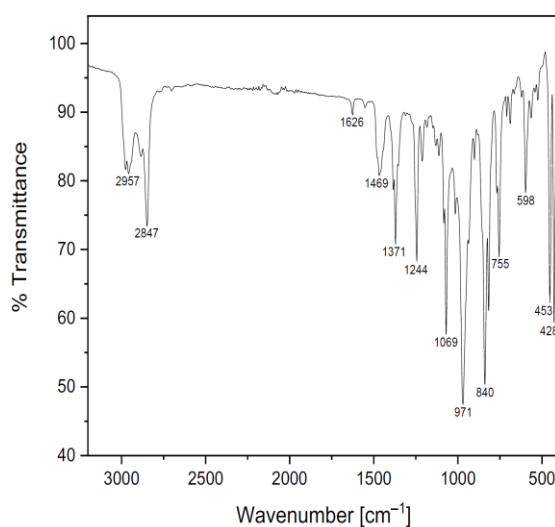


Figure S64. <sup>29</sup>Si{<sup>1</sup>H} NMR spectrum of (TMSO)(*Bu*<sub>3</sub>Si)Si=O(*i*Pr<sub>2</sub>Me<sub>2</sub>) (17) in THF-*d*<sub>8</sub> at 243 K.



**Figure S65.** Solid-state FT-IR spectrum of (TMSO)(tBu<sub>3</sub>Si)Si=O(I'Pr<sub>2</sub>Me<sub>2</sub>) (**17**).

## 2. X-ray Crystallographic Data

### General Information

The X-ray intensity data of **1**, **5**, **17** and **19** were collected on an X-ray single crystal diffractometer equipped with a CMOS detector (Bruker Photon-100), an IMS microsource with MoK $\alpha$  radiation ( $\lambda = 0.71073 \text{ \AA}$ ) and a Helios mirror optic by using the APEX III software package.<sup>[S10]</sup> The X-ray intensity data of **2**, **13** and **14** were collected on an X-ray single crystal diffractometer equipped with a CMOS detector (Bruker Photon-100), a rotating anode (Bruker TXS) with MoK $\alpha$  radiation ( $\lambda = 0.71073 \text{ \AA}$ ) and a Helios mirror optic by using the APEX III software package.<sup>[S10]</sup> The measurements were performed on single crystals coated with the perfluorinated ether Fomblin<sup>®</sup> Y. The crystals were fixed on the top of a microsampler, transferred to the diffractometer and frozen under a stream of cold nitrogen. A matrix scan was used to determine the initial lattice parameters. Reflections were merged and corrected for Lorenz and polarization effects, scan speed, and background using SAINT.<sup>[S11]</sup> Absorption corrections, including odd and even ordered spherical harmonics were performed using SADABS.<sup>[S11]</sup> Space group assignments were based upon systematic absences, E statistics, and successful refinement of the structures. Structures were solved by direct methods with the aid of successive difference Fourier maps, and were refined against all data using the APEX III software in conjunction with SHELXL-2014<sup>[S12]</sup> and

SHELXL<sup>[S13]</sup> All H atoms were placed in calculated positions and refined using a riding model, with methylene and aromatic C–H distances of 0.99 and 0.95 Å, respectively, and  $U_{\text{iso}}(\text{H}) = 1.2 \cdot U_{\text{eq}}(\text{C})$ . Full-matrix least-squares refinements were carried out by minimizing  $\Delta w(F_o^2 - F_c^2)^2$  with SHELXL-97<sup>[S14]</sup> weighting scheme. Neutral atom scattering factors for all atoms and anomalous dispersion corrections for the non-hydrogen atoms were taken from International Tables for Crystallography.<sup>[S15]</sup> The images of the crystal structures were generated by Mercury.<sup>[S16]</sup> The CCDC numbers CCDC-1915626 (**1**), CCDC-1915627 (**4**), CCDC-1915631 (**5**), CCDC-1915629 (**13**), CCDC-1915628 (**14**), CCDC-1915630 (**17**) and CCDC-1915625 (**19**) contain the supplementary crystallographic data for the structures. These data can be obtained free of charge from the Cambridge Crystallographic Data Centre via <https://www.ccdc.cam.ac.uk/structures/>.

### Single Crystal X-ray Structure Determinations

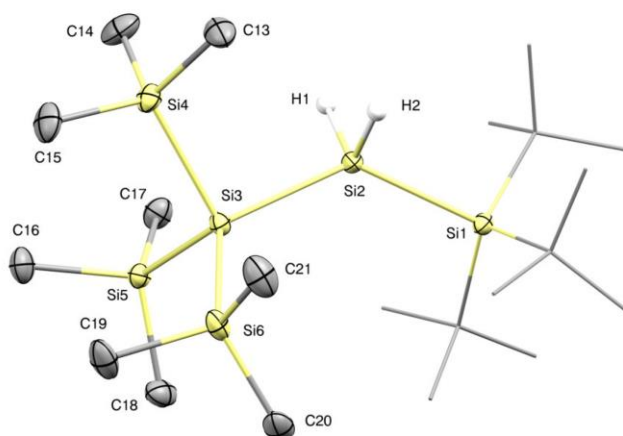


**Figure S66.** Molecular structure of **1** with ellipsoids set at 50% probability. Hydrogen atoms are omitted for clarity, except for the Si–H nuclei. Selected bond lengths [Å] and angles [°]: Si1–Si2 2.369(1), Si2–Si3 2.350(1), Si3–Si4 2.364(1), Si3–Si5 2.356(1), Si3–Si6 2.351(1); Si1–Si2–Si3 132.1(1), Si2–Si3–Si4 99.0(1), Si2–Si3–Si5 113.6(1), Si2–Si3–Si6 118.9(1), Si4–Si3–Si5 106.3(1), Si4–Si3–Si6 108.2(1), Si5–Si3–Si6 109.5(1).

Table S1. Crystal data and structure refinement for compound 1.

<b>Chemical formula</b>	C <sub>21</sub> H <sub>56</sub> Si <sub>6</sub>	
<b>Formula weight</b>	477.19 g/mol	
<b>Temperature</b>	100(2) K	
<b>Wavelength</b>	0.71073 Å	
<b>Crystal size</b>	0.231 × 0.278 × 0.384 mm	
<b>Crystal habit</b>	clear colourless fragment	
<b>Crystal system</b>	orthorhombic	
<b>Space group</b>	P 21 21 21	
<b>Unit cell dimensions</b>	a = 9.4966(3) Å	α = 90°
	b = 13.7852(5) Å	β = 90°
	c = 24.0165(9) Å	γ = 90°
<b>Volume</b>	3144.06(19) Å <sup>3</sup>	
<b>Z</b>	4	
<b>Density (calculated)</b>	1.008 g/cm <sup>3</sup>	
<b>Absorption coefficient</b>	0.272 mm <sup>-1</sup>	
<b>F(000)</b>	1064	
<b>Diffractometer</b>	Bruker D8 Venture Duo IMS	
<b>Radiation source</b>	IMS microsource, Mo	
<b>Theta range for data collection</b>	2.25 to 25.02°	
<b>Index ranges</b>	-11 ≤ h ≤ 11, -16 ≤ k ≤ 16, -28 ≤ l ≤ 28	
<b>Reflections collected</b>	72550	
<b>Independent reflections</b>	5546 [R(int) = 0.0601]	
<b>Coverage of independent reflections</b>	99.9%	
<b>Absorption correction</b>	Multi-Scan	
<b>Max. and min. transmission</b>	0.9400 and 0.9030	
<b>Refinement method</b>	Full-matrix least-squares on F <sup>2</sup>	
<b>Refinement program</b>	SHELXL-2014/7 (Sheldrick, 2014)	
<b>Function minimized</b>	Σ w(F <sub>o</sub> <sup>2</sup> - F <sub>c</sub> <sup>2</sup> ) <sup>2</sup>	
<b>Data / restraints / parameters</b>	5546 / 0 / 271	
<b>Goodness-of-fit on F<sup>2</sup></b>	1.046	
<b>Δ/σ<sub>max</sub></b>	0.001	
<b>Final R indices</b>	5293 data; I > 2σ(I)	R1 = 0.0236, wR2 = 0.0572
	all data	R1 = 0.0259, wR2 = 0.0581
<b>Weighting scheme</b>	w = 1/[σ <sup>2</sup> (F <sub>o</sub> <sup>2</sup> ) + (0.0328P) <sup>2</sup> + 0.5764P] where P = (F <sub>o</sub> <sup>2</sup> + 2F <sub>c</sub> <sup>2</sup> )/3	
<b>Largest diff. peak and hole</b>	0.266 and -0.188 eÅ <sup>-3</sup>	
<b>R.M.S. deviation from mean</b>	0.036 eÅ <sup>-3</sup>	

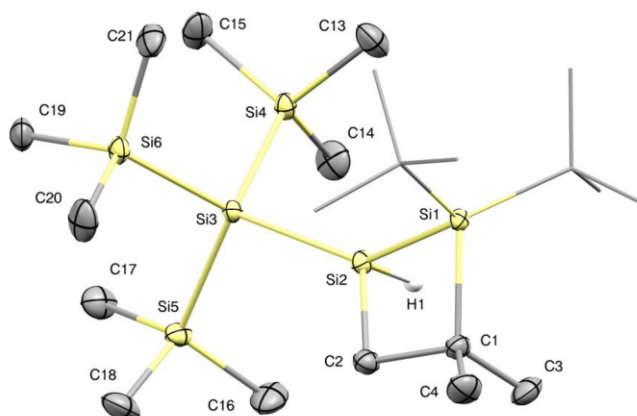


**Figure S67.** Molecular structure of **4** with ellipsoids set at 50% probability. Hydrogen atoms are omitted for clarity, except for the Si–H nucleus. Selected bond lengths [Å] and angles [°]: Si1–Si2 2.345(1), Si1–C1 1.957(2), C1–C2 1.572(2), Si2–C2 1.916(2), Si2–Si3 2.346(1); C1–Si1–Si2 76.3(1), Si1–Si2–C2 76.6(1), Si1–C1–C2 97.3(1), C1–C2–Si2 99.7(1).

Table S2. Crystal data and structure refinement for compound 4.

<b>Chemical formula</b>	C <sub>21</sub> H <sub>34</sub> Si <sub>6</sub>	
<b>Formula weight</b>	475.17 g/mol	
<b>Temperature</b>	100(2) K	
<b>Wavelength</b>	0.71073 Å	
<b>Crystal size</b>	0.116 × 0.157 × 0.166 mm	
<b>Crystal habit</b>	clear colourless fragment	
<b>Crystal system</b>	monoclinic	
<b>Space group</b>	P 1 21/n 1	
<b>Unit cell dimensions</b>	a = 12.4962(10) Å	α = 90°
	b = 14.8445(10) Å	β = 108.895(3)°
	c = 17.5284(14) Å	γ = 90°
<b>Volume</b>	3076.3(4) Å <sup>3</sup>	
<b>Z</b>	4	
<b>Density (calculated)</b>	1.026 g/cm <sup>3</sup>	
<b>Absorption coefficient</b>	0.278 mm <sup>-1</sup>	
<b>F(000)</b>	1056	
<b>Diffractometer</b>	Bruker D8 Venture	
<b>Radiation source</b>	TXS rotating anode, Mo	
<b>Theta range for data collection</b>	2.42 to 25.03°	
<b>Index ranges</b>	-14 ≤ h ≤ 14, -17 ≤ k ≤ 17, -20 ≤ l ≤ 20	
<b>Reflections collected</b>	55818	
<b>Independent reflections</b>	5430 [R(int) = 0.0490]	
<b>Coverage of independent reflections</b>	99.9%	
<b>Absorption correction</b>	Multi-Scan	
<b>Max. and min. transmission</b>	0.9690 and 0.9550	
<b>Refinement method</b>	Full-matrix least-squares on F <sup>2</sup>	
<b>Refinement program</b>	SHELXL-2014/7 (Sheldrick, 2014)	
<b>Function minimized</b>	Σ w(F <sub>o</sub> <sup>2</sup> - F <sub>c</sub> <sup>2</sup> ) <sup>2</sup>	
<b>Data / restraints / parameters</b>	5430 / 0 / 265	
<b>Goodness-of-fit on F<sup>2</sup></b>	1.037	
<b>Δ/σ<sub>max</sub></b>	0.001	
<b>Final R indices</b>	4777 data; I > 2σ(I)	R1 = 0.0282, wR2 = 0.0661
	all data	R1 = 0.0348, wR2 = 0.0692
<b>Weighting scheme</b>	w = 1/[σ <sup>2</sup> (F <sub>o</sub> <sup>2</sup> ) + (0.0267P) <sup>2</sup> + 2.0069P] where P = (F <sub>o</sub> <sup>2</sup> + 2F <sub>c</sub> <sup>2</sup> )/3	
<b>Largest diff. peak and hole</b>	0.732 and -0.272 eÅ <sup>-3</sup>	
<b>R.M.S. deviation from mean</b>	0.043 eÅ <sup>-3</sup>	

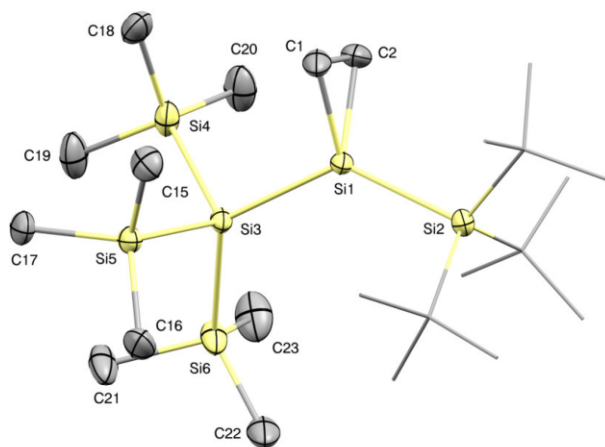


**Figure S68.** Molecular structure of **5** with ellipsoids set at 50% probability. Hydrogen atoms are omitted for clarity. Selected bond lengths [Å] and angles [°]: Si1–C1 1.885(2), Si1–C2 1.890(2), C1–C2 1.542(3), Si1–Si2 2.372(1), Si1–Si3 2.371(1); Si1–C1–C2 66.1(1), C1–C2–Si1 65.7(1), C2–Si1–C1 48.2(1).



Table S3. Crystal data and structure refinement for compound 5.

<b>Chemical formula</b>	C <sub>23</sub> H <sub>38</sub> Si <sub>6</sub>	
<b>Formula weight</b>	503.23 g/mol	
<b>Temperature</b>	100(2) K	
<b>Wavelength</b>	0.71073 Å	
<b>Crystal size</b>	0.108 × 0.204 × 0.288 mm	
<b>Crystal habit</b>	clear colourless fragment	
<b>Crystal system</b>	orthorhombic	
<b>Space group</b>	F d d 2	
<b>Unit cell dimensions</b>	a = 31.226(4) Å	α = 90°
	b = 33.796(4) Å	β = 90°
	c = 12.2692(14) Å	γ = 90°
<b>Volume</b>	12948(3) Å <sup>3</sup>	
<b>Z</b>	16	
<b>Density (calculated)</b>	1.033 g/cm <sup>3</sup>	
<b>Absorption coefficient</b>	0.267 mm <sup>-1</sup>	
<b>F(000)</b>	4480	
<b>Diffractometer</b>	Bruker D8 Venture Duo IMS	
<b>Radiation source</b>	IMS microsource, Mo	
<b>Theta range for data collection</b>	2.41 to 25.35°	
<b>Index ranges</b>	-37 ≤ h ≤ 37, -40 ≤ k ≤ 40, -14 ≤ l ≤ 14	
<b>Reflections collected</b>	40402	
<b>Independent reflections</b>	5919 [R(int) = 0.0269]	
<b>Coverage of independent reflections</b>	99.9%	
<b>Absorption correction</b>	Multi-Scan	
<b>Max. and min. transmission</b>	0.9720 and 0.9370	
<b>Refinement method</b>	Full-matrix least-squares on F <sup>2</sup>	
<b>Refinement program</b>	SHELXL-2014/7 (Sheldrick, 2014)	
<b>Function minimized</b>	Σ w(F <sub>o</sub> <sup>2</sup> - F <sub>c</sub> <sup>2</sup> ) <sup>2</sup>	
<b>Data / restraints / parameters</b>	5919 / 1 / 280	
<b>Goodness-of-fit on F<sup>2</sup></b>	1.072	
<b>Δ/σ<sub>max</sub></b>	0.002	
<b>Final R indices</b>	5870 data; I > 2σ(I)	R1 = 0.0180, wR2 = 0.0484
	all data	R1 = 0.0182, wR2 = 0.0485
<b>Weighting scheme</b>	w = 1/[σ <sup>2</sup> (F <sub>o</sub> <sup>2</sup> ) + (0.0283P) <sup>2</sup> + 6.4105P] where P = (F <sub>o</sub> <sup>2</sup> + 2F <sub>c</sub> <sup>2</sup> )/3	
<b>Largest diff. peak and hole</b>	0.226 and -0.135 eÅ <sup>-3</sup>	
<b>R.M.S. deviation from mean</b>	0.035 eÅ <sup>-3</sup>	

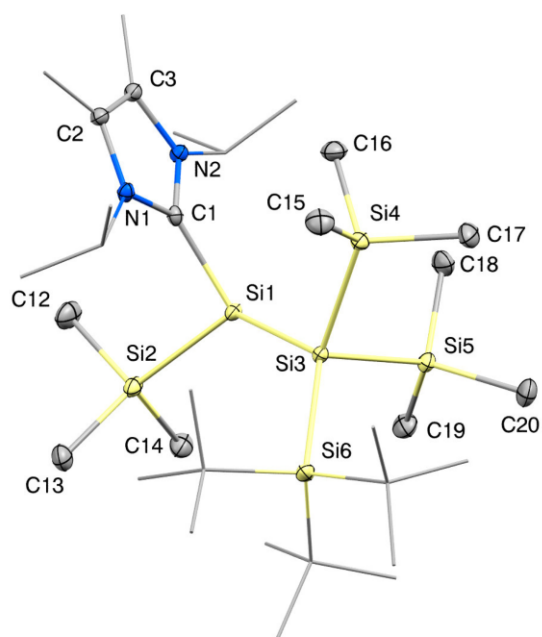


**Figure S69.** Molecular structure of **13** with ellipsoids set at 50% probability. Hydrogen atoms are omitted for clarity. Selected bond lengths [Å] and angles [°]: Si1–Si2 2.360(1), Si1–Si3 2.437(1), Si1–C1 1.961(2); C1–Si1–Si2 99.3(1), C1–Si1–Si3 115.6(1), Si2–Si1–Si3 126.0(1).

## 15. Appendix

Table S4. Crystal data and structure refinement for compound 13.

<b>Chemical formula</b>	C <sub>32</sub> H <sub>74</sub> N <sub>2</sub> Si <sub>6</sub>	
<b>Formula weight</b>	655.47 g/mol	
<b>Temperature</b>	100(2) K	
<b>Wavelength</b>	0.71073 Å	
<b>Crystal size</b>	0.096 × 0.139 × 0.162 mm	
<b>Crystal habit</b>	purple-red fragment	
<b>Crystal system</b>	triclinic	
<b>Space group</b>	P -1	
<b>Unit cell dimensions</b>	a = 11.3385(4) Å	α = 90.739(2)°
	b = 12.1541(4) Å	β = 97.371(2)°
	c = 16.6351(6) Å	γ = 116.9890(10)°
<b>Volume</b>	2019.35(12) Å <sup>3</sup>	
<b>Z</b>	2	
<b>Density (calculated)</b>	1.078 g/cm <sup>3</sup>	
<b>Absorption coefficient</b>	0.229 mm <sup>-1</sup>	
<b>F(000)</b>	728	
<b>Diffractometer</b>	Bruker D8 Venture	
<b>Radiation source</b>	TXS rotating anode, Mo	
<b>Theta range for data collection</b>	2.22 to 25.03°	
<b>Index ranges</b>	-13 ≤ h ≤ 13, -14 ≤ k ≤ 14, -19 ≤ l ≤ 19	
<b>Reflections collected</b>	43501	
<b>Independent reflections</b>	7143 [R(int) = 0.0466]	
<b>Coverage of independent reflections</b>	99.9%	
<b>Absorption correction</b>	Multi-Scan	
<b>Max. and min. transmission</b>	0.9780 and 0.9640	
<b>Refinement method</b>	Full-matrix least-squares on F <sup>2</sup>	
<b>Refinement program</b>	SHELXL-2014/7 (Sheldrick, 2014)	
<b>Function minimized</b>	Σ w(F <sub>o</sub> <sup>2</sup> - F <sub>c</sub> <sup>2</sup> ) <sup>2</sup>	
<b>Data / restraints / parameters</b>	7143 / 0 / 385	
<b>Goodness-of-fit on F<sup>2</sup></b>	1.044	
<b>Δ/σ<sub>max</sub></b>	0.001	
<b>Final R indices</b>	6168 data; I > 2σ(I)	R1 = 0.0306, wR2 = 0.0678
	all data	R1 = 0.0393, wR2 = 0.0711
<b>Weighting scheme</b>	w = 1/[σ <sup>2</sup> (F <sub>o</sub> <sup>2</sup> ) + (0.0220P) <sup>2</sup> + 1.3289P] where P = (F <sub>o</sub> <sup>2</sup> + 2F <sub>c</sub> <sup>2</sup> )/3	
<b>Largest diff. peak and hole</b>	0.328 and -0.271 eÅ <sup>-3</sup>	
<b>R.M.S. deviation from mean</b>	0.045 eÅ <sup>-3</sup>	

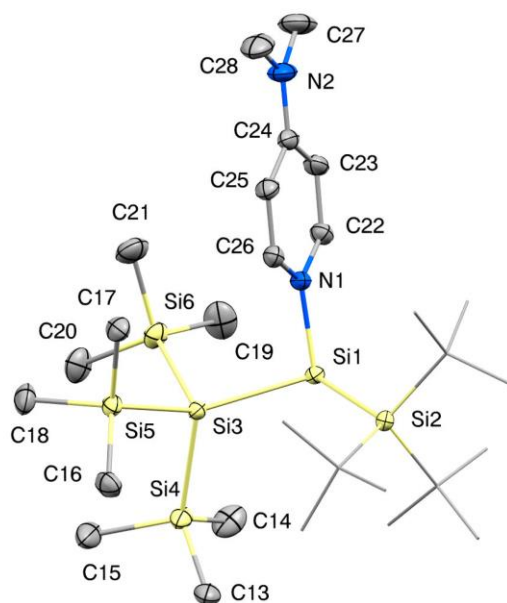


**Figure S70.** Molecular structure of **14** with ellipsoids set at 50% probability. Hydrogen atoms and solvent molecules are omitted for clarity. Selected bond lengths [Å] and angles [°]: Si1–Si2 2.433(1), Si1–Si3 2.420(1), Si1–N1 1.942(2); N1–Si1–Si2 104.5(1), N1–Si1–Si3 98.1(1), Si2–Si1–Si3 116.1(1).

Table S5. Crystal data and structure refinement for compound 14.

<b>Chemical formula</b>	C <sub>28</sub> H <sub>64</sub> N <sub>2</sub> Si <sub>6</sub>	
<b>Formula weight</b>	597.34 g/mol	
<b>Temperature</b>	100(2) K	
<b>Wavelength</b>	0.71073 Å	
<b>Crystal size</b>	0.188 × 0.261 × 0.306 mm	
<b>Crystal habit</b>	clear orange-red fragment	
<b>Crystal system</b>	triclinic	
<b>Space group</b>	P -1	
<b>Unit cell dimensions</b>	a = 11.8830(19) Å	α = 94.596(6)°
	b = 12.9036(19) Å	β = 105.116(5)°
	c = 15.496(3) Å	γ = 110.563(5)°
<b>Volume</b>	2108.6(6) Å <sup>3</sup>	
<b>Z</b>	2	
<b>Density (calculated)</b>	1.054 g/cm <sup>3</sup>	
<b>Absorption coefficient</b>	0.222 mm <sup>-1</sup>	
<b>F(000)</b>	740	
<b>Diffractometer</b>	Bruker D8 Venture	
<b>Radiation source</b>	TXS rotating anode, Mo	
<b>Theta range for data collection</b>	2.30 to 25.66°	
<b>Index ranges</b>	-14 ≤ h ≤ 14, -15 ≤ k ≤ 15, -18 ≤ l ≤ 18	
<b>Reflections collected</b>	82436	
<b>Independent reflections</b>	7972 [R(int) = 0.0755]	
<b>Coverage of independent reflections</b>	99.6%	
<b>Absorption correction</b>	Multi-Scan	
<b>Max. and min. transmission</b>	0.9590 and 0.9340	
<b>Refinement method</b>	Full-matrix least-squares on F <sup>2</sup>	
<b>Refinement program</b>	SHELXL-2014/7 (Sheldrick, 2014)	
<b>Function minimized</b>	Σ w(F <sub>o</sub> <sup>2</sup> - F <sub>c</sub> <sup>2</sup> ) <sup>2</sup>	
<b>Data / restraints / parameters</b>	7972 / 180 / 436	
<b>Goodness-of-fit on F<sup>2</sup></b>	1.038	
<b>Δ/σ<sub>max</sub></b>	0.005	
<b>Final R indices</b>	7075 data; I > 2σ(I)	R1 = 0.0358, wR2 = 0.0920
	all data	R1 = 0.0407, wR2 = 0.0950
<b>Weighting scheme</b>	w = 1/[σ <sup>2</sup> (F <sub>o</sub> <sup>2</sup> ) + (0.0391P) <sup>2</sup> + 1.4350P] where P = (F <sub>o</sub> <sup>2</sup> + 2F <sub>c</sub> <sup>2</sup> )/3	
<b>Largest diff. peak and hole</b>	0.335 and -0.380 eÅ <sup>-3</sup>	
<b>R.M.S. deviation from mean</b>	0.051 eÅ <sup>-3</sup>	

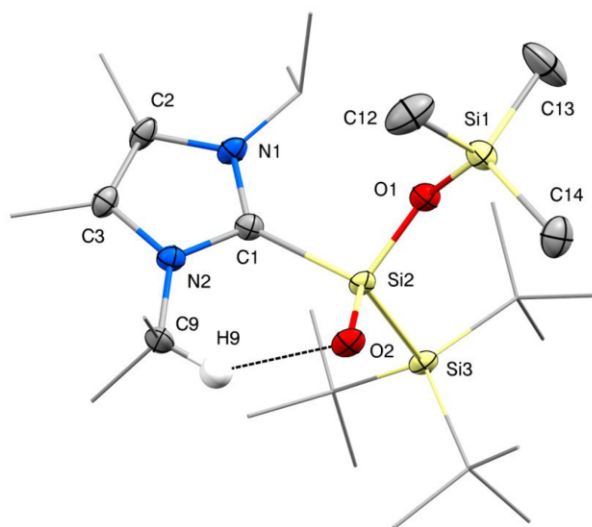


**Figure S71.** Molecular structure of **17** with ellipsoids set at 50% probability. Hydrogen atoms, except for H9 involved in hydrogen bonding (visualized by the dashed line), are omitted for clarity. Selected bond lengths [Å] and angles [°]: Si1–O1 1.641(2), Si2–O2 1.556(2), Si2–O1 1.655(3), Si2–Si3 2.415(1), Si2–C1 1.984(3); O2–Si2–O1 115.5(1), O2–Si2–C1 106.9(1), O1–Si2–C1 101.2(1), O2–Si2–Si3 111.7(1), O1–Si2–Si3 107.0(1), C1–Si2–Si3 114.3(1).

Table S6. Crystal data and structure refinement for compound 17.

<b>Chemical formula</b>	C <sub>26</sub> H <sub>56</sub> N <sub>2</sub> O <sub>2</sub> Si <sub>3</sub>	
<b>Formula weight</b>	513.00 g/mol	
<b>Temperature</b>	100(2) K	
<b>Wavelength</b>	0.71073 Å	
<b>Crystal size</b>	0.334 × 0.458 × 0.527 mm	
<b>Crystal habit</b>	clear pale brown fragment	
<b>Crystal system</b>	orthorhombic	
<b>Space group</b>	P n a 21	
<b>Unit cell dimensions</b>	a = 17.0644(9) Å	α = 90°
	b = 10.4534(6) Å	β = 90°
	c = 18.0274(9) Å	γ = 90°
<b>Volume</b>	3215.7(3) Å <sup>3</sup>	
<b>Z</b>	4	
<b>Density (calculated)</b>	1.060 g/cm <sup>3</sup>	
<b>Absorption coefficient</b>	0.170 mm <sup>-1</sup>	
<b>F(000)</b>	1136	
<b>Diffractometer</b>	Bruker D8 Venture Duo IMS	
<b>Radiation source</b>	IMS microsource, Mo	
<b>Theta range for data collection</b>	2.25 to 25.02°	
<b>Index ranges</b>	-20 ≤ h ≤ 20, -12 ≤ k ≤ 12, -21 ≤ l ≤ 20	
<b>Reflections collected</b>	90131	
<b>Independent reflections</b>	5615 [R(int) = 0.0660]	
<b>Coverage of independent reflections</b>	100.0%	
<b>Absorption correction</b>	Multi-Scan	
<b>Max. and min. transmission</b>	0.9450 and 0.9160	
<b>Refinement method</b>	Full-matrix least-squares on F <sup>2</sup>	
<b>Refinement program</b>	SHELXL-2014/7 (Sheldrick, 2014)	
<b>Function minimized</b>	Σ w(F <sub>o</sub> <sup>2</sup> - F <sub>c</sub> <sup>2</sup> ) <sup>2</sup>	
<b>Data / restraints / parameters</b>	5615 / 1 / 317	
<b>Goodness-of-fit on F<sup>2</sup></b>	1.085	
<b>Final R indices</b>	5362 data; I > 2σ(I)	R1 = 0.0352, wR2 = 0.0860
	all data	R1 = 0.0376, wR2 = 0.0877
<b>Weighting scheme</b>	w = 1/[σ <sup>2</sup> (F <sub>o</sub> <sup>2</sup> ) + (0.0388P) <sup>2</sup> + 2.1487P] where P = (F <sub>o</sub> <sup>2</sup> + 2F <sub>c</sub> <sup>2</sup> )/3	
<b>Largest diff. peak and hole</b>	0.404 and -0.222 eÅ <sup>-3</sup>	
<b>R.M.S. deviation from mean</b>	0.048 eÅ <sup>-3</sup>	



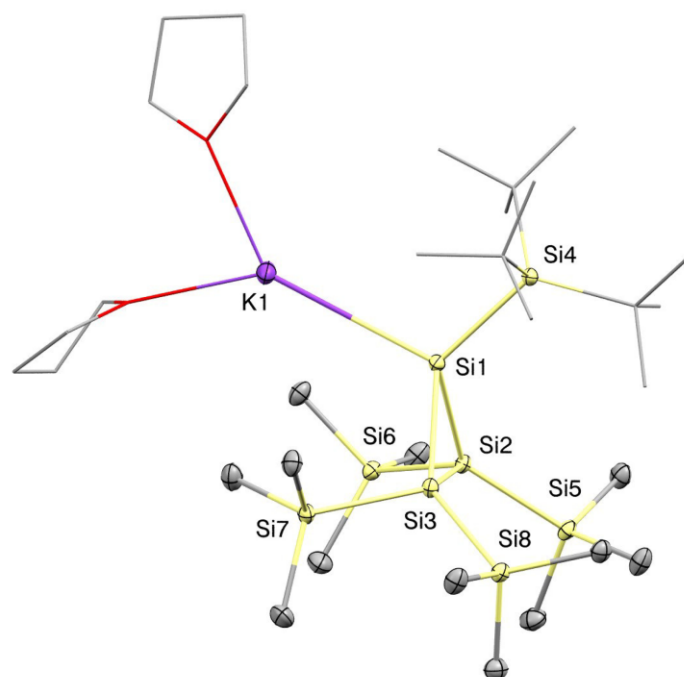


**Figure S72.** Molecular structure of **19** with ellipsoids set at 50% probability. Hydrogen atoms are omitted for clarity. Selected bond lengths [Å] and angles [°]: K1–Si1 3.465(1), Si1–Si2 2.364(1), Si1–Si3 2.364(1), Si1–Si4 2.378(1), Si2–Si3 2.358(1), Si2–Si5 2.357(1), Si2–Si6 2.348(1), Si3–Si7 2.342(1), Si3–Si8 2.367(1); Si2–Si1–Si3 59.8(1), Si2–Si1–Si4 123.6(1), Si2–Si1–K1 116.4(1), Si3–Si1–Si4 122.3(1), Si3–Si1–K1 115.6(1), Si4–Si1–K1 110.7(1).

Table S7. Crystal data and structure refinement for compound 19.

<b>Chemical formula</b>	C <sub>32</sub> H <sub>79</sub> KO <sub>2</sub> Si <sub>8</sub>	
<b>Formula weight</b>	759.76 g/mol	
<b>Temperature</b>	100(2) K	
<b>Wavelength</b>	0.71073 Å	
<b>Crystal size</b>	0.217 × 0.286 × 0.293 mm	
<b>Crystal habit</b>	clear colourless fragment	
<b>Crystal system</b>	monoclinic	
<b>Space group</b>	P 21/n	
<b>Unit cell dimensions</b>	a = 14.4278(13) Å	α = 90°
	b = 21.935(2) Å	β = 91.076(3)°
	c = 14.7814(14) Å	γ = 90°
<b>Volume</b>	4677.1(7) Å <sup>3</sup>	
<b>Z</b>	4	
<b>Density (calculated)</b>	1.079 g/cm <sup>3</sup>	
<b>Absorption coefficient</b>	0.343 mm <sup>-1</sup>	
<b>F(000)</b>	1672	
<b>Diffractometer</b>	Bruker D8 Venture Duo IMS	
<b>Radiation source</b>	IMS microsource, Mo	
<b>Theta range for data collection</b>	2.20 to 25.03°	
<b>Index ranges</b>	-17 ≤ h ≤ 17, -26 ≤ k ≤ 26, -17 ≤ l ≤ 17	
<b>Reflections collected</b>	184640	
<b>Independent reflections</b>	8263 [R(int) = 0.0510]	
<b>Coverage of independent reflections</b>	99.9%	
<b>Absorption correction</b>	Multi-Scan	
<b>Max. and min. transmission</b>	0.9290 and 0.9060	
<b>Refinement method</b>	Full-matrix least-squares on F <sup>2</sup>	
<b>Refinement program</b>	SHELXL-2014/7 (Sheldrick, 2014)	
<b>Function minimized</b>	Σ w(F <sub>o</sub> <sup>2</sup> - F <sub>c</sub> <sup>2</sup> ) <sup>2</sup>	
<b>Data / restraints / parameters</b>	8263 / 0 / 409	
<b>Goodness-of-fit on F<sup>2</sup></b>	1.039	
<b>Final R indices</b>	7411 data; I > 2σ(I)	R1 = 0.0242, wR2 = 0.0552
	all data	R1 = 0.0296, wR2 = 0.0575
<b>Weighting scheme</b>	w = 1/[σ <sup>2</sup> (F <sub>o</sub> <sup>2</sup> ) + (0.0236P) <sup>2</sup> + 2.5040P] where P = (F <sub>o</sub> <sup>2</sup> + 2F <sub>c</sub> <sup>2</sup> )/3	
<b>Largest diff. peak and hole</b>	0.284 and -0.200 eÅ <sup>-3</sup>	
<b>R.M.S. deviation from mean</b>	0.039 eÅ <sup>-3</sup>	

### 3. DFT Calculations

#### General Information

Geometry optimizations and harmonic frequency calculations were performed using *Gaussian09*<sup>[S17]</sup> employing the M06-2X/6-31+G(d,p)<sup>[S18]</sup> level of density functional theory. The SMD polarizable continuum model was used to account for solvent effects of benzene.<sup>[S19]</sup> The “ultrafine” grid option was used for numerical integrations.<sup>[S20]</sup> Stationary points are characterized as minima by analysis of computed Hessians. The connectivity between minima and transition states was validated by IRC calculations<sup>[S21]</sup> or displacing the geometry along the transition mode, followed by unconstrained optimization. For improved energies, single point calculations were conducted at the SMD-M06-2X/6-311+G(d,p)<sup>[S22]</sup> level of theory; wave functions used for bonding analysis were obtained at the M06-2X/6-311++G(2d,2p) level.<sup>[S22]</sup> Natural Bond Orbital (NBO) and Natural Resonance Theory (NRT) analyses were performed using the *NBO 6.0* program<sup>[S23]</sup>, interfaced with *Gaussian09*<sup>[S24]</sup>. NMR chemical shift values were calculated using the Gauge-Independent Atomic Orbital (GIAO) method implemented in *Gaussian09* and the M06-L<sup>[S25]</sup> functional along with the 6-311G(2d,p) basis set and the SMD solvent model for the structures obtained at the M06-2X/6-31+G(d,p) level of theory. <sup>29</sup>Si {<sup>1</sup>H} NMR spectroscopic chemical shifts  $\delta$  are reported in ppm relative to tetramethylsilane ( $\delta(^{29}\text{Si}(\text{SiMe}_4)) = 0$  ppm). Pictures of molecular structures were generated with the ChemCraft<sup>[S26]</sup>, Cylview<sup>[S27]</sup> or GaussView<sup>[S28]</sup> programs.

## Comparison of calculated and experimental structures

**Table S8.** Comparison of selected bond lengths [Å] and angles [°] for the computed and experimental structures of **4**, **5**, **13**, **14** and **17**. Geometries are calculated at the M06-2X/6-31+G(d,p) level of theory. Experimental data are taken from SC-XRD analyses.

Compound	bond/angle	exp.	calc.	$\Delta(\text{calc.-exp.})$
<b>4</b>	Si1–Si2	2.345(1)	2.35	0.01
	Si1–C1	1.957(2)	1.96	0.00
	C1–C2	1.572(2)	1.57	0.00
	Si2–C2	1.916(2)	1.93	0.01
	Si2–Si3	2.346(1)	2.34	0.01
	C1–Si1–Si2	76.3(1)	76.5	0.20
	Si1–Si2–C2	76.6(1)	76.3	0.30
	Si1–C1–C2	97.3(1)	97.3	0.00
	C1–C2–Si2	99.7(1)	99.8	0.10
<b>5</b>	Si1–C1	1.885(2)	1.89	0.01
	Si1–C2	1.890(2)	1.90	0.01
	C1–C2	1.542(3)	1.53	0.01
	Si1–Si2	2.372(1)	2.36	0.01
	Si1–Si3	2.371(1)	2.36	0.01
	Si1–C1–C2	66.1(1)	66.3	0.20
	C1–C2–Si1	65.7(1)	66.1	0.40
	C2–Si1–C1	48.2(1)	47.5	0.70
<b>13</b>	Si1–Si2	2.360(1)	2.36	0.00
	Si1–Si3	2.437(1)	2.42	0.02
	Si1–C1	1.961(2)	1.99	0.03
	C1–Si1–Si2	99.3(1)	99.1	0.20
	C1–Si1–Si3	115.6(1)	112.6	3.00
	Si2–Si1–Si3	126.0(1)	125.4	0.60
	<b>14</b>	Si1–Si2	2.433(1)	2.43
Si1–Si3		2.420(1)	2.42	0.00
Si1–N1		1.942(2)	1.99	0.05
N1–Si1–Si2		104.5(1)	101.8	2.70
N1–Si1–Si3		98.1(1)	93.3	4.80
Si2–Si1–Si3		116.1(1)	116.0	0.10
<b>17</b>	Si1–O1	1.641(2)	1.68	0.04
	Si2–O2	1.556(2)	1.57	0.01
	Si2–O1	1.655(3)	1.68	0.03
	Si2–Si3	2.415(1)	2.39	0.02
	Si2–C1	1.984(3)	2.01	0.02
	O2–Si2–O1	115.5(1)	115.7	0.20
	O2–Si2–C1	106.9(1)	105.1	1.80
	O1–Si2–C1	101.2(1)	99.7	1.50
	O2–Si2–Si3	111.7(1)	114.4	2.70
	O1–Si2–Si3	107.0(1)	107.4	0.40
	C1–Si2–Si3	114.3(1)	113.8	0.50

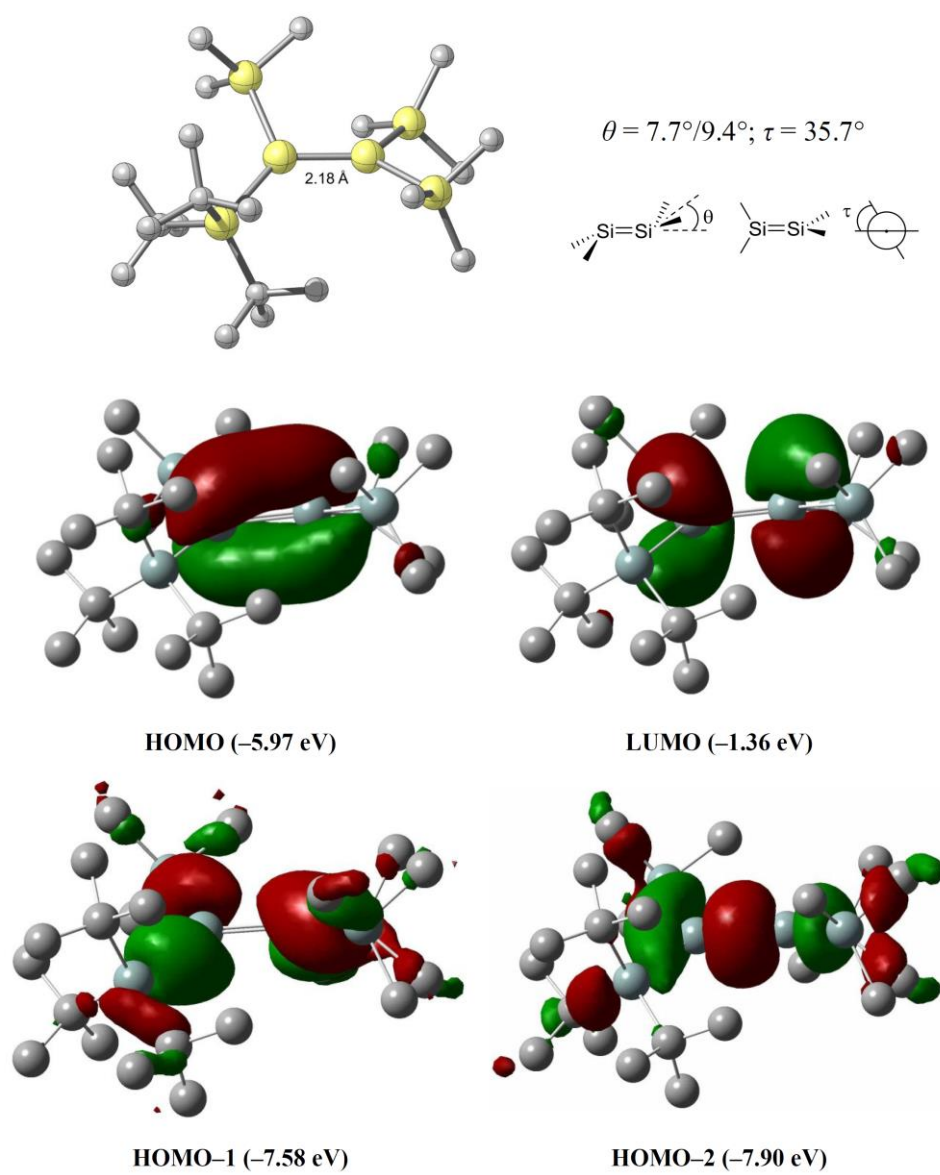
Calculated  $^{29}\text{Si}\{^1\text{H}\}$  NMR Resonances

Table S9. Comparison of experimental and calculated NMR chemical shifts.

Compound	Si	Exp. $\delta(^{29}\text{Si})$ [ppm]	Calc. $\delta(^{29}\text{Si})$ [ppm]	$\Delta\delta$ [ppm]
3'	$\underline{\text{Si}}\text{TMS}_2$	161.9	162.5	0.6
	$\underline{\text{Si}}(\text{TMS})\text{Si}^t\text{Bu}_3$	132.4	140.5	8.1
	$\underline{\text{Si}}^t\text{Bu}_3$	31.7	22.4	9.3
	$\underline{\text{TMS}}$	-6.8	-6.3	0.5
	$\underline{\text{TMS}}$	-7.7	-7.2	0.5
4	$\underline{\text{Si}}^t\text{Bu}_2$	35.6	21.8	13.8
	$\underline{\text{TMS}}$	-9.2	-10.2	1.0
	$\underline{\text{Si}}\text{H}$	-60.4	-59.8	0.6
	$\underline{\text{Si}}(\text{TMS})_3$	-133.8	-143.9	10.1
5	$\underline{\text{Si}}^t\text{Bu}_3$	20.2	7.4	12.8
	$\underline{\text{TMS}}$	-8.3	-9.4	1.1
	$\underline{\text{Si}}(\text{TMS})_3$	-113.7	-124.8	11.1
	$\underline{\text{Si}}\text{CH}_2\text{CH}_2$	-164.3	-162.1	2.2
6	$\underline{\text{Si}}^t\text{Bu}_3$	29.6	23.2	6.4
	$\underline{\text{TMS}}$	-11.5	-11.0	0.5
	$\underline{\text{TMS}}$	-12.2	-13.9	1.7
	$\underline{\text{TMS}}$	-12.9	-14.5	1.6
	$\underline{\text{Si}}\text{NH}_2$	-35.7	-36.8	0.9
	$\underline{\text{Si}}\text{H}$	-119.9	-116.6	3.3
13	$\underline{\text{Si}}^t\text{Bu}_3$	29.4	18.2	11.2
	$\underline{\text{TMS}}$	-9.1	-11.6	2.5
	$\underline{\text{TMS}}$	-11.9	-12.6	0.7
	<i>silylene Si</i>	-104.7	-109.6	4.9
	$\underline{\text{Si}}(\text{TMS})_2$	-117.4	-128.8	11.4
14	<i>silylene Si</i>	68.8	75.0	6.2
	$\underline{\text{Si}}^t\text{Bu}_3$	20.4	9.7	10.7
	$\underline{\text{TMS}}$	-9.3	-9.5	0.2
	$\underline{\text{Si}}(\text{TMS})_3$	-121.6	-126.9	5.3
15	$\underline{\text{Si}}^t\text{Bu}_3$	31.2	23.5	7.7
	$\underline{\text{TMS}}$	-9.9	-9.3	0.6
	$\underline{\text{Si}}(\text{TMS})_3$	-115.2	-117.5	2.3
	<i>silylene Si</i>	-120.6	-127.4	6.8
16	$\underline{\text{Si}}^t\text{Bu}_3$	30.6	22.1	8.5
	$\underline{\text{TMS}}$	-9.2	-9.6	0.4
	$\underline{\text{TMS}}$	-11.4	-10.5	0.9
	<i>silylene Si</i>	-117.1	-115.2	1.8
	$\underline{\text{Si}}(\text{TMS})_2$	-118.9	-132.7	13.8
17	$\underline{\text{Si}}^t\text{Bu}_3$	6.6	8.0	1.4
	$\underline{\text{TMS}}$	-3.4	-10.6	7.2
	$\underline{\text{Si}}=\text{O}$	-50.8	-50.8	0.0

**Tetrasilyldisilene 3': Calculated structure, comparison and NMR shifts**

A huge number of stable disilenes has already been reported up to date<sup>[S29]</sup>, but to the best of our knowledge none of the type  $ABSi=SiA_2$  ( $A, B =$  different silyl groups) is known. The calculated structure of **3'** has Si=Si bond length of 2.18 Å, located on the lower limit for silyl-substituted disilenes:  $d_{(Si-Si)} = 2.19-2.26$  Å.<sup>[S30]</sup> It further exhibits a bent and twisted structure (Figure S73). Reported disilenes have shown to have either a bent or a twisted geometry, with the distortion mode being mainly determined by the size and shape of the silyl substituents. There are only two examples with both distortions reported: (*E*)-[('Bu<sub>2</sub>MeSi)<sub>2</sub>MeSi]('Bu<sub>2</sub>MeSi)Si=SiMe(SiMe'Bu<sub>2</sub>) and (*Z*)-('BuN)(TMS<sub>3</sub>Si)Si=Si(SiTMS<sub>3</sub>)('BuN).<sup>[S31]</sup> With regard to a comparable huge difference in the steric demand of the silyl groups in **3'**, we assume the calculated structure to be reasonable. The calculated NMR shifts are in good agreement with other tetrasilyl-substituted disilenes<sup>[S30]</sup> as well as with the measured experimental values (Table S9). The splitting of the NMR signals between the two sp<sup>2</sup> hybridized Si atoms is only slightly higher than in known A<sub>2</sub>Si=SiB<sub>2</sub> disilenes ( $A, B =$  different silyl groups).<sup>[S30]</sup> For completion, relaxed potential energy scans of the dihedral angle revealed **3'** as the global minimum with several other local minima located at least 2.5 kcal/mol higher in energy in addition to non-matching NMR shifts.



**Figure S73.** Calculated molecular structure of tetrasilyldisilene 3' with its frontier orbitals and their corresponding energy values; *trans*-bent angle  $\theta$  and twist angle  $\tau$ .



**Table S10.** Calculated transitions and UV-Vis absorption bands using TD-DFT (time-dependent-DFT).

Wavelength [nm]	MO contributions	Transition	f	Contribution
467.3	HOMO→LUMO	$\pi \rightarrow \pi^*$	0.1109	95.7%
334.9	HOMO-1→LUMO	$\sigma(\text{silyl}) \rightarrow \pi^*$	0.0571	86.5%
332.9	HOMO-2→LUMO	$\sigma(\text{silyl}) \rightarrow \pi^*$	0.0030	90.5%

**Bis(silyl)silylenes 3/3'': calculated structures**

The donor-free silylene **3** has a singlet-triplet energy gap  $\Delta E_{S-T}$  of 2.5 kcal/mol, higher than the value calculated for silylene **3''** (0.6 kcal/mol). This is also reflected in an increase of the Si-Si-Si bond angle at the silylene center. Only the most stable conformer is reported in each case.

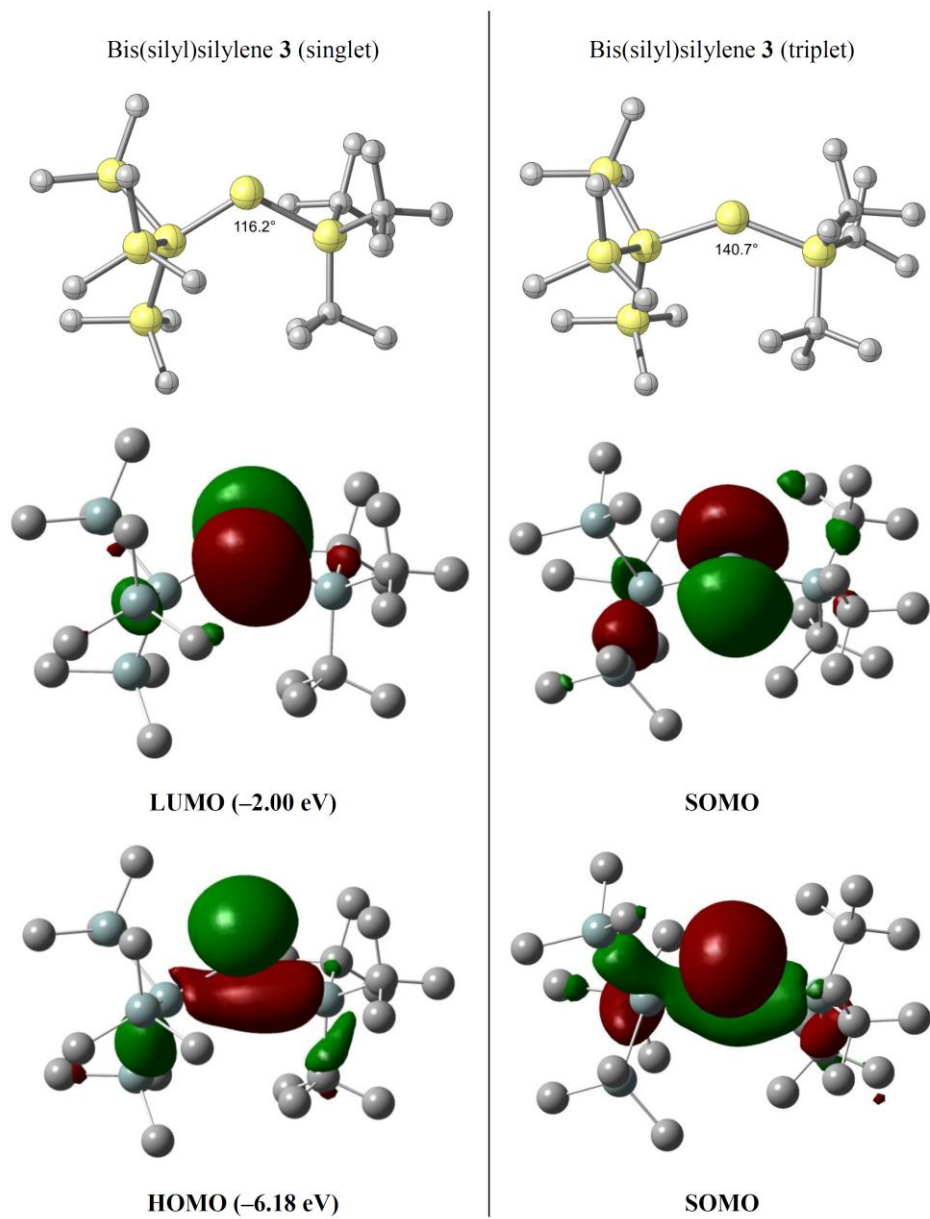


Figure S74. Calculated molecular structures of bis(silyl)silylenes 3 with their corresponding frontier orbitals.

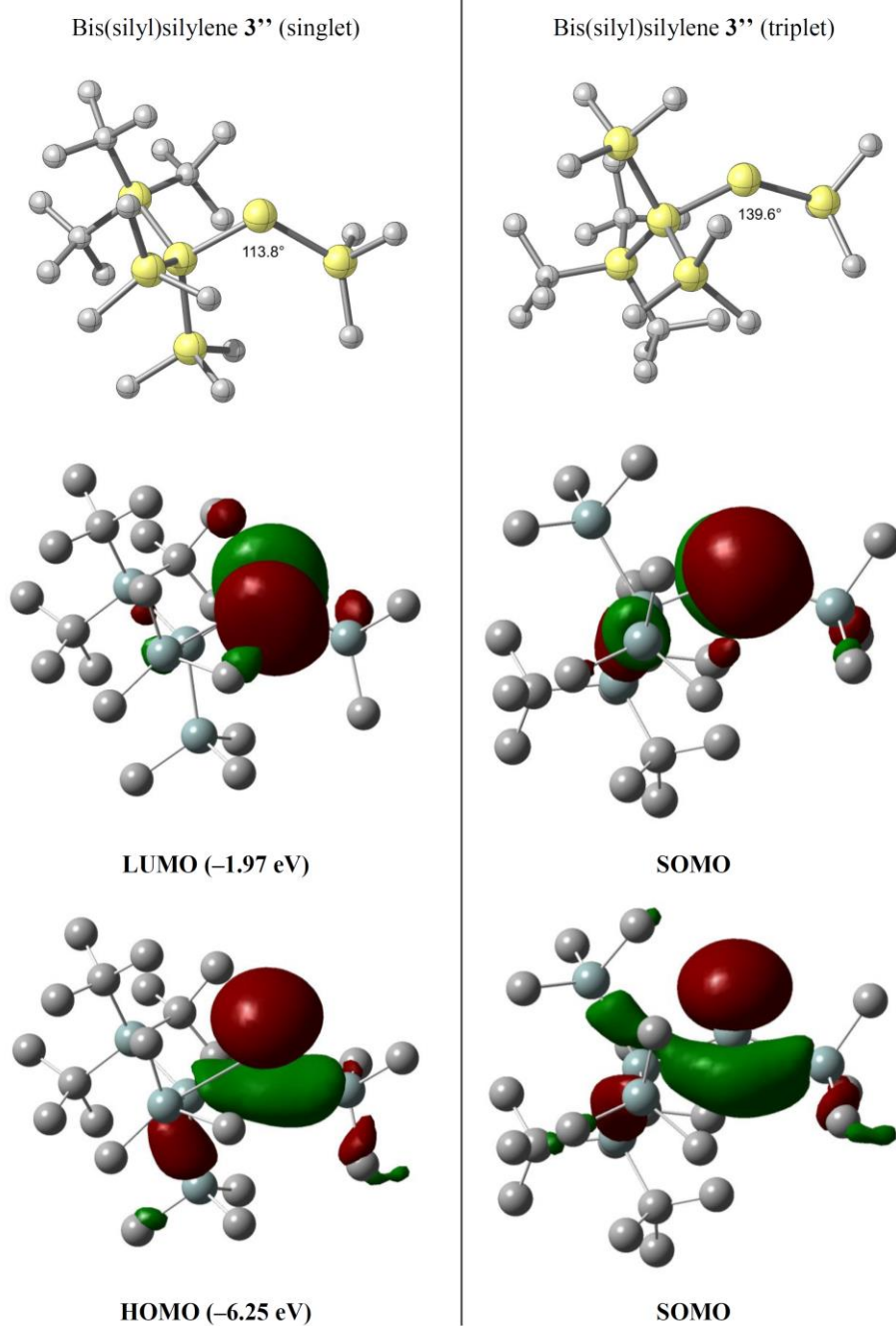
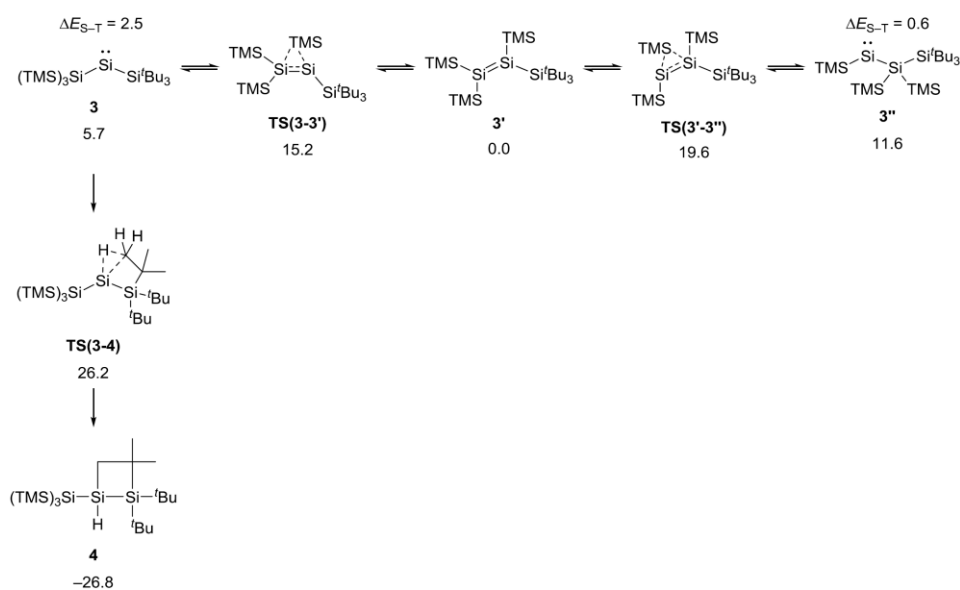


Figure S75. Calculated molecular structures of bis(silyl)silylenes **3''** with their corresponding frontier orbitals.

**Mechanism for the interconversion between the silylenes **3** and **3''**, disilene **3'** and the C–H activation product (disiletane **4**) at 298 K**

Based on recent reports on reactions of silyl-substituted silylenes occurring on the singlet potential energy surface<sup>[S32]</sup>, only pathways occurring from the singlet silylenes have been investigated. As shown in Figure S68, rearrangement of **3'** (the most stable isomer) to **3** is accompanied with a barrier of 15.2 kcal/mol to yield **3** located 5.7 kcal/mol higher in energy. The effective barrier for the migration of the second TMS group to give **3''** is slightly higher with 19.6 kcal/mol. Thus, all isomerization reactions can be described as reactions in equilibrium with **3'** being the kinetic product. Decomposition of **3** *via* C–H activation, providing the thermodynamic product **4**, possesses an effective barrier of 26.2 kcal/mol, thus being in line with the experimentally observed reaction time of 4 days at r.t. for full conversion to **4**. Accordingly, we have proven the intermediacy of disilene **3'** as the kinetic product, which gives access to the very reactive bis(silyl)silyene **3**.



**Figure S76.** Computed pathway for the silylene-disilene-silylene interconversion at 298 K; the Gibbs Free energies  $\Delta G_{298}$  and the singlet-triplet energy gap  $\Delta E_{S-T}$  are reported in kcal/mol.

### Mechanism for the interconversion between the silylenes **3** and **3''**, disilene **3'** and the C–H activation product (disiletane **4**) at 133 K

In addition to the computed pathway for the silylene-disilene-silylene interconversion at 298 K, we calculated the same at 133 K, since we also performed EPR spectroscopy at this temperature. Here, we obtained comparable results with only slightly different energy values and effective barriers.

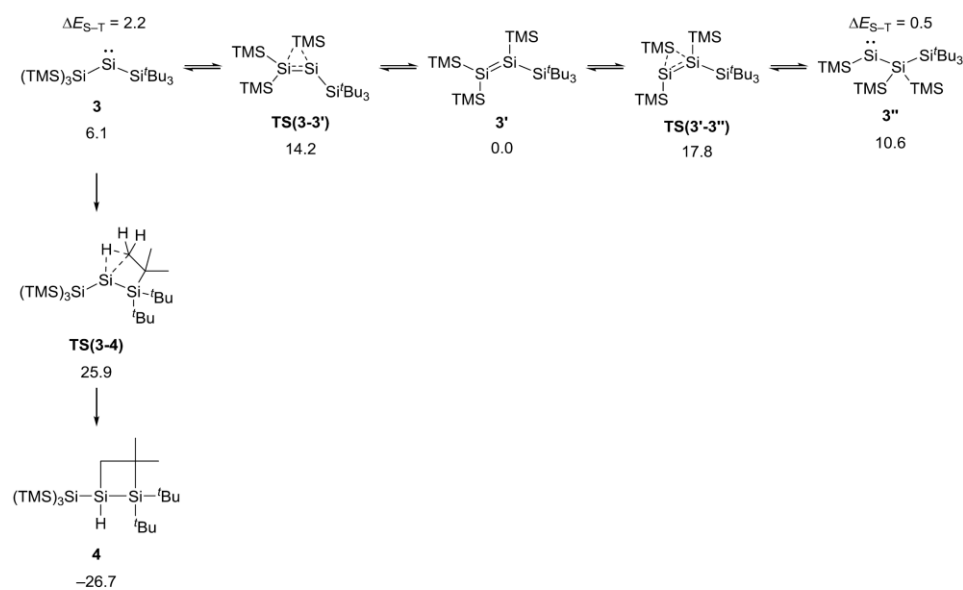


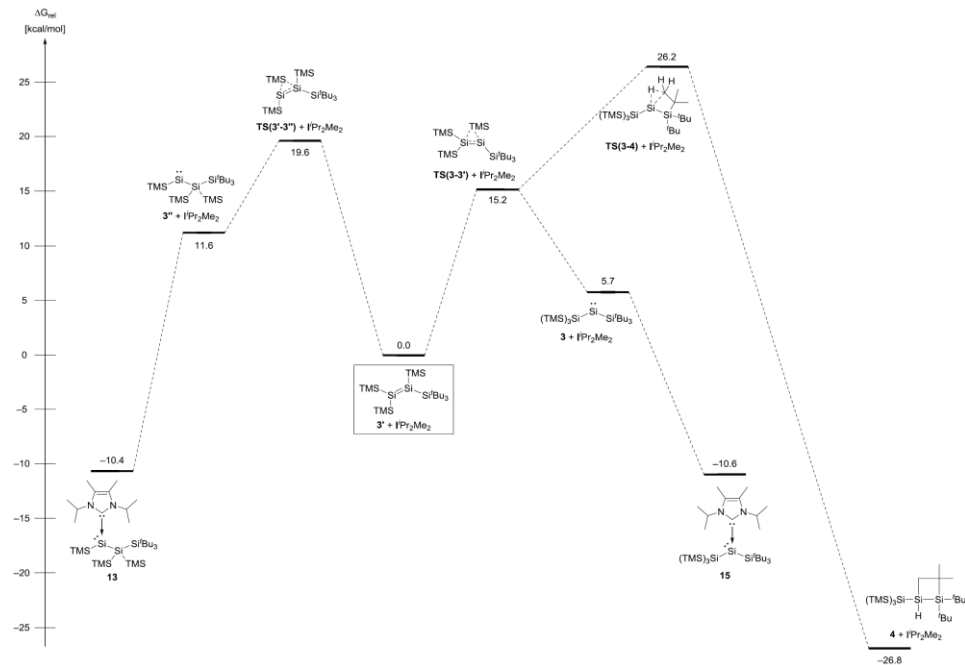
**Figure S77.** Computed pathway for the silylene-disilene-silylene interconversion at 133 K; the Gibbs Free energies  $\Delta G_{133}$  and the singlet-triplet energy gap  $\Delta E_{S-T}$  are reported in kcal/mol.

### Bond dissociation energies for all Lewis base-stabilized silylenes

**Table S11.** Calculated bond dissociation energies for all plausible donor-stabilized bis(silyl)silylenes.

Compound	$\Delta G_{298}$ [kcal/mol]*	$D^0(0)$ [kcal/mol]*	$\Delta G_{298}^{\text{iso}}$ [kcal/mol]	$\Delta G_{298}^{\text{base}}$ [kcal/mol]
<b>15</b> ( <b>3</b> · $\text{I}^t\text{Pr}_2\text{Me}_2$ )	16.3	44.6	0.0	0.0
<b>13</b> ( <b>3''</b> · $\text{I}^t\text{Pr}_2\text{Me}_2$ )	22.0	47.4	0.3	0.3
<b>3</b> · $\text{IMe}_4$	22.5	47.6	0.0	-6.2
<b>16</b> ( <b>3''</b> · $\text{IMe}_4$ )	27.6	50.7	0.9	-5.4
<b>14</b> ( <b>3</b> ·DMAP)	15.3	33.5	0.0	1.0
<b>3''</b> ·DMAP	17.4	33.1	3.8	4.9

\* all dissociation energies are referenced to the singlet ground state of the corresponding donor-free silylene;  
 $\Delta G_{298}^{\text{iso}}$  relative energy between the respective two isomeric Lewis base-stabilized silylenes;  
 $\Delta G_{298}^{\text{base}}$  relative energy between all donor-stabilized silylenes, referenced to **15**.

Rearrangement of  $\text{IPr}_2\text{Me}_2$ -stabilized bis(silyl)silylene **13**

**Figure S78.** Computed pathway for the interconversion of the  $\text{IPr}_2\text{Me}_2$ -stabilized silylenes **13** and **15** at 298 K.

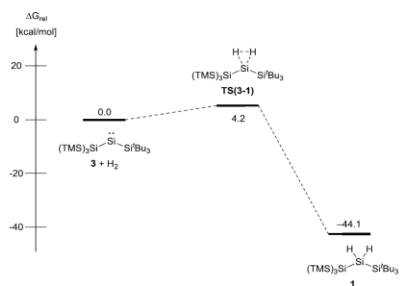


**Figure S79.** Computed pathway for the dihydrogen activation by singlet bis(silyl)silylene **3**.

### Calculated IR Stretching Frequencies

**Table S12.** Selected experimentally determined and theoretically calculated IR frequencies.

Compound	Mode	Exp. $\tilde{\nu}$ [cm <sup>-1</sup> ]	Calc. $\tilde{\nu}$ [cm <sup>-1</sup> ]
17	<i>Si–O sym. stretch</i>	1069	1118
	<i>Si–O–Si asym. stretch</i>	971	948

### Bonding analysis of the NHC-stabilized silanoic ester 17

There had been a lot of discussion in the community recently, concerning the formulation of Lewis structures with dative bonds or with a zwitterionic representation.<sup>[S33]</sup> We know that this is also the case for **17**, but for consistency, all structural representations in this report are given with dative C<sub>NHC</sub>–Si bonds. Possible multiple bonding in four-coordinate silanoic esters and related thioesters has already been discussed in detail by Driess, Apeloig and co-workers in a combined theoretical and solid state NMR study.<sup>[S34]</sup> In contrast to their study, our silanoic ester **17** bears solely silyl substituents and one coordinating NHC. Thus, the NHC-stabilized silanoic ester **17** is prone for a more detailed investigation of its bonding situation.

**Table S13.** Selected results of the NBO analysis of the NHC-stabilized silanoic ester **17**.

Bond in <b>17</b>	NBO analysis (NLMOs) <sup>[a]</sup>		WBI
	pol.	hybr.	
Si <sup>2</sup> –Si <sup>3</sup>	49% (Si <sup>2</sup> )	sp <sup>1.74</sup> (Si <sup>2</sup> )	0.85
	51% (Si <sup>3</sup> )	sp <sup>2.44</sup> (Si <sup>3</sup> )	
Si <sup>2</sup> –O <sup>2</sup>	16% (Si <sup>2</sup> )	sp <sup>2.75</sup> (Si <sup>2</sup> )	0.91
	84% (O <sup>2</sup> )	sp <sup>1.02</sup> (O <sup>2</sup> )	
Si <sup>2</sup> –O <sup>1</sup>	12% (Si <sup>2</sup> )	sp <sup>3.85</sup> (Si <sup>2</sup> )	0.47
	88% (O <sup>1</sup> )	sp <sup>1.40</sup> (O <sup>1</sup> )	
Si <sup>2</sup> –C <sup>1</sup>	19% (Si <sup>2</sup> )	sp <sup>4.60</sup> (Si <sup>2</sup> )	0.54
	81% (C <sup>1</sup> )	sp <sup>1.34</sup> (C <sup>1</sup> )	

### Comparison to calculated less sterically encumbered silanoic ester derivatives

We calculated a collection of model systems with (**E-H**) and without (**A-D**) coordination of a stabilizing NHC as well as varying the number and position of silyl substituents. All model systems, as well as **17**, contain highly polarized Si–O bonds, whereas the WBIs of the Si<sup>2</sup>–O<sup>2</sup> bond within the series **A-D** and **E-H** show only minor dependency on the substituents. Nevertheless, within **A-D** a less pronounced polarization of the Si<sup>2</sup>–O<sup>2</sup> bond upon R<sup>3</sup> bearing a silyl group can be identified,

S78



clearly evident by decrease of the difference of NPA charges  $\Delta q(\text{Si}^2\text{O}^2)$ . Furthermore, silyl groups at  $\text{R}^1$  clearly increase the polarization of the  $\text{Si}^2\text{-O}^1$  bond. Coordination of a NHC in **E-H** decreases the WBI of both Si-O bonds as expected, however polarizations of the  $\text{Si}^2\text{-O}^2$  bond remain unchanged and only slightly reduced for  $\text{Si}^2\text{-O}^1$ . Comparison of model **A** to its NHC-stabilized congener **E** revealed quite similar polarization ( $\Delta q(\text{Si}^2\text{O}^2)$  and  $\Delta q(\text{Si}^2\text{O}^1)$ ) for both Si-O bonds upon NHC coordination.

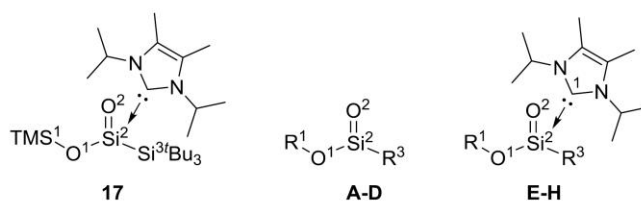


**Figure S80.** NHC-stabilized silanoic ester **17** and investigated simple donor-free and NHC-supported derivatives.

**Table S14.** Calculated structural parameters for the comparison of **17** with the smaller model systems **A-H**.

Compound	$\text{R}^1/\text{R}^3$	$q(\text{Si}^2)$	$q(\text{O}^2)$	$q(\text{O}^1)$	$\Delta q(\text{Si}^2\text{O}^2)$	$\Delta q(\text{Si}^2\text{O}^1)$	WBI( $\text{Si}^2\text{O}^2$ )	WBI( $\text{Si}^2\text{O}^1$ )
<b>17</b>	TMS/ $\text{Si}^i\text{Bu}_3$	1.79	-1.36	-1.34	3.15	3.13	0.91	0.47
<b>A</b>	$\text{SiH}_3/\text{SiH}_3$	1.83	-1.17	-1.28	3.00	3.11	1.30	0.61
<b>B</b>	$\text{CH}_3/\text{CH}_3$	2.19	-1.19	-0.94	3.38	3.13	1.27	0.65
<b>C</b>	$\text{CH}_3/\text{SiH}_3$	1.81	-1.18	-0.94	2.99	2.75	1.28	0.65
<b>D</b>	$\text{SiH}_3/\text{CH}_3$	2.21	-1.18	-1.27	3.39	3.48	1.29	0.62
<b>E</b>	$\text{SiH}_3/\text{SiH}_3$	1.74	-1.28	-1.29	3.02	3.03	1.04	0.52
<b>F</b>	$\text{CH}_3/\text{CH}_3$	2.09	-1.30	-0.95	3.39	3.04	1.04	0.53
<b>G</b>	$\text{CH}_3/\text{SiH}_3$	1.74	-1.29	-0.96	3.03	2.70	1.04	0.54
<b>H</b>	$\text{SiH}_3/\text{CH}_3$	2.09	-1.29	-1.28	3.38	3.37	1.04	0.52

The same situation is also present in our silanoic ester **17**, although both WBIs are further decreased to 0.47 and 0.91 for the two Si-O bonds. Aiming on an explanation for the differences in the Si-O bond lengths for **17**, we used NBO analysis. Accordingly, the natural localized molecular orbitals (NLMOs, Figure S71), corresponding to the  $\sigma(\text{Si}^2\text{-Si}^3)$ ,  $\sigma(\text{Si}^2\text{-O}^1)$ ,  $\sigma(\text{Si}^2\text{-O}^2)$  and  $\sigma(\text{Si}^2\text{-C}^1)$  bonds, as well as three NLMOs, representing the electron lone pairs at  $\text{O}^2$ , are consistent with the zwitterionic representation as the major resonance structure within NRT analysis (Table S15). This analysis further revealed negative hyperconjugation of the lone pairs at  $\text{O}^2$  into the  $\sigma^*(\text{Si}^2\text{-C}^1)$  and  $\sigma^*(\text{Si}^2\text{-O}^1)$ . Both antibonding orbitals are partly populated ( $\text{Si}^2\text{-C}^1$ : 0.12 e,  $\text{Si}^2\text{-O}^1$ : 0.13 e) with decreased occupancy of the  $\text{LP}(\text{O}^2)$  NBOs (1.83 e, 1.87 e). These results clearly rationalize the results found within SC-XRD structure: a short  $\text{Si}^2\text{-O}^2$  bond length, being in the range of a Si=O double bond, and an elongated  $\text{Si}^2\text{-O}^1$  bond, located on the upper end of reported Si-O single

bonds, together with an elongated  $C_{\text{NHC}}\text{-Si}$  bond. All in all, the bonding situation of our silanoic ester can be summarized as following: **17** possesses a zwitterionic representation with two highly polarized  $\text{Si-O}$  bonds and additional weakened  $\text{Si}^2\text{-O}^1$  and  $\text{Si}^2\text{-C}^1$   $\sigma$  bonds by negative hyperconjugation. Thus, it is not astonishing that **17** possesses only limited thermal stability and is prone for the occurrence of side reactions.

**Table S15.** Results of NRT analysis of **17**.

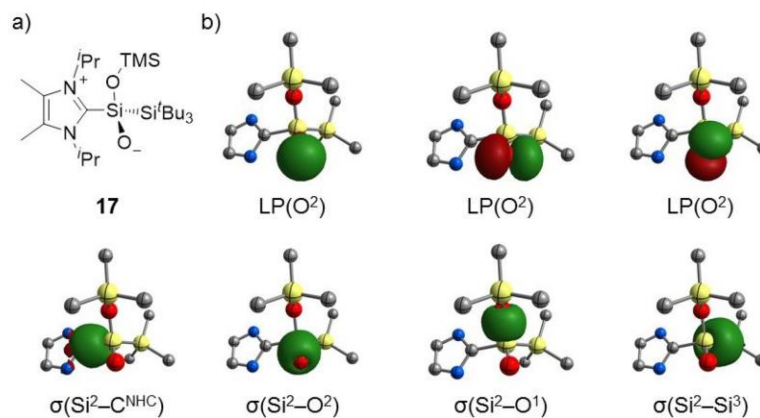
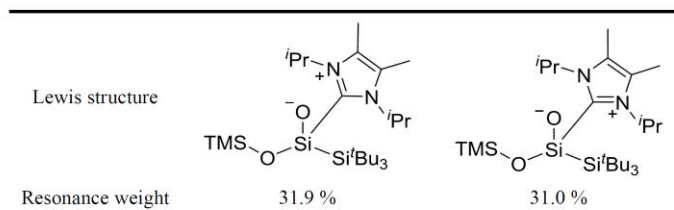


**Figure S81.** Results of the bonding analysis of **17**. (a) Dominant Lewis resonance structure according to NRT analysis; (b) NLMOs representing the electron lone pairs at  $\text{O}^2$  and the  $\text{C}_{\text{NHC}}\text{-Si}^2$ ,  $\text{Si}^2\text{-O}^1$ ,  $\text{Si}^2\text{-O}^2$ ,  $\text{Si}^2\text{-Si}^3$  bonds.

## 15. Appendix

### Calculated energies at the M06-2X/6-311+G(d,p)(SMD: benzene) level of theory

**Table S16.** DFT-derived energies for the respective analyzed compounds.

Structure	E(SCF) [H/particle]
<b>1</b>	-2570.803718
<b>TS(3-1)</b>	-2570.722088
<b>3 (singlet)</b>	-2568.908465
<b>3 (triplet)</b>	-2568.912373
<b>TS(3-4)</b>	-2568.875705
<b>TS(3-3')</b>	-2568.893194
<b>3'</b>	-2568.917479
<b>TS(3'-3'')</b>	-2568.886242
<b>3'' (singlet)</b>	-2568.899001
<b>3'' (triplet)</b>	-2568.899965
<b>4</b>	-2568.960237
<b>5</b>	-2647.494162
<b>6</b>	-2625.496807
<b>13</b>	-3109.279400
<b>14</b>	-2951.000770
<b>15</b>	-3109.279819
<b>16</b>	-2952.175198
<b>3''·DMAP</b>	-2950.994669
<b>3''·IME<sub>4</sub></b>	-2952.176611
<b>17</b>	-2152.162045
<b>IME<sub>4</sub></b>	-383.232221
<b>I'Pr<sub>2</sub>Me<sub>2</sub></b>	-540.345382
<b>DMAP</b>	-382.067974

### Cartesian coordinates (x,y,z) for the optimized structures

1	TS(3-1)	3 (singlet)
Si 2.56893 -0.01769 0.12410	Si -2.55727 0.00360 0.14027	Si 2.47938 -0.05132 0.09767
H 0.41078 1.34809 2.00641	H -0.48522 -1.49944 1.18760	Si 0.42074 -1.10324 0.75962
Si 0.46790 0.09189 1.19642	Si -0.43396 0.18045 1.20696	Si -1.55478 -0.04566 0.06096
H 0.47762 -1.00674 2.20927	H -0.38356 -1.16962 2.07720	Si -2.94912 -0.24307 1.96382
Si -1.64474 0.00353 0.14058	Si 1.67450 -0.01175 0.12703	Si -2.21260 1.95823 -1.00816
Si -2.96190 -0.69425 1.97177	Si 3.05226 0.17605 2.03741	Si -2.22928 -1.89831 -1.26928
Si -2.33456 2.18854 -0.40498	Si 2.27617 -2.01908 -0.94146	C 2.80727 0.97019 1.73859
Si -2.24383 -1.39956 -1.66160	Si 2.31223 1.77550 -1.26713	C 3.91811 2.02178 1.57850
C 3.88807 0.61779 1.40737	C -3.74763 -0.94601 1.36517	H 4.86827 1.57014 1.27499
C 3.84731 2.15068 1.53688	C -3.58954 -2.47173 1.23671	H 4.08636 2.52666 2.54080
H 4.18092 2.65781 0.62737	H -3.93719 -2.84928 0.27140	H 3.66680 2.79437 0.84744
H 4.52399 2.45855 2.34593	H -4.19449 -2.95994 2.01306	C 1.50688 1.67707 2.17466
H 2.84573 2.51638 1.79079	H -2.55256 -2.79893 1.37798	H 0.72580 0.95142 2.45366
C 3.59509 0.06101 2.81404	C -3.45520 -0.60231 2.83862	H 1.08530 2.33434 1.41048
H 3.60077 -1.02958 2.85714	H -3.49876 0.46750 3.04998	H 1.69824 2.28305 3.07162
H 2.62642 0.40810 3.19044	H -2.46919 -0.95774 3.15345	C 3.20643 0.05285 2.90944
H 4.36435 0.42223 3.51085	H -4.20121 -1.09867 3.47507	H 4.17877 -0.42243 2.75740
C 5.31895 0.21802 1.00420	C -5.22464 -0.61078 1.08067	H 2.46764 -0.73611 3.09200
H 5.58712 0.58147 0.00669	H -5.50953 -0.80958 0.04287	H 3.27870 0.65516 3.82602
H 5.46923 -0.86504 1.01735	H -5.46379 0.43296 1.30134	C 3.78726 -1.48657 -0.12196
H 6.03431 0.65345 1.71614	H -5.86570 -1.23181 1.72217	C 3.54971 -2.64083 0.87102
C 2.82679 -1.89863 -0.31289	C -3.04026 1.89266 -0.00482	H 4.33900 -3.39389 0.73635
C 3.21719 -2.72588 0.92518	C -3.37910 2.48103 1.37649	H 2.58862 -3.13518 0.69764
H 3.24386 -3.78898 0.64812	H -3.52529 3.56550 1.27720	H 3.57117 -2.32661 1.91621
H 2.48875 -2.61812 1.73630	H -2.56895 2.32290 2.09758	C 5.23231 -0.98724 0.06139
H 4.20570 -2.46887 1.31387	H -4.29950 2.06920 1.79796	H 5.47906 -0.15296 -0.60206
C 3.90974 -2.11037 -1.38502	C -4.23695 2.14251 -0.93978	H 5.93268 -1.80447 -0.16282
H 3.63719 -1.66638 -2.34676	H -4.00790 1.89068 -1.97948	H 5.43018 -0.66788 1.08887
H 4.05452 -3.18680 -1.55340	H -4.50255 3.20869 -0.91609	C 3.67223 -2.10859 -1.52525

S81

## 15. Appendix

H 4.87650 -1.69270 -1.08418  
 C 1.50020 -2.49977 -0.81532  
 H 1.07871 -1.96253 -1.66734  
 H 0.74441 -2.51163 -0.01977  
 H 1.66094 -3.54222 -1.12549  
 C 2.48652 1.11557 -1.45242  
 C 3.86445 1.41022 -2.06717  
 H 4.40817 0.49722 -2.33019  
 H 4.49843 1.99735 -1.39607  
 H 3.73772 1.99566 -2.98872  
 C 1.80404 2.45165 -1.10464  
 H 2.35080 3.04341 -0.36878  
 H 0.79059 2.28883 -0.71966  
 H 1.70954 3.06095 -2.01505  
 C 1.59770 0.46275 -2.52194  
 H 1.45840 1.16011 -3.36086  
 H 0.60318 0.23049 -2.12329  
 H 2.02367 -0.45714 -2.93282  
 C -2.28318 -2.29230 2.72458  
 H -2.11694 -3.06359 1.96558  
 H -2.99927 -2.68595 3.45531  
 H -1.33459 -2.11873 3.23985  
 C -2.91432 0.65105 3.30175  
 H -1.88313 0.89522 3.57877  
 H -3.43652 0.31164 4.20362  
 H -3.39822 1.57202 2.96009  
 C -4.76964 -1.02121 1.51374  
 H -5.23563 -0.16703 1.01323  
 H -5.33764 -1.22908 2.42818  
 H -4.86323 -1.89461 0.85972  
 C -4.21063 2.35238 -0.20472  
 H -4.52686 3.35282 -0.52263  
 H -4.51059 2.22495 0.84080  
 H -4.75679 1.61880 -0.80538  
 C -1.55008 3.46726 0.74660  
 H -0.46335 3.52642 0.63770  
 H -1.76536 3.22880 1.79361  
 H -1.96696 4.45812 0.53176  
 C -1.91338 2.59740 -2.20533  
 H -0.85270 2.44476 -2.42819  
 H -2.15932 3.64276 -2.42478  
 H -2.49300 1.96826 -2.88972  
 C -4.01931 -0.90369 -2.10588  
 H -4.04281 0.08593 -2.57486  
 H -4.68745 -0.88451 -1.24087  
 H -4.42177 -1.62240 -2.82966  
 C -1.29383 -1.24480 -3.29145  
 H -0.29276 -1.68120 -3.26238  
 H -1.20372 -0.20245 -3.61383  
 H -1.86930 -1.78234 -4.05504  
 C -2.26347 -3.21734 -1.14216  
 H -2.59449 -3.83794 -1.98287  
 H -2.95906 -3.38028 -0.31211  
 H -1.27514 -3.56881 -0.83076

### 3 (triplet)

Si -2.58012 0.03072 0.12361  
 Si -0.35244 0.19389 0.86002  
 Si 1.81936 0.02655 0.06243  
 Si 3.00954 -0.39703 2.04603  
 Si 2.19524 -1.75010 -1.42446  
 Si 2.54285 2.09079 -0.78935  
 C -3.32436 -1.54936 0.99225  
 C -4.68500 -1.94715 0.38996  
 H -5.41488 -1.13234 0.42299  
 H -5.10416 -2.78708 0.96140  
 H -4.59616 -2.27738 -0.64910  
 C -2.37554 -2.75787 0.87797  
 H -1.41511 -2.56685 1.37044  
 H -2.17082 -3.04746 -0.15484  
 H -2.83683 -3.62240 1.37526  
 C -3.52201 -1.30199 2.49822  
 H -4.29036 -0.55255 2.70571  
 H -2.59122 -0.98787 2.98626  
 H -3.84337 -2.23776 2.97585

H -5.12578 1.57679 -0.64379  
 C -1.84781 2.71193 -0.53385  
 H -1.53173 2.40348 -1.53102  
 H -0.97813 2.65087 0.13397  
 H -2.12897 3.77280 -0.59008  
 C -2.50568 -0.85739 -1.60783  
 C -3.90468 -1.14938 -2.17933  
 H -4.53819 -0.25898 -2.22942  
 H -4.43567 -1.90839 -1.59697  
 H -3.80434 -1.53961 -3.20191  
 C -1.72508 -2.17999 -1.54926  
 H -2.16652 -2.91890 -0.87740  
 H -0.69563 -2.00470 -1.22760  
 H -1.68923 -2.62665 -2.55340  
 C -1.74291 0.03170 -2.60342  
 H -1.59294 -0.51729 -3.54431  
 H -0.75046 0.29949 -2.21995  
 H -2.27791 0.95322 -2.84994  
 C 2.42004 1.53865 3.18517  
 H 2.30695 2.49249 2.65970  
 H 3.12852 1.68635 4.00862  
 H 1.44682 1.27552 3.60902  
 C 3.00288 -1.45861 2.99428  
 H 1.97342 -1.74299 3.23973  
 H 3.55459 -1.36119 3.93632  
 H 3.45388 -2.27755 2.42440  
 C 4.86053 0.57172 1.63564  
 H 5.29677 -0.13412 0.92246  
 H 5.45178 0.52988 2.55794  
 H 4.96197 1.58113 1.22276  
 C 4.15319 -2.24828 -0.81751  
 H 4.44994 -3.14599 -1.37266  
 H 4.47292 -2.37816 0.22166  
 H 4.69978 -1.39738 -1.23564  
 C 1.49928 -3.51511 -0.07999  
 H 0.40762 -3.53041 -0.14417  
 H 1.77566 -3.52833 0.98018  
 H 1.87548 -4.43906 -0.53439  
 C 1.83993 -2.00079 -2.78401  
 H 0.79045 -1.75463 -2.96900  
 H 2.04443 -2.97976 -3.23276  
 H 2.45493 -1.26013 -3.30741  
 C 4.05882 1.39680 -1.89665  
 H 4.04713 0.55571 -2.59830  
 H 4.75907 1.15772 -1.09184  
 H 4.44512 2.27074 -2.43452  
 C 1.27351 2.03904 -2.82513  
 H 0.27541 2.42810 -2.61027  
 H 1.16443 1.11310 -3.39951  
 H 1.78814 2.76986 -3.46057  
 C 2.36842 3.39243 -0.28851  
 H 2.63319 4.22508 -0.95012  
 H 3.12069 3.34206 0.50580  
 H 1.40392 3.62223 0.17591

### TS(3-4)

Si 2.60661 0.10179 0.02442  
 H 0.65283 2.27272 -0.33511  
 Si 0.48122 0.98013 0.48466  
 Si -1.63815 0.06589 0.06817  
 Si -2.19516 -0.87035 2.15395  
 Si -3.02153 1.96233 -0.15868  
 Si -2.26504 -1.42351 -1.64901  
 C 2.74949 1.53711 -1.28107  
 C 1.24875 1.64671 -1.60108  
 H 0.83827 0.83782 -2.20454  
 H 0.96385 2.60244 -2.06234  
 C 3.19102 2.88627 -0.68588  
 H 2.59184 3.18355 0.17906  
 H 3.07446 3.66452 -1.45383  
 H 4.24256 2.88072 -0.38587  
 C 3.60399 1.29464 -2.53233  
 H 4.66632 1.24243 -2.26349  
 H 3.48152 2.12690 -3.23952  
 H 3.35030 0.37383 -3.06012

H 3.96736 -1.41966 -2.32074  
 H 2.65391 -2.45879 -1.73694  
 H 4.33537 -2.98250 -1.58842  
 C 2.42645 1.08725 -1.48022  
 C 3.81433 1.49185 -2.00356  
 H 4.38502 0.63699 -2.37642  
 H 4.41739 1.99235 -1.23859  
 H 3.69702 2.19342 -2.84173  
 C 1.63777 2.36559 -1.16848  
 H 2.14041 3.01886 -0.45023  
 H 0.64821 2.11880 -0.77358  
 H 1.49474 2.94638 -2.09153  
 C 1.65158 0.37898 -2.60673  
 H 1.58959 1.04140 -3.48262  
 H 0.62535 0.15488 -2.29203  
 H 2.11459 -0.55397 -2.93508  
 C -2.29183 -1.53901 3.17110  
 H -2.12853 -2.50562 2.68522  
 H -3.00878 -1.67751 3.98896  
 H -1.33548 -1.22687 3.60389  
 C -2.99476 1.42016 2.86982  
 H -1.98552 1.76146 3.12495  
 H -3.56423 1.32313 3.80146  
 H -3.47147 2.20005 2.26713  
 C -4.73158 -0.70596 1.52031  
 H -5.17259 -0.00783 0.80297  
 H -5.34586 -0.69008 2.42846  
 H -4.79544 -1.71211 1.09437  
 C -1.70329 2.03876 -2.82773  
 H -2.20471 2.88546 -3.31077  
 H -1.99436 1.12723 -3.36125  
 H -0.62520 2.16843 -2.94994  
 C -4.10732 2.01173 -0.95493  
 H -4.45378 2.87986 -1.52853  
 H -4.47422 2.12535 0.07034  
 H -4.56816 1.11753 -1.38418  
 C -1.64298 3.52568 -0.10748  
 H -1.76638 3.42641 0.97568  
 H -2.26537 4.36564 -0.43820  
 H -0.60056 3.78494 -0.30725  
 C -3.84763 -1.52991 -2.17571  
 H -3.74968 -0.67329 -2.85040  
 H -4.66232 -1.32188 -1.47497  
 H -4.13140 -2.40155 -2.77739  
 C -0.91686 -2.30331 -2.57414  
 H 0.05670 -2.52340 -2.11778  
 H -0.77368 -1.47478 -3.27531  
 H -1.22040 -3.18559 -3.14968  
 C -2.47492 -3.44739 -0.21379  
 H -2.77660 -4.28212 -0.85759  
 H -3.25249 -3.31079 0.54371  
 H -1.55071 -3.72727 0.30146

### TS(3-3')

Si -0.24192 -1.07655 0.69185  
 Si 1.19206 -2.05129 -1.22810  
 Si 1.55670 0.15262 0.22067  
 Si 3.40794 -0.70999 1.41593  
 C 3.94858 0.17567 2.54653  
 H 4.75952 0.37242 3.19995  
 H 4.30805 1.59263 2.00104  
 H 3.11765 1.03201 3.18668  
 C 4.89361 -1.21790 0.35574  
 H 5.69099 -1.59459 1.00711  
 H 4.65243 -2.00342 -0.36612  
 H 5.29302 -0.36471 -0.20040  
 C 2.89048 -2.11611 2.56545  
 H 2.24781 -2.85534 2.08314  
 H 3.77824 -2.62560 2.95804  
 H 2.33110 -1.70277 3.41102  
 Si 2.32264 2.17914 -0.78708  
 C 4.20121 2.12455 -1.01891  
 H 4.49337 1.34401 -1.72880  
 H 4.52187 3.08736 -1.43510  
 H 4.75123 1.96531 -0.08820



## 15. Appendix

C -3.42130 1.67570 0.75261	C 3.90841 0.19420 1.45624	C 1.93741 3.58921 0.41675
C -2.96200 2.03587 2.17933	C 3.62960 1.40407 2.36461	H 2.39469 4.51473 0.04704
H -3.49122 2.94186 2.50595	H 2.63528 1.34810 2.82006	H 0.86361 3.76516 0.52708
H -1.88852 2.25448 2.21202	H 3.69813 2.35586 1.83375	H 2.34928 3.38587 1.41099
H -3.16665 1.25361 2.91272	H 4.37193 1.42514 3.17446	C 1.64280 2.57392 -2.50411
C -4.95829 1.57634 0.75228	C 5.32327 0.33897 0.86455	H 2.02925 1.86304 -3.24152
H -5.36308 1.30288 -0.22738	H 6.05844 0.40705 1.67876	H 0.55379 2.57662 -2.56528
H -5.38562 2.55171 1.02371	H 5.42510 1.24403 0.25771	H 2.00278 3.57113 -2.78676
H -5.32493 0.84983 1.48325	H 5.60432 -0.51454 0.24018	C -0.24374 -2.74724 -2.25189
C -3.01907 2.86820 -0.13379	C 3.88215 -1.05158 2.35600	H -0.80180 -1.97330 -2.78314
H -3.41561 2.79547 -1.14989	H 4.19538 -1.95741 1.82949	H 0.21299 -3.40673 -3.00196
H -1.92955 2.98058 -0.19397	H 2.88782 -1.22812 2.78331	H -0.93685 -3.34318 -1.65229
H -3.42030 3.79155 0.30603	H 4.57733 -0.90608 3.19428	C 2.08525 -3.57766 -0.56097
C -2.61812 -0.11618 -1.82077	C 2.51644 -1.65826 -0.78307	H 1.40974 -4.15900 0.07396
C -4.00907 0.20066 -2.40011	C 1.63310 -1.64709 -2.03883	H 2.36571 -4.19623 -1.42291
H -4.30047 1.24176 -2.23622	H 1.51283 -2.67522 -2.40996	H 2.99125 -3.36770 0.00894
H -4.79293 -0.43916 -1.98195	H 2.04378 -1.05468 -2.85986	C 2.29802 -1.24703 -2.55785
H -3.99505 0.03555 -3.48664	H 0.63565 -1.26637 -1.80069	H 1.75148 -0.44528 -3.06607
C -2.22940 -1.53298 -2.27562	C 3.90220 -2.20444 -1.16265	H 3.23163 -0.83311 -2.16384
H -2.96859 -2.28678 -1.99218	H 4.53312 -2.37927 -0.28614	H 2.55108 -2.00770 -3.30728
H -1.25620 -1.83766 -1.87451	H 4.44028 -1.52923 -1.83806	Si -2.32113 0.05534 0.20231
C -2.15179 -1.54919 -3.37197	H 3.78943 -3.16830 -1.67856	C -3.67983 -1.33359 -0.06158
C -1.59199 0.83691 -2.45823	C 1.82858 -2.63135 0.19284	C -2.36356 1.34768 -1.25858
H -1.62070 0.72521 -3.55188	H 1.74549 -3.62202 -0.27713	C -2.59078 0.94511 1.93619
H -0.57254 0.60405 -2.13049	H 0.81203 -2.29289 0.42728	C -3.77382 1.93103 1.91501
H -1.77995 1.88819 -2.23028	H 2.36538 -2.76058 1.13427	H -3.94033 2.31737 2.93089
C 2.31506 0.65581 3.45362	C -0.86676 -2.08504 2.73884	H -3.58150 2.79472 1.27219
H 2.30221 1.71995 3.19719	H -1.11528 -2.45847 3.73903	H -4.70718 1.46776 1.58372
H 2.91991 0.52873 4.35879	H 0.11685 -1.60407 2.79476	C -1.33873 1.72575 2.38836
H 1.28695 0.35617 3.68598	H -0.78167 -2.94641 2.06806	H -0.99177 2.45725 1.65518
C 2.82243 -2.21654 2.52569	C -2.32178 0.50540 3.44594	H -1.57461 2.27101 3.31320
H 1.76349 -2.49347 2.58392	H -2.50230 0.07624 4.43822	H -0.50040 1.05740 2.60961
H 3.27593 -2.40162 3.50602	H -3.14235 1.19528 3.22377	C -2.85866 -0.08967 3.04634
H 3.30704 -2.87868 1.80065	H -1.39581 1.08893 3.49000	H -2.06050 -0.83843 3.11348
C 4.84666 0.00013 1.82424	C -3.84345 -1.79692 2.08633	H -2.90310 0.42851 0.01463
H 5.27868 -0.55154 0.98278	H -3.79323 -2.65276 1.40468	H -3.80753 -0.61568 2.91737
H 5.40485 -0.26904 2.72815	H -4.65908 -1.14647 1.75422	C -3.78684 1.79279 -1.64109
H 5.00180 1.06868 1.64132	H -4.09760 -2.17690 3.08256	H -4.32951 2.22208 -0.79326
C 1.67425 -1.29892 -3.18511	C -2.36422 3.42325 0.84188	H -3.72713 2.56743 -2.41929
H 1.92392 -2.11488 -3.87307	H -2.19502 3.15221 1.88857	H -4.38938 0.97633 -2.04628
H 2.19683 -0.39898 -3.52777	H -3.08690 4.24711 0.81073	C -1.57703 2.60839 -0.87150
H 0.59880 -1.11162 -3.26002	H -1.41227 3.78403 0.44099	H -2.06561 3.18041 -0.07850
C 4.05145 -2.12405 -1.43725	C -4.78414 1.60235 0.43457	H -0.56477 2.36007 -0.53833
H 4.27672 -2.90512 -2.17246	H -5.22457 0.73925 -0.07337	H -1.49110 3.27181 -1.74440
H 4.38985 -2.47853 -0.45779	H -5.42343 2.47187 0.24193	C -1.68217 0.76163 -2.50782
H 4.63899 -1.23680 -1.69569	H -4.80523 1.40629 1.51175	H -2.20398 -0.11594 -2.89824
C 1.27832 -3.29975 -0.85425	C -3.09805 2.48782 -1.97704	H -1.66480 1.51597 -3.30820
H 1.60752 -3.59912 0.14611	H -2.09285 2.65286 -2.38072	H -0.64342 0.47539 -2.29881
H 1.47081 -4.13277 -1.53997	H -3.66074 3.42284 -2.07886	C -3.33565 -2.59697 0.75132
H 0.19700 -3.13881 -0.80858	H -3.58953 1.73182 -2.59822	H -4.14484 -3.33208 0.66363
C 4.23586 1.87542 -1.60802	C -4.16001 -1.42917 -1.70458	H -2.41133 -3.06458 0.39551
H 4.16223 1.23548 -2.49420	H -4.49868 -2.19582 -2.41166	H -3.21174 -2.40567 1.81986
H 4.96070 1.42185 -0.92420	H -4.55245 -0.46569 -2.04625	C -3.75086 -1.78299 -1.53197
H 4.63216 2.84577 -1.92806	H -4.60396 -1.64968 -0.72895	H -4.12914 -1.00347 -2.19782
C 1.34595 2.81008 -2.06062	C -1.69653 -0.89021 -3.37578	H -2.78041 -2.11276 -1.90947
H 0.36769 3.00208 -1.60679	H -1.92099 0.16669 -3.55212	H -4.43834 -2.63696 -1.61152
H 1.19652 2.13908 -2.91291	H -2.23967 -1.47635 -4.12661	C -5.09431 -0.87355 0.33746
H 1.73632 3.76140 -2.44023	H -0.62752 -1.04252 -3.54457	H -5.18806 -0.68427 1.40980
C 2.67921 3.32183 0.63899	C -1.71557 -3.20030 -1.30258	H -5.40507 0.03186 -0.19390
H 2.94781 4.31590 0.26412	H -2.09403 -3.53805 -0.33134	H -5.81458 -1.66501 0.08556
H 3.43984 3.01832 1.36569	H -0.62773 -3.30790 -1.29410	
H 1.72177 3.40507 1.16642	H -2.11803 -3.87118 -2.07046	

### 3'

Si -0.08770 0.64733 0.13933
Si 0.05441 2.94401 0.72126
Si 1.89926 -0.25231 0.11257
Si 3.70451 0.97158 -0.76992
C 4.63637 -0.26330 -1.86929
H 5.43926 0.26401 -2.39860
H 5.09198 -1.08246 -1.30568
H 3.96886 -0.69765 -2.62089
C 4.95031 1.65459 0.47695
H 5.77891 2.13404 -0.05724
H 4.51187 2.38741 1.15789

### TS(3'-3'')

Si -0.20080 -0.25697 -0.11440
Si -1.00502 -2.25855 -1.15555
Si -1.63794 1.05039 1.00004
Si -1.40162 1.95361 -1.37017
C -0.80219 3.74459 -1.23316
H -1.19565 4.28088 -2.10645
H -1.19360 4.21905 -0.32902
H 0.28383 3.85474 -1.23585
C -3.26918 2.08423 -1.68419
H -3.41248 2.56852 -2.65852
H -3.78675 1.12210 -1.70393

### 3'' (singlet)

Si 0.24862 0.57217 -0.03316
Si 1.18092 1.09319 2.09349
Si 1.67620 -0.56867 -1.54414
Si 0.46931 2.60670 -1.26761
C -0.26896 2.72524 -3.00706
H -0.00488 3.71941 -3.38907
H 0.18071 1.98413 -3.67566
H -1.35400 2.62160 -3.06063
C 3.32722 2.84452 -1.59658
H 2.46990 3.75248 -2.19506
H 2.92657 2.94116 -0.69051
H 2.73360 2.01237 -2.18975
C -0.16650 4.07249 -0.25590

S83

## 15. Appendix

H 5.36581 0.84072 1.07977	H -3.73574 2.70948 -0.91738	H -1.24117 3.98708 -0.06263
C 3.09422 2.30601 -1.96608	C -0.64889 1.30697 -2.99712	H 0.34388 4.14763 0.70960
H 2.62370 1.81710 -2.82556	H 0.44384 1.34514 -2.99544	H 0.00746 5.00647 -0.80268
H 2.36102 2.99293 -1.53863	H -0.95312 0.28664 -3.24235	Si 3.64330 -1.47499 -0.51781
H 3.94254 2.89574 -2.33315	H -1.00356 1.96532 -3.80092	C 4.68208 -0.66471 0.84246
Si 2.63668 -2.42325 0.64743	Si -3.76634 0.00553 1.26514	H 4.12297 -0.44688 1.75499
C 4.31273 -2.13370 1.48480	C -4.66018 -1.24006 0.14693	H 5.49404 -1.35691 1.09751
H 4.20059 -1.49497 2.36726	H -4.08179 -2.14307 -0.05984	H 5.14077 0.26488 0.49090
H 4.72506 -3.09459 1.81470	H -5.57740 -1.53913 0.66955	C 4.82895 -1.74561 -1.97153
H 5.04567 -1.66618 0.82144	H -4.95773 -0.79748 -0.80874	H 4.35139 -2.32913 -2.76481
C 2.89527 -3.56954 -0.83134	C -5.02233 1.40152 1.53822	H 5.15112 -0.79393 -2.40754
H 1.95242 -3.80486 -1.33256	H -4.60415 2.20297 2.15547	H 5.72461 -2.28377 -1.63984
H 3.56896 -3.11988 -1.56671	H -5.35260 1.83909 0.59094	C 3.10870 -3.19583 0.09463
H 3.34373 -4.50999 -0.49048	H -5.90836 1.00579 2.04890	H 2.66481 -3.15370 1.09366
C 1.56246 -3.27689 1.94466	C -3.52655 -0.82392 2.96004	H 2.38722 -3.67874 -0.57378
H 1.34300 -2.59890 2.77545	H -2.78219 -1.62651 2.93704	H 3.99561 -3.83851 0.14521
H 0.61649 -3.64283 1.54104	H -3.19856 -0.09052 3.70455	C 0.16604 2.18946 3.26624
H 2.11219 -4.13693 2.34511	H -4.47547 -1.25074 3.30545	H -0.73486 1.71251 3.65866
C -0.43993 4.16826 -0.63587	C 0.05529 -3.39781 -2.24107	H 0.81268 2.43859 4.11692
H -1.51637 4.14952 -0.83212	H 0.69090 -4.07171 -1.66165	H -0.13045 3.13032 2.79151
H -0.17606 5.18107 -0.30936	H -0.64743 -4.01696 -2.81259	C 2.76042 2.10611 1.82054
H 0.07767 3.96977 -1.57952	H 0.68439 -2.86346 -2.95887	H 2.51185 3.13841 1.55108
C 1.80692 3.36720 1.29595	C -2.43609 -1.76175 -2.29383	H 3.32789 2.13593 2.75861
H 2.54267 3.39944 0.49145	H -2.06533 -1.61585 -3.31351	H 3.41142 1.69547 1.04652
H 1.77748 4.36168 1.75770	H -3.17488 -2.57087 -2.32420	C 1.64440 -0.46493 3.07057
C 2.15103 2.65288 2.05057	H -2.94704 -0.85066 -1.97743	H 0.76988 -0.92561 3.54001
C -0.98937 3.32947 2.25705	C -1.61147 -3.32693 0.28569	H 2.12510 -1.22435 2.44697
H -2.06677 3.21488 2.12510	H -0.76058 -3.80053 0.78678	H 2.34400 -0.18868 3.86859
H -0.68156 2.70598 3.10242	H -2.16583 -2.75242 1.03251	Si -1.87360 -0.58616 -0.05016
H -0.79549 4.37523 2.52582	H -2.26532 -4.12304 -0.08998	C -2.92206 0.11136 1.44155
Si -2.20021 -0.43239 -0.17257	Si 2.15063 0.08675 0.32757	C -1.46558 -2.48261 0.19982
C -3.28349 0.89551 -1.11408	C 3.17612 -0.85012 -1.04121	C -2.79006 -0.28651 -1.74010
C -2.93362 -0.87358 1.57770	C 2.30325 -0.79453 2.06780	C -3.95300 -1.26830 -1.97614
C -1.97226 -2.02004 -1.28274	C 2.65998 1.95999 0.42621	H -4.48459 -0.97996 -2.89403
C -3.22953 -2.91046 -1.27991	C 4.01619 2.15384 1.13154	H -3.60400 -2.29508 -2.11829
H -3.08138 -3.74112 -1.98414	H 4.29990 3.21389 1.07068	H -4.68309 -1.26869 -1.16128
H -3.41758 -3.35223 -0.29697	H 3.96605 1.89642 2.19336	C -1.82073 -0.41286 -2.92828
H -4.13321 -2.37738 -1.58814	H 4.82406 1.57229 0.67852	H -1.42083 -1.42179 -3.04709
C -0.79515 -2.87773 -0.79879	C 1.61989 2.80552 1.18138	H -2.35087 -0.15727 -3.85695
H -0.94261 -3.26127 0.21071	H 1.51941 2.52084 2.22980	H -0.96965 0.26431 -2.83832
H -0.67708 -3.74353 -1.46631	H 1.92930 3.86034 1.15279	C -3.36910 1.13975 -1.77338
H 0.14207 -2.31257 -0.82508	H 0.62598 2.74173 0.73549	H -2.62988 1.89697 -1.49053
C -1.65495 -1.63936 -2.73993	C 2.77709 2.54668 -0.99201	H -3.70727 1.37118 -2.79311
H -0.79105 -0.96813 -2.80862	H 1.87397 2.37344 -1.58716	H -4.23329 1.25157 -1.11320
H -1.41031 -2.55231 -3.30014	H 2.92184 3.63382 -0.92318	C -2.69907 -3.30013 0.63019
H -2.50219 -1.17034 -3.24615	H 3.62845 2.14147 -1.54497	H -3.53331 -3.20428 -0.07092
C -4.44928 -1.14041 1.53955	C 3.76231 -1.15823 2.40272	H -2.42938 -4.36450 0.67693
H -4.72245 -1.92709 0.82977	H 4.42569 -0.28843 2.37470	H -3.05915 -3.01668 1.62268
H -4.78540 -1.46439 2.53450	H 3.80529 -1.56916 3.42109	C -0.92802 -3.11113 -1.09628
H -5.02054 -0.24313 1.28370	H 4.17477 -1.91625 1.73228	H -1.68627 -3.17993 -1.88023
C -2.23770 -2.12012 2.15170	C 1.78091 0.11056 3.19807	H -0.07436 -2.55807 -1.51487
H -2.49399 -3.03398 1.60862	H 2.42791 0.97472 3.37051	H -0.57834 -4.13137 -0.88645
H -1.14624 -2.01146 2.15518	H 0.76408 0.47198 3.00686	C -0.36876 -2.67785 1.25928
H -2.55708 -2.26240 3.19327	H 1.75795 -0.46719 4.13242	H -0.66171 -2.32718 2.25060
C -2.67067 0.26122 2.58290	C 1.45296 -2.07960 2.12194	H -0.12705 -3.74683 1.34486
H -3.12542 1.20889 2.28805	H 1.70039 -2.80138 1.33941	H 0.55432 -2.15702 0.98069
H -3.09227 -0.01581 3.55918	H 1.61150 -2.57690 3.08896	C -2.83717 1.64912 1.49376
H -1.59709 0.43019 2.72326	H 0.38044 -1.85440 2.05736	H -3.32950 2.01070 2.40772
C -2.48995 1.56837 -2.25158	C 2.63013 -0.51457 -2.44145	H -1.80271 2.00508 1.51838
H -3.11196 2.35211 -2.70711	H 3.17373 -1.10097 -3.19559	H -3.33414 2.12568 0.64633
H -1.57505 2.04785 -1.89035	H 1.56764 -0.76711 -2.53345	C -2.36904 -0.42028 2.77554
H -2.20631 0.87470 -3.04396	H 2.74598 0.53985 -2.70246	H -2.56453 -1.48735 2.90994
C -3.71242 2.02058 -0.15807	C 3.03596 -2.37095 -0.86671	H -1.29134 -0.26149 2.87307
H -4.40016 1.67596 0.61896	H 3.55332 -2.74199 0.02116	H -2.85603 0.10707 3.60790
H -2.85375 2.49052 0.33056	H 1.99033 -2.67680 -0.80262	C -4.41025 -0.27851 1.37566
H -4.23071 2.80338 -0.72943	H 3.47211 -2.88050 -1.73743	H -4.92281 0.17768 0.52473
C -4.56227 0.29176 -1.72350	C 4.67988 -0.52223 -1.01596	H -4.55971 -1.36108 1.31945
H -4.34466 -0.41206 -2.53142	H 4.88814 0.51841 -1.27760	H -4.91611 0.07601 2.28490
H -5.18123 -0.22351 -0.98229	H 5.13415 -0.72392 -0.04045	
H -5.17042 1.09932 -2.15489	H 5.19678 -1.15075 -1.75467	

### 3\*\* (triplet)

Si 2.11636 0.42605 -0.87163  
 Si 3.95248 -0.94775 -0.38431  
 Si -0.04350 0.85544 -0.08735

### 4

Si -2.61188 -0.07367 -0.07455  
 H -0.37107 -2.29044 -0.46696  
 Si -0.44030 -0.80124 -0.58293

### S84

### 5

Si -0.47225 -1.05292 -0.02451  
 C -0.39963 -2.75728 0.79492  
 H 0.53107 -3.04492 1.27958  
 H -1.27226 -3.13929 1.32025  
 Si -2.58063 0.01757 -0.04846



# 15. Appendix

Si -0.64512 2.58123 -1.62010	Si 1.70161 -0.07065 0.01609	C -0.41925 -2.81143 -0.73071
Si 0.40137 2.04571 1.93410	Si 1.99579 -0.77619 2.23650	H -1.31159 -3.21472 -1.20189
Si -1.39803 -1.12671 0.03955	Si 3.15503 -1.35906 -1.31590	H 0.48983 -3.15528 -1.21703
C 5.39723 -0.14811 -1.30068	Si 2.32920 2.17776 -0.25675	C -2.76356 0.70630 -1.86295
H 5.56418 0.87615 -0.95352	C -2.70862 -0.50083 -1.98968	Si 1.67039 -0.05737 0.02288
H 5.21072 -0.11352 -2.37849	C -1.18276 -0.34233 -2.30578	C -1.39985 1.20573 -2.37712
H 6.31561 -0.72198 -1.13154	H -0.93050 0.69723 -2.54338	H -1.52625 1.66671 -3.36717
C 3.76962 -2.72059 -1.01363	H -0.87057 -0.95894 -3.15947	H -0.69298 0.37485 -2.49232
H 4.73470 -3.23168 -0.91304	C -3.06219 -1.97500 -2.25567	H -0.93639 1.94819 -1.72388
H 3.47976 -2.74565 -2.06858	H -2.39875 -2.66775 -1.72931	Si 3.05283 -1.66849 -1.02375
H 3.02865 -3.28825 -0.44309	H -2.94778 -2.17311 -3.33070	Si 2.36046 0.17935 2.26402
C 4.36272 -1.00481 1.45815	H -4.09433 -2.21950 -1.98745	C -3.18925 -0.40776 -2.83648
H 4.58284 -0.00472 1.84437	C -3.61527 0.35663 -2.87888	H -4.20555 -0.76683 -2.65564
H 5.25095 -1.62970 1.61047	H -4.67245 0.19619 -2.63232	H -2.50582 -1.26416 -2.79486
H 3.54493 -1.42992 2.04834	H -3.47630 0.08242 -3.93417	H -3.16115 -0.01546 -3.86262
C -1.31025 2.08188 -3.32136	H -3.41361 1.42682 -2.79010	C -3.78061 1.85573 -1.96998
H -2.28029 1.58045 -3.30402	C -3.84102 -1.05530 1.05096	H -4.77263 1.57098 -1.60547
H -0.60182 1.44297 -3.85714	C -3.41359 -2.53167 1.12204	H -3.88935 2.15192 -3.02279
H -1.42385 3.00789 -3.89872	H -2.41103 -2.63799 1.55218	H -3.46219 2.74390 -1.41620
C 0.90917 3.57804 -2.04497	H -3.41154 -3.01817 0.14419	Si 2.26416 1.94885 -1.08805
H 0.61028 4.49015 -2.57581	H -4.11384 -3.08413 1.76392	C -4.02146 -1.21947 0.39603
H 1.55030 2.99468 -2.71570	C -5.26221 -0.96824 0.46411	C -5.39004 -0.62312 0.01220
H 1.50853 3.86492 -1.17931	H -5.95666 -1.54611 1.09030	H -5.56110 0.36308 0.45426
C -1.92312 3.73610 -0.83145	H -5.31875 -1.37562 -0.54929	H -6.18627 -1.28838 0.37475
H -1.58232 4.12805 0.13222	H -5.63112 0.06216 0.43023	H -5.51459 -0.53229 -1.07034
H -2.88232 3.23241 -0.67122	C -3.88885 -0.53169 2.49473	C -3.88028 -2.57986 -0.31226
H -2.10077 4.58948 -1.49614	H -4.29838 0.48053 2.55830	H -4.78174 -3.17716 -0.11623
C 1.35508 3.62256 1.49726	H -2.90134 -0.53323 2.96974	H -3.03064 -3.14749 0.07624
H 1.63675 4.12251 2.43162	H -4.54134 -1.18408 3.09155	H -3.76968 -2.50012 -1.39539
H 0.76075 4.32749 0.90815	C -2.61082 1.83047 0.27896	C -4.05129 -1.52523 1.90437
H 2.27369 3.39678 0.94477	C -1.72471 2.56927 -0.73610	H -4.33731 -0.65613 2.50235
C 1.53441 1.10464 3.12441	H -1.66900 3.63377 -0.46576	H -3.08632 -1.89216 2.27140
H 1.83968 1.79725 3.91797	H -2.09700 2.51168 -1.76175	H -4.79801 -2.30857 2.09452
H 2.44129 0.75908 2.61737	H -0.70158 2.17728 -0.72317	C -2.45038 1.43481 1.28245
H 1.05774 0.24233 3.59826	C -4.02482 2.43000 0.22984	C -1.84341 0.89387 2.59113
C -1.11307 2.61058 2.92429	H -4.66762 2.03108 1.02092	H -1.71734 1.72388 3.30113
H -0.75997 3.26710 3.72869	H -4.51691 2.24279 -0.73153	H -0.85284 0.45581 2.42271
H -1.65451 1.78049 3.38597	H -3.97375 3.51895 0.37041	H -2.46082 0.13747 3.07767
H -1.82360 3.17884 2.31644	C -1.98197 2.10200 1.65786	C -3.79500 2.10643 1.60922
C -3.25365 -0.54168 0.20530	H -1.91322 3.18743 1.82072	H -4.49193 1.42264 2.10213
C -3.78301 -0.01033 -1.13736	H -0.96482 1.69543 1.71243	H -4.28958 2.50926 0.71950
H -4.78988 0.40429 -0.98917	H -2.55542 1.68387 2.48673	H -3.62379 2.94544 2.29826
H -3.86028 -0.78371 -1.90575	C 0.56446 -0.20156 3.33019	C -1.48031 2.51733 0.78781
H -3.15319 0.79685 -1.52649	H 0.67761 -0.60336 4.34367	H -1.85172 3.05689 -0.08817
C -3.36363 0.63126 1.19514	H -0.39606 -0.54913 2.93255	H -0.50102 2.09374 0.53716
H -3.07772 0.35967 2.21269	H 0.52199 0.89013 3.40184	H -1.31861 3.25977 1.58303
H -4.40473 0.98242 1.22967	C 2.03371 -2.66681 2.28173	C 3.15257 -3.25968 0.00116
H -2.74340 1.48083 0.88866	H 2.10947 -3.02078 3.31618	H 3.47099 -3.04958 1.02817
C -4.19809 -1.65873 0.68446	H 2.88642 -3.06906 1.72534	H 3.89751 -3.92762 -0.44736
H -3.96727 -1.98610 1.70211	H 1.12065 -3.08662 1.84552	H 2.20311 -3.79989 0.04628
H -4.17738 -2.53849 0.03489	C 3.60866 -0.10221 2.95817	C 4.23964 -0.00949 2.40074
H -5.23030 -1.28094 0.69381	H 3.58338 0.99092 3.02426	H 4.77430 0.72123 1.78672
C -0.82238 -2.11637 1.61787	H 4.47255 -0.38432 2.34762	H 4.55900 -1.01078 2.09226
C 0.71539 -2.15011 1.69705	H 3.76436 -0.49552 3.96919	H 4.54858 0.13293 3.44294
H 1.13611 -1.14250 1.76917	C 2.42049 -3.07175 -1.62934	C 1.90250 1.89558 2.92093
H 1.17676 -2.64088 0.83658	H 2.16396 -3.58220 -0.69560	H 0.83035 2.09778 2.83513
H 1.02373 -2.70058 2.59795	H 3.14094 -3.69347 -2.17328	H 2.43582 2.67843 2.37088
C -1.31391 -1.43540 2.90688	H 1.50796 -3.00283 -2.23080	H 2.18009 1.98164 3.97785
H -0.84552 -1.92074 3.77483	C 4.83727 -1.57065 -0.47362	C 1.59570 -1.14849 3.37193
H -2.39668 -1.51689 3.03582	H 5.29306 -0.60583 -0.22954	H 1.86608 -0.95821 4.41704
H -1.04693 -0.37431 2.94288	H 5.52273 -2.11152 -1.13624	H 1.97733 -2.13916 3.10177
C -1.34048 -3.56639 1.63597	H 4.74776 -2.14475 0.45455	H 0.50476 -1.18368 3.29742
H -1.04102 -4.04526 2.57899	C 3.42113 -0.52826 -2.99529	C 4.84064 -1.07531 -1.22966
H -0.92662 -4.16897 0.82347	H 2.46423 -0.33496 -3.49238	H 4.91348 -0.22990 -1.92086
H -2.43174 -3.62214 1.57365	H 4.01640 -1.17755 -3.64744	H 5.43039 -1.89883 -1.65003
C -1.13024 -2.18793 -1.57707	H 3.95073 0.42511 -2.89864	H 5.29931 -0.78401 -0.27975
C 0.20629 -2.94917 -1.55475	C 4.21688 2.22362 -0.10488	C 2.40757 -2.06304 -2.76753
H 1.05566 -2.27452 -1.40908	H 4.56702 3.26197 -0.13460	H 1.35183 -1.80399 -2.89249
H 0.34997 -3.44589 -2.52477	H 4.69633 1.68665 -0.93007	H 2.52081 -3.13113 -2.98590
H 0.24632 -3.72586 -0.78635	H 4.56144 1.77704 0.83350	H 2.98094 -1.50924 -3.51776
C -1.07708 -1.28072 -2.81773	C 1.88779 2.86616 -1.96226	C 2.32561 1.67878 -2.95868
H -1.97282 -0.66988 -2.94320	H 0.80859 2.95635 -2.11359	H 1.34914 1.39379 -3.36238
H -0.97118 -1.90169 -3.71848	H 2.28744 2.23010 -2.75794	H 3.03993 0.89261 -3.22311
H -0.21134 -0.60972 -2.78047	H 2.32706 3.86416 -2.07627	H 2.64261 2.60276 -3.45596
C -2.25265 -3.22300 -1.78091	C 1.62038 3.30783 1.08301	C 1.29833 3.54345 -0.75381
H -2.36398 -3.89762 -0.92611	H 1.82974 2.91651 2.08466	H 0.31095 3.57407 -1.21954



## 15. Appendix

H -2.01577 -3.84126 -2.65810  
H -3.22270 -2.75564 -1.97025

### 6

Si -0.18427 0.49074 0.60395  
Si 0.17194 2.83076 0.68409  
N 1.79778 -0.39555 -0.39409  
Si 3.79438 0.87781 -0.52817  
H -0.04746 0.07549 2.03964  
N 1.40847 -0.91697 -2.04937  
H 1.11048 -0.19806 -2.70128  
H 2.09516 -1.50689 -2.50893  
C 4.80622 -0.09589 -1.80938  
H 5.84802 0.24472 -1.80551  
H 4.80548 -1.17605 -1.63475  
H 4.40192 0.08006 -2.81221  
C 4.73819 0.93813 1.12498  
H 5.08646 1.95714 1.32499  
H 4.12763 0.62480 1.97815  
H 5.61514 0.28415 1.08711  
C 3.74929 2.63822 -1.22605  
H 3.28581 2.67365 -2.21694  
H 3.22871 3.34753 -0.57785  
H 4.78671 2.97775 -1.33502  
Si 2.47107 -2.37504 0.74466  
C 4.33290 -2.49172 1.08767  
H 4.64225 -1.79288 1.86963  
H 4.54180 -3.50603 1.44921  
H 4.95966 -2.31878 0.20900  
C 2.04349 -3.85343 -0.36084  
H 1.05099 -3.78056 -0.81295  
H 2.77594 -3.92560 -1.17336  
H 2.09567 -4.78509 0.21402  
C 1.68544 -2.50552 2.46188  
H 2.01980 -1.66702 3.08323  
H 0.59351 -2.49791 2.45658  
H 2.02176 -3.43127 2.94326  
C 0.45209 3.51229 -1.06233  
H -0.50509 3.67558 -1.56873  
H 0.97295 4.47556 -1.01387  
H 1.05067 2.84043 -1.68442  
C 1.71008 3.05829 1.76862  
H 2.53210 2.38337 1.52071  
H 2.08204 4.08737 1.69619  
H 1.43756 2.87351 2.81361  
C -1.11585 3.96015 1.49346  
H -2.05262 4.03488 0.93578  
H -1.34973 3.65290 2.51676  
H -0.67658 4.96446 1.53958  
Si -2.33180 -0.33121 -0.10284  
C -2.84016 0.70015 -1.67292  
C -3.52217 0.00613 1.41142  
C -2.26904 -2.23725 -0.50424  
C -3.66371 -2.88955 -0.50179  
H -3.56304 -3.94503 -0.79122  
H -4.13957 -2.86985 0.48188  
H -4.34668 -2.41969 -1.21708  
C -1.39041 -2.94791 0.53688  
H -1.75453 -2.84483 1.56134  
H -1.33820 -4.02238 0.30863  
H -0.36924 -2.55851 0.50144  
C -1.62318 -2.52433 -1.87146  
H -0.62337 -2.08629 -1.95795  
H -1.52299 -3.61353 -1.98860  
H -2.23407 -2.17212 -2.70757  
C -5.00704 -0.03657 1.00534  
H -5.29181 -0.98052 0.53209  
H -5.63136 0.08363 1.90204  
H -5.26950 0.77521 0.32053  
C -3.30314 -1.01629 2.54163  
H -3.60876 -2.02854 2.26691  
H -2.25705 -1.04838 2.86760  
H -3.90761 -0.72039 3.41032  
C -3.24297 1.38433 2.03383  
H -3.35848 2.20623 1.32521

H 0.53767 3.42863 0.98815  
H 2.07936 4.30047 1.00797

### 13

Si 1.10519 0.14246 1.12423  
Si 1.37654 -1.79212 2.45020  
C 2.62986 -0.11464 -0.12275  
Si -0.93422 0.78782 -0.01560  
Si -0.29365 1.99669 -1.96362  
Si -1.30228 2.60708 1.51559  
Si -2.88886 -0.61552 -0.30585  
N 2.97818 -1.07561 -1.02196  
N 3.71256 0.71341 -0.05874  
C 4.26137 -0.85925 -1.50609  
C 4.72642 0.26574 -0.88800  
C 2.14724 -2.26278 -1.30710  
H 1.19219 -2.03012 -0.82664  
C 2.73609 -3.51070 -0.65068  
H 2.91095 -3.35385 0.41494  
H 3.67847 -3.80874 -1.11760  
H 2.03082 -4.33924 -0.76649  
C 1.91287 -2.47242 -2.80081  
H 1.60861 -1.54647 -3.29476  
H 1.10740 -3.20008 -2.92336  
H 2.79428 -2.87181 -3.30605  
C 4.95208 -1.67090 -2.55518  
H 4.53609 -1.47906 -3.54843  
H 4.89555 -2.74321 -2.36397  
H 6.00800 -1.39886 -2.58246  
C 6.06175 0.91915 -1.04614  
H 6.00865 1.82197 -1.66034  
H 6.75071 0.22472 -1.52850  
H 6.49290 1.19057 -0.08047  
C 3.78989 1.94045 0.82096  
H 2.74379 2.08768 1.07940  
C 4.52051 1.56207 2.11403  
H 5.53434 1.19402 1.92612  
H 3.96374 0.79913 2.66348  
H 4.59025 2.45785 2.73821  
C 4.35425 3.14324 0.12388  
H 3.96829 4.02602 0.64209  
H 4.03218 3.20506 -0.91841  
H 5.44496 3.19069 0.16609  
C 3.28025 -1.95828 2.63423  
H 3.62302 -1.31315 3.45019  
H 3.84973 -1.68582 1.73782  
H 3.54607 -2.98830 2.90056  
C 0.72209 -3.57180 2.18583  
H 1.30152 -4.23434 2.84163  
H 0.80150 -3.95436 1.16653  
H -0.32596 -3.65386 2.48925  
C 0.77193 -1.36432 4.19884  
H 1.22288 -0.42650 4.53931  
H 1.06330 -2.16031 4.89514  
H -0.31549 -1.25377 4.25230  
C -0.16690 1.09373 -3.63029  
H -1.11827 0.73724 -4.03059  
H 0.51688 0.24192 -3.57462  
H 0.25291 1.80843 -4.34940  
C 1.46746 2.66564 -1.73440  
H 1.64461 3.48135 -2.44663  
H 2.19724 1.87404 -1.94072  
H 1.65138 3.04459 -0.72692  
C -1.41348 3.49583 -2.28554  
H -1.53866 4.11930 -1.39475  
H -2.40856 3.20225 -2.63412  
H -0.95597 4.11458 -3.06708  
C 0.10232 3.87445 1.32595  
H -0.03969 4.65165 2.08663  
H 0.10416 4.36302 0.34621  
H 1.07883 3.41150 1.49413  
C -1.23313 2.04680 3.32789  
H -1.12610 2.94003 3.95552  
H -0.37042 1.39922 3.51554  
H -2.13962 1.52338 3.64708

H 1.89083 4.36433 -1.17644  
H 1.17937 3.73562 0.31717  
C 4.01528 2.36825 -0.48896  
H 4.41686 3.17545 -1.11342  
H 4.71043 1.52730 -0.53610  
H 3.99338 2.73197 0.54418

### 14

Si -0.37732 -0.40628 -1.18161  
N 1.50459 -0.79129 -0.64954  
C -3.16486 -2.31376 -1.20631  
Si -1.58611 -2.17831 -0.04416  
N 5.54426 -1.49442 0.17861  
C -2.79235 -2.88347 -2.58758  
H -3.66860 -2.81813 -3.24843  
H -2.50211 -3.93688 -2.54503  
H -1.98108 -2.31541 -3.05604  
Si -0.39051 1.74944 -0.09233  
C -3.73870 -0.90856 -1.46138  
H -4.56248 -0.97165 -2.18726  
H -2.99159 -0.22334 -1.88409  
H -4.13982 -0.46179 -0.55199  
Si -2.28698 3.03263 -0.68344  
C -4.30349 -3.17573 -0.63249  
H -5.12074 -3.23281 -1.36641  
H -4.72499 -2.74925 0.28231  
H -3.99085 -2.20029 -0.41172  
Si 0.06316 2.43450 2.13937  
C -0.56213 -3.85489 -0.14965  
Si 1.33359 2.80799 -1.33490  
C 0.23494 -3.94739 -1.46438  
H -0.38290 -3.82594 -2.35569  
H 0.71967 -4.93328 -1.52458  
H 1.02764 -3.19649 -1.50399  
C 6.46096 -1.81773 -0.90239  
H 6.15930 -2.73891 -1.41325  
H 7.45695 -1.96785 -0.48936  
H 6.51067 -1.00614 -1.63753  
C 1.99083 -0.71136 0.60490  
H 1.27083 -0.45248 1.37047  
C 3.30841 -0.94043 0.92919  
C 3.60311 -0.84570 1.96623  
C 4.23530 -1.27489 -0.08889  
C 3.71385 -1.35691 -1.40392  
H 4.34014 -1.60063 -2.25139  
C 2.37717 -1.10875 -1.62695  
H 1.95207 -1.16305 -2.62527  
C 3.04392 2.47133 -0.57220  
H 3.32878 1.42071 -0.69174  
H 3.08174 2.71047 0.49599  
H 3.80018 3.08150 -1.08091  
C 1.18115 4.69387 -1.48921  
H 2.05904 5.06814 -2.03004  
H 1.13725 5.20331 -0.52280  
H 0.29337 4.97598 -2.06475  
C -1.46211 -5.10209 -0.06735  
H -2.10968 -5.20063 -0.94241  
H -2.09671 -5.10925 0.82342  
H -0.83075 -6.00232 -0.02996  
C 0.47081 -3.96341 0.98620  
H 1.07964 -4.86703 0.83496  
H 0.00622 -4.04911 1.97215  
H 1.15700 -3.10967 1.00545  
C -2.14723 -1.86161 1.80775  
C -3.21612 -0.75674 1.85492  
H -2.89181 0.14315 1.31634  
H -3.39826 -0.46824 2.90090  
H -4.17536 -1.07825 1.44090  
C -0.96246 -1.32141 2.62387  
H -0.10476 -2.00052 2.65176  
H -1.27450 -1.13844 3.66335  
H -0.63468 -0.36414 2.20734  
C -2.70871 -3.09885 2.52879  
H -3.54852 -3.55146 1.99346  
H -3.07228 -2.80692 3.52509

S86

## 15. Appendix

H -3.94810 1.55960 2.85871  
H -2.23272 1.43723 2.45356  
C -1.64512 0.78158 -2.64163  
H -1.92837 1.37182 -3.52476  
H -0.78974 1.28678 -2.17566  
H -1.31078 -0.19953 -2.98611  
C -3.20481 2.14652 -1.30173  
H -4.13001 2.21213 -0.72237  
H -2.41035 2.63403 -0.72819  
H -3.35181 2.73183 -2.22055  
C -4.03925 0.09557 -2.42479  
H -3.81907 -0.89228 -2.83684  
H -4.92522 0.00468 -1.78858  
H -4.30610 0.74775 -3.26845

### 15

Si 1.67558 1.98198 0.06229  
Si 0.34632 0.11555 -0.73843  
Si -1.94902 -0.06990 -0.12454  
Si -2.51620 -2.14518 -1.15790  
Si -3.12278 0.20229 1.95491  
Si -3.10835 1.41039 -1.58763  
C 3.56432 1.46357 0.27663  
C 4.41203 2.57761 0.92077  
H 4.31064 3.53818 0.40961  
H 5.47347 2.29189 0.87745  
H 4.16438 2.72884 1.97507  
C 3.75673 0.19926 1.13583  
H 3.41939 -0.70255 0.61797  
H 3.23561 0.25260 2.09409  
H 4.82831 0.06882 1.34808  
C 4.18672 1.15361 -1.09516  
H 4.32855 2.05329 -1.69935  
H 3.57463 0.45408 -1.67450  
H 5.17804 0.69678 -0.95372  
C 1.53756 3.24822 -1.44077  
C 1.65854 2.56514 -2.81821  
H 1.54143 3.32848 -3.60146  
H 0.88891 1.80317 -2.96503  
H 2.62811 2.08610 -2.97409  
C 2.56970 4.39065 -1.41207  
H 2.59150 4.92832 -0.46049  
H 2.31988 5.12079 -2.19566  
H 3.58305 4.03465 -1.62134  
C 0.13487 3.87906 -1.40030  
H 0.02424 4.60076 -0.58598  
H -0.64935 3.12118 -1.28980  
H -0.06092 4.41645 -2.33977  
C 1.05532 2.86833 1.71130  
C 1.58403 4.29855 1.92398  
H 1.19030 4.99531 1.17873  
H 2.67509 4.36114 1.90252  
H 1.25326 4.66176 2.90826  
C 1.47878 2.02887 2.92850  
H 2.55855 2.05005 3.10085  
H 1.17557 0.98256 2.82091  
H 0.99418 2.42019 3.83493  
C -0.48033 2.94772 1.74887  
H -0.80762 3.29960 2.73843  
H -0.93858 1.97074 1.57275  
H -0.87889 3.64366 1.00895  
C -2.37038 -1.96749 -3.04273  
H -3.19461 -1.37737 -3.45514  
H -2.41052 -2.96319 -3.50147  
H -1.43379 -1.48460 -3.33635  
C -1.42529 -3.64297 -0.70156  
H -0.35310 -3.42869 -0.67495  
H -1.59093 -4.41881 -1.45981  
H -1.70873 -4.06858 0.26613  
C -4.28184 -2.75939 -0.82610  
H -4.37873 -3.17847 0.17964  
H -4.51267 -3.55586 -1.54438  
H -5.03491 -1.97471 -0.94019  
C -4.25101 1.72512 1.90399  
H -4.81230 1.76732 2.84568

C -2.86384 3.69012 1.39237  
H -2.73146 4.50877 2.11084  
H -3.78593 3.16749 1.65759  
H -3.00308 4.13717 0.40367  
C -4.29081 0.30177 -1.31861  
C -3.93378 0.39304 -2.81109  
H -4.67841 1.01931 -3.32266  
H -3.93484 -0.58079 -3.30795  
H -2.95498 0.85821 -2.96656  
C -4.45106 1.74900 -0.82812  
H -4.80992 1.80869 0.20024  
H -5.18185 2.27302 -1.46142  
H -3.50860 2.30120 -0.88437  
C -5.66162 -0.39084 -1.20932  
H -6.05733 -0.36956 -0.19046  
H -5.63737 -1.43366 -1.53875  
H -6.38461 0.13858 -1.84676  
C -3.53492 -1.06789 1.48144  
C -2.34067 -1.32942 2.41316  
H -1.70851 -0.44177 2.51925  
H -1.70535 -2.14569 2.06607  
H -2.70536 -1.59378 3.41711  
C -4.32253 0.09539 2.10735  
H -4.52229 -0.13197 3.16433  
H -5.28892 0.26102 1.62395  
H -3.76110 1.03390 2.07734  
C -4.44247 -2.31095 1.50513  
H -4.82160 -2.46222 2.52603  
H -3.90710 -3.22173 1.22336  
H -5.30980 -2.21214 0.84510  
C -2.32553 -2.22513 -1.25775  
C -1.45390 -3.10177 -0.34563  
H -0.65863 -2.51758 0.12858  
H -0.98014 -3.89810 -0.94249  
H -2.02404 -3.59426 0.44752  
C -1.43801 -1.83819 -2.44991  
H -1.94944 -1.21588 -3.18514  
H -1.10903 -2.75042 -2.96833  
H -0.54522 -1.29516 -2.11952  
C -3.48610 -3.08265 -1.78966  
H -4.18991 -3.37497 -1.00506  
H -3.08141 -4.00594 -2.22965  
H -4.05035 -2.57296 -2.57601

### 16

Si -1.36567 0.56683 1.19160  
Si -1.73036 2.89403 1.09407  
C -2.85039 0.08767 -0.01025  
Si 0.58221 -0.62661 0.39959  
Si -0.25957 -2.59158 -0.64706  
Si 1.03529 -1.46165 2.61090  
Si 2.52098 0.37075 -0.66688  
N -3.08080 0.28565 -1.33284  
N -3.97059 -0.54321 0.42885  
C -4.30735 -0.22797 -1.72195  
C -4.87250 -0.75591 -0.60034  
C -2.24021 1.06901 -2.22132  
H -1.32716 1.31864 -1.68487  
C -4.79091 -0.15530 -3.13015  
H -4.11954 -0.69196 -3.80836  
H -4.86369 0.88051 -3.47620  
H -5.78073 -0.60673 -3.21062  
C -6.16908 -1.46125 -0.39391  
H -6.01195 -2.48913 -0.05131  
H -6.72697 -1.50035 -1.33057  
H -6.78956 -0.94857 0.34744  
C -4.22775 -0.98811 1.79177  
H -3.35734 -0.72954 2.39718  
C -3.63621 2.98167 1.16040  
H -4.03696 2.32219 1.93837  
H -4.08612 2.68677 0.20375  
H -3.96259 4.00452 1.38192  
C -1.25886 4.15597 -0.25716  
H -1.80385 5.08374 -0.04180  
H -1.52749 3.83863 -1.26967

H -1.95022 -3.87276 2.67801  
C 6.03694 -1.36341 1.54063  
H 5.54413 -2.07756 2.20971  
H 5.87451 -0.34982 1.92462  
H 7.10630 -1.56724 1.55143  
C -3.94406 2.45817 0.03291  
H -4.68716 3.24143 -0.16086  
H -3.89525 2.30434 1.11581  
H -4.30327 1.53655 -0.42788  
C -2.43975 3.06856 -2.57034  
H -2.44259 2.05681 -2.98956  
H -1.60325 3.61306 -3.02168  
H -3.36816 3.56925 -2.86870  
C -2.14496 4.82489 -0.07313  
H -1.21095 5.31365 -0.35880  
H -2.23981 4.87709 1.01712  
H -2.97438 5.40019 -0.50269  
C -1.49876 2.42955 3.21118  
H -2.26483 3.08715 2.78654  
H -1.26181 2.79620 4.21706  
H -1.93142 1.42935 3.30589  
C 0.71454 4.21817 2.13098  
H 1.69392 4.28558 1.64540  
H 0.83118 4.55774 3.16751  
H 0.03741 4.90959 1.62292  
C 1.40835 1.48774 3.10211  
H 1.12541 0.46519 3.37192  
H 1.59274 2.03285 4.03586  
H 2.35183 1.45826 2.54556  
C 1.40779 2.17665 -3.11973  
H 0.43495 2.25783 -3.61434  
H 1.70287 1.12495 -3.16945  
H 2.13744 2.76807 -3.68643

### 3''-DMAP

Si -0.83138 1.65282 1.03042  
Si -1.05285 3.41088 -0.54796  
Si 0.85960 -0.06326 0.81931  
Si -0.22082 -1.85468 1.96583  
Si 2.19680 0.85549 2.58128  
Si 2.10810 -0.68956 -1.15831  
C -3.85071 -0.35293 -1.23760  
C -4.57546 -0.24777 1.05155  
C -2.79223 4.05211 -0.10486  
H -2.88394 4.24109 0.96933  
H -3.56667 3.32754 -0.38608  
H -3.00247 4.98642 -0.63881  
C -1.09365 3.34465 -2.45571  
H -1.45189 4.32228 -2.80194  
H -1.78395 2.58871 -2.84627  
H -0.11284 3.17308 -2.90668  
C 0.18040 4.77987 -0.10178  
H 0.14892 4.99917 0.97048  
H -0.07398 5.69849 -0.64338  
H 1.20900 4.50945 -0.36255  
C -1.42444 -2.89825 0.92576  
H -0.94175 -3.47744 0.13455  
H -2.20066 -2.27460 0.46439  
H -1.92236 -3.60202 1.60447  
C -1.31298 -1.18973 3.38607  
H -0.94736 -1.56813 4.34689  
H -2.34006 -1.55133 3.25638  
H -1.33204 -0.09910 3.44538  
C 0.97421 -3.07959 2.79524  
H 1.67587 -2.55314 3.45554  
H 1.55746 -3.66899 2.08569  
H 0.38929 -3.76784 3.41365  
C 1.20416 0.86349 4.19557  
H 1.80407 1.37970 4.95513  
H 1.00156 -0.14799 4.56212  
H 0.25501 1.39468 4.08601  
C 2.61812 2.67359 2.23462  
H 3.00173 3.12587 3.15705  
H 1.72732 3.23814 1.93498  
H 3.37882 2.79921 1.45817



# 15. Appendix

H -4.97336 1.69342 1.08308  
H -3.67304 2.65018 1.81376  
C -4.29547 -1.24934 2.30494  
H -4.79500 -1.07641 3.26598  
H -3.78832 -2.21788 2.35652  
H -5.06800 -1.31564 1.53249  
C -2.07918 0.47257 3.53786  
H -0.99862 0.39058 3.40347  
H -2.38435 -0.23372 4.31829  
H -2.27140 1.48330 3.91364  
C -4.86303 0.74389 -1.89144  
H -5.38755 0.52921 -0.95349  
H -4.86036 -0.17222 -2.48970  
H -5.44466 1.49758 -2.43577  
C -3.35107 3.19130 -0.95002  
H -2.64660 3.48333 -0.16837  
H -4.36180 3.32615 -0.55359  
H -3.22163 3.88497 -1.78930  
C -2.27930 1.58722 -3.28209  
H -2.97932 2.09489 -3.95782  
H -1.99991 0.63159 -3.72876  
H -1.37484 2.19855 -3.21576  
C 1.21776 -1.50631 -0.02061  
N 1.18146 -2.14637 1.17856  
N 2.01261 -2.28830 -0.80907  
C 2.45648 -3.40123 -0.11265  
C 1.93160 -3.31235 1.14405  
C 2.28088 -2.01708 -2.23990  
H 1.95197 -0.98224 -2.37242  
C 0.41861 -1.65626 2.33942  
H 0.12658 -0.64805 2.03338  
C 2.14595 -4.24347 2.29408  
H 1.22127 -4.45902 2.83103  
H 2.53741 -5.19190 1.92385  
H 2.86866 -3.84071 3.00956  
C 3.35815 -4.46164 -0.65764  
H 3.34887 -5.32232 0.01222  
H 3.03625 -4.80809 -1.64139  
H 4.39144 -4.11375 -0.74023  
C 3.76522 -2.11507 -2.59538  
H 4.07411 -3.13694 -2.82714  
H 3.94858 -1.50711 -3.48592  
H 4.39681 -1.72709 -1.79104  
C 1.39158 -2.89108 -3.11785  
H 0.33968 -2.70443 -2.88894  
H 1.56595 -2.64582 -4.16958  
H 1.59490 -3.95706 -2.97656  
C 1.26316 -1.56523 3.61103  
H 0.77107 -0.87598 4.30405  
H 1.35149 -2.52804 4.11902  
H 2.26489 -1.18002 3.40284  
C -0.84765 -2.48182 2.54684  
H -1.36684 -2.13633 3.44437  
H -1.51759 -2.37030 1.69237  
H -0.62521 -3.54550 2.66943

### 3'''Ime4

Si -2.31866 -1.05271 0.01871  
Si -0.37642 0.10575 -0.83920  
Si 1.81044 -0.37362 -0.02410  
Si 3.04726 1.43252 -0.94156  
Si 2.68830 -0.87365 2.14389  
Si 2.50520 -2.15485 -1.43077  
C -3.84294 0.17586 0.23522  
C -5.06068 -0.51684 0.87888  
H -5.34311 -1.44108 0.36856  
H -5.92542 0.16159 0.83403  
H -4.89470 -0.75237 1.93360  
C -3.51689 1.41835 1.09142  
H -2.94540 2.15652 0.52288  
H -2.95987 1.19242 2.00450  
H -4.45710 1.90532 1.38849  
C -4.29727 0.71176 -1.13389  
H -4.76795 -0.06106 -1.74731  
H -3.46132 1.13215 -1.70501

H -0.19077 4.39294 -0.25210  
C -1.08489 3.64456 2.71081  
H -1.47518 3.09159 3.57102  
H -1.39854 4.69146 2.79919  
H 0.00854 3.61491 2.76324  
C -0.60193 -2.53750 -2.51689  
H 0.28447 -2.39250 -3.13893  
H -1.32467 -1.74966 -2.76104  
H -1.05698 -3.49743 -2.79167  
C -1.96965 -3.05892 0.05526  
H -2.07257 -4.15082 0.05037  
H -2.75854 -2.64619 -0.58541  
H -2.13371 -2.70622 1.07527  
C 0.86432 -0.09477 -0.36015  
H 1.07913 -4.24213 0.70378  
H 1.81968 -4.01195 -0.88697  
H 0.35596 -4.99464 -0.72706  
C -0.40072 -2.58776 3.14042  
H -0.22645 -2.88988 4.18020  
H -0.46944 -3.49782 2.53512  
H -1.35724 -2.05925 3.09563  
C 1.08924 -0.06977 3.90078  
H 1.03381 -0.52880 4.89553  
H 0.23476 0.60674 3.79504  
H 2.00969 0.51994 3.85784  
C 2.56632 -2.53501 2.96840  
H 2.46373 -2.88836 4.00203  
H 3.51256 -1.99306 2.89923  
H 2.63369 -3.41589 2.32277  
C 3.84352 -0.99340 -1.12662  
C 3.38784 -1.78438 -2.36508  
H 4.04668 -2.65341 -2.50292  
H 3.44096 -1.19128 -3.28176  
H 2.36438 -2.16222 -2.26041  
C 3.99566 -2.01472 0.00984  
H 4.40839 -1.57366 0.91834  
H 4.67863 -2.81722 -0.30500  
C 3.03875 -2.46759 0.26873  
C 5.23609 -0.41130 -1.43041  
H 5.69452 0.04632 -0.54943  
H 5.21872 0.33793 -2.22722  
H 5.90339 -1.22250 -1.75614  
C 3.24829 1.64292 0.62763  
C 2.11398 2.39843 1.34588  
H 1.45875 1.71899 1.90185  
H 1.48537 2.97918 0.66554  
H 2.54778 3.09944 2.07424  
C 4.04076 0.90573 1.72126  
H 4.29960 1.61357 2.52164  
H 4.97715 0.48337 1.34676  
H 3.46204 0.09697 2.17637  
C 4.19404 2.68181 -0.00174  
H 4.63580 3.29786 0.79458  
H 3.67457 3.36191 -0.68211  
H 5.01868 2.21816 -0.55241  
C 1.95691 1.30027 -2.29182  
C 1.14728 2.54259 -1.89374  
H 0.37730 2.30324 -1.15431  
H 0.64912 2.96708 -2.77877  
H 1.77406 3.33257 -1.47030  
C 1.02218 0.40709 3.12356  
H 1.54777 -0.41709 -3.60893  
H 0.55043 1.00570 -3.91799  
H 0.22797 -0.02584 -2.51094  
C 3.10756 1.75283 -3.20660  
H 3.83841 2.38051 -2.68894  
H 2.69569 2.34451 -4.03737  
H 3.64159 0.90707 -3.64913  
H -2.76125 1.98855 -2.50520  
H -1.99555 0.49488 -3.11786  
H -5.11231 -0.47891 2.18255  
H -4.38732 -2.06957 1.80048

### 17

Si 0.01326 3.38173 -0.89553

### S88

C 3.81971 0.00183 3.08294  
H 4.19844 0.53729 3.96252  
H 4.60147 0.02245 2.32073  
H 3.66146 -1.04128 3.37492  
C 3.14155 -2.31337 -0.82622  
C 2.21328 -3.54067 -0.82540  
H 2.76872 -4.41661 -0.46092  
H 1.84496 -3.78524 -1.82538  
H 1.34748 -3.40495 -0.16792  
C 3.80386 -2.26026 0.55958  
H 4.55671 -1.47370 0.63518  
H 4.30614 -3.21696 0.76479  
H 3.07018 -2.09458 1.35371  
C 4.24369 -2.56162 -1.87133  
H 5.02669 -1.79899 -1.83528  
H 3.85608 -2.59711 -2.89385  
H 4.72566 -3.52896 -1.66785  
C 3.28373 0.81309 -1.59396  
C 2.55066 2.15382 -1.40350  
H 2.15971 2.26291 -0.38730  
H 1.71357 2.28472 -2.09188  
H 3.25280 2.98258 -1.57780  
C 4.49047 0.84287 -0.64047  
H 5.06432 1.76495 -0.81068  
H 5.17267 0.00304 -0.79762  
H 4.18285 0.84037 0.40896  
C 3.83395 0.76763 -3.03088  
H 4.54821 1.59185 -3.17049  
H 3.04986 0.89328 -3.78245  
H 4.36390 -0.16479 -3.24907  
C 0.84766 -1.00043 -2.62301  
C 0.27276 0.35033 -3.07264  
H -0.05764 0.95091 -2.21959  
H -0.59058 0.18948 -3.73733  
H 0.99642 0.94925 -3.63244  
C -0.34136 -1.84882 -2.14360  
H -0.06534 -2.88496 -1.93912  
H -1.11976 -1.86690 -2.92250  
H -0.79088 -1.44352 -1.23254  
C 1.45442 -1.69368 -3.85483  
H 2.32375 -1.16250 -4.25292  
H 0.70000 -1.73487 -4.65449  
H 1.75623 -2.72390 -3.64534  
C -4.83862 -0.67288 -0.27316  
C -3.40104 0.41308 1.33879  
C -2.70614 0.30718 -0.85217  
H -3.96110 -0.62050 -2.28011  
H -1.94128 0.55262 -1.57915  
H -3.18019 0.75664 2.34390  
H -5.27454 -0.42650 1.85738  
N -2.45292 0.68185 0.41887  
N -5.97004 -1.34103 -0.60188  
C -6.19118 -1.76085 -1.97623  
H -7.13961 -2.29206 -2.03600  
H -6.23636 -0.89937 -2.65224  
H -5.39696 -2.43503 -2.31615  
C -6.95454 -1.64618 0.42325  
H -7.35197 -0.73088 0.87650  
H -7.78167 -2.18960 -0.03036  
H -6.52286 -2.27203 1.21258

### Ime4

C -0.00001 1.56948 -0.00008  
N -1.05666 0.70877 -0.00007  
N 1.05666 0.70879 -0.00004  
C -0.67982 -0.63285 -0.00001  
C 0.67984 -0.63285 -0.00002  
C -2.43479 1.15630 0.00015  
H -2.42088 2.24530 -0.00106  
C -1.66694 -1.75075 -0.00013  
H -2.31176 -1.71953 -0.88499  
H -2.31316 -1.71843 0.88367  
H -1.14952 -2.71231 0.00089  
C 1.66695 -1.75075 0.00015  
H 2.31324 -1.71842 -0.88360

## 15. Appendix

H -5.04003 1.50995 -0.98590  
 C -2.69404 -2.29871 -1.46131  
 C -2.54942 -1.64270 -2.84989  
 H -2.78978 -2.39124 -3.61894  
 H -1.53147 -1.28628 -3.02594  
 H -3.22394 -0.79560 -2.99740  
 C -4.09094 -2.94496 -1.41576  
 H -4.32189 -3.41126 -0.45462  
 H -4.15141 -3.72932 -2.18419  
 H -4.88168 -2.22133 -1.63799  
 C -1.64410 -3.42421 -1.41842  
 H -1.80314 -4.11649 -0.58693  
 H -0.62375 -3.02736 -1.34122  
 H -1.69401 -4.01274 -2.34586  
 C -2.07974 -2.08097 1.68394  
 C -3.10859 -3.20597 1.90130  
 H -3.01161 -4.00118 1.15732  
 H -4.14206 -2.84944 1.88266  
 H -2.93714 -3.66501 2.88611  
 C -2.16896 -1.14010 2.89809  
 H -3.17489 -0.73888 3.04690  
 H -1.47850 -0.29481 2.81434  
 H -1.90074 -1.69304 3.81011  
 C -0.68531 -2.72934 1.72885  
 H -0.50719 -3.16067 2.72549  
 H 0.10671 -2.00097 1.53193  
 H -0.57990 -3.53789 1.00287  
 C 2.80084 1.49656 -2.82017  
 H 3.32037 0.67269 -3.32059  
 H 3.21056 2.43665 -3.20940  
 H 1.73978 1.43635 -3.08541  
 C 2.52563 3.14914 -0.30398  
 H 1.55174 3.45804 -0.69747  
 H 3.26921 3.88179 -0.64112  
 H 2.48684 3.19908 0.79022  
 C 4.92294 1.37336 -0.64569  
 H 5.18239 1.77210 0.33901  
 H 5.40880 2.00437 -1.40017  
 H 5.34483 0.36839 -0.72619  
 C 3.13914 -2.70993 2.25193  
 H 3.55017 -2.92359 3.24584  
 H 3.89814 -2.97803 1.50987  
 H 2.26980 -3.35638 2.09451  
 C 4.28759 0.08879 2.47677  
 H 4.65622 -0.16039 3.47919  
 H 4.12786 1.17225 2.43565  
 H 5.07016 -0.16297 1.75490  
 C 1.59799 -0.53321 3.66596  
 H 0.58016 -0.92136 3.57463  
 H 1.54523 0.53169 3.91336  
 H 2.06753 -1.03871 4.51862  
 C 4.38397 -2.11104 -1.70018  
 H 4.93410 -2.08931 -0.75249  
 H 4.68709 -1.23738 -2.28670  
 H 4.69457 -3.00816 -2.24887  
 C 2.11100 -3.90132 -0.79057  
 H 1.18671 -3.95182 -0.20947  
 H 2.92018 -4.28798 -0.16483  
 H 2.00102 -4.57127 -1.65189  
 C 1.69589 -2.02048 -3.13800  
 H 2.20745 -2.70166 -3.82954  
 H 1.74039 -1.00769 -3.54605  
 H 0.64061 -2.30733 -3.09743  
 C -0.62748 1.94687 -0.23820  
 N -0.40163 2.57669 0.94084  
 N -1.05989 2.93873 -1.06526  
 C -1.11759 4.15771 -0.40759  
 C -0.69171 3.92716 0.86599  
 C -1.38434 2.79684 -2.47882  
 H -1.17846 1.76421 -2.76854  
 C 0.07546 1.93411 2.14826  
 H 0.09021 0.86059 1.97077  
 C -0.49916 4.84752 2.02160  
 H 0.54359 4.84249 2.35593  
 H -0.75544 5.86861 1.73588  
 H -1.12994 4.56547 2.87044

Si -0.10969 0.40665 -0.69858  
 Si -1.99122 -0.75625 0.20818  
 O -0.09999 1.95071 -0.02691  
 O -0.00092 0.34465 -2.26106  
 N 2.29900 0.02142 1.13046  
 N 2.51876 -1.01409 -0.75158  
 C 1.65738 -0.26379 -0.02610  
 C 3.57397 -0.52140 1.12712  
 C 3.71190 -1.17688 -0.06439  
 C 1.69702 0.85877 2.18885  
 H 0.64407 0.90154 1.91855  
 C 1.80901 0.23788 3.58100  
 H 2.78353 0.41778 4.04046  
 H 1.62007 -0.83884 3.56222  
 H 1.05318 0.70099 4.22183  
 C 2.24426 2.28068 2.13446  
 H 2.12233 2.68986 1.13035  
 H 3.30119 2.32224 2.41485  
 H 1.68122 2.90794 2.83228  
 C 4.55997 -0.40547 2.24395  
 H 4.63736 0.61828 2.61600  
 H 5.54769 -0.70142 1.88761  
 H 4.30079 -1.05512 3.08472  
 C 4.89657 -1.94045 -0.56198  
 H 5.10949 -1.71922 -1.60922  
 H 4.75614 -3.02033 -0.46350  
 H 5.77685 -1.66287 0.01993  
 C 2.20311 -1.55980 -2.09984  
 H 1.12658 -1.41914 -2.20127  
 C 2.84460 -0.69782 -3.18051  
 H 2.43578 0.31237 -3.11588  
 H 2.58210 -1.10533 -4.16094  
 H 3.93628 -0.67169 -3.10049  
 C 2.53437 -3.04706 -2.21791  
 H 2.25082 -3.59724 -1.31554  
 H 3.58884 -3.23486 -2.43281  
 H 1.95472 -3.45427 -3.05073  
 C 1.66656 3.43810 -1.78412  
 H 1.81113 4.39386 -2.29936  
 H 1.67815 2.63551 -2.52935  
 H 2.51322 3.28987 -1.10486  
 C -0.13169 4.75607 0.37768  
 H -0.15724 5.73718 -0.10834  
 H 0.70552 4.75190 1.08283  
 H -1.05726 4.64029 0.95237  
 C -1.36405 3.51858 -2.15456  
 H -2.35219 3.43722 -1.68929  
 H -1.26076 2.71135 -2.88653  
 H -1.31526 4.48023 -2.67763  
 C -1.42228 -2.49944 0.89037  
 C -0.74343 -2.33529 2.26009  
 H 0.07183 -1.60247 2.21153  
 H -0.30469 -3.29478 2.57159  
 H -1.43724 -2.02228 3.04498  
 C -0.35613 -3.12815 -0.02764  
 H -0.66713 -3.21314 -1.07103  
 H -0.11632 -4.13981 0.33280  
 H 0.57227 -2.55016 0.00099  
 C -2.57494 -3.50629 1.04208  
 H -3.39069 -3.12258 1.66192  
 H -2.20018 -4.42391 1.51904  
 H -2.99597 -3.79364 0.07446  
 C -2.86034 0.29121 1.61574  
 C -1.84740 0.88033 2.61659  
 H -1.21838 1.63166 2.12755  
 H -1.20644 0.12512 3.08112  
 C -2.39553 1.38364 3.42646  
 C -3.58238 1.50682 1.00608  
 H -3.95487 2.14760 1.81843  
 H -4.44322 1.22413 0.39530  
 H -2.90379 2.11151 0.39263  
 C -3.89404 -0.52743 2.41002  
 H -4.42950 0.13695 3.10376  
 H -3.42584 -1.31157 3.01312  
 H -4.64147 -1.00091 1.76639  
 C -3.17630 -0.96617 -1.32986

H 1.14953 -2.71231 -0.00096  
 H 2.31171 -1.71957 0.88505  
 C 2.43477 1.15632 -0.00004  
 H 2.42086 2.24531 0.00012  
 H -2.96030 0.80043 0.89160  
 H -2.96118 0.79838 -0.88994  
 H 2.96075 0.79929 0.89067  
 H 2.96070 0.79956 -0.89088

### I'Pr<sub>2</sub>Me<sub>2</sub>

C 0.00002 -1.23722 -0.32495  
 N 1.06479 -0.40314 -0.16304  
 N -1.06478 -0.40314 -0.16324  
 C 0.68163 0.91113 0.10850  
 C -0.68168 0.91114 0.10827  
 C 2.42663 -0.94655 -0.20393  
 H 2.27099 -1.95910 -0.58512  
 C 3.02439 -1.05210 1.19835  
 H 2.35951 -1.62855 1.84644  
 H 3.17900 -0.06692 1.64869  
 H 3.99463 -1.55626 1.15404  
 C 3.33721 -0.20100 -1.17853  
 H 2.83105 -0.04209 -2.13475  
 H 4.23545 -0.79808 -1.36027  
 H 3.66113 0.76643 -0.78623  
 C 1.61154 2.06769 0.29230  
 H 2.05181 2.39358 -0.65566  
 H 2.42988 1.83461 0.97820  
 H 1.06627 2.91582 0.71146  
 C -1.61162 2.06769 0.29187  
 H -2.05284 2.39261 -0.65597  
 H -1.06603 2.91633 0.70958  
 H -2.42925 1.83515 0.97882  
 C -2.42661 -0.94662 -0.20390  
 H -2.27102 -1.95916 -0.58513  
 C -3.02400 -1.05217 1.19852  
 H -3.17850 -0.06697 1.64886  
 H -2.35896 -1.62864 1.84642  
 H -3.99427 -1.55632 1.15447  
 C -3.33752 -0.20107 -1.17817  
 H -4.23550 -0.79848 -1.36011  
 H -2.83149 -0.04152 -2.13434  
 H -3.66191 0.76603 -0.78541

### DMAP

C -1.95018 -1.12991 0.01301  
 C -0.56378 -1.19658 -0.02258  
 C 0.18286 0.00001 -0.05137  
 C -0.56379 1.19660 -0.02239  
 C -1.95019 1.12990 0.01318  
 N -2.66335 -0.00001 0.02958  
 H -2.52346 -2.05434 0.03259  
 H -0.08365 -2.16685 -0.02668  
 H -0.08368 2.16688 -0.02626  
 H -2.52348 2.05433 0.03294  
 N 1.55377 -0.00001 -0.10669  
 C 2.26982 1.25150 0.04183  
 H 1.99555 1.95367 -0.75240  
 H 2.07179 1.72990 1.01149  
 H 3.33969 1.06008 -0.03769  
 C 2.26981 -1.25150 0.04216  
 H 3.33970 -1.06012 -0.03722  
 H 2.07159 -1.72964 1.01189  
 H 1.99569 -1.95389 -0.75193

### A

Si -2.49638 -0.42362 0.00007  
 Si 0.42252 0.52760 -0.00005  
 Si 2.41838 -0.67989 0.00005  
 O -0.81526 -0.53474 -0.00026  
 O 0.26856 2.04481 0.00003  
 H -2.93650 0.29138 -1.21352  
 H -2.93601 0.29073 1.21423



## 15. Appendix

C -1.55780 5.41110 -1.08327  
H -1.56535 6.23658 -0.37018  
H -0.88631 5.68142 -1.90444  
H -2.56793 5.30923 -1.49184  
H -2.43844 3.03103 -2.64701  
H -0.75911 3.47627 -3.06401  
H -0.59042 2.16451 2.98490  
H 1.09075 2.27204 2.38013

### B

Si -0.44944 0.20942 0.00000  
O 0.86077 -0.76051 -0.00000  
O -0.39056 1.73278 0.00000  
C -1.93582 -0.88862 -0.00000  
H -1.92178 -1.53491 0.88153  
H -2.84699 -0.29023 -0.00020  
H -1.92156 -1.53519 -0.88132  
C 2.20117 -0.26199 0.00000  
H 2.21356 0.83121 0.00001  
H 2.70758 -0.63866 0.89060  
H 2.70757 -0.63864 -0.89061

### E

Si 2.66457 -1.75975 0.55812  
Si 0.85262 0.29644 -0.60324  
Si 1.02862 2.61624 -0.30417  
O 1.71286 -0.39501 0.66773  
O 1.02505 -0.31340 -2.02310  
N -1.49965 0.04627 1.25325  
N -2.00596 -0.52190 -0.75772  
C -0.98448 -0.09657 0.01271  
C -2.83592 -0.28399 1.26228  
C -3.15416 -0.64401 -0.00885  
C -0.76253 0.51632 2.42600  
H 0.30268 0.36897 2.25051  
C -1.93098 -0.83121 -2.19187  
H -0.88495 -0.73977 -2.50335  
H -2.28881 -1.85070 -2.34440  
H -2.56443 -0.12850 -2.73641  
H -3.43252 -0.24231 2.15985  
H -0.97425 1.57332 2.59748  
H -1.07391 -0.07123 3.29076  
H 3.81096 -1.55184 -0.34968  
H 1.86772 -2.92388 0.10633  
H 3.16518 -2.02939 1.92657  
H 0.64988 3.03015 1.07885  
H 2.40584 3.10977 -0.55067  
H 0.10358 3.32963 -1.22407  
H -4.08382 -0.98160 -0.43910

### H

Si 2.67069 -0.32480 -1.46306  
Si 0.91372 0.49166 0.77062  
O 1.80793 -0.65717 -0.07992  
O 1.14996 1.98472 0.40970  
N -1.42968 -1.22195 -0.00331  
N -1.83067 0.86136 -0.34266  
C -0.88796 0.01054 0.10930  
C -2.70560 -1.14648 -0.51557  
C -2.95700 0.17135 -0.73066  
C -0.76872 -2.46530 0.38781  
H 0.31001 -2.31662 0.33464  
C -1.69559 2.32116 -0.43346  
H -0.66280 2.57886 -0.17134  
H -1.92078 2.62511 -1.45705  
H -2.40379 2.78396 0.25658  
H -3.30985 -2.02296 -0.68852  
H -1.06547 -2.74240 1.40164  
H -1.06343 -3.25057 -0.30945  
H 3.81714 0.56944 -1.20364  
H 1.79159 0.27223 -2.49818  
H 3.17251 -1.62498 -1.96984  
H -3.82432 0.67205 -1.13103

C -2.60075 -2.01512 -2.29984  
H -3.22361 -2.03825 -3.20540  
H -2.60523 -3.02625 -1.88156  
H -1.58306 -1.74807 -2.60803  
C -4.60238 -1.39734 -0.94509  
H -5.13118 -0.62240 -0.38185  
H -4.62615 -2.31854 -0.35392  
H -5.18192 -1.58012 -1.86145  
C -3.26529 0.34203 -2.14245  
H -3.65668 1.18337 -1.56654  
H -3.94859 0.18430 -2.98985  
H -2.28457 0.61301 -2.54453

### C

Si -0.05998 0.42979 -0.00554  
O -1.08280 -0.84303 -0.00632  
O -0.48967 1.89453 0.00307  
C -2.50918 -0.72290 0.00521  
H -2.81440 0.32659 0.02337  
H -2.90105 -1.20787 -0.89059  
H -2.88832 -1.23540 0.89109  
Si 2.10528 -0.43759 0.00158  
H 2.21064 -1.45098 -1.06969  
H 3.05405 0.67045 -0.22286  
H 2.33977 -1.06812 1.31888

### F

Si 1.30750 0.42869 0.37914  
O 1.97886 -0.75963 -0.60523  
O 1.48966 1.92393 -0.00490  
N -1.21464 -1.19497 0.07278  
N -1.61156 0.90917 -0.09636  
C -0.61902 0.01814 0.10363  
C -2.56972 -1.06710 -0.13656  
C -2.81878 0.26425 -0.24438  
C -0.52738 -2.47044 0.26730  
H 0.52172 -2.34173 -0.00251  
C -1.45200 2.36773 -0.15794  
H -0.37767 2.58669 -0.13493  
H -1.90057 2.72532 -1.08635  
H -1.96278 2.81474 0.69728  
H -3.22631 -1.92055 -0.19834  
H -0.61608 -2.78530 1.30941  
H -0.98733 -3.21659 -0.38208  
H -3.73671 0.80231 -0.42105  
C 1.64245 -0.21250 2.10537  
H 2.70132 -0.06603 2.34044  
H 1.05608 0.34023 2.84547  
H 1.42406 -1.28065 2.20848  
C 2.09018 -0.50536 -1.99441  
H 2.43805 0.51579 -2.18052  
H 2.80202 -1.21792 -2.41915  
H 1.11993 -0.64018 -2.49606

H -3.00431 -1.80834 -0.00019  
H 2.43906 -1.53011 1.20999  
H 2.43950 -1.53007 -1.20992  
H 3.54863 0.26861 0.00023

### D

Si -2.12513 -0.11918 -0.00009  
Si 0.88946 0.20200 -0.00005  
O -0.51718 -0.62054 0.00032  
O 0.98526 1.72223 0.00006  
H -2.38411 0.69418 -1.20394  
H -2.39402 0.66084 1.22353  
H -2.94034 -1.34848 -0.02014  
C 2.27296 -1.02313 -0.00012  
H 2.19873 -1.66862 -0.87942  
H 3.23376 -0.50841 -0.00360  
H 2.20291 -1.66375 0.88309

### G

Si -1.15233 0.54403 0.05872  
O -1.70628 -0.52367 1.23381  
O -1.18230 2.07716 0.31757  
N 1.29041 -1.23247 0.03460  
N 1.81722 0.84372 -0.14485  
C 0.76439 0.01261 0.00052  
C 2.66023 -1.18373 -0.09277  
C 2.99174 0.12924 -0.20520  
C 0.52414 -2.47304 0.15465  
H -0.45660 -2.23654 0.56782  
C 1.75022 2.30880 -0.22455  
H 0.71240 2.60825 -0.04157  
H 2.41208 2.72683 0.53576  
H 2.07924 2.62251 -1.21712  
H 3.27066 -2.07293 -0.08495  
H 0.41592 -2.93727 -0.82749  
H 1.05642 -3.14691 0.82762  
H 3.95003 0.61250 -0.31272  
C -1.52076 -0.18777 2.60043  
H -1.78257 0.85841 2.78658  
H -2.16086 -0.83773 3.20173  
H -0.47486 -0.34658 2.90274  
Si -2.00133 -0.36278 -1.92871  
H -3.47055 -0.19920 -2.04970  
H -1.36207 0.28813 -3.10353  
H -1.70245 -1.82032 -2.04292

C 0.90929 -0.10964 2.54328  
H 1.89601 0.07149 2.98138  
H 0.17518 0.44300 3.13736  
H 0.69900 -1.18067 2.63094

#### 4. References

- [S1] G. R. Fulmer, A. J. M. Miller, N. H. Sherden, H. E. Gottlieb, A. Nudelman, B. M. Stoltz, J. E. Bercaw, K. I. Goldberg, *Organometallics* **2010**, *29*, 2176-2179.
- [S2] C. Kayser, R. Fischer, J. Baumgartner, C. Marschner, *Organometallics* **2002**, *21*, 1023-1030.
- [S3] N. Wiberg, K. Amelunxen, H.-W. Lerner, H. Schuster, H. Nöth, I. Krossing, M. Schmidt-Amelunxen, T. Seifert, *J. Organomet. Chem.* **1997**, *542*, 1-18.
- [S4] N. Kuhn, T. Kratz, *Synthesis* **1993**, 561-562.
- [S5] K. Fredenhagen, G. Cadenbach, *Z. Anorg. Allg. Chem.* **1926**, *158*, 249-263.
- [S6] T. Gross, H. Reinke, H. Oehme, *Can. J. Chem.* **2000**, *78*, 1399-1404.
- [S7] a) A. Sekiguchi, T. Tanaka, M. Ichinohe, K. Akiyama, S. Tero-Kubota, *J. Am. Chem. Soc.* **2003**, *125*, 4962-4963; b) A. Sekiguchi, T. Tanaka, M. Ichinohe, K. Akiyama, P. P. Gaspar, *J. Am. Chem. Soc.* **2008**, *130*, 426-427.
- [S8] H. Cui, J. Zhang, C. Cui, *Organometallics* **2013**, *32*, 1-4.
- [S9] a) W. Ando, M. Fujita, H. Yoshida, A. Sekiguchi, *J. Am. Chem. Soc.* **1988**, *110*, 3310-3311; b) S. Zhang, P. E. Wagenseller, R. T. Conlin, *J. Am. Chem. Soc.* **1991**, *113*, 4278-4281.
- [S10] *APEX suite of crystallographic software*, APEX 3 version 2015.5-2; Bruker AXS Inc.: Madison, Wisconsin, USA, **2015**.
- [S11] *SAINT*, Version 7.56a and *SADABS* Version 2008/1; Bruker AXS Inc.: Madison, Wisconsin, USA, **2008**.
- [S12] G. M. Sheldrick, *SHELXL-2014*, University of Göttingen, Göttingen, Germany, **2014**.
- [S13] C. B. Hübschle, G. M. Sheldrick, B. Dittrich, *J. Appl. Cryst.* **2011**, *44*, 1281-1284.
- [S14] G. M. Sheldrick, *SHELXL-97*, University of Göttingen, Göttingen, Germany, **1998**.
- [S15] A. J. C. Wilson, *International Tables for Crystallography*, Vol. C, Tables 6.1.1.4 (pp. 500-502), 4.2.6.8 (pp. 219-222), and 4.2.4.2 (pp. 193-199); Kluwer Academic Publishers: Dordrecht, The Netherlands, **1992**.
- [S16] C. F. Macrae, I. J. Bruno, J. A. Chisholm, P. R. Edgington, P. McCabe, E. Pidcock, L. Rodriguez-Monge, R. Taylor, J. van de Streek, P. A. Wood, *J. Appl. Cryst.* **2008**, *41*, 466-470.
- [S17] M. J. Frisch, G. W. Trucks, H. B. Schlegel, G. E. Scuseria, M. A. Robb, J. R. Cheeseman, G. Scalmani, V. Barone, B. Mennucci, G. A. Petersson, H. Nakatsuji, M. Caricato, X. Li, H. P. Hratchian, A. F. Izmaylov, J. Bloino, G. Zheng, J. L. Sonnenberg, M. Hada, M. Ehara, K. Toyota, R. Fukuda, J. Hasegawa, M. Ishida, T. Nakajima, Y. Honda, O. Kitao, H. Nakai, T. Vreven, J. A. Montgomery, Jr., J. E. Peralta, F. Ogliaro, M. Bearpark, J. J. Heyd, E. Brothers, K. N. Kudin, V. N. Staroverov, R. Kobayashi, J. Normand, K. Raghavachari, A. Rendell, J. C. Burant, S. S. Iyengar, J. Tomasi, M. Cossi, N. Rega, J. M. Millam, M. Klene, J. E. Knox, J. B. Cross, V. Bakken, C. Adamo, J. Jaramillo, R. Gomperts, R. E. Stratmann, O. Yazyev, A. J. Austin, R. Cammi, C. Pomelli, J. W. Ochterski, R. L. Martin, K. Morokuma, V. G. Zakrzewski, G. A. Voth, P. Salvador, J. J. Dannenberg, S. Dapprich, A. D. Daniels, Ö. Farkas, J. B. Foresman, J. V. Ortiz, J. Cioslowski, D. J. Fox, *Gaussian 09, Revision E.01*, Gaussian, Inc., Wallingford CT, **2009**.

- [S18] a) R. Ditchfield, W. J. Hehre, J. A. Pople, *J. Chem. Phys.* **1971**, *54*, 724-728; b) W. J. Hehre, R. Ditchfield, J. A. Pople, *J. Chem. Phys.* **1972**, *56*, 2257-2261; c) Y. Zhao, D. G. Truhlar, *Theor. Chem. Acc.* **2008**, *120*, 215-241.
- [S19] A. V. Marenich, C. J. Cramer, D. G. Truhlar, *J. Phys. Chem. B* **2009**, *113*, 6378-6396.
- [S20] S. E. Wheeler, K. N. Houk, *J. Chem. Theory Comput.* **2010**, *6*, 395-404.
- [S21] K. Fukui, *Acc. Chem. Res.* **1981**, *14*, 363-368.
- [S22] a) R. Krishnan, J. S. Binkley, R. Seeger, J. A. Pople, *J. Chem. Phys.* **1980**, *72*, 650-654; b) A. D. McLean, G. S. Chandler, *J. Chem. Phys.* **1980**, *72*, 5639-5648.
- [S23] E. D. Glendening, J. K. Badenhoop, A. E. Reed, J. E. Carpenter, J. A. Bohmann, C. M. Morales, C. R. Landis, F. Weinhold, *Vol. 34* **2013**, *Theoretical Chemistry Institute, University of Wisconsin, Madison*, 1429-1437.
- [S24] a) E. D. Glendening, C. R. Landis, F. Weinhold, *Wiley Interdiscip. Rev. Comput. Mol. Sci.* **2011**, *2*, 1-42; b) E. D. Glendening, C. R. Landis, F. Weinhold, *J. Comput. Chem.* **2013**, *34*, 1429-1437.
- [S25] Y. Zhao, D. G. Truhlar, *J. Chem. Phys.* **2006**, *125*, 194101.
- [S26] G. A. Andrienko, <http://www.chemcraftprog.com>, **2015**.
- [S27] C. Y. Legault, *Université de Sherbrooke*, <http://www.cylview.org>, **2009**.
- [S28] R. Dennington, T. A. Keith, J. M. Millam, Version 5 ed., Semichem Inc., Shawnee Mission, KS, **2009**.
- [S29] V. Y. Lee, *Organosilicon Compounds: Theory and Experiment (Synthesis), Vol. 1*, 1st ed., Academic Press, New York, **2017**; and references therein.
- [S30] M. Kira, *Proc. Jpn. Acad. Ser. B* **201**, *88*, 167-191.
- [S31] a) M. Ichinohe, R. Kinjo, A. Sekiguchi, *Organometallics* **2003**, *22*, 4621-4623. b) D. Wendel, T. Szilvási, C. Jandl, S. Inoue, B. Rieger, *J. Am. Chem. Soc.* **2017**, *139*, 9156-9159.
- [S32] M. Kosa, M. Karni, Y. Apeloig, *J. Am. Chem. Soc.* **2013**, *135*, 9032-9040.
- [S33] a) D. Himmel, I. Krossing, A. Schnepf, *Angew. Chem. Int. Ed.* **2014**, *53*, 370-374; b) G. Frenking, *Angew. Chem. Int. Ed.* **2014**, *53*, 6040-6046; c) D. Himmel, I. Krossing, A. Schnepf, *Angew. Chem. Int. Ed.* **2014**, *53*, 6047-6048.
- [S34] J. D. Epping, S. Yao, M. Karni, Y. Apeloig, M. Driess, *J. Am. Chem. Soc.* **2010**, *132*, 5443-5455.



## 15.3 Supporting Information Chapter 9

Electronic Supplementary Material (ESI) for RSC Advances.  
This journal is © The Royal Society of Chemistry 2020

### Supporting Information

#### **DMAP-stabilized bis(silyl)silylenes as versatile synthons for organosilicon compounds**

*Richard Holzner,<sup>†</sup> Dominik Reiter,<sup>†</sup> Philipp Frisch, and Shigeyoshi Inoue\**

Department of Chemistry, WACKER-Institute of Silicon Chemistry, Technische Universität München, Lichtenbergstraße 4, 85748 Garching bei München (Germany) \*E-mail: [s.inoue@tum.de](mailto:s.inoue@tum.de)

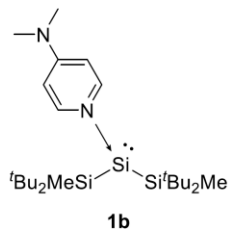
## Table of Contents

1. Experimental Section .....	3
1.1. General Methods and Instrumentation.....	3
1.2. (tBu <sub>2</sub> MeSi) <sub>2</sub> Si:←DMAP ( <b>1b</b> ).....	4
1.3. Bis(hypersilyl)silylene DMAP complex ( <b>1c</b> ).....	7
1.4. Silyl Radical <b>2</b> .....	9
1.5. Azasilepin <b>3</b> .....	10
1.6. Hexakis(trimethylsilyl)trisilirane ( <b>4</b> ).....	14
1.7. Hydrosilanes <b>5a-c</b> .....	16
1.8. Siliranes <b>6</b> .....	17
1.9. Silimine <b>7a</b> .....	18
1.10. Silimine <b>7b</b> .....	19
2. X-ray Crystallographic Data .....	22
2.1. General Information.....	22
2.2 SC-XRD structures.....	23
2.3 Crystal data and structural refinement parameters .....	25
3. References.....	26

## 1. Experimental Section

### 1.1. General Methods and Instrumentation

All manipulations were carried out under exclusion of water and oxygen under an atmosphere of argon 4.6 ( $\geq 99.996\%$ ) using standard Schlenk and glovebox techniques. The glassware used was heat dried under fine vacuum prior to use. All solvents were refluxed over sodium/benzophenone, freshly distilled under argon and deoxygenated prior to use. PTFE-based grease (*Triboflon III* from *Freudenberg & Co. KG*) was used as sealant. Deuterated benzene ( $C_6D_6$ ) was obtained from Sigma-Aldrich, dried over Na/K alloy, flask-to-flask condensed, deoxygenated by three freeze-pump-thaw cycles and stored over 3 Å molecular sieves in a glovebox. All NMR samples were prepared under argon in *J. Young* PTFE valve NMR tubes. The NMR spectra were recorded on a *Bruker DRX400* ( $^1H$ : 400.13 MHz,  $^{13}C$ : 100.62 MHz,  $^{29}Si$ : 79.49 MHz), *AV500* ( $^1H$ : 500.13 MHz) or *AV500C* ( $^1H$ : 500.36 MHz,  $^{13}C$ : 125.83 MHz,  $^{29}Si$ : 99.41 MHz) spectrometer at ambient temperature (300 K), unless otherwise stated. The  $^1H$ ,  $^{13}C\{^1H\}$  and  $^{29}Si\{^1H\}$  NMR spectroscopic chemical shifts  $\delta$  are reported in ppm relative to tetramethylsilane.  $^1H$  and  $^{13}C\{^1H\}$  NMR spectra are calibrated against the residual proton and natural abundance carbon resonances of the respective deuterated solvent as internal standard ( $C_6D_6$ :  $\delta(^1H) = 7.16$  ppm and  $\delta(^{13}C) = 128.1$  ppm).<sup>[S1]</sup> The following abbreviations are used to describe signal multiplicities: s = singlet, d = doublet, dd = doublet of doublets, m = multiplet, br = broad. In some NMR spectra, signals from silicone oil ( $C_6D_6$ :  $\delta(^1H) = 0.29$  ppm,  $\delta(^{13}C) = 1.4$  ppm and  $\delta(^{29}Si) = -21.8$  ppm), originating from the cannulas used (*B. Braun Melsungen AG Sterican®*), can be observed. EPR spectra were recorded on a *Jeol JES-Fa200* esr spectrometer with a spectrometer frequency of 9.267 GHz (X-band). Quantitative elemental analyses (EA) were measured with a *EURO EA (HEKAtech)* instrument equipped with a CHNS combustion analyzer at the *Laboratory for Microanalysis* at the *TUM Catalysis Research Center*. Melting Points (m.p.) were determined in sealed glass capillaries under inert gas by a *Büchi M-565* melting point apparatus. Unless otherwise stated, all commercially available chemicals were purchased from *abcr GmbH* or *Sigma-Aldrich* and used without further purification. Hydrogen ( $H_2$ ) 5.0 ( $\geq 99.999\%$ ) and ethylene 3.5 ( $\geq 99.95\%$ ) were purchased from *Westfalen AG* and used as received. The compounds  $((TMS)_3Si)_2SiBr_2$ ,<sup>[S2]</sup>  $(^tBu_2MeSi)_2SiBr_2$ ,<sup>[S3]</sup>  $(^tBu_3Si)_2SiBr_2$ <sup>[S4]</sup> and  $((TMS)_3Si)(^tBu_3Si)Si\leftarrow DMAP$  (**1a**)<sup>[S5]</sup> were prepared as described in the corresponding references. Potassium graphite ( $KC_8$ ) was synthesized following a literature reported procedure upon heating a 1:8 mixture of potassium and graphite in a thick-walled, PTFE-capped pressurize-able Schlenk flask to 500 °C until a homogenous bronze powder was obtained.<sup>[S6]</sup>

1.2. (<sup>t</sup>Bu<sub>2</sub>MeSi)<sub>2</sub>Si←DMAP (**1b**)Si<sub>3</sub>C<sub>25</sub>H<sub>52</sub>N<sub>2</sub>

464.96 g/mol

THF (10 mL) was added to a mixture of (<sup>t</sup>Bu<sub>2</sub>MeSi)<sub>2</sub>SiBr<sub>2</sub> (300 mg, 597 μmol, 1.0 eq.), KC<sub>8</sub> (169 mg, 1.25 mmol, 2.1 eq.) and DMAP (72.9 mg, 597 μmol, 1.0 eq.) at ambient temperature. After stirring for 3 hours, the solvent was removed under reduced pressure and the residue was extracted with toluene (3 × 2 mL) to remove KBr and graphite. The solvent was evaporated *in vacuo* and compound **1b** was obtained as red-brown, crystalline solid (233 mg, 551 μmol, 92%). Crystals suitable for SC-XRD analysis were obtained from a cooled (-35 °C) toluene solution of **1b**.

**m.p.** = 140 °C (decomposition; color change from red-brown to black)

**<sup>1</sup>H NMR (500 MHz, C<sub>6</sub>D<sub>6</sub>, 300 K):** δ [ppm] = 8.66 (d, <sup>3</sup>J = 7.5 Hz, 2H, *o*-C<sup>DMAP</sup>H), 5.42 (d, <sup>3</sup>J = 7.5 Hz, 2H, *m*-C<sup>DMAP</sup>H), 1.76 (s, 6H, N(CH<sub>3</sub>)<sub>2</sub>), 1.41 (s, 36H, C(CH<sub>3</sub>)<sub>3</sub>), 0.42 (s, 6H, Si(CH<sub>3</sub>)<sub>2</sub>).

**<sup>13</sup>C{<sup>1</sup>H} NMR (126 MHz, C<sub>6</sub>D<sub>6</sub>, 300 K):** δ [ppm] = 154.3 (*p*-C<sup>DMAP</sup>), 153.0 (*o*-C<sup>DMAP</sup>), 105.2 (*m*-C<sup>DMAP</sup>), 38.1 (N(CH<sub>3</sub>)<sub>2</sub>), 31.2 (C(CH<sub>3</sub>)<sub>3</sub>), 22.9 (C(CH<sub>3</sub>)<sub>3</sub>), -3.7 (Si(CH<sub>3</sub>)<sub>2</sub>).

**<sup>29</sup>Si{<sup>1</sup>H} NMR (99 MHz, C<sub>6</sub>D<sub>6</sub>, 300 K):** δ [ppm] = 61.5 (Si:), 11.8 (Si<sup>t</sup>Bu<sub>2</sub>Me).

Note: The chemical shifts of DMAP-stabilized silylenes **1** and silaimines **7** are dependent on the concentration of the NMR sample.

<b>EA:</b>	Si <sub>3</sub> C <sub>25</sub> H <sub>52</sub> N <sub>2</sub>	Calculated [%]:	C (64.58), H (11.27), N (6.03)
		Experimental [%]:	C (64.34), H (11.33), N (5.98)

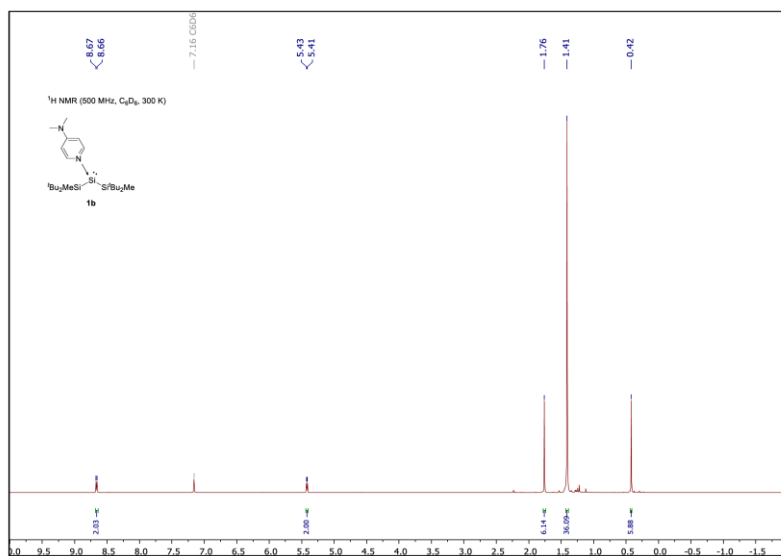


Fig. S1: <sup>1</sup>H NMR spectrum (500 MHz) of compound **1b** in C<sub>6</sub>D<sub>6</sub> at 300 K.

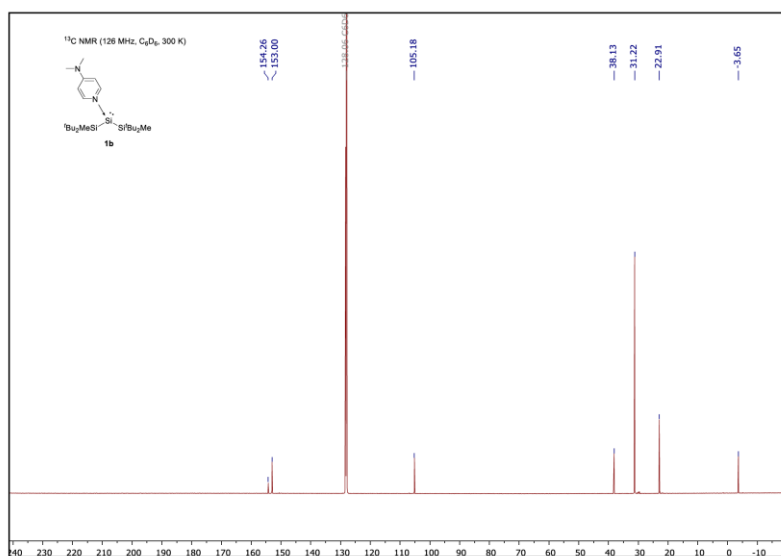


Fig. S2: <sup>13</sup>C NMR spectrum (126 MHz) of compound **1b** in C<sub>6</sub>D<sub>6</sub> at 300 K.

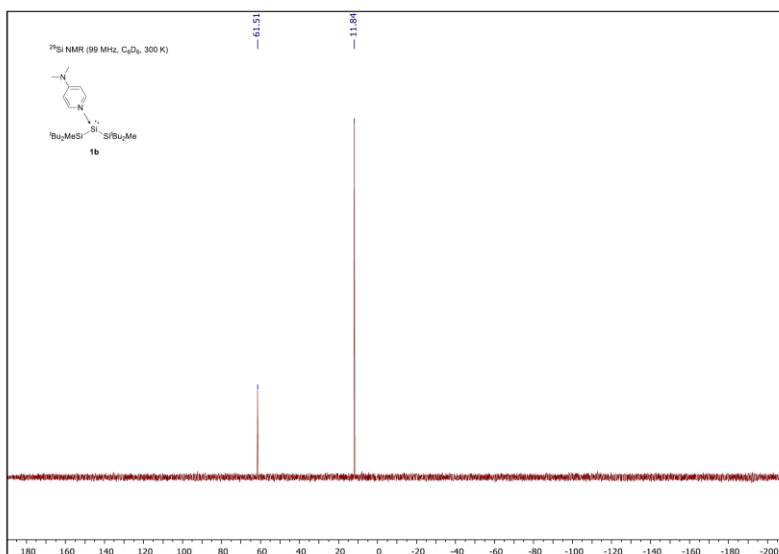


Fig. S3:  $^{29}\text{Si}$  NMR spectrum (99 MHz) of compound **1b** in  $\text{C}_6\text{D}_6$  at 300 K.

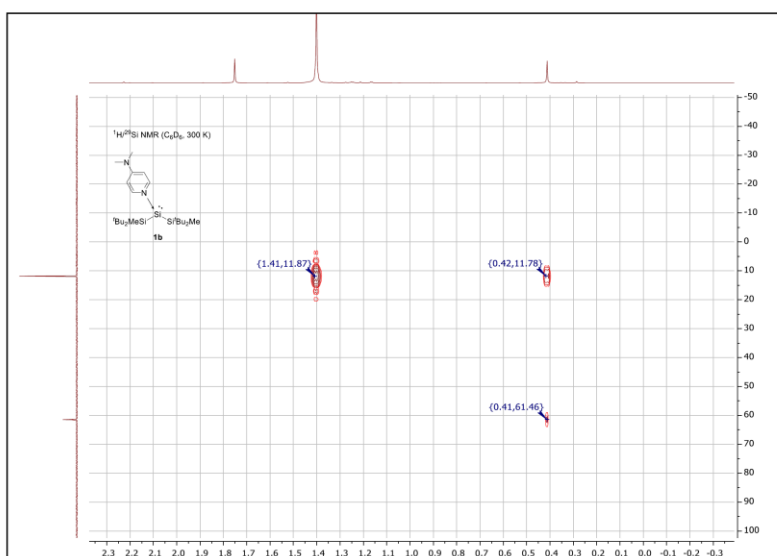
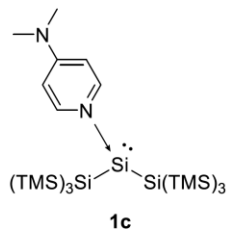


Fig. S4:  $^1\text{H}/^{29}\text{Si}$  HMBC NMR spectrum of compound **1b** in  $\text{C}_6\text{D}_6$  at 300 K.



1.3. Bis(hypersilyl)silylene DMAP complex (**1c**)
 $\text{Si}_9\text{C}_{25}\text{H}_{64}\text{N}_2$ 

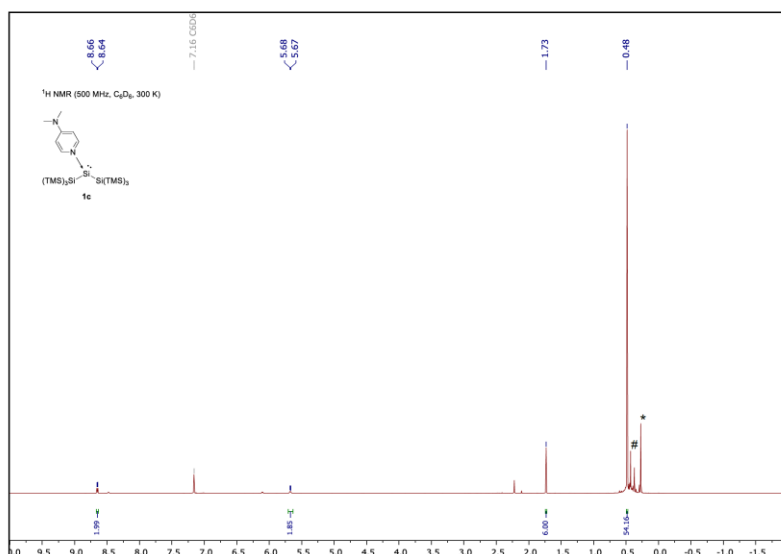
645.57 g/mol

THF (10 mL) was added to a mixture of  $((\text{TMS})_3\text{Si})_2\text{SiBr}_2$  (300 mg, 439  $\mu\text{mol}$ , 1.0 eq.),  $\text{KC}_8$  (125 mg, 922  $\mu\text{mol}$ , 2.1 eq.) and DMAP (53.7 mg, 439  $\mu\text{mol}$ , 1.0 eq.) at ambient temperature. After stirring for 3 hours, the solvent was removed under reduced pressure and the residue was extracted with toluene ( $3 \times 2$  mL) to remove KBr and graphite. The solvent was evaporated *in vacuo* and compound **1c** was obtained as dark-brown solid.

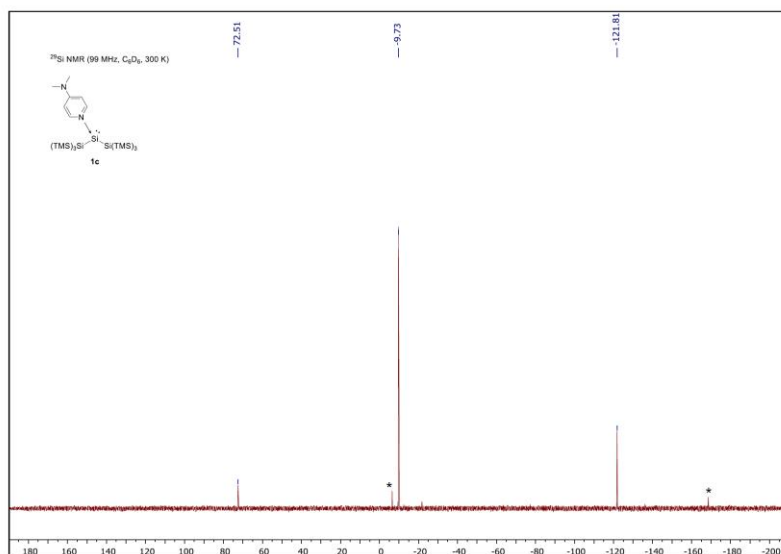
Note: During the synthesis of **1c**, the concomitant formation of hexakis(trimethylsilyl)trisilirane (**4**) and  $\text{Si}(\text{TMS})_4$  was observed. Therefore, no sample of **1c** with sufficient purity for elemental analysis was obtained and the yield was not determined.

$^1\text{H}$  NMR (500 MHz,  $\text{C}_6\text{D}_6$ , 300 K):  $\delta$  [ppm] = 8.65 (d,  $^3J = 7.1$  Hz, 2H, *o*- $\text{C}^{\text{DMAP}}\text{H}$ ), 5.67 (d,  $^3J = 6.6$  Hz, 2H, *m*- $\text{C}^{\text{DMAP}}\text{H}$ ), 1.73 (s, 6H,  $\text{N}(\text{CH}_3)_2$ ), 0.48 (s, 54H,  $\text{Si}(\text{CH}_3)_3$ ).

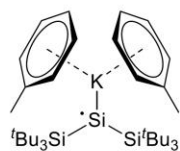
$^{29}\text{Si}\{^1\text{H}\}$  NMR (99 MHz,  $\text{C}_6\text{D}_6$ , 300 K):  $\delta$  [ppm] = 72.5 (*Si*), -9.7 (*Si*( $\text{CH}_3$ )<sub>3</sub>), -121.8 (*Si*( $\text{TMS}$ )<sub>3</sub>).



**Fig. S5:**  $^1\text{H}$  NMR spectrum (500 MHz) of compound **1c** in  $\text{C}_6\text{D}_6$  at 300 K. Signals labeled with \* and # belong to  $\text{Si}(\text{TMS})_4$  and hexakis(trimethylsilyl)trisilirane (**4**), respectively.



**Fig. S6:** <sup>29</sup>Si NMR spectrum (99 MHz) of compound **1c** in C<sub>6</sub>D<sub>6</sub> at 300 K. Signals labeled with \* belong to hexakis(trimethylsilyl)trisilirane (**4**).

1.4. Silyl Radical **2****2**Si<sub>3</sub>C<sub>38</sub>H<sub>70</sub>K

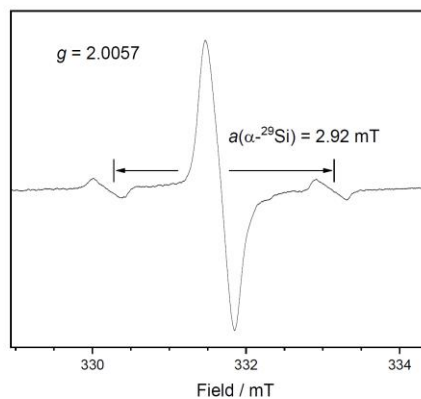
650.33 g/mol

Precooled THF (10 mL, -78 °C) was added to a mixture of (t-Bu<sub>3</sub>Si)<sub>2</sub>SiBr<sub>2</sub> (100 mg, 170 μmol, 1.0 eq.) and KC<sub>8</sub> (92.2 mg, 682 μmol, 3.5 eq.). The reaction mixture was allowed to warm to room temperature over 16 hours and the solvent was subsequently removed under reduced pressure. Concomitantly formed KBr and graphite were separated by extracting the residue with toluene (3 × 4 mL). Evaporation of the solvent *in vacuo* and subsequent washing of the residue with *n*-hexane (3 × 2 mL) afforded compound **2** as orange-brown solid (54.1 mg, 88.5 μmol, 52%). Crystals suitable for SC-XRD analysis were obtained from a cooled (-35 °C) solution of **2** in toluene.

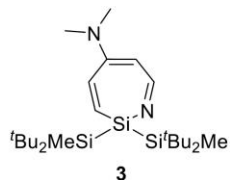
**m.p.** = 60 °C (decomposition; color change to dark red)

**EPR** (toluene, 286 K)  $g = 2.0056$ ,  $a(\alpha\text{-}^{29}\text{Si}) = 2.92$  mT

Note: Compound **2** is completely NMR silent. Elemental analysis was not matching, presumably because an unquantifiable amount of coordinating toluene was removed during drying compound **2** in fine vacuum. Due to its extreme air and moisture sensitivity and the fact, that it is not stable in toluene, no satisfactory spectroscopic data of **2** was obtained before addition of crown ether (18-C-6). With crown ether however, one signal in the EPR spectrum was observed (Fig. **S7**). Hyperfine coupling with the β-<sup>29</sup>Si nuclei was not visible.



**Fig. S7:** X-band EPR spectrum of compound **2** + crown ether (18-C-6) in toluene ( $1 \times 10^{-4}$ M, 286 K).

1.5. Azasilepin **3**
 $\text{Si}_3\text{C}_{25}\text{H}_{52}\text{N}_2$ 

464.96 g/mol

A solution of DMAP-stabilized silylene **1b** (36.0 mg, 85.1  $\mu\text{mol}$ ) in benzene (2 mL) was heated to 65 °C for 16 h. The color changed from deep-brown to yellow. Evaporation of the solvent, afforded compound **3** as yellow solid (36.0 mg, 85.1  $\mu\text{mol}$ , quant.). Crystals suitable for SC-XRD analysis were obtained from a cooled (-35 °C) solution of **3** in *n*-hexane.

**$^1\text{H}$  NMR (500 MHz,  $\text{C}_6\text{D}_6$ , 300 K):**  $\delta$  [ppm] = 8.34 (d,  $^3J = 4.7$  Hz, 1H, NCH), 6.27 (dd,  $^3J = 15.5$  Hz,  $^4J = 2.5$  Hz, 1H, SiCHCH), 6.01 (d,  $^3J = 15.5$  Hz, 1H, SiCH), 4.68 (dd,  $^3J = 4.7$  Hz,  $^4J = 2.5$  Hz, 1H, NCHCH), 2.27 (s, 6H, N(CH $_3$ ) $_2$ ), 1.29 (s, 18H, C(CH $_3$ ) $_3$ ), 1.19 (s, 18H, C(CH $_3$ ) $_3$ ), 0.37 (s, 6H, Si(CH $_3$ )).

**$^{13}\text{C}\{^1\text{H}\}$  NMR (126 MHz,  $\text{C}_6\text{D}_6$ , 300 K):**  $\delta$  [ppm] = 165.4 (SiNCH), 156.2 (CNMe $_2$ ), 138.2 (NCHCH), 137.4 (SiCHCH), 105.8 (SiCHCH), 40.3 (N(CH $_3$ ) $_2$ ), 30.4 (Si(C(CH $_3$ ) $_3$ ), 30.1 (Si(C(CH $_3$ ) $_3$ ), 22.5 (Si(C(CH $_3$ ) $_3$ ), 21.6 (Si(C(CH $_3$ ) $_3$ ), -4.9 (Si(CH $_3$ )).

**$^{29}\text{Si}\{^1\text{H}\}$  NMR (99 MHz,  $\text{C}_6\text{D}_6$ , 300 K):**  $\delta$  [ppm] = 2.0 (Si $^t$ Bu $_2$ Me), -28.1 (SiN).

<b>EA:</b>	$\text{Si}_3\text{C}_{25}\text{H}_{52}\text{N}_2$	Calculated [%]:	C (64.58), H (11.27), N (6.03)
		Experimental [%]:	C (64.62), H (11.47), N (5.99)

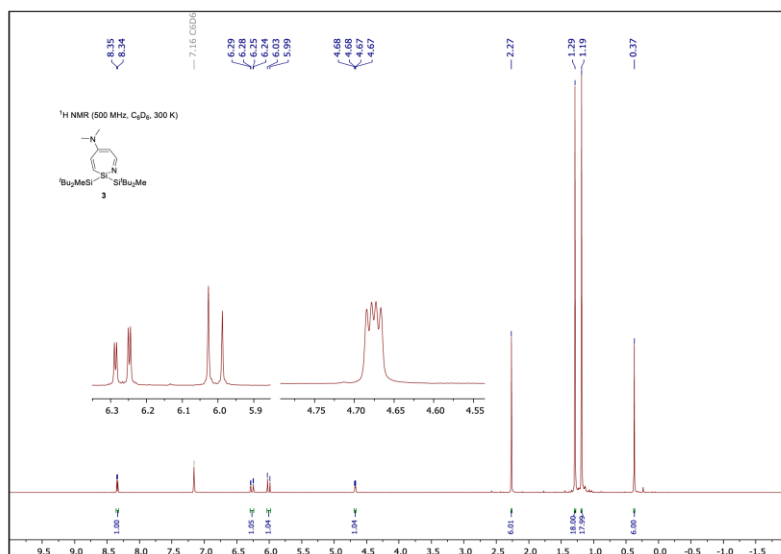


Fig. S8: <sup>1</sup>H NMR spectrum (500 MHz) of compound **3** in C<sub>6</sub>D<sub>6</sub> at 300 K.

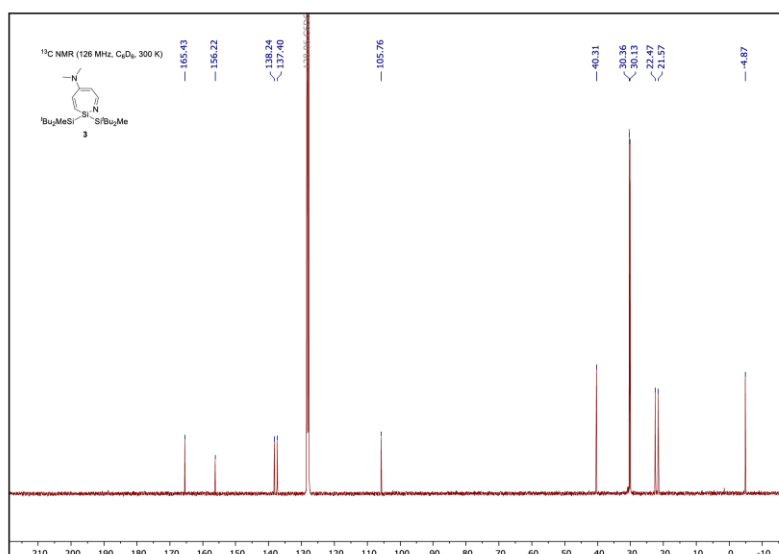


Fig. S9: <sup>13</sup>C NMR spectrum (126 MHz) of compound **3** in C<sub>6</sub>D<sub>6</sub> at 300 K.

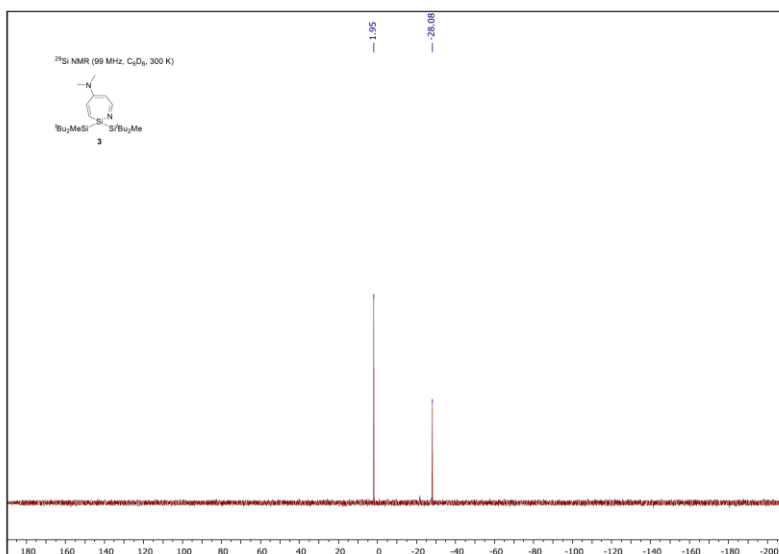


Fig. S10: <sup>29</sup>Si NMR spectrum (99 MHz) of compound **3** in C<sub>6</sub>D<sub>6</sub> at 300 K.

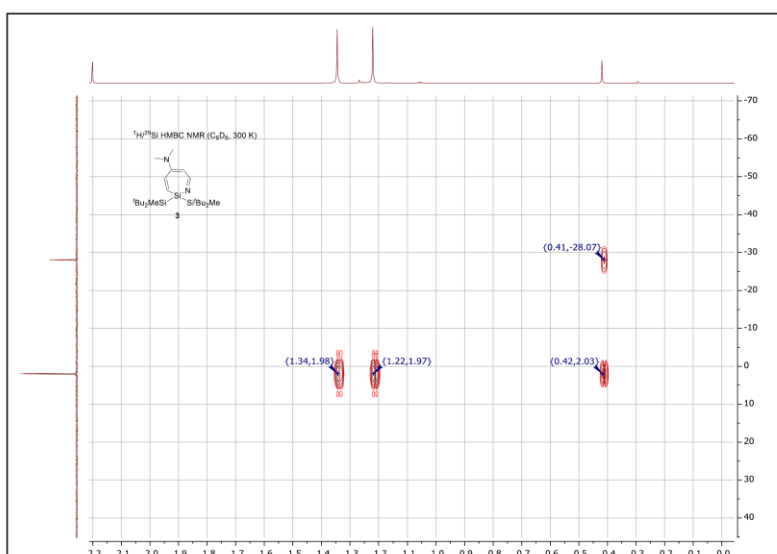


Fig. S11: <sup>1</sup>H/<sup>29</sup>Si HMBC NMR spectrum of compound **3** in C<sub>6</sub>D<sub>6</sub> at 300 K.

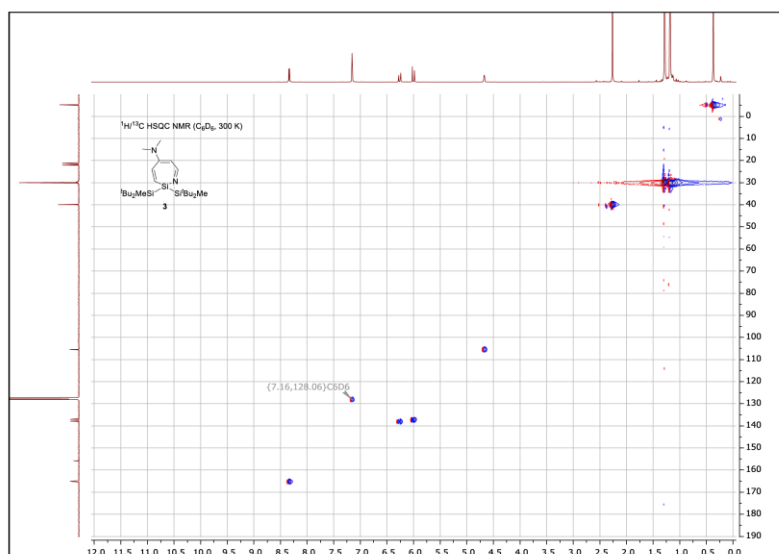
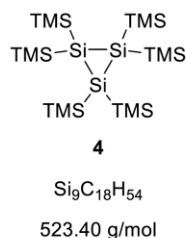


Fig. S12:  $^1\text{H}/^{13}\text{C}$  HSQC NMR spectrum of compound **3** in  $\text{C}_6\text{D}_6$  at 300 K.



1.6. Hexakis(trimethylsilyl)trisilirane (**4**)

A toluene solution of crude silylene **1c** (50 mg) was heated to 65 °C for 16 hours. After cooling down to ambient temperature, liberated DMAP was separated by precipitation with  $\text{SiBr}_4$  (26.9 mg, 77.5  $\mu\text{mol}$ , 1.0 eq.) and subsequent filtration. The resulting solution was concentrated under reduced pressure and compound **4** was obtained by crystallization at -35 °C as colorless solid (30.1 mg).

Note: Compound **4** has already been reported by Klinkhammer *et al.* from the attempted synthesis of the free silylene  $((\text{TMS})_3\text{Si})_2\text{Si}$ .<sup>[S7]</sup> Therefore, we did not analyze it further. DMAP forms an unidentified adduct with  $\text{SiBr}_4$  which is insoluble in common organic solvents. Thus, this adduct was not further analyzed.

$^1\text{H}$  NMR (500 MHz,  $\text{C}_6\text{D}_6$ , 300 K):  $\delta$  [ppm] = 0.43 (s, 54H,  $\text{Si}(\underline{\text{C}}\text{H}_3)_3$ ).

$^{13}\text{C}\{^1\text{H}\}$  NMR (126 MHz,  $\text{C}_6\text{D}_6$ , 300 K):  $\delta$  [ppm] = 4.7 ( $\text{Si}(\underline{\text{C}}\text{H}_3)_3$ ).

$^{29}\text{Si}\{^1\text{H}\}$  NMR (99 MHz,  $\text{C}_6\text{D}_6$ , 300 K):  $\delta$  [ppm] = -6.5 ( $\underline{\text{S}}\text{i}(\text{C}\text{H}_3)_3$ ), -168.6 ( $\underline{\text{S}}\text{i}(\text{TMS})_2$ ).

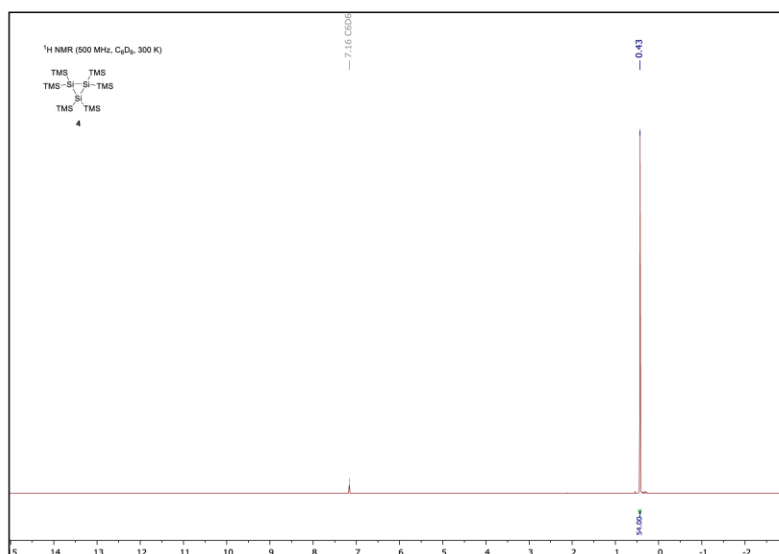


Fig. S13:  $^1\text{H}$  NMR spectrum (500 MHz) of compound **4** in  $\text{C}_6\text{D}_6$  at 300 K.

## 15. Appendix

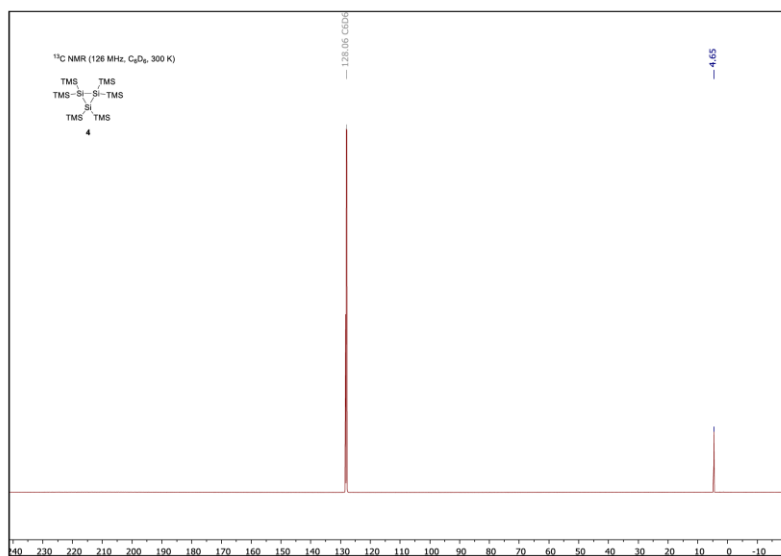


Fig. S14: <sup>13</sup>C NMR spectrum (126 MHz) of compound 4 in C<sub>6</sub>D<sub>6</sub> at 300 K.

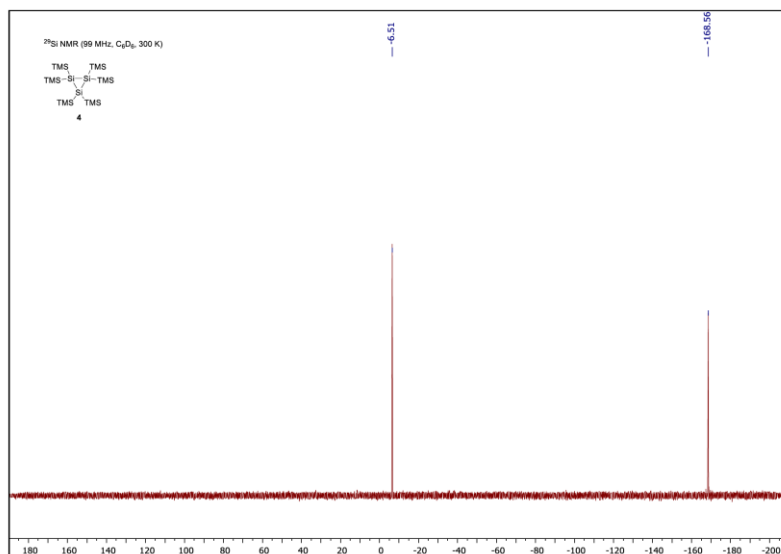
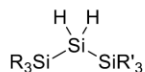


Fig. S15: <sup>29</sup>Si NMR spectrum (99 MHz) of compound 4 in C<sub>6</sub>D<sub>6</sub> at 300 K.

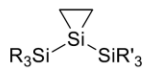
1.7. Hydrosilanes **5a-c**

**5a** R = Si<sup>t</sup>Bu<sub>3</sub>, R' = Si(TMS)<sub>3</sub>

**5b** R = R' = Si(TMS)<sub>3</sub>

**5c** R = R' = Si<sup>t</sup>Bu<sub>2</sub>Me

In a pressurizable Schlenk flask, a solution of the respective DMAP-stabilized silylenes **1a-c** (100 μmol, 1.0 eq.) in toluene (5 mL) was frozen in liquid nitrogen, degassed and exposed to dihydrogen (1 bar). The reaction mixture was subsequently heated to 65 °C for 2 hours. Decolorization indicated full conversion. Concomitantly formed free DMAP was separated by precipitation with SiBr<sub>4</sub> (100 μmol, 1.0 eq.) and filtration. The solvent was removed under reduced pressure to afford hydrosilanes **5** as colorless solids in quantitative yields. Compounds **5a-c** were identified by comparison of NMR spectral data with corresponding literature reports (**5a**,<sup>[S5]</sup> **5b**,<sup>[S2]</sup> **5c**<sup>[S3]</sup>).

1.8. Siliranes **6**

**6a** R = Si<sup>t</sup>Bu<sub>3</sub>, R' = Si(TMS)<sub>3</sub>

**6b** R = R' = Si<sup>t</sup>Bu<sub>2</sub>Me

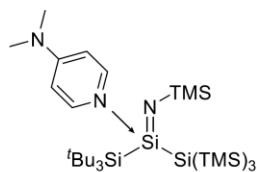
The synthesis of siliranes **6** was conducted by a similar procedure than that for hydrosilanes **5** (*vide supra*). Instead of H<sub>2</sub>, the DMAP-silylene complexes **1a** and **1b** were exposed to ethylene (1 bar). The compounds **6** were obtained as colorless solids. Silirane **6a** was identified by comparison of NMR spectral data with literature reports.<sup>[S5]</sup> Compound **6b** was identified by multinuclear NMR spectroscopy.

**6b**

<sup>1</sup>H NMR (500 MHz, C<sub>6</sub>D<sub>6</sub>, 300 K): δ [ppm] = 1.10 (s, 36H, C(CH<sub>3</sub>)<sub>3</sub>), 0.81 (s, 4H, CH<sub>2</sub>), 0.10 (s, 6H, Si(CH<sub>3</sub>)).

<sup>13</sup>C NMR (126 MHz, C<sub>6</sub>D<sub>6</sub>, 300 K): δ [ppm] = 29.9 (C(CH<sub>3</sub>)<sub>3</sub>), 21.8 (C(CH<sub>3</sub>)<sub>3</sub>), -0.7 (CH<sub>2</sub>), -6.3 (SiCH<sub>3</sub>)

<sup>29</sup>Si{<sup>1</sup>H} NMR (99 MHz, C<sub>6</sub>D<sub>6</sub>, 300 K): δ [ppm] = 11.2 (Si<sup>t</sup>Bu<sub>2</sub>Me), -174.5 (SiCH<sub>2</sub>).

1.9. Silaimine **7a****7a**Si<sub>7</sub>C<sub>31</sub>H<sub>73</sub>N<sub>3</sub>

684.54 g/mol

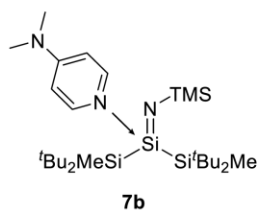
Trimethylsilyl azide (11.6 mg, 100 μmol, 1.0 eq.) was added to a solution of silylene **1a** (60.0 mg, 100 μmol, 1.0 eq.) in benzene (2 mL) at ambient temperature. Decolorization from dark-brown to yellow and concomitant N<sub>2</sub> evolution was observed. After stirring the mixture for 1 hour, evaporation of the solvent under reduced pressure afforded compound **7a** as yellow solid (53.8 mg, 78.6 μmol, 78%). Crystals suitable for SC-XRD analysis were obtained from a cooled (-35 °C) *n*-hexane solution of **7a**.

Note: Compound **7a** decomposes in solution under liberation of DMAP. Presumably, the donor-free silaimine is formed that decomposes further to an unidentified mixture of products.

**<sup>1</sup>H NMR (500 MHz, C<sub>6</sub>D<sub>6</sub>, 300 K):** δ [ppm] = 9.42 (br. s, 1H, *o*-C<sup>DMAP</sup>H), 8.50 (br. s, 1H, *o*-C<sup>DMAP</sup>H), 6.06 (d, <sup>3</sup>J = 6.9 Hz, 2H, *m*-C<sup>DMAP</sup>H), 1.83 (s, 6H, N(CH<sub>3</sub>)<sub>2</sub>), 1.41 (s, 27H, Si(C(CH<sub>3</sub>)<sub>3</sub>)), 0.69 (s, 9H, NSi(CH<sub>3</sub>)<sub>3</sub>), 0.47 (s, 27H, Si(Si(CH<sub>3</sub>)<sub>3</sub>)<sub>3</sub>).

**<sup>13</sup>C NMR (126 MHz, C<sub>6</sub>D<sub>6</sub>, 300 K):** δ [ppm] = 155.9 (*p*-C<sup>DMAP</sup>), 150.6 (*o*-C<sup>DMAP</sup>), 106.9 (*m*-C<sup>DMAP</sup>), 38.3 (N(CH<sub>3</sub>)<sub>2</sub>), 33.3 (C(CH<sub>3</sub>)<sub>3</sub>), 25.1 (C(CH<sub>3</sub>)<sub>3</sub>), 7.7 (NSi(CH<sub>3</sub>)), 5.3 (Si(Si(CH<sub>3</sub>)<sub>3</sub>)).

**<sup>29</sup>Si{<sup>1</sup>H} NMR (99 MHz, C<sub>6</sub>D<sub>6</sub>, 300 K):** δ [ppm] = 2.0 (Si<sup>t</sup>Bu<sub>3</sub>), -9.4 (Si(SiMe<sub>3</sub>)<sub>3</sub>), -25.1 (N(SiMe<sub>3</sub>)), -25.9 (Si=N), -121.3 (Si(SiMe<sub>3</sub>)<sub>3</sub>).

1.10. Silaimine **7b**Si<sub>4</sub>C<sub>28</sub>H<sub>61</sub>N<sub>3</sub>

552.16 g/mol

Analog to the synthesis of **7a** (*vide supra*) silylene **1b** (25 mg, 53.8 μmol, 1.0 eq.) was treated with trimethylsilyl azide (6.19 mg, 53.8 μmol, 1.0 eq.) to afford silaimine **7b** as yellow, crystalline solid (28.4 mg, 51.4 mmol, 96%).

**<sup>1</sup>H NMR (500 MHz, C<sub>6</sub>D<sub>6</sub>, 300 K):** δ [ppm] = 8.82-8.81 (m, 2H, *o*-C<sup>DMAP</sup>H), 5.79 (d, <sup>3</sup>J = 7.3 Hz, 2H, *m*-C<sup>DMAP</sup>H), 1.80 (s, 6H, N(CH<sub>3</sub>)<sub>2</sub>), 1.34 (s, 18H, C(CH<sub>3</sub>)<sub>3</sub>), 1.16 (s, 18H, C(CH<sub>3</sub>)<sub>3</sub>), 0.72 (s, 9H, Si(CH<sub>3</sub>)<sub>3</sub>), 0.42 (s, 6H, Si(CH<sub>3</sub>)<sub>2</sub>).

**<sup>13</sup>C{<sup>1</sup>H} NMR (126 MHz, C<sub>6</sub>D<sub>6</sub>, 300 K):** δ [ppm] = 155.8 (*p*-C<sup>DMAP</sup>), 145.7 (*o*-C<sup>DMAP</sup>), 106.3 (*m*-C<sup>DMAP</sup>), 38.3 (N(CH<sub>3</sub>)<sub>2</sub>), 31.1 (C(CH<sub>3</sub>)<sub>3</sub>), 31.1 (C(CH<sub>3</sub>)<sub>3</sub>), 22.5 (C(CH<sub>3</sub>)<sub>3</sub>), 22.3 (C(CH<sub>3</sub>)<sub>3</sub>), -4.5 (Si(CH<sub>3</sub>)<sub>2</sub>).

**<sup>29</sup>Si{<sup>1</sup>H} NMR (99 MHz, C<sub>6</sub>D<sub>6</sub>, 300 K):** δ [ppm] = -8.8 (Si<sup>i</sup>Bu<sub>2</sub>Me), -24.9 (Si<sup>i</sup>Me<sub>3</sub>), -25.5 (Si=N).

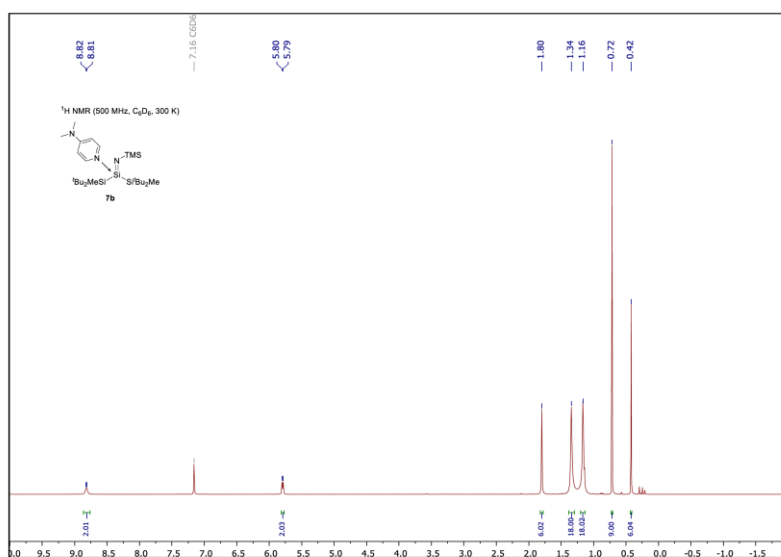


**Fig. S16:** <sup>1</sup>H NMR spectrum (500 MHz) of compound **7b** in C<sub>6</sub>D<sub>6</sub> at 300 K.

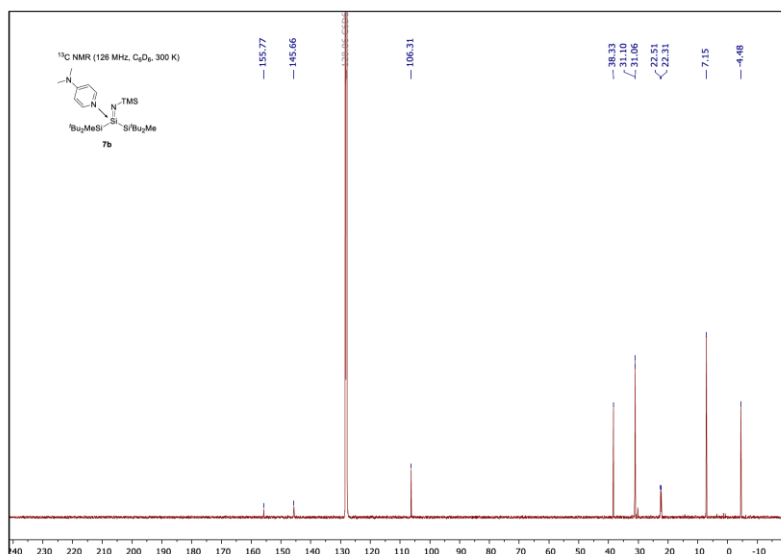


Fig. S17: <sup>13</sup>C NMR spectrum (126 MHz) of compound **7b** in C<sub>6</sub>D<sub>6</sub> at 300 K.

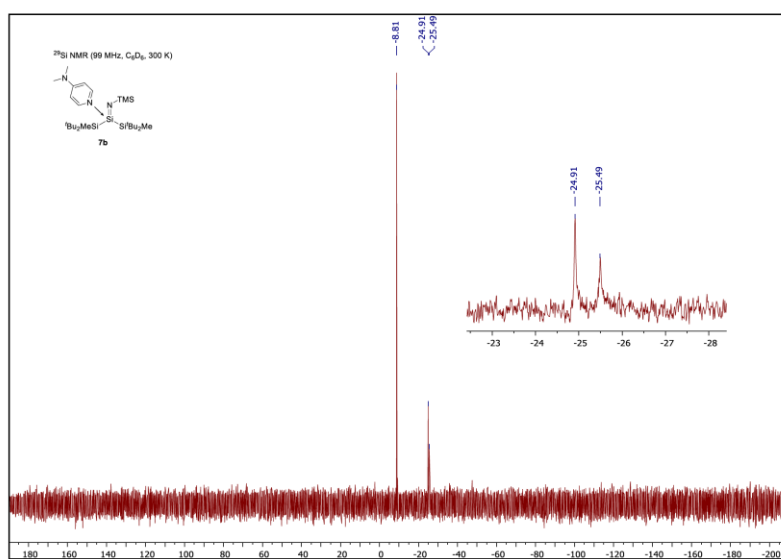


Fig. S18: <sup>29</sup>Si NMR spectrum (99 MHz) of compound **7b** in C<sub>6</sub>D<sub>6</sub> at 300 K.



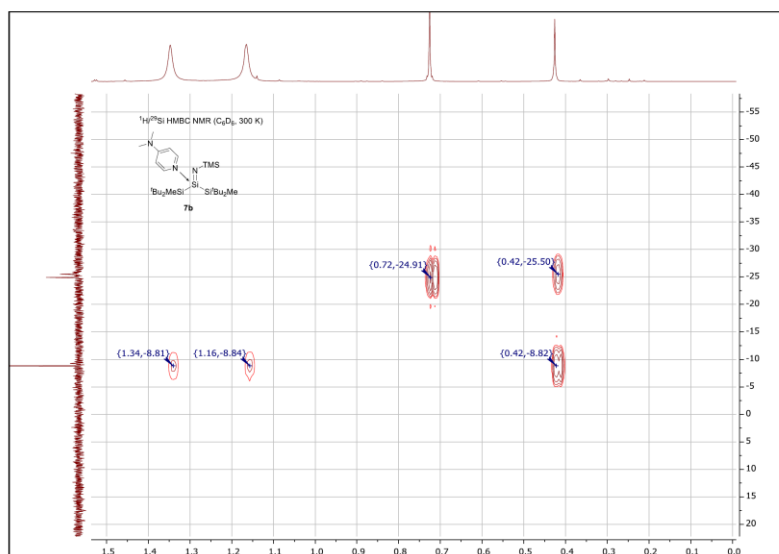


Fig. S19:  $^1\text{H}/^{29}\text{Si}$  HMBC NMR spectrum of compound **7b** in  $\text{C}_6\text{D}_6$  at 300 K.

## 2. X-ray Crystallographic Data

### 2.1. General Information

The X-ray intensity data of **2** were collected on an X-ray single crystal diffractometer equipped with a CMOS detector (*Bruker Photon-100*), a rotating anode (*Bruker TXS*) with MoK $\alpha$  radiation ( $\lambda = 0.71073 \text{ \AA}$ ) and a *Helios* mirror optic by using the *APEX III* software package.<sup>[S8]</sup> The X-ray intensity data of **1b** and **7a** were collected on an X-ray single crystal diffractometer equipped with a CMOS detector (*Bruker Photon-100*), an IMS microsource with MoK $\alpha$  radiation ( $\lambda = 0.71073 \text{ \AA}$ ) and a *Helios* mirror optic by using the *APEX III* software package.<sup>[S8]</sup> The X-ray intensity data of **3** was collected on an X-ray single crystal diffractometer equipped with a CCD detector (*Apex II CCD*), a fine-focus sealed tube with MoK $\alpha$  radiation ( $\lambda = 0.71073 \text{ \AA}$ ) and a *Triumph* monochromator by using the *APEX III/III* software package.<sup>[S8]</sup> The measurements were performed on single crystals coated with the perfluorinated ether *Fomblin*<sup>®</sup> Y. The crystal was fixed on the top of a micro sampler, transferred to the diffractometer and frozen under a stream of cold nitrogen. A matrix scan was used to determine the initial lattice parameters. Reflections were merged and corrected for Lorentz and polarization effects, scan speed, and background using *SAINTE*.<sup>[S9]</sup> Absorption corrections, including odd and even ordered spherical harmonics were performed using *SADABS*.<sup>[S9]</sup> Space group assignments were based upon systematic absences, E statistics, and successful refinement of the structures. Structures were solved by direct methods with the aid of successive difference Fourier maps, and were refined against all data using the *APEX III* software in conjunction with *SHELXL-2014*<sup>[S10]</sup> and *SHELXLE*.<sup>[S11]</sup> All H atoms were placed in calculated positions and refined using a riding model, with methylene and aromatic C–H distances of 0.99 and 0.95  $\text{\AA}$ , respectively, and  $U_{\text{iso}}(\text{H}) = 1.2 \cdot U_{\text{eq}}(\text{C})$ . Full-matrix least-squares refinements were carried out by minimizing  $\Delta w(F_o^2 - F_c^2)$ <sup>[S9]</sup> with *SHELXL-97* weighting scheme.<sup>[S12]</sup> Neutral atom scattering factors for all atoms and anomalous dispersion corrections for the non-hydrogen atoms were taken from International Tables for Crystallography.<sup>[S13]</sup> The images of the crystal structures were generated by *Mercury*.<sup>[S14]</sup> The CCDC numbers CCDC-1967942 (**1b**), CCDC-1967943 (**2**), CCDC-1967944 (**3**) and CCDC-1967945 (**7a**) contain the supplementary crystallographic data for the structures. These data can be obtained free of charge from the Cambridge Crystallographic Data Centre via <https://www.ccdc.cam.ac.uk/structures/>.

## 2.2 SC-XRD structures

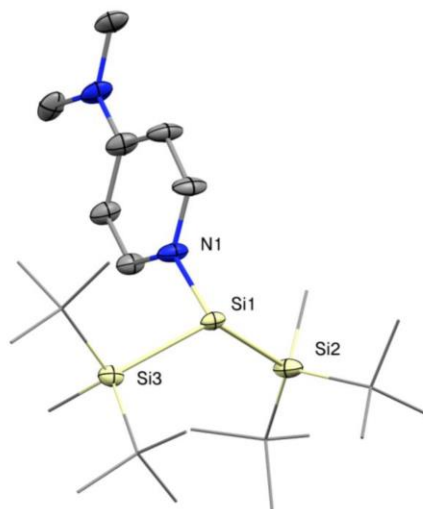


**Fig. S20:** SC-XRD structure of silylene **1b** with thermal ellipsoids drawn at the 30% probability level. Hydrogen atoms are omitted for clarity, <sup>t</sup>Bu- and Me-groups are simplified as wireframes. Selected bond lengths [Å] and angles [°]: Si1–N1 1.937(5), Si1–Si2 2.390(3), Si1–Si3 2.378(3), Si2–Si1–Si3 123.1(1), Si2–Si1–N1 96.2(2), Si3–Si1–N1 98.8(2).

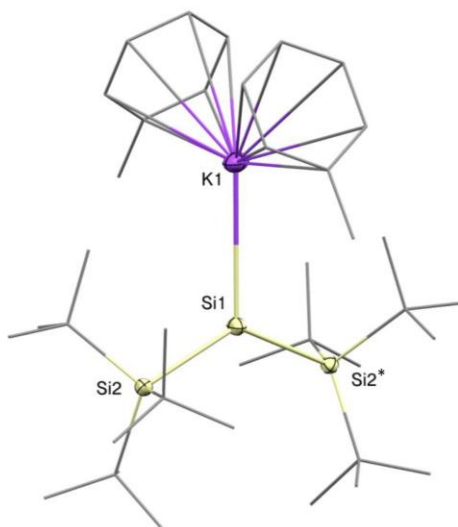


**Fig. S21:** SC-XRD structure of silyl radical **2** with thermal ellipsoids drawn at the 30% probability level. Hydrogen atoms are omitted for clarity, <sup>t</sup>Bu-groups and toluene molecules are simplified as wireframes. Selected bond lengths [Å] and angles [°]: Si1–Si2 2.3936(14), Si1–K1 3.315(2), K1–Si1–Si2 114.91(2), Si2–Si1–Si2\* 130.19(3).

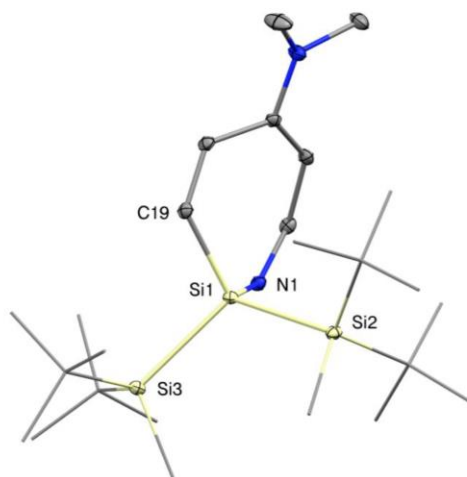


**Fig. S22:** SC-XRD structure of azasilepin **3** with thermal ellipsoids drawn at the 30% probability level. Hydrogen atoms are omitted for clarity, 'Bu- and Me-groups are simplified as wireframes. Selected bond lengths [Å] and angles [°]: Si1–N1 1.750(1), Si1–C19 1.878(1), Si1–Si2 2.4144(6), Si2–Si1–Si3 113.74(2), Si2–Si1–N1 109.08(4), N1–Si1–C19 104.71(5).

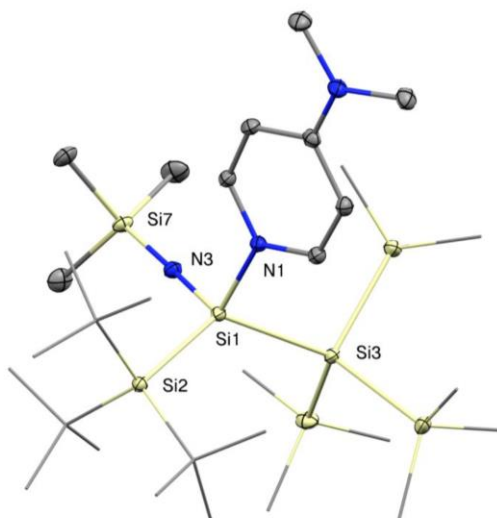


**Fig. S23:** SC-XRD structure of silaimine **7a** with thermal ellipsoids drawn at the 30% probability level. Hydrogen atoms are omitted for clarity, 'Bu- and Me-groups are simplified as wireframes. Selected bond lengths [Å] and angles [°]: Si1–Si2 2.453(1), Si1–N1 1.928(2), Si1–N3 1.616(2), N3–Si7 1.660(2), Si2–Si1–Si3 125.08(3), N1–Si1–N3 106.08(8), Si1–N3–Si7 177.1(1).

# 15. Appendix

## 2.3 Crystal data and structural refinement parameters

Table S1: Crystal data and structural refinement parameters for compounds 1, 3, 4 and 7a.

Compound #	1b	2	3	7a
CCDC #	1967942	1967943	1967944	1967945
Chemical formula	C <sub>10</sub> H <sub>10</sub> N <sub>2</sub> Si <sub>3</sub>	C <sub>10</sub> H <sub>10</sub> KSi <sub>3</sub>	C <sub>10</sub> H <sub>10</sub> N <sub>2</sub> Si <sub>3</sub>	C <sub>10</sub> H <sub>10</sub> N <sub>2</sub> Si <sub>3</sub>
Formula weight	464.96	650.31	464.96	684.55
Temperature	100(2) K	100(2) K	100(2) K	100(2) K
Wavelength	0.71073 Å	0.71073 Å	0.71073 Å	0.71073 Å
Crystal size	0.209 × 0.235 × 0.373 mm	0.176 × 0.299 × 0.302 mm	0.268 × 0.342 × 0.398 mm	0.059 × 0.153 × 0.213 mm
Crystal habit	clear dark red-brown fragment	clear yellow fragment	clear yellow fragment	clear yellow fragment
Crystal system	monoclinic	monoclinic	orthorhombic	triclinic
Space group	C 2/c	C 2/c	P b c a	P -1
Unit cell dimensions	a = 28.128(4) Å, α = 90° b = 15.312(2) Å, β = 110.180(4)° c = 14.673(19) Å, γ = 90°	a = 20.678(7) Å, α = 90° b = 12.877(5) Å, β = 120.067(10)° c = 17.566(10) Å, γ = 90°	a = 11.9770(13) Å, α = 90° b = 16.9418(17) Å, α = 90° c = 28.631(3) Å, α = 90°	a = 11.515(9) Å, α = 97.728(17)° b = 11.940(9) Å, β = 92.844(18)° c = 16.100(7) Å, γ = 104.175(19)°
Volume	5933.4(14) Å <sup>3</sup>	4049(3) Å <sup>3</sup>	5809.6(11) Å <sup>3</sup>	2119(2) Å <sup>3</sup>
Z	8	4	8	2
Density (calculated)	1.041 g/cm <sup>3</sup>	1.067 g/cm <sup>3</sup>	1.063 g/cm <sup>3</sup>	1.073 g/cm <sup>3</sup>
Absorption coefficient	0.174 mm <sup>-1</sup>	0.243 mm <sup>-1</sup>	0.178 mm <sup>-1</sup>	0.248 mm <sup>-1</sup>
F(000)	2064	1436	2064	756
Diffractometer	Bruker D8 Venture Duo IMS	Bruker D8 Venture	Bruker D8 Kappa Apex II	Bruker D8 Venture Duo IMS
Radiation source	IMS microsource, Mo	TXS rotating anode, Mo	fine-focus sealed tube, Mo	IMS microsource, Mo
Theta range for data collection	1.94 to 25.35°	2.28 to 25.68°	2.20 to 26.37°	2.03 to 25.35°
Index ranges	-33<h<=33, -18<k<=18, -17<l<=17	-25<h<=25, -15<k<=15, -21<l<=20	-14<h<=14, -21<k<=21, -35<l<=35	-13<h<=13, -14<k<=14, -18<l<=19
Reflections collected	36869	68970	188411	89033
Independent reflections	5424 [R(int) = 0.0913]	3797 [R(int) = 0.0742]	5931 [R(int) = 0.0304]	7757 [R(int) = 0.0458]
Coverage of independent reflections	99.8%	98.6%	99.8%	99.9%
Absorption correction	Multi-Scan	Multi-Scan	Multi-Scan	Multi-Scan
Refinement method	Full-matrix least-squares on F <sup>2</sup>	Full-matrix least-squares on F <sup>2</sup>	Full-matrix least-squares on F <sup>2</sup>	Full-matrix least-squares on F <sup>2</sup>
Refinement program	SHELXL-2017/1 (Sheldrick, 2017)	SHELXL-2016/6 (Sheldrick, 2016)	SHELXL-2016/6 (Sheldrick, 2016)	SHELXL-2016/6 (Sheldrick, 2016)
Function minimized	Σ w(F <sub>o</sub> <sup>2</sup> - F <sub>c</sub> <sup>2</sup> ) <sup>2</sup>	Σ w(F <sub>o</sub> <sup>2</sup> - F <sub>c</sub> <sup>2</sup> ) <sup>2</sup>	Σ w(F <sub>o</sub> <sup>2</sup> - F <sub>c</sub> <sup>2</sup> ) <sup>2</sup>	Σ w(F <sub>o</sub> <sup>2</sup> - F <sub>c</sub> <sup>2</sup> ) <sup>2</sup>
Data / restraints / parameters	5424 / 8 / 328	3797 / 0 / 202	5931 / 0 / 287	7757 / 0 / 393
Goodness-of-fit on F <sup>2</sup>	1.172	1.040	1.045	1.123
Final R indices	4238 data, I>2σ(I) R1 = 0.1217, wR2 = 0.2651 all data: R1 = 0.1445, wR2 = 0.2780	3472 data, I>2σ(I) R1 = 0.0305, wR2 = 0.0855 all data: R1 = 0.0341, wR2 = 0.0886	5356 data, I>2σ(I) R1 = 0.0289, wR2 = 0.0771 all data: R1 = 0.0334, wR2 = 0.0802	7180 data, I>2σ(I) R1 = 0.0402, wR2 = 0.0992 all data: R1 = 0.0439, wR2 = 0.1016
Weighting scheme	w=1/[σ <sup>2</sup> (F <sub>o</sub> <sup>2</sup> )+108.1245P] where P=(F <sub>o</sub> <sup>2</sup> +2F <sub>c</sub> <sup>2</sup> )/3	w=1/[σ <sup>2</sup> (F <sub>o</sub> <sup>2</sup> )+0.0477P <sup>2</sup> +2.4242P] where P=(F <sub>o</sub> <sup>2</sup> +2F <sub>c</sub> <sup>2</sup> )/3	w=1/[σ <sup>2</sup> (F <sub>o</sub> <sup>2</sup> )+(0.0388P <sup>2</sup> +3.2781P)] where P=(F <sub>o</sub> <sup>2</sup> +2F <sub>c</sub> <sup>2</sup> )/3	w=1/[σ <sup>2</sup> (F <sub>o</sub> <sup>2</sup> )+(0.0445P <sup>2</sup> +1.7142P)] where P=(F <sub>o</sub> <sup>2</sup> +4F <sub>c</sub> <sup>2</sup> )/3
Largest diff. peak and hole	0.560 and -0.742 eÅ <sup>-3</sup>	0.263 and -0.218 eÅ <sup>-3</sup>	0.366 and -0.261 eÅ <sup>-3</sup>	0.634 and -0.268 eÅ <sup>-3</sup>
R.M.S. deviation from mean	0.104 eÅ <sup>-3</sup>	0.040 eÅ <sup>-3</sup>	0.042 eÅ <sup>-3</sup>	0.058 eÅ <sup>-3</sup>

### 3. References

- [S1] G. R. Fulmer, A. J. M. Miller, N. H. Sherden, H. E. Gottlieb, A. Nudelman, B. M. Stoltz, J. E. Bercaw, K. I. Goldberg, *Organometallics* **2010**, *29*, 2176-2179.
- [S2] T. Gross, H. Reinke, H. Oehme, *Can. J. Chem.* **2000**, *78*, 1399-1404.
- [S3] A. Sekiguchi, T. Fukawa, M. Nakamoto, V. Y. Lee, M. Ichinohe, *J. Am. Chem. Soc.* **2002**, *124*, 9865-9869.
- [S4] N. Wiberg, W. Niedermayer, H. Nöth, J. Knizek, W. Ponikwar, K. Polborn, D. Fenske, G. Baum, *Z. Anorg. Allg. Chem.* **2001**, *627*, 594-606.
- [S5] D. Reiter, R. Holzner, A. Porzelt, P. J. Altmann, P. Frisch, S. Inoue, *J. Am. Chem. Soc.* **2019**, *141*, 13536-13546.
- [S6] K. Fredenhagen, G. Cadenbach, *Z. Anorg. Allg. Chem.* **1926**, *158*, 249-263.
- [S7] a) K. W. Klinkhammer, *Chem. Eur. J.* **1997**, *3*, 1418-1431. ; b) K. W. Klinkhammer, *Organosilicon Chemistry III - From Molecules to Materials* (Eds.: N. Auner, J. Weis), Wiley-VCH, **1997**.
- [S8] *APEX suite of crystallographic software*, APEX 3 version 2015.5-2; Bruker AXS Inc.: Madison, Wisconsin, USA, 2015.
- [S9] *SAINT*, Version 7.56a and *SADABS* Version 2008/1; Bruker AXS Inc.: Madison, Wisconsin, USA, 2008.
- [S10] G. M. Sheldrick, *SHELXL-2014*, University of Göttingen, Göttingen, Germany, 2014.
- [S11] C. B. Hübschle, G. M. Sheldrick, B. Dittrich, *J. Appl. Cryst.* **2011**, *44*, 1281-1284.
- [S12] G. M. Sheldrick, *SHELXL-97*, University of Göttingen, Göttingen, Germany, 1998.
- [S13] A. J. C. Wilson, *International Tables for Crystallography*, Volume C, Tables 6.1.1.4 (pp. 500-502), 4.2.6.8 (pp. 219-222), and 4.2.4.2 (pp. 193-199), Kluwer Academic Publishers: Dordrecht, The Netherlands, **1992**.
- [S14] C. F. Macrae, I. J. Bruno, J. A. Chisholm, P. R. Edgington, P. McCabe, E. Pidcock, L. Rodriguez-Monge, R. Taylor, J. van de Streek, P. A. Wood, *J. Appl. Cryst.* **2008**, *41*, 466-470.

## 15.4 Supporting Information Chapter 10

### Supporting Information

#### **Iminosilyldisilenes: Striking Reactivity in Small Molecule Activation**

*Richard Holzner, Philipp Frisch, Daniel Wendel, and Shigeyoshi Inoue\**

Department of Chemistry, WACKER-Institute of Silicon Chemistry, Technische Universität München, Lichtenbergstraße 4, 85748 Garching bei München (Germany) \*E-mail: s.inoue@tum.de



**Table of Contents**

<b>1. Experimental Section</b>	<b>3</b>
1.1. General Methods and Instrumentation.....	3
1.3. Iminodisilene I <sup>t</sup> BuN( <sup>t</sup> Bu <sub>2</sub> MeSi)Si=Si(Si <sup>t</sup> Bu <sub>2</sub> Me)NI <sup>t</sup> Bu ( <b>1</b> ).....	5
1.2 Iminodisilene I <sup>t</sup> BuN( <sup>t</sup> Bu <sub>2</sub> MeSi)Si=Si(Si <sup>t</sup> Bu <sub>2</sub> Me)NI <sup>t</sup> Bu ( <b>2</b> ).....	9
1.4 I <sup>t</sup> BuN( <sup>t</sup> Bu <sub>2</sub> MeSi)HSi-SiH(Si <sup>t</sup> Bu <sub>2</sub> Me)NI <sup>t</sup> Bu ( <b>3</b> ).....	16
1.4. Dioxadisiletane <b>4</b> .....	19
1.4. Disilaoxirane <b>5-f</b> .....	21
1.4 I <sup>t</sup> BuN( <sup>t</sup> Bu <sub>2</sub> MeSi)BrSi-SiBr( <sup>t</sup> Bu <sub>2</sub> MeSi) I <sup>t</sup> BuN ( <b>6</b> ).....	25
1.4 I <sup>t</sup> BuN( <sup>t</sup> Bu <sub>2</sub> MeSi) <sub>2</sub> SiBr ( <b>7</b> ).....	28
1.4. Radical Cation of I <sup>t</sup> BuN( <sup>t</sup> Bu <sub>2</sub> MeSi)Si=Si(Si <sup>t</sup> Bu <sub>2</sub> Me)NI <sup>t</sup> Bu <b>8</b> .....	30
1.4. Compound <b>9</b> .....	32
<b>2. X-ray Crystallographic Data</b>	<b>36</b>
2.1. General Information.....	36
2.2 SC-XRD structures.....	37
2.3 Crystal data and structural refinement parameters.....	41
<b>3. References</b>	<b>43</b>

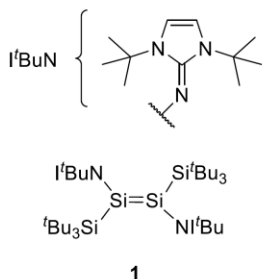
## 1. Experimental Section

### 1.1. General Methods and Instrumentation

All manipulations were carried out under exclusion of water and oxygen under an atmosphere of argon 4.6 ( $\geq 99.996\%$ ) using standard Schlenk and glovebox techniques. The glassware used was heat dried under high vacuum prior to use. All solvents were refluxed over sodium/benzophenone, freshly distilled under argon and deoxygenated prior to use. PTFE-based grease (*Triboflon III* from *Freudenberg & Co. KG*) was used as sealant. Deuterated benzene ( $C_6D_6$ ), toluene ( $Tol-d_6$ ) and THF ( $THF-d_6$ ) were obtained from Sigma-Aldrich, dried over Na/K alloy, flask-to-flask condensed, deoxygenated by three freeze-pump-thaw cycles and stored over 4 Å molecular sieves in a glovebox. All NMR samples were prepared under argon in *J. Young* PTFE valve NMR tubes. The NMR spectra were recorded on a *Bruker DRX400* ( $^1H$ : 400.13 MHz,  $^{13}C$ : 100.62 MHz,  $^{29}Si$ : 79.49 MHz), *AV500* ( $^1H$ : 500.13 MHz) or *AV500C* ( $^1H$ : 500.36 MHz,  $^{13}C$ : 125.83 MHz,  $^{29}Si$ : 99.41 MHz) spectrometer at ambient temperature (300 K), unless otherwise stated. The  $^1H$ ,  $^{13}C\{^1H\}$  and  $^{29}Si\{^1H\}$  NMR spectroscopic chemical shifts  $\delta$  are reported in ppm relative to tetramethylsilane.  $^1H$  and  $^{13}C\{^1H\}$  NMR spectra are calibrated against the residual proton and natural abundance carbon resonances of the respective deuterated solvent as internal standard ( $C_6D_6$ :  $\delta(^1H) = 7.16$  ppm and  $\delta(^{13}C) = 128.1$  ppm,  $Tol-d_6$ :  $\delta(^1H) = 2.08$  ppm and  $\delta(^{13}C) = 20.4$  ppm),  $THF-d_6$ :  $\delta(^1H) = 1.73$  ppm and  $\delta(^{13}C) = 25.4$  ppm).<sup>[S1]</sup> The following abbreviations are used to describe signal multiplicities: s = singlet, d = doublet, dd = doublet of doublets, dt = doublet of triplets, t = triplet, sept = septet, m = multiplet, br = broad. In some NMR spectra, signals from silicone grease ( $C_6D_6$ :  $\delta(^1H) = 0.29$  ppm,  $\delta(^{13}C) = 1.4$  ppm and  $\delta(^{29}Si) = -21.8$  ppm), originating from the cannulas used (*B. Braun Melsungen AG Sterican®*), can be observed. UV/VIS spectra were recorded on a *Varian, Inc. Cary 50* spectrophotometer with a Schlenk quartz cuvette. EPR spectra were recorded on a *Jeol JES-Fa200 esr* spectrometer with a spectrometer frequency of 9.267 GHz (X-band). Quantitative elemental analyses (EA) were measured with a *EURO EA (HEKAtech)* instrument equipped with a CHNS combustion analyzer at the *Laboratory for Microanalysis* at the *TUM Catalysis Research Center*. Melting Points (m.p.) were determined in sealed glass capillaries under inert gas by a *Büchi M-565* melting point apparatus. Unless otherwise stated, all commercially available chemicals were purchased from *abcr GmbH* or *Sigma-Aldrich* and used without further purification. Hydrogen ( $H_2$ ) 5.0 ( $\geq 99.999\%$ ), oxygen ( $O_2$ ) 5.0 ( $\geq 99.999\%$ ), carbon dioxide ( $CO_2$ ) 5.0 ( $\geq 99.999\%$ ), dinitrogen monoxide ( $N_2O$ ) 5.0 ( $\geq 99.999\%$ ) and carbon monoxide ( $CO$ ) 4.7 ( $\geq 99.997\%$ ) were purchased from *Westfalen AG* and used as received. The compounds bis(*tert*-butyl)imidazolin-2-iminotribromosilane ( $(^tBuNSiBr_3)^{[S2]}$ ), supersilyl sodium ( $(^tBu_3SiNa \cdot 2THF)^{[S3]}$ ), bis(*tert*-butyl)methylsilyl sodium ( $(^tBu_2MeSiNa)^{[S4]}$ ) and the functionalized trityl (fluoroaryl)borate  $[Ph_3C][B(4-(^iPr_3Si)-C_6F_4)_4]^{[S5]}$  were prepared as described in the corresponding references. Potassium graphite ( $KC_8$ ) was

synthesized following a literature reported procedure upon heating a 1:8 mixture of potassium and graphite in a thick-walled, PTFE-capped pressurize-able Schlenk flask to 500 °C until a homogenous bronze powder was obtained.<sup>[S6]</sup>

The cyclic voltammetry (CV) measurements were performed in an Ar-filled glovebox (*MBraun*, oxygen and water content < 0.1 ppm). The electrochemical three-electrode glass cell was custom made with a gold (*Alfa Aesar*, 99.999% purity) working electrode (WE), a platinum (*Advent*, 99.99+% purity) counter electrode (CE), and a lithium (99.9%, foil, *Rockwood Lithium*, 0.45 mm thickness) reference electrode (RE). The electrolyte in the main and the CE compartment consisted of THF (*Sigma-Aldrich*) and 0.1 M tetrabutylammonium bis(trifluoromethane)sulfonimide (TBATFSI). For the RE compartment a solution of 0.1 M LiTFSI in THF was used. The cell compartments were separated by porous glass frits. For the separation of the RE compartment a *Vycor 7930* frit (*Advanced Glass & Ceramics, Holden, MA*) was used in order to diminish the diffusion between the Li-ion containing RE electrolyte and the electrolyte in the main compartment. The electrodes of the cell compartments were connected *via* fused-in tungsten wires. Before the first CV was recorded, the high frequency resistance (HFR) of the glass cell setup was measured *via* Electrochemical Impedance Spectroscopy (EIS) and used for ohmic drop correction of the measured WE potential. At the end of the CVs, about 10 mg of ferrocenium hexafluorophosphate ( $\text{FcPF}_6$ , *Sigma-Aldrich*) were added to the electrolyte in the main compartment in order to calibrate the potential of the Li RE versus the  $\text{Fc}/\text{Fc}^+$  couple. The CVs were recorded using a *Biologic VMP3* potentiostat/galvanostat.

1.3. Iminodisilene  $t\text{BuN}(\text{Bu}_2\text{MeSi})\text{Si}=\text{Si}(\text{Si}^t\text{Bu}_2\text{Me})\text{N}^t\text{Bu}$  (**1**)
 $\text{Si}_4\text{C}_{46}\text{H}_{94}\text{N}_6$ 

843.64 g/mol

A solution of  $t\text{Bu}_3\text{SiNa}\cdot 2\text{THF}$  (833 mg, 2.27 mmol, 2.10 eq.) in *n*-hexane (10 mL) was added to a suspension of  $t\text{BuNSiBr}_3$  (500 mg, 1.08 mmol, 1.00 eq.) in *n*-hexane (5 mL). The color changed to dark green. After filtration, compound **1** was obtained by crystallization from toluene at  $-35\text{ }^\circ\text{C}$  (251 mg, 297  $\mu\text{mol}$ , 55% yield). These crystals were also suitable for SC-XRD analysis.

**m.p.:**  $161\text{ }^\circ\text{C}$  (decomposition, color change to brown).

**$^1\text{H}$  NMR (500 MHz,  $\text{C}_6\text{D}_6$ , 300 K):**  $\delta$  [ppm] = 6.08 (s, 4H,  $\text{CH-N}$ ), 1.58 – 1.50 (m\*, 90H,  $t\text{Bu}$ ).

\* The signal of  $t\text{BuN}$  overlaps with the signal of  $t\text{Bu}_3\text{Si}$

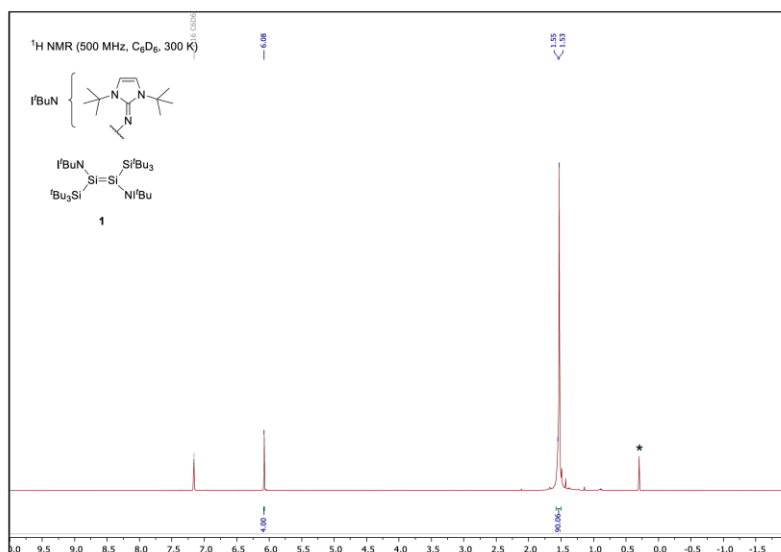
**$^1\text{H}$  NMR (500 MHz,  $\text{THF-}d_6$ , 300 K):**  $\delta$  [ppm] = 6.46 (s, 4H,  $\text{CH-N}$ ), 1.61 (s, 36H,  $\text{N}^t\text{Bu}$ ), 1.26 (s, 54H,  $t\text{Bu}_3\text{Si}$ ).

**$^{13}\text{C}\{^1\text{H}\}$  NMR (126 MHz,  $\text{THF-}d_6$ , 193 K):**  $\delta$  [ppm] = 145.7 ( $\text{C}=\text{N}$ ), 110.5 ( $\text{CH-N}$ ), 57.2 ( $\text{NC}(\text{CH}_3)_3$ ), 31.3 ( $\text{Si}(\text{C}(\text{CH}_3)_3)_3$ ), 31.1 ( $\text{NC}(\text{CH}_3)_3$ ), 21.7 ( $\text{Si}(\text{C}(\text{CH}_3)_3)_3$ ).

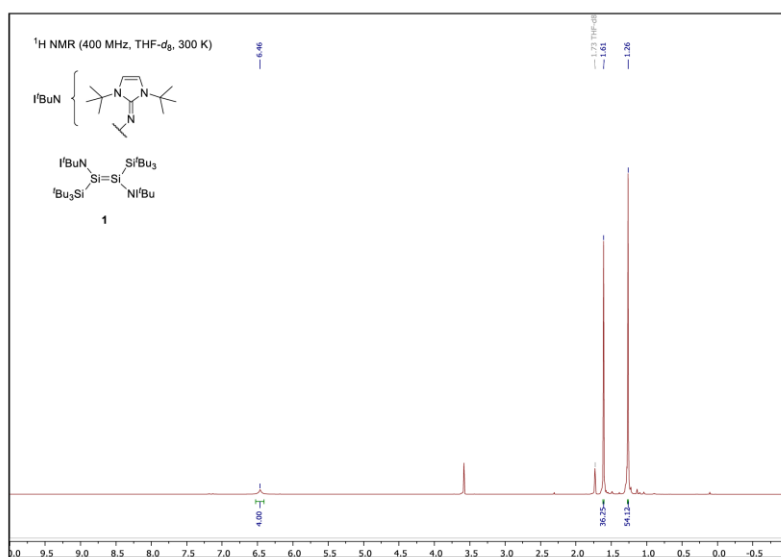
**$^{29}\text{Si}\{^1\text{H}\}$  NMR (99 MHz,  $\text{THF-}d_6$ , 193 K):**  $\delta$  [ppm] = 74.3 ( $\text{Si}=\text{Si}$ ), 23.1 ( $t\text{Bu}_3\text{Si}$ ).

Note: Compound **1** is only slightly soluble in *n*-hexane, benzene and toluene, however, it shows good solubility in THF. No additional sets of signals for the (*Z*)-isomer were observed in the multinuclear NMR spectra of compound **1**. Similar to reports for disilenes **III** and **VI** the signal intensities in the  $^{29}\text{Si}$  NMR spectrum of **1** at room temperature are very weak, presumably due to the biradical character of these disilenes.<sup>[S2.7]</sup> Therefore, the  $^{13}\text{C}$  and  $^{29}\text{Si}$  NMR spectra of **1** were recorded at  $-80\text{ }^\circ\text{C}$ .

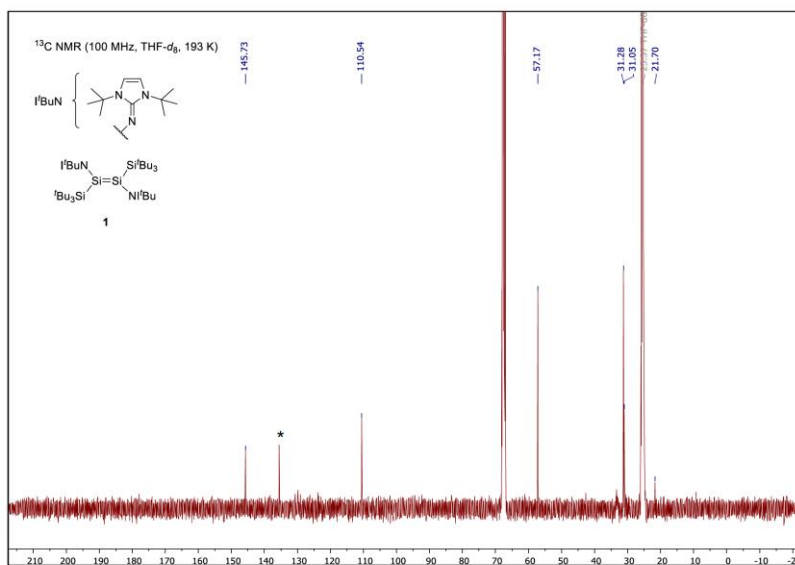
**EA:**  $\text{Si}_4\text{C}_{40}\text{H}_{82}\text{N}_6$  Calculated [%]: C (65.49), H (11.23), N (9.96)  
Experimental [%]: C (65.02), H (11.14), N (9.59)



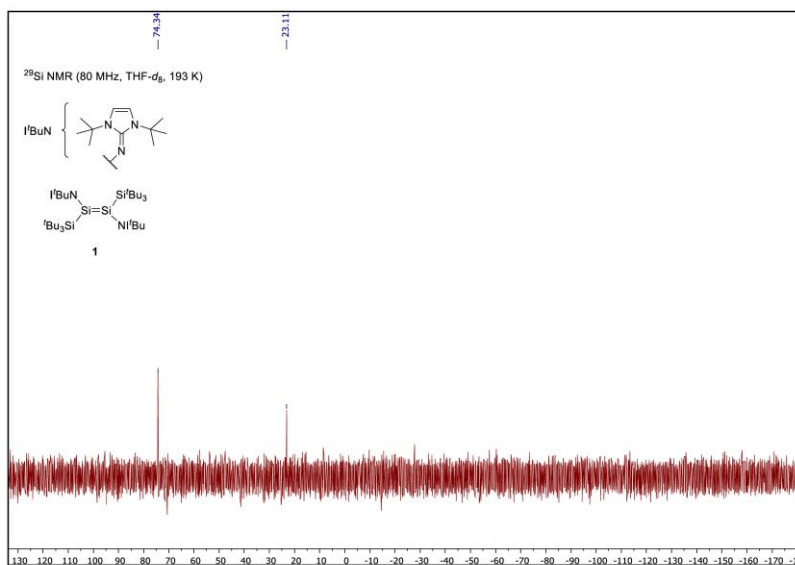
**Figure S1:** <sup>1</sup>H NMR spectrum (500 MHz) of compound **1** in C<sub>6</sub>D<sub>6</sub> at 300 K. Signal labeled with \* belongs to silicone grease.



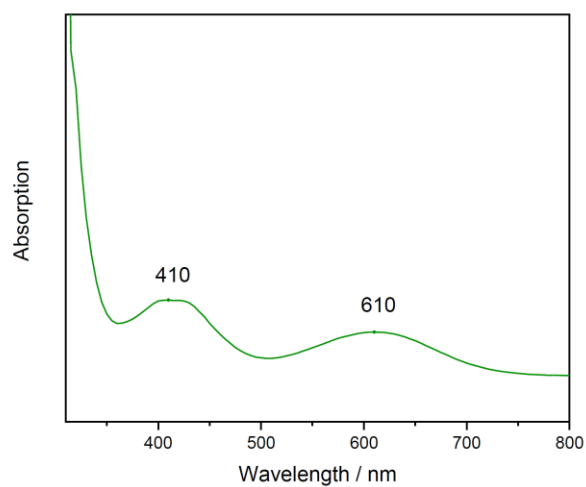
**Figure S2:** <sup>1</sup>H NMR spectrum (400 MHz) of compound **1** in THF-*d*<sub>6</sub> at 300 K.



**Figure S3:** <sup>13</sup>C NMR spectrum (100 MHz) of compound 1 in THF-*d*<sub>8</sub> at 193 K. Signal labeled with \* belongs to residual toluene.



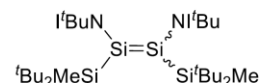
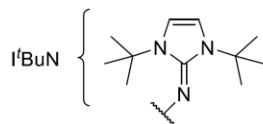
**Figure S4:** <sup>29</sup>Si NMR spectrum (80 MHz) of compound 1 in THF-*d*<sub>8</sub> at 193 K.



**Figure S5:** UV/VIS spectrum of green disilene **1** in *n*-hexane ( $2.5 \times 10^{-3}$  M), measured at room temperature ( $\lambda_{\text{max}} = 410$  nm; 610 nm).

Similar to the observations for compound **VI**, the UV/VIS spectrum of **1** contains two peaks. The peaks of disilene **VI** were assigned by theoretical calculations to be the HOMO→LUMO+1 transition (435 nm) and the  $\pi \rightarrow \pi^*$  transition (518 nm).<sup>[S2]</sup> Presumably, the absorption maximum of **1** at the lower wavelength of 410 nm also derives from the HOMO→LUMO+1 transition and the second peak (610 nm) can be assigned to the  $\pi \rightarrow \pi^*$  transition.



1.2 Iminodisilene  $t\text{BuN}(t\text{Bu}_2\text{MeSi})\text{Si}=\text{Si}(t\text{Bu}_2\text{Me})\text{N}i\text{Bu}$  (**2**)**2** $\text{Si}_4\text{C}_{40}\text{H}_{82}\text{N}_6$ 

759.48 g/mol

A solution of  $t\text{Bu}_2\text{MeSiNa}$  (684 mg, 3.79 mmol, 2.15 eq.) in THF (15 mL) was added dropwise to a solution of  $t\text{BuNSiBr}_3$  (815 mg, 1.76 mmol, 1.00 eq.) in THF (20 mL) at room temperature. An immediate color change to deep red was observed. After stirring the mixture for 1 h, the solvent was removed under reduced pressure and the residue extracted with toluene ( $3 \times 4$  mL). The solvent was evaporated *in vacuo* and the byproduct  $t\text{Bu}_2\text{MeSiBr}$  was removed by sublimation in high vacuum ( $70^\circ\text{C}$ ,  $2 \times 10^{-5}$  mbar). Compound **2** was obtained as crystalline deep red solid (550 mg, 724  $\mu\text{mol}$ , 82%) and is stable at ambient and elevated ( $90^\circ\text{C}$ ) temperatures in solid state

and in solution (benzene, toluene, *n*-hexane, THF). Single crystals suitable for XRD analysis were obtained from cooling a concentrated solution of **2** in *n*-hexane to  $-35^\circ\text{C}$ . In solution, temperature-dependent (*E/Z*)-isomerization of **2** with **2-(Z)** as major species can be observed.

**m.p.:**  $211^\circ\text{C}$  (decomposition, color change to brown).

**2-(Z):**

**$^1\text{H}$  NMR (500 MHz,  $\text{C}_6\text{D}_6$ , 300 K):**  $\delta$  [ppm] = 6.04 (s, 4H,  $\text{CH-N}$ ), 1.47 (s, 36H,  $t\text{Bu}_2\text{MeSi}$ ), 1.43 (s, 36H,  $\text{N}i\text{Bu}$ ), 0.52 (s, 6H,  $t\text{Bu}_2\text{MeSi}$ ).

**$^{13}\text{C}\{^1\text{H}\}$  NMR (126 MHz,  $\text{C}_6\text{D}_6$ , 300 K):**  $\delta$  [ppm] = 144.1 ( $\text{C}=\text{N}$ ), 107.9 ( $\text{CH-N}$ ), 54.9 ( $\text{N}(\text{C}(\text{CH}_3)_3)$ ), 31.2 ( $\text{Si}(\text{C}(\text{CH}_3)_3)_2(\text{CH}_3)$ ), 29.6 ( $\text{NC}(\text{CH}_3)_3$ ), 21.2 ( $\text{Si}(\text{C}(\text{CH}_3)_3)_2(\text{CH}_3)$ ),  $-3.9$  ( $\text{Si}(\text{C}(\text{CH}_3)_3)_2(\text{CH}_3)$ ).

**$^{29}\text{Si}\{^1\text{H}\}$  NMR (99 MHz,  $\text{C}_6\text{D}_6$ , 300 K):**  $\delta$  [ppm] = 67.4 ( $\text{Si}=\text{Si}$ ), 20.4 ( $t\text{Bu}_2\text{MeSi}$ ).

**2-(E):**

**$^1\text{H}$  NMR (500 MHz,  $\text{C}_6\text{D}_6$ , 300 K):**  $\delta$  [ppm] = 6.11 (s, 4H,  $\text{CH-N}$ ), 1.59 (s, 36H,  $t\text{Bu}_2\text{MeSi}$ ), 1.46 (s, 36H,  $\text{N}i\text{Bu}$ ), 0.18 (s, 6H,  $t\text{Bu}_2\text{MeSi}$ ).

**$^{13}\text{C}\{^1\text{H}\}$  NMR (126 MHz,  $\text{C}_6\text{D}_6$ , 300 K):**  $\delta$  [ppm] = 144.8 ( $\text{C}=\text{N}$ ), 108.6 ( $\text{CH-N}$ ), 55.8 ( $\text{N}(\text{C}(\text{CH}_3)_3)$ ), 31.1 ( $\text{Si}(\text{C}(\text{CH}_3)_3)_2(\text{CH}_3)$ ), 29.9 ( $\text{NC}(\text{CH}_3)_3$ ), 21.9 ( $\text{Si}(\text{C}(\text{CH}_3)_3)_2(\text{CH}_3)$ ),  $-7.0$  ( $\text{Si}(\text{C}(\text{CH}_3)_3)_2(\text{CH}_3)$ ).

**$^{29}\text{Si}\{^1\text{H}\}$  NMR (99 MHz,  $\text{C}_6\text{D}_6$ , 300 K):**  $\delta$  [ppm] = 71.4 ( $\text{Si}=\text{Si}$ ), 7.9 ( $t\text{Bu}_2\text{MeSi}$ ).

**EA:**  $\text{Si}_4\text{C}_{40}\text{H}_{82}\text{N}_6$  Calculated [%]: C (63.26), H (10.88), N (11.07)  
Experimental [%]: C (63.08), H (10.97), N (10.79)

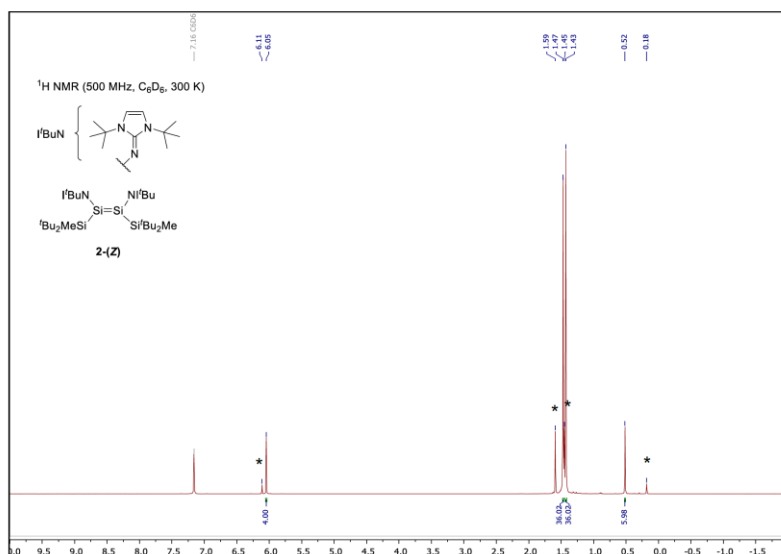


**Figure S6:** <sup>1</sup>H NMR spectrum (500 MHz) of compound **2-(Z)** in C<sub>6</sub>D<sub>6</sub> at 300 K. Signals labeled with \* belong to **2-(E)**.

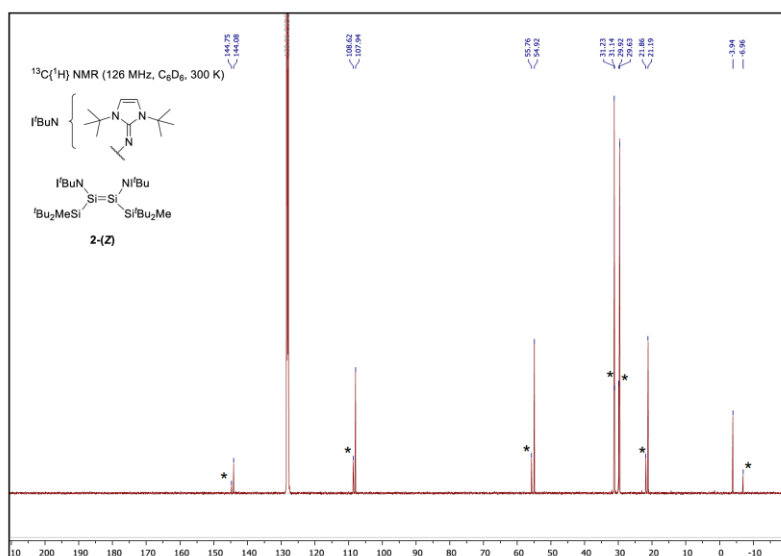


**Figure S7:** <sup>13</sup>C{<sup>1</sup>H} spectrum (126 MHz) of compound **2-(Z)** in C<sub>6</sub>D<sub>6</sub> at 300 K. Signals labeled with \* belong to **2-(E)**.

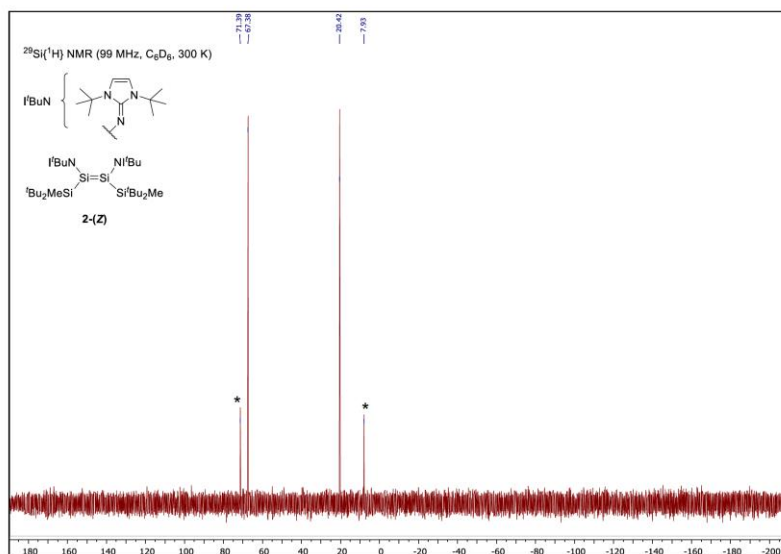


**Figure S8:**  $^{29}\text{Si}\{^1\text{H}\}$  NMR spectrum (99 MHz) of compound **2-(Z)** in  $\text{C}_6\text{D}_6$  at 300 K. Signals labeled with \* belong to **2-(E)**.

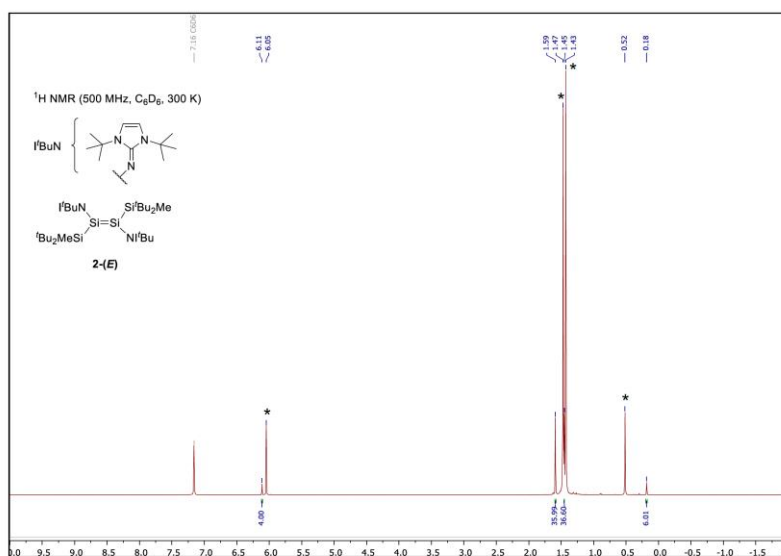


**Figure S9:**  $^1\text{H}$  NMR spectrum (500 MHz) of compound **2-(E)** in  $\text{C}_6\text{D}_6$  at 300 K. Signals labeled with \* belong to **2-(Z)**.

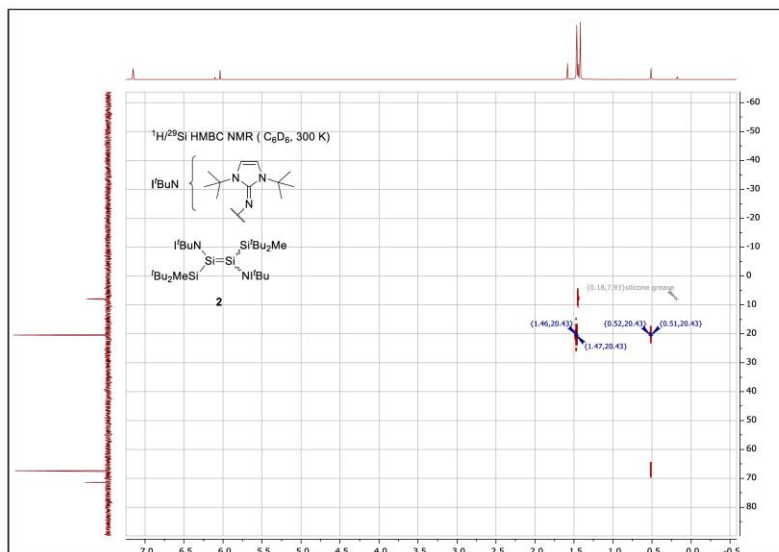


Figure S10:  $^1\text{H}/^{29}\text{Si}$  HMBC NMR spectrum of disilene **2** in  $\text{C}_6\text{D}_6$  at 300 K.

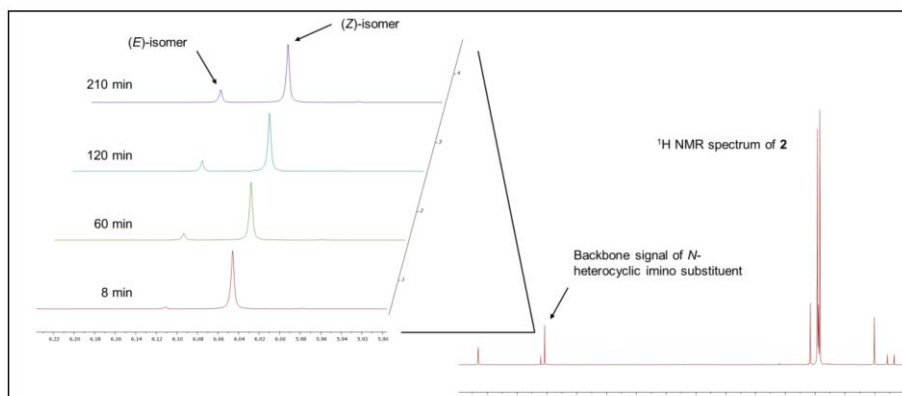
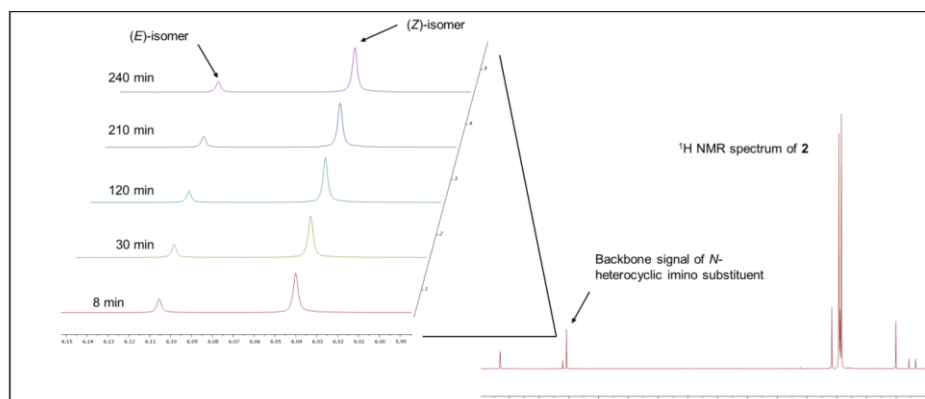


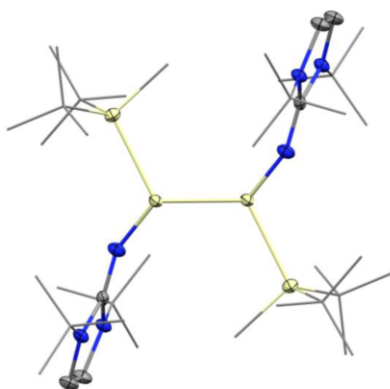
Figure S11:  $^1\text{H}$  NMR kinetic studies of (*E/Z*)-isomerization of **2** in solution at room temperature.

Note: Crystals of **2** (5 mg) were dissolved in  $\text{C}_6\text{D}_6$  and the isomerization process was monitored by  $^1\text{H}$  NMR spectroscopy. Since 8 minutes after dissolving the crystals, almost no (*E*)-isomer is observable, we assume that **2** adopts solely (*Z*)-configuration in the solid state. Equilibrium is reached at room temperature after 3.5 hours with a ratio of (*E*):(*Z*) = 18:82. The concentration of **2**, as well as exposure to visible light have no influence on the kinetic of this isomerization reaction.



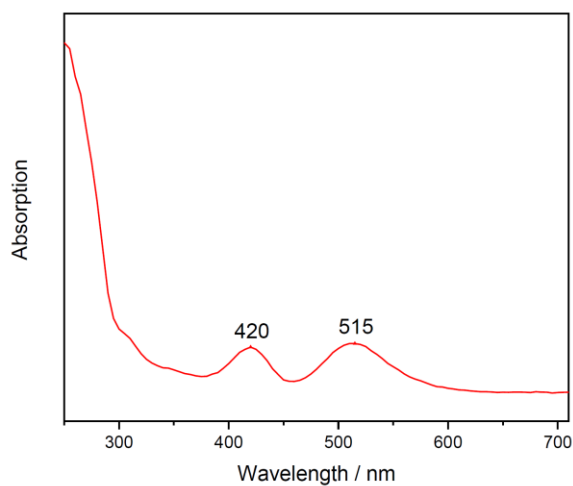
**Figure S12:**  $^1\text{H}$  NMR kinetic studies of (*E/Z*)-isomerization of **2** after heating to 80 °C in solution at room temperature.

Note: A solution of **2** in  $\text{C}_6\text{D}_6$  was heated to 80 °C for 6 hours. Subsequently, the (*E/Z*)-isomerization process was monitored at room temperature by  $^1\text{H}$  NMR spectroscopy. The initially (after 8 min) observed ratio (*E*):(*Z*) = 24:76 changed within 3.5 hours to (*E*):(*Z*) = 18:82, the same value, which was previously observed from isomerization of crystalline **2** at room temperature. This process can be repeated in cycles and is fully reversible. No decomposition products were observed.



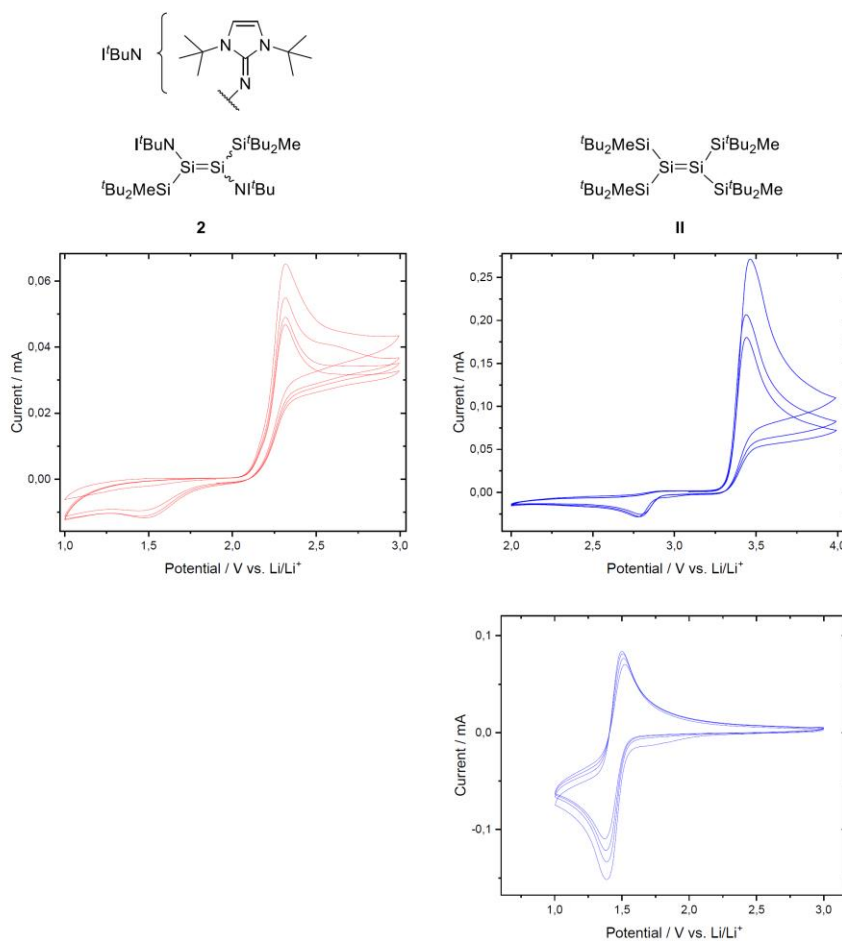
**Figure S13:** Solid state structure of **2-(E)**.

Note: This solid state structure was surprisingly obtained from a reactivity test of **2** and contains a minor, unknown, co-crystallized compound. Therefore, no satisfactory structure was obtained and structural parameters cannot be discussed. Nonetheless, this structure is an unambiguous evidence for the existence of the (*E*)-isomer of **2**.



**Figure S14:** UV/VIS spectrum of red disilene **2** in *n*-hexane ( $2.5 \times 10^{-3}$  M), measured at room temperature ( $\lambda_{\text{max}} = 420$  nm; 515 nm).

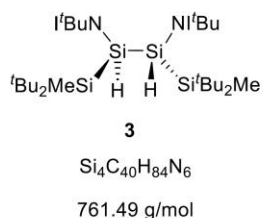
Similar to the observations for compound **VI**, the UV/VIS spectrum of **2** contains two peaks. The peaks of disilene **VI** were assigned by theoretical calculations to be the HOMO→LUMO+1 transition (435 nm) and the  $\pi \rightarrow \pi^*$  transition (518 nm).<sup>[S2]</sup> Presumably, the absorption maximum of **2** at the lower wavelength of 420 nm also derives from the HOMO→LUMO+1 transition and the second peak (515 nm) can be assigned to the  $\pi \rightarrow \pi^*$  transition.



**Figure S15:** Cyclic voltammograms displaying the oxidation waves of **2** (left) and (tBu<sub>2</sub>MeSi)<sub>2</sub>Si=Si(Si<sup>t</sup>Bu<sub>2</sub>Me)<sub>2</sub> (**II**) (right, top) and the reduction wave of **II** (right, bottom), measured in multiple cycles in a three-electrode setup using a lithium metal reference electrode (0.1 M (*n*-Bu<sub>4</sub>N)TFSI in THF at room temperature).

Note: Since the only disilene radical cation reported so far derives from one-electron oxidation of **II**, we measured the cyclic voltammograms of **II** and iminodisilene **2** under the same conditions for comparison. Apparently, the oxidation of **2** occurs at lower potentials than required for the oxidation of **II** (~1 V vs. Li/Li<sup>+</sup>). This result already indicates the accessibility of a cationic species, from oxidation of **2**.



1.4  $t\text{BuN}(t\text{Bu}_2\text{MeSi})\text{HSi-SiH}(\text{Si}^t\text{Bu}_2\text{Me})\text{N}^t\text{Bu}$  (**3**)

A toluene (8 mL) solution of disilene **1** (60.0 mg, 79.0  $\mu\text{mol}$ , 1.00 eq.) in a pressurizable Schlenk flask was degassed (freeze-pump-thaw) and subsequently exposed to hydrogen gas (1 bar) at room temperature. Complete decolorization occurred within 2 hours. After concentrating the solution under reduced pressure, silane **3** was obtained by crystallization at  $-35\text{ }^\circ\text{C}$  as colorless crystals (47.6 mg, 62.5  $\mu\text{mol}$ , 79% yield). These crystals were also suitable for SC-XRD analysis.

**m.p.:** 195  $^\circ\text{C}$  (decomposition).

**$^1\text{H}$  NMR (500 MHz,  $\text{C}_6\text{D}_6$ , 300 K):**  $\delta$  [ppm] = 6.53 (s, 2H,  $\text{SiH}$ ), 6.05 (d, 2H,  $^3J = 3.3\text{ Hz}$ ,  $\text{CH-N}$ ), 6.03 (d, 2H,  $^3J = 3.3\text{ Hz}$ ,  $\text{CH-N}$ ), 1.49 (s, 18H,  $t\text{BuN}$ ), 1.45 (s, 18H,  $t\text{Bu}_2\text{MeSi}$ ), 1.37 (s, 18H,  $t\text{Bu}_2\text{MeSi}$ ), 1.36 (s, 18H,  $t\text{BuN}$ ), 0.42 (s, 6H,  $t\text{Bu}_2\text{MeSi}$ ).

**$^{13}\text{C}\{^1\text{H}\}$  NMR (126 MHz,  $\text{C}_6\text{D}_6$ , 300 K):**  $\delta$  [ppm] = 141.7 ( $\text{C}=\text{N}$ ), 107.5 ( $\text{CH-N}$ ), 107.2 ( $\text{CH-N}$ ), 55.0 ( $\text{N}(\text{C}(\text{CH}_3)_3)$ ), 54.4 ( $\text{N}(\text{C}(\text{CH}_3)_3)$ ), 31.0 ( $\text{Si}(\text{C}(\text{CH}_3)_3)_2(\text{CH}_3)$ ), 30.1 ( $\text{Si}(\text{C}(\text{CH}_3)_3)_2(\text{CH}_3)$ ), 29.9 ( $\text{N}(\text{C}(\text{CH}_3)_3)$ ), 29.5 ( $\text{N}(\text{C}(\text{CH}_3)_3)$ ), 21.6 ( $\text{Si}(\text{C}(\text{CH}_3)_3)_2(\text{CH}_3)$ ), 21.5 ( $\text{Si}(\text{C}(\text{CH}_3)_3)_2(\text{CH}_3)$ ),  $-4.8$  ( $\text{Si}(\text{C}(\text{CH}_3)_3)_2(\text{CH}_3)$ ).

**$^{29}\text{Si}\{^1\text{H}\}$  NMR (99 MHz,  $\text{C}_6\text{D}_6$ , 195 K):**  $\delta$  [ppm] = 6.1 ( $t\text{Bu}_2\text{MeSi}$ ),  $-69.1$  ( $\text{SiH}$ ).

**EA:** Si<sub>4</sub>C<sub>40</sub>H<sub>82</sub>N<sub>6</sub> Calculated [%]: C (63.09), H (11.12), N (11.04)  
Experimental [%]: C (62.69), H (11.22), N (10.62)

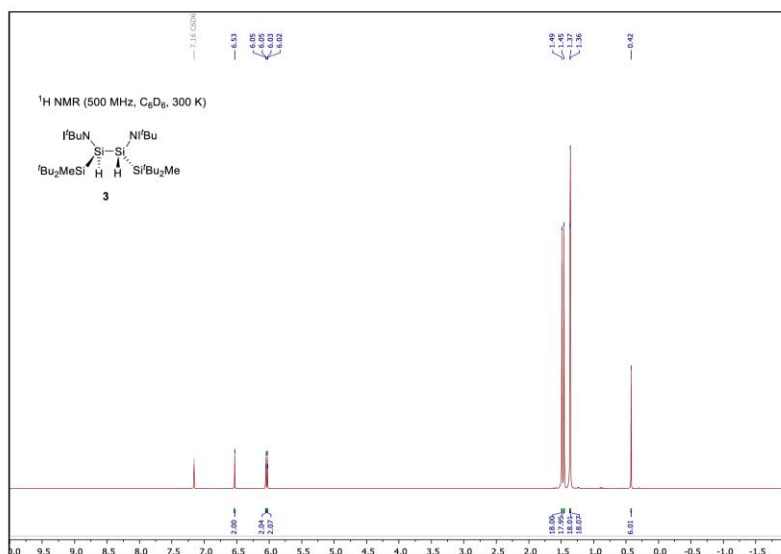


Figure S16: <sup>1</sup>H NMR spectrum (500 MHz) of compound **3** in C<sub>6</sub>D<sub>6</sub> at 300 K.

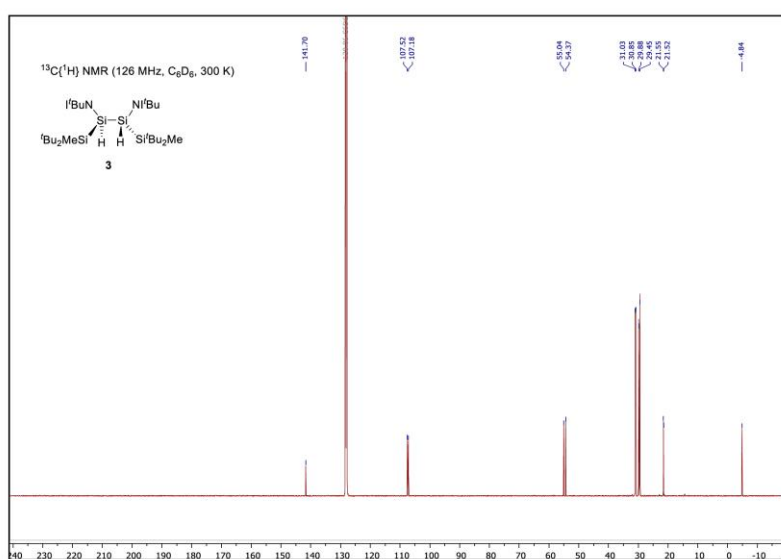
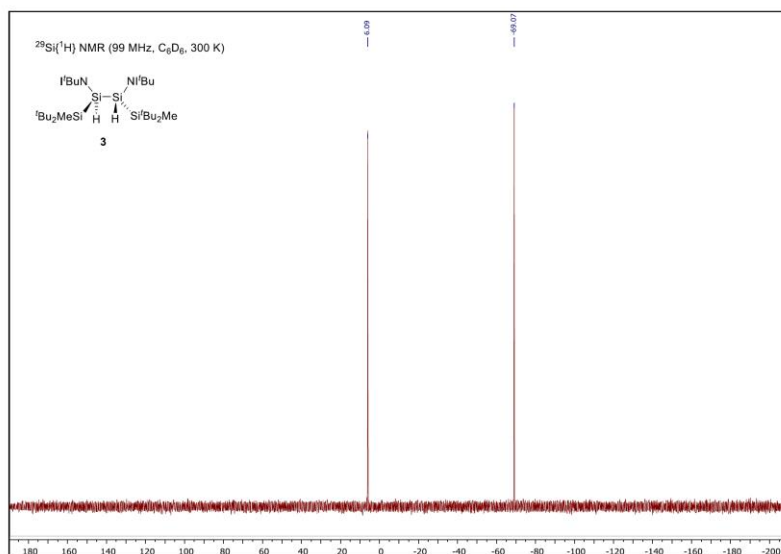
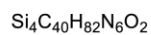
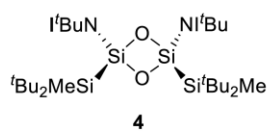


Figure S17: <sup>13</sup>C{<sup>1</sup>H} NMR spectrum (126 MHz) of compound **3** in C<sub>6</sub>D<sub>6</sub> at 300 K.



**Figure S18:**  $^{29}\text{Si}\{^1\text{H}\}$  NMR spectrum (99 MHz) of compound **3** in  $\text{C}_6\text{D}_6$  at 300 K.

1.4. Dioxadisiletane **4**

791.48 g/mol

In a pressurizeable Schlenk flask, a solution of disilene **2** (70.0 mg, 92.2  $\mu\text{mol}$ ) in *n*-pentane (10 mL) was cooled to  $-130\text{ }^\circ\text{C}$  and exposed to oxygen (1.2 bar) under stirring. The deep red color rapidly vanished and the solution was allowed to warm to room temperature. After evaporation of all volatiles *in vacuo*, compound **4** was obtained from recrystallization of the residue in *n*-hexane at  $-35\text{ }^\circ\text{C}$  as colorless crystals (61.4 mg, 76.3  $\mu\text{mol}$ , 83%).

m.p.: 266  $^\circ\text{C}$ 

$^1\text{H NMR}$  (500 MHz,  $\text{C}_6\text{D}_6$ , 300 K):  $\delta$  [ppm] = 5.98 (s, 4H,  $\text{CH-N}$ ), 1.48 (s, 36H,  $\text{N}^t\text{Bu}$ ), 1.44 (s, 36H,  $^t\text{Bu}_2\text{MeSi}$ ), 0.53 (s, 6H,  $^t\text{Bu}_2\text{MeSi}$ ).

$^{13}\text{C}\{^1\text{H}\}$  NMR (126 MHz,  $\text{C}_6\text{D}_6$ , 300 K):  $\delta$  [ppm] = 140.1 ( $\text{C=N}$ ), 108.0 ( $\text{CH-N}$ ), 55.7 ( $\text{N}(\text{C}(\text{CH}_3)_3)$ ), 30.8 ( $\text{Si}(\text{C}(\text{CH}_3)_3)_2(\text{CH}_3)$ ), 29.9 ( $\text{NC}(\text{CH}_3)_3$ ), 21.1 ( $\text{Si}(\text{C}(\text{CH}_3)_3)_2(\text{CH}_3)$ ),  $-3.6$  ( $\text{Si}(\text{C}(\text{CH}_3)_3)_2(\text{CH}_3)$ ).

$^{29}\text{Si}\{^1\text{H}\}$  NMR (99 MHz,  $\text{C}_6\text{D}_6$ , 195 K):  $\delta$  [ppm] =  $-0.2$  ( $^t\text{Bu}_2\text{MeSi}$ ),  $-47.3$  ( $\text{SiO}$ ).

EA:  $\text{Si}_4\text{C}_{40}\text{H}_{82}\text{Br}_2\text{N}_6$       Calculated [%]:      C (60.70), H (10.44), N (10.62)  
 Experimental [%]:      C (59.66), H (10.44), N (10.18)

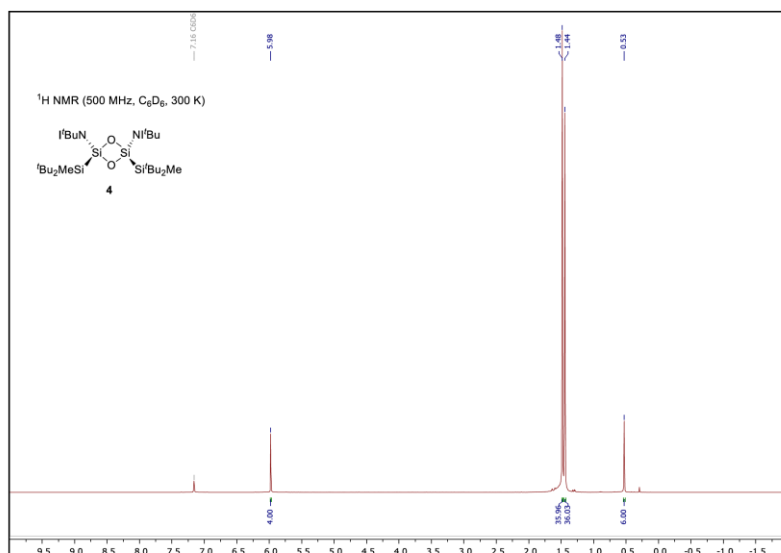


Figure S19:  $^1\text{H NMR}$  spectrum (500 MHz) of compound **4** in  $\text{C}_6\text{D}_6$  at 300 K.

S19

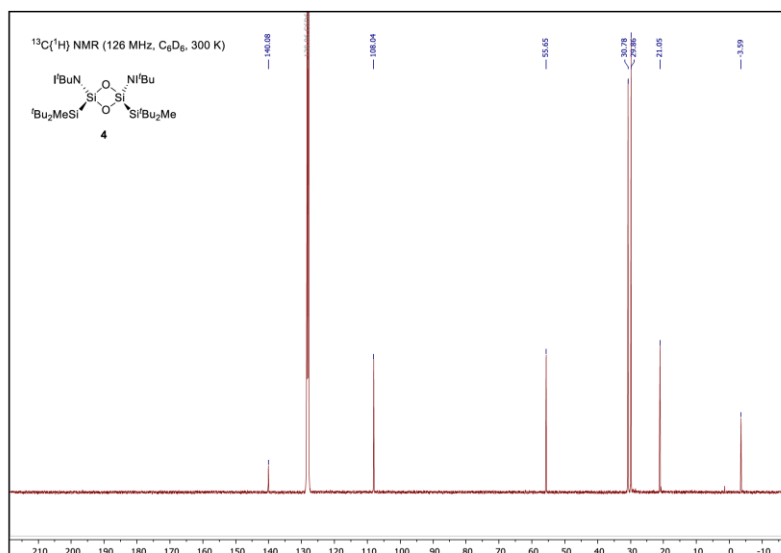


Figure S20:  $^{13}\text{C}$  NMR spectrum (126 MHz) of compound **4** in  $\text{C}_6\text{D}_6$  at 300 K.

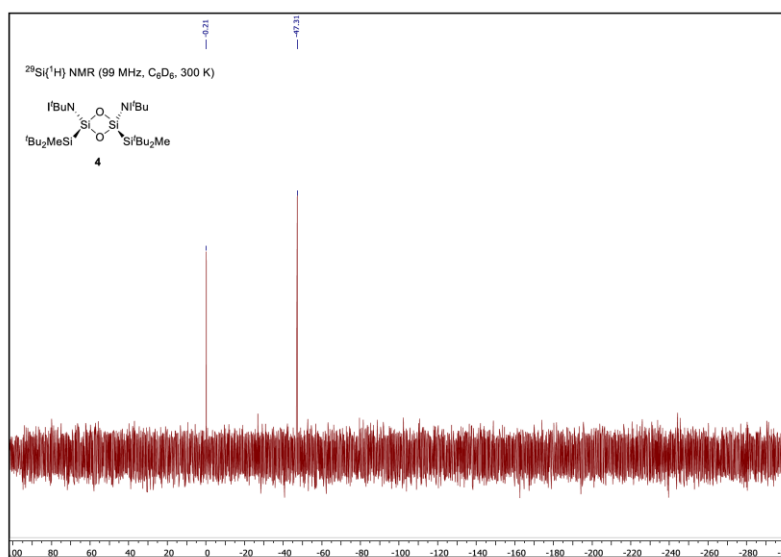
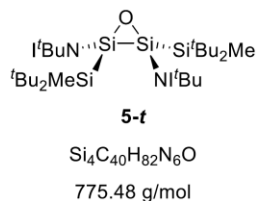


Figure S21:  $^{29}\text{Si}$  NMR spectrum (99 MHz) of compound **4** in  $\text{C}_6\text{D}_6$  at 300 K.

1.4. Disilaoxirane **5-f**

An *n*-pentane (8 mL) solution of **2** (70.0 mg, 92.2 μmol) in a pressurizeable Schlenk flask was cooled to  $-78\text{ }^{\circ}\text{C}$  and exposed to N<sub>2</sub>O (1 bar) under stirring. The red solution turned yellow and was allowed to warm to ambient temperature after 20 minutes. All volatiles were removed under reduced pressure and the yellow solid residue was purified by recrystallization from *n*-hexane to give yellow crystals (57.3 mg). Multinuclear NMR spectroscopy revealed the composition of this crystals to be 25% **4** and 75% **5-c** (77% yield). Various separation attempts were unsuccessful. Heating of a sample of **5-c** in C<sub>6</sub>D<sub>6</sub> to 70 °C for 16 hours lead to quantitative isomerization to **5-f**.

Note: Neither the crystals of **5-c**, nor that of **5-f** were suitable for SC-XRD analysis due to co-crystallization with compound **4**. Compounds **5** were identified by comparison of multinuclear NMR spectroscopic data with literature reported disilaoxiranes.<sup>[S8]</sup>

**5-c:**

**<sup>1</sup>H NMR (500 MHz, C<sub>6</sub>D<sub>6</sub>, 300 K):** δ [ppm] = 6.02 (d, <sup>3</sup>J = 3.2 Hz, 2H, CH-N), 6.00 (d, <sup>3</sup>J = 3.2 Hz, 2H, CH-N), 1.48 (s, 18H, N<sup>i</sup>Bu), 1.47 (s, 18H, N<sup>t</sup>Bu), 1.43 (s, 18H, <sup>t</sup>Bu<sub>2</sub>MeSi), 1.41 (s, 18H, <sup>i</sup>Bu<sub>2</sub>MeSi), 0.50 (s, 6H, <sup>t</sup>Bu<sub>2</sub>MeSi).

**5-f**

**<sup>1</sup>H NMR (500 MHz, C<sub>6</sub>D<sub>6</sub>, 300 K):** δ [ppm] = 6.08 (d, <sup>3</sup>J = 3.2 Hz, 2H, CH-N), 6.06j (d, <sup>3</sup>J = 3.2 Hz, 2H, CH-N), 1.48 (s, 18H, N<sup>i</sup>Bu), 1.47 (s, 18H, N<sup>t</sup>Bu), 1.43 (s, 18H, <sup>t</sup>Bu<sub>2</sub>MeSi), 1.41 (s, 18H, <sup>i</sup>Bu<sub>2</sub>MeSi), 0.50 (s, 6H, <sup>t</sup>Bu<sub>2</sub>MeSi).

**<sup>13</sup>C{<sup>1</sup>H} NMR (126 MHz, C<sub>6</sub>D<sub>6</sub>, 300 K):** δ [ppm] = 143.1 (C=N), 108.4 (CH-N), 108.3 (CH-N), 55.9 (NC(CH<sub>3</sub>)<sub>3</sub>), 55.3 (NC(CH<sub>3</sub>)<sub>3</sub>), 30.9 (Si(C(CH<sub>3</sub>)<sub>3</sub>)<sub>2</sub>(CH<sub>3</sub>)), 30.7 (Si(C(CH<sub>3</sub>)<sub>3</sub>)<sub>2</sub>(CH<sub>3</sub>)), 29.5 (NC(CH<sub>3</sub>)<sub>3</sub>), 22.1 (Si(C(CH<sub>3</sub>)<sub>3</sub>)<sub>2</sub>(CH<sub>3</sub>)), 21.9 (Si(C(CH<sub>3</sub>)<sub>3</sub>)<sub>2</sub>(CH<sub>3</sub>)), -6.4 (Si(C(CH<sub>3</sub>)<sub>3</sub>)<sub>2</sub>(CH<sub>3</sub>)).

**<sup>29</sup>Si{<sup>1</sup>H} NMR (99 MHz, C<sub>6</sub>D<sub>6</sub>, 195 K):** δ [ppm] = 5.3 (<sup>t</sup>Bu<sub>2</sub>MeSi), -48.8 (SiO).

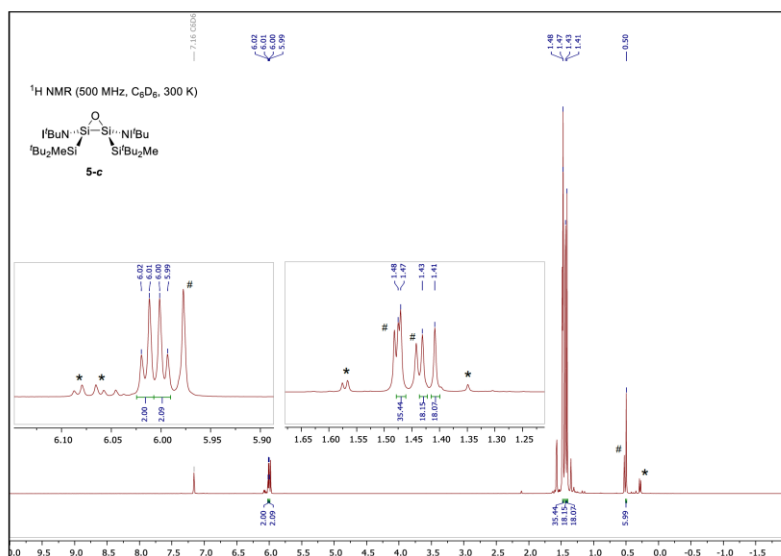


**Figure S22:** <sup>1</sup>H NMR spectrum (500 MHz) of compound **5-c** in C<sub>6</sub>D<sub>6</sub> at 300 K. Signals labeled with \* and # belong to compounds **5-t** (\*) and **4** (#).

Note: The signals at 1.48 ppm and 1.47 ppm are overlapping. Thus, no separate integration was possible.

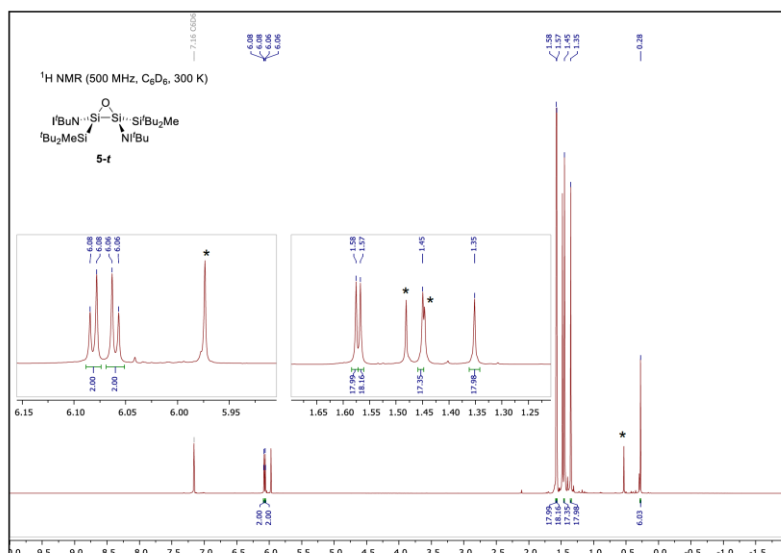


**Figure S23:** <sup>1</sup>H NMR spectrum (500 MHz) of compound **5-c** in C<sub>6</sub>D<sub>6</sub> at 300 K. Signals labeled with \* belong to compound **4**.



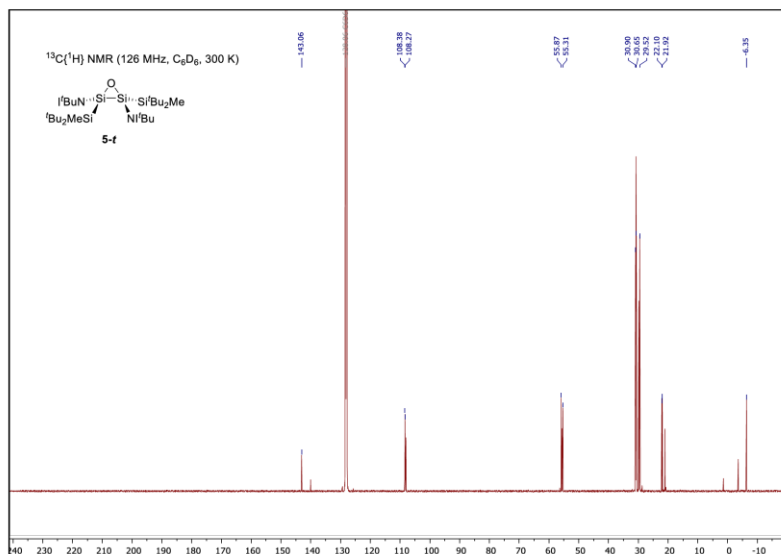


**Figure S24:** <sup>13</sup>C NMR spectrum (126 MHz) of compound **5-t** in C<sub>6</sub>D<sub>6</sub> at 300 K. Unlabeled signals belong to compound **4**.

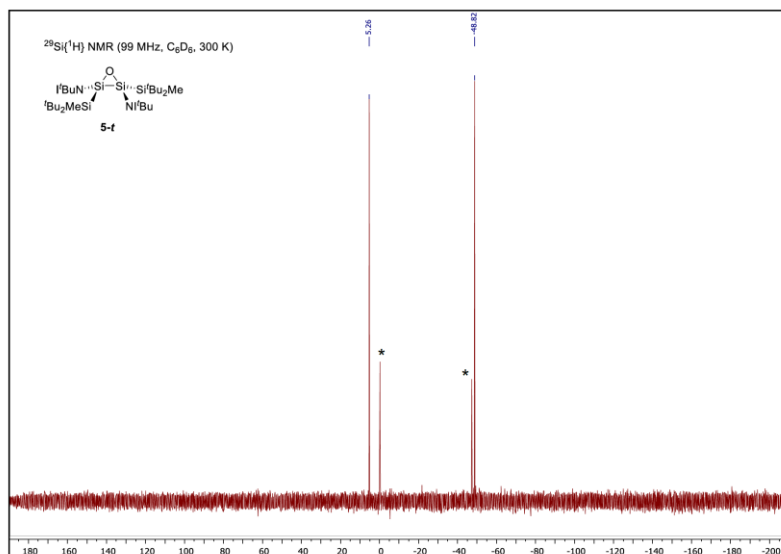


**Figure S25:** <sup>29</sup>Si NMR spectrum (99 MHz) of compound **5-t** in C<sub>6</sub>D<sub>6</sub> at 300 K. Signals labeled with \* belong to compound **4**.

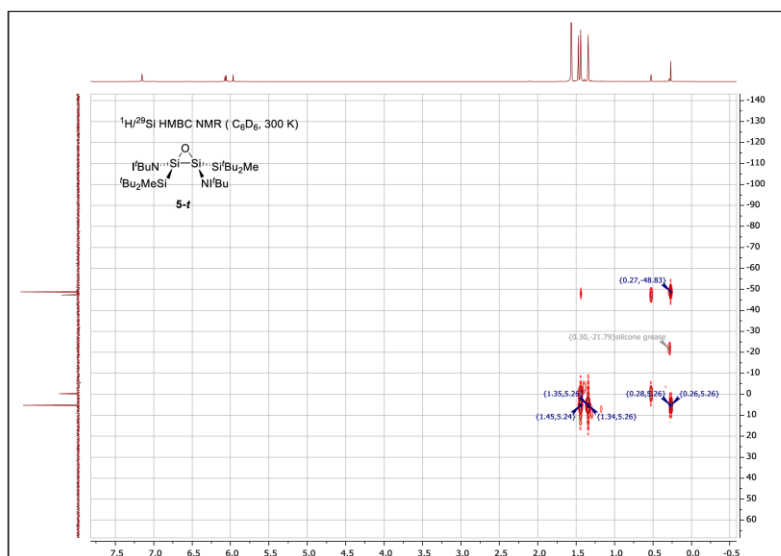
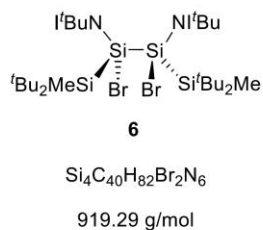


Figure S26:  $^1\text{H}/^{29}\text{Si}$  HMBC NMR spectrum of mixture of compounds **5-t** and **4** in  $\text{C}_6\text{D}_6$  at 300 K.

1.4  $t\text{BuN}(t\text{Bu}_2\text{MeSi})\text{BrSi-SiBr}(t\text{Bu}_2\text{MeSi}) t\text{BuN}$  (**6**)

A solution of  $\text{SiBr}_4$  (22.9 mg, 65.8  $\mu\text{mol}$ , 1.00 eq.) in *n*-hexane (2 mL) was added dropwise to a solution of iminodisilene **2** (50.0 mg, 65.8  $\mu\text{mol}$ , 1.00 eq.) in *n*-hexane at ambient temperature. Full decolorization occurred and a colorless precipitate was formed. This precipitate was separated, washed with *n*-hexane ( $3 \times 1$  mL) and dried under high vacuum to afford 1,2-dibromosilane **6** as colorless solid (58.1 mg, 63.2  $\mu\text{mol}$ , 96%). Compound **6** is almost insoluble in *n*-hexane and only poorly soluble in benzene, toluene or THF. Crystals, suitable for SC XRD analysis were grown from a saturated solution of **6** in THF / toluene (1:1) at  $-35$  °C.

**m.p.:** 185 °C (decomposition, color change to brown).

**$^1\text{H}$  NMR (500 MHz,  $\text{C}_6\text{D}_6$ , 300 K):**  $\delta$  [ppm] = 6.09 (d,  $^3J = 3.3$  Hz, 2H,  $\text{CH-N}$ ), 6.01 (d,  $^3J = 3.3$  Hz, 2H,  $\text{CH-N}$ ), 1.64 (s, 36H,  $\text{N}^i\text{Bu}$ ), 1.43 (s, 18H,  $t\text{Bu}_2\text{MeSi}$ ), 1.40 (s, 18H,  $t\text{Bu}_2\text{MeSi}$ ), 0.67 (s, 6H,  $t\text{Bu}_2\text{MeSi}$ ).

**$^{13}\text{C}\{^1\text{H}\}$  NMR (126 MHz,  $\text{C}_6\text{D}_6$ , 300 K):**  $\delta$  [ppm] = 142.8 ( $\text{C}=\text{N}$ ), 109.5 ( $\text{CH-N}$ ), 109.3 ( $\text{CH-N}$ ), 57.7 ( $\text{NC}(\text{CH}_3)_3$ ), 56.5k ( $\text{NC}(\text{CH}_3)_3$ ), 31.9 ( $\text{Si}(\text{C}(\text{CH}_3)_3)_2(\text{CH}_3)$ ), 31.6 ( $\text{Si}(\text{C}(\text{CH}_3)_3)_2(\text{CH}_3)$ ), 31.2 ( $\text{NC}(\text{CH}_3)_3$ ), 30.9 ( $\text{NC}(\text{CH}_3)_3$ ), 24.3 ( $\text{Si}(\text{C}(\text{CH}_3)_3)_2(\text{CH}_3)$ ), 22.1 ( $\text{Si}(\text{C}(\text{CH}_3)_3)_2(\text{CH}_3)$ ),  $-3.5$  ( $\text{Si}(\text{C}(\text{CH}_3)_3)_2(\text{CH}_3)$ ).

**$^{29}\text{Si}\{^1\text{H}\}$  NMR (99 MHz,  $\text{C}_6\text{D}_6$ , 195 K):**  $\delta$  [ppm] = 5.5 ( $t\text{Bu}_2\text{MeSi}$ ),  $-51.9$  ( $\text{SiBr}$ ).

<b>EA:</b>	$\text{Si}_4\text{C}_{40}\text{H}_{82}\text{Br}_2\text{N}_6$	Calculated [%]:	C (52.26), H (8.99), N (9.14)
		Experimental [%]:	C (51.50), H (9.24), N (8.77)

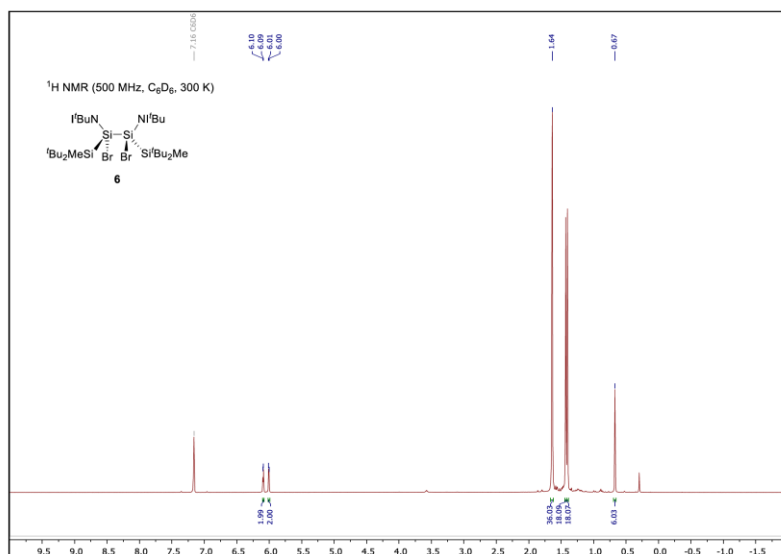


Figure S27: <sup>1</sup>H NMR spectrum (500 MHz) of compound **6** in C<sub>6</sub>D<sub>6</sub> at 300 K.

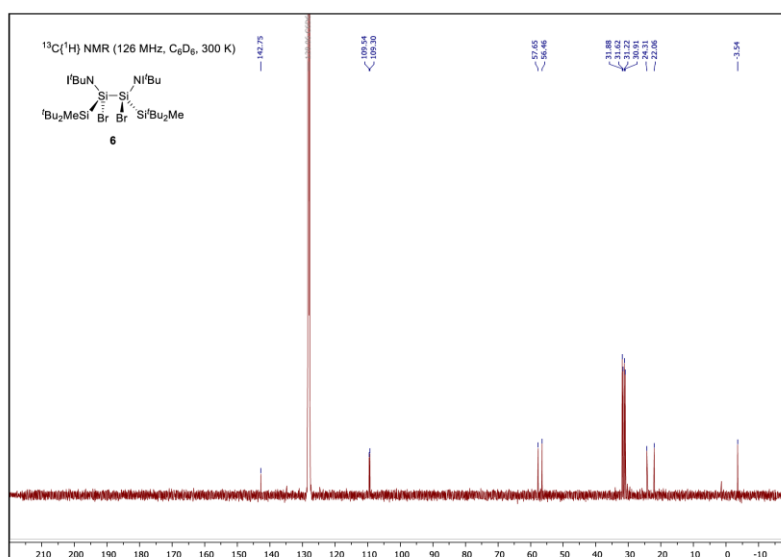


Figure S28: <sup>13</sup>C{<sup>1</sup>H} NMR spectrum (126 MHz) of compound **6** in C<sub>6</sub>D<sub>6</sub> at 300 K.

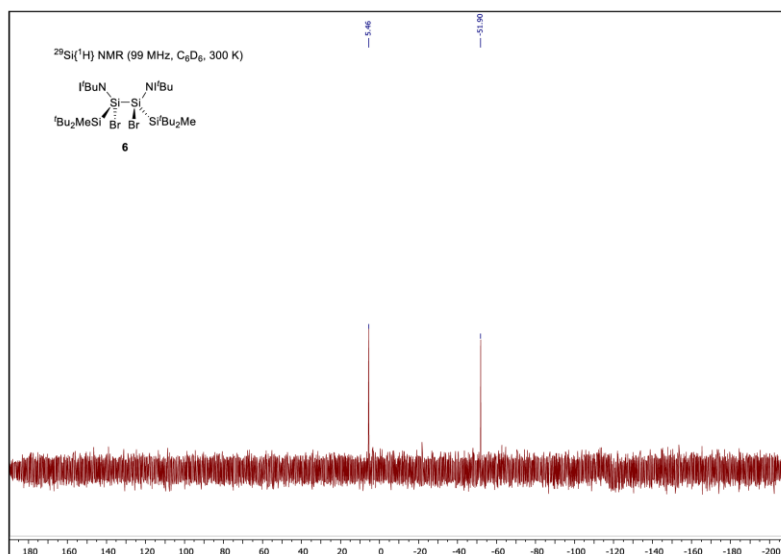


Figure S29:  $^{29}\text{Si}\{^1\text{H}\}$  NMR spectrum (99 MHz) of compound **6** in  $\text{C}_6\text{D}_6$  at 300 K.

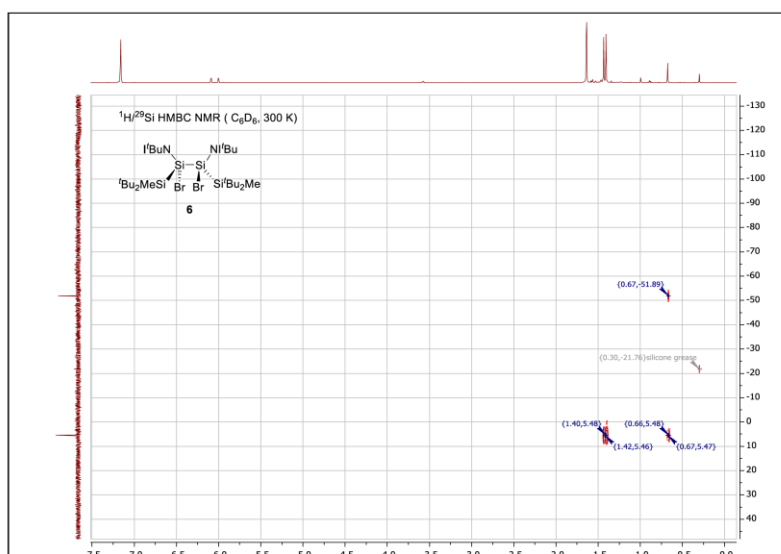


Figure S30:  $^1\text{H}/^{29}\text{Si}$  HMBC NMR spectrum of compound **6** in  $\text{C}_6\text{D}_6$  at 300 K.

1.4  ${}^1\text{BuN}(\text{}^t\text{Bu}_2\text{MeSi})_2\text{SiBr}$  (**7**)

Compound **2** (25.0 mg, 32.9  $\mu\text{mol}$ , 1.00 eq.) was dissolved in toluene (0.2 mL) and a solution of IDipp-SiBr<sub>2</sub> (19.0 mg, 32.9  $\mu\text{mol}$ , 1.00 eq.) in toluene (0.4 mL) was added at ambient temperature. Within 30 minutes of stirring, complete decolorization to a cloudy mixture was observable. Free NHC was removed by precipitation with CO<sub>2</sub> and subsequent filtration. After evaporation of the solvent under reduced pressure, compound **7** was afforded as colorless solid (11.0 mg, 17.8  $\mu\text{mol}$ , 54%). Crystals suitable for SC XRD analysis were obtained from cooling a concentrated toluene solution to  $-35^\circ\text{C}$ .

**m.p.:** 169  $^\circ\text{C}$  (decomposition, color change to orange).

**${}^1\text{H}$  NMR (500 MHz, C<sub>6</sub>D<sub>6</sub>, 300 K):**  $\delta$  [ppm] = 6.04 (d,  ${}^3J = 3.3$  Hz, 1H,  $\underline{\text{C}}\text{H-N}$ ), 5.90 (d,  ${}^3J = 3.3$  Hz, 1H,  $\underline{\text{C}}\text{H-N}$ ), 1.58 (s, 9H, N $\underline{\text{B}}\text{u}$ ), 1.40 (s, 18H,  $\underline{\text{B}}\text{u}_2\text{MeSi}$ ), 1.39 (s, 9H, N $\underline{\text{B}}\text{u}$ ), 1.34 (s, 18H,  $\underline{\text{B}}\text{u}_2\text{MeSi}$ ), 0.53 (s, 6H,  $\underline{\text{B}}\text{u}_2\text{MeSi}$ ).

**${}^{13}\text{C}\{{}^1\text{H}\}$  NMR (126 MHz, C<sub>6</sub>D<sub>6</sub>, 300 K):**  $\delta$  [ppm] = 142.8 ( $\underline{\text{C}}=\text{N}$ ), 110.0 ( $\underline{\text{C}}\text{H-N}$ ), 108.8 ( $\underline{\text{C}}\text{H-N}$ ), 56.9 (N $\underline{\text{C}}(\text{CH}_3)_3$ ), 56.5 (N $\underline{\text{C}}(\text{CH}_3)_3$ ), 31.3 (Si( $\underline{\text{C}}(\text{CH}_3)_3$ )<sub>2</sub>(CH<sub>3</sub>)), 31.2 (Si( $\underline{\text{C}}(\text{CH}_3)_3$ )<sub>2</sub>(CH<sub>3</sub>)), 31.0 (N $\underline{\text{C}}(\text{CH}_3)_3$ ), 30.3 (N $\underline{\text{C}}(\text{CH}_3)_3$ ), 23.5 (Si( $\underline{\text{C}}(\text{CH}_3)_3$ )<sub>2</sub>(CH<sub>3</sub>)), (Si( $\underline{\text{C}}(\text{CH}_3)_3$ )<sub>2</sub>(CH<sub>3</sub>)),  $-2.9$  (Si( $\underline{\text{C}}(\text{CH}_3)_3$ )<sub>2</sub>( $\underline{\text{C}}\text{H}_3$ )).

**${}^{29}\text{Si}\{{}^1\text{H}\}$  NMR (99 MHz, C<sub>6</sub>D<sub>6</sub>, 300 K):**  $\delta$  [ppm] = 1.7 ( $\underline{\text{B}}\text{u}_2\text{MeSi}$ ),  $-35.6$  ( $(\underline{\text{B}}\text{u}_2\text{MeSi})_2\text{}^t\text{BuNSiBr}$ ).

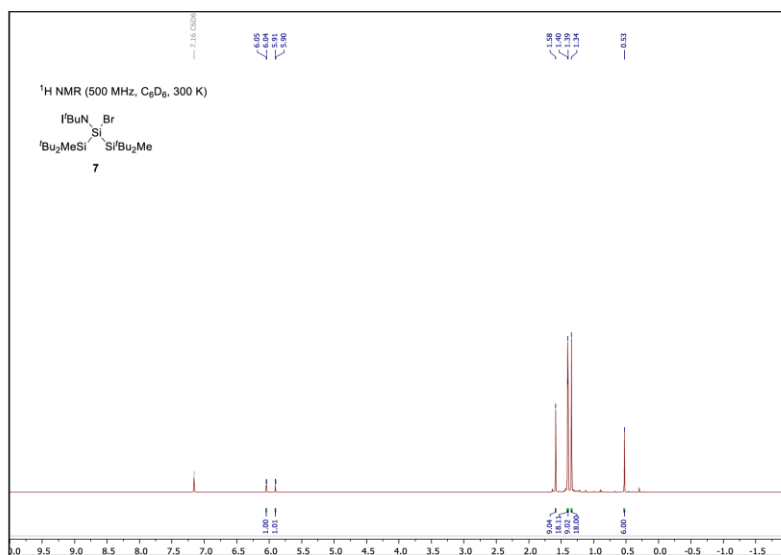


**Figure S31:**  ${}^1\text{H}$  NMR spectrum (500 MHz) of compound **7** in C<sub>6</sub>D<sub>6</sub> at 300 K.

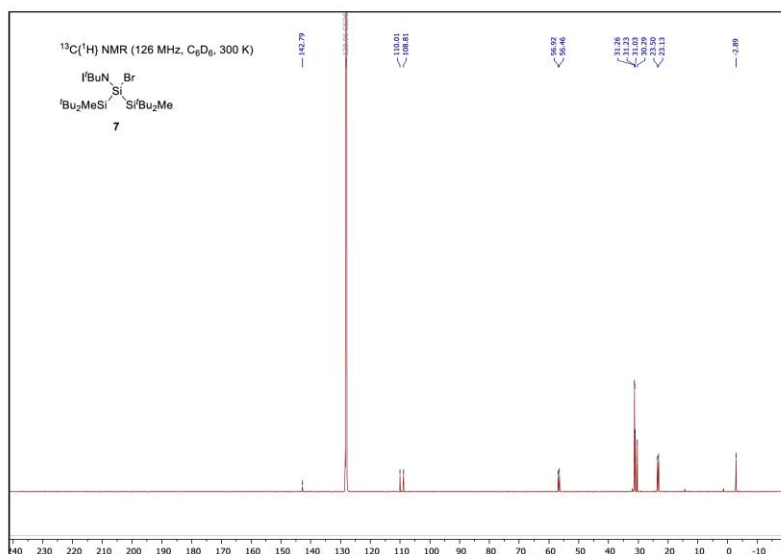


Figure S32:  $^{13}\text{C}\{^1\text{H}\}$  NMR spectrum (126 MHz) of compound 7 in  $\text{C}_6\text{D}_6$  at 300 K.

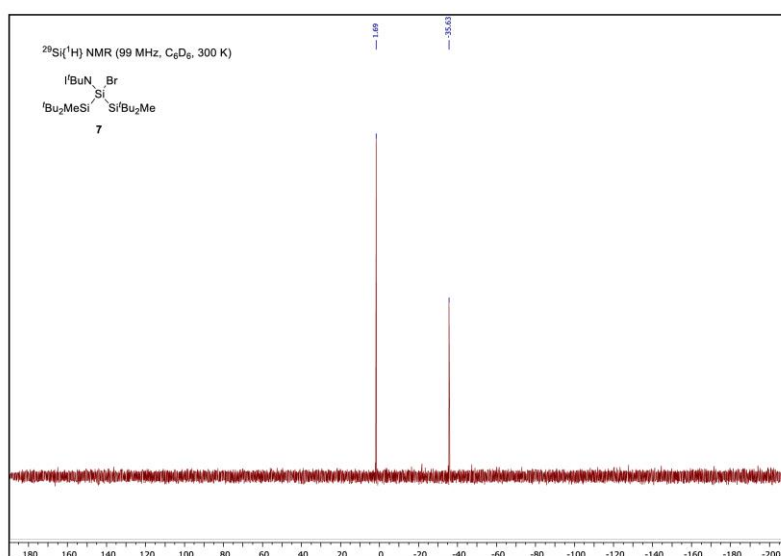
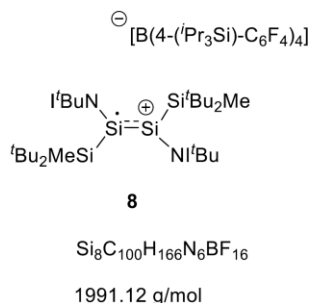


Figure S33:  $^{29}\text{Si}\{^1\text{H}\}$  NMR spectrum (99 MHz) of compound 7 in  $\text{C}_6\text{D}_6$  at 300 K.



1.4. Radical Cation of  $t\text{BuN}(t\text{Bu}_2\text{MeSi})\text{Si}=\text{Si}(\text{Si}^t\text{Bu}_2\text{Me})\text{N}^t\text{Bu}$  **8**

To a mixture of iminodisilene **2** (39.0 mg, 51.4  $\mu\text{mol}$ , 1.00 eq.) and the functionalized trityl (fluoroaryl)borate  $[\text{Ph}_3\text{C}][\text{B}(4-(t\text{Pr}_3\text{Si})\text{-C}_6\text{F}_4)_4]$  (75.8 mg, 51.4  $\mu\text{mol}$ , 1.00 eq.) toluene (4 mL) was added at room temperature. The reaction mixture turned dark green and a phase separation to a lower oily green layer and a top brown layer was observed. After evaporation of all volatile compounds *in vacuo*, the oily residue was washed with *n*-hexane ( $5 \times 3$  mL) to give radical cation **8** as extremely air and moisture sensitive green powder (67.0 mg, 33.4  $\mu\text{mol}$ , 66% yield). Crystals almost suitable for SC-XRD analysis were obtained from diffusion of *n*-hexane into a difluorobenzene solution of **8** at ambient temperature.

Note: The TIPS-functionalized borate anion was only used, in order to facilitate crystallization. Utilization of the commercially available  $\text{B}(\text{C}_6\text{F}_5)_4$  anion also provides the disilene radical cation.

<b>EA:</b>	$\text{Si}_8\text{C}_{100}\text{H}_{166}\text{BF}_{16}\text{N}_6$	Calculated [%]:	C (60.30), H (8.40), N (4.22)
		Experimental [%]:	C (59.15), H (7.93), N (3.57)

Note: Because of the extreme sensitivity of **8**, no better matching elemental analysis was obtained. The carbon value however was reproducibly low, presumably due to the formation of incombustible silicon carbides.

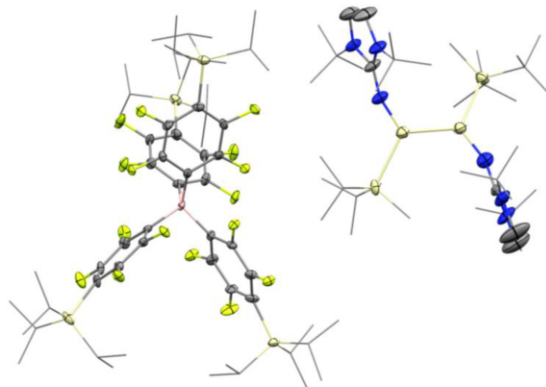


**Figure S34:** Solid state structure of compound **8**.

Note: Because of twinning and disorder, no satisfactory structure was obtained. Therefore, structural parameters cannot be discussed. Nonetheless, this structure is an unambiguous evidence for the existence of **8**.

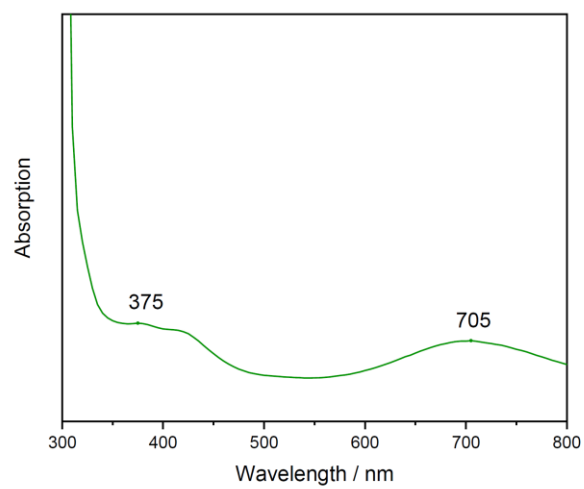
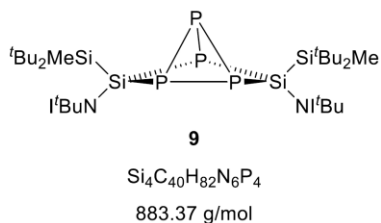


**Figure S35:** UV/VIS spectrum of disilene radical cation **8** in 1,2-difluorobenzene, measured at room temperature.

## 1.4. Compound 9



Under exclusion of light, white phosphorus (4.89 mg, 39.5  $\mu$ mol, 1.00 eq.) was added to a solution of disilene **2** (30.0 mg, 39.5  $\mu$ mol, 1.00 eq.) in toluene (2 mL) at room temperature. The dark red color completely vanished within 18 hours stirring to give a slightly cloudy, pale yellow mixture. After filtration and evaporation of the solvent, compound **9** was obtained as colorless crystalline solid (32.9 mg, 37.2  $\mu$ mol, 94%). Crystals suitable for SC-XRD analysis were obtained from a cooled ( $-35$  °C) solution of **9** in a toluene / *n*-hexane (1:1) mixture.

**m.p.:** 218 °C (decomposition, color change to yellow).

**<sup>1</sup>H NMR (500 MHz, C<sub>6</sub>D<sub>6</sub>, 300 K):**  $\delta$  [ppm] = 5.86 (d,  $^3J = 3.2$  Hz, 2H, CH-N), 5.78 (d,  $^3J = 3.2$  Hz, 2H, CH-N), 1.65 (s, 18H, Bu<sub>2</sub>MeSi), 1.61 (s, 18H, Bu<sub>2</sub>MeSi), 1.35 (s, 18H, N<sup>t</sup>Bu), 1.29 (s, 18H, N<sup>t</sup>Bu), 0.73 (s, 6H, Bu<sub>2</sub>MeSi).

**<sup>13</sup>C{<sup>1</sup>H} NMR (100 MHz, C<sub>6</sub>D<sub>6</sub>, 300 K):**  $\delta$  [ppm] = 140.7 (C=N), 108.8 (CH-N), 108.1 (CH-N), 55.9 (NC(CH<sub>3</sub>)<sub>3</sub>), 55.2 (NC(CH<sub>3</sub>)<sub>3</sub>), 31.8 (Si(C(CH<sub>3</sub>)<sub>3</sub>)<sub>2</sub>(CH<sub>3</sub>)), 31.6 (Si(C(CH<sub>3</sub>)<sub>3</sub>)<sub>2</sub>(CH<sub>3</sub>)), 30.6 (NC(CH<sub>3</sub>)<sub>3</sub>), 30.3 (NC(CH<sub>3</sub>)<sub>3</sub>), 23.0 (Si(C(CH<sub>3</sub>)<sub>3</sub>)<sub>2</sub>(CH<sub>3</sub>)), 23.0 (Si(C(CH<sub>3</sub>)<sub>3</sub>)<sub>2</sub>(CH<sub>3</sub>)),  $-1.7$  (Si(C(CH<sub>3</sub>)<sub>3</sub>)<sub>2</sub>(CH<sub>3</sub>)).

**<sup>29</sup>Si{<sup>1</sup>H} NMR (99 MHz, C<sub>6</sub>D<sub>6</sub>, 300 K):**  $\delta$  [ppm] = 11.9 (s, Bu<sub>2</sub>MeSi),  $-52.2$  (m, SiP<sub>2</sub>).

**<sup>31</sup>P{<sup>1</sup>H} NMR (162 MHz, C<sub>6</sub>D<sub>6</sub>, 300 K):**  $\delta$  [ppm] = 106.6 (dt,  $^1J_{P-P} = 126.9$  Hz,  $^2J_{P-P} = 8.5$  Hz, 1P, PSi<sub>2</sub>),  $-44.0$  (dd,  $^1J_{P-P} = 158.1$  Hz,  $^2J_{P-P} = 8.9$  Hz, 2P, PSiP<sub>2</sub>),  $-217.6$  (dt,  $^1J_{P-P} = 157.9$  Hz,  $^1J_{P-P} = 129.0$  Hz, 1P, PP<sub>3</sub>).

<b>EA:</b>	Si <sub>4</sub> C <sub>40</sub> H <sub>82</sub> N <sub>6</sub> P <sub>4</sub>	Calculated [%]:	C (54.39), H (9.36), N (9.51)
		Experimental [%]:	C (54.14), H (9.25), N (9.35)

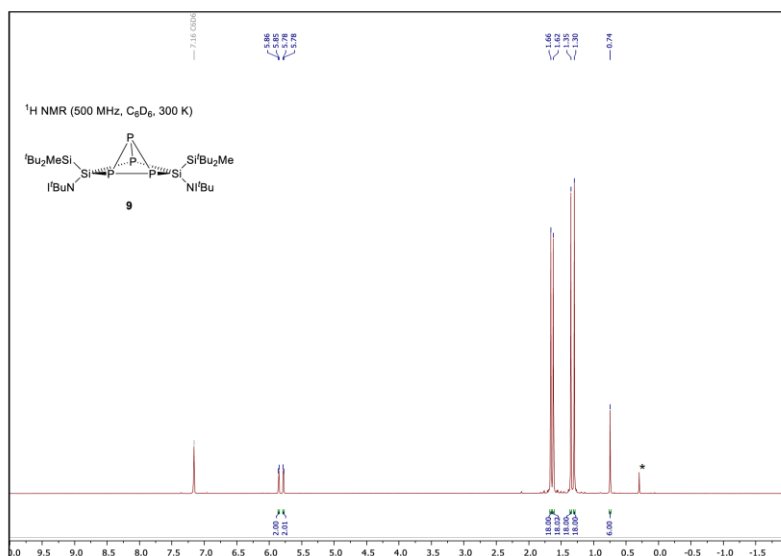


**Figure S36:** <sup>1</sup>H NMR spectrum (500 MHz) of compound **9** in C<sub>6</sub>D<sub>6</sub> at 300 K. The signal labeled with \* belongs to silicone grease.

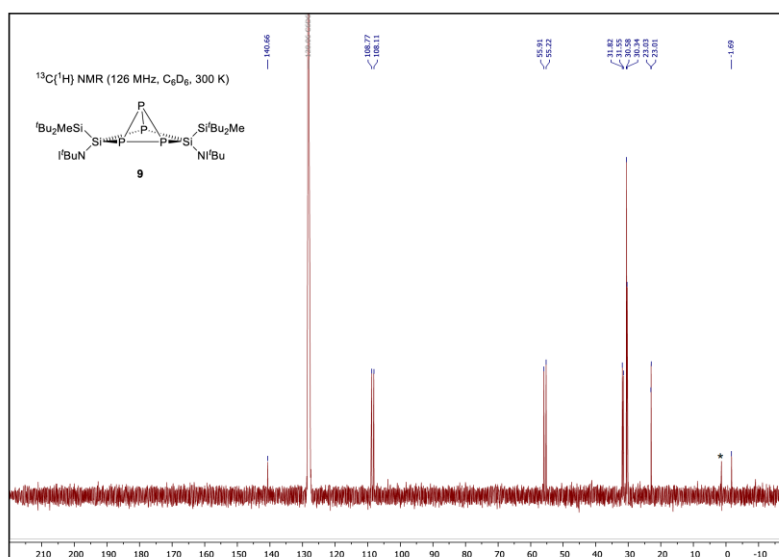


**Figure S37:** <sup>13</sup>C{<sup>1</sup>H} spectrum (126 MHz) of compound **9** in C<sub>6</sub>D<sub>6</sub> at 300 K. The signal labeled with \* belongs to silicone grease.



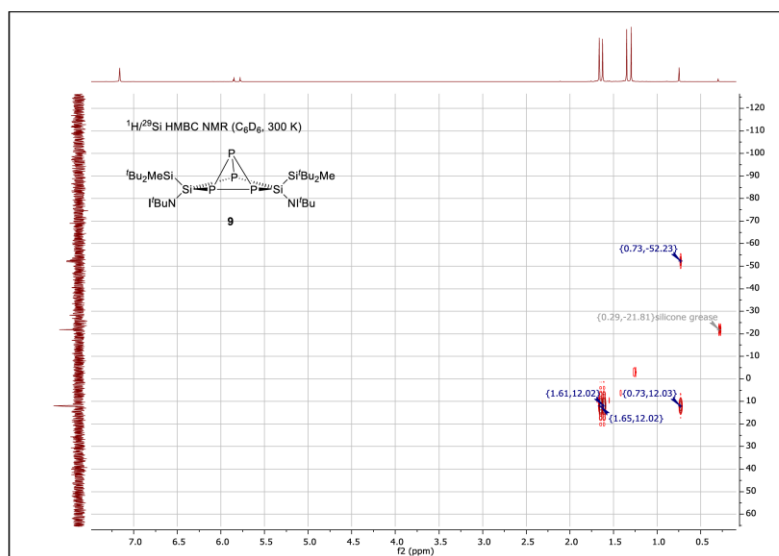


Figure S40:  $^1\text{H}/^{29}\text{Si}$  HMBC NMR spectrum of compound **9** in  $\text{C}_6\text{D}_6$  at 300 K.

## 2. X-ray Crystallographic Data

### 2.1. General Information

The X-ray intensity data of **4** and **7** were collected on an X-ray single crystal diffractometer equipped with a CMOS detector (*Bruker Photon-100*), a rotating anode (*Bruker TXS*) with MoK $\alpha$  radiation ( $\lambda = 0.71073 \text{ \AA}$ ) and a *Helios* mirror optic by using the *APEX III* software package.<sup>[S9]</sup> The X-ray intensity data of **1**, **2-(Z)**, **3**, **6** and **9** were collected on an X-ray single crystal diffractometer equipped with a CMOS detector (*Bruker Photon-100*), an IMS microsource with MoK $\alpha$  radiation ( $\lambda = 0.71073 \text{ \AA}$ ) and a *Helios* mirror optic by using the *APEX III* software package.<sup>[S9]</sup> The measurements were performed on single crystals coated with the perfluorinated ether *Fomblin*<sup>®</sup> Y. The crystal was fixed on the top of a micro sampler, transferred to the diffractometer and frozen under a stream of cold nitrogen. A matrix scan was used to determine the initial lattice parameters. Reflections were merged and corrected for Lorentz and polarization effects, scan speed, and background using *SAINT*.<sup>[S10]</sup> Absorption corrections, including odd and even ordered spherical harmonics were performed using *SADABS*.<sup>[S10]</sup> Space group assignments were based upon systematic absences, E statistics, and successful refinement of the structures. Structures were solved by direct methods with the aid of successive difference Fourier maps, and were refined against all data using the *APEX III* software in conjunction with *SHELXL-2014*<sup>[S11]</sup> and *SHELXLE*.<sup>[S12]</sup> All H atoms (except Si-H) were placed in calculated positions and refined using a riding model, with methylene and aromatic C-H distances of 0.99 and 0.95  $\text{\AA}$ , respectively, and  $U_{\text{iso}}(\text{H}) = 1.2 \cdot U_{\text{eq}}(\text{C})$ . H atoms bound to Si atoms could be located in the difference Fourier maps and were allowed to refine freely. Full-matrix least-squares refinements were carried out by minimizing  $\Delta w(F_o^2 - F_c^2)$ <sup>[S10]</sup> with *SHELXL-97* weighting scheme.<sup>[S13]</sup> Neutral atom scattering factors for all atoms and anomalous dispersion corrections for the non-hydrogen atoms were taken from International Tables for Crystallography.<sup>[S14]</sup> The images of the crystal structures were generated by *Mercury*.<sup>[S15]</sup> The CCDC numbers - contain the supplementary crystallographic data for the structures. These data can be obtained free of charge from the Cambridge Crystallographic Data Centre via <https://www.ccdc.cam.ac.uk/structures/>.



## 2.2 SC-XRD structures

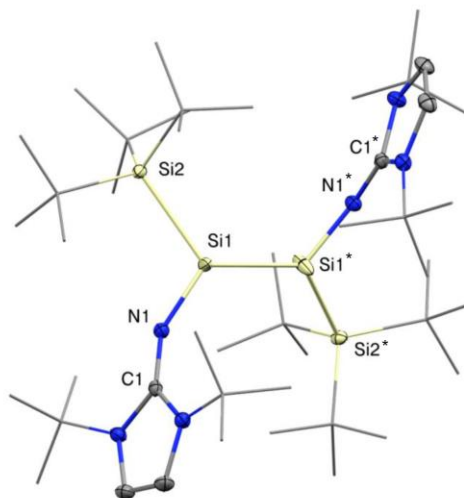


**Figure S41:** SC-XRD structure of disilene **1** with thermal ellipsoids drawn at the 50% probability level. Hydrogen atoms are omitted for clarity, 'Bu- and Me-groups are simplified as wireframes. Selected bond lengths [Å] and angles [°]: Si1–Si1\* 2.2534(7), Si1–Si2 2.4142(6), Si1–N1 1.682(1), N1–C1 1.285(2), N1–Si1–Si1\* 122.97(5), Si2–Si1–Si1\* 124.52(3), Si2–Si1–N1 110.56(4).

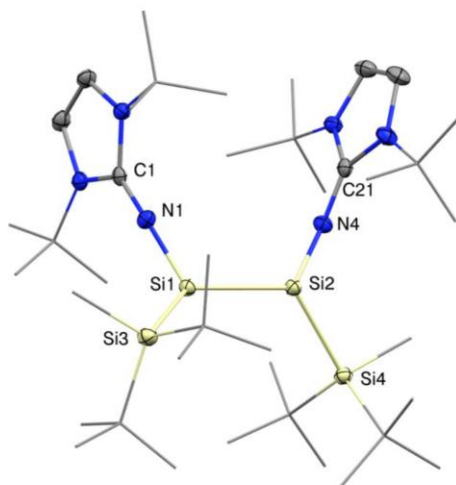


**Figure S42:** SC-XRD structure of disilene **2-Z** with thermal ellipsoids drawn at the 50% probability level. Hydrogen atoms are omitted for clarity, 'Bu- and Me-groups are simplified as wireframes. Selected bond lengths [Å] and angles [°]: Si1–Si2 2.2844(7), Si1–Si3 2.3922(7), Si2–Si4 2.4001(7), Si1–N1 1.683(1), Si2–N4 1.680(1), N1–C1 1.283(2), N4–C21 1.278(2), Si3–Si1–N1 104.35(5), Si4–Si2–N4 103.84(5), Si2–Si1–Si3 121.28(2), Si2–Si1–N1 119.25(5).

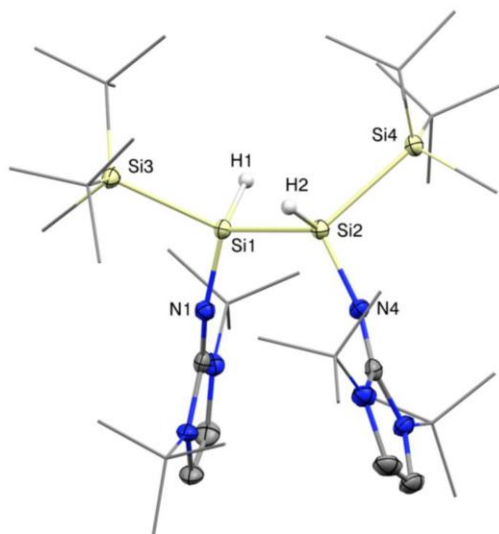


**Figure S43:** SC-XRD structure of hydrosilane **3** with thermal ellipsoids drawn at the 50% probability level. Hydrogen atoms are omitted for clarity, Bu- and Me-groups are simplified as wireframes. Selected bond lengths [Å] and angles [°]: Si1–Si2 2.4184(6), Si1–H1 1.43(1), Si1–Si3 2.4085(6), Si1–N1 1.682(1), Si2–H2 1.42(2), H1–Si1–Si3 101.1(6), N1–Si1–H1 113.9(6), N1–Si1–Si2 111.91(4), Si2–Si1–Si3 120.40(2).

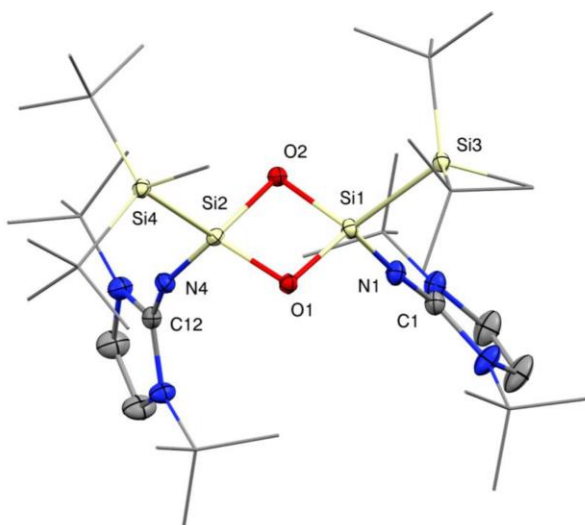


**Figure S44:** SC-XRD structure of compound **4** with thermal ellipsoids drawn at the 50% probability level. Hydrogen atoms are omitted for clarity, Bu- and Me-groups are simplified as wireframes. Selected bond lengths [Å] and angles [°]: Si1–O1 1.686(1), Si1–O2 1.695(1), Si1–Si3 2.3897(6), Si1–N1 1.641(1), N1–C1 1.274(2), Si2–O1 1.698(1), Si2–O2 1.691(1), Si3–Si1–O1 119.63(4), Si3–Si1–O2 114.96(4), Si3–Si1–N1 106.06(5), Si1–O1–Si2 91.77(5).

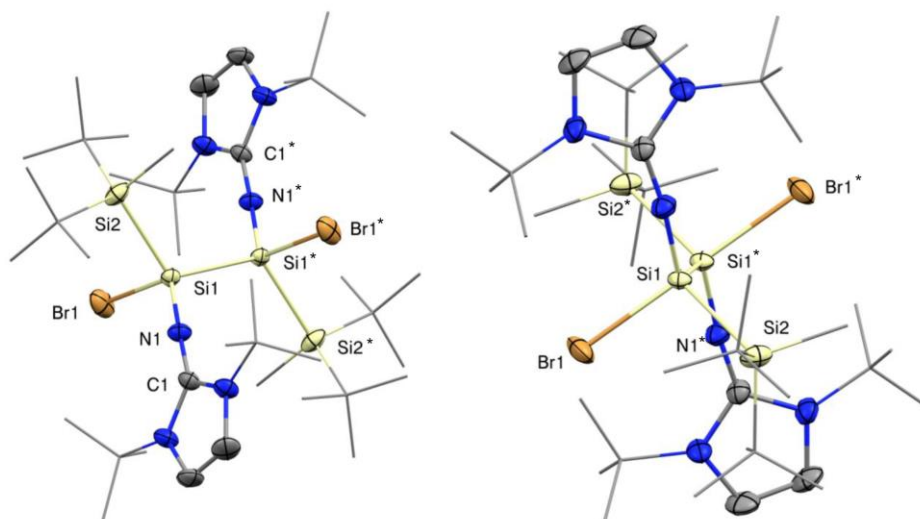


**Figure S45:** SC-XRD structure of compound **6** with thermal ellipsoids drawn at the 50% probability level. Side view (left), front view (right). Hydrogen atoms are omitted for clarity, 'Bu- and Me-groups are simplified as wireframes. Selected bond lengths [Å] and angles [°]: Si1–Si1\* 2.479(2), Si1–N1 1.658(3), Si1–Br1 2.340(2), Si1–Si2 2.427(3), Br1–Si1–Si2 99.32(8), Br1–Si1–N1 111.1(2), Br1–Si1–Si1\* 100.14(8).

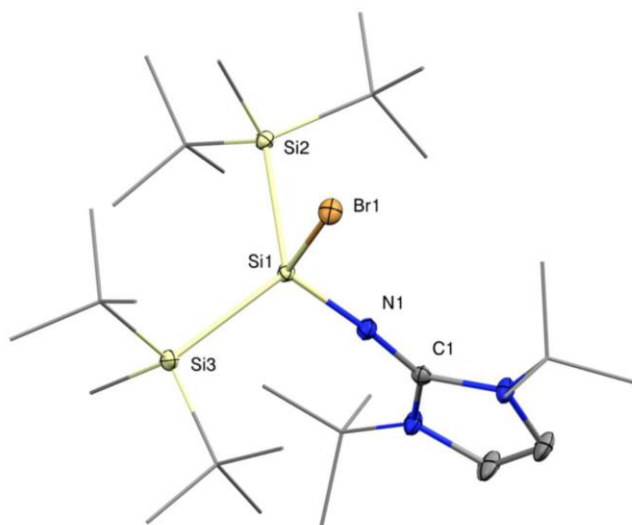


**Figure S46:** SC-XRD structure of compound **7** with thermal ellipsoids drawn at the 50% probability level. Hydrogen atoms are omitted for clarity, 'Bu- and Me-groups are simplified as wireframes. Selected bond lengths [Å] and angles [°]: Si1–Br1 2.3555(5), Si1–Si2 2.4663(5), Si1–Si3 2.4637(6), Si1–N1 1.651(1), Br1–Si1–Si2 98.30(2), Br1–Si1–Si3 98.33(2), Br1–Si1–N1 106.53(5), Si2–Si1–Si3 123.75(2).

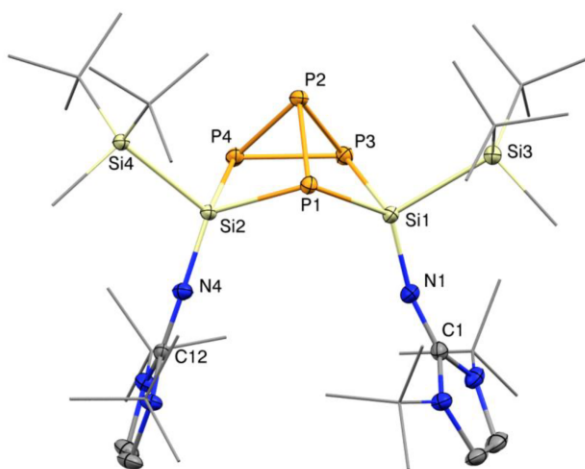


**Figure S47:** SC-XRD structure of compound **9** with thermal ellipsoids drawn at the 50% probability level. Hydrogen atoms are omitted for clarity, 'Bu- and Me-groups are simplified as wireframes. Selected bond lengths [Å] and angles [°]: Si1–P1 2.2785(8), Si1–P3 2.2723(7), P1–P2 2.2937(7), P3–P2 2.2301(8), N1–Si1–Si3 109.32(4), P1–Si1–P3 94.22(2), P1–P2–P3 94.95(2), Si1–P1–Si2 106.69(2).

# 15. Appendix

## 2.3 Crystal data and structural refinement parameters

Table S1: Crystal data and structural refinement parameters for compounds 1, 2-(Z), 3 and 4.

Compound #	1	2-(Z)	3	4
CCDC #	-	-	-	-
Chemical formula	Si <sub>3</sub> C <sub>10</sub> H <sub>8</sub> N <sub>6</sub>	Si <sub>3</sub> C <sub>10</sub> H <sub>8</sub> N <sub>6</sub>	Si <sub>3</sub> C <sub>10</sub> H <sub>8</sub> N <sub>6</sub>	Si <sub>3</sub> C <sub>10</sub> H <sub>8</sub> N <sub>6</sub> O <sub>2</sub>
Formula weight	843.62	759.47	761.49	791.47
Temperature	100(2) K	100(2) K	100(2) K	100(2) K
Wavelength	0.71073 Å	0.71073 Å	0.71073 Å	0.71073 Å
Crystal size	0.155 × 0.162 × 0.186 mm	0.185 × 0.228 × 0.254 mm	0.266 × 0.333 × 0.487 mm	0.169 × 0.201 × 0.294 mm
Crystal habit	clear dark green fragment	clear red fragment	clear colourless fragment	clear colourless fragment
Crystal system	Monoclinic	triclinic	triclinic	triclinic
Space group	C 1 2/c 1	P -1	P -1	P -1
Unit cell dimensions	a = 21.5194(19) Å, α = 90° b = 10.3978(9) Å, β = 91.393(3)° c = 23.024(2) Å, γ = 90°	a = 10.4102(19) Å, α = 81.153(7)° b = 12.363(2) Å, β = 76.718(7)° c = 21.101(4) Å, γ = 65.519(7)°	a = 10.6636(5) Å, α = 80.983(2)° b = 12.0948(6) Å, β = 83.783(2)° c = 21.0663(11) Å, γ = 65.412(2)°	a = 11.8823(10) Å, α = 103.907(3)° b = 12.5801(10) Å, β = 97.451(3)° c = 17.6952(13) Å, γ = 109.909(3)°
Volume	5150.2(5) Å <sup>3</sup>	2400.2(8) Å <sup>3</sup>	2437.5(2) Å <sup>3</sup>	2366.1(3) Å <sup>3</sup>
Z	8	2	2	2
Density (calculated)	1.088 g/cm <sup>3</sup>	1.051 g/cm <sup>3</sup>	1.038 g/cm <sup>3</sup>	1.111 g/cm <sup>3</sup>
Absorption coefficient	0.151 mm <sup>-1</sup>	0.156 mm <sup>-1</sup>	0.153 mm <sup>-1</sup>	0.163 mm <sup>-1</sup>
F(000)	1872	940	844	872
Diffractometer	Bruker D8 Venture Duo IMS	Bruker D8 Venture Duo IMS	Bruker D8 Venture Duo IMS	Bruker D8 Venture
Radiation source	IMS microsource, Mo	IMS microsource, Mo	IMS microsource, Mo	TXS rotating anode, Mo
Theta range for data collection	2.17 to 26.02° -26<math>\leq\theta\leq 26</math>	2.21 to 25.35° -12<math>\leq\theta\leq 12</math>	1.96 to 25.35° -12<math>\leq\theta\leq 12</math>	2.33 to 25.68° -14<math>\leq\theta\leq 14</math>
Index ranges	-12<math>\leq h\leq 12</math> -28<math>\leq k\leq 28</math> 72253	-14<math>\leq h\leq 14</math> -25<math>\leq k\leq 25</math> 55819	-14<math>\leq h\leq 14</math> -25<math>\leq k\leq 25</math> 106559	-15<math>\leq h\leq 15</math> -21<math>\leq k\leq 21</math> 104064
Reflections collected	5073 [R(int) = 0.0311]	8777 [R(int) = 0.0309]	8902 [R(int) = 0.0274]	8998 [R(int) = 0.0373]
Independent reflections	100.0%	99.9%	99.7%	99.9%
Absorption correction	Multi-scan	Multi-Scan	Multi-Scan	Multi-Scan
Max. and min. transmission	0.9770 and 0.9720	0.9610 and 0.9720	0.9600 and 0.9410	0.9730 and 0.9610
Refinement method	Full-matrix least-squares on F <sup>2</sup>	Full-matrix least-squares on F <sup>2</sup>	Full-matrix least-squares on F <sup>2</sup>	Full-matrix least-squares on F <sup>2</sup>
Refinement program	SHELXL-2014/7 (Sheldrick, 2014)	SHELXL-2016/6 (Sheldrick, 2016)	SHELXL-2016/6 (Sheldrick, 2016)	SHELXL-2016/6 (Sheldrick, 2016)
Function minimized	$\sum w(F_o^2 - F_c^2)^2$	$\sum w(F_o^2 - F_c^2)^2$	$\sum w(F_o^2 - F_c^2)^2$	$\sum w(F_o^2 - F_c^2)^2$
Data / restraints / parameters	5073 / 0 / 268	8777 / 0 / 477	8902 / 0 / 485	8998 / 204 / 690
Goodness-of-fit on F <sup>2</sup>	1.061	1.040	1.046	1.040
$\Delta\sigma_{max}$	0.001	0.001	0.001	0.046
Final R indices	4598 data; I>2σ(I); R1 = 0.0342, wR2 = 0.0834 all data: R1 = 0.0388, wR2 = 0.0860	7672 data; I>2σ(I); R1 = 0.0333, wR2 = 0.0820 all data: R1 = 0.0403, wR2 = 0.0861	8372 data; I>2σ(I); R1 = 0.0281, wR2 = 0.0694 all data: R1 = 0.0302, wR2 = 0.0714	8093 data; I>2σ(I); R1 = 0.0320, wR2 = 0.0811 all data: R1 = 0.0368, wR2 = 0.0843
Weighting scheme	w=1/[σ <sup>2</sup> (F <sub>o</sub> ) + (0.0348P) <sup>2</sup> + 7.2742P] where P=(F <sub>o</sub> <sup>2</sup> +2F <sub>c</sub> <sup>2</sup> )/3	w=1/[σ <sup>2</sup> (F <sub>o</sub> ) + (0.0379P) <sup>2</sup> + 1.3913P] where P=(F <sub>o</sub> <sup>2</sup> +2F <sub>c</sub> <sup>2</sup> )/3	w=1/[σ <sup>2</sup> (F <sub>o</sub> ) + (0.0260P) <sup>2</sup> + 1.2312P] where P=(F <sub>o</sub> <sup>2</sup> +2F <sub>c</sub> <sup>2</sup> )/3	w=1/[σ <sup>2</sup> (F <sub>o</sub> ) + (0.0376P) <sup>2</sup> + 1.5234P] where P=(F <sub>o</sub> <sup>2</sup> +2F <sub>c</sub> <sup>2</sup> )/3
Largest diff. peak and hole	0.456 and -0.374 eÅ <sup>-3</sup>	0.615 and -0.295 eÅ <sup>-3</sup>	0.305 and -0.200 eÅ <sup>-3</sup>	0.457 and -0.314 eÅ <sup>-3</sup>
R.M.S. deviation from mean	0.044 eÅ <sup>-3</sup>	0.047 eÅ <sup>-3</sup>	0.034 eÅ <sup>-3</sup>	0.046 eÅ <sup>-3</sup>

S41

Table S2: Crystal data and structural refinement parameters for compounds 6, 7, and 9.

Compound #	6	7	9
CCDC #	-	-	-
Chemical formula	Si <sub>3</sub> C <sub>10</sub> H <sub>8</sub> BrN <sub>6</sub>	Si <sub>3</sub> C <sub>10</sub> H <sub>8</sub> BrN <sub>6</sub>	Si <sub>3</sub> C <sub>10</sub> H <sub>8</sub> N <sub>6</sub> P <sub>4</sub>
Formula weight	459.85	459.89	883.35
Temperature	100(2) K	100(2) K	100(2) K
Wavelength	0.71073 Å	0.71073 Å	0.71073 Å
Crystal size	0.072 × 0.072 × 0.144 mm	0.074 × 0.094 × 0.163 mm	0.256 × 0.319 × 0.339 mm
Crystal habit	clear colourless fragment	clear colourless fragment	clear colourless fragment
Crystal system	triclinic	Monoclinic	Triclinic
Space group	P -1	P 1 21h 1	P -1
Unit cell dimensions	a = 10.0850(5) Å, α = 64.783(2)° b = 11.8820(6) Å, β = 74.656(2)° c = 12.0647(6) Å, γ = 69.356(2)°	a = 15.9826(9) Å, α = 90° b = 12.7552(7) Å, β = 97.970(3)° c = 17.0612(10) Å, γ = 90°	a = 10.0360(17) Å, α = 90.316(6)° b = 11.430(2) Å, β = 100.375(6)° c = 24.720(4) Å, γ = 115.781(5)°
Volume	1212.73(11) Å <sup>3</sup>	3444.5(3) Å <sup>3</sup>	2500.4(8) Å <sup>3</sup>
Z	2	4	2
Density (calculated)	1.259 g/cm <sup>3</sup>	1.190 g/cm <sup>3</sup>	1.173 g/cm <sup>3</sup>
Absorption coefficient	1.803 mm <sup>-1</sup>	1.319 mm <sup>-1</sup>	0.281 mm <sup>-1</sup>
F(000)	490	1336	960
Diffractometer	Bruker D8 Venture Duo IMS	Bruker D8 Venture	Bruker D8 Venture Duo IMS
Radiation source	IMS microsource, Mo	TXS rotating anode, Mo	IMS microsource, Mo
Theta range for data collection	2.44 to 25.68°	2.00 to 25.68°	2.28 to 25.68°
Index ranges	-12<math>\leq h\leq 12</math> -14<math>\leq k\leq 14</math> -14<math>\leq l\leq 14</math>	-19<math>\leq h\leq 19</math> -15<math>\leq k\leq 15</math> -20<math>\leq l\leq 20</math>	-12<math>\leq h\leq 12</math> -13<math>\leq k\leq 13</math> -30<math>\leq l\leq 30</math>
Reflections collected	43948	74911	69988
Independent reflections	4618 [R(int) = 0.0594]	6550 [R(int) = 0.0530]	9439 [R(int) = 0.0232]
Coverage of independent reflections	99.9%	100.0%	99.6%
Absorption correction	Multi-Scan	Multi-scan	Multi-Scan
Max. and min. transmission	0.8780 and 0.8560	0.9070 and 0.8620	0.9320 and 0.9110
Refinement method	Full-matrix least-squares on F <sup>2</sup>	Full-matrix least-squares on F <sup>2</sup>	Full-matrix least-squares on F <sup>2</sup>
Refinement program	SHELXL-2016/6 (Sheldrick, 2016)	SHELXL-2016/6 (Sheldrick, 2016)	SHELXL-2016/6 (Sheldrick, 2016)
Function minimized	$\sum w(F_o^2 - F_c^2)^2$	$\sum w(F_o^2 - F_c^2)^2$	$\sum w(F_o^2 - F_c^2)^2$
Data / restraints / parameters	4618 / 174 / 442	6550 / 0 / 345	9439 / 0 / 513
Goodness-of-fit on F <sup>2</sup>	1.237	1.032	1.030
$\Delta\sigma_{max}$	0.018	0.002	0.002
Final R indices	4034 data; I>2σ(I); R1 = 0.0637, wR2 = 0.1353 all data: R1 = 0.0733, wR2 = 0.1390	5719 data; I>2σ(I); R1 = 0.0225, wR2 = 0.0511 all data: R1 = 0.0300, wR2 = 0.0538	8839 data; I>2σ(I); R1 = 0.0245, wR2 = 0.0609 all data: R1 = 0.0267, wR2 = 0.0626
Weighting scheme	w=1/[σ <sup>2</sup> (F <sub>o</sub> ) + 5.1304P] where P=(F <sub>o</sub> <sup>2</sup> +2F <sub>c</sub> <sup>2</sup> )/3	w=1/[σ <sup>2</sup> (F <sub>o</sub> ) + (0.0222P) <sup>2</sup> + 1.9334P] where P=(F <sub>o</sub> <sup>2</sup> +2F <sub>c</sub> <sup>2</sup> )/3	w=1/[σ <sup>2</sup> (F <sub>o</sub> ) + (0.0251P) <sup>2</sup> + 1.4676P] where P=(F <sub>o</sub> <sup>2</sup> +2F <sub>c</sub> <sup>2</sup> )/3
Largest diff. peak and hole	1.293 and -0.844 eÅ <sup>-3</sup>	0.304 and -0.262 eÅ <sup>-3</sup>	0.335 and -0.266 eÅ <sup>-3</sup>
R.M.S. deviation from mean	0.081 eÅ <sup>-3</sup>	0.047 eÅ <sup>-3</sup>	0.038 eÅ <sup>-3</sup>

S42



### 3. References

- [S1] G. R. Fulmer, A. J. M. Miller, N. H. Sherden, H. E. Gottlieb, A. Nudelman, B. M. Stoltz, J. E. Bercaw, K. I. Goldberg, NMR Chemical Shifts of Trace Impurities: Common Laboratory Solvents, Organics, and Gases in Deuterated Solvents Relevant to the Organometallic Chemist. *Organometallics*, **2010**, *29*, 2176-2179.
- [S2] D. Wendel, T. Szilvási, C. Jandl, S. Inoue, B. Rieger, Twist of a Silicon–Silicon Double Bond: Selective *Anti*-Addition of Hydrogen to an Iminodisilene. *J. Am. Chem. Soc.*, **2017**, *139*, 9156-9159.
- [S3] N. Wiberg, K. Amelunxen, H. W. Lerner, H. Schuster, H. Nöth, I. Krossing, M. Schmidt-Amelunxen, T. Seifert, Donorfreie und donorhaltige Supersilylalkalimetalle  $t\text{Bu}_3\text{SiM}$ : Synthesen, Charakterisierung, Strukturen. *J. Organomet. Chem.*, **1997**, *542*, 1-18.
- [S4] A. Sekiguchi, T. Fukawa, M. Nakamoto, V. Y. Lee, M. Ichinohe, Isolable Silyl and Germyl Radicals Lacking Conjugation with  $\pi$ -Bonds: Synthesis, Characterization, and Reactivity. *J. Am. Chem. Soc.*, **2002**, *124*, 9865-9869.
- [S5] L. Jia, X. Yang, A. Ishihara, T. J. Marks, Protected (Fluoroaryl)borates as Effective Counteranions for Cationic Metallocene Polymerization Catalysts. *Organometallics*, **1995**, *14*, 3135-3137.
- [S6] K. Fredenhagen, G. Cadenbach, Die Bindung von Kalium durch Kohlenstoff. *Z. Anorg. Allg. Chem.*, **1926**, *158*, 249-263.
- [S7] A. Sekiguchi, S. Inoue, M. Ichinohe, Y. Arai, Isolable Anion Radical of Blue Disilene  $(t\text{Bu}_2\text{MeSi})_2\text{Si}=\text{Si}(\text{SiMe}^t\text{Bu}_2)_2$  Formed upon One-Electron Reduction: Synthesis and Characterization. *J. Am. Chem. Soc.*, **2004**, *126*, 9626-9629.
- [S8] D. Wendel, T. Szilvási, D. Henschel, P. J. Altmann, C. Jandl, S. Inoue, B. Rieger, Precise Activation of Ammonia and Carbon Dioxide by an Iminodisilene. *Angew. Chem. Int. Ed.*, **2018**, *57*, 14575-14579.
- [S9] *APEX suite of crystallographic software*, APEX 3 version 2015.5-2; Bruker AXS Inc.: Madison, Wisconsin, USA, **2015**.
- [S10] *SAINTE*, Version 7.56a and *SADABS* Version 2008/1; Bruker AXS Inc.: Madison, Wisconsin, USA, **2008**.
- [S11] G. M. Sheldrick, SHELXL-2014, University of Göttingen, Göttingen, Germany, **2014**.
- [S12] C. B. Hübschle, G. M. Sheldrick, B. Dittrich, ShelXle: a Qt graphical user interface for SHELXL. *J. Appl. Cryst.*, **2011**, *44*, 1281-1284.
- [S13] G. M. Sheldrick, SHELXL-97, University of Göttingen, Göttingen, Germany, **1998**.
- [S14] A. J. C. Wilson, *International Tables for Crystallography*, Volume C, Tables 6.1.1.4 (pp. 500-502), 4.2.6.8 (pp. 219-222), and 4.2.4.2 (pp. 193-199), Kluwer Academic Publishers: Dordrecht, The Netherlands, **1992**.
- [S15] C. F. Macrae, I. J. Bruno, J. A. Chisholm, P. R. Edgington, P. McCabe, E. Pidcock, L. Rodriguez-Monge, R. Taylor, J. van de Streek, P. A. Wood, Mercury CSD 2.0 - new features for the visualization and investigation of crystal structures. *J. Appl. Cryst.*, **2008**, *41*, 466-470.

## 15.5 Supporting Information Chapter 11

### Supporting Information

#### **Formation of a Silene through CO Activation by a Polarized Iminodisilene**

*Richard Holzner, Philipp Frisch and Shigeyoshi Inoue\**

Department of Chemistry, WACKER-Institute of Silicon Chemistry, Technische Universität München, Lichtenbergstraße 4, 85748 Garching bei München (Germany) \*E-mail: s.inoue@tum.de



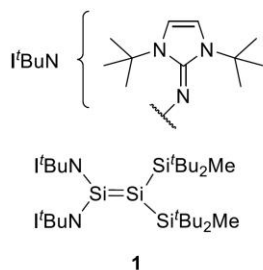
**Table of Contents**

<b>1. Experimental Section</b>	<b>3</b>
1.1. General Methods and Instrumentation.....	3
1.3. (tBuN) <sub>2</sub> Si=Si(Si <sup>t</sup> Bu <sub>2</sub> Me) <sub>2</sub> ( <b>1</b> ) .....	4
1.3. Silene <b>2a</b> .....	8
1.4 Silene <b>2b</b> .....	12
1.5 Reaction of disilene <b>V</b> with CO (Silyl Radical <b>S1</b> ) .....	15
<b>2. X-ray Crystallographic Data</b>	<b>18</b>
2.1. General Information.....	18
2.2 SC-XRD structures.....	19
<b>3. References</b>	<b>20</b>

## 1. Experimental Section

### 1.1. General Methods and Instrumentation

All manipulations were carried out under exclusion of water and oxygen under an atmosphere of argon 4.6 ( $\geq 99.996\%$ ) using standard Schlenk and glovebox techniques. The glassware used was heat dried under high vacuum prior to use. All solvents were refluxed over sodium/benzophenone, freshly distilled under argon and deoxygenated prior to use. PTFE-based grease (*Triboflon III* from *Freudenberg & Co. KG*) was used as sealant. Deuterated benzene ( $C_6D_6$ ) was obtained from Sigma-Aldrich, dried over Na/K alloy, flask-to-flask condensed, deoxygenated by three freeze-pump-thaw cycles and stored over 4 Å molecular sieves in a glovebox. All NMR samples were prepared under argon in *J. Young* PTFE valve NMR tubes. The nuclear magnetic resonance spectra (NMR) were recorded on a *Bruker DRX400* ( $^1H$ : 400.13 MHz,  $^{13}C$ : 100.62 MHz,  $^{29}Si$ : 79.49 MHz), *AV500* ( $^1H$ : 500.13 MHz) or *AV500C* ( $^1H$ : 500.36 MHz,  $^{13}C$ : 125.83 MHz,  $^{29}Si$ : 99.41 MHz) spectrometer at ambient temperature (300 K), unless otherwise stated. The  $^1H$ ,  $^{13}C\{^1H\}$  and  $^{29}Si\{^1H\}$  NMR spectroscopic chemical shifts  $\delta$  are reported in ppm relative to tetramethylsilane.  $^1H$  and  $^{13}C\{^1H\}$  NMR spectra are calibrated against the residual proton and natural abundance carbon resonances of the respective deuterated solvent as internal standard ( $C_6D_6$ :  $\delta(^1H) = 7.16$  ppm and  $\delta(^{13}C) = 128.1$  ppm, *Tol- $d_8$* :  $\delta(^1H) = 2.08$  ppm and  $\delta(^{13}C) = 20.4$  ppm), *THF- $d_6$* :  $\delta(^1H) = 1.73$  ppm and  $\delta(^{13}C) = 25.4$  ppm).<sup>[S1]</sup> The following abbreviations are used to describe signal multiplicities: s = singlet, d = doublet, dd = doublet of doublets, dt = doublet of triplets, t = triplet, sept = septet, m = multiplet, br = broad. In some NMR spectra, signals from silicone grease ( $C_6D_6$ :  $\delta(^1H) = 0.29$  ppm,  $\delta(^{13}C) = 1.4$  ppm and  $\delta(^{29}Si) = -21.8$  ppm), originating from the cannulas used (*B. Braun Melsungen AG Sterican®*), can be observed. UV/VIS spectra were recorded on a *Varian, Inc. Cary 50* spectrophotometer with a Schlenk quartz cuvette. EPR spectra were recorded on a *Jeol JES-Fa200 esr* spectrometer with a spectrometer frequency of 9.267 GHz (X-band). Quantitative elemental analyses (EA) were measured with a *EURO EA (HEKAtech)* instrument equipped with a CHNS combustion analyzer at the *Laboratory for Microanalysis* at the *TUM Catalysis Research Center*. Melting Points (m.p.) were determined in sealed glass capillaries under inert gas by a *Büchi M-565* melting point apparatus. Unless otherwise stated, all commercially available chemicals were purchased from *abcr GmbH* or *Sigma-Aldrich* and used without further purification. Carbon monoxide (CO) 4.7 ( $\geq 99.997\%$ ) was purchased from *Westfalen AG* and used as received. The compounds  $l^tBuN(^tBu_2MeSi)Si=Si(Si^tBu_2Me)Ni^tBu$  and  $(^tBu_2MeSi)_2Si=Si(Si^tBu_2Me)_2$ <sup>[S2]</sup> were prepared as described in the corresponding references.

1.3. ( $i^t$ BuN) $_2$ Si=Si(Si $^i$ Bu $_2$ Me) $_2$  (**1**)Si $_4$ C $_{40}$ H $_{82}$ N $_6$ 

759.48 g/mol

A solution of disilene  $i^t$ BuN( $^i$ Bu $_2$ MeSi)Si=Si(Si $^i$ Bu $_2$ Me)N $^i$ Bu (**V**) (100 mg, 132  $\mu$ mol) in toluene (5 mL) was heated in a pressurizable Schlenk flask to 115  $^\circ$ C for 4 days. After filtration, the solution was concentrated *in vacuo* and cooled to  $-35$   $^\circ$ C for crystallization. Compound **1** was obtained as purple crystals (75.4 mg, 75% yield). These crystals were also suitable for SC-XRD analysis.

Note: The crystals are only slightly soluble in *n*-hexane, however they show good solubility in toluene and benzene. Although the crystals are purple, the resulting solution is deep red.

m.p.: 65  $^\circ$ C (decomposition, color change to black).

$^1$ H NMR (500 MHz, C $_6$ D $_6$ , 300 K):  $\delta$  [ppm] = 6.00 (s, 4H,  $\underline{CH}$ -N), 1.54 (s, 36H,  $\underline{Bu}$ N), 1.50 (s, 36H,  $\underline{Bu}_2$ MeSi), 0.36 (s, 6H,  $\underline{Bu}_2$ MeSi).

$^{13}$ C{ $^1$ H} NMR (126 MHz, C $_6$ D $_6$ , 300 K):  $\delta$  [ppm] = 139.2 ( $\underline{C}$ =N), 108.3 ( $\underline{CH}$ -N), 55.9 (N $\underline{C}$ (CH $_3$ ) $_3$ ), 31.4 (Si(C( $\underline{C}$ H $_3$ ) $_3$ ) $_2$ (CH $_3$ )), 29.5 (NC( $\underline{C}$ H $_3$ ) $_3$ ), 22.6 (Si( $\underline{C}$ (CH $_3$ ) $_3$ ) $_2$ (CH $_3$ )),  $-3.0$  (Si(C(CH $_3$ ) $_3$ ) $_2$ ( $\underline{C}$ H $_3$ )).

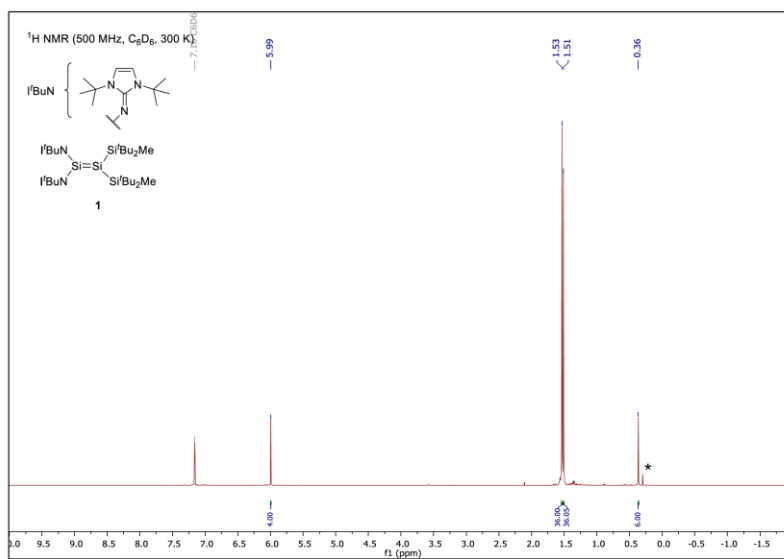
$^{29}$ Si{ $^1$ H} NMR (99 MHz, C $_6$ D $_6$ , 300 K):  $\delta$  [ppm] = 30.4 (=SiN $_2$ ), 23.0 ( $^i$ Bu $_2$ MeSi),  $-176.1$  (=SiSi $_2$ ).

EA: Si $_4$ C $_{40}$ H $_{82}$ N $_6$  Calculated: C (63.26), H (10.88), N (11.07)

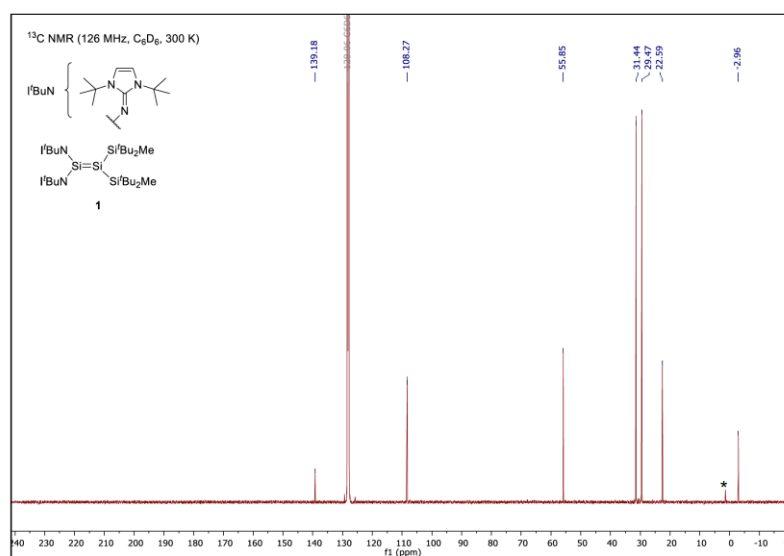
Experimental: C (63.12), H (10.93), N (11.05)



Figure S1: Depiction of iminodisilene **1** in solid state (left) and in benzene solution (right).



**Figure S2:** <sup>1</sup>H NMR spectrum (500 MHz) of compound **1** in C<sub>6</sub>D<sub>6</sub> at 300 K. Signal labeled with \* belongs to silicone grease.



**Figure S3:** <sup>13</sup>C NMR spectrum (126 MHz) of compound **1** in C<sub>6</sub>D<sub>6</sub> at 300 K. Signal labeled with \* belongs to silicone grease.

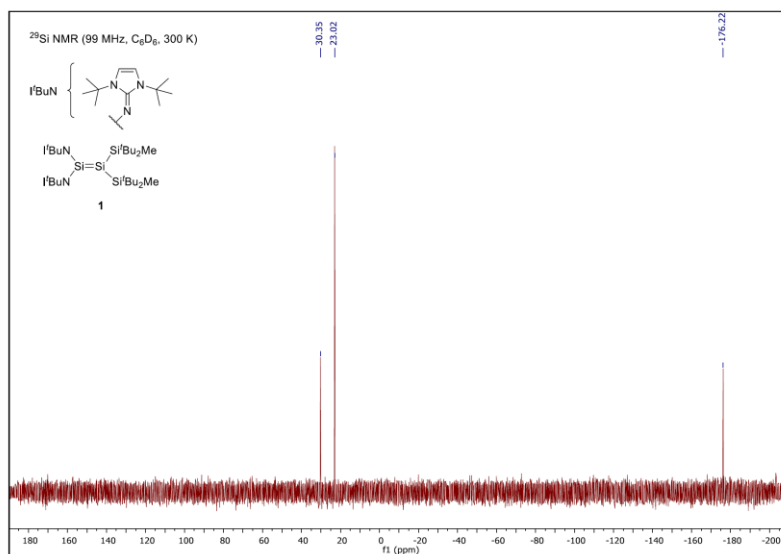


Figure S4: <sup>29</sup>Si NMR spectrum (99 MHz) of compound 1 in C<sub>6</sub>D<sub>6</sub> at 300 K.

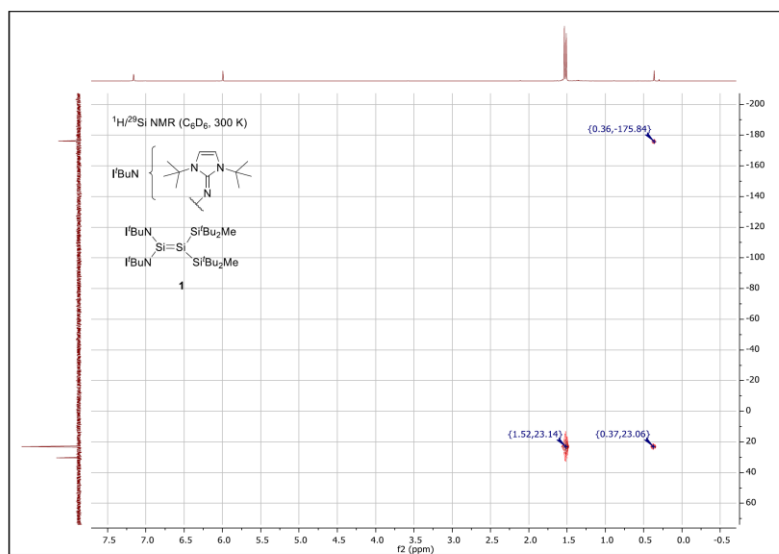


Figure S5: <sup>1</sup>H/<sup>29</sup>Si HMBC NMR spectrum of compound 1 in C<sub>6</sub>D<sub>6</sub> at 300 K.

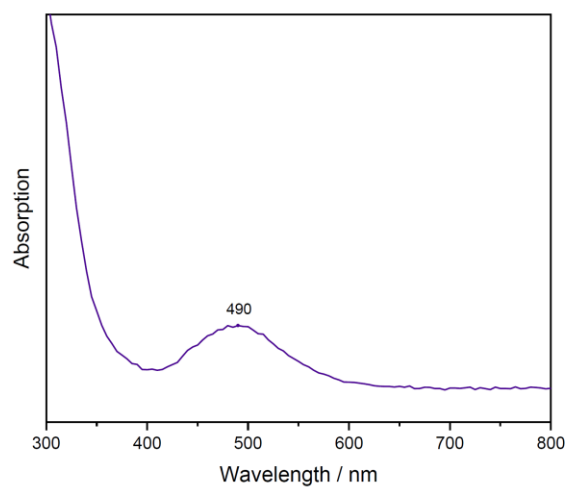
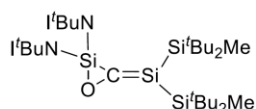


Figure S 6: UV/VIS spectrum of disilene **1** in toluene ( $2.5 \times 10^{-3}$  M), measured at room temperature ( $\lambda_{\text{max}} = 490$  nm).

## 1.3. Silene 2a

**2a**Si<sub>4</sub>C<sub>41</sub>H<sub>82</sub>N<sub>6</sub>O

787.49 g/mol

A solution of disilene **1** (40.0 mg, 52.2 μmol) in toluene (4 mL) in a pressurizable Schlenk flask was degassed in one freeze-pump-thaw cycle. After exposure to carbon monoxide (1.3 bar) at room temperature, the red color vanished within 1 hour to give a clear, colorless solution. All volatiles were removed in vacuo and compound **2a** was obtained as colorless solid (41.4 mg, 52.2 μmol, quant.). Crystals, suitable for SC-XRD analysis were obtained from a cooled

(−35 °C) *n*-hexane solution of **2a**.

**m.p.:** 88 °C (decomposition, color change to red).

**<sup>1</sup>H NMR (500 MHz, C<sub>6</sub>D<sub>6</sub>, 300 K):** δ [ppm] = 5.99 (s, 4H, CH-N), 1.55 (s, 36H, <sup>t</sup>BuN), 1.41 (s, 18H, <sup>t</sup>Bu<sub>2</sub>MeSi), 1.34 (s, 18H, <sup>t</sup>Bu<sub>2</sub>MeSi), 0.52 (s, 3H, <sup>t</sup>Bu<sub>2</sub>MeSi), 0.42 (s, 3H, <sup>t</sup>Bu<sub>2</sub>MeSi).

**<sup>13</sup>C{<sup>1</sup>H} NMR (126 MHz, C<sub>6</sub>D<sub>6</sub>, 300 K):** δ [ppm] = 231.4 (CO), 139.6 (C=N), 107.5 (CH-N), 55.1 (NC(CH<sub>3</sub>)<sub>3</sub>), 30.4 (Si(C(CH<sub>3</sub>)<sub>3</sub>)<sub>2</sub>(CH<sub>3</sub>)), 30.3 (Si(C(CH<sub>3</sub>)<sub>3</sub>)<sub>2</sub>(CH<sub>3</sub>)), 28.9 (NC(CH<sub>3</sub>)<sub>3</sub>), 22.0 (Si(C(CH<sub>3</sub>)<sub>3</sub>)<sub>2</sub>(CH<sub>3</sub>)), 21.3 (Si(C(CH<sub>3</sub>)<sub>3</sub>)<sub>2</sub>(CH<sub>3</sub>)), −4.8 (Si(C(CH<sub>3</sub>)<sub>3</sub>)<sub>2</sub>(CH<sub>3</sub>)), −4.8 (Si(C(CH<sub>3</sub>)<sub>3</sub>)<sub>2</sub>(CH<sub>3</sub>)).

**<sup>29</sup>Si{<sup>1</sup>H} NMR (99 MHz, C<sub>6</sub>D<sub>6</sub>, 300 K):** δ [ppm] = 16.8 (<sup>t</sup>Bu<sub>2</sub>MeSi), 13.9 (<sup>t</sup>Bu<sub>2</sub>MeSi), 10.1 (C=SiSi<sub>2</sub>), −116.6 (SiN<sub>2</sub>).



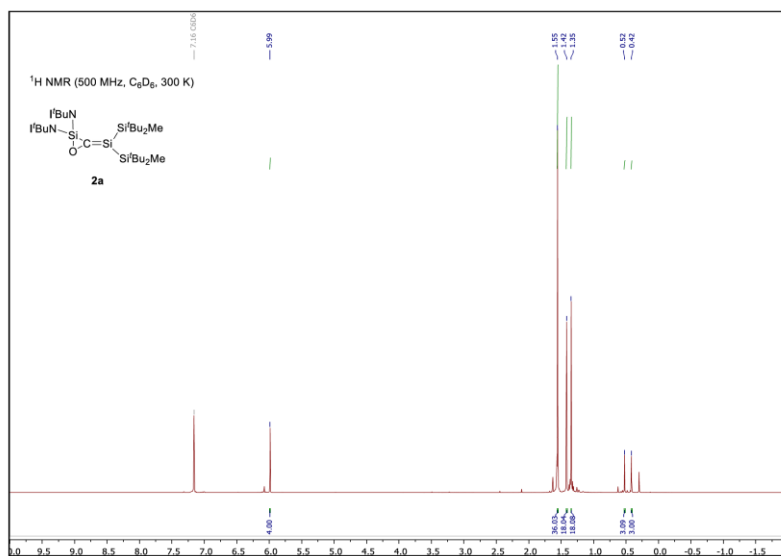


Figure S7: <sup>1</sup>H NMR spectrum (500 MHz) of compound **2a** in C<sub>6</sub>D<sub>6</sub> at 300 K.

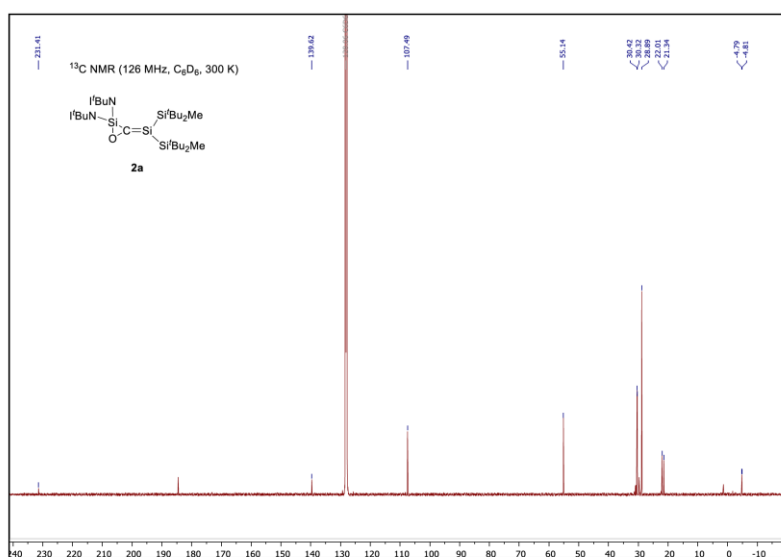
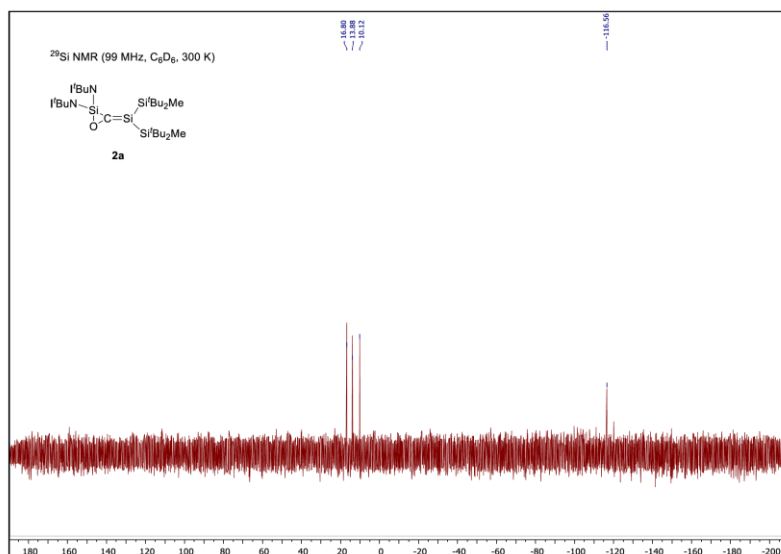
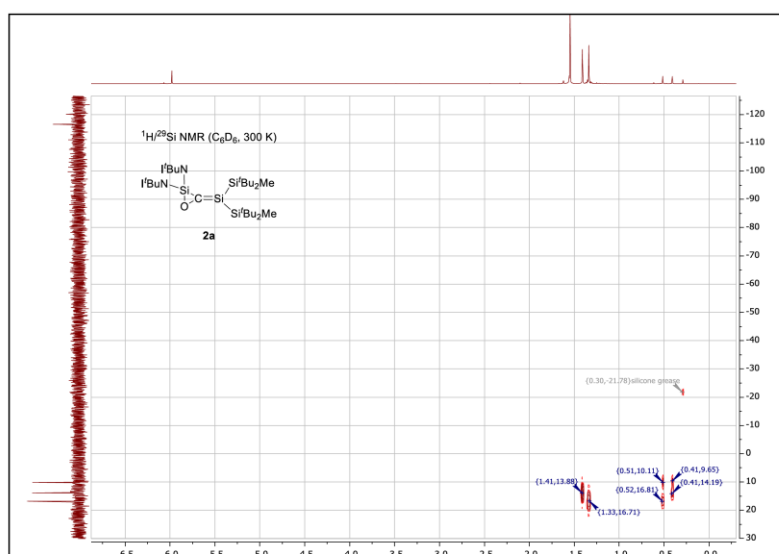


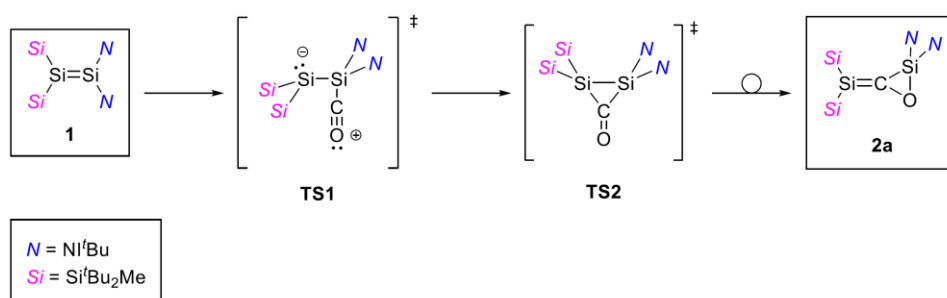
Figure S8: <sup>13</sup>C NMR spectrum (126 MHz) of compound **2a** in C<sub>6</sub>D<sub>6</sub> at 300 K.



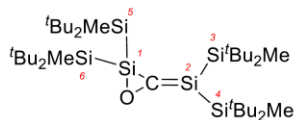
**Figure S9:**  $^{29}\text{Si}$  NMR spectrum (99 MHz) of compound **2a** in  $\text{C}_6\text{D}_6$  at 300 K.



**Figure S10:**  $^1\text{H}/^{29}\text{Si}$  HMBC NMR spectrum of silene **2a** in  $\text{C}_6\text{D}_6$  at 300 K.



**Scheme S1:** Proposed mechanism for the Formation of silene **2a** from the activation of CO by disilene **1**.

1.4 Silene **2b****2b**Si<sub>6</sub>C<sub>37</sub>H<sub>84</sub>O

713.59 g/mol

A solution of disilene (<sup>t</sup>Bu<sub>2</sub>MeSi)<sub>2</sub>Si=Si(Si'<sup>t</sup>Bu<sub>2</sub>Me)<sub>2</sub> (**VI**) (200 mg, 333 μmol) in toluene (10 mL) in a pressurizable Schlenk flask was exposed to carbon monoxide (1.3 bar). Upon heating the mixture to 80 °C for 5 days, the deep blue color vanished slowly to give a pale yellow, slightly cloudy solution. After filtration and evaporation of all volatiles under reduced pressure and recrystallization from *n*-hexane, compound **2b** was obtained as yellow, crystalline solid (242 mg, 316 μmol, 95% yield). Single crystals of **2b** can be obtained from a cooled (−35 °C) solution in toluene or *n*-hexane, however, the crystal quality was too poor for SC-XRD analysis because of twinning and disorder.

m.p.: 237 °C

<sup>1</sup>H NMR (500 MHz, C<sub>6</sub>D<sub>6</sub>, 300 K): δ [ppm] = 1.32 (s, 18H, <sup>t</sup>Bu<sub>2</sub>MeSi<sup>3/4</sup>), 1.26 (s, 18H, <sup>t</sup>Bu<sub>2</sub>MeSi<sup>3/4</sup>), 1.16 (s, 18H, <sup>t</sup>Bu<sub>2</sub>MeSi<sup>5/6</sup>), 1.15 (s, 18H, <sup>t</sup>Bu<sub>2</sub>MeSi<sup>5/6</sup>), 0.54 (s, 3H, <sup>t</sup>Bu<sub>2</sub>MeSi<sup>3/4</sup>), 0.40 (s, 3H, <sup>t</sup>Bu<sub>2</sub>MeSi<sup>3/4</sup>), 0.32 (s, 3H, <sup>t</sup>Bu<sub>2</sub>MeSi<sup>5/6</sup>).

<sup>13</sup>C{<sup>1</sup>H} NMR (126 MHz, C<sub>6</sub>D<sub>6</sub>, 300 K): δ [ppm] = 197.1 (CO), 30.5 (Si(C(CH<sub>3</sub>)<sub>3</sub>)<sub>2</sub>(CH<sub>3</sub>)), 30.4 (Si(C(CH<sub>3</sub>)<sub>3</sub>)<sub>2</sub>(CH<sub>3</sub>)), 30.2 (Si(C(CH<sub>3</sub>)<sub>3</sub>)<sub>2</sub>(CH<sub>3</sub>)), 29.8 (Si(C(CH<sub>3</sub>)<sub>3</sub>)<sub>2</sub>(CH<sub>3</sub>)), 22.6 (Si(C(CH<sub>3</sub>)<sub>3</sub>)<sub>2</sub>(CH<sub>3</sub>)), 22.4 (Si(C(CH<sub>3</sub>)<sub>3</sub>)<sub>2</sub>(CH<sub>3</sub>)), 21.7 (Si(C(CH<sub>3</sub>)<sub>3</sub>)<sub>2</sub>(CH<sub>3</sub>)), 21.4 (Si(C(CH<sub>3</sub>)<sub>3</sub>)<sub>2</sub>(CH<sub>3</sub>)), −4.5 (Si(C(CH<sub>3</sub>)<sub>3</sub>)<sub>2</sub>(CH<sub>3</sub>)), −4.6 (Si(C(CH<sub>3</sub>)<sub>3</sub>)<sub>2</sub>(CH<sub>3</sub>)), −5.7 (Si(C(CH<sub>3</sub>)<sub>3</sub>)<sub>2</sub>(CH<sub>3</sub>)).

<sup>29</sup>Si{<sup>1</sup>H} NMR (99 MHz, C<sub>6</sub>D<sub>6</sub>, 300 K): δ [ppm] = 19.1 (Si<sup>3/4</sup>), 14.6 (Si<sup>3/4</sup>), 14.1 (Si<sup>2</sup>), 9.2 (Si<sup>5,6</sup>), −50.0 (Si<sup>1</sup>).

EA: Si<sub>6</sub>C<sub>37</sub>H<sub>84</sub>O Calculated: C (62.28), H (11.87), N (-)

Experimental: C (61.10), H (11.94), N (-)

Note: The carbon value was reproducibly low, presumably due to the formation of incombustible silicon carbides.

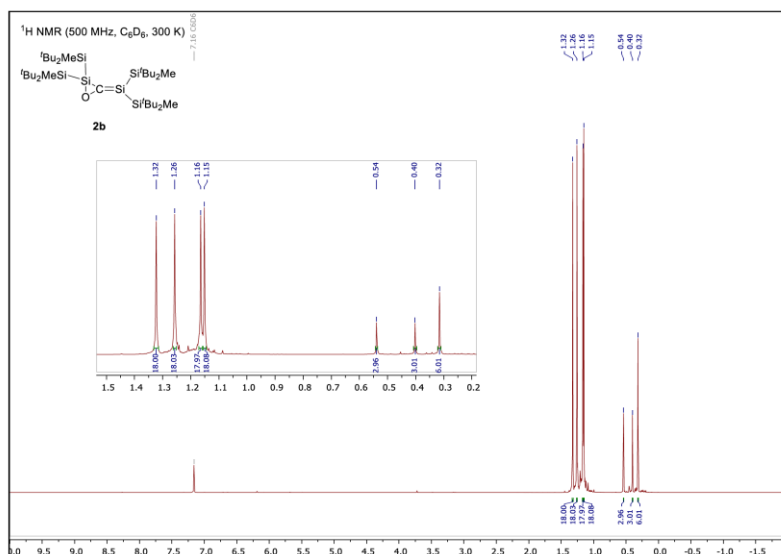


Figure S11: <sup>1</sup>H NMR spectrum (500 MHz) of compound **2b** in C<sub>6</sub>D<sub>6</sub> at 300 K.

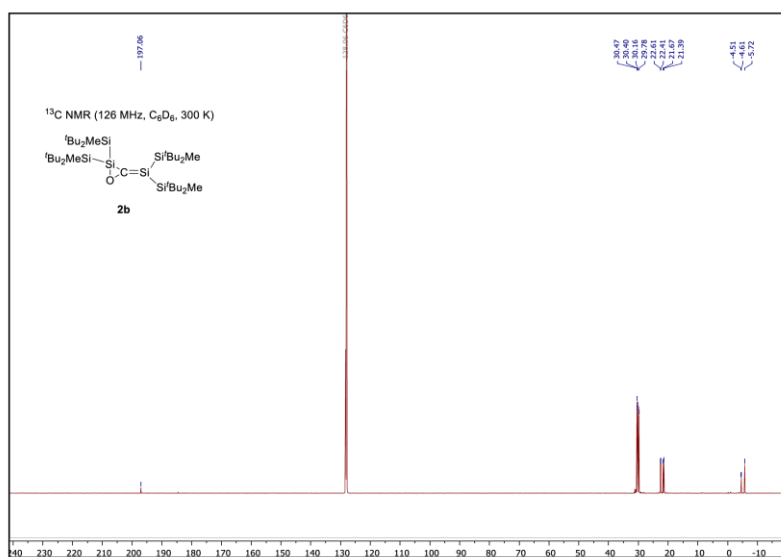


Figure S12: <sup>13</sup>C NMR spectrum (126 MHz) of compound **2b** in C<sub>6</sub>D<sub>6</sub> at 300 K.

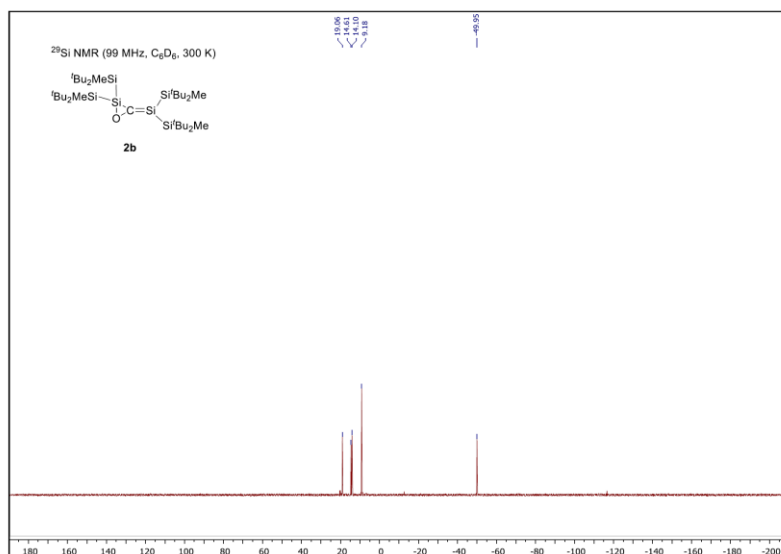


Figure S13: <sup>29</sup>Si NMR spectrum (99 MHz) of compound **2b** in C<sub>6</sub>D<sub>6</sub> at 300 K.

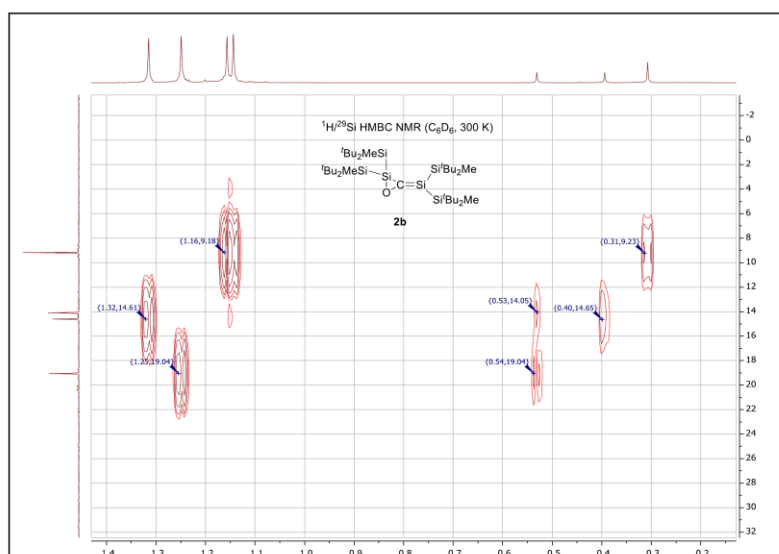
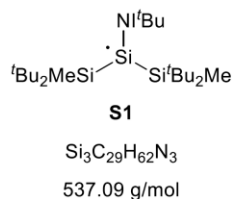


Figure S14: <sup>1</sup>H/<sup>29</sup>Si HMBC NMR spectrum of silene **2b** in C<sub>6</sub>D<sub>6</sub> at 300 K.

1.5 Reaction of disilene **V** with CO (Silyl Radical **S1**)

Disilene  $\text{I}^t\text{BuN}({}^t\text{Bu}_2\text{MeSi})\text{Si}=\text{Si}(\text{Si}^t\text{Bu}_2\text{Me})\text{Ni}^t\text{Bu}$  (**V**) (100 mg, 132  $\mu\text{mol}$ , 1.00 eq.) was dissolved in toluene (5 mL) and degassed in a pressurizeable Schlenk flask. The mixture was exposed to carbon monoxide (1 bar) at  $-40^\circ\text{C}$ . Within 30 minutes, the mixture turned orange and slightly cloudy. All volatiles were removed in vacuo and the residue was extracted with *n*-hexane ( $3 \times 1 \text{ mL}$ ). The resulting solution was concentrated under reduced pressure and cooled to  $-35^\circ\text{C}$ . Compound **S1** was obtained as orange crystals (6.00 mg, 11.2 mmol, 8% yield). These crystals were also suitable for SC-XRD analysis.

**EA:**  $\text{Si}_3\text{C}_{29}\text{H}_{62}\text{N}_3$  Calculated [%]: C (64.85), H (11.64), N (7.82)  
 Experimental [%]: C (62.46), H (11.64), N (7.88)

Note: The carbon value was reproducibly low, presumably due to the formation of incombustible silicon carbides.

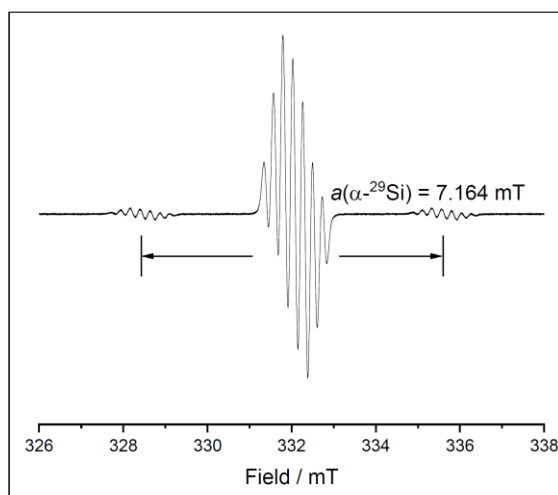


**Figure S15:** X-band EPR spectrum of **S1** in *n*-hexane ( $2 \times 10^{-3} \text{ M}$ ) at 286 K.



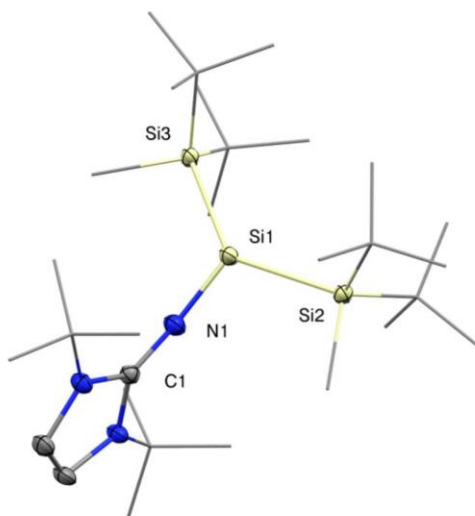


**Figure S16:** SC-XRD structure of the silyl radical **S1**, with thermal ellipsoids drawn at the 50% probability level. Hydrogen atoms are omitted for clarity, <sup>t</sup>Bu- and Me-groups are simplified as wireframes. Selected bond lengths [Å] and angles [°]: Si1–Si2 2.3843(7), Si1–Si3 2.3790(8), Si1–N1 1.676(2), N1–C1 1.280(3), Si2–Si1–Si3 132.98(3), Si3–Si1–N1 108.91(7), N1–Si1–Si2 111.62(7).

Note: Compound **S1** was obtained in a poor yield and the synthesis was not perfectly reproducible. Nonetheless, it was fully characterized by EPR spectroscopy, SC XRD analysis and elemental analysis. The EPR spectrum of **S1** displays a strong signal and two satellite signals with a hyperfine coupling constant (hfcc) of  $a(\alpha\text{-}^{29}\text{Si}) = 7.16$  mT, deriving from coupling of the unpaired electron with the central  $\alpha\text{-}^{29}\text{Si}$  nucleus (Figure S15). This  $\alpha\text{-}^{29}\text{Si}$  coupling constant is larger than in a silyl radical bearing three <sup>t</sup>Bu<sub>2</sub>MeSi substituents ( $a(\alpha\text{-}^{29}\text{Si}) = 5.80$  mT) and thus indicates a higher s-character.<sup>[S3]</sup> Furthermore, signal splitting, presumably from the contribution of the <sup>14</sup>N nuclei of the NHI substituent ( $a(^{14}\text{N}^{\text{exocyclic}})$ ,  $a(^{14}\text{N}^{\text{endocyclic}})$ ) and the  $\beta\text{-}^{29}\text{Si}$  nuclei ( $a(\beta\text{-}^{29}\text{Si})$ ) is observable. In the solid state, silyl radical **S1** exhibits a three-coordinate silicon center with a sum of bond angles of  $\Sigma\theta = 353.5^\circ$  (Figure S16), which is slightly more pyramidal than Sekiguchi's planar silyl radical (<sup>t</sup>Bu<sub>2</sub>MeSi)<sub>3</sub>Si<sup>•</sup>, and thus perfectly in line with the larger observed  $\alpha\text{-}^{29}\text{Si}$  hfcc in the EPR spectrum.<sup>[S3]</sup> The reasons for this higher degree of pyramidalization are of steric and electronic nature. On the one hand, the lower steric demand of the NHI ligand, compared to the bulky silyl groups, which is reflected in the wide Si2–Si1–Si3 angle of 133.0° does not force the silicon center to adopt a planar geometry. On the other hand, calculations predict, that electronegative substituents, which possess lone-pair electrons, such as nitrogen increase the pyramidalization of silyl radicals.<sup>[S4]</sup>

Although the presented synthesis of **S1** is not a suitable approach for the preparation of larger amounts of silyl radicals, it is a definite prove for the accessibility and stability of neutral, NHI-substituted silyl radicals.

## 2. X-ray Crystallographic Data

### 2.1. General Information

The X-ray intensity data of **1** and **2a** were collected on an X-ray single crystal diffractometer equipped with a CMOS detector (*Bruker Photon-100*), a rotating anode (*Bruker TXS*) with MoK $\alpha$  radiation ( $\lambda = 0.71073 \text{ \AA}$ ) and a *Helios* mirror optic by using the *APEX III* software package.<sup>[S5]</sup> The measurements were performed on single crystals coated with the perfluorinated ether *Fomblin*<sup>®</sup> Y. The crystal was fixed on the top of a micro sampler, transferred to the diffractometer and frozen under a stream of cold nitrogen. A matrix scan was used to determine the initial lattice parameters. Reflections were merged and corrected for Lorentz and polarization effects, scan speed, and background using *SAINT*.<sup>[S6]</sup> Absorption corrections, including odd and even ordered spherical harmonics were performed using *SADABS*.<sup>[S6]</sup> Space group assignments were based upon systematic absences, E statistics, and successful refinement of the structures. Structures were solved by direct methods with the aid of successive difference Fourier maps, and were refined against all data using the *APEX III* software in conjunction with *SHELXL-2014*<sup>[S7]</sup> and *SHELXLE*.<sup>[S8]</sup> All H atoms were placed in calculated positions and refined using a riding model, with methylene and aromatic C–H distances of 0.99 and 0.95  $\text{\AA}$ , respectively, and  $U_{\text{iso}}(\text{H}) = 1.2 \cdot U_{\text{eq}}(\text{C})$ . Full-matrix least-squares refinements were carried out by minimizing  $\Delta w(F_o^2 - F_c^2)$ <sup>[S6]</sup> with *SHELXL-97* weighting scheme.<sup>[S9]</sup> Neutral atom scattering factors for all atoms and anomalous dispersion corrections for the non-hydrogen atoms were taken from International Tables for Crystallography.<sup>[S10]</sup> The images of the crystal structures were generated by *Mercury*.<sup>[S11]</sup> The CCDC numbers - contain the supplementary crystallographic data for the structures. These data can be obtained free of charge from the Cambridge Crystallographic Data Centre via <https://www.ccdc.cam.ac.uk/structures/>.

## 2.2 SC-XRD structures

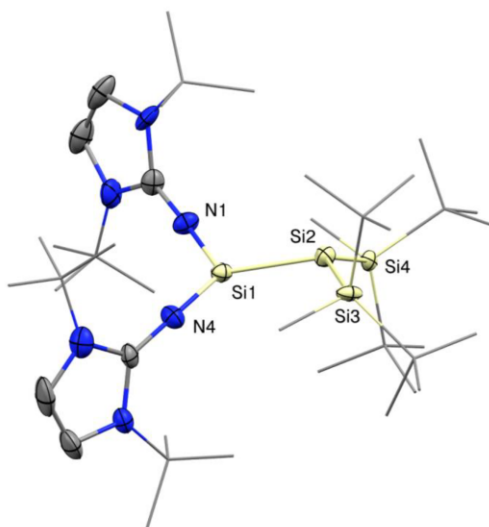


**Figure S17:** SC-XRD structure of disilene **1** with thermal ellipsoids drawn at the 30% probability level. Hydrogen atoms are omitted for clarity, <sup>t</sup>Bu- and Me-groups are simplified as wireframes. Selected bond lengths [Å] and angles [°]: Si1–Si2 2.219(4), Si1–N1 1.659(4), Si1–N4 1.604(4), Si2–Si3 2.360(6), Si2–Si4 2.343(5), N1–Si1–N4 113.1(2), Si3–Si2–Si4 138.2(2), Si1–Si2–Si3 106.3(2), Si2–Si1–N1 115.4(2).

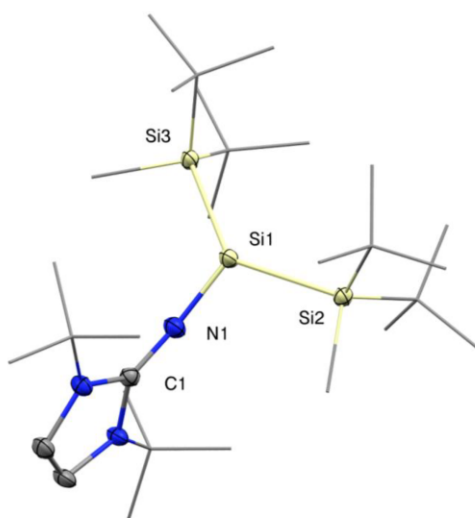


**Figure S18:** SC-XRD structure of the silyl radical **S1**, with thermal ellipsoids drawn at the 50% probability level. Hydrogen atoms are omitted for clarity, <sup>t</sup>Bu- and Me-groups are simplified as wireframes. Selected bond lengths [Å] and angles [°]: Si1–Si2 2.3843(7), Si1–Si3 2.3790(8), Si1–N1 1.676(2), N1–C1 1.280(3), Si2–Si1–Si3 132.98(3), Si3–Si1–N1 108.91(7), N1–Si1–Si2 111.62(7).

S19

### 3. References

- [S1] G. R. Fulmer, A. J. M. Miller, N. H. Sherden, H. E. Gottlieb, A. Nudelman, B. M. Stoltz, J. E. Bercaw, K. I. Goldberg, NMR Chemical Shifts of Trace Impurities: Common Laboratory Solvents, Organics, and Gases in Deuterated Solvents Relevant to the Organometallic Chemist. *Organometallics*, **2010**, *29*, 2176-2179.
- [S2] A. Sekiguchi, S. Inoue, M. Ichinohe, Y. Arai, Isolable Anion Radical of Blue Disilene ( $\text{Bu}_2\text{MeSi}$ )<sub>2</sub>Si=Si(SiMe'Bu<sub>2</sub>)<sub>2</sub> Formed upon One-Electron Reduction: Synthesis and Characterization. *J. Am. Chem. Soc.*, **2004**, *126*, 9626-9629.
- [S3] A. Sekiguchi, T. Fukawa, M. Nakamoto, V. Y. Lee, M. Ichinohe, Isolable Silyl and Germyl Radicals Lacking Conjugation with  $\pi$ -Bonds: Synthesis, Characterization, and Reactivity. *J. Am. Chem. Soc.*, **2002**, *124*, 9865-9869.
- [S4] B. Tumanskii, M. Karni, Y. Apeloig, *Encyclopedia of Radicals in Chemistry, Biology and Materials*, **2012**.
- [S5] *APEX suite of crystallographic software*, APEX 3 version 2015.5-2; Bruker AXS Inc.: Madison, Wisconsin, USA, **2015**.
- [S6] *SAINTE*, Version 7.56a and *SADABS* Version 2008/1; Bruker AXS Inc.: Madison, Wisconsin, USA, **2008**.
- [S7] G. M. Sheldrick, SHELXL-2014, University of Göttingen, Göttingen, Germany, **2014**.
- [S8] C. B. Hübschle, G. M. Sheldrick, B. Dittrich, ShelXle: a Qt graphical user interface for SHELXL. *J. Appl. Cryst.*, **2011**, *44*, 1281-1284.
- [S9] G. M. Sheldrick, SHELXL-97, University of Göttingen, Göttingen, Germany, **1998**.
- [S10] A. J. C. Wilson, *International Tables for Crystallography*, Volume C, Tables 6.1.1.4 (pp. 500-502), 4.2.6.8 (pp. 219-222), and 4.2.4.2 (pp. 193-199), Kluwer Academic Publishers: Dordrecht, The Netherlands, **1992**.
- [S11] C. F. Macrae, I. J. Bruno, J. A. Chisholm, P. R. Edgington, P. McCabe, E. Pidcock, L. Rodriguez-Monge, R. Taylor, J. van de Streek, P. A. Wood, Mercury CSD 2.0 - new features for the visualization and investigation of crystal structures. *J. Appl. Cryst.*, **2008**, *41*, 466-470.

## 15.6 Licenses for Copyrighted Content

### 15.6.1 License for Chapter 7: “Isolation of a Relatively Air-stable, Bulky Silyl-substituted, Neutral Silicon-centered Radical”

Dear Mr. Holzner,

**We hereby grant permission for the requested use expected that due credit is given to the original source.**

If material appears within our work with credit to another source, authorisation from that source must be obtained.

Credit must include the following components:

- Journals: Author(s) Name(s); Title of the Article. Name of the Journal. Publication year. Volume. Page(s). Copyright Wiley-VCH Verlag GmbH & Co. KGaA. Reproduced with permission.

If you also wish to publish your thesis in electronic format, you may use the article according to the Copyright transfer agreement:

#### 3. Final Published Version.

Wiley-VCH hereby licenses back to the Contributor the following rights with respect to the final published version of the Contribution:

a. [...]

b. Re-use in other publications. The right to re-use the final Contribution or parts thereof for any publication authored or edited by the Contributor (excluding journal articles) where such re-used material constitutes less than half of the total material in such publication. In such case, any modifications should be accurately noted.

Kind regards

Bettina Loycke  
Senior Rights Manager  
Rights & Licenses


Wiley-VCH Verlag GmbH & Co. KGaA  
Boschstraße 12  
69469 Weinheim  
Germany  
www.wiley-vch.de

T + (49) 6201 606-280  
F + (49) 6201 606-332  
rightsDE@wiley.com

**WILEY**

Journal: European Journal of Inorganic Chemistry  
Authors: R. Holzner, A. Kaushansky, B. Tumanskii, P. Frisch, F. Linsenmann, S. Inoue  
Volume Number: 25  
Year of Publication: 2019  
Title: Isolation of a Relatively Air-stable, Bulky Silyl-substituted, Neutral Silicon-centered Radical  
Pages: 2977-2981  
DOI: 10.1002/ejic.201900522

## 15.6.2 License for Chapter 8: “Disilene–Silylene Interconversion: A Synthetically Accessible Acyclic Bis(silyl)silylene”

 ACS Publications  
Disilene–Silylene Interconversion: A Synthetically Accessible Acyclic Bis(silyl)silylene

Author: Dominik Reiter, Richard Holzner, Amelie Porzelt, et al  
Publication: Journal of the American Chemical Society  
Publisher: American Chemical Society  
Date: Aug 1, 2019  
Copyright © 2019, American Chemical Society

**PERMISSION/LICENSE IS GRANTED FOR YOUR ORDER AT NO CHARGE**

This type of permission/license, instead of the standard Terms & Conditions, is sent to you because no fee is being charged for your order. Please note the following:

- Permission is granted for your request in both print and electronic formats, and translations.
- If figures and/or tables were requested, they may be adapted or used in part.
- Please print this page for your records and send a copy of it to your publisher/graduate school.
- Appropriate credit for the requested material should be given as follows: "Reprinted (adapted) with permission from (COMPLETE REFERENCE CITATION). Copyright (YEAR) American Chemical Society." Insert appropriate information in place of the capitalized words.
- One-time permission is granted only for the use specified in your request. No additional uses are granted (such as derivative works or other editions). For any other uses, please submit a new request.

[BACK](#) [CLOSE WINDOW](#)

© 2020 Copyright - All Rights Reserved | Copyright Clearance Center, Inc. | [Privacy statement](#) | [Terms and Conditions](#)  
Comments? We would like to hear from you. E-mail us at [customer-care@copyright.com](mailto:customer-care@copyright.com)



### 15.6.3 License for Chapter 9: “DMAP-stabilized bis(silyl)silylenes as versatile synthons for organosilicon compounds”

Dear Richard

The Royal Society of Chemistry (RSC) hereby grants permission for the use of your paper(s) specified below in the printed and microfilm version of your thesis. You may also make available the PDF version of your paper(s) that the RSC sent to the corresponding author(s) of your paper(s) upon publication of the paper(s) in the following ways: in your thesis via any website that your university may have for the deposition of theses, via your university's Intranet or via your own personal website. We are however unable to grant you permission to include the PDF version of the paper(s) on its own in your institutional repository. The Royal Society of Chemistry is a signatory to the STM Guidelines on Permissions (available on request).

Please note that if the material specified below or any part of it appears with credit or acknowledgement to a third party then you must also secure permission from that third party before reproducing that material.

Please ensure that the thesis includes the correct acknowledgement (see <http://rsc.li/permissions> for details) and a link is included to the paper on the Royal Society of Chemistry's website.

Please also ensure that your co-authors are aware that you are including the paper in your thesis.

Regards

Gill Cockhead  
Contracts & Copyright Executive

Gill Cockhead  
Contracts & Copyright Executive  
Royal Society of Chemistry,  
Thomas Graham House,  
Science Park, Milton Road,  
Cambridge, CB4 0WF, UK  
Tel +44 (0) 1223 432134

Journal: RSC Advances  
Authors: R. Holzner, D. Reiter, P. Frisch, S. Inoue  
Volume Number: 10  
Year of Publication: 2020  
Title: DMAP-stabilized bis(silyl)silylenes as versatile synthons for organosilicon compounds  
Pages: 3402-3406  
DOI: 10.1039/C9RA10628F